Final Report

Correlation of Slag Cement Composition with Durability of Portland Cement-Slag Concrete

FDOT Contract Number BDV25-977-63

Date: April 2021

Submitted To: Jose Armenteros, MSc, PE

Concrete Materials Engineer

Florida Department of Transportation

State Materials Office

5007 NE 39th Avenue

Gainesville, FL 32609

Phone: 352-955-6666

Email: Jose.Armenteros@dot.state.fl.us

Submitted By: Dr. Abla Zayed

Department of Civil and Environmental Engineering

University of South Florida

4202 E Fowler Avenue

Tampa, FL 33620

Phone: 813-974-5823

zayed@usf.edu

Disclaimer

The opinions, findings, and conclusions expressed in this publication are those of the authors and not necessarily those of the State of Florida Department of Transportation (FDOT) or the U.S. Department of Transportation (USDOT) or the Federal Highway Administration (FHWA).

		Approximate Conversions to SI Units (from FHWA)			
Symbol	**When You Know**	**Multiply By**	**To Find**	**Symbol**
Length				
in	inches	25.4	millimeters	mm
ft	feet	0.305	meters	m
yd	yards	0.914	meters	m
mi	miles	1.61	kilometers	km
Area				
in^2	square inches	645.2	square millimeters	mm^2
ft^2	square feet	0.093	square meters	m^2
yd^2	square yard	0.836	square meters	m^2
mi^2	square miles	2.59	square kilometers	km^2
Volume				
fl oz	fluid ounces	29.57	milliliters	mL
gal	gallons	3.785	liters	L
ft^3	cubic feet	0.028	cubic meters	m^3
yd^3	cubic yards	0.765	cubic meters	m^3
NOTE: volumes greater than 1000 L shall be shown in m^3				
Mass				
oz	ounces	28.35	grams	g
lb	pounds	0.454	kilograms	kg
Temperature (exact degrees)				
°F	Fahrenheit	5 (F-32)/9 or (F-32)/1.8	Celsius	°C
Illumination				
fc	foot-candles	10.76	lux	lx
fl	foot-Lamberts	3.426	candela/m^2	cd/m^2
Force and Pressure or Stress				
lbf	pound-force	4.45	newtons	N
lbf/in^2	pound-force per square inch	6.89	kilopascals	kPa

Technical Report Documentation Page

1. Report No.	2. Government Accession No.	3. Recipient's Catalog No.

4. Title and Subtitle	5. Report Date
Correlation of Slag Cement Composition with Durability of Portland Cement-Slag Concrete	
	6. Performing Organization Code

7. Author(s)	8. Performing Organization Report No.
Abla Zayed, Kyle Riding, Dhanushika Mapa, Hai Zhu, Jair Burgos, Farzaneh Nosouhian, Yuri Stetsko	

9. Performing Organization Name and Address	10. Work Unit No. (TRAIS)
Department of Civil and Environmental Engineering University of South Florida 4202 E Fowler Avenue; ENB 118 Tampa, FL 33620-5350	
	11. Contract or Grant No. BDV25-977-63

12. Sponsoring Agency Name and Address	13. Type of Report and Period Covered
Florida Department of Transportation 605 Suwannee St, MS 30 Tallahassee, FL 32399	Final Report April 30, 2019-April 30, 2021
	14. Sponsoring Agency Code

15. Supplementary Notes

16. Abstract

Three ordinary portland cements (OPC), three limestone cements (IL), and seven ground granulated blast furnace slags (GGBFS/slag) were used to investigate the heat generation, adiabatic temperature rise, sulfate optimization, sulfate durability (external and internal), and chloride durability in slag-blended cementitious systems. The as-received materials were characterized for their physical, chemical, and mineralogical composition using Blaine fineness, particle size distribution, specific gravity, X-ray fluorescence, and X-ray diffraction coupled with Rietveld refinement. The selected cements varied in their tricalcium aluminate, tricalcium silicate, sulfates, alkali, calcite contents, and fineness. Alumina content, magnesia-to-alumina ratio, sulfate levels and fineness were varied in the selected slags. A single slag substitution level of 60% was used throughout this study, as it is the most commonly used replacement level in massive concrete structural elements in the state of Florida. Adiabatic temperature rise of plain and slag blended concrete of a cementitious content of 665 lb/yd^3 was measured using Type II(MH) cement, Type IL cement and their blends with slags of variable alumina content for a total of 10 concrete mixtures. Slag blended cementitious systems were optimized for sulfate content based on heat of hydration measurements according to ASTM C563 and adding hemihydrate as a partial replacement of slag. External sulfate durability was assessed using ASTM C1012 at a constant water-to-cementitious materials (w/cm) ratio. Delayed ettringite formation (DEF) was investigated using heat-cured mortar bars. Sulfate-optimized mixtures were also studied for sulfate durability. Chloride binding experiments were conducted on selected plain mixtures as well as slag-blended mixtures. Phase assemblage studies using quantitative X-ray diffraction and thermodynamic modeling were performed on pastes and mortars. The findings indicate the significance of the slag alumina content and magnesia-to-alumina ratio on adiabatic temperature rise. Limestone cement concrete generated lower adiabatic temperature rise than Type II(MH); however, for the slag-blended mixtures, incorporation of the same slag generated similar adiabatic temperature rise when blended with either cements. Sulfate demand of the slag-blended cementitious mixtures was influenced by cement C_3A, C_4AF and calcite contents, and slag alumina and magnesia contents as well as their particle size. External sulfate durability of the system appeared to be affected by the cement C_3A and calcite content, and the slag alumina and the sulfate content. Expansion caused by DEF was suppressed when slag was used at 60% replacement level. Chloride binding was enhanced with increasing slag alumina levels and was negatively affected by the alkalis and limestone content of cement.

17. Key Word	18. Distribution Statement
Slag chemical and physical characteristics, adiabatic temperature rise, sulfate optimization in slag blended systems, delayed ettringite formation, chloride binding isotherms, sulfate durability	

19. Security Classif. (of this report)	20. Security Classif. (of this page)	21. No. of Pages	22. Price
None	None	335	

Form DOT F 1700.7 (8-72)   Reproduction of completed page authorized

Acknowledgment

Executive Summary

E.1   Background

In general, supplementary cementitious materials (SCMs) such as fly ash and slag are widely used in structural concrete elements in the state of Florida to enhance durability performance and service life. Recent field data of drilled shafts [1], however, showed high core temperatures. These mixtures incorporated ground granulated blast furnace slag (GGBFS, slag) at 60% replacement levels. Additionally, recent research [2] conducted by the Concrete Construction Materials Group at the University of South Florida identified higher cracking risks and poor sulfate resistance in slag-blended concrete mixtures with several portland cement-slag combinations. The slag-blended concrete mixtures used in the conducted research were similar to those approved for use in structural concrete elements in Florida. The findings indicated that slag fineness, alumina content, and alumina-to-magnesia ratio have significant influence on shrinkage, heat evolution, cracking potential, and sulfate durability. Furthermore, there is a concern about whether current FDOT Standard Specifications on slag source acceptance provide adequate reporting requirements to specify the appropriate slag replacement levels for different concrete types and service conditions to sustain durability and service life. Additionally, there were questions about the accuracy of the adiabatic temperature rise in massive concrete elements, specifically for mixtures incorporating currently available cements and slags in the state of Florida. This study highlights the importance of material characteristics of cements and slags on the durability performance of slag-blended concrete mixtures to prevent or minimize structural damage and extend the service life of concrete structures in the state of Florida.

E.2   Research Objectives

The objectives of this investigation were:

1. Assess adiabatic temperature rise in slag-blended concrete mixtures.
2. Identify methods to ensure sulfate optimization in slag-blended cementitious systems.
3. Establish the effects of sulfate-optimized slag-blended cementitious systems on durability.

Satisfying these objectives provides the Florida Department of Transportation (FDOT) with the scientific knowledge required to modify the specifications pertaining to slag and slag use in structural concrete exposed to variable environmental conditions. This will ensure appropriate use of slag-blended systems to ensure sustainable and durable structural concrete elements in the state of Florida.

In order to achieve the objectives, several slags and cements with different chemical and physical characteristics were identified. The as-received materials were characterized using X-ray fluorescence analysis, X-ray diffraction coupled with Rietveld refinement, Blaine fineness, laser particle size distribution, and specific gravity. The blended systems used a single cement replacement level of 60% by mass of slag as identified by the State Materials Office (SMO) of the Florida Department of Transportation (FDOT). Sulfate optimization was conducted in duplicates using isothermal calorimetry for the slag-blended cementitious mixtures with a total of 160 batches. Subsequently, mortar bars were prepared using the as-received sulfate content for the control as well as the slag-blended mixtures and tested for internal and external sulfate durability. To verify the effectiveness of optimizing the slag sulfate content on concrete sulfate durability, additional mortar mixtures were prepared using the optimized slag sulfate content and tested for internal and external sulfate attack. A total of approximately 140 mortar batches (six specimens in each mixture) were prepared to assess sulfate durability and phase assemblage evolution. Chloride binding isotherms for selected cementitious systems were also determined.

To address the challenge in assessing the adiabatic temperature rise in concrete typically used in the state of Florida for massive structural elements, two cements were used: ASTM C150 Type II(MH) and ASTM C595 Type IL cements. A total of ten (10) concrete mixtures were prepared including slag-blended concrete mixtures. The slags were selected to reflect variability in alumina, alumina-to-magnesia ratio and fineness. Adiabatic temperature rise experiments were conducted at the United States Bureau of Reclamation (USBR) laboratory in Denver, CO.

E.3   Main Findings

The findings indicate that adiabatic temperature rise and the rate of temperature rise of slag-blended mixtures depend on slag chemical composition; namely, alumina and magnesia content as well as the cement type. The findings also indicate that adiabatic temperature rise

predictions using ACI 207.2R underestimate the adiabatic temperature rise in mass concrete using Type II(MH) and Type IL(10) cements. Concrete mixtures made with Type IL cement showed lower adiabatic temperature rise during the first 48 hours compared to Type II(MH) concrete mixture. At 60% slag replacement, concrete blended with high alumina slag did not provide significant reduction in the adiabatic temperature rise compared to the control mixtures. The findings indicate the significance of the cement and slag chemical and physical characteristics on adiabatic temperature rise in slag-blended concrete mixtures. Mass concrete control plans (MCCP) must be developed based on the specific cement and slag used in the mixture.

The findings of the current research developed adiabatic temperature rise curves for concrete made with Type IL(10) and Type II(MH) cements which can be implemented in the approval process of MCCP and subsequently offer a better prediction for field concrete temperature rise in structural elements. Additionally, the current research provided values for equivalent cement factors for different slags (B), which are required for adiabatic temperature prediction in concrete mixtures incorporating slags of variable chemical composition. Again, the provided scientific data, when implemented in MCCP approval protocols, would minimize if not eliminate field issues related to underpredicting temperature rise in mass concrete elements and therefore enhance the service life of massive structural elements.

Sulfate optimization studies indicated that the sulfate balance of slag-blended cementitious mixtures was affected by the cementitious materials particle size as well as the cement composition (alumina-bearing compounds and calcite content) and slag composition (alumina, magnesia and calcite). Isothermal calorimetry was found to be an accurate technique to identify optimum sulfate contents for slag-blended cementitious systems.

In terms of external sulfate durability, slags blended with Type IL(10 or 14) cements showed better durability than mixtures with Type II(MH) or Type I cements. The limestone content was also found to affect durability with higher limestone content showing better durability (up to 11% calcite content). Additionally, sulfate durability experiments conducted on sulfate-optimized slag mixtures suggested that sulfate durability assessed using ASTM C1012 for a period of 6 months improved with sulfate optimization. However, extending the exposure time to 18 months might be critical for proper classification of the appropriate sulfate exposure class.

Internal sulfate attack or delayed ettringite formation (DEF) studies were conducted on plain and slag-blended mortar (60% replacement). The findings indicate that for the control mixtures prepared with Type I (moderate and high alkali content (HA)), Type II moderate heat (MH), Type IL(10), or Type IL(14) cements all showed expansion from DEF within 120 days. No signs of delayed ettringite formation (DEF) were identified for mixtures incorporating slag at 60% replacement level whether the slag had the as-received or optimized sulfate content. However, longer monitoring times are needed to verify this conclusion.

The findings also indicated that high alumina slag cementitious systems have higher chloride binding capacities than low alumina slag systems. Further research is needed to assess the effectiveness of slags of variable chemical composition, at different replacement levels, on chloride diffusivity in slag-blended concrete (FDOT Road and Bridge Construction Specification). This is a critical study which is necessary for specifying the minimum slag replacement levels in reinforced structural elements to minimize incidence of reinforcement corrosion and enhance corrosion performance and durability of the infrastructure in the state of Florida.

E.4 Recommendations

Based on the findings of this study, the following recommendations can be made:

1. Proposed specification changes to the following current FDOT specifications:

   a. Specification 929 Supplementary Cementitious Materials, Sub-article 929-4 Ground Granulated Blast Furnace Slag:

   Ground granulated blast furnace slag (GGBFS, slag cement, slag) is the quenched, ground byproduct of the iron ore refinement process conducted in blast furnaces. It is primarily an amorphous material of calcium aluminosilicate constituents.

   929-4 Slag Cement.

   Sub-article 929-4.1 General: Slag and reference cement used for the determination of slag activity tests shall meet the requirements of ASTM C989. Sampling and testing procedures shall follow the requirements of ASTM C989. Calcium sulfate or calcium sulfate and limestone additions are required for slags with alumina content greater than 11%. Addition amounts shall be determined in accordance with ASTM C563 using isothermal calorimetry and a 50:50 cement-GGBFS blend.

Sub-article 929-4.2 Acceptance Testing of Slag: Acceptance of slag from sources operating under an accepted QC Plan shall be based on the monthly test reports meeting the chemical and physical requirements of ASTM C989 and this Section. Acceptance testing documentation shall include:

1. Reporting results of all testing listed under Section 10 of ASTM C989.
2. Report results of the following elemental oxide content: CaO, SiO_2, Al_2O_3, MgO, MnO, TiO_2, total SO_3, Fe_2O_3, Na_2O, and K_2O.
3. Report any limestone addition content, including $CaCO_3$ content.
4. Report any calcium sulfate addition content, including SO_3 content.
5. Report any inorganic processing additions content. If inorganic processing additions are used, report compliance with Section 6.1.2. of ASTM C989.

Corresponding samples along with monthly test reports shall be submitted to the Department, upon request.

Sub-article 929-4.3 Exceptions: Slag alumina content shall not exceed 18%. Slags with alumina content $\geq 15\%$ but not exceeding 18% must have an expansion $\leq 0.1\%$ at 365 days when tested in accordance with ASTM C1012 using Type I/II portland cement with an equivalent alkali content of $\leq 0.6\%$, fixed w/cm of 0.485, and slag content of 50% to be approved for use.

b. Recommended modifications for Standard Specification, Section 346 Table 346-2 for Structural Portland Cement Concrete: The recommended changes to Tables 346-2 and 346-3 are shown below in red, bold, and underlined:

				Highly Reactive Pozzolans [4]		
Application	Portland Cement	Fly Ash Type F	Slag	Silica Fume	Metakaolin	Ultra-Fine Fly Ash
General Use	70-82	18-30				
	66-78	15-25		7-9		
	66-78	15-25			8-12	
	66-78	15-25				8-12
	30-40	10-20	50-60			
	30-75 [1]		25-70 [1]			
	41-50		**50-59 [5]**			
	30-40		**60-70**			
	36-43		50-55	7-9		
	33-42		50-55		8-12	
	33-42		50-55			8-12
Precast / Prestressed	70-85 [1]	15-30 [1]				
	70-82	18-30				
	66-78	15-25		7-9		
	66-78	15-25			8-12	
	66-78	15-25				8-12
	30-40	10-20	50-60			
	41-50		**50-59 [5]**			
	30-40		**60-70**			
	36-43		50-55	7-9		
	33-42		50-55		8-12	
	33-42		50-55			8-12
Drilled Shaft	63-67	33-37				
	38-42		58-62			
	30-40	10-20	50-60			
Mass Concrete	50-82 [2]	18-50 [2]				
	50-65 [3]	35-50 [3]				
	66-78	15-25		7-9		
	66-78	15-25			8-12	
	66-78	15-25				8-12
	30-40	10-20	50-60			
	41-50		**50-59 [5]**			
	30-40		**60-70**			
	36-43		50-55	7-9		
	33-42		50-55		8-12	
	33-42		50-55			8-12

Recommended Modifications to Table 346-2
Cementitious Materials Concrete Mix Proportions (%)
(Environmental classification is extremely aggressive, unless otherwise noted)

Notes:
(1) Slightly Aggressive and Moderately Aggressive environments. **For Moderately Aggressive environment, water to cementitious materials ratio (w/cm) must be less than or equal to 0.50**.
(2) For Concrete with Core Temperature T≤**160**°F.
(3) For Concrete with Core Temperature T>**160**°F.
(4) Highly reactive pozzolans may be used below the specified ranges to enhance strength and workability.
(5) Concrete in contact with soil or water using slag with $Al_2O_3 \geq 15\%$, requires maximum w/cm = 0.40 and minimum $f_c' = 5,000$ psi or demonstrate that slag at 50% replacement of Type II portland cement (ASTM C150), tested in accordance to ASTM C1012 at a fixed w/cm ratio of 0.485, does not exceed 0.1% expansion at 12 months. Report the chemical and physical properties of the cement and slag (according to relevant FDOT reporting requirements on cement and slag) used in ASTM C1012 testing.

Recommended Modifications to Table 346-3 Master Proportion Table			
Class of Concrete	28-day Specified Minimum Compressive Strength [7] (f_c') (psi)	Maximum Water to Cementitious Materials Ratio [7] (pounds per pounds)	Target Slump Value (inches) [3]
I [1]	3,000	0.53[8]	3 [2]
I (Pavement)	3,000	0.50	1.5 or 3 [5]
II [1]	3,400	0.53[8]	3 [2]
II (Bridge Deck)	4,500	0.44	3 [2]
III [4]	5,000	0.44	3 [2]
III (Seal)	3,000	0.53[8]	8
IV	5,500	0.41[6]	3 [2]
IV (Drilled Shaft)	4,000	0.41	8.5
V (Special)	6,000	0.37[6]	3 [2]
V	6,500	0.37[6]	3 [2
VI	8,500	0.37[6]	3 [2]
VII	10,000	0.37[6]	3 [2]

Notes:

(1) For precast three-sided culverts, box culverts, endwalls, inlets, manholes and junction boxes, the target slump value and air content will not apply. The maximum allowable slump is 6 inches, except as noted in (2). The Contractor is permitted to use concrete meeting the requirements of ASTM C478 (4,000 psi) in lieu of the specified Class I or Class II concrete for precast endwalls, inlets, manholes and junction boxes.

(2) The Engineer may allow a maximum target slump of 7 inches when a Type F, G, I or II admixture is used.

(3) For a reduction in the target slump for slip-form operations, submit a revision to the mix design to the Engineer. The target slump for slip-form mix is 1.50 inches.

(4) When precast three-sided culverts, box culverts, endwalls, inlets, manholes or junction boxes require a Class III concrete, the minimum cementitious materials content is 470 pounds per cubic yard. Do not apply the air content range and the maximum target slump shall be 6 inches, except as allowed in (2).

(5) Meet the requirements of Section 350.

(6) When silica fume or metakaolin is required, the maximum water to cementitious material ratio will be 0.35. When ultrafine fly ash is used, the maximum water to cementitious material ratio will be 0.30.

(7) When slag is used as supplementary cementitious materials in structures located in a very severe sulfate environment (S3) according to ACI 201.2 classification, use slag with $Al_2O_3 \leq 15\%$, $f_c' > 5,000$ psi and maximum w/cm of 0.40.

(8) When used in structures located in a moderate sulfate environment (S1) according to ACI 201.2, the w/cm must not exceed 0.50. When used in structures located in a severe sulfate environment (S2) according to ACI 201.2, the w/cm must not exceed 0.45 and fc' > 4500.

2. For structural concrete elements, where temperature rise is a concern, require use of Figure B2 in Appendix B (Adiabatic temperature rise as a function of placement temperature for Type IL cement content of 665 lb/yd^3) for concrete mixtures made with ASTM C595 Type IL cement and Figure B3 (Adiabatic temperature rise as a function of placement temperature for Type II(MH) cement content of 665 lb/yd^3) for concrete mixtures made with an ASTM C150 Type II(MH) cement in the MCCP in lieu of

Figure 4.3 of ACI 207.2R. Use of this data can be enforced during MCCP approval process.

3. When using the adiabatic temperature rise curves in Figures B2 and B3, require use of B values in MCCP analysis of 0.85 for slags with alumina content of 8% and 14% and 1.0 for slags with alumina content of 10% and 17%. Use of the specified B values can be enforced during the MCCP approval process.

4. In lieu of Figure B2 or Figure B3 and use of B values, allow specialty engineers to use adiabatic temperature rise values taken from test data from adiabatic or semi-adiabatic temperature rise tests conducted by USBR or a licensed professional engineer. This allowance can be enforced during the MCCP approval process.

5. Approval process of slag-blended concrete mixtures must include testing for sulfate balance of the cementitious constituents of the submitted mixture including all chemical admixtures. Testing should occur at the identified replacement level as well as the identified w/cm ratio according to ASTM C563.

6. Require testing for external sulfate durability according to ASTM C1012, for a period of 18 months, as part of the approval process for sulfate-optimized slag mixtures.

E.5   Recommendations for Future Study

Based on the findings of this study, the following is recommended:

1. Initiate a study to assess chloride ingress in slag-blended concrete using slag sources of different chemical composition. In addition to assessing the effectiveness of slags of different chemical composition on chloride ingress, the study must also assess the effectiveness of different slag replacement levels on chloride diffusivity. This is a critical study that will directly impact the current specifications pertaining to minimum slag content and subsequently the appropriate use of slag-blended concrete mixture proportions.

2. Initiate a study to assess the degree of slag reactivity and its relationship to chemical, physical, and mineralogical characteristics of slags. This will be beneficial to further improve the adiabatic temperature rise prediction for slag-blended concrete mixtures.

3. Initiate a study to assess the sulfate optimization with an expanded matrix of slags and cements currently available in the state of Florida. The study must cover, at a minimum, the currently approved replacement levels of slags in slag-blended concrete under FDOT Road and Bridge Construction Specification.

4. Initiate a study to investigate the effect of sulfate and limestone content in slag on sulfate durability (external and internal (DEF)) and chloride ingress in slag-blended systems at different replacement levels.

E.6   References

[1]   G. Mullins, "Personal Communications." 2019.

[2]   A. Zayed, K. A. Riding, Y. Stetsko, N. Shanahan, A. Markandeya, F. Nosouhian, D. Mapa and M. Fincan, "Final Report Effects of Blast Furnace Slag Characteristics on Durability of Cementitious Systems for Florida Concrete Structures FDOT Contract Number : BDV25-977-28," University of South Florida, Tampa, FL, 2019.

Table of Contents

List of Figures

List of Tables

xxx

Chapter 1   Literature Review

1.1   Introduction

Supplementary cementitious materials (SCMs) are widely used in the state of Florida to enhance the durability and service life of concrete structures. Ground granulated blast furnace slag (GGBFS, slag, slag cement) is extensively used as an SCM in concrete mixtures to improve durability performance. Typically, concrete mixtures made with slag are expected to minimize the initial temperature rise and provide better resistance to sulfate attack and chloride ingress. The findings of a recent investigation conducted by the University of South Florida – Concrete Construction Materials Group [1] indicated that certain combinations of portland cements and slags experience higher cracking risks and provided poor sulfate resistance. It was further demonstrated that the fineness, alumina content, and alumina-to-magnesia ratio of slags have significant influence on temperature rise, cracking potential, and sulfate durability of slag-blended systems.

The concrete mixtures used in the field or the laboratory investigation that experienced durability issues, contained slags in compliance with the current standard specifications for slags: ASTM C989 and AASHTO-M302. While the current slag specifications allow for calcium sulfate and processing additions, they do not require the slag source (supplier) to provide this information on the Mill Certificate. The information is only provided if the end user requests optional chemical and physical data. No limitation is provided on the chemical requirements for slags other than sulfide sulfur (S) at a maximum of 2.5%. Therefore, it is evident that the technical guidance provided by the current specifications as it pertains to the slag's chemical and physical characteristics necessary to sustain concrete durability is not adequate. Among the chemical and physical characteristics of GGBFS, sulfate additions are important especially for high alumina slags, as this will affect the sulfate balance of the cementitious system. In the following sections, the findings of the literature review on the characteristics of slags that affect the durability of concrete incorporating slag will be presented.

1.1.1 Slag Characteristics

Slag is a by-product of iron ore refinement. It is a latent hydraulic material and therefore it does not require the presence of portland cement to develop cementing properties, but it can be used on its own in the presence of an alkali activator [2]. In an OPC-slag system, the high pH of the pore solution, alkalis and sulfates resulting from cement particles hydrolysis and dissolution activate slag hydration [3]–[5]. Slag is widely used as an SCM because it is known to improve the workability and reduce the initial temperature rise during the early stages of hydration. It is also known to reduce permeability and subsequently provide high resistance to sulfate attack and chloride penetration.

ASTM C989 [6] divides slags into three grades based on a strength activity index (SAI): grades 80, 100 and 120. This SAI is defined based on the compressive strength of a 50/50 OPC-BFS blend to that of unblended reference cement. The average 28-day SAI from the last 5 consecutive samples must be at least 75 for Grade 80, 95 for Grade 100, and 115 for Grade 120. Grades 100 and 120 are more commonly used in concrete than Grade 80 because of the early strength gain [3].

Slag is mainly comprised of lime, silica, alumina and magnesia [3], [7]. However, its chemical composition can vary depending on the nature of the iron ore, the composition of the limestone flux, the coke consumption and the kind of iron being made. The range of the chemical compositions of different slags [7], available globally, is summarized in Table 1-1. Slag contains both amorphous and crystalline phases. In order to use slag as a SCM in concrete, it should have 90-100% amorphous content [8]. This is achieved by rapid cooling or quenching of molten slag to temperatures below 800°C (1,472°F) from 1,400°C–1,500°C (2,552°F–2,732°F) [7], [8]. The crystalline phases in slags can form in cases where molten slag is cooled at a slower rate. These phases remain inert [9] and do not contribute significantly to the development of concrete mechanical properties.

Table 1-1: Typical global slag composition

Analyte	Content (weight %)
CaO	30-50
SiO_2	28-38
Al_2O_3	8-24
MgO	1-18
Fe_2O_3	1-3
MnO	1-3
S	1-2.5
TiO_2	<4
Na_2O+K_2O	<2

The reactivity of slag is affected by its main chemical oxide composition CaO (C), SiO_2 (S), Al_2O_3, (A) and MgO (M). Several chemical hydraulic moduli or activity indices are defined, using the weight percentages of these oxides, to predict the hydraulicity of slags [10], [11]. The most common index is the basicity ratio CaO/SiO_2 and a good reactivity is expected in slags if this ratio is greater than 1 [12]. However, it is reported that these indices do not correlate well with the mechanical properties of slag-blended systems [10], [11].

Ben Haha et al. [13] studied the effect of MgO on the hydration of alkali-activated slag using three slags with MgO contents varying from 7.7% to 13.2%. The slags were ground to approximately similar fineness of 500 ± 10 m^2/kg and the Al_2O_3 content was very similar (11.3-12.0%). The slags were activated by sodium metasilicate pentahydrate (waterglass) and sodium hydroxide. It was found that higher MgO contents in slag generally results in faster hydration and higher compressive strengths. Increasing the MgO content increased the amount of hydrotalcite formed and decreased the Al uptake by C-S-H, resulting in a higher volume of hydrates, which in turn contributed to higher compressive strength. However, they also reported an increase in slag reactivity at early ages with decreasing MgO content (at the same Al_2O_3 content)

Ben Haha et al. [14] also investigated the effect of Al_2O_3 on the hydration of alkali-activated slags using the same activators mentioned before. Three slags, of approximately similar fineness of 500 ± 10 m^2/kg and varying Al_2O_3 contents of 7.0-16.7%, were used in the study. The

MgO contents were similar (6.4% - 7.2%). The findings indicate that higher Al_2O_3 contents in slags increase the Al uptake by C-S-H in the hydrated paste. The Al_2O_3 content in the hydrotalcite also increased with increasing the slag Al_2O_3 content thus lowering the Mg/Al ratios of the hydrotalcite. Although the Al_2O_3 content of slags, in the presence of NaOH or waterglass, modified the composition of the hydrate assemblage, no significant effect is observed on the hydrate volume or the compressive strength. Whittaker et al. [12] also noted that the increase in Al_2O_3 content does not have significant effect on the compressive strength, although it results in small increases in hydrate volume. The slags they studied had Al_2O_3 contents of 7.4% and 12.3%. Increasing the Al_2O_3 content in slag leads to the formation of Aluminate-Ferrite-monosubstituted (AFm) phases (monocarboaluminate and hemicarboaluminate) and a decrease in the volume of C-S-H.

As with all cementitious materials, the reactivity of slag is dependent on its surface area. Typically, slags with higher fineness are expected to enhance early-age strength development. In general, slags with Blaine fineness values between $350 – 450$ m^2/kg are available worldwide. In the United States, there are slags with surface areas varying between $450 – 550$ m^2/kg or even higher [10]. Binici et al. [15] investigated the effect of fineness on the compressive strength and heat of hydration of slag-blended systems. The blends were prepared using 66% clinker, 4% gypsum, 20% ground basaltic pumice (GBP), and 20% slag. The materials were ground to obtain Blaine fineness values of 250 ± 5 m^2/kg, 400 ± 5 m^2/kg and 550 ± 5 m^2/kg. The total heat measured by isothermal calorimetry increased with the Blaine fineness. An increase in the compressive and flexural strengths with increasing fineness was observed as well. However, the effect of slag fineness is not entirely clear, as the fineness of clinker, slag, and GBP were also varied in this study.

In addition to the slag chemical, mineralogical and physical characteristics, sulfate content of high alumina slags have their significance on performance of the slag-blended cementitious systems. This effect will be addressed in detail in a separate section of this literature review. With the availability of high alumina slags, calcium sulfate additions are necessary to ensure durability of the slag-blended cementitious system.

As slag-blended cementitious systems incorporate cements of different mineralogy, chemistry and physical characteristics, a summary of cement characteristics that affect performance of slag-blended cementitious systems will be discussed next.

1.1.2   Effect of Cement Composition on Blended Cementitious Systems Performance

In slag-blended cementitious systems, slags are activated by calcium hydroxide formed during cement hydration, as well as the alkalis and sulfates present in the cement [3], [16]. Therefore, cement composition is expected to influence the reactivity of slag. Currently, the published literature does not have clear agreement on cement composition and its effect on slag reactivity in slag-blended cementitious systems. Whittaker [17] investigated the impact of cement type on slag reactivity using heat evolution in blends containing 40% and 70% slag with two cements with 61.0% and 58.7% C_3S contents and 7.5% and 8.0% C_3A contents. It was concluded that clinker composition does not have any significant effect on hydration kinetics of slag; however, because of the similar C_3S, C_3A, alkali content (0.69 and 0.61%), and particle size, this conclusion may not be very strong.

Kocaba [18] reported that cement composition does affect hydration kinetics of slags in slag-blended cementitious systems. A slag replacement level of 40% was used in her study. The slags with one cement (cement A) indicated enhanced hydration of C_3S, while with two other cements (cements B and C), C_3S hydration was retarded. However, the X-ray diffraction (XRD) results did not indicate a significant difference in alite consumption in these systems and the reasons for this behavior was not clearly explained. C_3S content for cement A was 68%, while for Cements B and C it was 49.1% and 64.5%, respectively. Compared to cements B and C, cement A had the lowest C_3A content, alkali content and sulfate content. However, cement A had the highest fineness while cement C had the lowest fineness. The particle size (d_{50}) of cement A, B and C were 9, 14, 20 μm, respectively. As it appears, in the presence of reactive cements (high C_3S and high fineness) slag hydration is accelerated.

Additionally, a recent study [1] investigated the effect of slag-blended with different cement types on sulfate durability and cracking potential. Four cements of variable C_3S (48 – 54% XRD), C_3A (5.5-8.4% XRD), alkali content (0.35 -1.05%) and fineness (417 – 522 cm^2/g) were blended with slags of variable alumina, alumina-to-magnesia ratio and fineness. The findings

indicate the influence of cement composition, alkali content and fineness, on durability of the slag-blended cementitious system. The C_3A content and alkali content of cements were found to affect sulfate durability, temperature evolution and stress development in the slag-blended cementitious system. Irrespective of the slag composition, when slags were blended with low-C_3A, low-C_3S and low-alkali (Na_2O_{eq} <0.6%) cements, the slag-blended systems showed improved sulfate resistance and decreased cracking risks compared to those with high C_3A cements.

1.2   Effect of Slag on Concrete Temperature Rise

Cement hydration is an exothermic reaction which results in a temperature rise in concrete. Slag is extensively used to reduce heat of hydration of concrete and thereby reduce temperature rise in applications where thermal cracking is a concern [19]. In addition to the heat of hydration, the size of the concrete element, specific heat capacity, thermal diffusivity, and emissivity of the concrete also influence temperature rise [20]. In mass concrete such as dams, footings, and bridge piles, restrained volume change during or after a high temperature rise can cause cracking. When the heat being generated dissipates to the surrounding environment, the temperature at the surface becomes lower compared to that of the interior resulting in a temperature gradient. Tensile stresses can be induced when the concrete cools and this deformation is restrained either internally or externally. Cracking may result if the tensile stresses exceed the tensile strength. Thermal cracking problems are not limited to mass concrete, but can also occur in other concrete structures such as concrete pavements, walls etc.

The heat released during cement hydration is dependent on the cementitious system chemical composition, fineness, water/cementitious ratio (w/cm), and temperature. Although partial replacement of cement with slag is expected to reduce the heat of hydration and particularly the rate of heat release, several studies have stated that heat evolution during slag hydration varies depending on slag chemical composition, especially CaO, SiO_2, Al_2O_3, and MgO [12]–[14]. In general, reactivity of slag increased with increasing CaO/SiO_2 ratio [12]. Few studies have indicated the effect of Al_2O_3 and MgO on slag hydration. Isothermal calorimetry measurements of cement-slag systems and alkali activated slag systems indicated that increasing Al_2O_3 contents of slags would increase the aluminate hydration peak [12], [14]. Alkali activated slag systems with comparable Al_2O_3 contents and varying MgO contents have shown increased cumulative heat

during the first 2 days with low MgO contents; however, after 2 days, slags with higher MgO contents resulted in higher cumulative heat [13].

Several researchers have investigated the effect of slag inclusion on concrete cracking and the focus of most of the research was on the effect of cement replacement level with slag on concrete cracking potential [21], [22], [23]. Byard et al. [21] tested 50% slag-blended concrete in a rigid cracking frame (RCF) experiments. Inclusion of slag reduced and delayed the maximum temperature compared to the plain concrete mixture, which subsequently resulted in reduced stresses and delayed cracking. The Al_2O_3 and MgO content and CaO/SiO_2 ratio of the slag used in this study were 9%, 13% and 0.9 respectively, which indicated a lower reactivity. Wei and Hansen [22] also investigated cement replacement by slag at 30% and 50% on cracking tendencies. The slag used in their study had a chemical composition similar to that of the slag used by Byard et al [21]. The Blaine fineness of slag was 602 m^2/kg. Cracking was delayed in 50% slag-blended concrete. The authors reported that the cracking in the slag mix was caused by increased autogenous shrinkage whereas cracking in the OPC mix was due to thermal stresses.

Markandeya et al. [24] studied the effect of five slags with variable Al_2O_3 and MgO contents and similar CaO/SiO_2 ratios on early age cracking resistance using rigid cracking frame (RCF) experiment. These slags were blended with two cements with similar C_3S, equivalent-alkali (Na_2O_{eq}), and Blaine fineness, but variable C_3A content. Although incorporation of slag greatly reduced the concrete temperature compared to the control mixtures, as observed from semi-adiabatic calorimetry, the maximum temperatures of the slag-blended mixtures varied from 46°C to 53°C. This variation may appear small, but more significant temperature differences can be expected if these slags are used in mass concrete, where the element core can approach adiabatic conditions. The findings also indicated the dependence of concrete temperature and cracking potential on MgO content, Al_2O_3 content, MgO/Al_2O_3 ratio and fineness of slags. Low alumina slags resulted in reduced temperatures and decreased cumulative heat. Besides, for these slags with similar CaO/SiO_2 ratios, a linear relationship was observed between RCF indices and MgO/Al_2O_3 ratios. An increase in the MgO/Al_2O_3 ratio decreased the second zero stress temperature indicating a lower cracking risk. A relationship between MgO/Al_2O_3 and cracking temperature was also observed; however, the slag fineness also appeared to influence the cracking temperature.

As stated in the literature, incorporation of slag in concrete can reduce temperature rise and subsequently reduce thermal cracking. Changes in slag fineness and chemical composition can reduce this benefit substantially. Therefore, when selecting a slag for a particular application, attention should be given to its chemical composition and fineness. In order to provide guidance on slag selection for mass concrete, further research has to be conducted on a greater range of cement and slag compositions.

1.3   Sulfate Balance in Cement-Slag Cementitious Systems

Portland cements are generally optimized for their sulfate content based on strength and fresh properties. However, when working with binary cementitious systems of high-alumina slag and portland cements, further sulfate optimization of the binary system or calcium sulfate additions to the high-alumina slag is necessary to sustain durability and strength of the blended system. Gypsum ($CaSO_4.2H_2O$) or other forms of calcium sulfate are added to clinker during cement production to control the aluminate reaction during cement hydration. The appropriate gypsum addition is influenced by cement fineness, chemical composition and mineralogy. Additionally, the resulting aluminate hydration products can vary in nature depending on the sulfate content and the sulfate-to-aluminate ratio. Varying the sulfate content will influence the rate of early hydration and the phase assemblage which in turn will affect the hardened paste properties. Sulfates not only control the aluminate reaction, but also affect concrete strength, shrinkage and durability. Excess sulfate levels can have negative effects on hardened concrete properties. Therefore, it is important to add the appropriate amount of sulfate to optimize the strength and durability performance of not only plain cement systems but also of blended systems. While several studies in the literature discuss sulfate optimization in pure cement systems, not many studies are available on sulfate optimization in slag-blended cementitious systems.

Variability in sulfate level influences the concrete properties not only during the early stages of hydration, but also at later ages. If the SO_3 content in the system is inadequate to control aluminate hydration, it would react prior to the alite phase causing flash set. The initial reaction of sulfates with tricalcium aluminate results in the formation of ettringite. At room temperature, ettringite may transform to monosulfoaluminate if the sulfates in the system are depleted while there are still unreacted aluminates in the hydrating system. If monosulfoaluminate gets in contact

with a new sulfate source, it may reform ettringite resulting in expansion and unsoundness in concrete. On the other hand, if there is excess SO_3 present in the system, the surplus could be bound by the C-S-H gel resulting in a weaker structure in addition to extending ettringite formation after concrete has hardened. Additionally, adsorbed sulfates in C-S-H gel can be desorbed at later ages and can participate in internal sulfate attack.

The published literature identifies several parameters which affect the optimum SO_3 content in cementitious systems [25], [26], [27]. Availability of SO_3 (distribution, source, and solubility), C_3A, C_3S, and alkali contents, cement fineness, and curing temperature are the main contributing factors to the sulfate demand. Secondly, addition of SCMs, substitution levels, and physical and chemical characteristics would also influence the sulfate balance of the blended cementitious system [25], [28], [29]. In the case of slag, the alumina, alkali, and SO_3 content as well as fineness could affect the sulfate balance in the system and therefore a re-optimization might be required in the blended systems.

1.3.1   Determining the Sulfate Optimum

The sulfate content required to optimize the performance of different properties of hardened paste can vary. In other words, the optimum sulfate content which enhances strength in concrete may not be the same which controls shrinkage or improves durability performance (internal or external sulfate durability etc.). However, a strong correlation between the optimum SO_3 content determined based on compressive strength and heat of hydration obtained from isothermal calorimetry was reported by Lerch [30]. It was also reported that the same sulfate optimum correlates well with that determined from the length change of mortar bars stored in water. Evans [27] stated that the maximum strength and minimum expansion can be expected at approximately the same sulfate level.

In general, cement producers set the optimum sulfate level of a cement based on the maximum compressive strength of mortar cubes and/or heat of hydration of paste at 1 day in accordance with ASTM C563 [31]. The specification recommends considering optimum SO_3 content at 1, 3 and 7 days for compressive strengths. The literature indicates optimum SO_3 level in a cementitious system increases with age, with the increase at early ages more significant compared to that at a later age. As shown in Figure 1-1, the increase in optimum sulfate content

from 1 to 3 days is higher than that from 3 to 7 days. It has also been suggested that at least two optimum SO_3 levels should be defined for strength, one for the early-age and the other at 28 days [32]. The increase in the optimum sulfate content (determined based on strength) with age, is due to the increase in C-S-H volume and formation of ettringite which minimizes the paste porosity. According to Hawkins [33], [34] sulfate optimum determined based on 3-day compressive strength is a better indicator of the sulfate requirement in the system than that on 1-day strength, improving the strength, sulfate resistance and drying shrinkage. It was also suggested that slag-blended systems should follow a similar approach when determining the optimum SO_3 content.
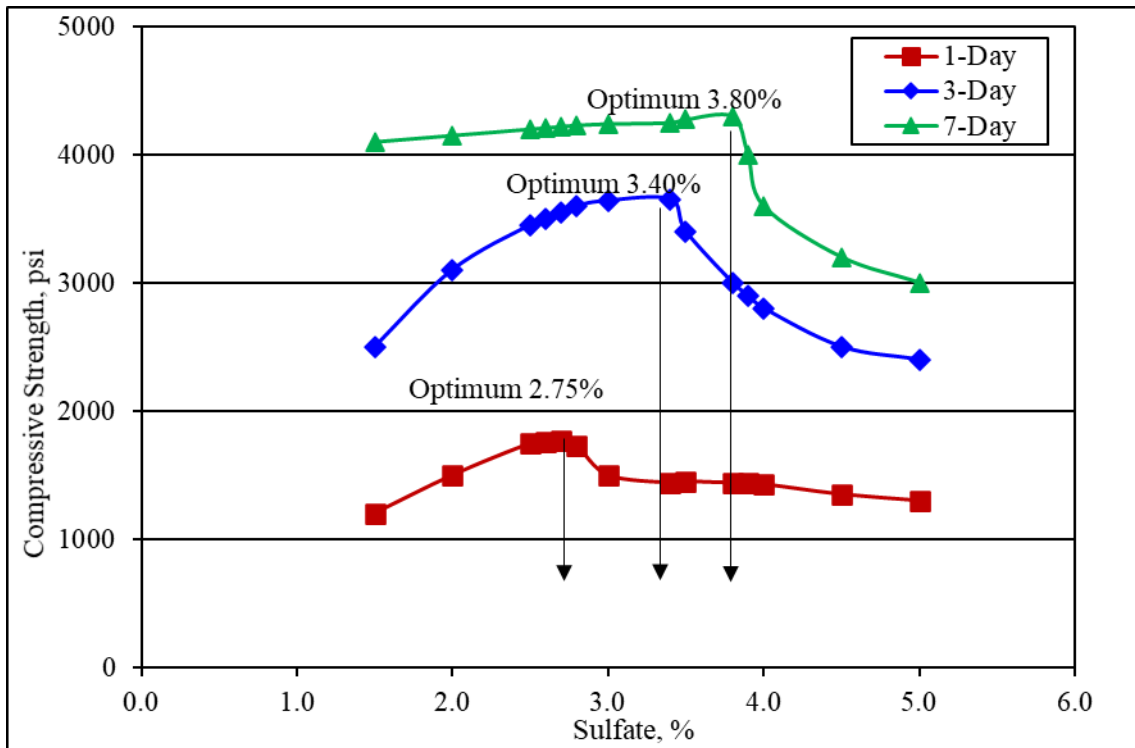
Figure 1-1: Optimum sulfate content as a function of curing time (adapted from [34])

In addition to mortar strength and heat, the most recent ASTM C563-18 [31] allows the use of mortar drying shrinkage tests to determine the optimum SO_3 level. It identifies three methods to approximate the SO_3 content to maximize performance based on the chosen parameter: namely, visual fit, least square parabolic fit, and asymmetric fit. However, Niemuth [25] stated that use of a mathematical fitting method is a better way of determining the optimum SO_3 level rather than the visual interpretation method.

10

1.3.2 Effects on Hardened Paste Properties

The optimum SO_3 level is the one which results in the least porosity and highest strength [27]. The heat of hydration and strengths increase with increasing SO_3 levels, reach a maximum, and then begin to decrease at higher SO_3 content [30]. This behavior is attributed to the aluminate reactions. Increasing SO_3 levels affect strength in two ways. First, an increase in SO_3 results in an ettringite formation which in turn increases the compressive strength. Second, the increase in SO_3 increases the density of C-S-H, giving a coarser pore system that reduces the strength. The optimum SO_3 level is dependent on the balance between these two competing mechanisms for a given material system [35]

While the formation of ettringite during early ages is beneficial for strength, ettringite formation at later ages can cause detrimental expansion in concrete [27], [36], as will be described in section 1.3.6. According to the literature, a smaller expansion is observed for a system which is optimized for sulfate based on maximizing strength and minimizing contraction. Sulfate optimum varies with fineness, alkali content and tricalcium aluminate of portland cement [30].

1.3.3 Sulfate Source and Solubility

The early aluminate hydration is influenced by the distribution and form of sulfates in the cementitious system. As mentioned in literature [27], the formation of aluminate phases vary depending on the sulfate contents in different regions with regions rich in sulfate forming well-defined ettringite needles, while regions low in sulfate forming a gel-like material identified as an AFm type phase [37]. A better physical distribution of sulfates can be achieved by inter-grinding gypsum with cement and results in a better control of aluminate hydration. The fineness and particle size of gypsum are also known to affect its solubility, which in turn would influence the optimum SO_3 content, with higher gypsum fineness resulting in a lower sulfate demand [32].

As the solubility of sulfates influences the hydration rate of aluminates, the source of sulfate and its dissolution rate would affect the sulfate requirement in the system [38]. In addition to gypsum, hemihydrate ($CaSO_4.xH_2O$ (x=0.5 and 0.6)) (α and β forms) and soluble anhydrite ($CaSO_4$ (III)) are added to clinker as sources of sulfate owing to their higher solubility. According to Pourchet et al. [38], during the early gypsum-C_3A reaction, monosulfoaluminate and ettringite form, while under the same experimental conditions, the hemihydrate-C_3A reaction prevents

formation of monosulfoaluminate during the first few minutes. Adu-Amankwah et al. [35] concluded that the quantities of hemi- and monocarboaluminate formed in a limestone-cement-slag ternary system are affected by the sulfate content.

1.3.4 Role of Alkalis

The presence of alkalis in cementitious systems is known to accelerate hydration [39] and therefore, higher sulfate levels are required for proper retardation of aluminate phases in these systems [30], [27], [32], [40]. The role of alkalis is dependent on the form in which they are present. Alkali oxides are typically incorporated in the crystal lattice of clinker minerals while the alkali sulfates are highly soluble and exist as a separate phase. Moreover, potassium and sodium oxides or sulfates have different effects on cement hydration. Potassium oxide is reported to accelerate hydration while sodium oxide slightly retards hydration [41]. Additionally, K_2SO_4 greatly reduces setting times compared to Na_2SO_4 due to the formation of syngenite ($K_2SO_4.CaSO_4.H_2O$) [40].

Several correlations exist between the optimum SO_3, C_3A and equivalent Na_2O in pure cement systems at a given fineness (Equation 1-1 and 1-2) [40]. These relationships clearly show that the optimum sulfate content of a system is highly dependent on its alkali content.

Opt (SO_3 %) = 1.841 + 0.0950 (C_3A %) + 1.6364 (Equivalent Na_2O %)　　　　Equation 1-1

Opt (SO_3 %) = 0.789 + 0.1149 (C_3A %) + 1.872 (Equivalent Na_2O %)　　　　Equation 1-2

1.3.5 Effect of Fineness

The fineness of the cementitious material certainly affects the sulfate demand in a particular system. It is reported that cement with high fineness (especially high C_3A cement) have higher sulfate demand to effectively control the aluminate hydration. This is due to the enhanced rate of hydration resulting from the increased surface area [30]. Hawkins [33], [34] used cement replacement levels of 30% and 50% using slag with Blaine fineness of 430 m^2/kg, 490 m^2/kg and 550 m^2/kg and reported that the strength-based optimum SO_3 content increased with slag fineness. However, the chemical compositions of the slags used in this study were not reported.

1.3.6   Delayed Ettringite Formation (DEF)

The sulfate demand in a cementitious system is affected by the curing temperature. As expected, higher temperatures accelerate the hydration and increases the sulfate demand for proper setting. Additionally, the adsorption of sulfates by C-S-H increases at higher temperatures. The optimum SO_3 level at high temperatures may exceed that identified at room temperature [25], [42]. High sulfate levels of 4%–5% were reported at a temperature of 65°C (149°F) [42]. However, increased adsorption of sulfate by C-S-H at high temperatures is not desirable as the eventual desorption of these sulfates may cause undesirable expansion at later ages due to delayed ettringite formation (DEF). DEF could occur in steam-cured concrete or concrete experiencing high temperature rise during curing. Ettringite decomposition can occur at high temperatures, and once temperature drops to ambient conditions and in the presence of moisture, ettringite reformation can occur, leading to DEF [43]. Reformation of ettringite is due to the reaction between monosulfoaluminate and sulfates released by C-S-H (desorption) [44], [45], [46].

Heinz et al. [44] investigated the effect of SO_3/Al_2O_3 ratio on expansion due to DEF. They reported that "Portland cements blended with appropriate amounts of alumina-bearing latent hydraulic slags (blast furnace slags) or pozzolans (siliceous fly ash, trass, calcined clays) must maintain SO_3/Al_2O_3 mass ratio < 0.45" in order to avoid DEF. The same mixtures showed increased early strengths and low or no loss of later strengths. It is further reported that sulfate contents ≥ 3 wt. % and SO_3/Al_2O_3 mass ratios > 0.45 in portland cements and blends with alumina-free admixtures are more susceptible to DEF. Hence, the consideration of the effect of SO_3 contents or SO_3/Al_2O_3 ratios on long-term durability performance of cementitious systems is also important when determining the optimum sulfate level for a particular system. The effect of alkali content on the sulfate to aluminate ratio was not discussed.

It is reported that DEF exacerbate in the presence of alkalis in the system [44], [47]. Several studies indicated increased expansions due to DEF, in the cementitious systems with high alkali contents [44], [45], [46]. However, the systems which showed increased expansion in these studies had SO_3 contents ≥ 3 wt. %. Taylor [36] reported that cements high in both SO_3 and alkalis show higher expansions, while for cements with low SO_3 contents, alkali content does not cause

significant effects. As it appears, a system with high alkali contents and high SO_3 contents are more susceptible to DEF.

1.4 External Sulfate Attack

External sulfate attack is caused by the penetration of sulfate ions into the concrete and is manifested by expansion, loss of strength, surface spalling, mass loss and eventually disintegration [34]. Sulfate ions react with the monosulfoaluminate present in concrete and form ettringite which causes expansion. Additionally, secondary gypsum forms due to the reaction between CH and sulfates, and decalcification of C-S-H which leads to loss of strength and disintegration of concrete.

In order to mitigate durability issues associated with sulfate attack, generally it is recommended to use cements low in C_3A content to control the formation of secondary ettringite [48]. It is also suggested to use cements low in C_3S and high in C_2S to decrease lime present in the system [48], [49]. Additionally, care should be given to make the concrete less permeable to control the penetration of sulfate ions [16]. SCMs such as slag also play a vital role in decreasing concrete permeability and enhancing lime consumption. Although the use of partial replacement of cement with slag is said to improve sulfate resistance, it is not necessarily true for all slags. According to ASTM C989 [6] high alumina slags (18% Al_2O_3) can lower sulfate durability of a cementitious system if incorporated at 50% or less.

1.4.1 Effect of Slag Alumina Content

As mentioned in ASTM C989 [6], slags containing Al_2O_3 contents less than 11% are able to provide adequate sulfate resistance irrespective of the C_3A contents in cements. Although the specification comments on sulfate durability of slag-blended systems using slags with Al_2O_3 content of less than 11% or at 18%, it is vague on slags with Al_2O_3 contents between 11-18%. Nevertheless, several researchers have investigated the effect of increasing alumina contents of slags on sulfate durability as explained in the following paragraphs [17], [50]–[53].

Hooton and Emery [50] studied the sulfate resistance of slag-blended cementitious systems with Al_2O_3 contents of slag varying from 8.39% to 11.39% at a cement replacement level of 50%. The Blaine fineness of these slags varied between $388 - 443$ m^2/kg. It was found that the expansion increased with increasing slag Al_2O_3 content. They also confirmed that low alumina slags can

provide adequate resistance for sulfate attack. Ogawa et al. [51] evaluated two slags of approximately similar fineness with Al_2O_3 contents of 10.7% and 15.2% with Type V cement and reported that a high alumina slag-blended cementitious system, even with a low C_3A cement, cannot improve sulfate resistance.

Whittaker [17], [54] studied the effect of increasing Al_2O_3 contents of slags on sulfate resistance. Three slags with Al_2O_3 contents of 7.36% (slag A), 11.6% (slag B) and 12.33% (slag C) at cement replacement level of 40% were used. Although all the slag-blended systems showed greater resistance to sulfate attack compared to the neat cement system when assessed by expansion measurements, visual observations indicated that alumina-rich slags performed poorly. Decalcification of C-S-H was also noted to occur in slag blends at earlier age compared to the plain cement system. Yu et al. [55] stated that the failure mechanism of slag blends exposed to sodium sulfate solutions are dominated by the loss of surface rather than macroscopic expansion. Additionally, Whittaker [17], [54] noted that a slag rich in Mg may increase sulfate resistance by binding Al to hydrotalcite and making it less available for ettringite formation. Hydrotalcite appeared to be relatively stable during sulfate attack because more alumina was bound to it as hydration progressed.

Gollop and Taylor [52] investigated three slags (X, Y, Z) with Al_2O_3 contents of 11.2%, 13.4% and 16.0%, respectively for sulfate resistance. A replacement level of 69% was used for the 3 slags. An additional replacement level of 92% was used for slag Y. The visual observations as well as the scanning electron microscope (SEM) observations indicated that the deterioration increased with increasing Al_2O_3 content of slags, at a given level of substitution. The samples prepared with slags Y (13.4% Al_2O_3) and Z (16.0% Al_2O_3) showed the most damage while those with X (11.2% Al_2O_3) showed better sulfate resistance than that of OPC. However, slag Y at the replacement level of 92%, indicated the least amount of damage. Gollop and Taylor explained this as a consequence of the amount of Al that can be accommodated in C-S-H. At lower slag replacement levels in the system, the difference in Si/Ca and Al/Ca of C-S-H is not that significant compared to those in C-S-H of a plain PC system. On the other hand, at higher slag replacement levels, Si/Ca and Al/Ca of C-S-H are substantially different.

According to Osborne [53] it is recommended to use a minimum cement replacement level of 70% with slag in severe sulfate conditions with limitations on alumina content of slag and C_3A content of portland cement. Slags which exceed Al_2O_3 contents of 14% should only be used with cements of low to moderate C_3A contents (<10%).

1.4.2 Effect of Sulfate and Limestone Addition

Few studies in the literature discuss the addition of sulfate or limestone or both as means of improving sulfate durability in slag-cement systems. Gollop and Taylor [52] reported improved sulfate resistance as a result of 5% gypsum addition to a blend containing 65% slag (13.4% Al_2O_3). This is due to the higher amount of ettringite formed and retained during initial hydration. Based on SEM observation of cubes stored in Na_2SO_4 solution, decalcification of C-S-H at the cube surface was reduced in this mix compared to that of a blend with 69% of the same slag without gypsum addition. Moreover, it was suggested that lower sulfate expansion can be expected by the addition of finely ground limestone to Portland cement due to the formation of monocarboaluminate [56].

Ogawa et al. [51] reported that addition of both limestone and calcium sulfate to slag blended cementitious systems can improve the sulfate resistance. This was even achieved with a blend of 60% OPC and high alumina slag (15.2% Al_2O_3). Although it was reported that the addition of sulfates would improve sulfate resistance due to the increased initial ettringite formation, a smaller amount of monosulfoaluminate would still remain and could result in additional ettringite formation when exposed to external sulfate ions. However, when sulfate is added together with limestone fines, ettringite and monocarboaluminate are formed, but not monosulfoaluminate. This combined effect from sulfate and limestone addition results in better sulfate resistance. The effect of such higher sulfate content in the cementitious system on DEF was not studied.

1.4.3 Role of Fineness

Studies on the effect of slag fineness on sulfate resistance are rare in the published literature. Locher [57] studied the effect of increased slag fineness on sulfate resistance using two slags with Al_2O_3 contents of 11.0% and 17.7% separately ground to 300 m^2/kg and 500 m^2/kg. The slags were used with three clinkers with C_3A contents of 0%, 8% and 11%. The gypsum addition to the system was 5%. Cement replacement levels varying from 5% - 85% were studied. It was

found that the slag fineness can have adverse effects on sulfate durability, with finer ground slag decreasing sulfate resistance if the replacement level is below 65%.

1.4.4   Impact on Permeability

Typically, incorporation of slag in concrete is known to refine the pore structure, decrease porosity, and permeability [16], [58] thus effectively reducing sulfate ingress. However, this may not be true at all ages. According to Whittaker et al. [54] at 14 days, prior to sulfate exposure, 40% of slag-blended samples showed a higher porosity due to a lower degree of hydration. Despite the higher porosity at this age, a refined or finer pore size distribution was observed from mercury intrusion porosimetry (MIP) analysis in the slag-blended system and this effect was more visible in the slag with the highest reactivity. On the other hand, Yu et al. [55] reported a decrease in total porosity for a 40% slag replacement at the age of 90 days prior to sulfate exposure. The same slag with 70% replacement indicated a higher porosity than the plain cement system at 90 days. However, both systems incorporating slags clearly reduced the breakthrough radius compared to the plain cement system.

As it appears, slag-blended systems show increased early-age porosity due to a lower degree of hydration compared to OPC systems. However, at later ages these systems may show decreased porosity due to the continued slag hydration. This is concerning as the field concrete structures are exposed to sulfate environments soon after casting. According to Stroh et al. [59] this does not seem to be problematic, in fact slag-blended concrete showed higher sulfate resistance and therefore lower degradation compared to OPC after 19 years of exposure to sulfate bearing soils. The samples used in this study had 80% replacement of slag with an Al_2O_3 content of 13.30% and considerably lower fineness of 268 m^2/kg than the typical slag grind currently in use.

While a refined pore structure would decrease concrete permeability, minimize sulfate ingress and lower expansion, it may cause a different type of failure in slag-blended concrete. Yu et al. [55] stated that unlike pure cement systems, slag-blended systems deteriorate more through loss of surface than macroscopic expansion that results from the modified pore system. Slag-blended systems have a buffering effect close to the surface as incoming sulfates are fixed by aluminate phases such as AFm and anhydrous slag. Once the phases in the buffering region have reacted, sulfate ions in pore solution would increase and provide the driving force for further

ingress. Hence, ettringite formed in a thin layer results in expansion which leads to cracking and subsequently surface spalling. Studies have indicated that surface spalling is higher in slag blends with high alumina slags.

According to Müllauer et al. [60] ettringite crystallization in pores ranging between 10-50 nm causes deterioration due to sulfate attack. This formation of ettringite in the small pores generates a stress that could exceed the tensile strength of the hydrated system resulting in expansion and damage in concrete. Ettringite forming in large pores has negligible effect on expansion as the pressure generated in these pores is insufficient to cause damage. In a recent investigation on sulfate durability of cement-slag blends with varying slag alumina contents [1], prior to sulfate exposure, mercury intruded pore volumes in the range 10-50 nm were approximately similar at the same replacement levels. It was speculated that if this trend is maintained at later ages, slags with high alumina contents would be more susceptible for sulfate attack, as those would form more secondary ettringite.

1.5   Chloride Ingress

Corrosion of steel reinforcement in concrete due to chloride ingress is a major durability issue in Florida. Chloride induced corrosion results in a smaller reinforcement cross-sectional area, leading to a loss in its load carrying capacity. Penetration of chloride ions lowers the pH of the concrete pore solution and the passive iron oxide film covering the reinforcement is attacked, which initiates corrosion. Moreover, chlorides can be bound to cement by chemical reactions or physical adsorption and form phases such as Kuzel's salt $((CaO)_3 \bullet Al_2O_3 \bullet 0.5CaSO_4 \bullet 0.5CaCl_2 \bullet (H_2O)_{11})$ and Friedel's salt $((CaO)_3 \bullet Al_2O_3 \bullet CaCl_2 \bullet (H_2O)_{10}$ [61]. The phases which could bound chlorides include AFm phases, C-S-H and hydrotalcite [59]. The free chloride present in the pore solution causes steel depassivation. It is therefore expected that the higher the amount of bound chlorides, the lower the free chlorides available for steel depassivation.

Typical preventative measures of chloride induced corrosion include increasing concrete cover and decreasing concrete permeability [62]. Therefore, incorporation of slag in concrete is an excellent way of reducing the concrete permeability and preventing chloride ingress, which in turn would contribute significantly to controlling corrosion of reinforcement [63]. The presence of slag

in concrete also influences the chloride binding capacity of the paste and thereby affects the chloride ion transport in concrete. The chloride binding capacity of slag-blended systems are affected by slag replacement level, w/cm ratio, temperature, pH, carbonation, chloride desorption, sulfate content and fineness [64]. Moreover, the chemical composition of slag, especially its alumina content is reported to have effects on chloride resistance, as it increases the formation of Friedel's salt [61], [65]. As reported by several researchers, increasing slag replacement levels increased chloride resistance due to its effect on pore structure refinement and increased chloride binding capacity [63], [66], [67]. However, the effects of the slag chemical and physical characteristics on chloride ingress have not been studied in detail.

1.5.1   Impact on Permeability

As discussed previously, incorporation of slag in concrete is known to refine the pore structure and reduce concrete permeability. Several published literature have stated that slag-blended concrete performs well in chloride environments [61], [65], [68]. Reduced porosity is attributed to the denser microstructure from the filling of capillary pores with the additional formation of low-density C-S-H. The additional C-S-H contributes to blocking the chloride diffusion path. Moreover, the increase in chloride binding with the addition of slag, not only demobilizes chloride ions by forming Friedel's salt, but also partially blocks the chloride diffusion paths by filling pores [65].

Cheng et al. [69] observed large capillary pores ranging from 0.05-10 µm in OPC concrete using SEM after 91 days while capillary pores less than 10-50 nm were observed in slag-blended concrete. Slag replacement levels of 40% and 60% and w/cm ratio of 0.55 were used in this study. The permeability of the OPC mix, 40% slag blend and 60% slag blend were reported as 2.56×10^{-13}, 1.52×10^{-13}, and 1.32×10^{-13} m/s respectively. It was also reported that the chloride ion-diffusion coefficient of blended concrete with 60% slag and 0.5 w/cm ratio was ten times lower than that of plain OPC concrete.

Otieno et al. [65] studied the effect of slag replacement level on chloride penetration resistance measured using a chloride conductivity test and considering slag replacement levels of 20%, 35% and 50%. As expected, for a given w/cm ratio and type of slag, chloride ion penetration decreased with increasing replacement levels. This can be attributed to the increase in

microstructure densification and chloride binding with higher amounts of slag in the mixture. Additionally, Otieno et al. [65] also stated that increasing MgO content in slags results in lower porosity due to the increased formation of hydrotalcite, C(-A)-S-H, which has a higher degree of space filling than C-S-H due to their lower density.

The effect of curing temperature on chloride binding and diffusion in slag-blended systems was studied by Ogirigbo et al. [61] at 20° C (68°F) and 38° C (100.4°F). In spite of the fact that the higher temperature increased the chloride binding due to increased slag hydration, a greater chloride ingress was observed at 38° C. This was attributed to an increase in coarse porosity as denoted by SEM-BSE image analysis of paste samples at 28 days. The capillary porosity was observed to increase by about 36% with the higher temperature.

1.5.2   Effect of Alumina

Unlike for sulfate durability or temperature rise, high alumina contents in cementitious systems are favorable for chloride durability of concrete. According to the literature, high alumina contents bind more chlorides either by chemical reactions or adsorption and lowers free chloride available in the pore solution [63], [61], [65], which is a desirable outcome to prevent steel corrosion. While Type V cements are highly sulfate resistant, use of these cements in chloride environments is reported to aggravate corrosion in concrete due to their lower C_3A contents. Type I cements are recommended for such exposure conditions as it binds more chloride ions [70].

Ogirigbo et al. [61] investigated the effect of two slags, having alumina contents of 12.33% (S1) and 7.77% (S2) on chloride binding and diffusion in slag blends with 30% replacement. The experiments were conducted under two different temperature regimes, 20°C (68°F) and 38°C (100.4°F). As expected, blends with S1 had a higher chloride binding capacity, as indicated by the higher amount of Friedel's salt observed from XRD. The Friedel's salt formation increased further at 38°C (100.4°F) due to the accelerated slag hydration, and formation of higher amounts of C-S-H and aluminate phases for chloride binding.

1.5.3   Effect of Sulfate Addition

As discussed in section 1.4.2, addition of sulfate to the cementitious system is favorable for sulfate durability. On the contrary, sulfates can have adverse effects on chloride durability. According to Luo et al. [71], in slag-blended systems the pore structure and chloride diffusion

coefficient are influenced with additional sulfate as the chloride binding capacity of the system is greatly reduced. This is due to the fact that a lesser amount of Friedel's salt is formed due lower alumina availability in the presence of sulfates. Alumina reacts with sulfate and therefore, a lower amount of alumina is available to react with chloride ions. Luo et al. [71] compared 30% OPC and 70% GGBFS blended system with 30% OPC, 65% GGBFS and 5% gypsum system. Although the inclusion of slag decreased both the apparent chloride diffusion coefficient and the effective chloride diffusion coefficient at 60 days compared to the OPC system, chloride diffusion coefficients increased greatly with the addition of 5% gypsum to the slag-blended system. Moreover, the chloride binding capability of GGBFS blended mixes were greatly reduced by the sulfate addition and also the alkalinity of sulfates.

1.5.4 Role of Fineness

Only a few studies in the literature discuss the effect of slag fineness on chloride resistance. Typically, a higher fineness is expected to enhance hydration and subsequently result in a denser concrete microstructure, which is required to resist chloride ingress. It was also reported that to achieve better chloride penetration resistance, the fineness of GGBFS should be higher than that of cement [63]. Teng et al. [72] stated that a concrete with 50% slag replacement with 786 m^2/kg slag fineness has a lower diffusion coefficient than a normal OPC and this coefficient would drop substantially with increasing slag fineness. Kim et al. [73] investigated the chloride penetration of slag-blended concrete under tensile loading using three slags of fineness 398 m^2/kg, 612 m^2/kg and 782 m^2/kg. Although the chloride diffusivity coefficient showed only a small decrease with increasing slag fineness when no loading is applied, the diffusivity coefficient dropped considerably under tensile loading. Otieno et al. [65] reported the effect of fineness of the slag-blended system on chloride conductivity using ground granulated Corex slag (GGCS) at replacement levels of 20%, 35% and 50%. The fineness of the blends varied from 345 to 380 m^2/kg. The chloride conductivity decreased from 0.7 mS/cm to 0.2 mS/cm with increasing fineness at a w/cm ratio of 0.4.

1.6 Conclusions

The above review highlights the significance of chemical composition and fineness of GGBFS on its reactivity. It also indicates the importance of considering the cement replacement

levels, chemical and physical characteristics of GGBFS when selecting slags for concrete to enhance the durability of concrete. Evidently, inclusion of slag can render durable concrete, provided that the system is properly sulfated and optimized for heat generation, sulfate and chloride resistance. In all cases, Al_2O_3 content of slag appears to be a very important parameter. Additionally, slag fineness, sulfate content, and its MgO/Al_2O_3 ratio as well as cement characteristics are of significance for assessing durable performance of slag-blended concrete.

1.7 References

[1] A. Zayed, K. A. Riding, Y. Stetsko, N. Shanahan, A. Markandeya, F. Nosouhian, D. Mapa and M. Fincan, "Final Report Effects of Blast Furnace Slag Characteristics on Durability of Cementitious Systems for Florida Concrete Structures FDOT Contract Number : BDV25-977-28," University of South Florida, Tampa, FL, 2019.

[2] A. M. Neville, *Properties of Concrete*, 4th ed. Harlow, England: Pearson Education Limited, 2006.

[3] R. Siddique and M. I. Khan, *Supplementary Cementing Materials*. Springer Science {&} Business Media, 2011.

[4] P. K. Mehta, D. Pirtz, and M. Polivka, "Properties of alite cements," *Cem. Concr. Res.*, vol. 9, no. 4, pp. 439–450, Jul. 1979.

[5] B. Lothenbach, K. Scrivener, and R. D. Hooton, "Supplementary cementitious materials," *Cem. Concr. Res.*, vol. 41, no. 12, pp. 1244–1256, 2011.

[6] ASTM C989/C989M-17, "Standard Specification for Slag Cement for Use in Concrete and Mortars," West Conshohocken, PA: ASTM International, 2017.

[7] M. Morantville-Regourd, "Cements made from blastfurnace slag," in *Lea's Chemistry of Cement and Concrete*, 4th ed., P. C. Hewlett, Ed. New York, NY: Arnold, 1998, pp. 633–674.

[8] R. Snellings, G. Mertens, and J. Elsen, "Supplementary cementitious materials," *Rev. Mineral. Geochemistry*, vol. 74, no. 1, pp. 211–278, Dec. 2012.

[9] J. I. Escalante, L. Y. Gómez, K. K. Johal, G. Mendoza, H. Mancha, and J. Méndez, "Reactivity of blast-furnace slag in Portland cement blends hydrated under different conditions," *Cem. Concr. Res.*, vol. 31, no. 10, pp. 1403–1409, Oct. 2001.

[10] S. C. Pal, A. Mukherjee, and S. R. Pathak, "Investigation of hydraulic activity of ground granulated blast furnace slag in concrete," *Cem. Concr. Res.*, vol. 33, no. 9, pp. 1481–1486, Sep. 2003.

[11] A. A. Ramezanianpour, *Cement Replacement Materials*. Berlin, Germany: Springer Berlin

Heidelberg, 2014.

[12]   M. Whittaker, M. Zajac, M. Ben Haha, F. Bullerjahn, and L. Black, "The role of the alumina content of slag, plus the presence of additional sulfate on the hydration and microstructure of Portland cement-slag blends," *Cem. Concr. Res.*, vol. 66, pp. 91–101, Dec. 2014.

[13]   M. Ben Haha, B. Lothenbach, G. Le Saout, and F. Winnefeld, "Influence of slag chemistry on the hydration of alkali-activated blast-furnace slag — Part I: Effect of MgO," *Cem. Concr. Res.*, vol. 41, no. 9, pp. 955–963, Sep. 2011.

[14]   M. Ben Haha, B. Lothenbach, G. Le Saout, and F. Winnefeld, "Influence of slag chemistry on the hydration of alkali-activated blast-furnace slag — Part II: Effect of Al2O3," *Cem. Concr. Res.*, vol. 42, no. 1, pp. 74–83, Jan. 2012.

[15]   H. Binici, H. Temiz, and M. M. Köse, "The effect of fineness on the properties of the blended cements incorporating ground granulated blast furnace slag and ground basaltic pumice," *Constr. Build. Mater.*, vol. 21, no. 5, pp. 1122–1128, May 2007.

[16]   S. Mindess, F. J. Young, and D. Darwin, *Concrete*. Upper Saddle River, NJ: Pearson Education, Inc., 2003.

[17]   M. J. Whittaker, "The Impact of Slag Composition on the Microstructure of Composite Slag Cements Exposed to Sulfate Attack," The University of Leeds, 2014.

[18]   V. Kocaba, "Development and Evaluation of Methods to Follow Microstructural Development of Cementitious Systems Including Slags," École Polytechnique Fédérale de Lausanne, 2009.

[19]   ACI committee 207, "ACI 207.2R-07 Report on Thermal and Volume Change Effects on Cracking of Mass Concrete," American Concrete Institute, Farmington Hills, MI, 2007.

[20]   A. Lawrence, "A Finite Element Model for The Prediction of Thermal Stresses in Mass Concrete," University of Florida, 2009.

[21]   B. E. Byard, A. K. Schindler, R. W. Barnes, and A. Rao, "Cracking Tendency of Bridge Deck Concrete," *Transp. Res. Rec. J. Transp. Res. Board*, vol. 2164, no. 1, pp. 122–131, 2010.

[22] Y. Wei and W. Hansen, "Early-age strain-stress relationship and cracking behavior of slag cement mixtures subject to constant uniaxial restraint," *Constr. Build. Mater.*, vol. 49, pp. 635–642, 2013.

[23] K. A. Riding, J. L. Poole, A. K. Schindler, M. C. G. Juenger, and K. J. Folliard, "Statistical Determination of Cracking Probability for Mass Concrete," *J. Mater. Civ. Eng.*, vol. 26, no. 9, p. 04014058, 2013.

[24] A. Markandeya, N. Shanahan, D. Mapa, K. A. Riding, and A. Zayed, "Influence of slag composition on cracking potential of slag-portland cement concrete," *Constr. Build. Mater.*, vol. 164, pp. 820–829, 2018.

[25] M. D. Niemuth, "Effect of fly ash on the optimum sulfate of Portland cement," Purdue University, 2012.

[26] D. Tsamatsoulis and N. Nikolakakos, "Investigation of Some Basic Parameters Affecting the Optimum Sulfates Content of Cement," no. May, pp. 152–157, 2014.

[27] K. A. Evans, "The Optimum Sulphate Content in Portland Cement," University of Toronto, 1997.

[28] V. C. Campiteli and M. C. Florindo, "The Influence of Limestone Additions on Optimum Sulfur Trioxide Content in Portland Cements," in *Carbonate Additions to Cement, ASTM STP 1064*, P. Kleiger and R. D. Hooton, Eds. Philadelphia: American Society for Testing and Materials, 1990, pp. 30–40.

[29] M. Antoni, "Investigation of cement substitution by blends of calcined clays and limestone," École Polytechnique, 2013.

[30] W. Lerch, "The influence of gypsum on the hydration and properties of Portland cement pastes," Research Laboratory of the Portland Cement Association, Chicago, IL, 1946.

[31] ASTM C563 - 18, "Standard Guide for Approximation of Optimum SO3 in Hydraulic Cement," West Conshohocken, PA: ASTM International, 2018.

[32] F. J. Tang, *Optimization of sulfate form and content (No. RD105T)*. Skokie, IL: PCA Research and Development, 1992.

[33] P. Hawkins, "SO3 Optimization for Ground Granulated Blast Furnace Slag," in *Bulk Materials International Slag Symposium*, 2002.

[34] I. B. Javed and P. C. Taylor, "Sulfate Resistance of Concrete Using Blended Cements or Supplementary Cementitious Materials," Portlance Cement Association, Skokie, IL, 2006.

[35] S. Adu-Amankwah, L. Black, J. Skocek, M. Ben Haha, and M. Zajac, "Effect of sulfate additions on hydration and performance of ternary slag-limestone composite cements," *Constr. Build. Mater.*, vol. 164, pp. 451–462, 2018.

[36] H. F. W. Taylor, C. Famy, and K. L. Scrivener, "Delayed Ettringite Formation in Concrete," *Cem. Concr. Res.*, vol. 31, pp. 1–2, 2015.

[37] S. Kelham, "The Effect of Cement Composition and Fineness on Expansion Associated with Delayed Ettringite Formation," *Cem. Concr. Compos.*, vol. 18, pp. 171–179, 1996.

[38] S. Pourchet, L. Regnaud, J. P. Perez, and A. Nonat, "Early C3A hydration in the presence of different kinds of calcium sulfate," *Cem. Concr. Res.*, vol. 39, no. 11, pp. 989–996, 2009.

[39] C. D. Lawrence, "Physicochemical and mechanical properties of Portland cement," in *Lea's Chemistry of Cement and Concrete*, 4th ed., P. C. Hewlett, Ed. London: Arnold Publishers, 1998, pp. 343–419.

[40] I. Jawed and J. Skalny, "Alkalies in cement: a review: II. Effects of alkalies on hydration and performance of Portland cement.," *Cem. Concr. Res.*, vol. 8, no. 1, pp. 37–51, 1978.

[41] P. C. Hewlett, Ed., *Lea's Chemistry of Cement and Concrete*, 4th ed. New York, NY: Arnold, 1998.

[42] H. Zhang, Z. Lin, and D. Tong, "Influence of the type of calcium sulfate on the strength and hydration of portland cement under an initial steam-curing condition," *Cem. Concr. Res.*, vol. 26, no. 10, pp. 1505–1511, Oct. 1996.

[43] D. Heinz and H. M. Ludwig, "Heat Treatment and the Risk of DEF Delayed Ettringite Formation in UHPC," in *International Symposium on Ultra High Performance Concrete*, 2004, pp. 717–730.

[44] D. Heinz, M. Kalde, U. Ludwig, and I. Ruediger, "Present State of Investigation on

Damaging Late Ettringite Formation (DLEF) in Mortars and Concrete," in *SP-177: Ettringite-The Sometimes Host of Destruction*, B. Erlin, Ed. ACI Committee 201, 1999, pp. 1–13.

[45] S. Kelham, "Influence of Cement Composition on Volume Stability of Mortar," in *SP-177: Ettringite-The Sometimes Host of Destruction*, B. Erlin, Ed. ACI Committee 201, 1999, pp. 27–45.

[46] C. D. Lawrence, "Long-term Expansion of Mortars and Concretes," in *SP-177: Ettringite-The Sometimes Host of Destruction*, B. Erlin, Ed. ACI Committee 201, 1999, pp. 105–124.

[47] Z. Zhang, J. Olek, and S. Diamond, "Studies on delayed ettringite formation in heat-cured mortars II: Characteristics of cement that may be susceptible to DEF," *Cem. Concr. Res.*, vol. 32, no. 11, pp. 1737–1742, 2002.

[48] N. G. Shanahan, "Influence of C3S content of cement on concrete sulfate durability," University of South Florida, 2003.

[49] N. Shanahan and A. Zayed, "Cement composition and sulfate attack," *Cem. Concr. Res.*, vol. 37, no. 4, pp. 618–623, Apr. 2007.

[50] R. D. Hooton and J. Emery, "Sulfate Resistance of a Candian slag cement," *ACI Mater. J.*, no. 87, pp. 547–555, 1990.

[51] S. Ogawa, T. Nozaki, K. Yamada, H. Hirao, and R. D. Hooton, "Improvement on sulfate resistance of blended cement with high alumina slag," *Cem. Concr. Res.*, vol. 42, no. 2, pp. 244–251, Feb. 2012.

[52] R. Gollop and H. Taylor, "Microstructural and microanalytical studies of sulfate attack, V, comparison of different slag blends," *Cem. Concr. Res.*, vol. 27, no. 7, pp. 1029–1044, 1996.

[53] G. J. Osborne, "Durability of Portland blast-furnace slag cement concrete," *Cem. Concr. Compos.*, vol. 21, pp. 11–21, 1999.

[54] M. Whittaker, M. Zajac, M. Ben Haha, and L. Black, "The impact of alumina availability on sulfate resistance of slag composite cements," *Constr. Build. Mater.*, vol. 119, pp. 356–369, 2016.

[55] C. Yu, W. Sun, and K. Scrivener, "Degradation mechanism of slag-blended mortars immersed in sodium sulfate solution," *Cem. Concr. Res.*, vol. 72, pp. 37–47, Jun. 2015.

[56] S. K. Chatterji, "Mechanisms of sulphate expansion of hardened cement pastes," in *Proceedings of the fifth international symposium on the chemistry of cement*, 1968, pp. 336–34.

[57] F. W. Locher, "The Problems of the Sulfate Resistance of Slag Cements," *Zement-Kalk-Gips*, vol. 19, no. 9, pp. 395–401, 1966.

[58] E. Özbay, M. Erdemir, and H. I. Durmuş, "Utilization and efficiency of ground granulated blast furnace slag on concrete properties - A review," *Constr. Build. Mater.*, vol. 105, pp. 423–434, 2016.

[59] J. Stroh, M. C. Schlegel, E. F. Irassar, B. Meng, and F. Emmerling, "Applying high resolution SyXRD analysis on sulfate attacked concrete field samples," *Cem. Concr. Res.*, vol. 66, pp. 19–26, Dec. 2014.

[60] W. Müllauer, R. E. Beddoe, and D. Heinz, "Sulfate attack expansion mechanisms," *Cem. Concr. Res.*, vol. 52, pp. 208–215, Oct. 2013.

[61] O. R. Ogirigbo and L. Black, "Chloride binding and diffusion in slag blends: Influence of slag composition and temperature," *Constr. Build. Mater.*, vol. 149, pp. 816–825, Sep. 2017.

[62] R. Loser, B. Lothenbach, A. Leemann, and M. Tuchschmid, "Chloride resistance of concrete and its binding capacity – Comparison between experimental results and thermodynamic modeling," *Cem. Concr. Compos.*, vol. 32, no. 1, pp. 34–42, Jan. 2010.

[63] H. W. Song and V. Saraswathy, "Studies on the corrosion resistance of reinforced steel in concrete with ground granulated blast-furnace slag—An overview," *J. Hazard. Mater.*, vol. 138, no. 2, pp. 226–233, Nov. 2006.

[64] H. Zibara, "Binding of external chlorides by cement pastes," University of Toronto, 2001.

[65] M. Otieno, H. Beushausen, and M. Alexander, "Effect of chemical composition of slag on chloride penetration resistance of concrete," *Cem. Concr. Compos.*, vol. 46, pp. 56–64, Feb. 2014.

[66] F. Leng, N. Feng, and X. Lu, "An experimental study on the properties of resistance to diffusion of chloride ions of fly ash and blast furnace slag concrete," *Cem. Concr. Res.*, vol. 30, no. 6, pp. 989–992, Jun. 2000.

[67] K. Y. Yeau and E. K. Kim, "An experimental study on corrosion resistance of concrete with ground granulate blast-furnace slag," *Cem. Concr. Res.*, vol. 35, no. 7, pp. 1391–1399, Jul. 2005.

[68] H. J. Chen, S. S. Huang, C. W. Tang, M. A. Malek, and L. W. Ean, "Effect of curing environments on strength, porosity and chloride ingress resistance of blast furnace slag cement concretes: A construction site study," *Constr. Build. Mater.*, vol. 35, pp. 1063–1070, Oct. 2012.

[69] A. Cheng, R. Huang, J. K. Wu, and C. H. Chen, "Influence of GGBS on durability and corrosion behavior of reinforced concrete," *Mater. Chem. Phys.*, vol. 93, no. 2–3, pp. 404–411, Oct. 2005.

[70] T. M. El Sokkary, H. H. Assal, and A. M. Kandeel, "Effect of silica fume or granulated slag on sulphate attack of ordinary portland and alumina cement blend," *Ceram. Int.*, vol. 30, no. 2, pp. 133–138, Jan. 2004.

[71] R. Luo, Y. Cai, C. Wang, and X. Huang, "Study of chloride binding and diffusion in GGBS concrete," *Cem. Concr. Res.*, vol. 33, no. 1, pp. 1–7, Jan. 2003.

[72] S. Teng, T. Y. D. Lim, and B. Sabet Divsholi, "Durability and mechanical properties of high strength concrete incorporating ultra fine Ground Granulated Blast-furnace Slag," *Constr. Build. Mater.*, vol. 40, pp. 875–881, Mar. 2013.

[73] D. H. Kim, K. Shimura, and T. Horiguchi, "Effect of Tensile Loading on Chloride Penetration of Concrete Mixed with Granulated Blast Furnace Slag," *J. Adv. Concr. Technol.*, vol. 8, no. 1, pp. 27–34, 2010.

Chapter 2   Materials Characterization

2.1   Introduction

The main objective of the current study is to assess the correlation between ground granulated blast furnace slag (GGBFS, BFS, slag, slag cement) characteristics and concrete temperature rise and durability. Towards satisfying these objectives, several ordinary portland cements (OPC), limestone cements (IL) and slags were acquired. All as-received materials were selected based on the mill certificates provided by the State Materials Office or the materials supplier. As the mill certificate is typically provided for the most recent analysis performed, it does not necessarily reflect the characteristics of the collected material. A battery of mineralogical, chemical, and physical characterization tests was conducted on the as-received materials; namely, X-ray fluorescence (XRF), quantitative X-ray diffraction coupled with Rietveld refinement (QXRD), laser particle size distribution (PSD), Blaine fineness, and specific gravity.

Durability issues considered here include the potential of the slag-blended cementitious system to control/minimize concrete temperature rise, delayed ettringite formation (DEF), and enhancing the blended system resistance to the ingress of sulfate and chloride ions. The cements were selected based on the characteristics that are known to influence durability performance including, tricalcium aluminate (C_3A), tricalcium silicate (C_3S), alkali content, and Blaine fineness. As for slags, a previous study conducted by the Construction Materials Group at the University of South Florida [1], [2], indicates that the slag, alumina, magnesia, sulfate contents and Blaine fineness significantly affect durability performance of the slag-blended systems. The slags were therefore selected to include those variables. The following sections present the results of the characterization tests performed on the as-received materials.

2.2   Chemical Oxide Composition of the As-Received Materials

2.2.1   XRF Analysis of Cements

The as-received cements, selected based on their mill certificates, were analyzed for their elemental oxide composition using XRF according to ASTM C114 [3]. The results are presented in Table 2-1 where cements with an alkali content below 0.6% are referred to as low-alkali (La) while cements with alkali contents above 0.6% are referred to as high-alkali (Ha), ASTM C150-

18 [4]. The as-received cements included two Type I cements with cement BB of low alkali content and cement C with high alkali content, two Type II(MH) cements with cement Z having a higher alkali content compared to cement TTC, and three IL cements of variable limestone content: Cement TIL (IL(10)), Cement THIL (IL(14)), and GIL-OP (IL(10)). As shown in Table 2-1, the alumina, sulfate and alkali contents vary among different cements. Cement BB and C, which are Type I cements, have higher alumina and sulfate than the other cements analyzed here. Among these two cements, cement C has substantially higher alkali content than cement BB. Higher alkali content of cements, in addition to higher aluminates and sulfates, have significance when considering sulfate durability and the potential of a cement to experience delayed ettringite formation (DEF) if subjected to high curing temperatures.

As for the Type II(MH) cements, Z and TTC, the most significant differences between these cements are in the alkali and magnesia contents, where cement Z shows the higher alkali and magnesia contents. The MgO contents in cements C and Z are much higher than the rest, which correlates with their higher alkali content. For limestone cements, cements TIL and THIL were received from the same manufacturer. The supplier has indicated they contain different limestone contents while using the same clinker, which agrees with the chemical analyses conducted here.

The losses on ignition (LOI) are also reported here. LOI at 550°C reflects moisture loss and chemically-bound water in portlandite, while differences in the LOI between 550°C and 950°C reflect the decomposition of limestone and the release of CO_2 [3]. From the XRF analyses of the different limestones, it is clear that the purity of the limestone used by different cement manufacturers varies as reflected in the silica content and differences in LOI between 550°C and 950°C. The different CO_2 values determined by LOI correlate well with the different limestone contents in the IL cements. Processing additions used in manufacturing Type IL cements were also analyzed in order to provide higher accuracy in calcite quantification using QXRD. Additionally, a reagent-grade sulfate source, hemihydrate to be used in sulfate optimization studies, was also analyzed using XRF, (See Table 2-2).

Table 2-1: Oxide chemical composition of as-received cements

Analyte	BB I	C I(Ha)	Z II(MH)(Ha)	TTC II(MH)	GIL-OP IL(10)	TIL IL(10)	THIL IL(14)
SiO_2	19.53	19.00	19.41	20.21	18.43	19.16	19.14
Al_2O_3	5.51	5.90	4.64	5.00	4.56	4.61	4.52
Fe_2O_3	1.79	2.80	3.06	3.78	3.29	3.74	3.54
CaO	64.27	60.80	62.77	63.60	62.28	62.40	62.11
MgO	1.05	2.50	3.01	0.32	0.91	1.12	1.08
SO_3	3.93	4.00	3.25	2.55	2.93	2.47	2.44
Na_2O	0.11	0.32	0.02	0.01	0.18	0.17	0.17
K_2O	0.41	1.10	0.95	0.32	0.32	0.32	0.29
TiO_2	0.26	0.26	0.35	0.36	0.21	0.23	0.22
P_2O_5	0.27	0.26	0.05	0.10	0.43	0.09	0.09
Mn_2O_3	0.02	0.11	0.09	0.13	0.06	0.15	0.14
SrO	0.07	0.28	0.04	0.13	0.06	0.12	0.12
Cr_2O_3	0.01	0.01	0.01	0.03	0.02	0.02	0.02
ZnO	0.01	0.07	0.04	0.05	0.06	0.05	0.04
L.O.I. (550°C)	-	-	0.75	1.34	1.62	0.76	0.69
L.O.I. (950°C)	2.60	2.40	2.53	2.85	5.86	5.35	5.99
Total	99.84	99.82	100.21	99.44	99.62	99.98	99.91
Na_2O_{eq}	0.38	1.05	0.65	0.22	0.40	0.38	0.36

Table 2-2: Oxide chemical composition of processing additions

Analyte	Hemihydrate (AH)	Limestone				Kiln dust
		ZLS (Z)	TTCLS (TTC)	TLS (TIL) & (THIL)	ALS (GILOP)	CKD (GILOP)
SiO_2	0.00	2.21	11.81	12.90	0.86	8.73
Al_2O_3	0.00	0.80	0.40	0.41	0.13	4.03
Fe_2O_3	0.01	0.45	0.24	0.23	0.16	1.52
CaO	38.70	52.80	47.55	47.63	54.59	46.62
MgO	0.00	0.65	0.57	0.51	0.43	0.57
SO_3	55.34	0.39	0.05	0.10	0.05	0.40
Na_2O	0.02	0.07	0.00	0.04	0.02	0.15
K_2O	0.00	0.18	0.07	0.06	0.00	0.38
TiO_2	0.00	0.05	0.03	0.03	0.02	0.19
P_2O_5	0.00	0.00	0.01	0.04	0.10	0.34
Mn_2O_3	0.00	0.03	0.01	0.01	0.01	0.02
SrO	0.02	0.02	0.08	0.08	0.04	0.05
Cr_2O_3	0.00	0.00	0.00	0.00	0.01	0.01
ZnO	0.00	0.00	0.00	0.00	0.00	0.02
BaO	0.00	0.01	0.00	0.00	0.01	0.02
L.O.I. (550°C)	6.18	1.01	0.63	0.09	0.09	-
L.O.I. (950°C)	6.24	42.44	39.19	38.03	43.41	35.45
Total	100.34	100.08	100.00	100.07	99.84	98.49
Na_2O_{eq}	0.02	0.19	0.04	0.08	0.02	0.40

2.2.2 XRF Analysis of Slags

According to the literature and previous research, the durability of slag-blended cementitious systems is affected by slag composition, especially alumina and magnesia contents [1], [2]. Seven slags were selected for this study and the chemical oxide compositions were also characterized by XRF. These slags were named according to their alumina content as reported on their corresponding mill certificates provided by the suppliers as S8, S10C, S10F, S14A, S14B, S16 and S17. Within these slags, S10C and S10F were from the same supplier with S10F reflecting a finer grind of the same slag granules used in producing S10C. S14A and S14B were slags produced from the same slag granules but processed by different suppliers. The results are depicted in Table 2-3.

Table 2-3: Oxide chemical composition of slags

Analyte	S8	S10C	S10F	S14A	S14B	S16	S17
SiO_2	38.44	36.34	36.67	34.39	33.39	32.86	30.47
Al_2O_3	7.82	10.69	10.09	13.95	13.80	16.29	17.07
Fe_2O_3	0.47	0.79	1.06	0.54	0.84	0.36	0.46
CaO	39.18	39.23	38.33	42.15	42.00	37.98	35.49
MgO	10.71	10.70	10.81	5.14	5.60	8.88	10.96
Total SO_3	2.18	2.03	2.17	2.96	3.10	2.61	2.87
Sulfide, Sulfur	0.59	0.86	0.79	0.54	0.60	0.95	0.59
SO_3 as Sulfate	0.18	0.05	0.11	1.03	1.22	0.23	1.39
Na_2O	0.28	0.26	0.30	0.24	0.23	0.37	0.48
K_2O	0.42	0.22	0.33	0.29	0.28	0.44	0.30
TiO_2	0.39	0.44	0.41	0.57	0.53	1.21	1.63
P_2O_5	0.00	0.00	0.00	0.01	0.00	0.00	0.00
Mn_2O_3	0.53	0.28	0.28	0.25	0.19	0.25	0.35
SrO	0.05	0.04	0.05	0.07	0.07	0.10	0.07
Cr_2O_3	0.00	0.00	0.00	0.00	0.00	0.00	0.00
ZnO	0.00	0.00	0.00	0.00	0.00	0.00	0.00
BaO	0.04	0.03	0.03	0.08	0.06	0.08	0.08
L.O.I. (950°C)	-0.77	-1.20	-0.06	-0.73	0.09	-1.03	0.17
Total	99.73	99.84	100.21	99.89	100.17	100.41	100.39
Na_2O_{eq}	0.56	0.40	0.52	0.42	0.41	0.66	0.68

It is clear that, in general, the alumina contents of the analyzed slags corresponded to their mill certificates with minor differences. The alumina contents of the slags studied here, 7.82% to 17.07%, represented a wide range of commercially available slags approved for use in the state of

Florida. Such a wide range of alumina contents is expected to enable comprehensive assessment of the effects of the slag chemical composition on durability and performance of slag-blended concrete mixtures. Other than differences in the alumina contents, the chemical analyses of the selected slags reflect variability in their magnesia contents, 5.14% to 10.96%, as well as sulfate contents. The analyses indicate that slags with alumina contents of 14% and 17% incorporated a sulfate source during processing of their corresponding slag granules. The assessment of the nature and amount of the added sulfates is best determined by QXRD, presented in the following section.

2.3 Mineralogical Analysis through X-Ray Diffraction

Though elemental oxide composition renders valuable information, cement performance is controlled by its mineralogy. The mineralogical compositions of the as-received materials were analyzed using X-ray diffraction in accordance with ASTM C1365 [5]. The as-received materials studied here were cements, slags, processing additions, limestone, gypsum and hemihydrate. The as-received materials were ground in a McCrone micronizing mill to obtain an average particle size of less than 10 μm. Due to the potential of heat generated by dry-grinding resulting in thermal decomposition of gypsum to hemihydrate or anhydrite, wet grinding was selected to minimize temperature increase during the grinding process. Ethanol (200 proof) was added as a grinding medium. After grinding, the samples were dried in an oven maintained at 40°C prior to scanning. XRD scans were collected using a Phillips X'Pert PW3040 Pro diffractometer equipped with the X'Celerator Scientific detector and a Cu-Kα x-ray source. Tension and current were set to 45 kV and 40 mA respectively; 5-mm divergence and anti-scatter slits were used in the automatic mode. Scans were collected over a 2θ angular range of 7° to 70° and the samples were rotated at 30 rpm during data collection to improve counting statistics [6]. Three samples were analyzed for each as-received material and the average values are reported here.

Since the chemical oxide compositions of all as-received materials were determined using XRF, the external standard method was applied to ascertain the amorphous content in the as-received material. Corundum (Standard Reference Material 676a) obtained from the National Institute of Standards and Technology (NIST) was used as an external standard in this study. The mass absorption coefficient (MAC) of corundum, calculated using the MAC calculator functionality in the Panalytical HighScore Plus 4.5 software, was equal to 30.91 cm^2/g. MAC

values for cements and slags were calculated based on their elemental oxide composition (XRF analysis) [7], [8]. Due to the extensive peak overlap, typical for portland cements, salicylic acid-methanol (SAM) extractions were performed to dissolve the silicates and free lime, and isolate a concentrated residue of the aluminates and ferrites, in addition to other minor phases [9], [10]. Potassium hydroxide-sucrose (KOSH) extractions were also used to dissolve aluminates and ferrites and obtain a residue of C_3S, C_2S, alkali sulfates, and magnesia [9]. The crystalline structures used for the refinement analyses of the as-received materials are presented in Table 2-4.

Table 2-4: Crystalline structures used for weight fraction analysis

Phase	Formula	Crystal System	PDF codes	ICSD Code
Alite	Ca_3SiO_5-Mg, Al	Monoclinic/M3	01-070-8632	94742
Belite	Ca_2SiO_4	Monoclinic/β	01-086-0398	81096
Aluminate	$Ca_3Al_2O_6$	Cubic	01-070-0839	1841
Ferrite	Ca_2AlFeO_5	Orthorhombic	01-071-0667	9197
Portlandite	$Ca(OH)_2$	Rhombohedral	01-072-0156	15471
Quartz	SiO_2	Rhombohedral	00-046-1045	41414
Gypsum	$CaSO_4(H_2O)_2$	Monoclinic	00-033-0311	151692
Hemihydrate	$CaSO_4(H_2O)_{0.5}$	Monoclinic	01-083-0438	79528
Anhydrite	$CaSO_4$	Orthorhombic	01-086-2270	40043
Calcite	$CaCO_3$	Rhombohedral	01-086-0174	80869
Dolomite	$CaMg(CO_3)_2$	Rhombohedral	01-075-1711	31277
Periclase	MgO	Cubic	01-071-1176	9863
Syngenite	$K_2Ca(SO_4)_2H_2O$	Monoclinic	00-028-0739	157072
Aphthitalite	$K_3Na(SO_4)_2$	Rhombohedral	01-074-0398	26018
Melilite	$Ca_8 (Al_6Mg_1Si_5) O_{28}$	Tetragonal	00-004-0689	158173
Merwinite	$Ca_3Mg(SiO_4)_2$	Monoclinic	01-089-2432	43078

2.3.1 XRD Analysis of Cements, Limestone, Sulfates, and Processing Additions

The mineralogical compositions of the as-received cements are presented in Table 2-5 for cements, while

Table 2-6 presents the mineralogical analyses for the gypsum and hemihydrate that were used in the sulfate optimization experiments, the limestone that was used in IL cements, and cement processing additions that were used by the cement manufacturers. The results indicate that cements BB and C had the highest C_3A contents, which would imply a higher sulfate demand [11]

for those two cements. For the two Type II (MH) cements studied here, namely Z, and TTC, Cement Z had the highest alkali, C_3S, C_3A, periclase, and syngenite contents. It is therefore to be expected that Cement Z will have different durability performance than Cement TTC. All Type II(MH) cements studied here have a calcite content between 2.9-3.5%.

For the IL cements studied here, GIL-OP has the highest tricalcium silicate content and the highest tricalcium aluminate content. Both phases are known to affect the sulfate durability of concrete. Additionally, the calcite content varied among the IL(10) cements from 8.8 to 9.2%. Variation in calcite content is expected to affect cement hydration kinetics and phase assemblage [12], [13]. The high quartz content in TIL and THIL is due to the quality of the limestone (TLS) used in manufacturing TIL and THIL cements. Table 2-6 indicates that the calcite content in different limestone sources varied. Such variation agrees with differences in the CO_2 content reported from XRF analyses, thus indicating differences in purities of the limestone sources used by different cement manufacturers. However, it is to be noted that all limestone sources used here meet the minimum requirements of 70% $CaCO_3$, (ASTM C114 [3]). It is also to be noted that calcite is also present in processing additions, which will therefore affect the calcite content in cements. Finally, Table 2-6 indicates that the sulfate source analyzed show high purity, confirming their suitability to use as a source of sulfate for the sulfate balance experiments.

Table 2-5: Mineralogical analyses of as-received cements

Analyte	BB (I)	C I(Ha)	Z I/II (MH) (Ha)	TTC II (MH)	GIL -OP IL(10)	TIL IL(10)	THIL IL(14)
Alite	49.1	49.5	54	49.6	44.5	44.5	40.3
Belite	15.6	13.7	7.2	19.1	16.5	16.1	16.9
Aluminate	8.6	8.3	5.6	3.3	3.7	2.3	2.9
Ferrite	4.2	7.5	7.7	11.3	8.9	11.8	10.8
Gypsum	5.7	3.8	0.3	3.2	3.9	1.5	1.5
Hemihydrate	0.2	1.7	2.5	0.2	-	1.4	2
Anhydrite	0.1	-	-	-	-	-	-
Calcite	0.2	1.8	3.4	2.8	9.2	8.8	11.4
Portlandite	1.1	0.2	-	-	1.5		
Quartz	0	0.2	0.2	0.3	0.4	1.2	1.4
Dolomite	-	1.3	0.5	-	0.7	-	-
Periclase	0.1	1.3	1.8	-	-	-	-
Syngenite	0.5	0.9	1.1	-	-	-	-
Aphthitalite	0.3	0.6	-	-	-	-	-
Amorphous/ unidentified	14.2	9.4	15.7	10.2	10.6	12.5	12.8

Table 2-6: Mineralogical analyses of limestone, processing additions, and sulfates

| Analyte | Hemihydrate (AH) | Limestone in cements | | | | Kiln dust |
		ZLS (Z)	TTCLS (TTC)	TLS (TIL) & (THIL)	ALS (GIL-OP)	CKD (GILOP)
Gypsum	-	-	-	-	-	-
Hemihydrate	98.6	-	-	-	-	-
Anhydrite	-	-	-	-	-	-
Calcite	-	86.8	81.1	79.0	94.2	75.8
Quartz	-	1.2	8.5	9.5	1.4	1.7
Dolomite	-	-	-	-	-	1.4
Lime	-	-	-	-	-	-
Amorphous/ unidentified	1.4	11.9	10.4	11.6	4.4	21.1

2.3.2 XRD Analysis of Slags

The mineralogical analyses of the as-received slags are shown in Table 2-7. The amorphous contents of the slags varied from approximately 95% to 99%. In the high-alumina slags, with sulfate or sulfate and calcite additions, S14A, S14B and S17, the amorphous content was closer to the lower amorphous content of 95%. It is to be noted that S14B has a calcite content of 1.4%, indicating limestone addition.

Table 2-7: Mineralogical analyses of as-received slags

Analyte	S8	σ	S10C	σ	S10F	σ	S14A	σ	S14B	σ	S16	σ	S17	σ
Calcite	0.9	0.3	0.2	0.0	0.2	0.0	0.2	0.0	1.4	0.0	0.3	0.0	0.2	0.1
Melilite	0.4	0.0	0.4	0.1	0.3	0.0	0.3	0.0	0.3	0.1	0.7	0.0	1.4	0.1
Merwinite	-	-	1.1	0.0	1.1	0.0	-	-	0.1	0.0	-	-	-	-
Quartz	-	-	-	-	-	-	-	-	-	-	-	-	0.1	0.0
Gypsum	-	-	-	-	-	-	0.2	0.0	2.0	0.1	-	-	2.6	0.4
Hemihydrate	-	-	-	-	-	-	0.7	0.1	-	-	-	-	-	-
Amorphous/ unidentified	98.7	0.3	98.3	0.1	98.4	0.0	98.5	0.1	96.1	0.2	99.0	0.0	95.7	0.6

2.4 Physical Characteristics

2.4.1 Cement Physical Characteristics

The physical characteristics of the as-received materials determined in this study are specific gravity, Blaine fineness, and particle size distribution. Typical portland cement density is about 3.15 g/cm^3 [11] but variation can occur depending on processing additions and limestone content. Density measurements were conducted in triplicates and the standard deviations were within the limits specified in ASTM C188 [14]. The average values for the density measurements of cements are presented in Table 2-8.

Fineness is an important parameter that affects the hydration kinetics of cementitious materials, especially during the early stages of hydration. Typically, Type II(MH) cement has limits on its Blaine fineness (ASTM C150) due to the effect of fineness on the rate of reaction and heat release during the first 7-days of hydration. Fineness was measured using the Blaine air permeability method according to ASTM C204 [15]. It is considered an indirect method of assessing fineness, as the test actually measures the flow of air through a compacted bed of cement or other powdered material. The air permeability is first measured on a standard calibrating cement

with a certified value, SRM 114q, obtained from (NIST). The fineness of all subsequently analyzed materials is calculated based on the values obtained for the SRM114q. While this test is rapid and simple to perform, there are several drawbacks that have to be considered, especially when the Blaine test is used to measure fineness of powdered materials other than cement. Fineness measurements of the as-received materials were conducted in triplicates and the average values are reported in Table 2-8 for cements. It can be seen that IL cements generally have the highest fineness among the cements studied here.

An alternative method to assess particle size effects of powdered cementitious materials is laser particle size analysis. Cements of similar Blaine fineness or specific surface area, can have substantially different particle size distributions [16]. Particle size distribution (PSD) correlates better with heat of hydration of portland cements than Blaine fineness measurements. Therefore, particle size distributions of the as-received cements were measured using an LA-950 laser scattering particle size analyzer manufactured by HORIBA Instruments. Ethanol (200 proof) was used as the dispersing medium. Each as-received material was measured in triplicates and the average values are reported here. The incremental and cumulative particle size distributions are presented in Figure 2-1 and Figure 2-2, respectively. The mean particle size diameter (MPS), density, and Blaine fineness of the as-received cements are presented in Table 2-8.

Table 2-8: Particle size analysis, Blaine fineness, and density of cements

Physical properties	BB	C	Z	TTC	GIL-OP	TIL	THIL
	I	I(Ha)	II(MH) (Ha)	II(MH)	IL(10)	IL(10)	IL(14)
D_{10} (µm)	2.17	2.69	2.41	2.20	2.99	1.52	1.62
D_{50} (µm)	12.19	12.59	10.72	10.79	11.04	9.96	10.38
D_{90} (µm)	28.30	35.28	27.92	23.85	25.41	21.22	26.65
Mean size (MPS) (µm)	14.03	16.50	13.46	12.29	13.11	10.80	12.75
Density (g/cm^3)	3.04	3.15	3.08	3.12	3.06	3.11	3.13
Blaine Fineness (m^2/kg)	356	436	412	428	469	483	488

Generally, the Blaine fineness correlates with D_{50} particle size, but there are exceptions, such as the case of Cements C and GIL-OP. Cement GIL-OP shows a higher Blaine fineness indicating finer particle size while its D_{50} particle size indicates a coarser grind. Similarly, the D_{50} for Cement C indicates a coarser grind compared to the reported Blaine fineness.
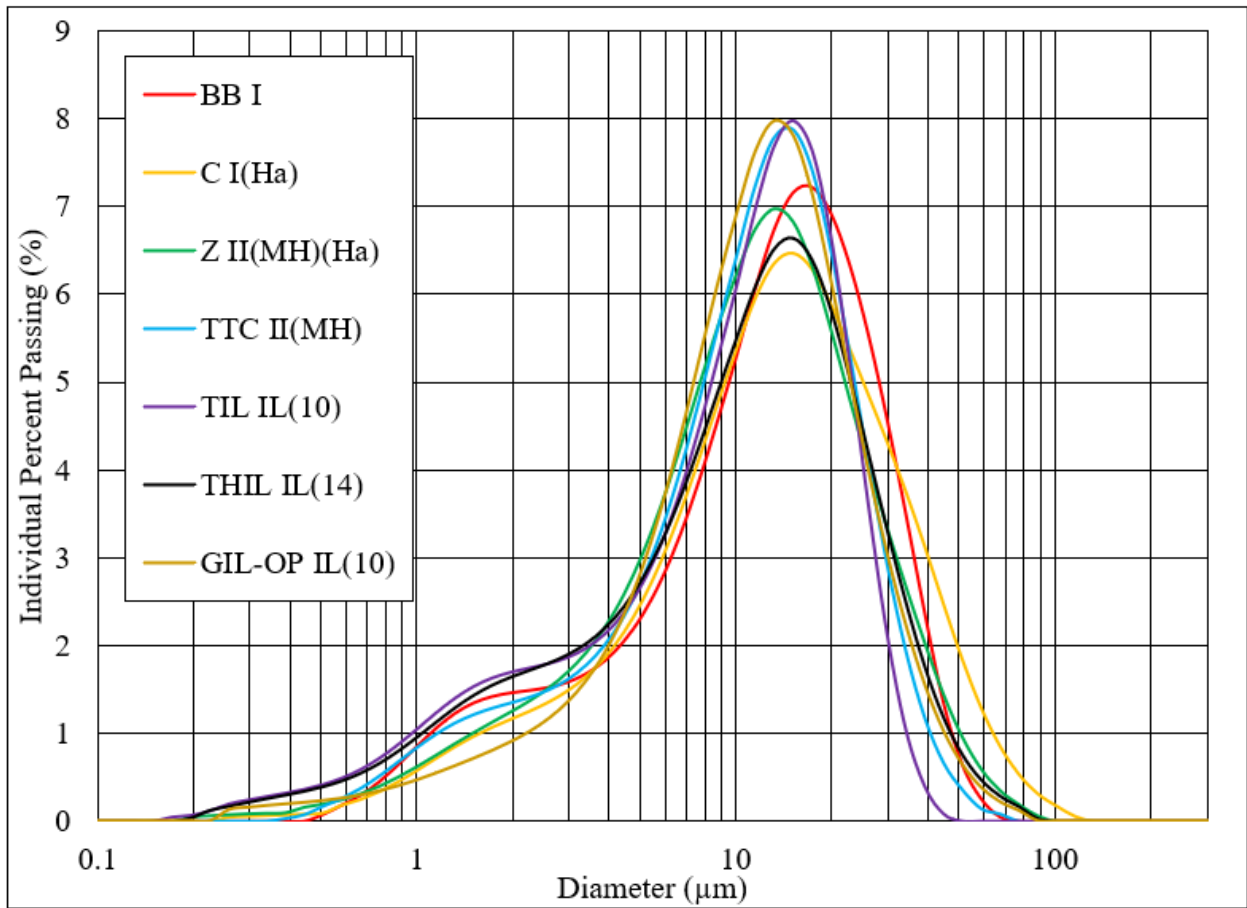
Figure 2-1: Incremental particle size distribution for as-received cements
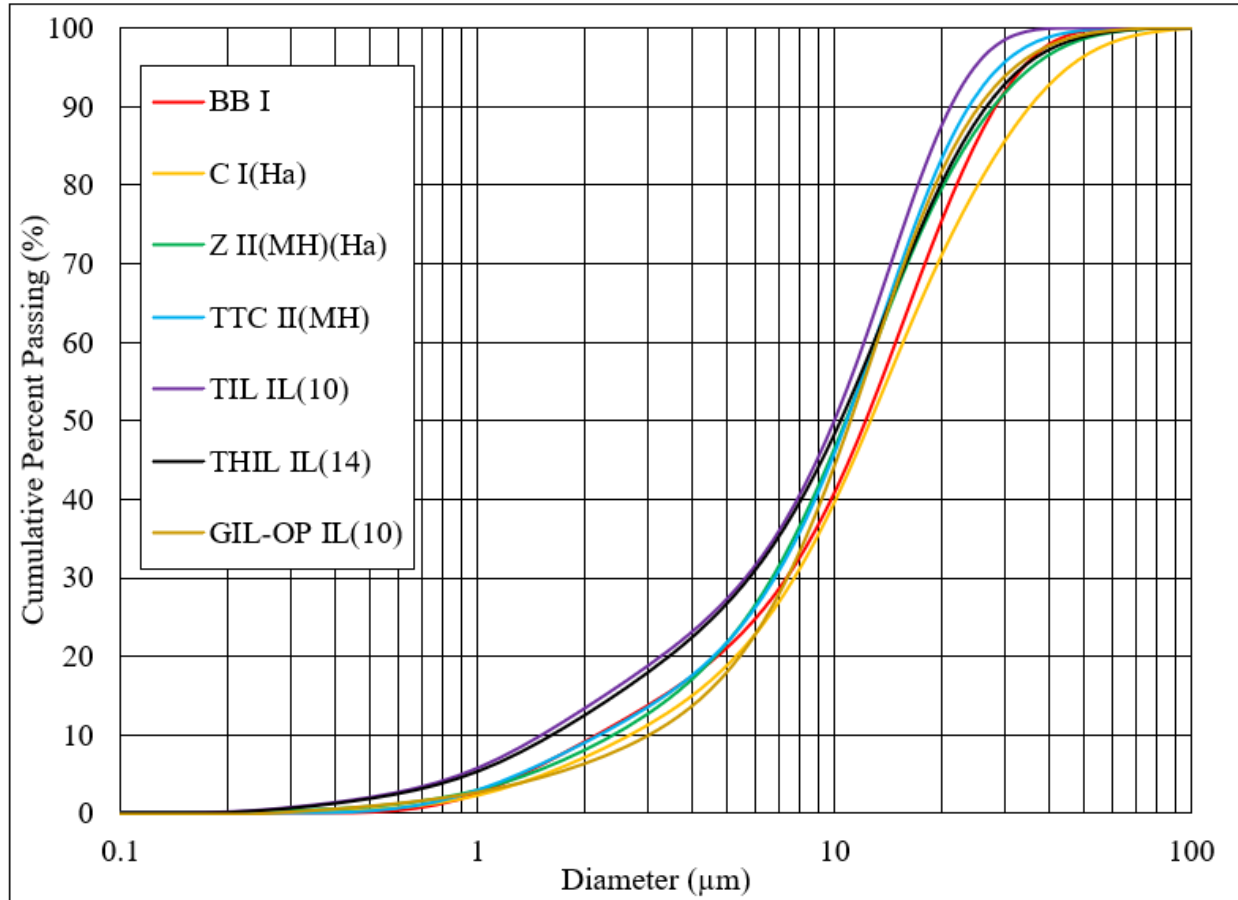
Figure 2-2: Cumulative particle size distribution for as-received cements

2.4.2 Slag Physical Characteristics

The published literature indicates the significance of the GGBFS fineness and physical characteristics on the durability of slag-blended cementitious systems [2]. All as-received slags were therefore subjected to the same physical testing conducted on the as-received cements and described previously in section 2.4.1. The results for the specific gravity, Blaine fineness, and particle size distribution tests are presented in Table 2-9. The incremental and cumulative particle size distributions are plotted in Figure 2-3 and Figure 2-4, respectively. The densities of the slags were very similar, ranging from 2.89 to 2.92 g/cm^3, but the fineness values showed significant differences. Within the selected seven slags, the Blaine fineness varied from 466 to 617 m^2/kg. In general, the low-alumina slags, except S10C, had a finer grind. Although the Blaine fineness has some correlation to the particle size distribution of the cement powder, the literature indicates drawbacks to using the Blaine fineness test as a tool to study the particle size of materials other

than cements due to differences in particle morphology and bed tortuosity [17], [18]. Particle size analyses conducted on the as-received slags indicated that though S14A and S14B had similar Blaine fineness values, though S14B had a coarser mean particle size than S14A. Additionally, S17 had a lower Blaine fineness than both S14A and S14B but particle size analysis indicated it had a smaller mean particle size.

Table 2-9: Particle size analysis, Blaine fineness, and density of slags

Physical properties	S8	S10C	S10F	S14A	S14B	S16	S17
D_{10} (μm)	1.23	1.71	1.56	1.63	2.08	1.57	1.52
D_{50} (μm)	8.28	9.25	8.28	9.33	10.92	10.04	9.09
D_{90} (μm)	18.90	19.72	16.87	21.73	24.44	23.68	18.84
Mean size (MPS) (μm)	9.49	10.29	9.03	10.97	12.55	11.80	9.79
Density (g/cm^3)	2.90	2.91	2.90	2.90	2.89	2.90	2.92
Blaine Fineness (m^2/kg)	617	485	600	551	553	466	510
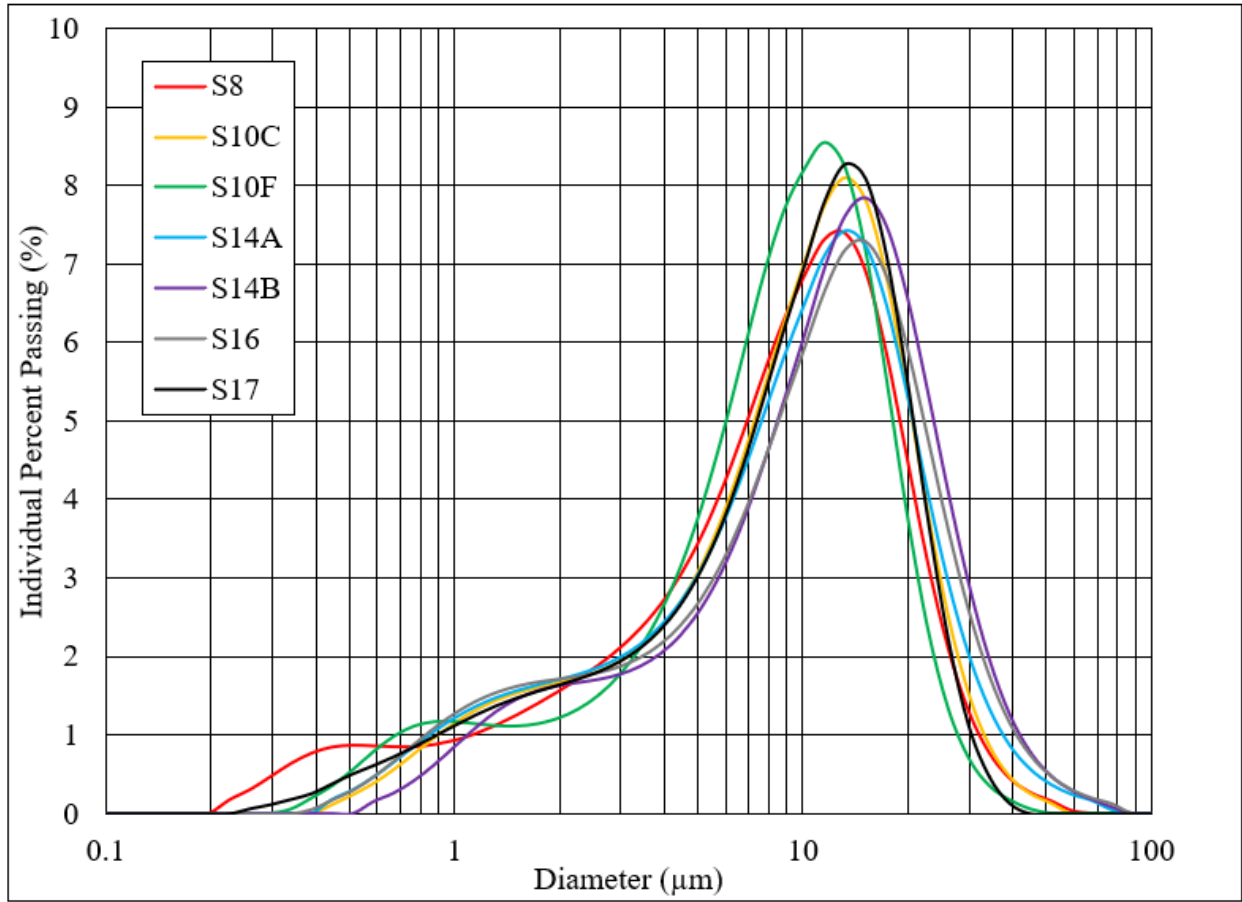
Figure 2-3: Incremental particle size distribution for slags
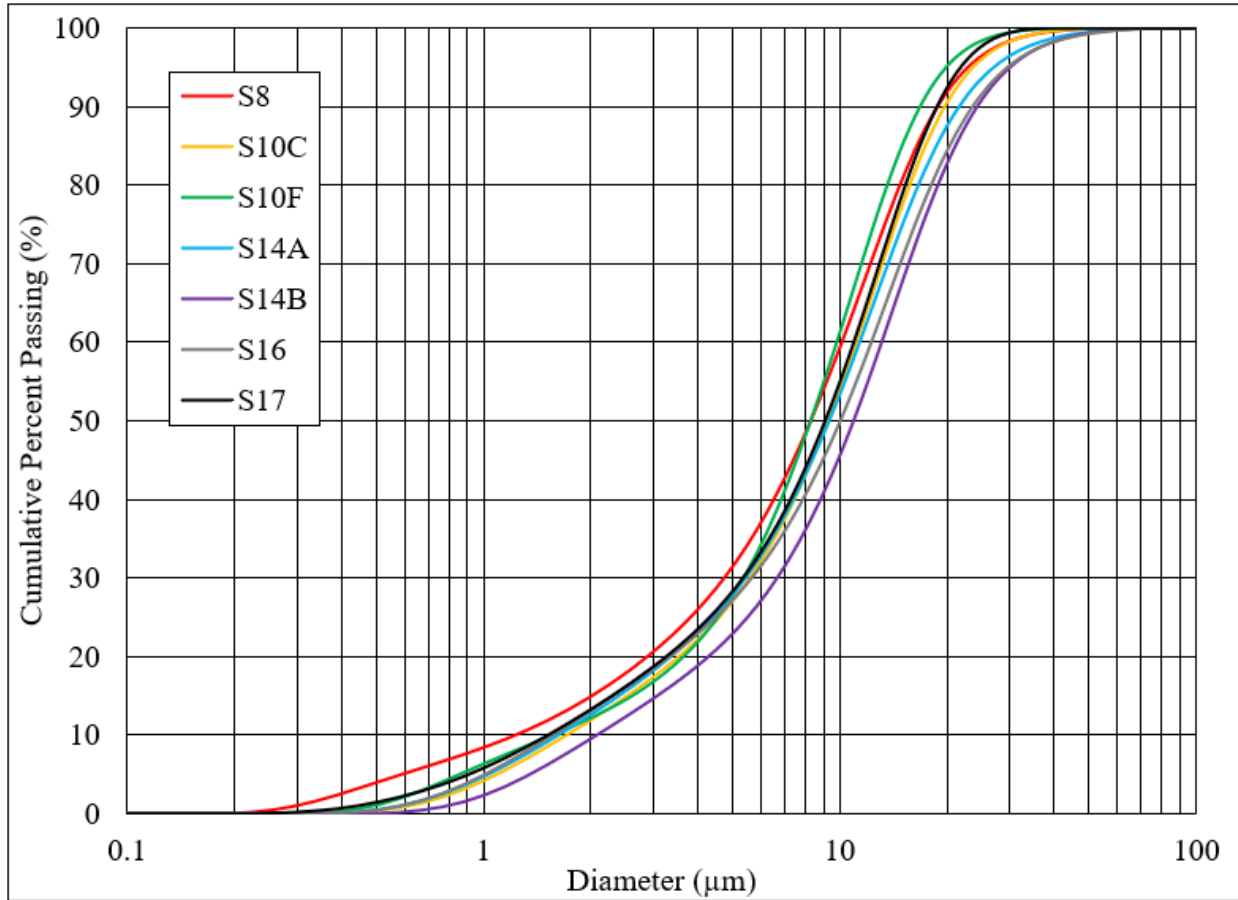
Figure 2-4: Cumulative particle size distribution for slags

2.5   Conclusions

A battery of chemical, mineralogical, and physical characterization testing of all as-received materials was conducted in this study. The findings indicate that the cements and slags selected for the current study reflect a wide range of materials characteristics, which is required for proper assessment of the performance and durability of slag-blended cementitious systems.

2.6 References

[1] A. Markandeya, N. Shanahan, D. Mapa, K. A. Riding, and A. Zayed, "Influence of slag composition on cracking potential of slag-portland cement concrete," *Constr. Build. Mater.*, vol. 164, pp. 820–829, 2018.

[2] F. Nosouhian, M. Fincan, N. Shanahan, Y. P. Stetsko, K. A. Riding, and A. Zayed, "Effects of slag characteristics on sulfate durability of Portland cement-slag-blended systems," *Constr. Build. Mater.*, vol. 229, p. 116882, Dec. 2019.

[3] ASTM C114−15, "Standard Test Methods for Chemical Analysis of Hydraulic Cement," West Conshohocken, PA: ASTM International, 2015.

[4] ASTM C150/C150M-18, "Standard Specification for Portland Cement," West Conshohocken, PA: ASTM International, 2018.

[5] ASTM C1365-06, "Standard Test Method for Determination of the Proportion of Phases in Portland Cement and Portland-Cement Clinker Using X-Ray Powder Diffraction Analysis," West Conshohocken, PA: ASTM International, 2016.

[6] D. Bish and R. J. Reynolds, "Sample Preparation for X-Ray Diffraction," in *Modern Powder Diffraction*, D. Bish and J. Post, Eds. Washington, DC: The Mineralogical Society of America, 1989, pp. 73–99.

[7] D. Jansen, C. Stabler, F. Goetz-Neunhoeffer, S. Dittrich, and J. Neubauer, "Does Ordinary Portland Cement Contain Amorphous Phase? A Quantitative Study Using an External Standard Method," *Powder Diffr.*, vol. 26, no. 1, pp. 31–38, Mar. 2011.

[8] M. A. G. Aranda, A. G. De la Torre, and L. Leon-Reina, "Rietveld Quantitative Phase Analysis of OPC Clinkers, Cements and Hydration Products," *Reviews in Mineralogy and Geochemistry*, vol. 74, no. 1. pp. 169–209, 2012.

[9] P. E. Stutzman, "Guide for X-Ray Powder Diffraction Analysis of Portland Cement and Clinker," Gaithersburg, MD, 1996.

[10] W. A. Gutteridge, "On the Dissolution of the Interstitial Phases in Portland Cement," *Cem. Concr. Res.*, vol. 9, no. 3, pp. 319–324, 1979.

[11]   S. Mindess, F. J. Young, and D. Darwin, *Concrete*. Upper Saddle River, NJ: Pearson Education, Inc., 2003.

[12]   M. Zajac, A. Rossberg, G. Le Saout, and B. Lothenbach, "Influence of limestone and anhydrite on the hydration of Portland cements," *Cem. Concr. Compos.*, vol. 46, pp. 99–108, 2014.

[13]   B. Lothenbach, G. Le Saout, E. Gallucci, and K. Scrivener, "Influence of limestone on the hydration of Portland cements," *Cem. Concr. Res.*, vol. 38, no. 6, pp. 848–860, 2008.

[14]   ASTM C188-15, "Standard Test Method for Density of Hydraulic Cement," West Conshohocken, PA: ASTM International, 2015.

[15]   ASTM C204-16, "Standard Test Methods for Fineness of Hydraulic Cement by Air-Permeability Apparatus," in *ASTM International*, 2016.

[16]   P. K. Mehta and P. J. M. Monteiro, *Concrete: Microstructure, Properties, and Materials*, Fourth Edi. McGraw-Hill Education, 2014.

[17]   E. C. Arvaniti, M. C. G. Juenger, S. A. Bernal, J. Duchesne, L. Courard, S. Leroy, J. L. Provis, A. Klemm, N. De Belie, "Determination of particle size, surface area, and shape of supplementary cementitious materials by different techniques," *Mater. Struct.*, vol. 48, no. 11, pp. 3687–3701, 2015.

[18]   E. C. Arvaniti, M. C. G. Juenger, S. A. Bernal, J. Duchesne, L. Courard, S. Leroy, J. L. Provis, A. Klemm, N. De Belie, "Physical characterization methods for supplementary cementitious materials," *Mater. Struct.*, vol. 48, no. 11, pp. 3675–3686, 2015.

Chapter 3   Effects of Cement-Slag Combinations on Sulfate Balance of Cementitious Systems

3.1   Introduction

During cement production, calcium sulfate is added to clinker to control and retard the aluminate reaction. To this end, gypsum ($CaSO_4 \bullet 2H_2O$) is the most widely used form of calcium sulfate in portland cement, but hemihydrate ($CaSO_4 \bullet 0.5H_2O$) and anhydrite ($CaSO_4$) can also be present. Typically, the optimum sulfate content for ordinary portland cement (OPC) is considered to be the one which gives the highest strength at one day [1]. In OPC systems, the strength development usually correlates well with the heat release during cement hydration. Lerch [2] reported a strong correlation between the optimum SO_3 content determined based on compressive strength and heat of hydration obtained from isothermal calorimetry. Supplementary cementitious materials (SCMs) such as ground granulated blast furnace slag (slag), fly ash, silica fume, and calcined clays are blended with cements to enhance concrete performance. Hence, when SCMs are incorporated, the hydration process in blended systems is influenced by the chemical and physical characteristics of the SCMs. SCMs can influence the correlation between heat of hydration and strength development because of the filler effect as well as the reactivity of the pozzolans [3], [4].

The filler effect can increase the sulfate demand in blended systems by accelerating the hydration process and consequently enhancing the adsorption of sulfate on the precipitated C-S-H [5]. In addition, high alumina contents in SCMs can enhance the reactivity and thereby increase the sulfate demand in blended systems [6]. Therefore, for blended cementitious systems such as cements with slags, sulfate optimization of the binary system or addition of extra sulfate to the slag may be required in order to sustain the strength and durability of the system. While several studies have reported on sulfate optimization in plain cement systems, studies on slag-blended systems are rare in the literature. Thus far, the optimum sulfate content which provides the best concrete performance in terms of both strength and durability is uncertain.

Few studies discussed the effect of sulfate addition on the performance of slag-blended cementitious systems. According to Whittaker et al. [7], the addition of anhydrite accelerated the hydration of alite, but did not affect the kinetics of slag hydration. In general, slag hydration forms a C-S-H phase with a lower Ca/Si ratio and a higher Al/Si ratio, and higher contents of ettringite, AFm phases (hydrated tetracalcium Al_2O_3–Fe_2O_3–mono phases) and hydrotalcite. Whittaker et al.

[7] observed an effect on the phase assemblage of the blends in presence of sulfates. It stabilized ettringite over other alumina bearing phases, affected the composition of C-S-H as sulfates adsorbed onto C-S-H, and also increased the Mg/Al ratio in hydrotalcite as more alumina was consumed to form ettringite. Similar findings were reported by Adu-Amankwah et al. [8] for ternary slag-limestone-composite cements. Increasing sulfate contents have two opposing effects on compressive strength; increased volume of ettringite increases the compressive strength and decreases water content in C-S-H which reduces the space filling capacity of the C-S-H and decreases the compressive strength.

Ogawa et al. [9] recommended the addition of sulfate to improve sulfate resistance in blended cements with high-alumina slag (15.2% Al_2O_3). When the total SO_3 content of plain OPC (8.7% C_3A) blended with 40% high-alumina slag increased from 2.6% to 4.2% and 5.8%, mortar bar expansion (ASTM C1012 [10]) was significantly suppressed. For the same system, incorporation of 4% limestone powder along with 4.2% sulfate content further improved the sulfate resistance of these blends as denoted by mortar bar expansion. Both these methods prevented the formation of ettringite at later age; increasing sulfate additions formed ettringite, initially minimizing monosulfoaluminate and in the presence of limestone formed carboaluminate phases that stabilized ettringite at early age. Moreover, Type V (4.9% C_3A) cement with 60% low-alumina slag (10.7% Al_2O_3) indicated stable sulfate resistance without any sulfate or limestone additions; however, use of high-alumina slag with the same cement required sulfate (4% total SO_3) and limestone (4%) additions to improve sulfate resistance.

Sufficient amounts of sulfate additions are needed to control the alumina reaction and to improve external sulfate durability. Sulfate present in the system can be adsorbed by C-S-H at high curing temperatures and later be desorbed causing internal sulfate attack. This can lead to detrimental expansion due to delayed ettringite formation (DEF). Ettringite decomposes at high temperatures with subsequent reformation (DEF) once temperatures drop to ambient condition and in the presence of moisture [11].

Sulfate addition can have adverse effects on chloride durability, especially at lower chloride concentrations [12]. Typically, incorporation of slags substantially decreases chloride ion ingress due to the refined pore structure [13]. As stated in the literature, high alumina contents bind more chloride either by chemical reactions or adsorption, which reduces the free chloride

available in the pore solution [14]–[17], which is desirable to prevent steel corrosion. However, addition of sulfates greatly reduces the alumina levels available to form Friedel's salt due to the formation of monosulfoaluminate and ettringite instead. At higher chloride concentrations, ettringite is again transformed to Friedel's salt [12]. Consequently, it is important to maintain proper sulfate balance in the system to sustain concrete durability.

Typically, cement producers decide on the optimum sulfate content based on the maximum compressive strength of mortar cubes and/or heat of hydration of paste at 1 day in accordance with ASTM C563 [18]. ASTM C563 [18] recommends four methods to determine the optimum amount of sulfate in cementitious systems; namely, isothermal calorimetry, mortar cube strength, drying shrinkage and concrete strength tests. Correlation between these four methods is not well established, but isothermal calorimetry appears to be the most repeatable test among those, because the rest of the test methods are more susceptible to operator-related variability issues. However, it is still debatable whether these sulfate amounts are sufficient to overcome concrete durability issues caused by sulfate attack, chloride ingress etc. It is possible that different sulfate levels may be required in order to achieve the greatest concrete performance in different categories. Moreover, the effect of sulfate content on short-term versus long-term performance of concrete is not yet well established. Therefore, the study of sulfate balance in cementitious systems remains with unresolved issues and consequently needs further investigation. One of the main objectives of this work is to determine the effect of different slags on concrete durability. Since the sulfate balance in the system is critical for concrete durability, the focus of this chapter is to assess sulfate optimization in slag-blended cementitious systems so that it can be related to durability performance.

3.2   Materials and Methods

3.2.1   Materials

Five cements and five slags with variable physical and chemical characteristics were used to investigate the sulfate balance in cementitious systems. These cements include ASTM C150 [19] Type I (Cement BB), ASTM C150 Type I with high alkali (Cement C), ASTM C150 Type II (MH) (Cement TTC), and two ASTM C595 [20] Type IL cements (TIL and THIL) with 10% and 14% limestone contents, respectively. Oxide chemical composition, Blaine fineness, mean particle

size (MPS) and mineralogical analysis of as-received cements are listed in Table 3-1 and Table 3-2 respectively.

Table 3-1: Oxide chemical composition, Blaine fineness, and mean particle size (MPS) of as-received cements

Analyte	BB I	C I(Ha)	TTC II(MH)	TIL IL(10)	THIL IL(14)
SiO_2	19.53	19.00	20.21	19.16	19.14
Al_2O_3	5.51	5.90	5.00	4.61	4.52
Fe_2O_3	1.79	2.80	3.78	3.74	3.54
CaO	64.27	60.80	63.60	62.40	62.11
MgO	1.05	2.50	0.32	1.12	1.08
SO_3	3.93	4.00	2.55	2.47	2.44
Na_2O	0.11	0.32	0.01	0.17	0.17
K_2O	0.41	1.10	0.32	0.32	0.29
TiO_2	0.26	0.26	0.36	0.23	0.22
P_2O_5	0.27	0.26	0.10	0.09	0.09
Mn_2O_3	0.02	0.11	0.13	0.15	0.14
SrO	0.07	0.28	0.13	0.12	0.12
Cr_2O_3	0.01	0.01	0.03	0.02	0.02
ZnO	0.01	0.07	0.05	0.05	0.04
L.O.I. (550°C)	-	-	1.34	0.76	0.69
L.O.I. (950°C)	2.60	2.40	2.85	5.35	5.99
Total	99.84	99.82	99.44	99.98	99.91
Na_2O_{eq}	0.38	1.05	0.22	0.38	0.36
Blaine Fineness (m^2/kg)	356	436	428	483	488
MPS (μm)	14.03	16.50	12.29	10.80	12.75

Table 3-2: Mineralogical analyses of as-received cements

Analyte	BB (I)	C I(Ha)	TTC II(MH)	TIL IL(10)	THIL IL(14)
Alite	49.1	49.5	49.6	44.5	40.3
Belite	15.6	13.7	19.1	16.1	16.9
Aluminate	8.6	8.3	3.3	2.3	2.9
Ferrite	4.2	7.5	11.3	11.8	10.8
Gypsum	5.7	3.8	3.2	1.5	1.5
Hemihydrate	0.2	1.7	0.2	1.4	2.0
Anhydrite	0.1	-	-	-	-
Calcite	0.2	1.8	2.8	8.8	11.4
Portlandite	1.1	0.2	-		
Quartz	0.0	0.2	0.3	1.2	1.4
Dolomite	-	1.3		-	-
Periclase	0.1	1.3	-	-	-
Syngenite	0.5	0.9	-	-	-
Aphthitalite	0.3	0.6		-	-
Amorphous/ unidentified	14.2	9.4	10.2	12.5	12.8

The five ASTM C989 [21] slags used in this study were selected based on different physical and chemical characteristics, with focus on alumina and magnesia content. These slags were named S8, S10C, S10F, S14B, and S17. Identified alumina content of the slags varies from approximately from 8% to 17% and fineness ranges from 466 to 617 m^2/kg. Oxide chemical composition, Blaine fineness and mean particle size (MPS) of the as-received slags are listed in Table 3-3. A reagent grade hemihydrate by Acros Organics was selected as an additional sulfate source to balance the sulfate demand in the blended system.

Table 3-3: Oxide chemical composition, Blaine fineness, and mean particle size (MPS) of as-received slags

Analyte	S8	S10C	S10F	S14B	S17
SiO_2	38.44	36.34	36.67	33.39	30.47
Al_2O_3	7.82	10.69	10.09	13.80	17.07
Fe_2O_3	0.47	0.79	1.06	0.84	0.46
CaO	39.18	39.23	38.33	42.00	35.49
MgO	10.71	10.70	10.81	5.60	10.96
Total SO_3	2.18	2.03	2.17	3.10	2.87
Sulfide, Sulfur	0.59	0.86	0.79	0.60	0.59
SO_3 as Sulfate	0.18	0.05	0.11	1.22	1.39
Na_2O	0.28	0.26	0.30	0.23	0.48
K_2O	0.42	0.22	0.33	0.28	0.30
TiO_2	0.39	0.44	0.41	0.53	1.63
P_2O_5	0.00	0.00	0.00	0.00	0.00
Mn_2O_3	0.53	0.28	0.28	0.19	0.35
SrO	0.05	0.04	0.05	0.07	0.07
Cr_2O_3	0.00	0.00	0.00	0.00	0.00
ZnO	0.00	0.00	0.00	0.00	0.00
BaO	0.04	0.03	0.03	0.06	0.08
L.O.I. (950°C)	-0.77	-1.20	-0.06	0.09	0.17
Total	99.73	99.84	100.21	100.17	100.39
Na_2O_{eq}	0.56	0.40	0.52	0.41	0.68
Blaine fineness (m^2/kg)	617	485	600	553	510
MPS (µm)	9.49	10.29	9.03	12.55	9.79

3.2.2 Mixture Designs

Ordinary portland cement pastes were prepared with a water-cement ratio (w/c) of 0.485 by mass. When incorporating slag, a 60% replacement level of cement by mass and a water-to-cementitious materials ratio (w/cm) of 0.485 was selected to investigate the effect of slag on hydration of blended systems.

When balancing the sulfate content in blended systems, ASTM C563 [18] requires the addition of extra sulfates as a partial replacement of cement content. However, in the United States, cements and slags are blended in the mixer at the ready-mix concrete plant, instead of at the cement plant, to give the ready-mix concrete producer more flexibility in SCM type and dosage. This results in the need for cement and slag sulfate levels to be determined independently. Adding extra sulfate to the cement to rebalance the system would thus not be appropriate since in practice extra

sulfate beyond what is needed for the cement would be added to the slag. Besides, depending on the slag composition, slag producers will add extra gypsum during the grinding process of the high-alumina slags. Consequently, a different adjustment method from ASTM C563 [18] was taken to rebalance the system. Hemihydrate was selected to vary the SO_3 level in the system.

When adding hemihydrate to estimate the optimum sulfate content in blended systems, ASTM C563 [18] requires the SO_3 levels to be at least 0.2% different unless more than five different sulfate levels are being tested. In addition, the difference between maximum and minimum sulfate content must be at least 2.0%. Hence, the slag-cement blended systems considered in this study had SO_3 level increments varying from 0.3% to 0.5%. This was decided based on the original sulfate content in the cement, alumina content in slags, and total sulfate content in the blended system. At least 8 sulfate levels were explored in each slag-cement system.

3.2.3 Experimental Methods

Isothermal conduction calorimetry was performed to measure the heat of hydration of the blended paste systems, according to ASTM C1702 [22], Method A, internal mixing using a TAM Air eight-channel calorimeter produced by TA instruments. When preparing samples, cement, slag and hemihydrate amounts were weighed in an ampoule and mixed using a spatula until the dry solids were evenly blended. The ampoule was then attached to the mixer containing the weighed amount of water which was dispersed through a syringe. All the ampoules were loaded in the calorimeter at the same time and kept in place before mixing until heat flow equilibrium was achieved. Once the heat flow became stable, mixing was started and water was injected over 10 seconds, followed by 1 minute of constant internal mixing. All the experiments were conducted in duplicates at 23°C for a period of 72 h. For each system, the optimum sulfate contents at 1, 2, and 3 days were determined. In some blends with high-alumina slags, the 3-day optimum could not be determined, even at approximately 5% total SO_3 levels. This was because the reaction was expansive and cracked the ampoule; therefore, the total SO_3 levels were not increased beyond 5% to avoid damaging the calorimeter. ASTM C563 [18] recommends three calculation methods to determine the optimum SO_3 content from the experimental results, namely, visual fit, least squares parabolic fit, or asymmetric fit. In the current study, heat of hydration at the specified ages were plotted against the total sulfate content in the blended system, and for each age, a polynomial was fit using the least squares method. Finally, the sulfate content corresponding to the maximum point

of the polynomial (highest heat of hydration) in the sulfate range considered (as-received SO_3 content to approximately 5% SO_3 content) was determined.

Phase assemblages of the slag-cement blended systems were determined by quantitative X-ray diffraction (XRD) using a Phillips X'Pert PW3040 Pro diffractometer equipped with the X'Celerator Scientific detector and a CuKα x-ray source. Tension and current were set to 45 kV and 40 mA, respectively. Scans were performed in the range of 7 - 70° 2θ, with a step size of 0.0167° 2θ. Samples were then loaded into the sample holder using a back-loading technique in order to minimize preferred orientation, and placed onto a spinner stage that rotated at 30 rpm in order to improve counting statistics [23]. Phase quantification was performed using the Rietveld refinement functionality of the PANalytical HighScore Plus 4.5 software. The samples were scanned immediately after removal from the calorimeter at 72 h. This included the as-received control cement pastes, as-received cement-slag pastes and four selected samples with varying SO_3 levels from each cement-slag paste system. The external standard method was used to quantify the amorphous content in the paste using corundum (Standard Reference Material (SRM 676a)) obtained from the National Institute of Standards and Technology (NIST). The mass absorption coefficient (MAC) of corundum was 30.91 cm^2/g.

Thermodynamic modeling was performed using the Gibbs free energy minimization software, GEMS 3 [24] to understand further the phases formed at 3 days in the slag-blended cementitious systems and the effect of varying sulfate contents on the phase assemblage. GEMS predicts phase assemblage based on equilibrium reactions. Therefore, the degree of hydration (DOH) of cement and slag fractions needed to be determined to scale the input parameters accordingly. The cement DOH was determined using XRD analysis by rescaling the quantification results on an anhydrous basis [25]. In the cement-slag blends, the slag degree of hydration was varied between 10% and 40% as slag DOH was unknown. The effect of varying sulfate content was modeled for slags S8 and S17 with cement BB. Hemihydrate was included as a partial replacement of slag. Therefore, the additional hemihydrate content in the blended system was varied from 0 to 4%. The DOH of slag was assumed to be a constant value of 40% for the analysis with varying sulfate content, although the slag DOH may vary depending on its chemical and physical properties as well as cement properties it is blended with. This assumption was made comparing the phase assemblage obtained from XRD analysis and GEMS modeling for as-

received slag-blended mixtures. While the slag DOH at early age still remains debatable, slag DOH varying between 30-40% between 1 and 7 days were reported for alkali-activated slags [26], [27]

3.3   Results and Discussion

3.3.1   Heat of Hydration Measurements of As-Received Cementitious Materials

3.3.1.1 As-Received Cement Systems

The measured heat flow and total heat evolution of as-received cements are shown in Figure 3-1:and Figure 3-2:, respectively. The total heat at 1, 2 and 3 days and the heat index ($C_3S+4.75C_3A$), determined based on phase quantification values determined via QXRD, are listed in Table 3-4:. The three cements, TTC, TIL and THIL have shown a faster hydration during the first 12 h even with their lower heat indices, but the reaction slowed down after 24 h, resulting in a higher total heat during the first 24 h than the cements BB, and C but lower heat of hydration after 24 h. This can be attributed to the combined effect of particle size and limestone content of the cement. As stated in the literature, a cement with higher Blaine fineness and/or lower MPS will increase its reactivity and consequently increase its heat of hydration at early age [28]. The smaller MPS of cements TTC, TIL and THIL compared to that of cements BB and C, along with the limestone content may have increased the initial hydration reaction. A slight acceleration of cement hydration is expected initially in the presence of limestone, as it provides additional nucleation sites for the growth of hydration products [29]. However, later hydration heat can be lower due to dilution effect as can be observed with cements TIL and THIL. Furthermore, cement THIL has the highest calcite content (11.4%) and the lowest heat of hydration at 72 h.

The highest heat of hydration at 72 h was observed for cement C (Type I (Ha)), and BB (Type I). Cements TTC, TIL and THIL were apparently under-sulfated as depicted by the closer silicate and aluminate peaks, with slight overlap. However, cements BB and C have shown well distinguished silicate and aluminate peaks due to proper sulfate adjustment. Cement BB has also shown a shoulder peak after the aluminate peak (sulfate depletion peak) which corresponds to monosulfate formation [30].
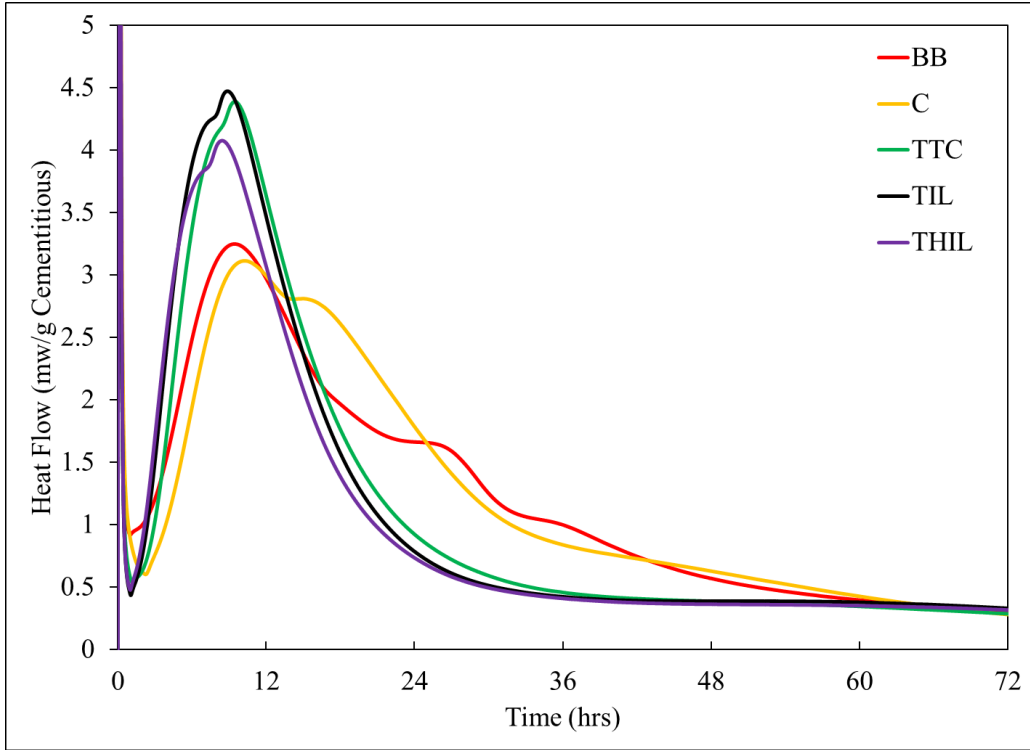
Figure 3-1: Heat flow of as-received cements
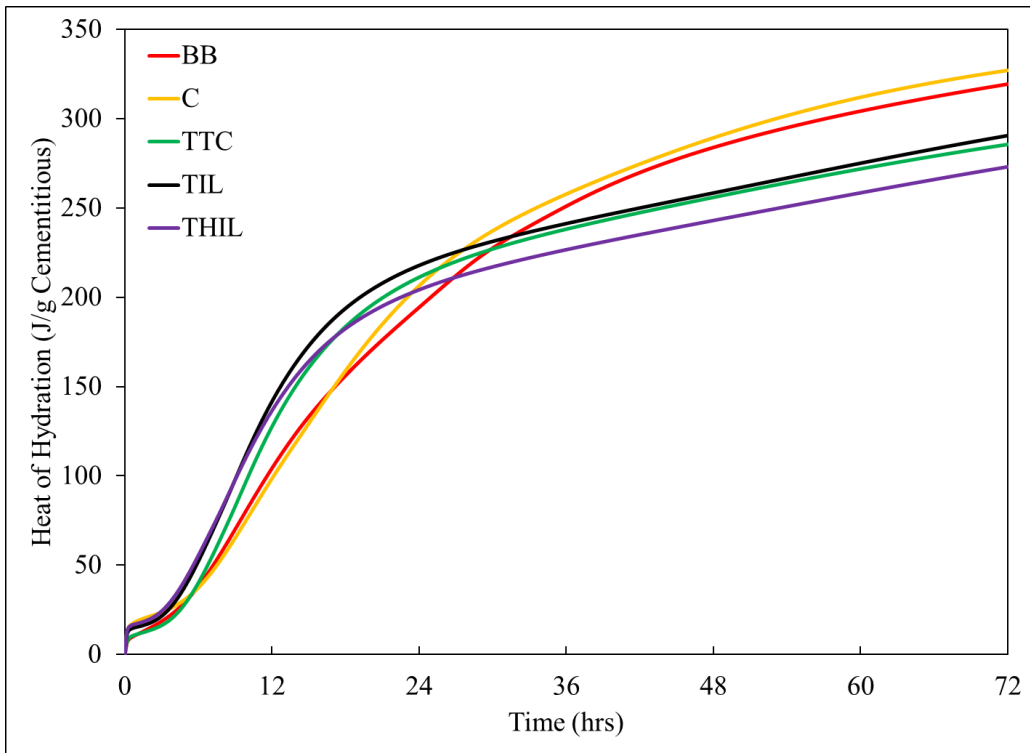
Figure 3-2: Total heat evolution of as-received cements

57

Table 3-4: Heat of hydration and heat indices of control cement pastes

Age	Heat of Hydration (J/g cement) and heat index (HI)*				
	BB (Type I)	C (Type I (Ha))	TTC (Type II(MH))	TIL (Type IL(10))	THIL (Type IL(14))
1 day	195	206	211	217	204
2 day	284	289	256	258	243
3 day	319	327	286	290	273
HI	90	89	65	55	54

*= Heat index determined based on phases quantification using XRD

3.3.1.2 As-Received Cement-Slag Blended Systems

Cement replacement with slags is known to influence the hydration kinetics of the blended system. The effect of varying the slag source on cement hydration as well as the effect of cement characteristics on slag hydration are investigated in this section.

Figure 3-3 and Figure 3-4 illustrate the measured heat flow and total heat of the slag-blended paste systems with cement BB (Type I). Addition of slag clearly resulted in a stronger aluminate peak. This can be attributed to the extra alumina in the slag or the acceleration of hydration. As it appears, slag S10F showed the highest aluminate peak intensity although its alumina content is not the highest, which is likely due to an increased early reactivity because of its higher fineness. Slag S10C, which has an alumina content similar to slag S10F but a coarser fineness, showed a slightly lower aluminate peak intensity as well as a lower hydration heat at 3 days than slag S10F. The lowest cumulative heat at 3 days was observed in slag S8 blend which has the lowest alumina content, although it has the highest fineness (617 m^2/kg) among all the slags considered in this study. This shows that the heat of hydration is affected by both the fineness and the alumina content.

The aluminate peaks in slag S14B and slag S17 appeared to be suppressed and delayed possibly due to the extra sulfate already added to the slags by the supplier; slag S17 showed the lowest aluminate peak intensity in spite of its highest alumina content. This indicates that the sulfate adjustment can also affect slag-alumina reaction and hydration kinetics in cementitious systems. In terms of heat of hydration, the slag S17 system appeared to have lower heat release during the first 24 hours, showing the effect of sulfate on delaying the alumina reaction. Afterwards, however, it surpassed the heat of hydration of all other slags.

Moreover, the slag S14B blend showed the highest cumulative heat until two days. Apart from the alumina content, the main difference between slag S14B and the other slags is its low MgO content (5.6%). According to Ben Haha et al. [26] during the first two days, the highest cumulative heat was observed for the slag with the lowest MgO content (at the same Al_2O_3 content). Therefore, as it appears, the system with slag S14B experienced an increased rate of reaction during the first two days after which hydration reaction appeared to slow down. Such observation needs to be further considered when conducting adiabatic temperature rise experiments on slag blended concrete mixtures.
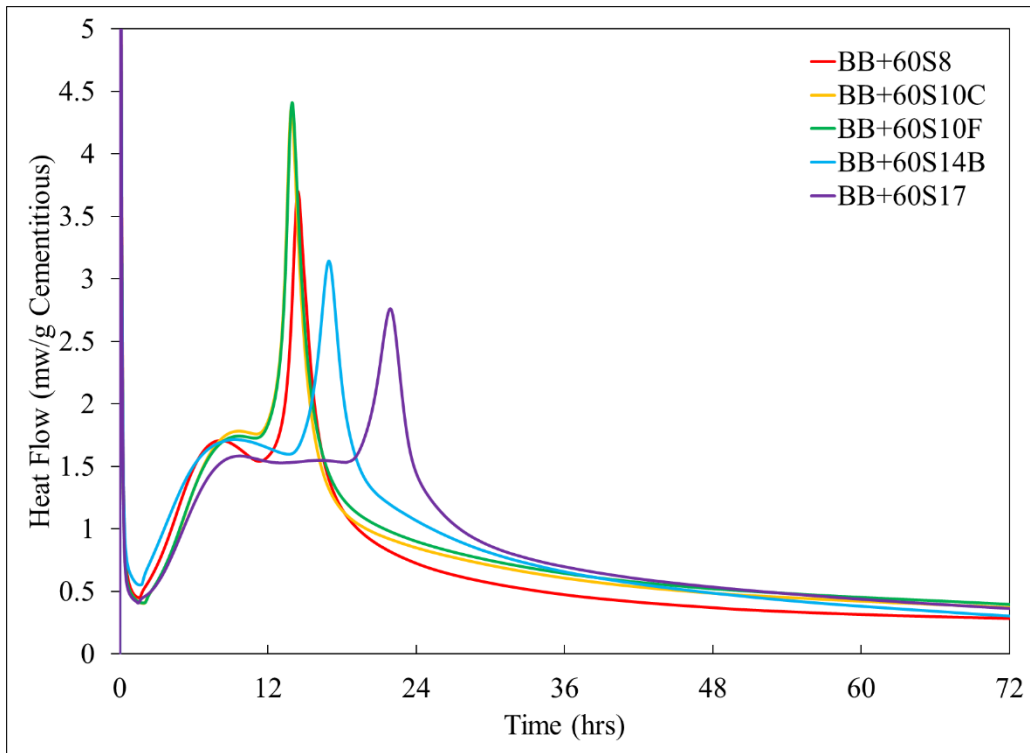
Figure 3-3: Heat flow of cement BB with slags
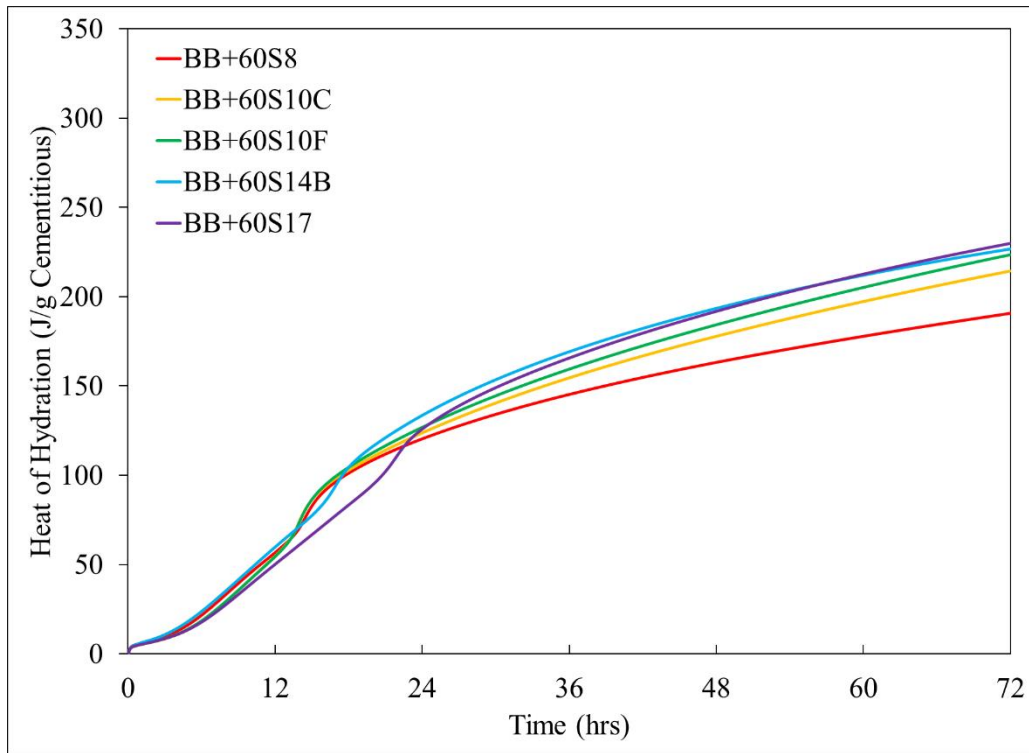
Figure 3-4: Total heat evolution of cement BB with slags

The measured heat flow and total heat evolutions of cement C (Type I with high alkali content) blended with slag are illustrated in Figure 3-5 and Figure 3-6 respectively. Both heat flow and total heat trends were similar to those of slags blended with cement BB, which again indicate the effect of slag alumina content on heat generation. Strong aluminate peaks can be observed in all the systems. In the heat flow curves of cement BB blends, a valley was clearly visible between the silicate and aluminate peaks; however, no such valley was observed between the two peaks in the heat flow curves of cement C blends. It is likely the sulfate in the system was consumed at a faster rate in the presence of alkalis and the aluminate peak occurred earlier as a result.
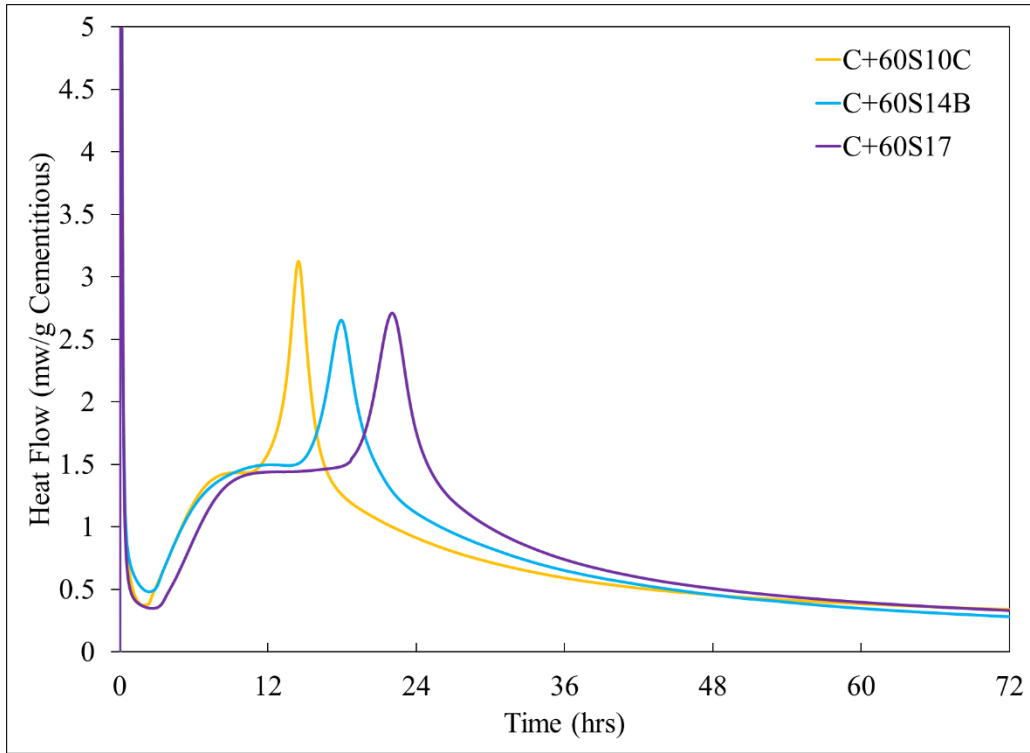
Figure 3-5: Heat flow of cement C with slags
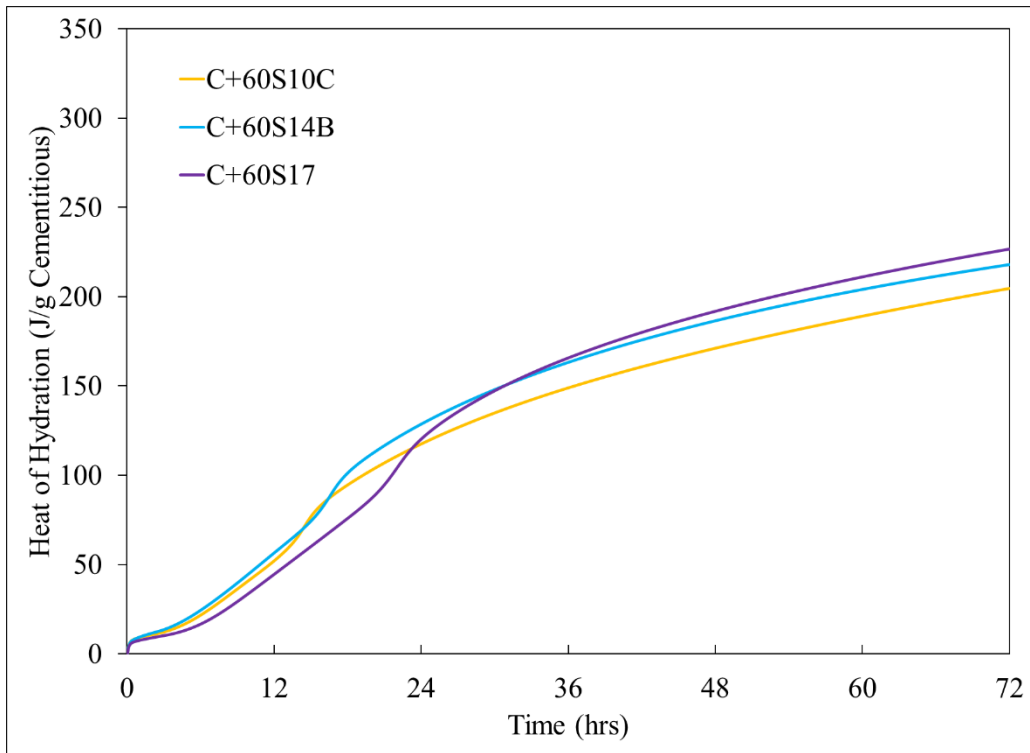
Figure 3-6: Total heat evolution of cement C with slags

61

Figure 3-7 shows the measured heat flow of cement TTC (Type II (MH)) blended with slags whereas Figure 3-8 illustrates the total heat released from the same mixtures. These slags blended with Type II(MH) cement did not result in alumina peaks as strong as that with Type I cements. This can be attributed to the lower C_3A content in Type II(MH) cements. The lowest cumulative heat at three days was observed in TTC+60S8 whereas the highest was seen in TTC+60S17, indicating the effect of slag alumina content on heat generation. Moreover, slags S10C and S10F with approximately similar alumina contents but different fineness, clearly showed the effect of slag fineness on hydration heat when blended with Type II (MH) cement as well. In terms of sulfate balance in the blended systems, blends with slags S10C, and S10F appeared to be under-sulfated as indicated by the slightly overlapped silicate and aluminate peaks. On the other hand, clearly distinguished silicate and aluminate peaks can be observed in the blends with slags S14B and S17, attributed to the extra sulfate blended by the supplier in these slags which delayed the aluminate peak.
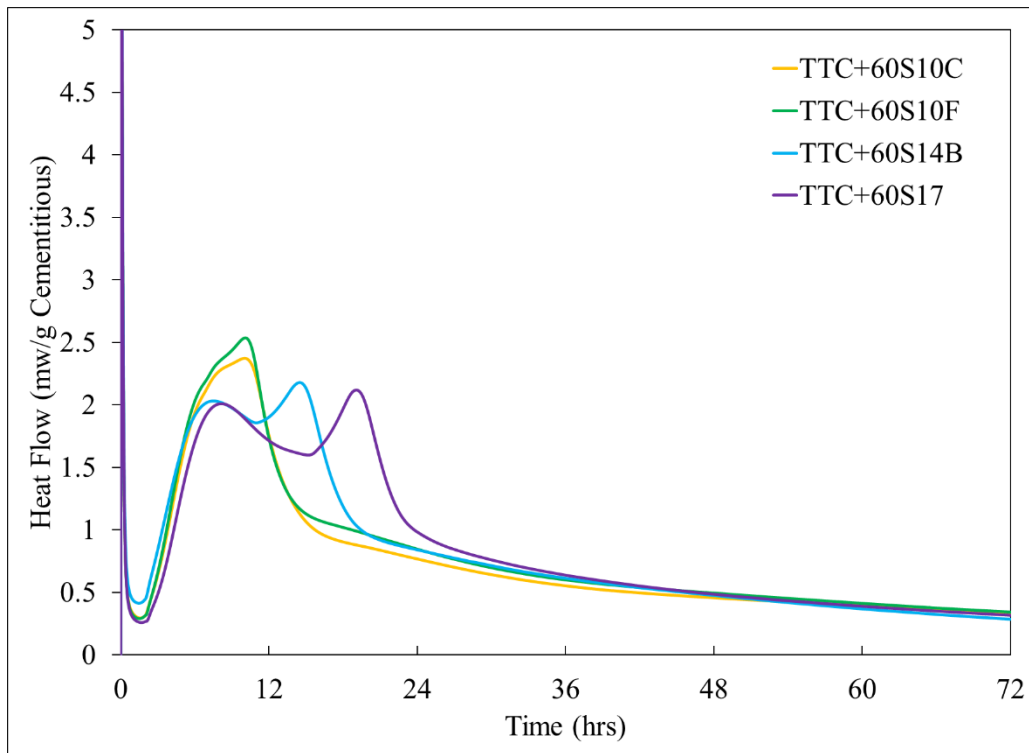
Figure 3-7: Heat flow of cement TTC with slags

62
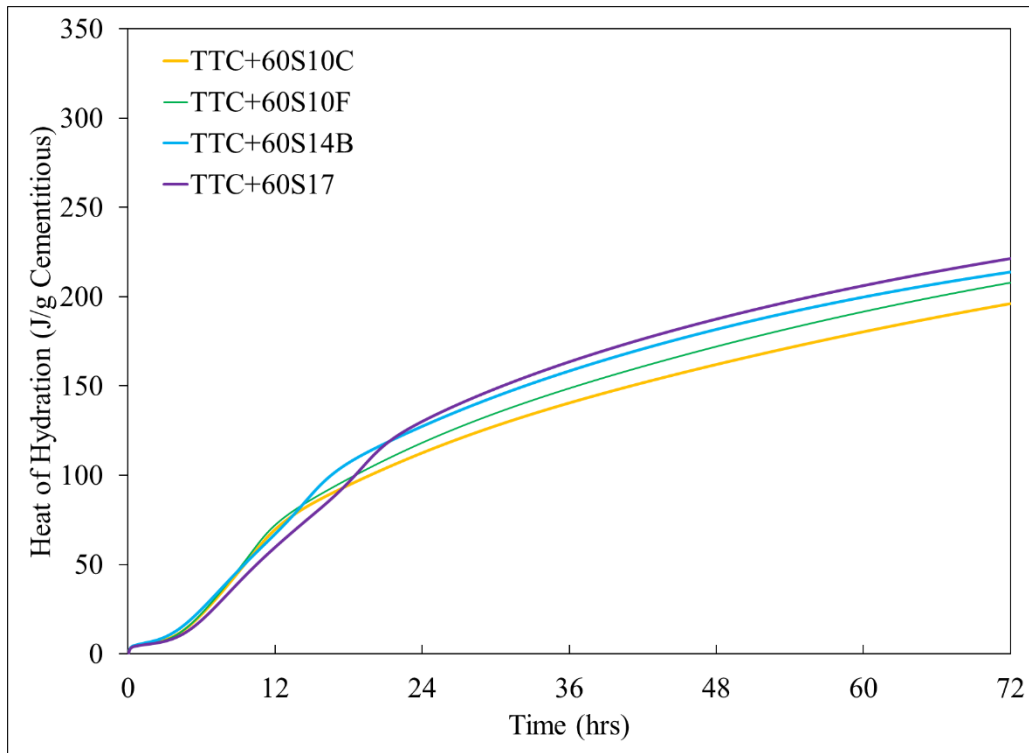
Figure 3-8: Total heat evolution of cement TTC with slags

Figure 3-9 and Figure 3-10 illustrate the measured heat flow and the total heat of slags blended with cement TIL, a Type IL cement which contains approximately 10% limestone content. Similar to Type I and Type II cements, the highest cumulative heat at three days was observed in the blend with slag S17, indicating the effect of slag alumina content on heat generation. However, heats of hydration of slag-cement TIL blends appeared to be slightly lower, due to the reduced clinker fraction in the cement. Moreover, it is noteworthy that the aluminate peak of the S10F blend was suppressed when blended with cement TIL, unlike with other cements, likely due to the high amount of calcite present in the system. The behavior of other slag blends appeared similar to those with cement TTC, but a slight shift in the peaks to the left can be observed, indicating a faster initial reaction. This can be due to the limestone effect on nucleation sites [29].
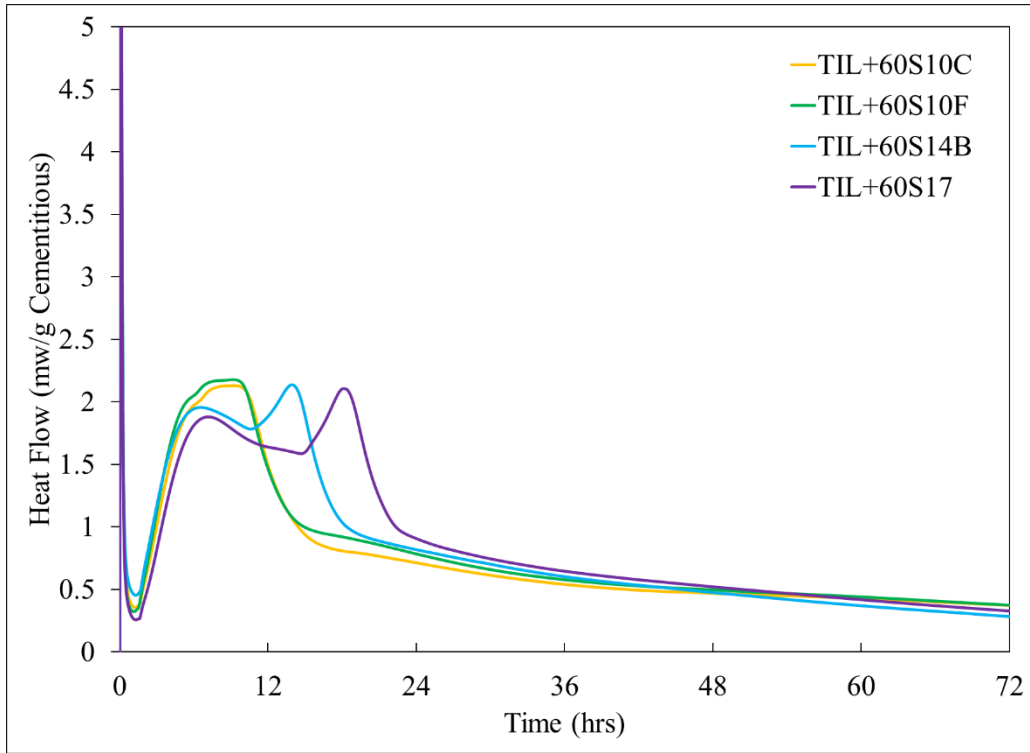
Figure 3-9: Heat flow of cement TIL with multiple slags
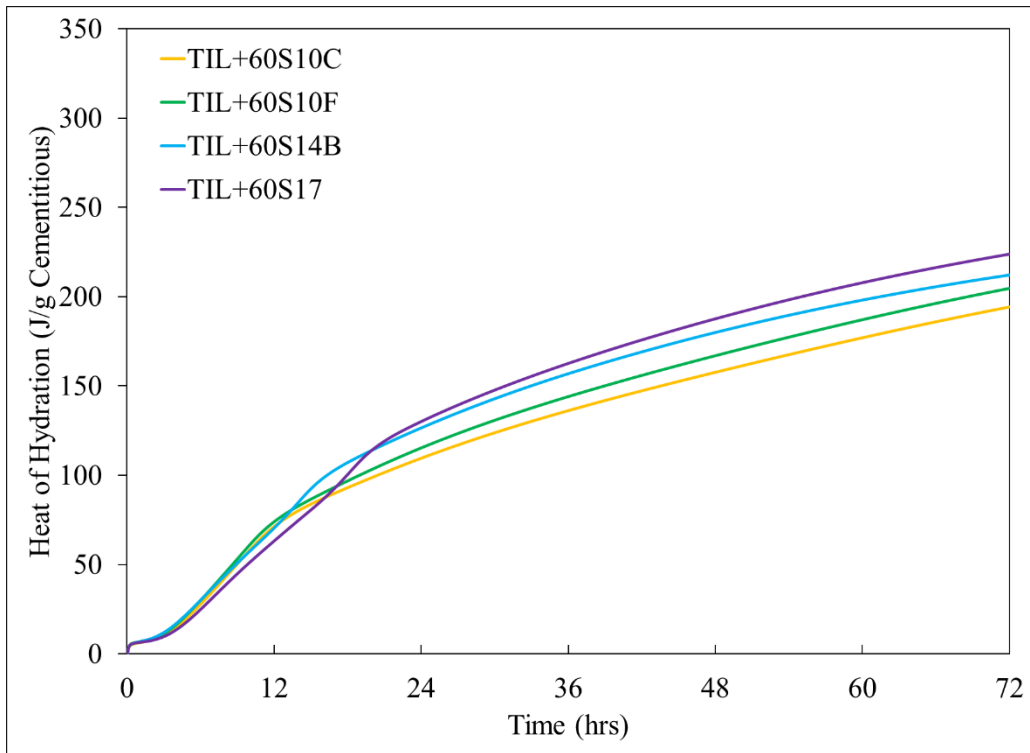
Figure 3-10: Total heat evolution of cement TIL with slags

64

The measured heat flow and total heat evolutions of cement THIL (Type IL with approximately 14% limestone) blended with slags are illustrated in Figure 3-11 and Figure 3-12, respectively. Only the slags S10C, S14B and S17 were studied here. Both heat flow and total heat trends were similar to those of slags blended with cement TIL. However, the heat of hydration of the cement-slag blends are lower due to reduced clinker fraction.
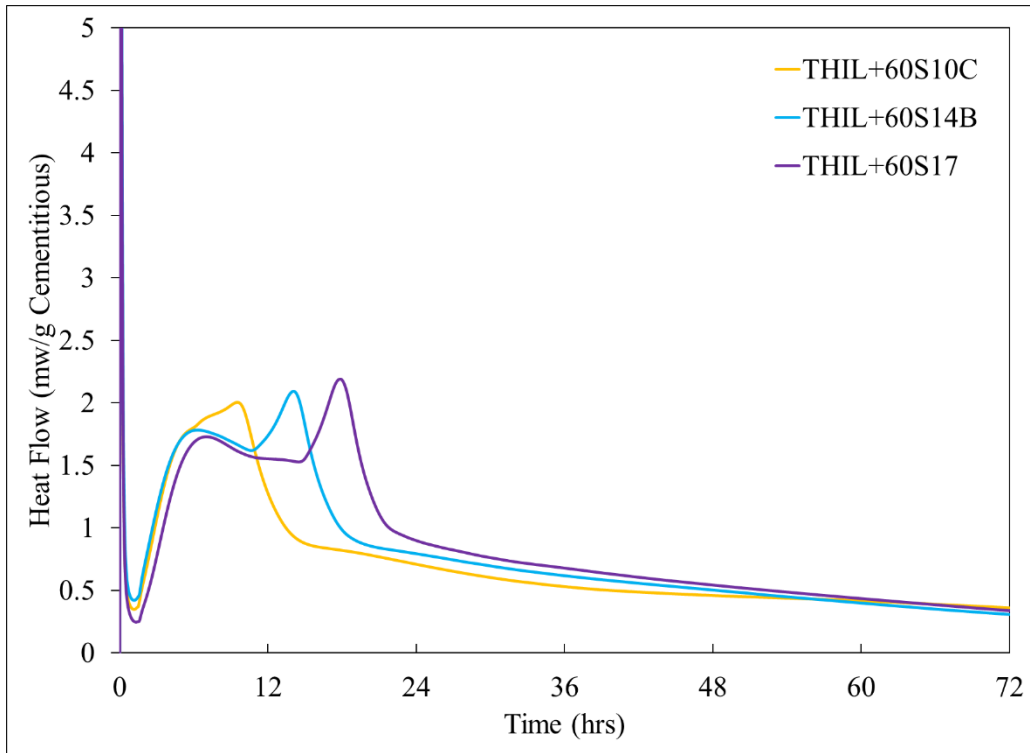
Figure 3-11: Heat flow of cement THIL with slags
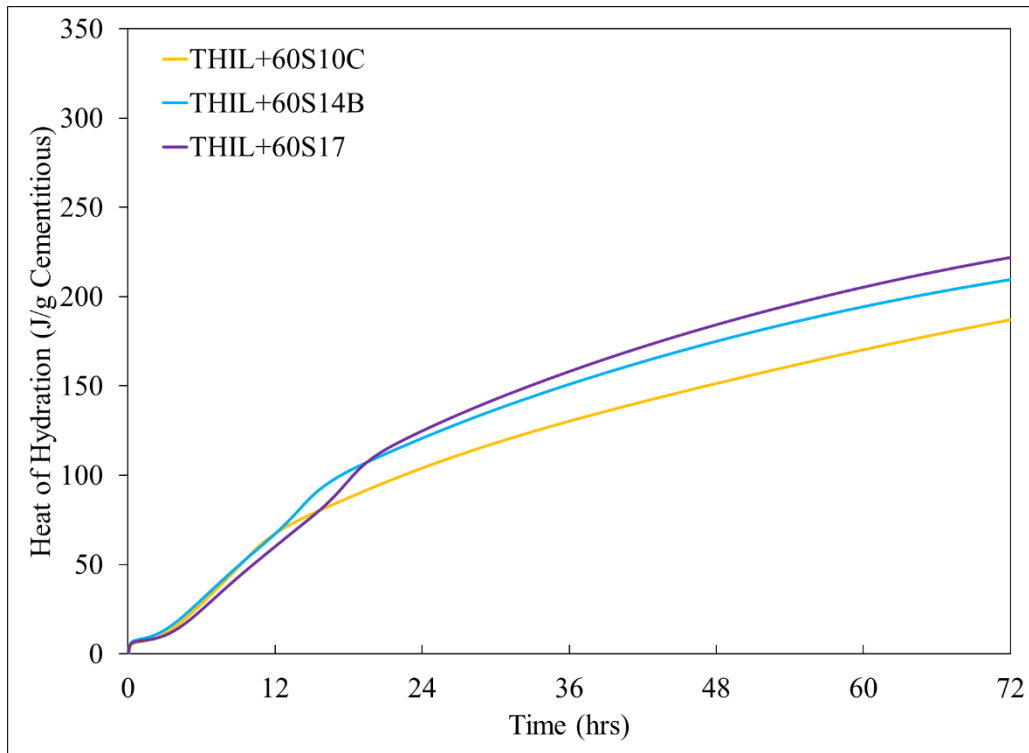
Figure 3-12: Total heat evolution of cement THIL with slags

As it is apparent from Figures Figure 3-3 through Figure 3-12, varying slag characteristics clearly affected the hydration kinetics of slag-cement blends. Increasing slag alumina contents resulted in increasing heats of hydration at the same age. In addition to the slag alumina content, slag fineness affected its reactivity; the finer the slag, the more reactive it was. On the other hand, when the same slag was blended with different cement sources, the effect on hydration kinetics was significant. Obviously, the heats of hydration at all ages varied with different cement types as can be seen from Table 3-5. The highest hydration heat can be observed when the slags were blended with cement BB which is a Type I cement due to its higher C_3A content. When the slags were combined with Type IL cements such as cement TIL and THIL, hydration heat was the lowest. This can be attributed to a reduced clinker factor in cement due to the dilution effect in the presence of limestone, and potentially poor sulfate balance. Expectedly, the heat of hydration of slags blended with Type II(MH) cements were in between those of Type I and Type IL cements, due to their moderate C_3A levels. Although, a faster hydration could be observed in the heat flow curves of cement C blends (Figure 3-5), heat of hydration values were still slightly lower than those of cement BB blends.

66

Table 3-5: Heat of hydration of as-received slag-cement blends at 1, 2, and 3 days

Slag	Cement	Heat of hydration (J/g cementitious)		
		1 day	2 days	3 days
S8	BB (Type I)	122	164	191
S10C	BB (Type I)	124	178	215
	C (Type I (Ha)	118	171	205
	TTC (Type II (MH))	113	162	197
	TIL (Type IL)	109	157	193
	THIL (Type IL)	104	152	187
S10F	BB (Type I)	128	185	224
	TTC (Type II (MH))	119	173	209
	TIL (Type IL)	115	168	205
S14B	BB (Type I)	132	193	226
	C (Type I (Ha)	127	186	217
	TTC (Type II (MH))	128	182	215
	TIL (Type IL)	127	180	212
	THIL (Type IL)	121	176	210
S17	BB (Type I)	126	192	230
	C (Type I (Ha)	124	192	228
	TTC (Type II (MH))	131	188	222
	TIL (Type IL)	130	188	224
	THIL (Type IL)	125	185	222

3.3.2   Phase Assemblage of As-Received Paste Systems

3.3.2.1 X-Ray Diffraction Analysis

The crystalline phases and amorphous content of the as-received cement pastes at 3 days are shown in Table 3-6. Amorphous content includes the C-S-H phase, which is the highest in cement TTC due to its higher C_3S content. The aluminates in IL cements completely reacted during the first 3 days, likely due to both physical and chemical effects of limestone. Monosulfoaluminate was only observed in cement BB due to its higher C_3A content. Although cement C had C_3A content similar to cement BB, hemicarboaluminate was observed instead of monosulfoaluminate because of the calcite content present in cement C. Both cement BB and C paste systems showed substantially higher amounts of ettringite than the rest of the cement pastes because of their higher C_3A contents along with higher sulfate contents. Among these, the highest ettringite content was

observed in cement C, which may have been affected by the high pH of the system due to its high alkali content. As reported by Stark and Bollmann [31], Na_2O_{eq} levels between 0.8% and 1.2% may lead to pH values between 13.5 and 14 during initial hydration which is desirable for ettringite stability. If the pH of the system is sustained, ettringite will remain stable. THIL showed the highest amount of hemicarboaluminate at 3 days, likely because it had the highest calcite content. Consequently, less C_3A may have been available for ettringite formation. Lower hemicarboaluminate content in cement TIL was somewhat surprising, since its calcite content is second only to that of cement THIL.

Table 3-6: Phase quantification of control cement pastes at 3 days by XRD

Cements / Phase (wt.%)	BB I	C I(Ha)	TTC II(MH)	TIL IL(10)	THIL IL(14)
Alite	5.5	4.2	4.2	3.3	2.5
Belite	6.8	3.7	4.1	3.9	5.3
Aluminate	0.7	0.6	0.2	0.0	0.0
Ferrite	0.1	0.8	2.8	2.4	2.0
Calcite	0.0	0.6	0.7	2.9	3.3
Quartz	0.0	0.0	0.0	0.3	0.6
Portlandite	10.0	8.7	7.0	8.1	7.4
Periclase	0.0	0.3	0.0	0.0	0.0
Dolomite	0.0	0.7	0.0	0.0	0.0
Ettringite	5.9	6.7	3.3	4.3	1.8
Monosulfate	0.3	0.0	0.0	0.0	0.0
Hemicarboaluminate	0.0	0.6	0.1	0.3	0.9
Amorphous content (AC)	70.7	73.3	77.5	74.6	76.2

In terms of the slag-blended cementitious systems, inclusion of slags affected the phase assemblage as can be seen from Table 3-7 and Table 3-8. Amorphous content in blends refers to the sum of C-S-H, C-A-S-H, and unhydrated slag. Aluminate from the clinker had completely hydrated by three days in all the systems except BB+60S14B and BB+60S17, where a small amount was still remaining. In terms of alumina bearing phases formed, monosulfoaluminate was only observed in blends with Type I cements (cements BB and C) owing to their high C_3A contents and also in TTC+60S17 but in low amounts. Ettringite can be observed in all the systems and hemicarboaluminate can be observed in all the systems except one (BB + 60S17) at three days. In slag blends with Type I cement, ettringite decreased and monosulfoaluminate increased with increasing the slag alumina contents except for the systems with slags S14B an S17, which were

already sulfated by the supplier. Higher monosulfoaluminate contents are not always desirable as it makes the system susceptible for external sulfate attack; therefore, a proper sulfate balance is required for high-alumina slags to overcome this. Evidently, the higher sulfate contents in high-alumina slags S14B and S17 contributed to the formation of ettringite. S14 showed higher content of hemicarboaluminate with cements BB and C because of the added calcite to the slag. For the other cements (TTC, TIL, THIL), the hemicarboaluminate level formed with S14 blends was not significantly higher than the other slags because those cements likely had sufficient calcite content to not limit the hemicarboaluminate formation at three days. In terms of cements, the ettringite contents formed in cement TTC blends were slightly lower than those of Type I cement blends, due to the moderate C_3A content in cement TTC (Type II (MH)). This also indicates the significance of the sulfate-to-aluminate ratio on the hydration products phase assemblage.

On the other hand, in the presence of calcite, more hemicarboaluminate was formed with increasing the slag alumina contents. Additionally, hemicarboaluminate contents increased with increasing calcite contents in the cements. The calcite contents in cements BB, C, TTC, TIL and THIL were 0.2%, 1.8%, 2.8%, 8.8% and 11.4%, respectively. Calcite reacts with the available alumina and forms hemicarboaluminate [7], which is known to have a stabilizing effect on ettringite lowering its potential conversion to monosulfoaluminates. The results also indicate that hemicarboaluminate formation was affected by the presence of sulfate and calcite in slags as well. The calcite present in S14B helped increase the hemicarboaluminate formed. On the other hand, the blends with the producer-sulfated slag S17 and low-calcite cements indicated substantially lower hemicarboaluminate contents than when S14B was used. The calcite and sulfate compete for alumina present in the system to form ettringite or hemicarboaluminate [8]. Formation of hemicarboaluminate stabilizes ettringite and subsequently limits the formation of monosulfoaluminate, which is desirable for sulfate durability.

In addition to ettringite and AFm phases (hemicarboaluminate and monosulfoaluminate), slag hydration formed small amounts of hydrotalcite, which can be observed in most of the blends with slags S10C, S10F, and S17. The systems with slag S14B, except TTC+60S14B, did not show any hydrotalcite due to the lower MgO content of slag S14B compared to the other slags studied [8].

Table 3-7: Phase quantification of as-received cements BB and C with slags at three days by

XRD

Mix ID Phase (wt.%)	BB+ 60S8	BB+ 60S10C	BB+ 60S10F	BB+ 60S14B	BB+ 60S17	C+ 60S10C	C+ 60S14B	C+ 60S17
Alite	0.4	0.5	0.4	0.9	0.8	0.7	1	0.7
Belite	2.7	2.7	2.8	2.7	2.6	1.8	1.3	1.3
Aluminate	0	0	0	0.1	0.1	0	0	0
Ferrite	0	0	0	0	0	0.1	0.2	0.2
Calcite	0.4	1.1	1.1	1.2	1.3	1.2	1.7	1.1
Quartz	0	0	0	0	0	0.1	0	0
Portlandite	1.9	1.3	1.4	1.3	1.2	1.2	1.2	1
Periclase	0	0	0	0	0	0.2	0.2	0.2
Dolomite	0	0	0	0	0	0.2	0.2	0.3
Melilite	0.1	0.1	0.1	0	0.3	0.1	0	0.3
Merwinite	0	0.1	0.1	0	0	0.1	0	0
Ettringite	2.3	1.7	1.8	4	3.3	2	4.2	3.8
Monosulfate	0.8	0.8	0.8	0.4	0.7	0.3	0	0.6
Hemicarboaluminate	0.2	0.1	0.3	1.1	0	0.5	1.5	0.3
Hydrotalcite	0	0.1	0.2	0	0.2	0	0	0.3
Amorphous content (AC)	91.1	91.4	90.9	88.3	89.6	91.5	88.5	90

Table 3-8: Phase quantification of as-received cements TTC, TIL, and THIL with slags at three days by XRD

Mix ID Phase (wt.%)	TTC+ 60S10C	TTC+ 60S10F	TTC+ 60S14B	TTC+ 60S17	TIL+ 60S10C	TIL+ 60S10F	TIL+ 60S14B	TIL+ 60S17	THIL+ 60S10C	THIL+ 60S14B	THIL+ 60S17
Alite	0.3	0.5	0.3	0.7	0.2	0.3	0.2	0.3	0.1	0.2	0.2
Belite	2.1	2.2	2.5	2	1.9	2.1	2	1.3	2	1.8	1.6
Aluminate	0	0	0	0	0	0	0	0	0	0	0
Ferrite	0.4	0.5	0.6	0.6	0.5	0.4	0.6	0.5	0.5	0.4	0.5
Calcite	1.5	0.5	1.5	1.3	2	2.3	2	1.7	2.5	2.7	2.3
Quartz	0.1	0	0.2	0.2	0.2	0.2	0.1	0.3	0.2	0.3	0.3
Portlandite	1.6	2.1	1.7	1.6	1.5	2.2	1.4	1.4	1.6	0.8	1
Periclase	0	0	0	0	0	0	0	0	0	0	0
Dolomite	0	0	0	0	0	0	0	0	0	0	0
Melilite	0.1	0.1	0	0.3	0.1	0	0	0.3	0.1	0	0.3
Merwinite	0.2	0.2	0	0	0.1	0.1	0	0	0.1	0	0
Ettringite	1.9	1.8	3.6	3.7	1.6	2.1	3.1	3.6	1.4	2.7	4.1
Monosulfate	0	0	0	0.1	0	0	0	0	0	0	0
Hemicarboaluminate	1.2	1.3	1.9	0.8	1.2	1.4	1.4	1.4	1.4	1.3	1.7
Hydrotalcite	0.1	0.2	0.1	0.2	0.1	0	0	0.2	0.1	0	0.2
AC	90.5	90.6	87.6	88.5	90.6	88.9	89.2	89.2	90	89.7	87.8

3.3.2.2 Thermodynamic Modeling

Figure 3-13 illustrates the predicted phase assemblage of as-received cements at three days using GEMS. The DOH of the cements BB, C, TTC, TIL and THIL were determined as 80.5%, 83.8%, 82.2%, 81.0% and 79.7% respectively. Ettringite was predicted in all systems. Monosulfoaluminate was only predicted in cement BB system similar to the findings from QXRD. However, a small amount of hemicarboaluminate was also predicted in the same system, which was not detected by XRD, possibly due to its low amounts. In both cement C and TTC systems, monocarboaluminate was predicted, not hemicarboaluminate as detected by QXRD. As stated by several researchers [7], [32], monocarboaluminate was calculated to be the more thermodynamically stable phase in the presence of calcite, while hemicarboaluminate was detected calculated only if no calcite was present (i.e. in hydrated cements which contain less than 2–3 wt% of calcite). But in contrast to the thermodynamic calculations, hemicarboaluminate was detected in early reactions, which later transformed to monocarboaluminate. Zajac et al. [32] stated that "It could be related either to the slow reaction kinetics of limestone at high pH values or to a faster formation kinetic of hemicarbonate when compared to the kinetics of monocarbonate formation". Furthermore, in contrast to QXRD analysis, no carboaluminate phases were predicted in cement TIL and THIL systems as well. This is unlikely as these two cements consist of higher calcite contents. Instead, a notable increase in the siliceous hydrogarnet phase can be observed. It is possible that the substantially higher amounts of ferrite present in both these cements resulted in predicting more siliceous hydrogarnet quantities instead of forming carboaluminate phases [33]. This behavior can be further explained by the unhydrated calcite observed in these two cements without reacting with the available alumina.
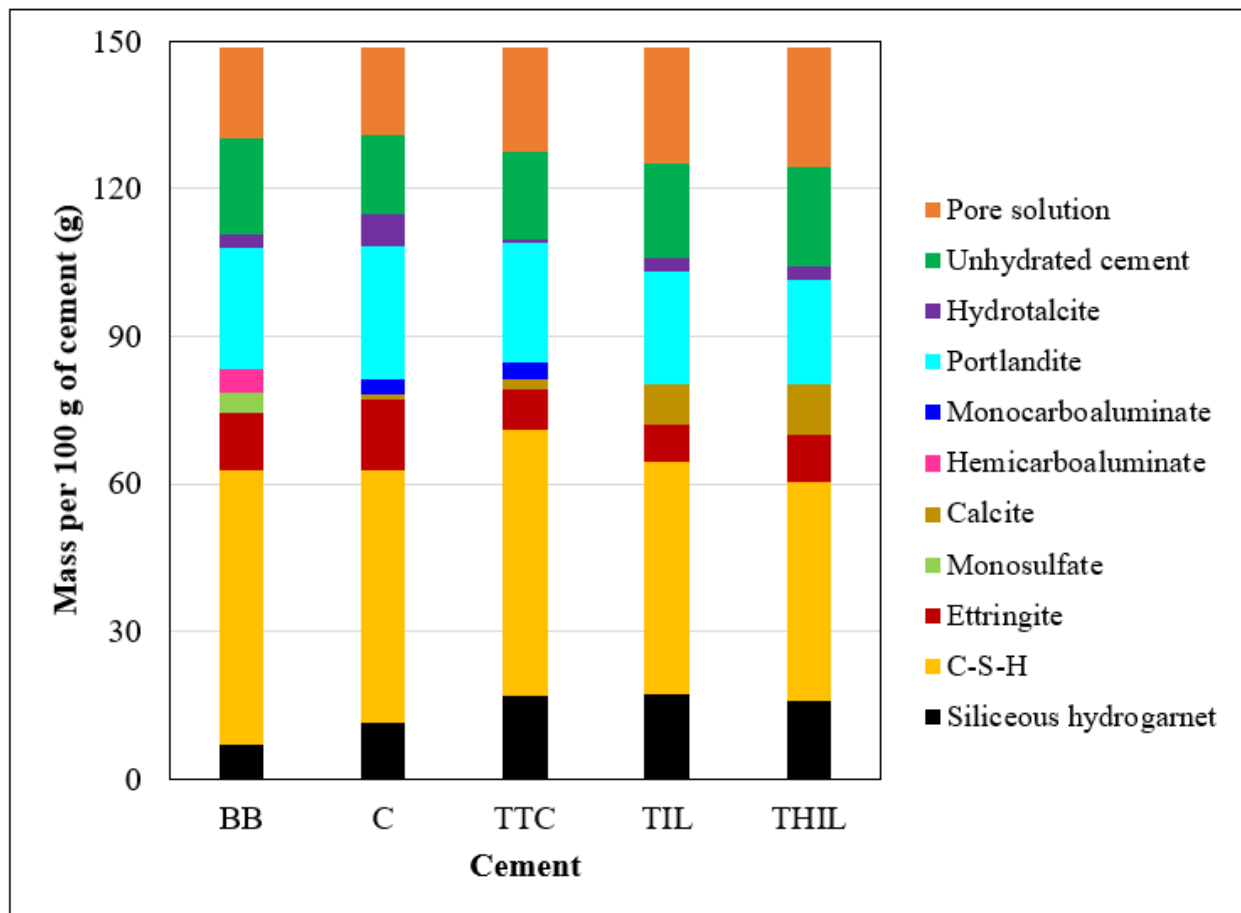
Figure 3-13: Phase assemblage prediction of as-received cement systems at three days using GEMS

Phase assemblage prediction of cements BB, C, TTC, and TIL blended with slags S8 and S17 are illustrated from Figure 3-14 through Figure 3-17. Slags with the highest and the lowest alumina contents were considered for better understanding of the changes in phase formation when blended with different cement types. As slag DOH is unknown, it was varied from 10%-40% keeping the cement DOH constant. When cement BB was blended with slag S8 and S17, phases such as C-(A)-S-H, ettringite, hemicarboaluminate, portlandite, hydrotalcite and siliceous hydrogarnet were formed in both systems (Figure 3-14). In the systems with slag S17, substantially higher monosulfoaluminate amounts were predicted at any DOH of slag, but only traces of monosulfoaluminate amounts were predicted in the blend with slag S8. QXRD analysis also detected a small amount of monosulfoaluminate in the BB+60S8 system. In the BB+S17 system, monosulfoaluminate content increased with increasing slag DOH and ettringite content gradually

disappeared as a result. Hemicarboaluminate was predicted for both systems and no traces of monocarboaluminate can be seen. As previously explained, monocarboaluminate is more thermodynamically stable if excess calcite is present in the system, unless hemicarboaluminate is predicted [32]. Cement BB contained the lowest calcite content (0.2%) among all cements studied here, hence a substantial amount of hemicarboaluminate was predicted in its blends. As it appears, the change in slag composition had the most significant effect on the alumina-bearing phases. Additionally, in both systems, portlandite content decreased and hydrotalcite content increased with slag DOH. Unlike in pure hydrotalcite (Mg/Al = 3), hydrotalcite formed in slag blends have a Mg/Al ratio of approximately 2 [7]. However, only traces of hydrotalcite contents were detected by QXRD.
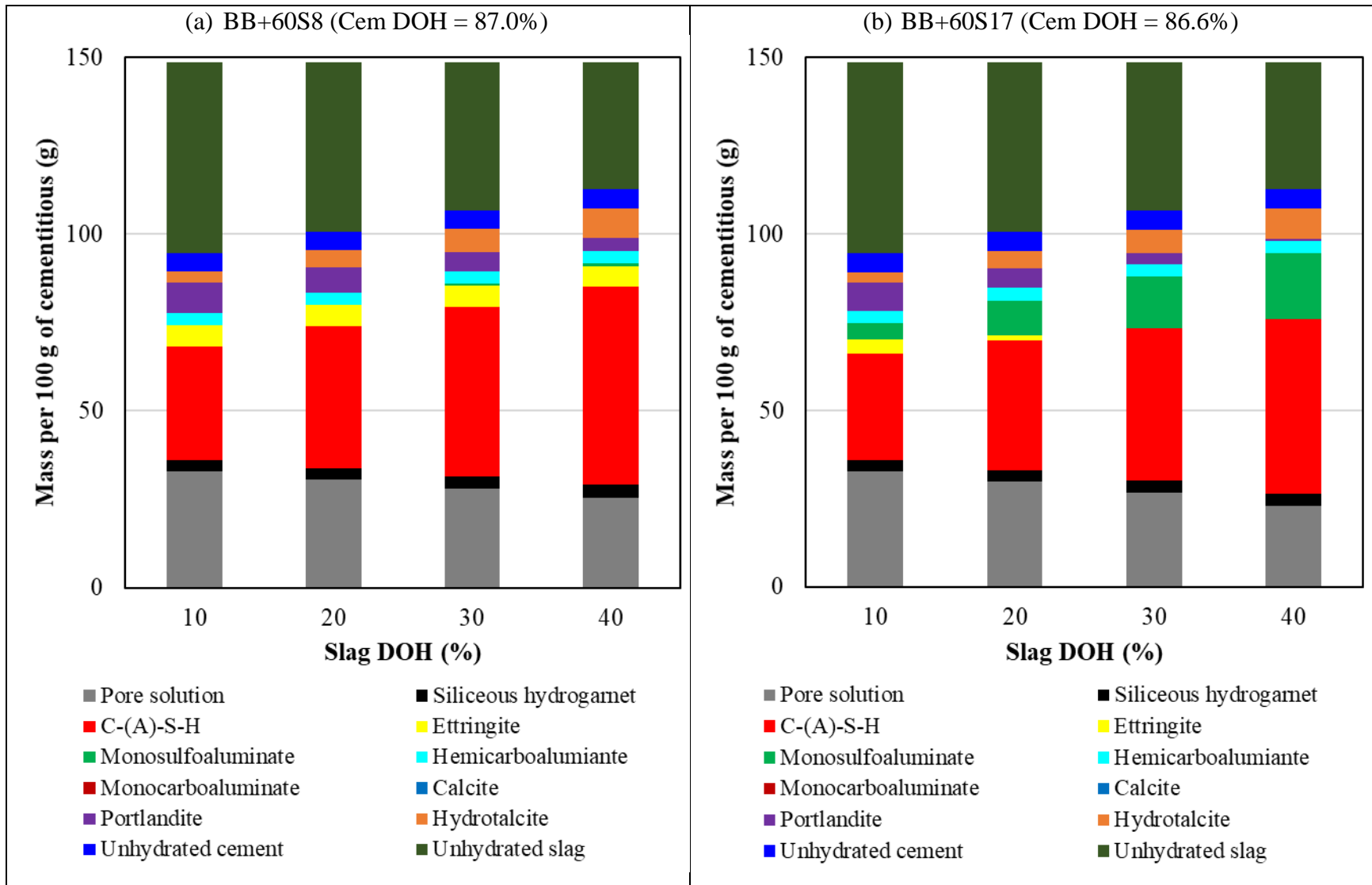
Figure 3-14: Phase assemblage prediction at three days using GEMS (a) BB+60S8 (b) BB+60S17

When S17 was blended with cement C, similar phases were formed, but significant differences can be observed in the quantities of the alumina-bearing phases (Figure 3-15). Ettringite was formed in the system at any slag DOH. However, ettringite content gradually decreased in C+60S17 when monosulfoaluminate started forming around 30% slag DOH. Ettringite contents were notably different in systems blended with slag S17 with more ettringite predicted in C+60S17 blend. Unlike in cement BB system, monocarboaluminate was predicted with cement C, which has a slightly higher calcite content (1.8%). However, as it appears, the calcite content in cement C was not sufficient in C+60S17 system to maintain the thermodynamic stability of monocarboaluminate, hence hemicarboaluminate was predicted at higher slag DOH due to the higher amount of alumina dissolved in the system. Evidently, the difference in calcite contents in the two cements BB and C had substantial effect on phase formation. On a different note, Cement C has a slightly higher alkali content compared to BB (1.05% vs. 0.38% Na_2O_{eq}). As stated in the literature [31], alkali contents affect the pH of the pore solution and consequently affect the stability of ettringite. Ettringite is more stable when the pH of the system is close to 13. Typically, alkali contents in the range between 0.8-1.2% Na_2O_{eq} in cement lead to pH values between 13.5 and 14 during initial hydration with low w/c ratios. The higher amount of ettringite predicted in C+60S17 compared to BB+60S17 can possibly be due to the higher pH of the system due to its higher alkali content. It is also stated that when the pH value is above 13.6, ettringite is less stable and transforms into low-sulfate compounds when the hydration progresses, and consequently increases the sulfate concentration in the pore solution [31]. However, later on, if the pH is lowered ettringite will re-crystallize. Nevertheless, such behavior was not observed in the predicted results.
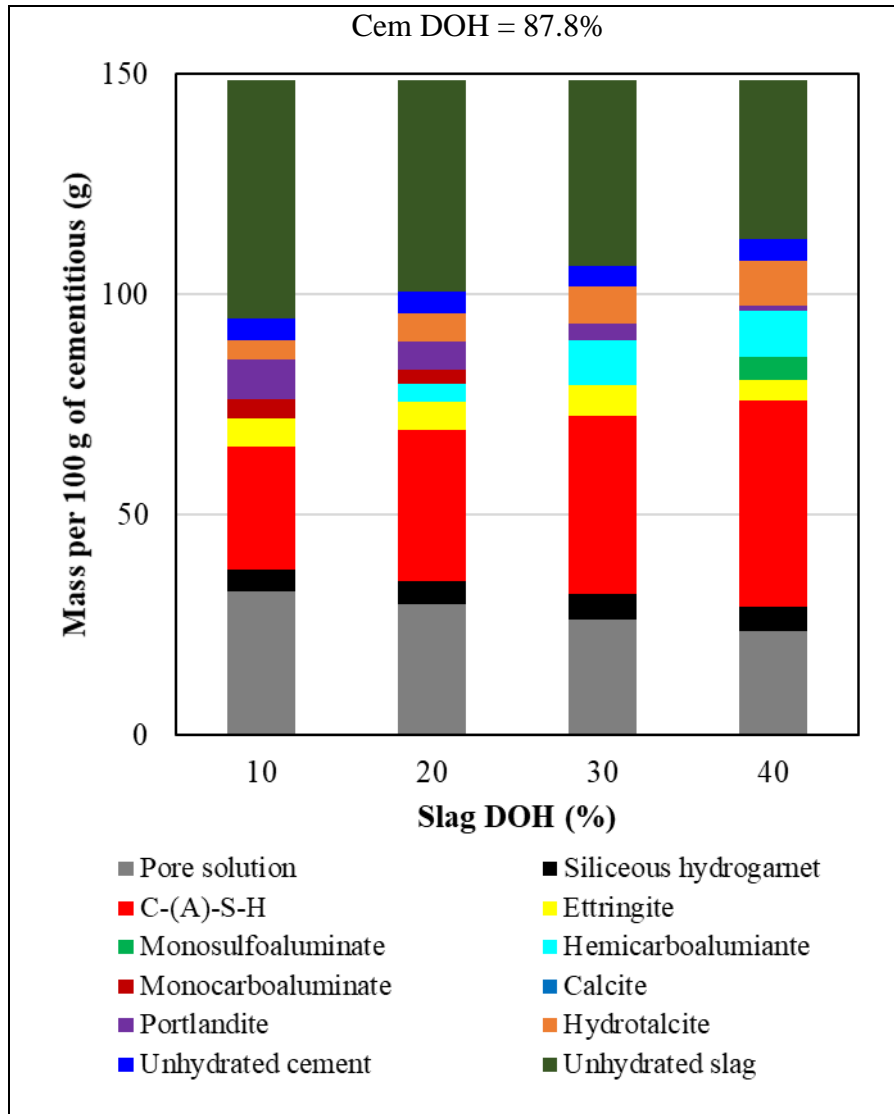
Figure 3-15: Phase assemblage prediction at three days using GEMS for C+60S17

Figure 3-16 illustrates the predicted phase assemblage of cement TTC blended with slag S17. It is noteworthy that cement TTC has a slightly higher calcite content of 2.8%. The phases formed were similar to those with cements BB and C but no monosulfoaluminate was observed in both the systems. However, XRD detected traces of monosulfoaluminate in TTC+60S17. While ettringite and monocarboaluminate were predicted in the system, at higher slag DOH, hemicarboaluminate was also predicted in TTC+60S17, due to the thermodynamic stability of carboaluminate phases in the presence of calcite. Although the ettringite content gradually increased with slag DOH, the increase in carboaluminate phases was significant as can be seen in TTC+60S17. Clearly, formation of carboaluminate phases stabilized ettringite.

77

However, predicted ettringite contents were lower than those of cement BB and C blends, which can be attributed to the lower C$_3$A content in cement TTC. Moreover, the increase in siliceous hydrogarnet phase is notable compared to that of cement BB and C blends, likely due to the considerably higher ferrite content in cement TTC. Additionally, the reduced portlandite content in TTC+60S17 can be attributed to the lower DOH of cement TTC at three days.
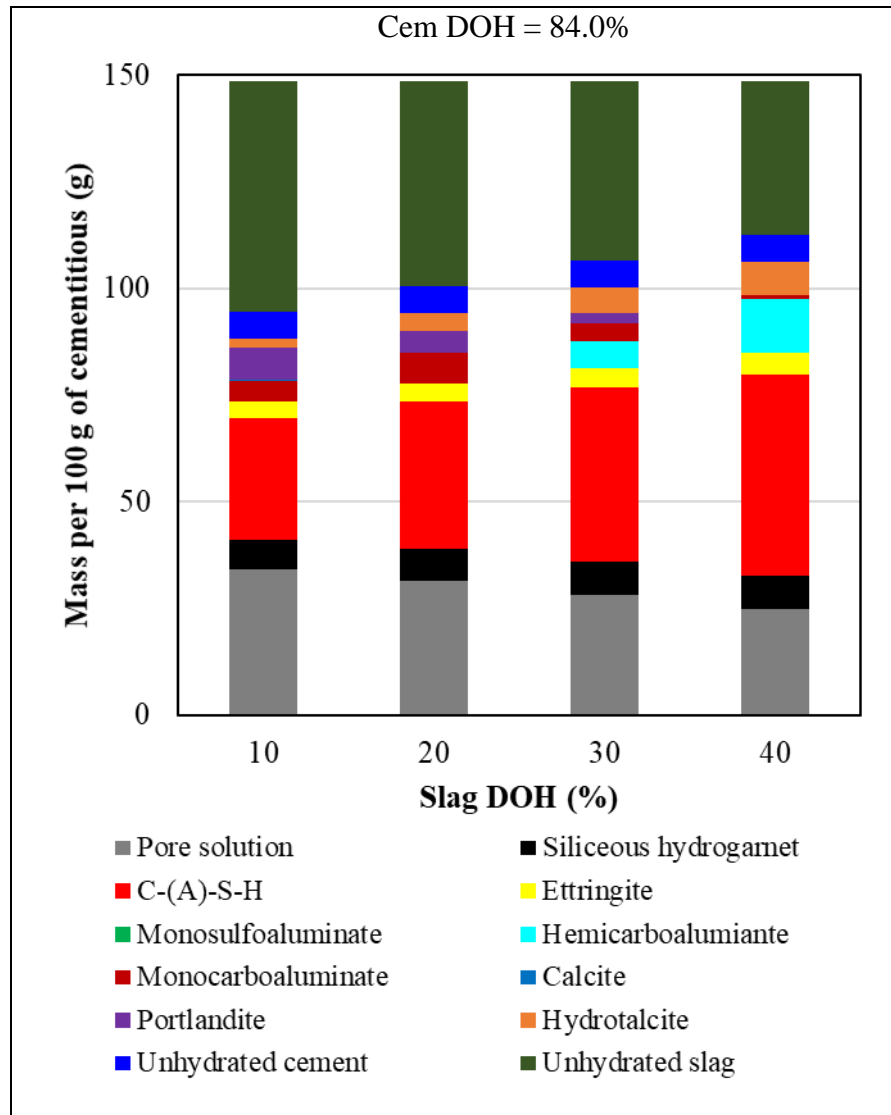
Figure 3-16: Phase assemblage prediction at three days using GEMS for TTC+60S17

Similar to XRD analysis, thermodynamic modeling of cement TIL blends did not predict monosulfoaluminate formation (Figure 3-17). Monocarboaluminate was predicted in the slag S17 blend. It is noteworthy that cement TIL has a higher calcite content (8.8%) and therefore a reduced clinker fraction. The lower C$_3$A content of the cement resulted in slightly lower ettringite

quantities. Moreover, similar to cement TTC blends, a notably higher amount of siliceous hydrogarnet was predicted which can be attributed to the higher ferrite content in cement TIL. It is likely the thermodynamic stability of carboaluminate phases is affected by the amount of alumina and iron in the system. Higher iron contents form more siliceous hydrogarnet making less alumina available to form carboaluminate phases [33].
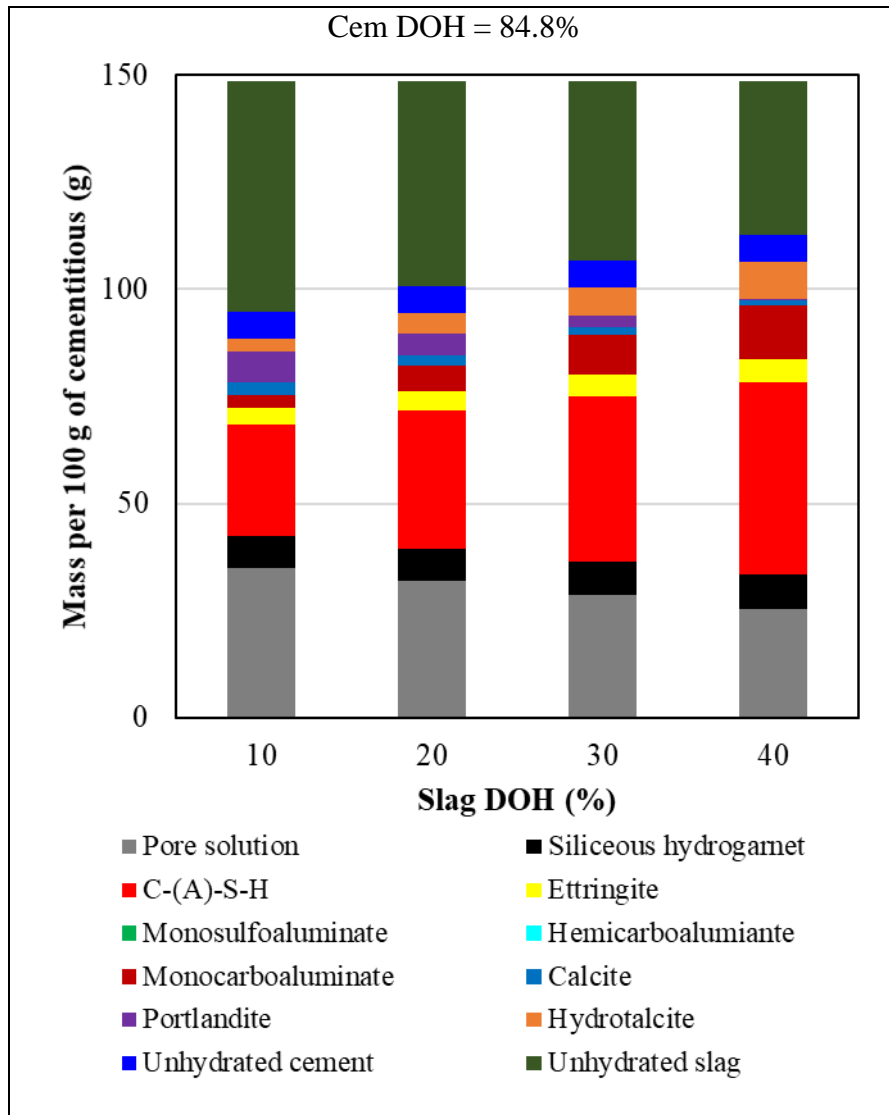
Figure 3-17: Phase assemblage prediction at three days using GEMS for TIL+60S17

According to thermodynamic modeling predictions, cement characteristics have significant effect on phases formed in cement-slag-blended systems. Changes in cement calcite content along with its aluminate content had substantial influence on the alumina-bearing phases formation. Moreover, the thermodynamic stability of the phases was affected by the amount of

ferrite, magnesia contents in the cements, as well as the slag DOH and its alumina and magnesia contents. Hence, Type I cements blended with high-alumina slag form high amounts of monosulfoaluminate which is not desirable for sulfate durability. This can be avoided, if low-alumina slags are used with Type I cements. However, sulfate addition may also increase ettringite stability. Additionally, use of Type II(MH) cements with slags could potentially reduce monosulfoaluminate formation and thereby make ettringite more stable. Furthermore, Type IL cements blended with slags of varying alumina levels is also desirable as it stabilizes ettringite by forming carboaluminate phases.

Figure 3-18 and Figure 3-19 show the phase assemblage prediction of slags blended with cements BB and TIL at slag DOH of 40%. Two Type I and Type IL cements were considered to observe the effect of calcite content on phase formation with different slag alumina contents. In cement BB blends, only traces of monosulfoaluminate were predicted with slag S8, but increasing slag alumina levels increased the formation of monosulfoaluminate. Ettringite were predicted in all the blends except in slag S14B and S17 systems which contradicts the XRD results. It is likely 40% slag DOH considered in the analysis is higher than in the actual system at three days and consequently predicted only monosulfoaluminate in these systems. Additionally, hemicarboaluminate was predicted in all systems. Portlandite content declined with increasing slag alumina content, likely consumed by slag hydration. While most of the systems predicted approximately similar hydrotalcite contents, BB+S14B showed a substantially lower amount of hydrotalcite that can be attributed to the lower MgO content of S14B. All other slags had similar MgO contents.

In terms of cement TIL systems (Figure 3-19), ettringite and monocarboaluminate were predicted in all the systems. Monocarboaluminate contents gradually increased with increasing slag alumina levels, while the calcite content declined. Moreover, the ettringite contents in TIL+60S14B and TIL+60S17 systems were slightly higher, due to the sulfate present in these two slags. Trends similar to that of cement BB blends can be seen with portlandite and hydrotalcite phases. Additionally, a substantial increase was predicted in the siliceous hydrogarnet content in all the systems, which can be attributed to considerably higher ferrite content in cement TIL, as stated before. Evidently, higher calcite contents in cements, stabilize ettringite formation and

reduce the formation of monosulfoaluminate when blended with any slag, which is desirable for sulfate durability.
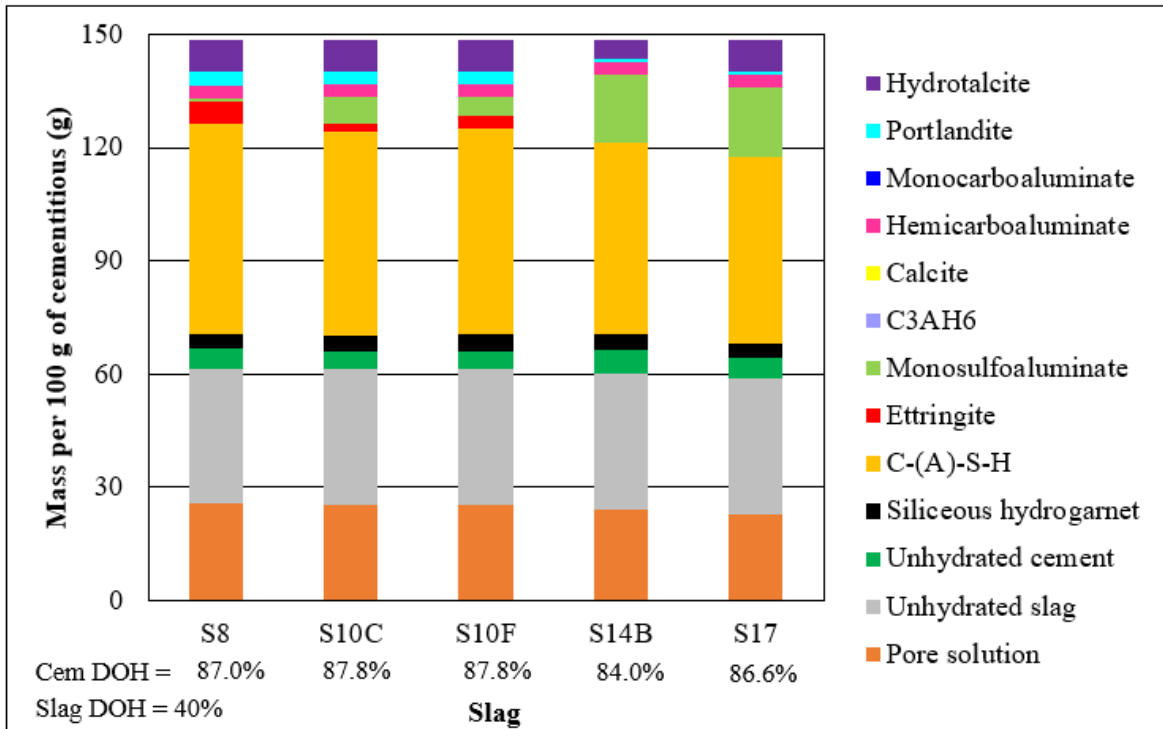
Figure 3-18: Phase assemblage prediction of cement BB-slag blends using GEMS
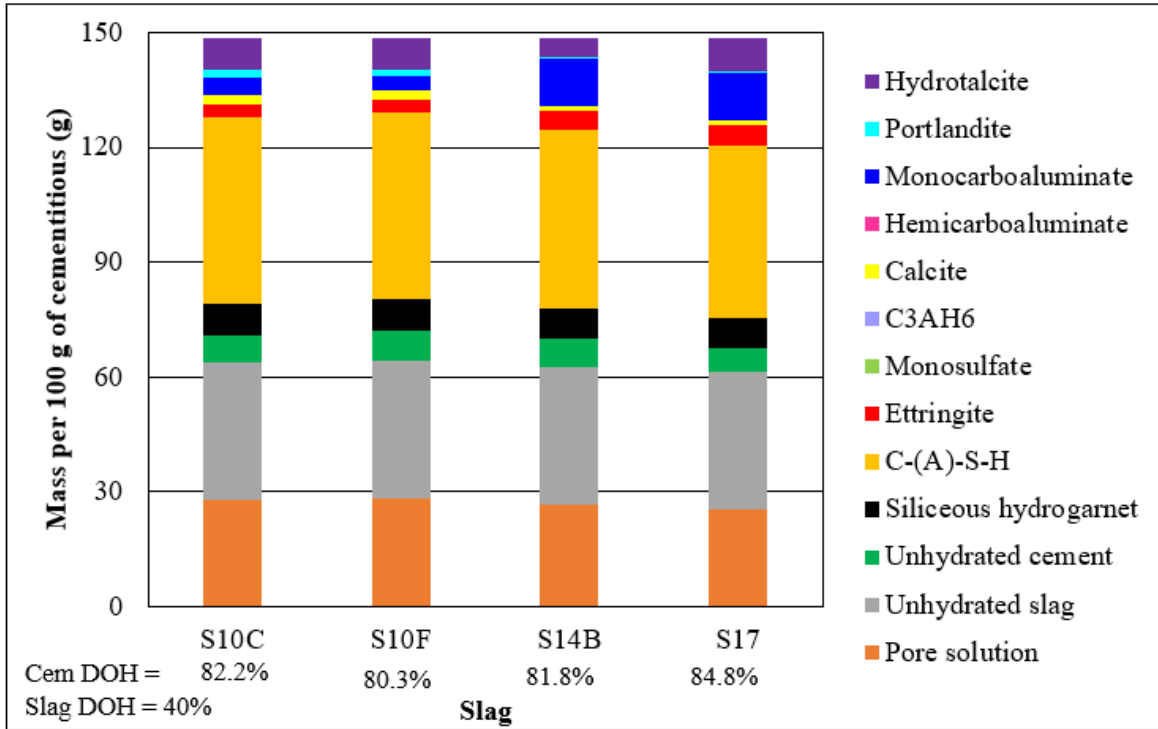
Figure 3-19: Phase assemblage prediction of cement TIL-slag blends using GEMS

3.3.3   Effect of Sulfate Additions on Cement-Slag Blended Systems

Based on the analysis of as-received cement and slag combinations, most of the cement-slag combinations appeared to be under-sulfated with the incorporation of slags. In other words, slags affect the sulfate demand in blended systems and therefore proper sulfate adjustment is required to maintain the desired performance in cementitious systems. Slags S14B and S17 are sulfated by the slag supplier to some extent and whether it is sufficient to achieve enhanced concrete durability performance remains unknown and needs further investigation. Nevertheless, phase assemblage and hydration kinetics are both affected by sulfate content present in the system [7], [8]. In addition, these will also impact the long-term durability of cementitious systems, such as strength development, sulfate durability and chloride ingress resistance. Therefore, a proper balance of total sulfate in blended systems and understanding its effect on hydration kinetics during sulfate adjustment are imperative. Thus, sulfate re-optimization of different cement and slag combinations will be discussed in subsequent sections.

3.3.3.1 Heat of Hydration Measurements and Optimum Sulfate Content Determination

The measured heat flow of cement-slag combinations with varying sulfate levels are presented in Appendix A. The total heat of each cement-slag combination with variable SO_3 levels at one, two and three days are demonstrated in Figures Figure 3-20 through Figure 3-26. The total SO_3 level in the system was varied until the aluminate peak was suppressed and delayed. The optimum sulfate content for any specified age was defined by the sulfate content that generated the highest total heat of hydration at that age [18]. While a similar behavior was observed in all the cement-slag blends, each system showed different optimum SO_3 content due to its unique chemical and physical characteristics. In general, the sulfate optimum increased with age, indicating a higher sulfate demand at later ages.

Figures Figure 3-20 through Figure 3-23 illustrate the differences in total heat at each age with cement BB-slag blends with variable SO_3 content. Clearly, increasing slag alumina contents resulted in an increased sulfate demand in the system.
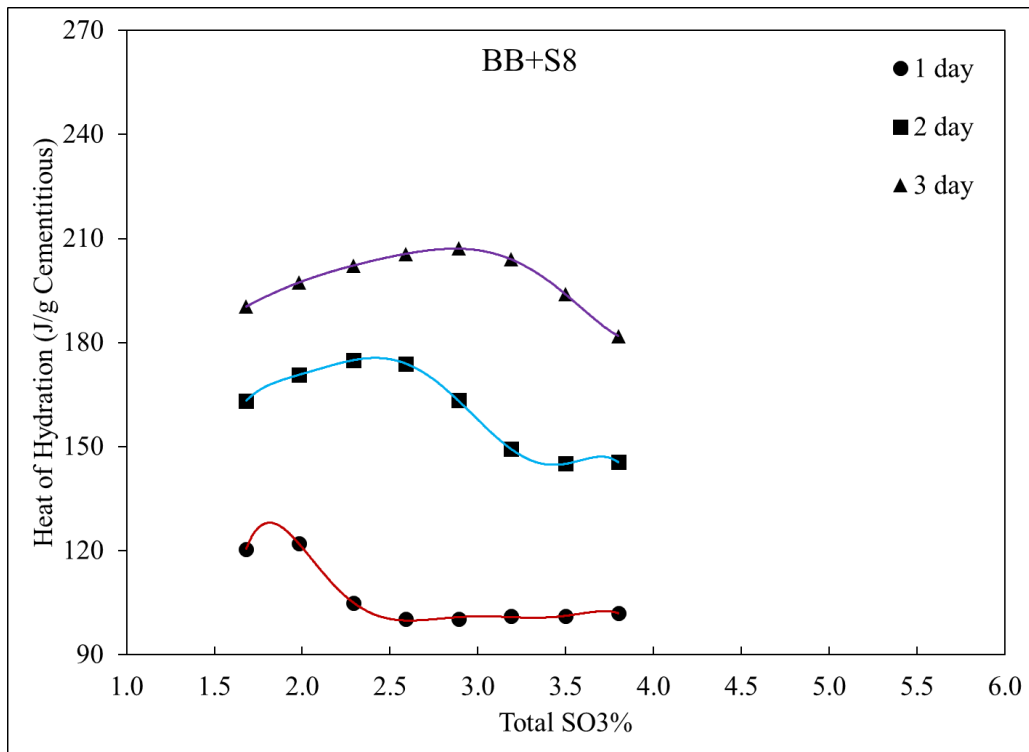
Figure 3-20: Total heat in cement BB and S8 with variable sulfate levels at different ages
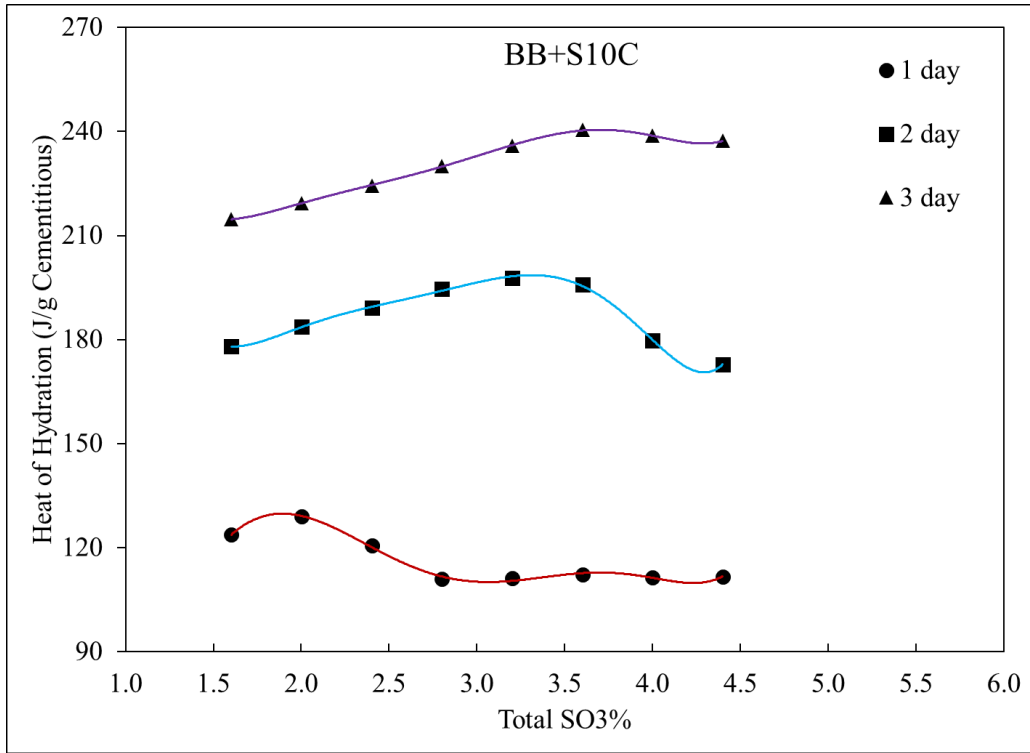
Figure 3-21: Total heat in cement BB and S10C with variable sulfate levels at different ages
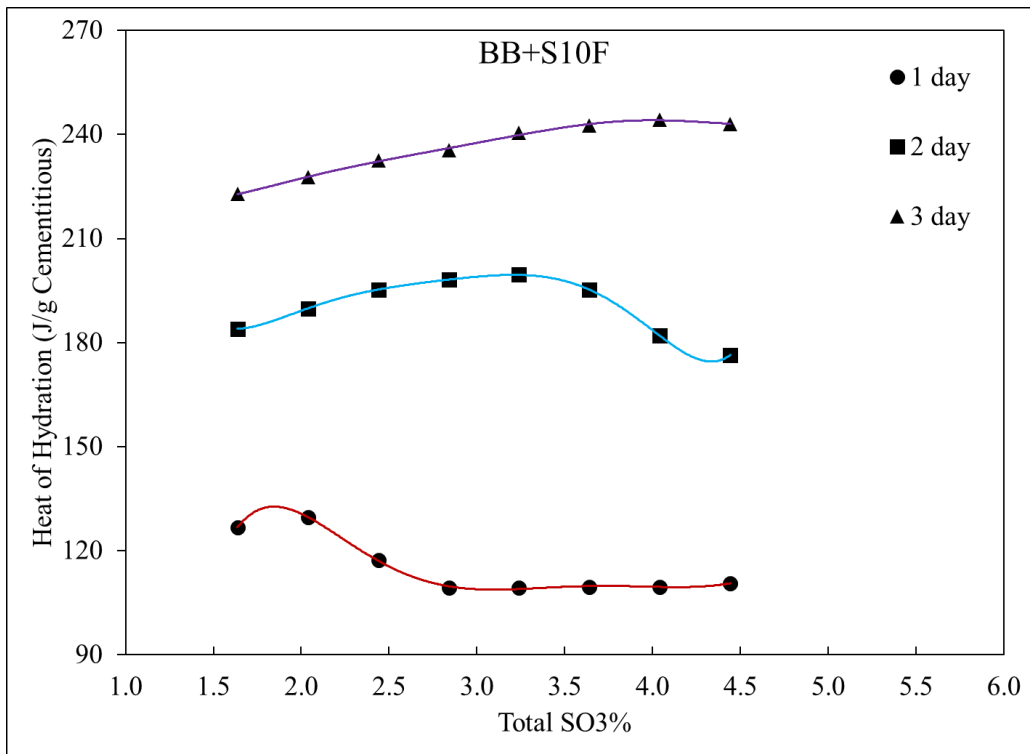
Figure 3-22: Total heat in cement BB and S10F with variable sulfate levels at different ages
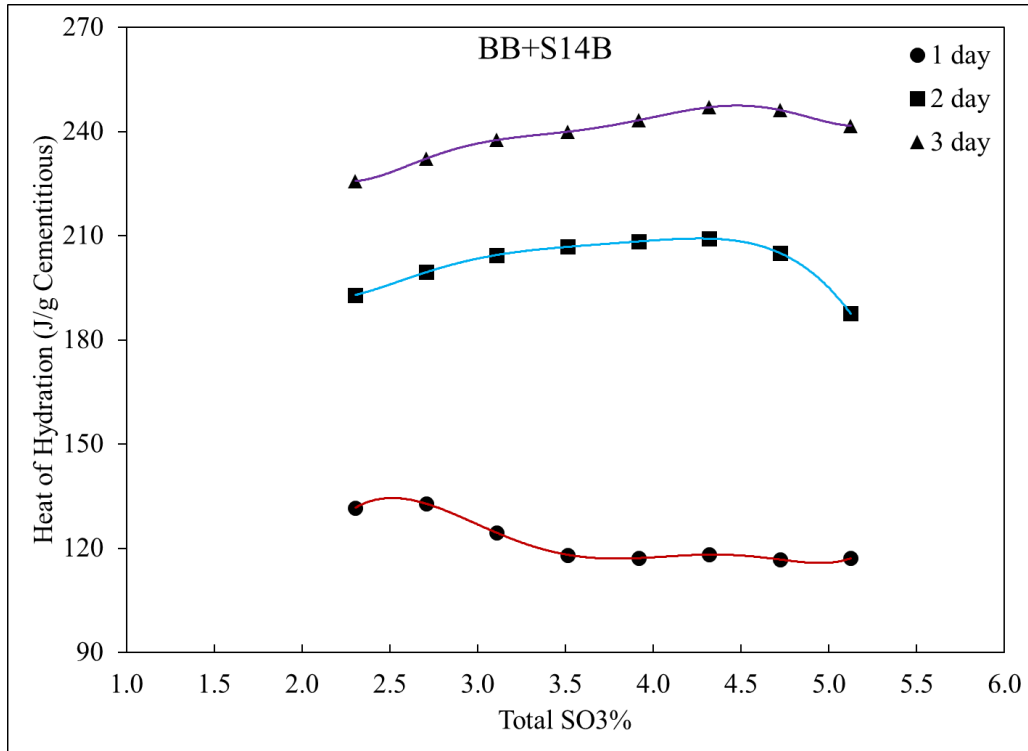
Figure 3-23: Total heat in cement BB and S14B with variable sulfate levels at different ages

Figure 3-24 shows the cement TTC- 60S10F slag blend with variable sulfate levels. The total SO$_3$ levels in the blend were slightly lower than that of Type I cement blends, which can be attributed to the lower C$_3$A and SO$_3$ contents of cement TTC, which is a Type II(MH) cement.
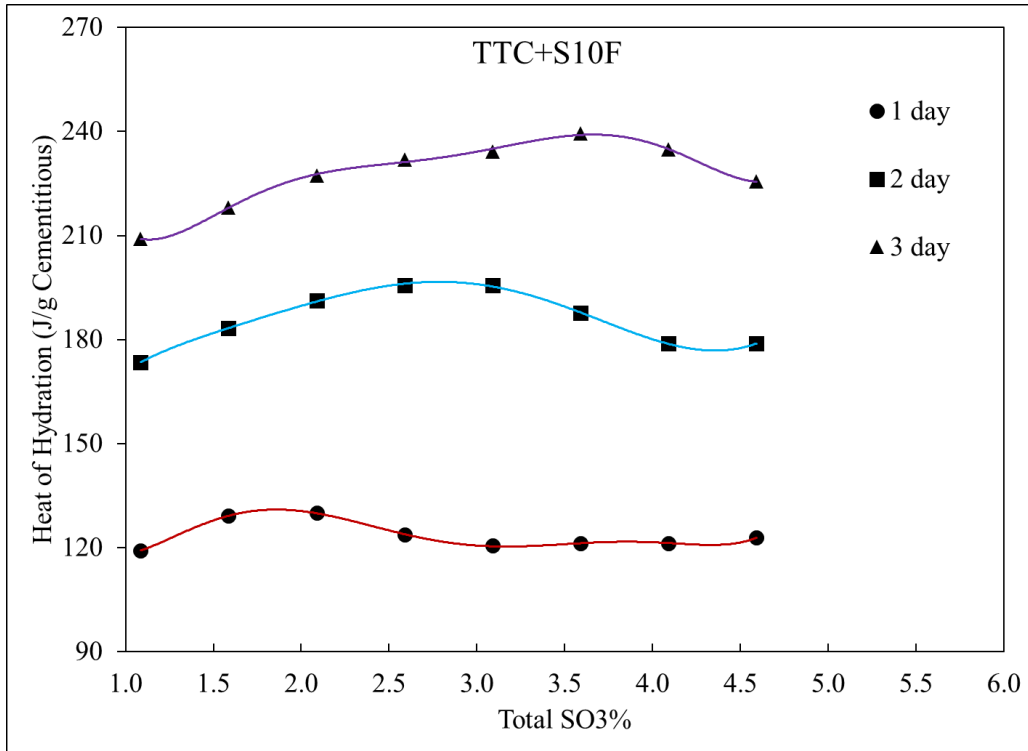
Figure 3-24: Total heat in cement TTC and S10F with variable sulfate levels at different ages

The total heat of cement TIL-slag-blended systems at variable sulfate levels are presented in Figure 3-25 and Figure 3-26. While the trends were similar to those of other cementitious systems, the total heat values obtained in slag-cement TIL blends were lower due to the reduced clinker fraction in cement TIL. Moreover, the total SO_3 levels investigated were slightly lower than those of Type I and Type II(MH) cement blends.
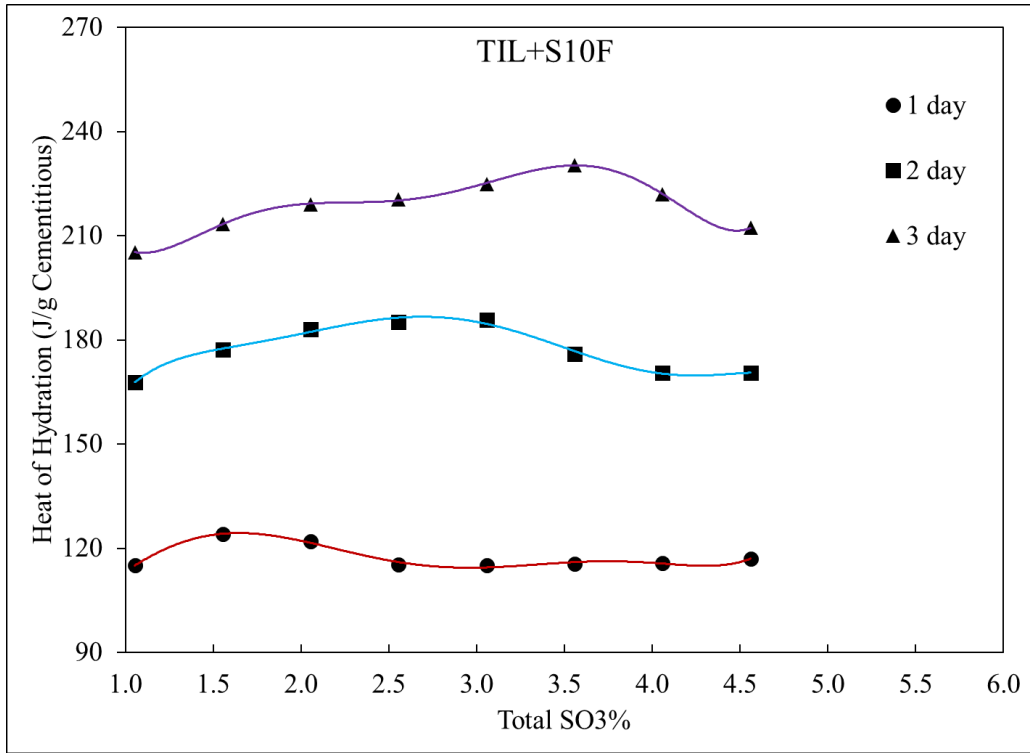
Figure 3-25: Total heat in cement TIL and S10F with variable sulfate levels at different ages
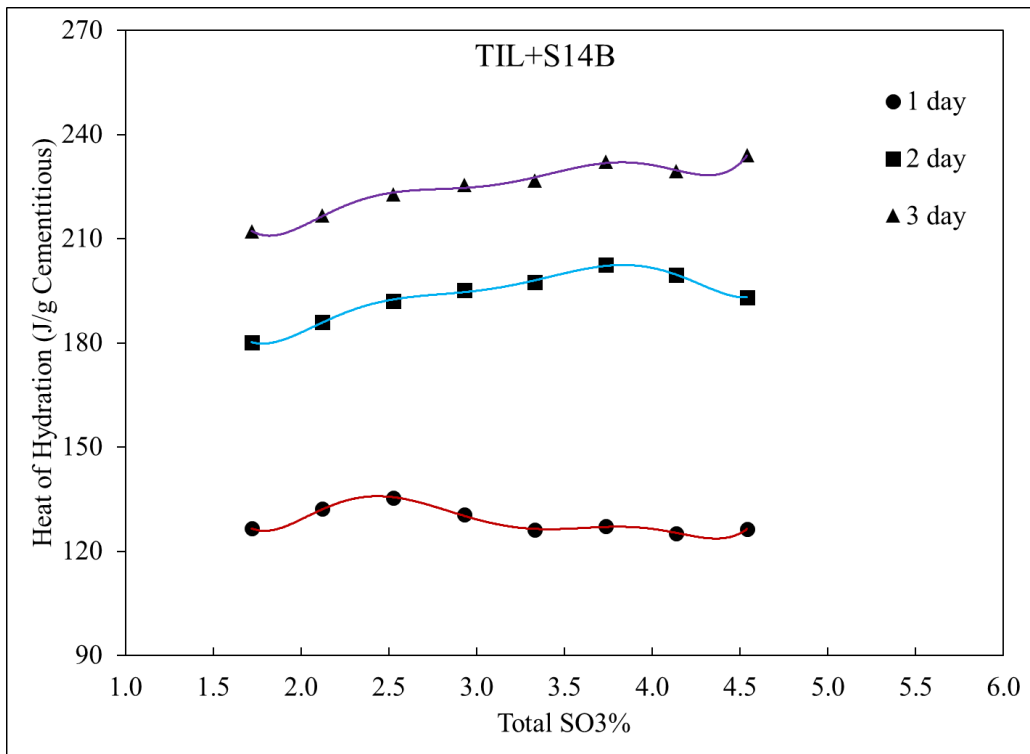
Figure 3-26: Total heat in cement TIL and S14B with variable sulfate levels at different ages

The optimum SO_3 content determined for each cement-slag system at 1, 2 and 3 days are listed in Table 3-9 and Table 3-10. Table 3-9 lists the optimum SO_3 content and SO_3/Al_2O_3 in the total system while Table 3-10 lists the optimum SO_3 content in the respective slag (considering extra sulfate is added to the slag); that is, the amount of sulfate that would have to be blended with the slag cement to achieve the optimum sulfate level when used with a particular cement. In few systems, the optimum SO_3 content could not be computed at some ages. The 3-day optimum SO_3 contents of TIL+S14B system could not be reached even with approximately 5% SO_3 present in the systems, as illustrated in Figure 3-26. Sulfate levels beyond 5% were not considered in the current study to avoid harm to the calorimeter. According to Table 3-9 and Table 3-10, the optimum sulfate content in cement-slag-blended systems are affected by the chemical and physical characteristics of both cement and slag. The sulfate balance in a cement-slag system may vary depending on the slag chemical and physical characteristics.

Table 3-9: Summary of determined optimum SO_3% and SO_3/Al_2O_3 in the total system at 1, 2, and 3 days

Slag [as-received SO_3 %]	Cement (Type) [as-received SO_3 %]	as-received SO_3 % (SO_3/Al_2O_3) in the system	Optimum SO_3% (SO_3/Al_2O_3) in the system		
			1 day	2 days	3 days
S8 [0.18]	BB (Type I) [3.93]	1.68 (0.24)	1.82 (0.26)	2.49 (0.37)	2.89 (0.43)
S10C [0.05]	BB (Type I) [3.93]	1.60 (0.19)	1.89 (0.22)	3.26 (0.39)	3.66 (0.45)
	C (Type I (Ha)) [4.00]	1.63 (0.19)	-	-	-
	TTC (Type II (MH)) [2.55]	1.05 (0.12)	-	-	-
	TIL (Type IL) [2.47]	1.02 (0.12)	-	-	-
	THIL (Type IL) [2.44]	1.01 (0.12)	-	-	-

Table 3-9(Continued): Summary of determined optimum SO_3% and SO_3/Al_2O_3 in the total system at 1, 2 and 3 days

Slag [as-received SO_3 %]	Cement (Type) [as-received SO_3 %]	as-received %SO_3 in mixture (SO_3/Al_2O_3)	Optimum %SO_3 in mixture (SO_3/Al_2O_3)		
			1 day	2 days	3 days
S10F [0.11]	BB (Type I) [3.93]	1.64 (0.20)	1.85 (0.23)	3.25 (0.41)	4.03 (0.52)
	TTC (Type II (MH)) [2.55]	1.09 (0.13)	1.86 (0.24)	2.79 (0.36)	3.65 (0.48)
	TIL (Type IL) [2.47]	1.05 (0.13)	1.65 (0.21)	2.68 (0.35)	3.57 (0.48)
S14B [1.22]	BB (Type I) [3.93]	2.30 (0.22)	2.51 (0.24)	4.31 (0.43)	4.34 (0.44)
	C (Type I (Ha)) [4.00]	2.33 (0.22)	-	-	-
	TTC (Type II (MH)) [2.55]	1.75 (0.17)	-	-	-
	TIL (Type IL) [2.47]	1.72 (0.17)	2.46 (0.25)	3.78 (0.39)	-
	THIL (Type IL) [2.44]	1.71 (0.17)	-	-	-
S17 [1.39]	BB (Type I) [3.93]	2.41 (0.19)	-	-	-
	C (Type I (Ha)) [4.00]	2.43 (0.19)	-	-	-
	TTC (Type II (MH)) [2.55]	1.85 (0.15)	-	-	-
	Z (Type II (MH)(Ha)) [3.25]	2.13 (0.18)	-	-	-
	TIL (Type IL) [2.47]	1.82 (0.15)	-	-	-

Table 3-10: Summary of determined optimum SO_3% in 100% slag at 1, 2, and 3 days

Slag	Cement	Optimum SO_3% in 100% slag		
		1 day	2 days	3 days
S8	BB (Type I)	0.41	1.53	2.20
S10C	BB (Type I)	0.53	2.81	3.48
S10F	BB (Type I)	0.46	2.80	4.10
	TTC (Type II (MH))	1.40	2.95	4.38
	TIL (Type IL)	1.10	2.82	4.30
S14B	BB (Type I)	1.56	4.56	4.61
	TIL (Type IL)	2.45	4.65	-

In general, the optimum sulfate content increased with increasing alumina contents in slags, as more sulfate is needed to control the alumina hydration. Two- and three-day optimums were found to be higher for all mixtures. This may be because the slag degree of hydration at one day is very low compared to that at two or three days, making the sulfate balance more dependent on the cement and particle size distribution than the slag composition. The highest 1-day optimum sulfate levels were observed in slag S14B blends. This can be attributed to the accelerated initial hydration due to the lower MgO content in slag S14B. It is noteworthy that 2-day and 3-day optimum values of slag S14B-cement BB were approximately similar, which implies that the system was approaching balanced sulfate level. Although S14B slag was already sulfated by the supplier, extra sulfate was needed to control the alumina reaction and maintain sulfate balance at two and three days for all cements used.

The effects of cement characteristics were more pronounced and less variable in the optimum SO_3 content values computed for 100% slag (Table 3-10). This is because extra sulfate was added to the system as a partial replacement of the slag and consequently, higher sulfate demand in the blended system resulted in a higher sulfate addition to the slag. In general, higher sulfate content was required to attain the sulfate optimum from 1 to 2 days than from 2 to 3 days [34]. Overall, slags blended with cement TIL (Type IL) also indicated a notably higher sulfate demand. Both as-received cements TTC and TIL were observed to be slightly under-sulfated, which explains the higher optimum sulfate values when blended with slag.

3.3.3.2 X-Ray Diffraction Analysis

Varying sulfate levels had significant effects on the hydration kinetics of cement-slag-blended systems as discussed previously. Hence, different sulfate levels may have significant influence on hydration, phases formed, and their quantities. Phase quantifications, using QXRD, for the slag-blended systems with variable sulfate levels at 3 days are presented in Table 3-11 through

Table 3-13. It appears that sulfate addition had the most significant influence on alumina bearing phases. Variation of ettringite, monosulfoaluminate, and hemicarboaluminate at different SO_3 levels are illustrated in Figure 3-27 through Figure 3-29. Additionally, notable changes can be observed in the clinker phases as well.

In cement BB-slag systems (Table 3-11), traces of aluminate can be observed at higher sulfate levels, and alite contents have also shown a small increase. This implies a retardation in alite and aluminate hydration. In contrast, the belite content notably decreased with increasing sulfate levels, indicating accelerated belite reaction. Moreover, a significant variation in ettringite and monosulfoaluminate contents can be observed with sulfate additions (Figure 3-27). Increasing the slag sulfate content increased ettringite content and decreased monosulfoaluminate and hemicarboaluminate contents. More ettringite was formed in systems with high-alumina slags. Higher amounts of sulfate present in the system stabilized ettringite, resulting in less alumina available to form other alumina-bearing phases [7]. According to Figure 3-27, a positive linear correlation was observed between the ettringite content and the total SO_3 content in the system. Moreover, there appears to be certain sulfate levels which completely eliminate monosulfoaluminate in the system. These levels may be of significance in controlling external sulfate attack in high-alumina slag-blended cementitious systems.

Table 3-11: Phase quantification of cement BB with slags at 3 days by XRD

Total sulfate % Phase (wt.%)	BB+60S8				BB+60S10C				BB+60S10F				BB+60S14B			
	1.68	2.29	2.89	3.50	1.60	2.40	3.20	4.00	1.64	2.44	3.24	4.04	2.30	3.11	3.92	4.72
Alite	0.4	0.5	0.6	0.7	0.5	0.5	0.9	1.0	0.4	0.6	1.0	1.1	0.9	0.9	0.9	0.8
Belite	2.7	2.3	2.1	1.7	2.7	2.6	2.2	1.8	2.8	2.4	2.1	1.6	2.7	2.2	2.1	2.2
Aluminate	0.0	0.0	0.1	0.4	0.0	0.0	0.3	0.4	0.0	0.0	0.1	0.3	0.1	0.1	0.1	0.2
Ferrite	0.0	0.0	0.0	0.0	0.0	0.0	0.0	0.0	0.0	0.0	0.0	0.0	0.0	0.0	0.0	0.0
Calcite	0.4	1.1	1.6	1.0	1.1	1.3	1.0	1.1	1.1	1.0	0.7	0.7	1.2	1.2	1.3	0.8
Quartz	0.0	0.0	0.0	0.0	0.0	0.0	0.0	0.0	0.0	0.0	0.0	0.0	0.0	0.0	0.0	0.0
Portlandite	1.9	1.7	1.4	1.4	1.3	1.3	1.2	1.3	1.4	1.3	1.2	1.2	1.3	1.1	0.9	1.0
Melilite	0.1	0.1	0.1	0.1	0.1	0.1	0.1	0.1	0.1	0.1	0.1	0.1	0.0	0.0	0.0	0.0
Merwinite	0.0	0.0	0.0	0.0	0.1	0.1	0.1	0.1	0.1	0.1	0.1	0.1	0.0	0.0	0.0	0.0
Ettringite	2.3	4.0	5.8	6.8	1.7	4.0	7.0	9.0	1.8	4.1	6.2	8.1	4.0	6.5	8.6	10.8
Monosulfate	0.8	0.3	0.1	0.0	0.8	0.1	0.0	0.0	0.8	0.3	0.0	0.0	0.4	0.1	0.0	0.0
Hemicarboaluminate	0.2	0.1	0.1	0.0	0.1	0.1	0.0	0.0	0.3	0.0	0.0	0.0	1.1	0.6	0.2	0.0
Hydrotalcite	0.0	0.0	0.0	0.0	0.1	0.1	0.0	0.0	0.2	0.0	0.0	0.0	0.0	0.0	0.0	0.0
Amorphous content (AC)	91.1	89.8	88.1	87.9	91.4	89.8	87.2	85.2	90.9	90.0	88.5	86.7	88.3	87.5	85.9	84.1
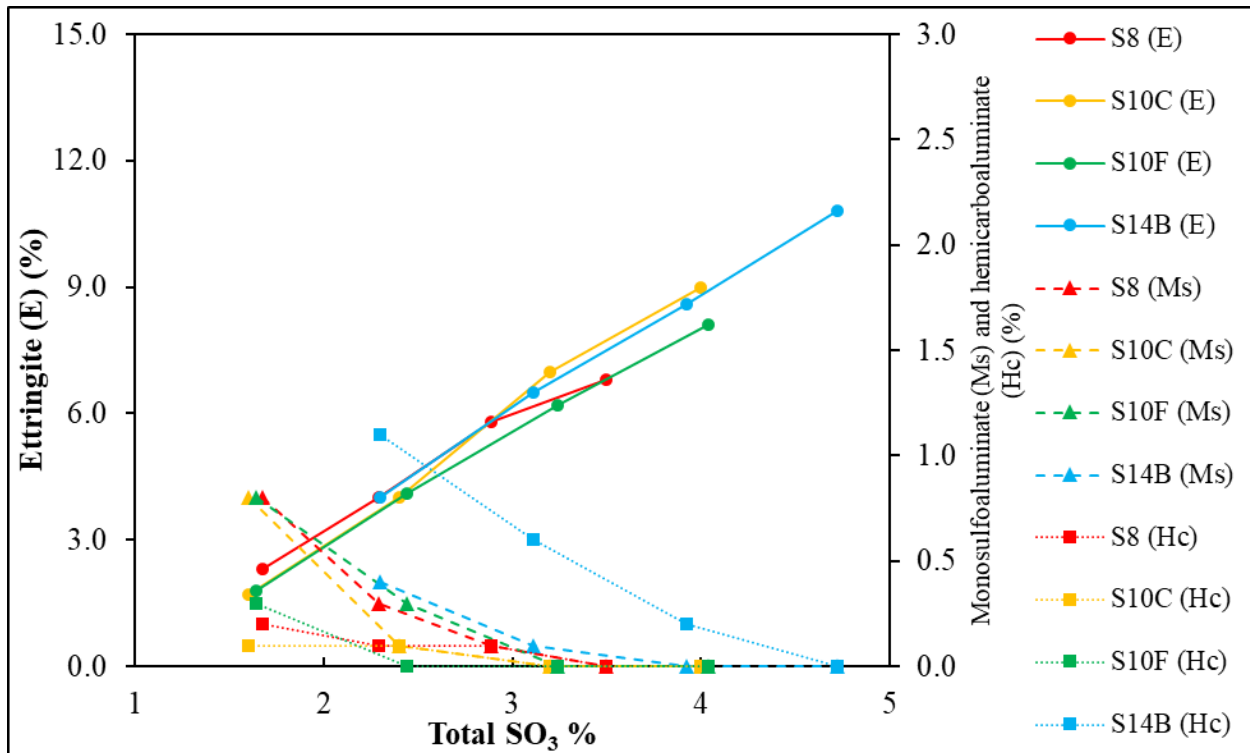
Figure 3-27: Ettringite, monosulfoaluminate, and hemicarboaluminate in cement BB-60% slag with variable sulfate levels as detected by XRD

The amorphous content (sum of C-S-H and unhydrated slag) in all systems showed a notable decrease with the increase in total sulfate contents. Addition of sulfates was reported to affect the composition of C-S-H by increasing the apparent Ca/Si ratio as calcium sulfates were adsorbed onto its surface [7]. Additionally, the presence of extra sulfates also affected hydrotalcite amounts in the systems. Hydrotalcite was detected only in several systems in small amounts and these quantities disappeared with increasing sulfate levels. According to Whittaker et al. [7], addition of extra sulfates increases the hydrotalcite Mg/Al ratio as more alumina is consumed to form ettringite.

The phase assemblage of the blends of cement TTC and slag S10F, at 3 days with variable sulfate levels are listed in Table 3-12. No traces of aluminate can be detected in any of the blends, but small amounts of ferrite can be observed, as cement TTC contains a considerably higher C_4AF content. Belite reaction appeared to accelerate with sulfate addition, similar to that with cement BB. Figure 3-28 shows the ettringite and monosulfoaluminate contents with varying sulfate content. As expected, ettringite content increased and portlandite content decreased with

increasing SO$_3$ levels. Hemicarboaluminate was observed at low sulfate contents due to the calcite content (2.8%) in cement TTC, and disappeared with increasing sulfate levels.

Table 3-12: Phase quantification of cement TTC with S10F at 3 days by XRD

Total sulfate % Phase (wt%)	TTC+60S10F			
	1.09	2.09	3.09	4.09
Alite	0.5	0.6	0.5	0.6
Belite	2.2	2.0	1.6	1.5
Aluminate	0.0	0.0	0.0	0.0
Ferrite	0.5	0.5	0.7	0.8
Calcite	0.5	0.6	0.8	0.6
Quartz	0.0	0.0	0.0	0.0
Portlandite	2.1	2.0	1.7	1.5
Melilite	0.1	0.1	0.0	0.1
Merwinite	0.2	0.1	0.1	0.1
Ettringite	1.8	4.0	6.0	7.9
Monosulfate	0.0	0.0	0.0	0.0
Hemicarboaluminate	1.3	0.7	0.0	0.0
Hydrotalcite	0.2	0.1	0.0	0.0
Amorphous content (AC)	90.6	89.4	88.5	87.0
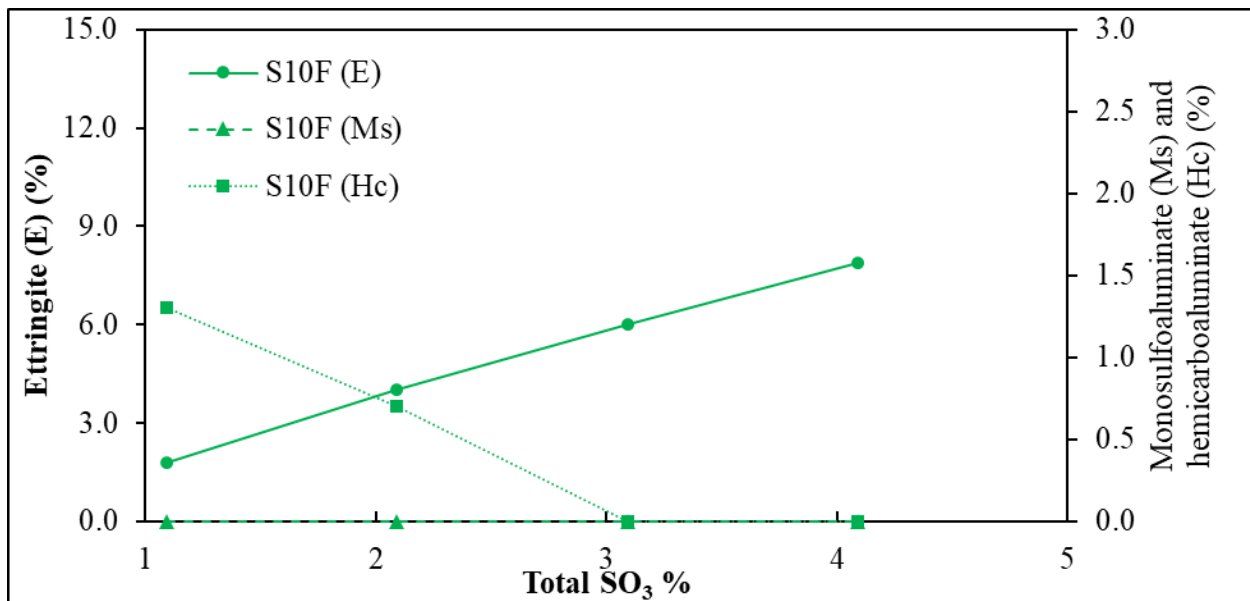
Figure 3-28: Alumina-bearing phases in TTC-S10F blends at variable sulfate levels

According to the phase quantification of cement TIL blends (

Table 3-13), small amounts of ferrite were observed, but no aluminate was detected. Additionally, belite content decreased with increasing SO_3 levels, indicating an accelerated hydration. As expected, no monosulfoaluminate was observed in any of the systems, but increased amounts of hemicarboaluminate amounts were detected compared to cement BB, which can be attributed to the higher calcite content (8.8%) present in cement TIL. Nevertheless, with increasing SO_3 levels, ettringite content increased linearly as depicted in Figure 3-29.

Table 3-13: Phase quantification of cement TIL with slags at 3 days by XRD

Total sulfate % Phase (wt.%)	TIL+60S10F				TIL+60S14B			
	1.05	2.06	3.06	4.06	1.72	2.53	3.33	4.14
Alite	0.3	0.2	0.4	0.4	0.2	0.5	0.4	0.6
Belite	2.1	1.9	1.4	1.3	2.0	1.7	1.5	1.4
Aluminate	0.0	0.0	0.0	0.0	0.0	0.0	0.0	0.0
Ferrite	0.4	0.6	0.7	0.9	0.6	0.8	0.7	0.8
Calcite	2.2	1.6	1.5	1.6	2.0	1.8	1.6	1.6
Quartz	0.2	0.2	0.2	0.2	0.1	0.2	0.1	0.2
Portlandite	2.2	1.5	1.6	1.5	1.4	1.2	1.5	1.5
Melilite	0.0	0.0	0.0	0.0	0.0	0.0	0.0	0.0
Merwinite	0.1	0.1	0.1	0.0	0.0	0.0	0.0	0.0
Ettringite	2.1	4.4	6.5	8.4	3.1	5.2	7.5	9.5
Monosulfate	0.0	0.0	0.0	0.0	0.0	0.0	0.0	0.0
Hemicarboaluminate	1.4	0.6	0.0	0.0	1.4	1.0	0.3	0.0
Hydrotalcite	0.0	0.1	0.0	0.0	0.0	0.0	0.0	0.0
AC	89.0	88.8	87.5	85.7	89.2	87.4	86.4	84.4
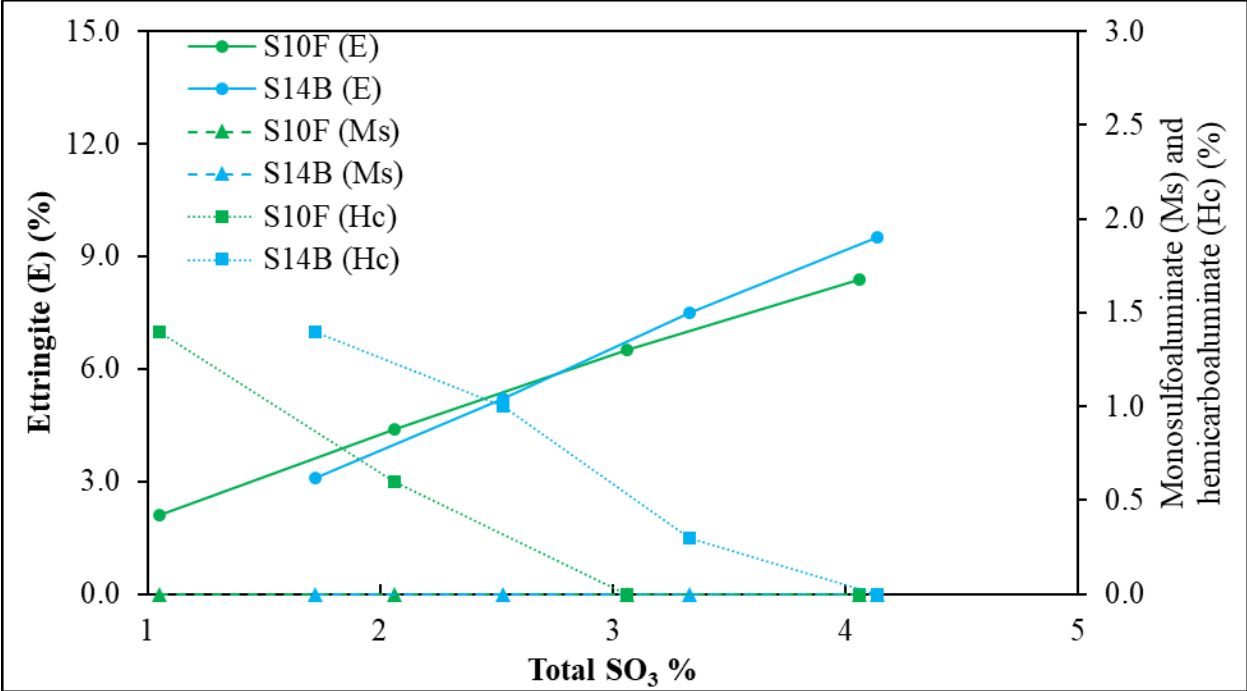
Figure 3-29: Ettringite, monosulfoaluminate, and hemicarboaluminate in cement TIL and slags with variable sulfate levels as detected by XRD

The acceleration of belite hydration with increasing sulfate levels was notable in all cement-slag systems. Based on the phase quantification results of the slag-blended cementitious systems with variable SO_3 content, alumina-bearing phases were most significantly affected by varying the sulfate content in the system. Higher sulfate contents led to stabilized ettringite formation, enhanced portlandite consumption, while eliminating monosulfoaluminate, even in cementitious systems blended with the high-alumina slags. A positive linear correlation was observed with ettringite and total SO_3 in the system. The presence of higher calcite contents from the cements resulted in the formation of hemicarboaluminate.

3.3.3.3 Thermodynamic Modeling

Figure 3-30 shows the predicted phase assemblage of cement BB with slag S8 and slag S17. Evidently increasing sulfate levels transformed the monosulfoaluminate to ettringite, thus increasing the ettringite contents. Although only traces of monosulfoaluminate were observed in BB+60S8 at low sulfate levels, in BB+60S17 a considerable amount of monosulfoaluminate remains even with sulfate addition. It is likely that the assumed slag DOH of 40% is high at 3 days, resulting in more alumina in the system, as ettringite was detected by XRD at low sulfate levels in

96

BB+60S17. In the system with slag S8, small amounts of carboaluminate phases were predicted at low sulfate levels, which decreased with increasing sulfate levels. However, the hemicarboaluminate formed in BB+60S17 appeared to be stable even with high sulfate levels, likely due to the high alumina present in the system. Moreover, the portlandite formed in S17 system was obviously lower than that in S8 system, indicating slag S17 reaction with cement consumed more portlandite.

The trends observed in thermodynamic modeling predictions of cement-slag blends at varying SO_3 levels appeared to be consistent with XRD phase quantification for most cases. However, an assumed slag DOH of 40% may have caused differences in the predicted phases. Addition of sulfate greatly affected the phase assemblage in slag-blended cementitious systems. In general, more ettringite was formed preferentially to monosulfoaluminate with extra sulfate present in the system. Additionally, in the presence of calcite, monosulfoaluminate formation was further reduced as calcite reacted with alumina in the system and formed hemicarboaluminate and subsequently stabilized ettringite. This is desirable in cement-slag systems because it can enhance long-term sulfate resistance of concrete as documented in the literature by Ogawa et al. [9]. Moreover, considerable amounts of hydrotalcite were predicted in all the systems, whereas QXRD analysis only detected traces of hydrotalcite in some systems. This may be again due to the difference between the assumed slag DOH used in the analysis and the actual DOH. In high-alumina slag-cement blended systems, portlandite consumption was higher, which implies an enhanced slag reactivity. Hence, for Type I cements and high-alumina slag blends, sulfate addition could minimize monosulfoaluminate formation, but cannot eliminate it entirely. When Type II(MH) and IL cements were blended with slag in the presence of extra sulfate, monosulfoaluminate formation was completely eliminated.
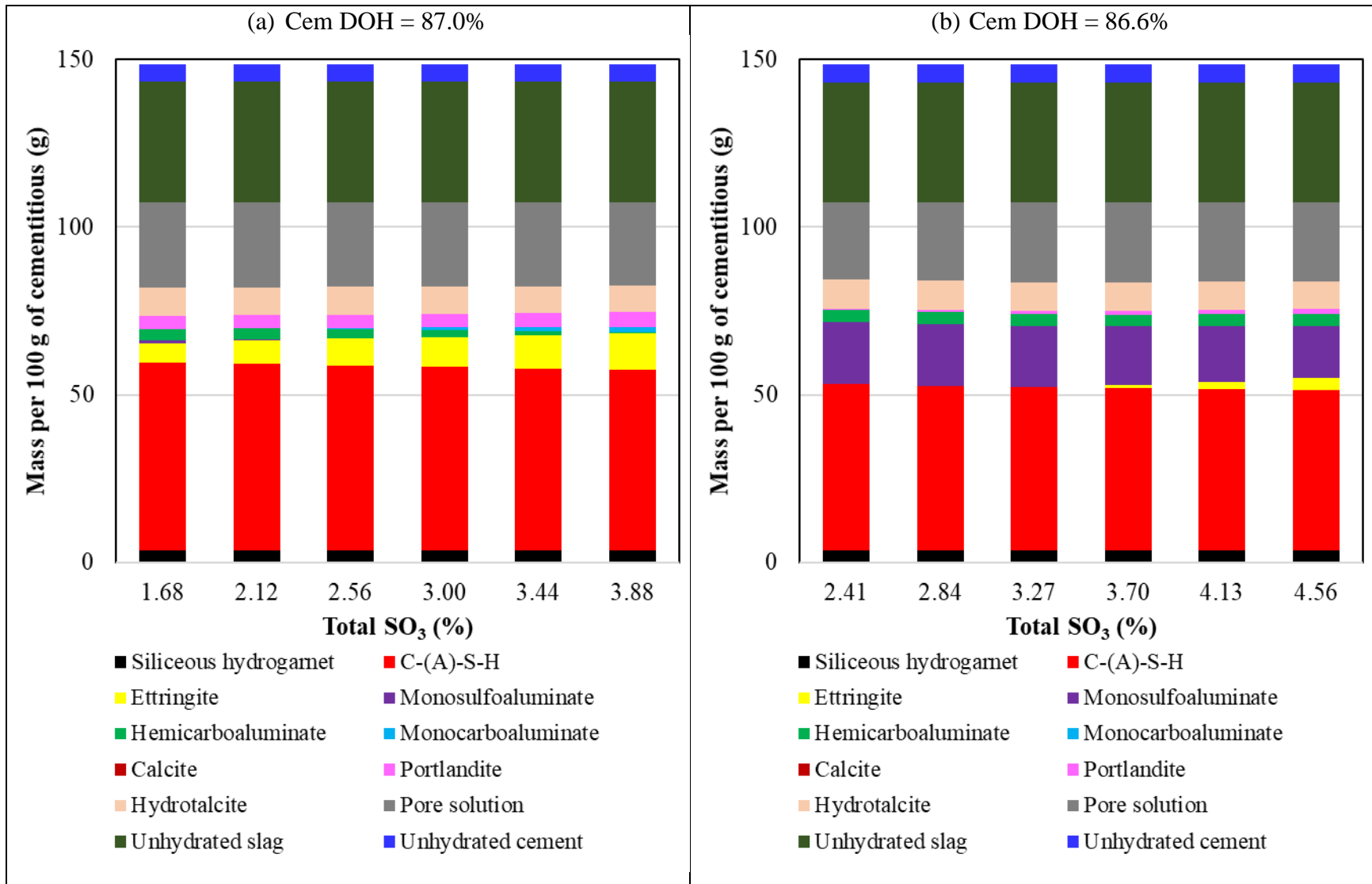
Figure 3-30: Phase assemblage prediction with varying SO$_3$ levels: (a) BB+60S8 (b) BB+60S17

3.3.4 Relationship between Optimum Sulfate Content and Cement and Slag Characteristics

Based on the optimum sulfate results obtained from all cement-slag combinations investigated here, 1-day optimums of some blends could not be determined as slags such as S14B were already sulfated. In some systems, 3-day optimums could not be computed as it was beyond the SO_3 levels (approximately 5%) considered in the current study. Figure 3-31 illustrates the 1-day, 2-day and 3-day optimum sulfate contents of all the optimized cement-slag-blended systems plotted against the slag alumina contents. Higher slag alumina content result in higher optimum sulfate contents at 2 and 3 days, with little difference seen at 1 day. Moreover, it is apparent that slags blended with Type I cements have the highest sulfate demand, which can be attributed to high alumina in Type I cements. Conversely, a lower sulfate demand was observed with slags blended with Type IL cement, due to incorporation of limestone and its subsequent dilution effect. However, when the SO_3 content is expressed as a percentage of 100% slag, the highest sulfate demand in slags was observed when slags are blended with under-sulfated cements TTC and TIL. Based on the trends observed in Figure 3-31, cement and slag characteristics that have a significant influence on the sulfate demand can be identified. For the cement, these characteristics are its fineness and the C_3A, C_4AF, and calcite contents, and for the slags, these characteristics are their finenesses and the alumina, magnesia, and calcite contents. The scope of the optimization matrix in this study was not sufficient to establish predictive relationships.
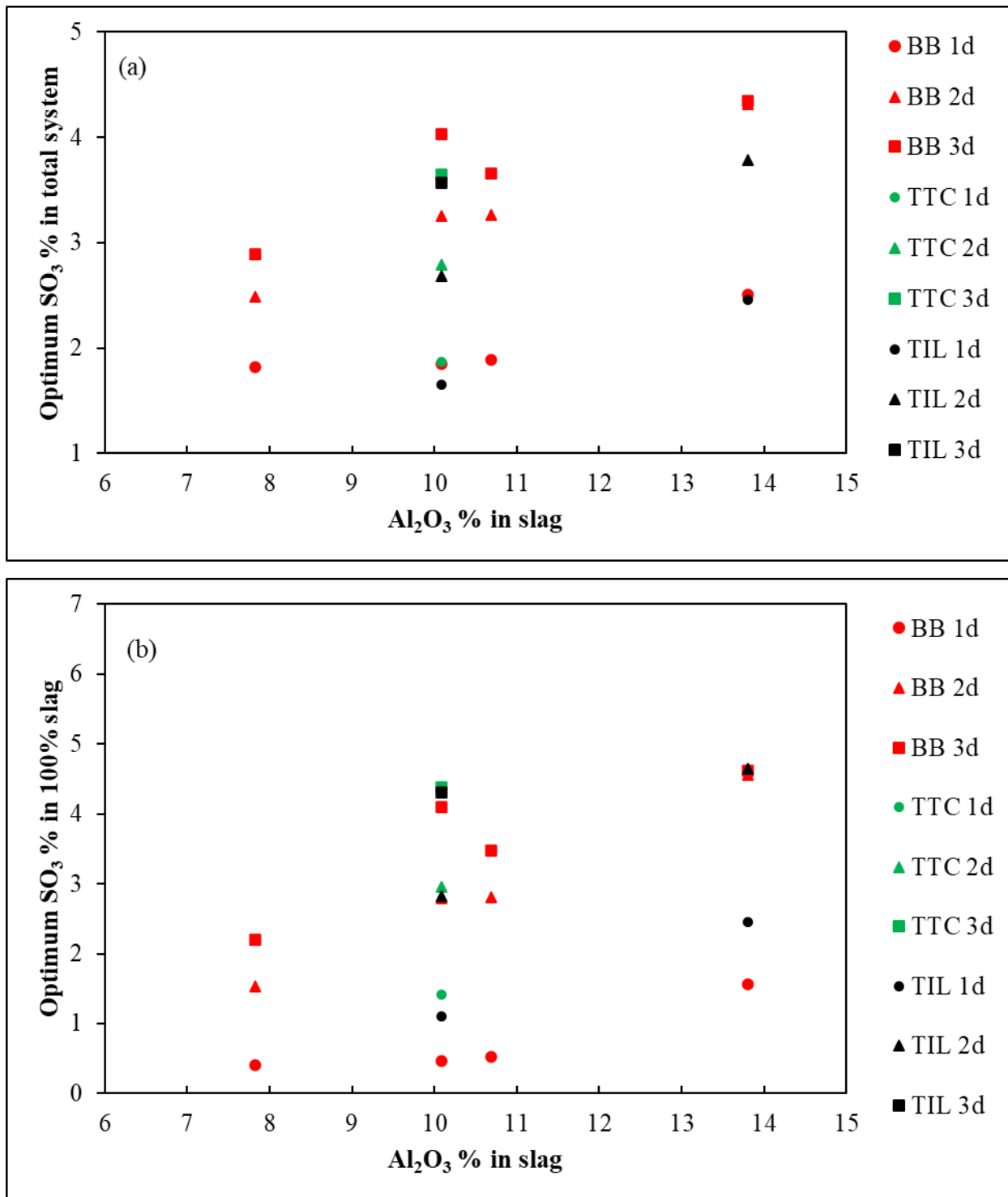
Figure 3-31: Optimum sulfate content versus alumina in slags: (a) total system (b) in 100% slag

3.4 Conclusions

Sulfate balance in cement-slag-blended systems plays an important role in sustaining the strength and durability performance of concrete. Based on the limited investigation performed on multiple cement-slag combinations, the optimum sulfate levels were affected by both cement and slag characteristics. XRD analysis and thermodynamic modeling of the cement-slag systems indicated significant changes in the phase assemblage at varying sulfate levels. With increasing sulfate levels more ettringite was formed and in high-alumina slag systems, ettringite was stabilized if higher amounts of calcite were present in the system due to the formation of carboaluminate phases. Hence, it is likely sulfate additions in the presence of limestone would be more effective in terms of sustaining external sulfate durability of concrete.

Two and three-day optimum sulfate levels of the blended systems were found to be more consistent across the cements compared to one-day optimums. The lower rate of hydration of the slag at early ages resulted in a lower DOH compared to the cement and 1 day was not long enough to reflect the contribution of slag to the hydration. In general, increasing slag alumina levels increased the optimum sulfate content in the blended system. Additionally, optimum sulfate content also increased with increasing C_3A contents in blended cements; the Type I cement required a higher optimum sulfate content, while the Type IL cement required a lower optimum. On the other hand, addition of extra sulfate to slag to reach the optimum sulfate content in the blended system was greatly affected by the cement characteristics. If the sulfate content in the as-received cement was insufficient, more sulfate had to be added to the slag in order to reach the optimum sulfate level in the blended system. Moreover, several properties of cements and slags were found to influence the optimum sulfate demand in slag-blended systems. Among those were the C_3A, C_4AF and calcite contents present in the cement, and the alumina, magnesia and calcite contents present in the slag. The particle size distribution of both cement and slag had a significant impact on sulfate balance as well. It is recommended that an expanded matrix be studied in order to establish a relationship between these properties and the measured 1, 2 and 3-day optimum sulfate demand in cement-slag-blended systems.

The optimum SO_3 content of cement-slag combinations was determined based on heat of hydration; however, the optimum sulfate content to ensure the long-term durability of the slag-blended cementitious systems needs to be assessed. Sulfate optimization using isothermal

calorimetry indicated that changing the cement source or the slag source for a given slag-cement combination changed the amount of sulfate required to optimize the blended system. It is recommended that an expanded matrix be studied to cover the slags and cements currently available in the state of Florida. It is also recommended to study the effect of slag replacement level (especially for the high-alumina slags) on sulfate optimum as the current study was limited to 60% slag replacement. It is expected that sulfate content in a slag-blended cementitious system will affect durability of the system when exposed to an external sulfate environment and/or subjected to high temperatures during curing.

3.5   Recommendations

- Allow the use of isothermal calorimetry to optimize slag sulfate levels on the specified slag-cement combination.

- Approval process of slag-blended concrete mixtures must include testing for sulfate balance of the cementitious constituents of the submitted mixture including chemical admixtures. Testing should occur at the identified replacement level as well as the identified w/cm ratio according to ASTM C543.

- Identify the correlation between sulfate optimum and variable slag replacement levels and sulfate durability and chloride penetrability in slag-blended cementitious mixtures.

3.6 References

[1] K. A. Evans, "The Optimum Sulphate Content in Portland Cement," University of Toronto, 1997.

[2] W. Lerch, "The influence of gypsum on the hydration and properties of Portland cement pastes," Research Laboratory of the Portland Cement Association, Chicago, IL, 1946.

[3] X. Li, R. Snellings, M. Antoni, N. M. Alderete, M. Ben Haha, S. Bishnoi, O. Cizer, M. Cyr, K. De Weerdt, Y. Dhandapani, J. Duchesne, J. Haufe, D. Hooton, M. Juenger, S. Kamali-Bernard, S.Kramar, M. Marroccoli, A. M. Joseph, A. Parashar, C. Patapy, J. L. Provis, S. Sabio, M. Santhanam, L. Steger, T. Sui, A. Telesca, A. Vollpracht, F. Vargas, B. Walkley, F. Winnefeld, G. Ye, M. Zajac, S. Zhang, K. L. Scrivener, "Reactivity tests for supplementary cementitious materials: RILEM TC 267-TRM phase 1," *Mater. Struct. Constr.*, vol. 51, no. 6, 2018.

[4] P. Suraneni, A. Hajibabaee, S. Ramanathan, Y. Wang, and J. Weiss, "New insights from reactivity testing of supplementary cementitious materials," *Cem. Concr. Compos.*, vol. 103, no. May, pp. 331–338, 2019.

[5] F. Zunino and K. Scrivener, "The influence of the filler effect on the sulfate requirement of blended cements," *Cem. Concr. Res.*, vol. 126, p. 105918, Dec. 2019.

[6] M. D. Niemuth, "Effect of fly ash on the optimum sulfate of Portland cement," Purdue University, 2012.

[7] M. Whittaker, M. Zajac, M. Ben Haha, F. Bullerjahn, and L. Black, "The role of the alumina content of slag, plus the presence of additional sulfate on the hydration and microstructure of Portland cement-slag blends," *Cem. Concr. Res.*, vol. 66, pp. 91–101, Dec. 2014.

[8] S. Adu-Amankwah, L. Black, J. Skocek, M. Ben Haha, and M. Zajac, "Effect of sulfate additions on hydration and performance of ternary slag-limestone composite cements," *Constr. Build. Mater.*, vol. 164, pp. 451–462, 2018.

[9] S. Ogawa, T. Nozaki, K. Yamada, H. Hirao, and R. D. Hooton, "Improvement on sulfate resistance of blended cement with high alumina slag," *Cem. Concr. Res.*, vol. 42, no. 2, pp. 244–251, Feb. 2012.

[10] ASTM C1012/C1012M-15, "Standard test method for length change of hydraulic-cement mortars exposed to sulfate solution," West Conshohocken, PA: ASTM International, 2015.

[11] D. Heinz and H. M. Ludwig, "Heat Treatment and the Risk of DEF Delayed Ettringite Formation in UHPC," in *International Symposium on Ultra High Performance Concrete*, 2004, pp. 717–730.

[12] H. Zibara, "Binding of external chlorides by cement pastes," University of Toronto, 2001.

[13] M. D. A. Thomas and P. B. Bamforth, "Modelling chloride diffusion in concrete: Effect of fly ash and slag," *Cem. Concr. Res.*, vol. 29, no. 4, pp. 487–495, 1999.

[14] H. W. Song and V. Saraswathy, "Studies on the corrosion resistance of reinforced steel in concrete with ground granulated blast-furnace slag—An overview," *J. Hazard. Mater.*, vol. 138, no. 2, pp. 226–233, Nov. 2006.

[15] O. R. Ogirigbo and L. Black, "Chloride binding and diffusion in slag blends: Influence of slag composition and temperature," *Constr. Build. Mater.*, vol. 149, pp. 816–825, Sep. 2017.

[16] M. Otieno, H. Beushausen, and M. Alexander, "Effect of chemical composition of slag on chloride penetration resistance of concrete," *Cem. Concr. Compos.*, vol. 46, pp. 56–64, Feb. 2014.

[17] M. D. A. Thomas, R. D. Hooton, A. Scott, and H. Zibara, "The effect of supplementary cementitious materials on chloride binding in hardened cement paste," *Cem. Concr. Res.*, vol. 42, no. 1, pp. 1–7, 2012.

[18] ASTM C563 - 18, "Standard Guide for Approximation of Optimum SO3 in Hydraulic Cement," West Conshohocken, PA: ASTM International, 2018.

[19] ASTM C150/C150M-18, "Standard Specification for Portland Cement," West Conshohocken, PA: ASTM International, 2018.

[20] ASTM C595/C595M-16, "Standard Specification for Blended Hydraulic Cements," West Conshohocken, PA: ASTM International, 2016.

[21] ASTM C989 / C989M-17, "Standard Specification for Slag Cement for Use in Concrete and Mortars," West Conshohocken, PA: ASTM International, 2017.

[22] ASTM C1702-17, "Standard Test Method for Measurement of Heat of Hydration of Hydraulic Cementitious Materials Using Isothermal Conduction Calorimetry," West Conshohocken, PA: ASTM International, 2017.

[23] D. Bish and R. J. Reynolds, "Sample Preparation for X-Ray Diffraction," in *Modern Powder Diffraction*, D. Bish and J. Post, Eds. Washington, DC: The Mineralogical Society of America, 1989, pp. 73–99.

[24] Paul Scherrer Institut (PSI), "GEMS 3 [Software]." .

[25] R. Snellings, "X-ray powder diffraction applied to cement," in *A Practical Guide to Microstructural Analysis of Cementitious Materials*, 2016, pp. 107–176.

[26] M. Ben Haha, B. Lothenbach, G. Le Saout, and F. Winnefeld, "Influence of slag chemistry on the hydration of alkali-activated blast-furnace slag — Part I: Effect of MgO," *Cem. Concr. Res.*, vol. 41, no. 9, pp. 955–963, Sep. 2011.

[27] B. Lothenbach and A. Gruskovnjak, "Hydration of alkali-activated slag: thermodynamic modelling," *Adv. Cem. Res.*, vol. 19, no. 2, pp. 81–92, 2007.

[28] A. Zayed, A. Sedaghat, A. J. Bien-Aime, and N. Shanahan, "Final Report Effects of portland cement particle size on heat of hydration FDOT Contract No: BDK84 977-13," University of South Florida, Tampa, FL, 2013.

[29] B. Lothenbach, G. Le Saout, E. Gallucci, and K. Scrivener, "Influence of limestone on the hydration of Portland cements," *Cem. Concr. Res.*, vol. 38, no. 6, pp. 848–860, Jun. 2008.

[30] J. W. Bullard, H. M. Jennings, R. A. Livingston, A. Nonat, G. W. Scherer, J. S. Schweitzer, K. L. Scrivener, J. J. Thomas, "Mechanisms of cement hydration," *Sci. Technol. Concr. Admixtures*, vol. 41, pp. 1208–1223, 2011.

[31] J. Stark and K. Bollmann, "Delayed Ettringite Formation in Concrete," *ZKG Int.*, vol. 53, no. 4, pp. 1–25, 2000.

[32] M. Zajac, A. Rossberg, G. Le Saout, and B. Lothenbach, "Influence of limestone and anhydrite on the hydration of Portland cements," *Cem. Concr. Compos.*, vol. 46, pp. 99–108, Feb. 2014.

[33] B. Z. Dilnesa, "Fe-containing Hydrates and their Fate during Cement Hydration:

Thermodynamic Data and Experimental Study," Swiss Federal Institute of Technology, 2012.

[34] I. B. Javed and P. C. Taylor, "Sulfate Resistance of Concrete Using Blended Cements or Supplementary Cementitious Materials," Portlance Cement Association, Skokie, IL, 2006.

Chapter 4   Effects of Slags Composition on Heat Generation in Blended Cementitious Systems

4.1   Introduction

Ground granulated blast furnace slag (GGBFS, slag) is a supplementary cementitious material (SCM) widely used in mass concrete to reduce concrete temperature rise and thereby increase resistance to thermal cracking [1]. In general, it is believed that cement replacement with slag would reduce the concrete temperature rise; however, several studies have reported that the heat generation during slag hydration is dependent on the chemical and physical characteristics of slags [2]–[5]. Moreover, recent construction projects of drilled shafts in Central and South Florida, which included high slag replacement levels in concrete, have reported temperature exceeding 195°F (90.6°C) at the reinforcement cage depth. Therefore, it is imperative to investigate the effect of slag chemical, physical and mineralogical composition on the temperature rise of concrete mixtures typically used in mass concrete. This information can help in designing thermal control plans used to minimize the risk of cracking and other durability-related issues.

In assessing concrete temperature rise, 5 slags, a Type II (MH) portland cement and a Type IL(10) cement were used. All adiabatic temperature measurements were conducted at the US Bureau of Reclamation (USBR) facilities. The primary focus of this task is to assess the effect of slag characteristics on heat generation by conducting adiabatic calorimetry experiments on slag-blended concrete.

CaO, SiO_2, Al_2O_3, and MgO have been identified in the literature to have significant effects on slag reactivity [2]–[4]. It is generally accepted that slag reactivity increases with CaO/SiO_2 ratio [2]; however, there are only few studies available in the literature that investigate the effects of Al_2O_3 and MgO on slag hydration. With increasing Al_2O_3 content, an increase in heat evolution has been observed by several researchers, especially at early ages [4], [6], [7]. Additionally, Ben Haha et al. [3] indicated that decreasing MgO content in slags at the same Al_2O_3 content increased the cumulative heat during the first 2 days. The reactivity affects heat evolution as well as the stress and mechanical property development of concrete.

While most of the studies in the literature assessed the effect of slag composition on heat evolution, Zayed et al.[5] studied the effect of slag chemistry and physical characteristics on

durability of slag-blended cementitious systems [8] as well as slag-blended concrete cracking potential [9]. All concrete mixtures containing slag performed better than the control portland cement mixture. They reported reduced temperatures and lower cracking risks in slag-blended concrete of low alumina content. A linear relationship was observed between rigid cracking frame (RCF) indices and slags' MgO/Al_2O_3 ratio (for slags with similar CaO/SiO_2); an increase in the MgO/Al_2O_3 ratio decreased the second zero stress temperature and thereby reduced cracking risks. The same MgO/Al_2O_3 ratio indicated a correlation with the cracking temperature as well. The findings indicate slag fineness also affect concrete cracking temperature.

Based on the current literature on slag hydration, the temperature sensitivity of slag-cement systems is dependent on the physical and chemical characteristics of the slags. The amount of heat that can be produced by a given slag also depends on its composition. As a result, the use of a single value to define or characterize the slag activation energy and ultimate heat of hydration of slag (461 J/g) [10] seems inadequate, given the wide variation of slag chemistry, Table 4-1 (Table 1.1 in [11]). .

Table 4-1: Range of chemical compositions of slags (adapted from Table 1.1 in [11])

Chemical constituents (as oxides) [*]	Range of composition, % by mass
SiO_2	32 to 42
Al_2O_3	7 to 16
CaO	32 to 45
MgO	5 to 15
S	0.7 to 2.2
Fe_2O_3	0.1 to 1.5
MnO	0.2 to 1.0

[*]Except for sulfur

4.2   Experimental Procedure

Two cements, and five slags were used to assess the effect of variable chemical, physical and mineralogical characteristics of the cementitious systems on heat generation. Cement Z is a Type II (MH) with a higher alkali content whereas cement GILOP is a Type IL cement with 9.1% calcite content. Mineralogical compositions of the as-received cements are listed in Table 4-2. The five slags were named according to their increasing alumina contents from 8% to 17%. S10C and

S10F have similar alumina contents but different fineness. Slag S10F was used to determine the effect of fineness on heat generation in concrete at a slag replacement level of 60%. The magnesia content of the slags was approximately 10% except for slag S14B, which had a lower MgO content of 5.6%. The mean particle size (MPS) of slags determined using laser scattering particle size analysis, Blaine fineness [12]and Al_2O_3[13], MgO, SO_3 and calcite content are listed in Table 4-3.

Table 4-2: Chemical, mineralogical analysis, and physical characteristics of as-received cements

Analyte	Z - I/II(MH)(Ha)	GIL-OP - IL(10)
Alite	54	44.5
Belite	7.2	16.5
Aluminate	5.6	3.7
Ferrite	7,7	8.9
Gypsum	0.3	3.9
Hemihydrate	2.5	-
Calcite	3.4	9.2
Portlandite	-	1.5
Quartz	0.2	0.4
Dolomite	0.5	0.7
Periclase	1.8	-
Syngenite	1.1	-
Amorphous/ unidentified	15.7	10.6
Na_2O_{eq}	0.65	0.40
Blaine fineness (m^2/kg)	412	469

Table 4-3: Slag chemical and physical characteristics

Slag	Al_2O_3 content (%)	MgO content (%)	SO_3 content (%)	Calcite content (%)	Blaine fineness (m^2/kg) b-value=0.9	Mean particle size (µm)
S8	7.82	10.71	0.18	0.9	617	9.49
S10C	10.69	10.70	0.05	0.2	485	10.29
S10F	10.09	10.81	0.11	0.2	600	9.03
S14B	13.80	5.60	1.22	1.4	553	12.55
S17	17.07	10.96	1.39	0.2	510	9.79

Table 4-4 gives the concrete mixture proportions used for adiabatic calorimetry measurements. The plain and slag-blended concrete mixtures were prepared using a constant

water-cementitious material ratio (w/cm) of 0.404 with a total cementitious content of 665 lb/yd^3 (395 kg/m^3). Control mixtures without slag cement were prepared with each cement and were designated as Control Z and Control GILOP. In the slag-blended mixtures, the cement replacement with slag was 60% by mass. Blended mixtures prepared were identified as GILOP-S8, GILOP-S14B, GILOP-S17, Z-S8, Z-S10C, Z-S10F, Z-S14B, and Z-S17. A water-reducing admixture (constant dosage) was used to maintain adequate workability. Coarse aggregates were soaked for a period of 24 hours prior to mixing and drained.

Table 4-4: Concrete mixture proportions per 1 yd^3 (1 m^3)

Material	Control mixes	Slag mixes
Cement, lb (kg)	665 (395)	266 (158)
Slag, lb (kg)	0	399 (237)
Coarse aggregate #57 limestone SSD, lb (kg)	1,719 (1,020)	1,719 (1,020)
Fine aggregate – SSD, lb (kg)	1,174 (697)	1,174 (697)
Water, lb (kg)	267 (158)	267 (158)
Air entraining admixture, fl oz (ml)	0.06 (2.3)	0.06 (2.3)
Water reducing admixture, fl oz (ml)	27.39 (1,059)	27.39 (1,059)
w/cm	0.404	0.404

Concrete mixtures were prepared in accordance with ASTM C192 [14]. Prior to mixing concrete, all the materials were pre-cooled to 50°F (10°C) to make sure that the concrete temperature would not reach beyond the maximum temperature that the chamber was capable of maintaining. Air content was determined in accordance to ASTM C231 [15], slump was measured per ASTM C143 [16], and unit weight was measured following ASTM C138 [17]. Fresh concrete properties are listed in Table 4-5.

Table 4-5: Concrete fresh properties

Mix ID / Fresh property	Control Z	Control GILOP	GILOP-S8	GILOP-S14B	GILOP-S17	Z-S8	Z-S10C	Z-S10F	Z-S14B	Z-S17
Unit Weight, lb/ft^3 (kg/m^3)	141.4 (2,265)	-	-	142.3 (2,279)	142.7 (2,286)	142.8 (2,287)	141.6 (2,268)	140.3 (2,247)	142.6 (2,284)	142.0 (2,275)
Slump, in. (mm)	5.0 (127)	3.25 (83)	4.0 (102)	2.0 (51)	4.75 (121)	5.0 (127)	4.25 (108)	6.5 (165)	2.75 (70)	3.5 (89)
Air Content, (%)	3.6	-	-	2.8	2.9	3.2	-	4.5	3.0	4.4
Temperature, °F (°C)	62.4 (16.9)	60.3 (15.7)	59.8 (15.4)	60.0 (15.6)	62.0 (16.7)	59.5 (15.3)	59.2 (15.2)	60.0 (15.6)	61.3 (16.3)	58.9 (14.9)

Concrete heat of hydration was measured using adiabatic calorimetry at the U.S. Bureau of Reclamation (USBR) according to USBR 4911-92 [18]. To perform this test, concrete was placed in a steel canister supported by foam blocks and a dolly to insulate the bottom of the sample and facilitate movement of the assembly, as shown in Figure 4-1. A steel plate with tubes attached, as shown in Figure 4-2, was placed on the canister opening and sealed to the canister using silicone. Two thermocouples were inserted into the steel tubes in the sample to measure the concrete temperature, as shown in Figure 4-3. Tight-fitting insulation was placed around the concrete sample and concrete temperature was recorded using two inserted temperature probes. The insulated concrete sample was placed in an environmental chamber shown in Figure 4-4. The chamber temperature was set to within 0.01°F (0.01°C) of the measured concrete temperature to greatly reduce the heat loss and to prevent any heat gain to the sample [19].

Figure 4-1: Concrete sample placed in steel canister set on insulated foam blocks and dolly

Figure 4-2: Picture of stainless steel plate with tubes attached that was inserted into concrete sample for thermocouple insertion

Figure 4-3: Thermocouple insertion into tubes on sample top

Figure 4-4: Concrete sample in adiabatic calorimeter

Apparent activation energy (E_a) of the cementitious material is needed when using modeling software to predict concrete temperature rise and cracking risks. The apparent activation energy (E_a) describes the temperature sensitivity of the hydration rate of a concrete mixture. Isothermal conduction calorimetry was performed to determine E_a for 10 cementitious mixtures. ASTM C1702 [20] offers 2 possible mixing procedures for assessing the temperature sensitivity of cementitious systems. The Method A internal mixing protocol was attempted first for all

mixtures at 3 temperatures (23, 30 and 40°C (73.4, 86, 104°F)) but later it was decided to implement Method B due to issues with the paste consistency at 40°C. ASTM C1702-Method B external mixing procedure [20] was used to measure the heat of hydration of the paste samples at 23, 30 and 40°C (73.4, 86, 104°F) and to determine E_a of the mixtures using the Arrhenius equations (Equation 4-1 and Equation 4-2). The k is obtained by taking the reciprocal of the hydration time parameter τ, determined at the 3 temperatures by performing isothermal calorimetry as will be discussed next.

$$k = Ae^{-(\frac{E_a}{RT})}$$

Equation 4-1

$$lnk = -\frac{E_a}{RT} + lnA$$

Equation 4-2

Where,

k = Specific rate of reaction

A = Pre-exponential term

E_a = Activation energy (kJ/mol)

R = Universal gas constant [8.314 J/(mol·K)]

T = Temperature (K)

A TAM Air eight-channel calorimeter produced by TA instruments was used to conduct heat flow measurements. All measurements were conducted in duplicates. The paste mixture design, Table 4-6, used the same paste proportions as the concrete mixtures, Table 4-4. A volumetric solution of the water reducing admixture was prepared. Air entraining admixture was not added in the paste mixtures as it was a small dosage and has been found not to significantly affect the activation energy [21]. When preparing samples, cement and slag were weighed in an ampoule and the water-reducing admixture solution was weighed in a separate syringe and preconditioned in an oven at the respective testing temperature for an hour. Chemical admixture solution was injected into the sample ampoule and mixed using a digital vortex mixer (Fisherbrand^{TM}) for 1 min at 1,000 rpm. The mixed sample ampoule was immediately loaded in the calorimeter and the experiment was started within 3 min. Heat flow measurements were collected for 72 h at 40°C (104°F), 120 h at 30°C (86°F) and 168 h at 23°C (73.4°F)

Table 4-6: Isothermal calorimetry paste mixture design

Material	Control mixes	Slag mixes
Cement (g)	4.0587	1.6037
Slag (g)	0	2.4055
Water (g)	1.6316	1.6117
Water reducing admixture (ml)	0.01089	0.01076
w/cm	0.404	0.404

Heat flow and cumulative heat of hydration were normalized per gram of cementitious materials in the sample. The data collected during the first 30 minutes were discarded to minimize the effect on data due to the disturbance caused to the signal when the samples were loaded in the calorimeter. The degree of hydration of the system was calculated from the measured heat of hydration using Equation 4-3, Equation 4-4 and Equation 4-5 [10], [22], [23]:

$$\alpha(t) = \frac{H(t)}{H_u} \qquad \text{Equation 4-3}$$

Where,

$\alpha(t)$ = Degree of hydration at time (t)

$H(t)$ = Heat evolved from time 0 to time t (J/g)

H_u = Total available heat (J/g)

$$H_{cem} = 500P_{C3S} + 260P_{C2S} + 866P_{C3A} + 420P_{C4AF} + 624P_{SO3} + 1186P_{FreeCaO} + \qquad \text{Equation 4-4}$$
$$850P_{MgO}$$

Where,

H_{cem} = Total heat of hydration of portland cement as described above (J/g)

P_i = Ratio of mass of ith component to total cement content

$$H_u = H_{cem} P_{cem} + 461P_{slag} \qquad \text{Equation 4-5}$$

For pastes without slag, $H_u = H_{cem}$. For the slag-blended systems, H_u was calculated using Equation 4-5 [10], [24]. The exponential function shown in Equation 4-6 was used to determine E_a:

$$\alpha_t = \alpha_u \cdot exp\left(-\left(\frac{\tau}{t}\right)\right)^{\beta}$$

<div align="right">Equation 4-6</div>

Where,

α_t = Degree of hydration at time 't'

α_u = Ultimate degree of hydration

τ = Time parameter

β = Shape parameter

The evolution of the degree of hydration values with time were fit to Equation 4-6 by the least-square method using the measured values of $\alpha(t)$ (Equation 4-3) and the corresponding α_u, τ, and β parameters were determined for each temperature, 23, 30 and 40°C (73.4, 86, 104°F). The E_a was determined by plotting $ln(k)$ ($k = 1/\tau$) determined at three temperatures against $1/T$, (Equation 4-2). E_a is the product of the negative slope and universal gas constant.

In addition to the activation energy, E_a, the hydration parameters of concrete, α_u*, $\tau*$, and $\beta*$ are required to predict temperature rise in concrete. The temperature development of a concrete element under adiabatic conditions can be determined from Equation 4-7. Therefore, using Equation 4-7 through Equation 4-10, the measured adiabatic temperature data were fitted by the least square method to obtain the hydration parameters, α_u*, $\beta*$ and $\tau*$ for each concrete mix [8], [21].

$$\frac{dT}{dt} = \frac{Q_h}{\rho \cdot c_p}$$

<div align="right">Equation 4-7</div>

Where,

T = Concrete temperature (°C)

ρ = Concrete density (kg/m^3)

c_p = Concrete specific heat capacity (J/kg/ °C)

Q_h = Rate of heat generation (W/m^3)

$$Q_h(t) = H_u \cdot W_c \cdot \left(\frac{\tau*}{t_e}\right)^{\beta*} \cdot \left(\frac{\beta*}{t_e}\right) \cdot \alpha_u^* exp\left(-\left(\frac{\tau*}{t_e}\right)\right)^{\beta*} \cdot \left(\frac{t_e}{\Delta t}\right)$$

<div align="right">Equation 4-8</div>

Where,

$Q_h(t)$ = Rate of heat generation (W/m^3)

<div align="center">118</div>

W_c = Weight of cement in the mixture (kg/m³)

t_e = Equivalent age at the reference temperature (h) (Equation 4-9)

Δt = Time interval

For concrete temperature histories which were not conducted at the reference temperature isothermally, equivalent age (Equation 4-9) is typically calculated and used instead of concrete age.

$$t_e(T_r) = \ exp\left[\left(\frac{-E_a}{R}\right)\left(\frac{1}{273 + T_c} - \frac{1}{273 + T_r}\right).\Delta t\right]$$

Equation 4-9

Where,

$t_e(T_r)$ = Equivalent age at the reference temperature (h)

T_r = Reference temperature (23ºC)

T_c = Concrete temperature at time interval Δt (ºC)

$$c_p(\alpha) = \frac{W_c\alpha(AT_c + B) + W_c(1 - \alpha)C_c + W_aC_a + W_wC_w}{\rho}$$

Equation 4-10

Where,

$c_p(\alpha)$ = Concrete specific heat (J/kg/°C) at degree of hydration α

W_c = Cementitious material content in the concrete (kg/m³)

A = A coefficient equal to 8.4 for metric

B = 339 for metric

ρ = Concrete density (kg/m³)

C_c = Specific heat of the cementitious materials (J/kg/°C)

W_a = Aggregate material content in the concrete (kg/m³)

C_a = Specific heat of the aggregate materials (J/kg/°C)

W_w = Water content in concrete (kg/m³)

C_w = Specific heat of water (J/kg/°C)

4.3 Results and Discussion

4.3.1 Adiabatic Calorimetry

Adiabatic temperature rise values at 168 h (7 days) are summarized in Table 4-7. Figure 4-5 illustrates the adiabatic temperature rise of the two control mixtures. Clearly, there is a substantial difference between the temperature rise of control GILOP and control Z, with temperature rise of control GILOP being lower. This was expected due to the reduced clinker fraction of cement GILOP compared to cement Z, which resulted in a lower reactivity. C_3S and C_3A contents of cement Z were 54% and 5.6% whereas for cement GILOP these values were 44.5% and 3.7% respectively. Although the higher limestone content in GILOP was expected to slightly accelerate the cement hydration due to the filler effect [25], the rate of the adiabatic temperature rise was slightly higher during the first 12 hours only.

Table 4-7: Concrete adiabatic temperature rise

Mix ID	Control Z (Type II (MH)	Control GILOP (IL cement)	GILOP-S8	GILOP-S14B	GILOP-S17	Z-S8	Z-S10C	Z-S10F	Z-S14B	Z-S17
168 h Adiabatic temp, °F(°C)	160.7 (71.5)	156.9 (69.4)	142.8 (61.6)	143.7 (62.1)	157.3 (69.6)	146.1 (63.4)	153.4 (67.4)	152.2 (66.8)	149.9 (65.5)	152.9 (67.2)
Adiabatic temp rise, °F(°C)	97.2 (54.0)	95.3 (52.9)	81.4 (45.2)	83.2 (46.2)	95.6 (53.1)	86.9 (48.3)	93.8 (52.1)	93.6 (52.0)	87.3 (48.5)	94.7 (52.6)

120
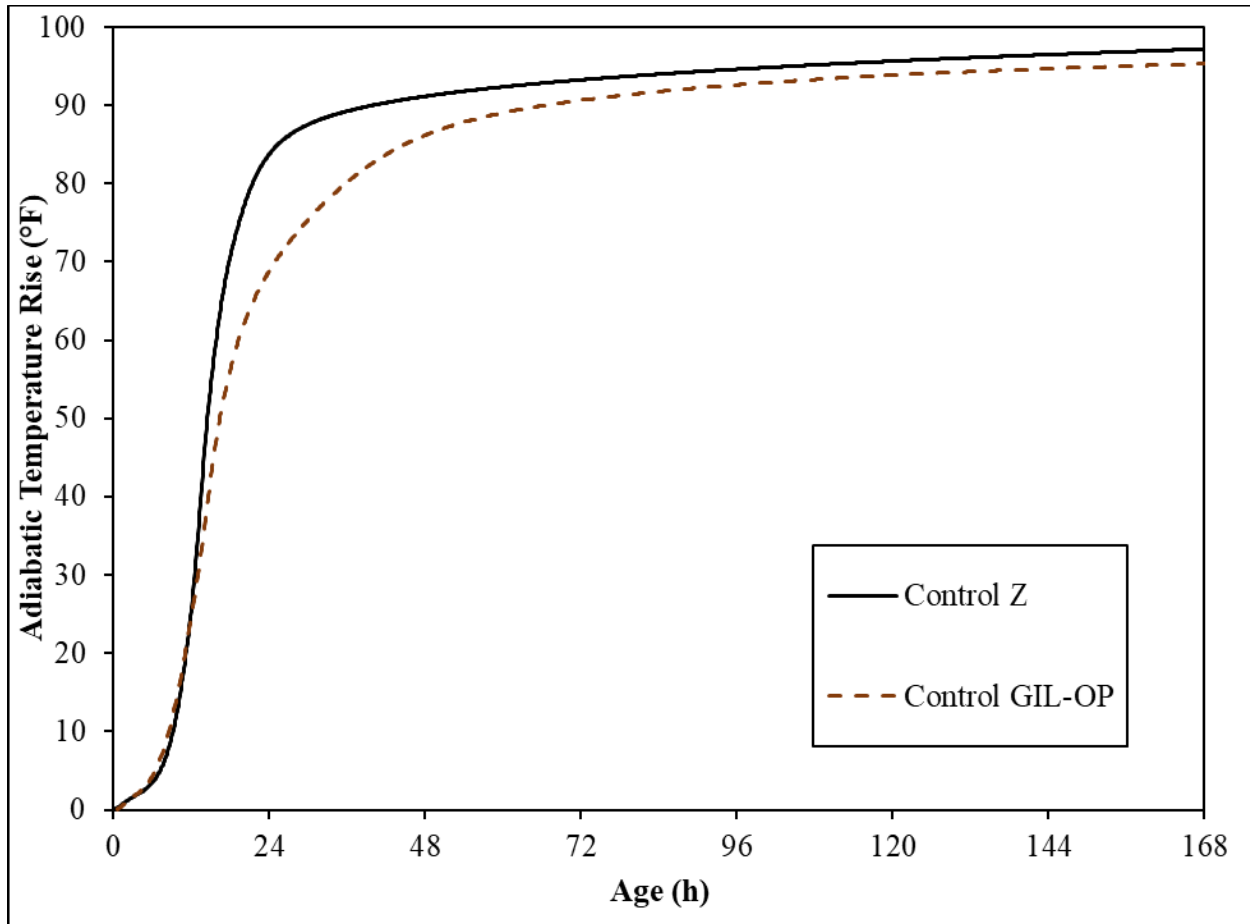
Figure 4-5: Adiabatic temperature rise of control Z (Type II(MH)) and control GIL-OP (IL(10))

Figure 4-6 and Figure 4-8 show the adiabatic temperature rise of the control and slag blended mixtures for a period of 168 h. As the temperature rise during the first 72 h increases rapidly, the rates of adiabatic temperature rise during this period are illustrated in Figure 4-8 and Figure 4-9. In general, the temperature rise of cement GILOP mixtures were lower than that of cement Z blended mixtures.
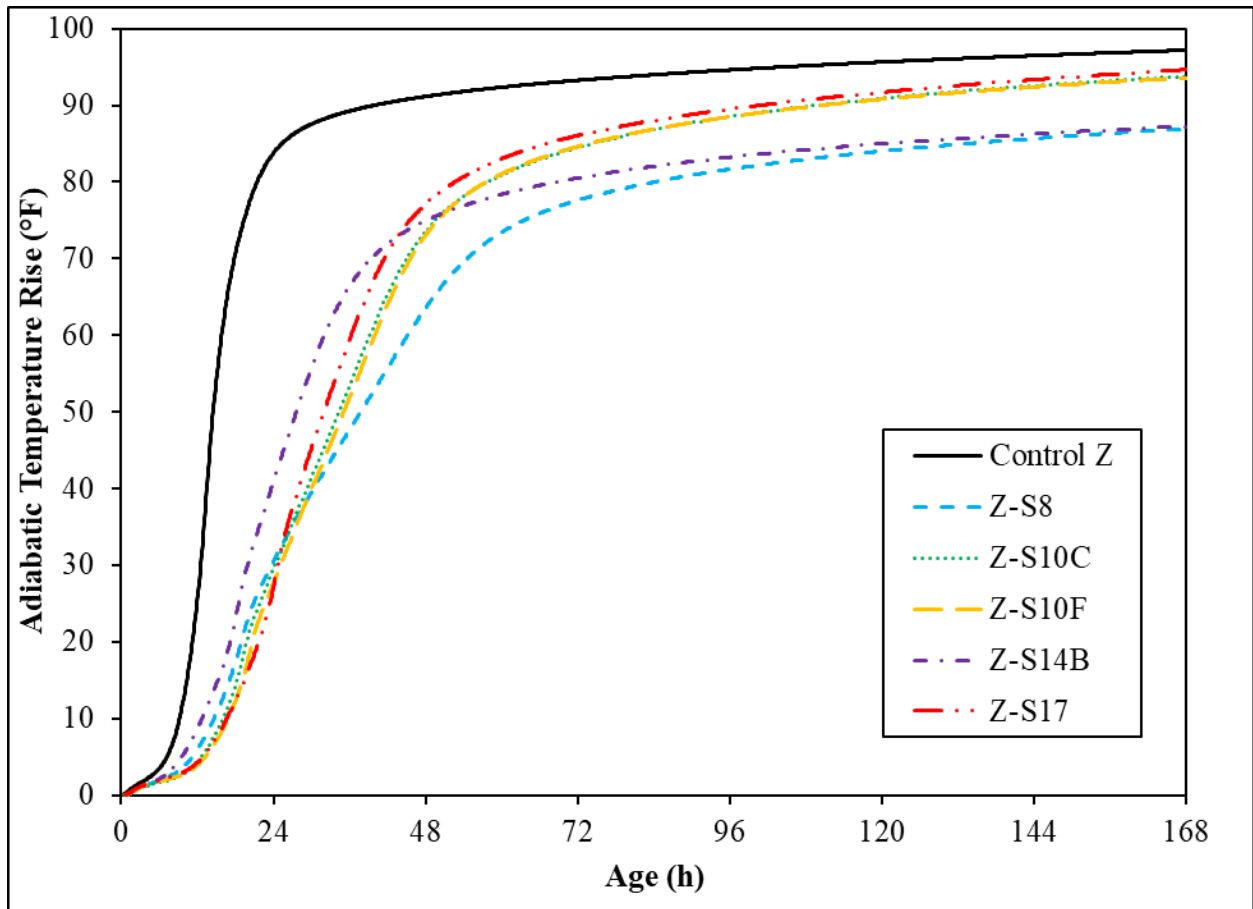
Figure 4-6: Adiabatic temperature rise of the slag-blended mixtures with Type II(MH) cement
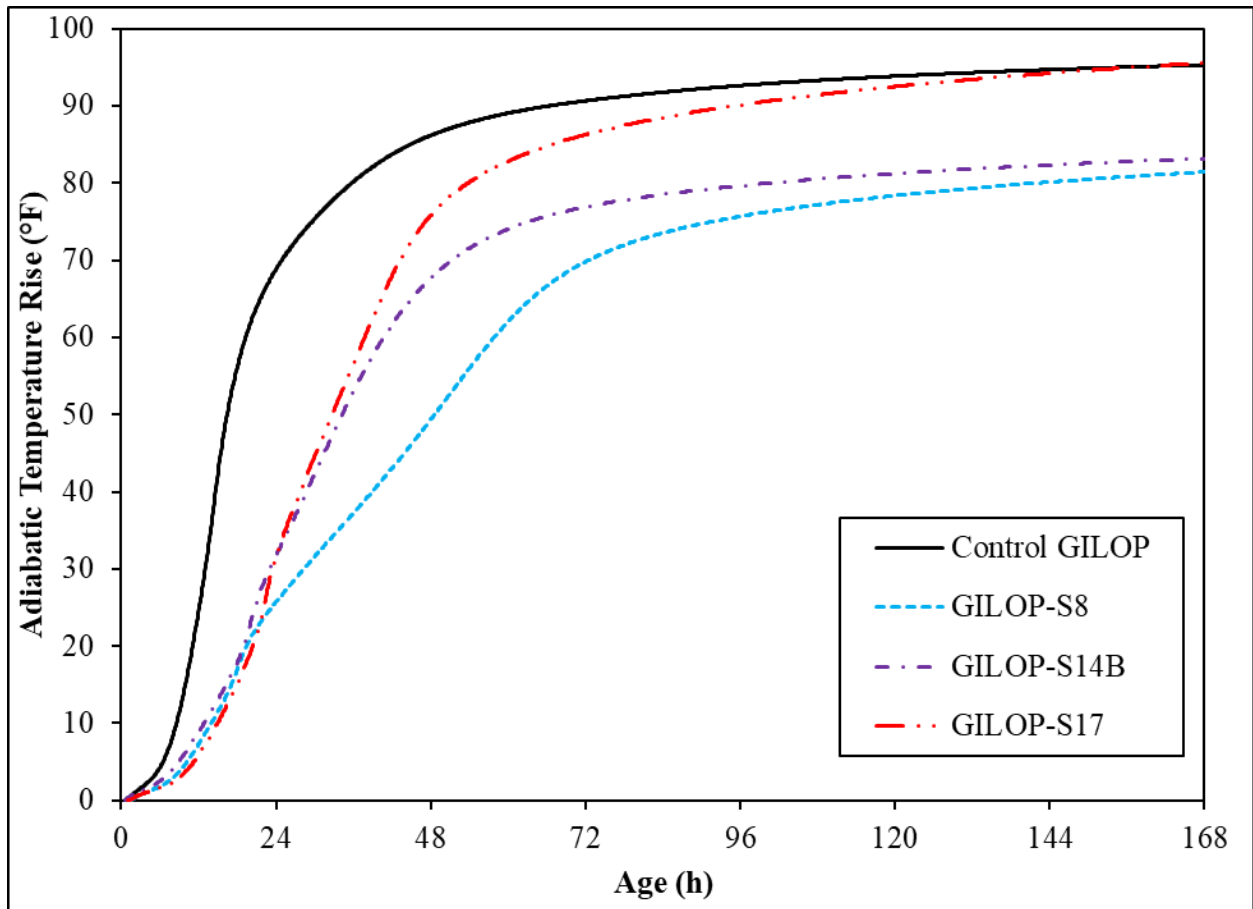
Figure 4-7: Adiabatic temperature rise of the slag-blended mixtures with IL(10) cement
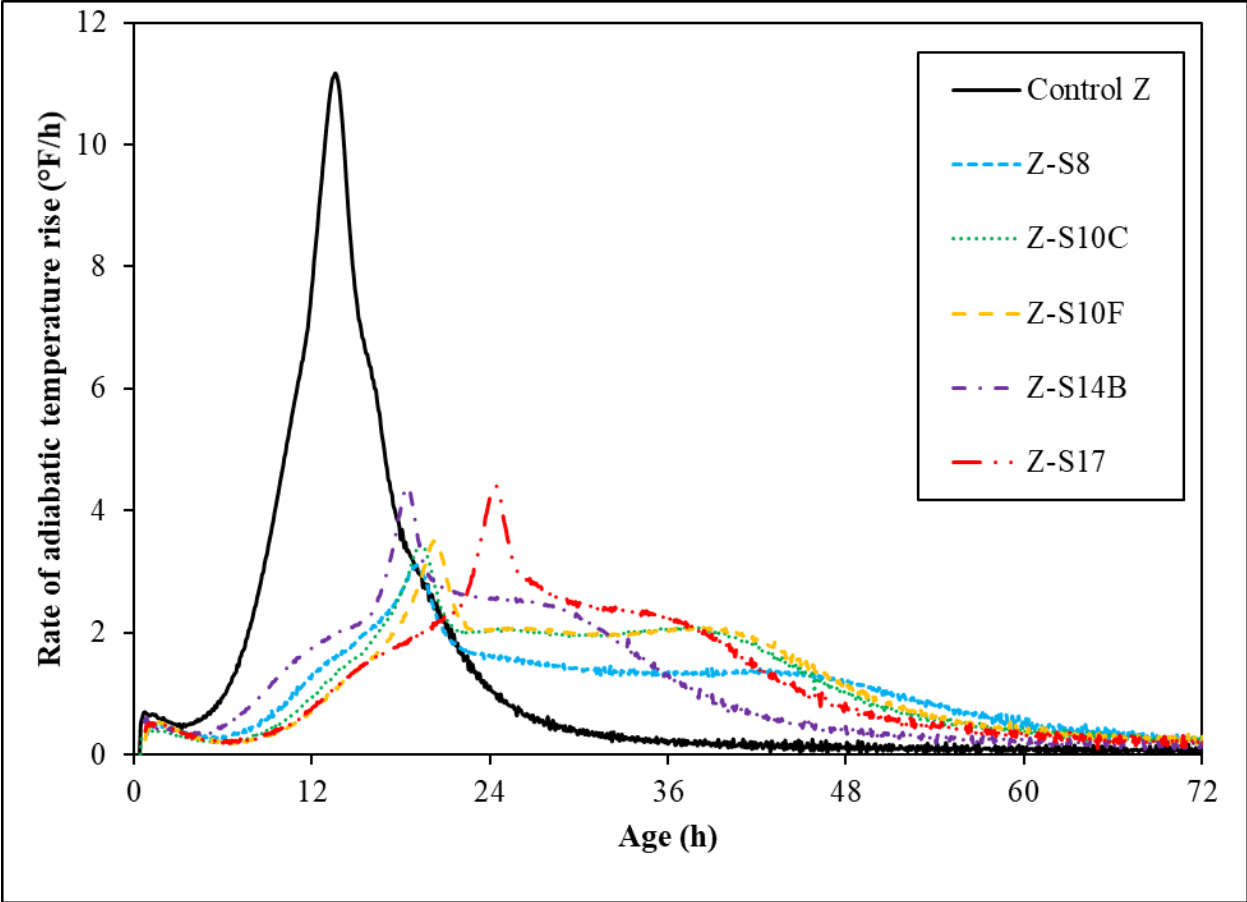
Figure 4-8: Rate of adiabatic temperature rise of slag-blended mixtures with Type II(MH) cement
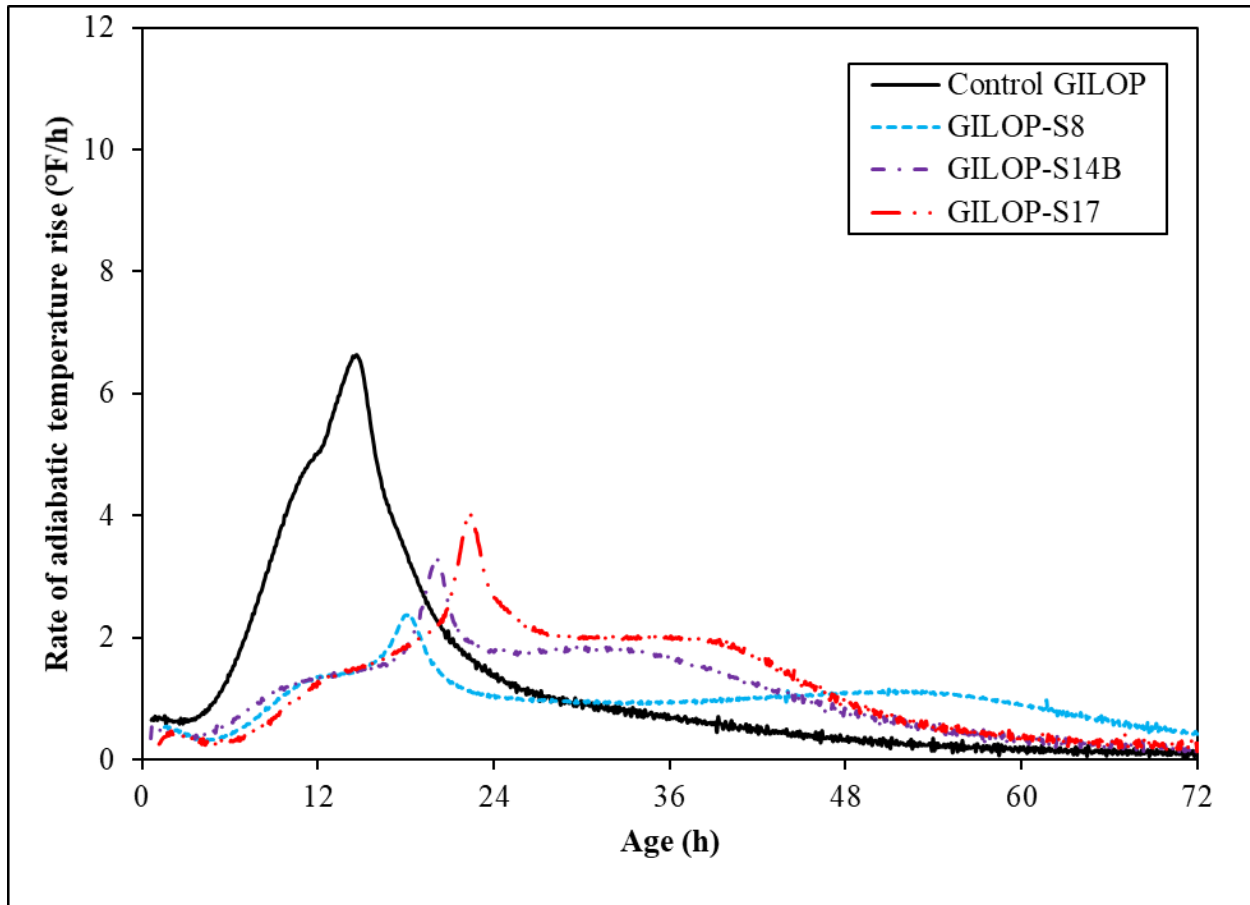
Figure 4-9: Rate of adiabatic temperature rise of the slag-blended mixtures with IL(10) cement

In the blended mixtures, incorporation of slag significantly reduced the temperature rise at 168 h as well as the rate of temperature rise compared to their respective control mixtures, except for GILOP-S17 which was higher than its control mixture. The 168-h adiabatic temperature rise values for the slag mixes with cement Z varied from 86.9°F (48.3°C) to 94.7°F (52.6°C), while this range for the slag mixes with cement GILOP was 81.4°F (45.2 °C) to 95.6°F (53.1°C). The lowest temperature rise was observed with S8 which had the lowest alumina content, while the highest was observed with S17 which had the highest alumina content. During the first 24 h, the lowest rate of temperature rise was observed in the mix with slag S17; however, between 24 and 36 h, the rate of temperature rise increased and surpassed the rest of the slag mixes as expected. This behavior was consistent with both cements, that is, cement Z (Type II(MH)) and GILOP (Type IL(10)). This phenomenon could be due to the higher gypsum content in this slag, which delayed the alumina reaction.

Slags S10C and S10F (about 10% Al_2O_3) showed substantially higher temperature rise at 168 h compared to that of S14B (about 14% Al_2O_3). However, slag S14B had the highest rate of temperature rise compared to all slag mixes as well as the highest temperature rise during the first 24 h. Apart from the Al_2O_3 content, the main difference between S14B and the other slags is the low MgO content (5.6%). Ben Haha et al. [3] calorimetry data showed that during the first 24 hours of hydration, the highest cumulative heat was observed for the slag with the lowest MgO content (at the same Al_2O_3 content). A similar behavior was observed in the stress development of slag-blended concrete mixtures using a slag with 14% Al_2O_3 and low MgO content [5] .

When slag-blended concrete mixtures are used in the field, similar differences between slag temperatures can be observed in the center of mass concrete as the interior of concrete approaches adiabatic conditions. This could cause high temperature differentials and consequently result in thermal cracking. Although several researchers [26]–[28] have suggested that cracking risks can be reduced in concrete with the use of slag (mainly by reducing the cement content), the variability observed in the adiabatic temperature rise of the slag mixtures studied here indicate that varying slag chemical compositions and physical characteristics contribute differently to concrete temperature rise, especially for slags with high alumina content.

4.3.2 Relationship between Adiabatic Temperature Rise and Slag Characteristics

Based on the adiabatic temperature rise profiles, the MgO and Al_2O_3 contents of slags influenced their reactivity, especially during early ages. Therefore, the differences of adiabatic temperature rise of slag mixes compared to their respective control mixes at the age of 36 and 48 h were plotted against the slag Al_2O_3 content as illustrated in Figure 4-10. The temperature difference of slag mixes with cement GILOP correlated well with the slag Al_2O_3 content unlike those with cement Z. However, the MgO/Al_2O_3 ratio of the slags indicated a better correlation with temperature difference for slag mixes with cement Z, as shown in Figure 4-11. An increased MgO/Al_2O_3 ratio appeared to increase the temperature difference compared to the control mixture with both cements. Higher temperature difference indicates a lower adiabatic temperature rise in the slag-blended mixtures.

126
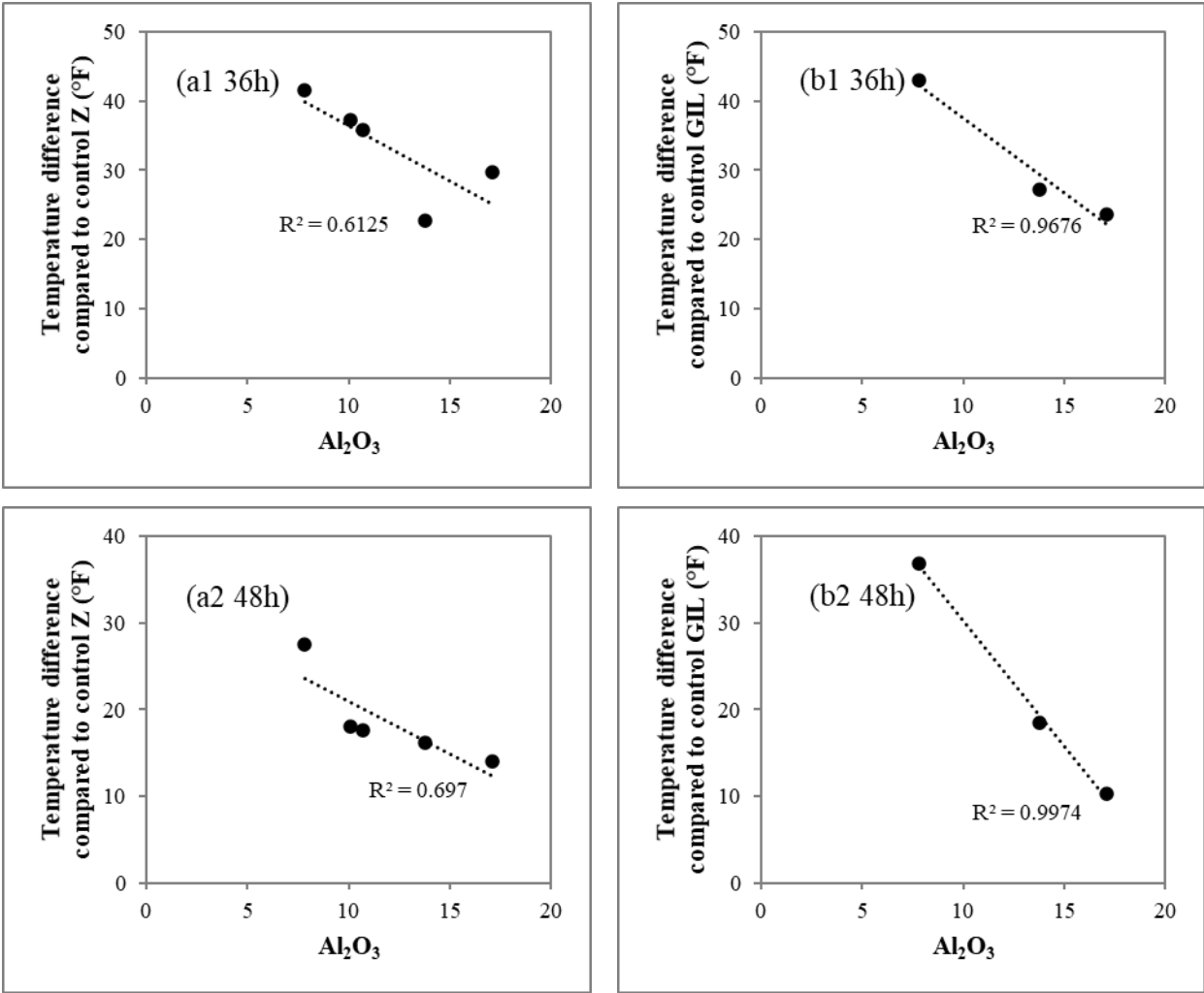
Figure 4-10: Temperature difference of slag mixes compared to the respective control mixes vs. slag Al_2O_3 content: (a) with cement Z (b) with cement GILOP at 36 and 48h
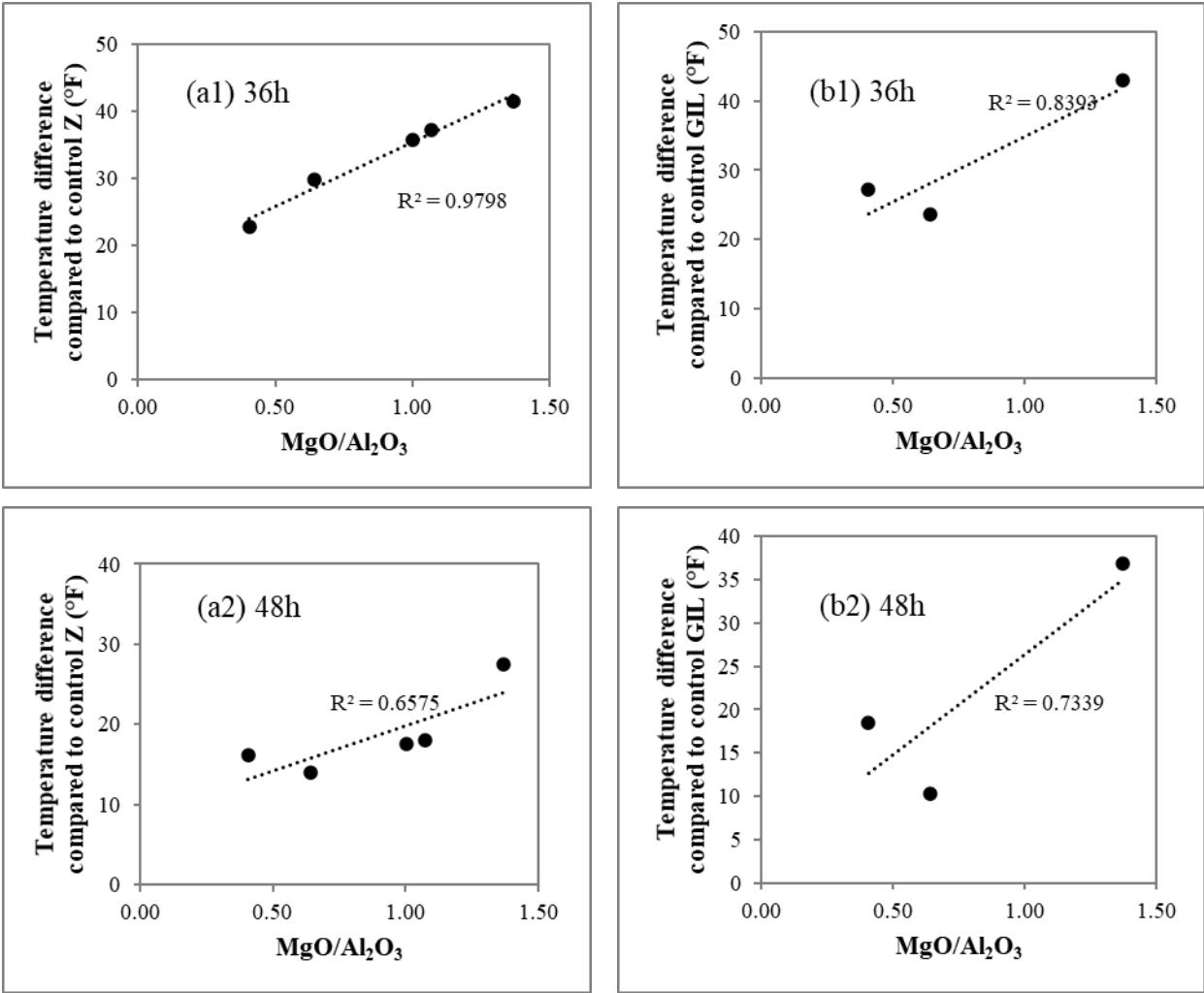
Figure 4-11: Temperature difference of slag mixes compared to the respective control mixes vs. slag MgO/Al_2O_3 ratio: (a) with cement Z (b) with cement GILOP at 36 and 48h

Linear relationships were also observed between the maximum rate of temperature rise of slag mixes and slag Al_2O_3 content and slag MgO/Al_2O_3 ratios, as shown in Figure 4-12 and Figure 4-13, respectively. This indicates the effect of slag chemistry on slag reactivity and hence temperature rise. Since particle size is also known to influence the reactivity of cementitious materials, MgO/Al_2O_3 ratio was scaled by the MPS (mean particle size), and the product of MPS and MgO/Al_2O_3 ratio was compared to the maximum rate of temperature rise, as shown in Figure 4-14. The R^2 of the linear relationship between the maximum rate of temperature rise and the calculated parameter improved from 0.95 to 0.96 for cement Z mixes and 0.58 to 0.67 for cement GILOP mixes.

128
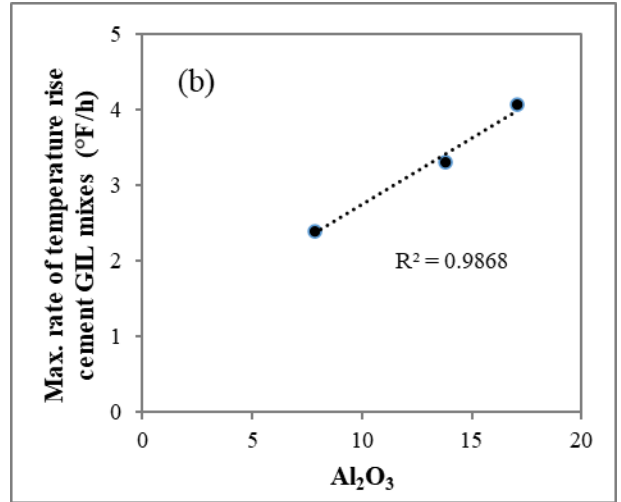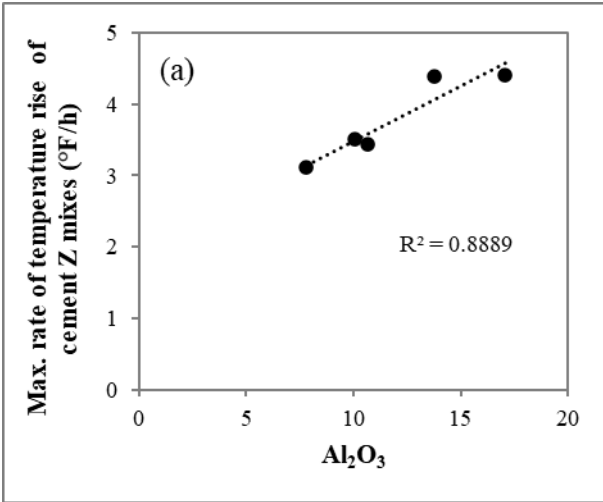
Figure 4-12: Max. rate of temperature rise of slag-blended mixes vs. slag Al_2O_3 contents: (a) with cement Z (b) with cement GILOP
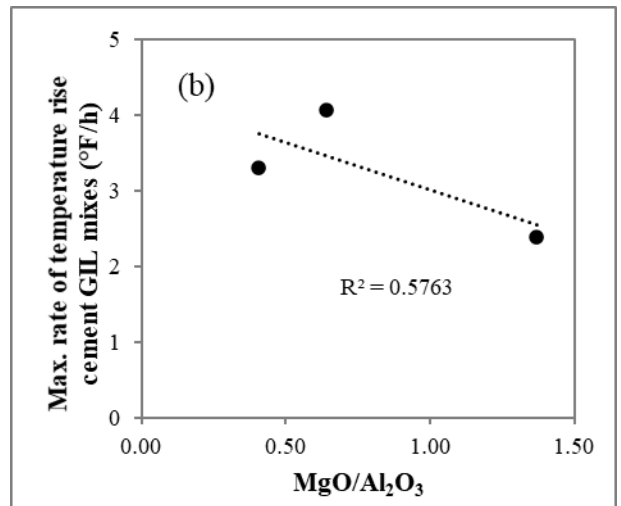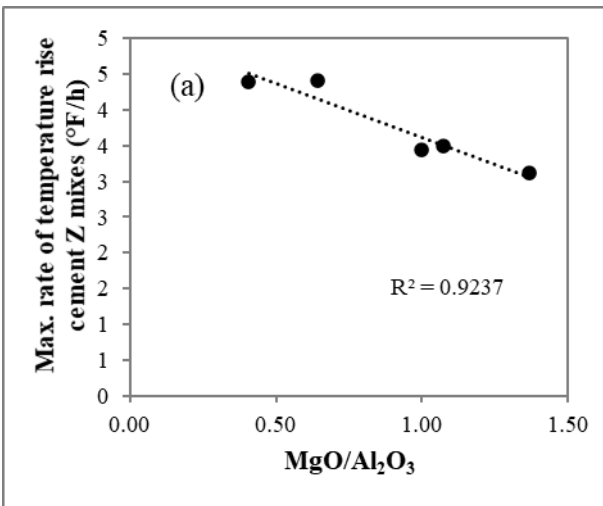
Figure 4-13: Max. rate of temperature rise of slag-blended mixes vs. slag MgO/Al_2O_3 ratios: (a) with cement Z (b) with cement GILOP
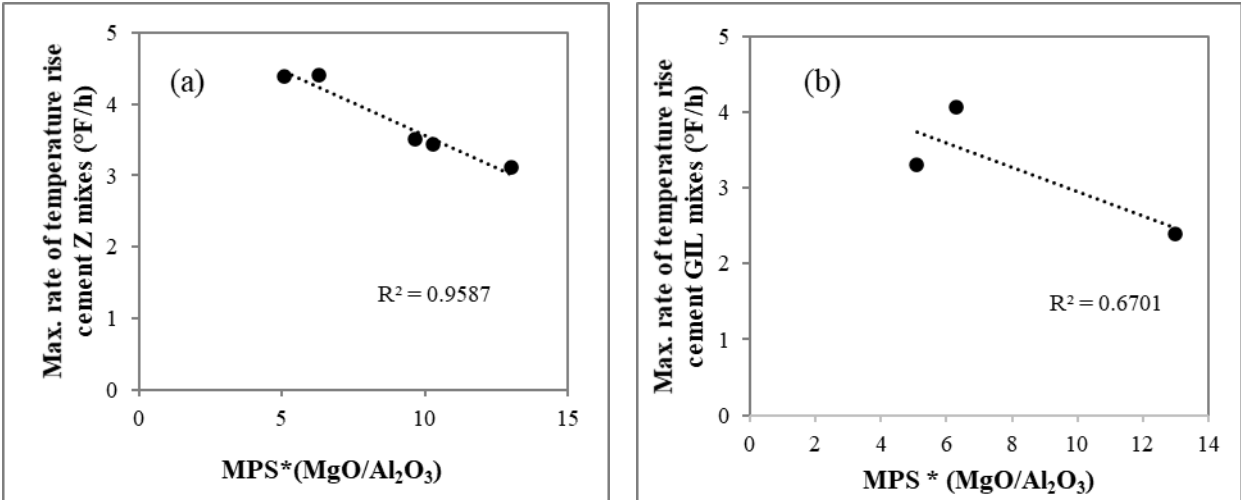
Figure 4-14: Max. rate of temperature rise of slag-blended mixes vs. slag $MPS*(MgO/Al_2O_3)$ ratios: (a) with cement Z (b) with cement GILOP

Figure 4-14 clearly indicates the effect of cement properties on the reactivity of the cementitious system. Therefore, the influence of cement was incorporated into the relationship considering its C_3S, C_3A and $CaCO_3$ (calcite) contents, determined using quantitative X-ray diffraction coupled with Rietveld refinement. The maximum rate of temperature rise of all mixtures considered in this study (inclusive of the control mixtures) was included in this linear relationship as illustrated in Figure 4-15. The P_{cem} and P_{slag} parameters indicate the fractions of cement and slag in the system. The max. rate of temperature rise correlated well with the parameter $[P_{cem}*(C_3S+4C_3A-CaCO_3) + P_{slag}*(Al_2O_3)]$ with an R^2 value of 0.96. A better relationship could be established using statistical means. It is also to be remembered that the relationship was established for 10 cementitious mixtures with 60% cement substitution using Type II(MH) and IL(10) cements and slags with alumina content between 8% to 17%. The relationship is therefore limited to those conditions.
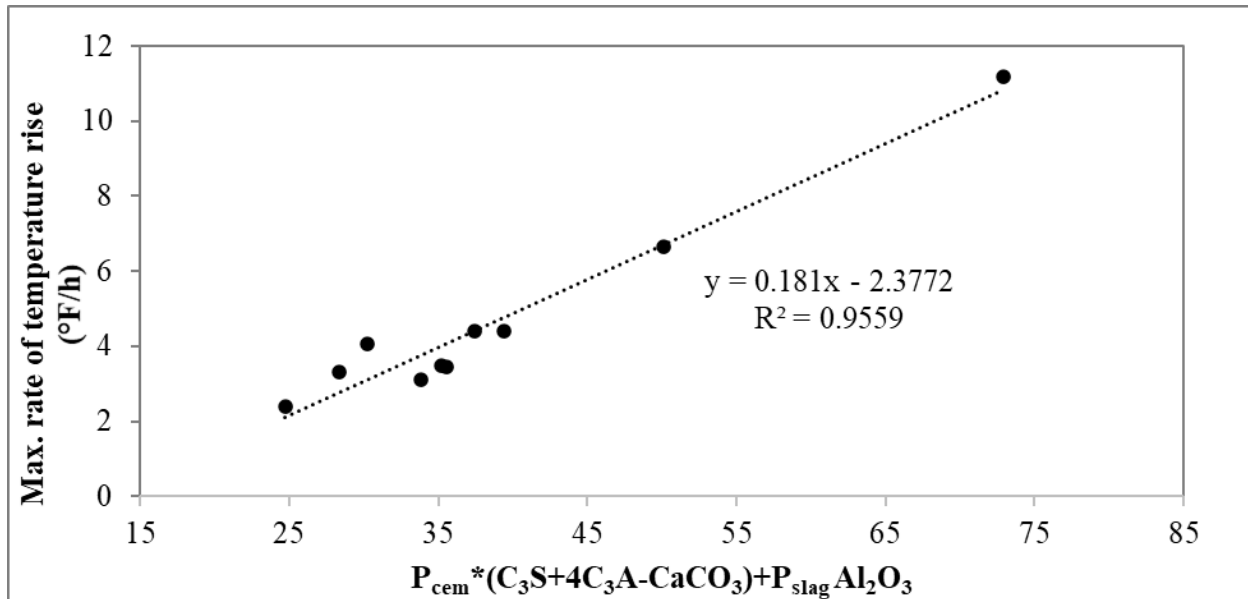
Figure 4-15: Max. rate of temperature rise of concrete mixes vs. $P_{cem}*(C_3S+4C_3A-CaCO_3)$ + $P_{slag}*(Al_2O_3)$

4.3.3 Isothermal Calorimetry

Isothermal calorimetry tests were essential to conduct in order to accurately perform sensitivity studies on the mixtures studied here. Isothermal calorimetry were conducted in duplicate for each mixture. The heat of hydration results of the paste mixtures are shown in Figures Figure 4-16 through Figure 4-21 at the respective temperatures of 23, 30, and 40°C (73.4, 86, and 104°F). Table 4-8 provides the total heat generated by the mixtures at an age of 3 days and an isothermal temperature of 23°C. At all temperatures, mixes with slag S8 yielded the lowest cumulative heat of hydration when blended with both cement Z and cement GILOP. As observed from the adiabatic temperature rise results, both cement Z with slag S14B and cement GILOP with slag S14B had slightly higher reactivity during the first 20 hours compared to all other slag blends, which can be attributed to the lower MgO content of S14B. Afterwards however, their rates of hydration slowed down and leveled off at lower cumulative heats of hydration than those of slag with 10% alumina. In terms of cement GILOP mixes, GILOP with S17 showed the highest heat of hydration at all temperatures, indicating the significance of its high alumina content on reactivity. With cement Z mixes, Z+S17 showed the highest cumulative heat at 23°C (73.4°F at 168 h), but cumulative heat was similar to Z+S10F at 30°C (86°F) at 120 h. At 40°C (104°F)

however, the cumulative heat at 72h was the highest for the Z+S10F mix. This indicates the significance of curing temperature on slag reactivity. Unlike adiabatic calorimetry temperature profiles, there is a clear distinction between the heat of hydration of S10F and S10C mixes at all temperatures. Z+S10F mixes showed slightly higher total heats, which can be attributed to the higher fineness of S10F compared to S10C at similar alumina content. The effect of fineness cannot be extrapolated from this limited work as there can be a combined effect of fineness and alumina content that can be also affected by the cement replacement level.
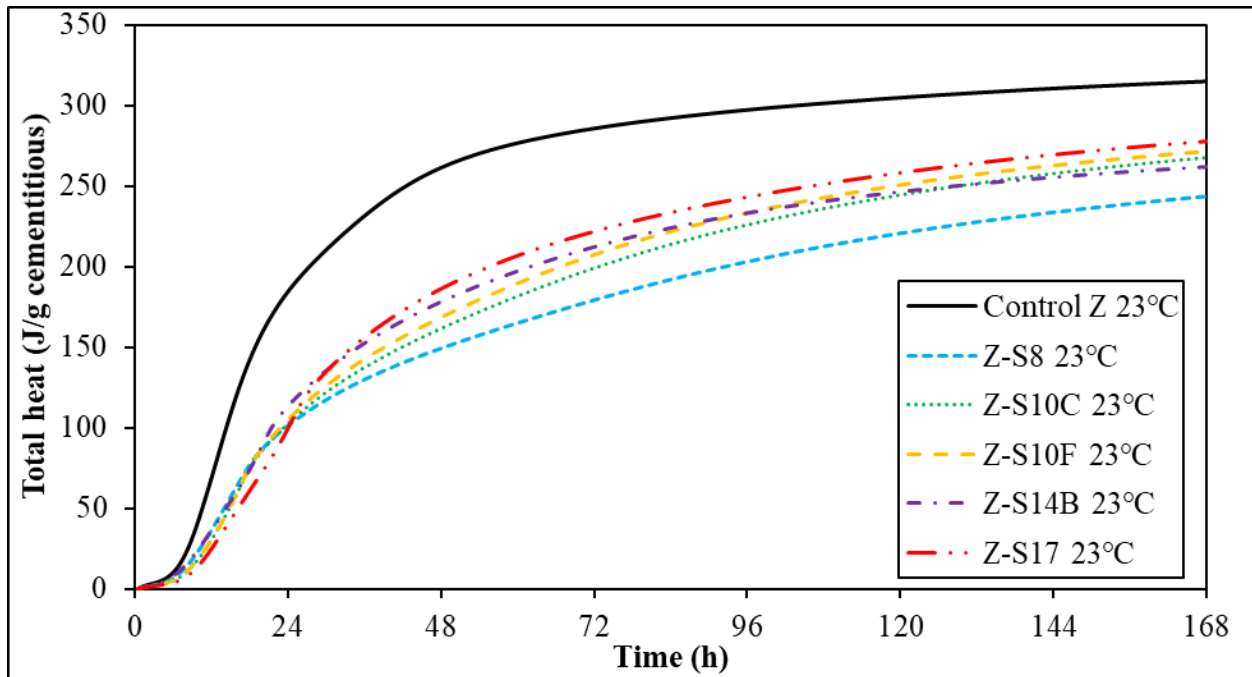
Figure 4-16: Heat of hydration of paste mixtures with cement Z at 23°C (73.4°F)
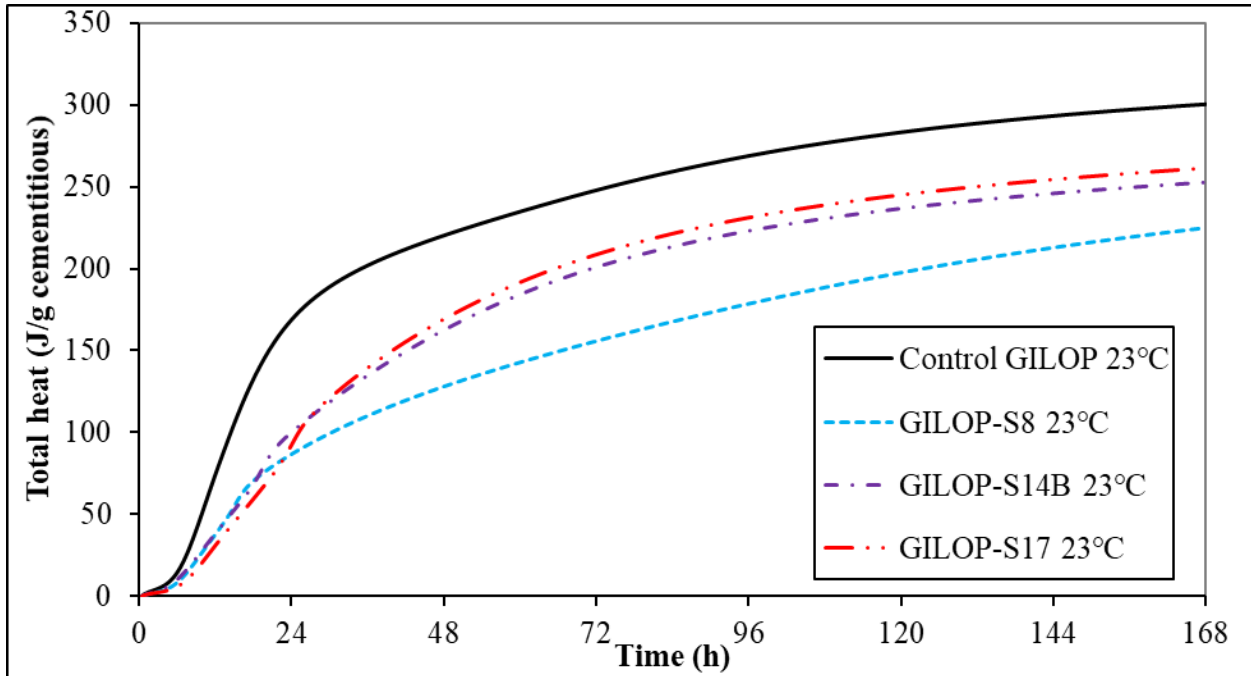
Figure 4-17: Heat of hydration of paste mixtures with cement GIL-OP at 23°C (73.4°F)
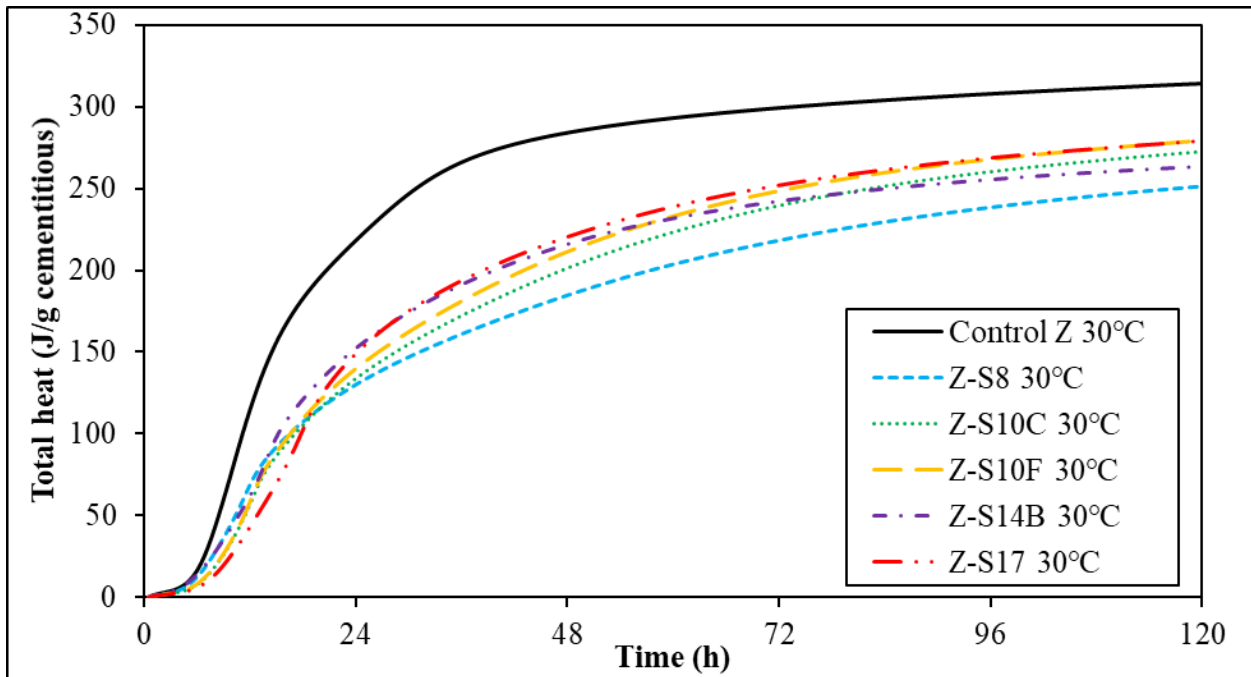
Figure 4-18: Heat of hydration of paste mixtures with cement Z at 30°C (86°F)

133
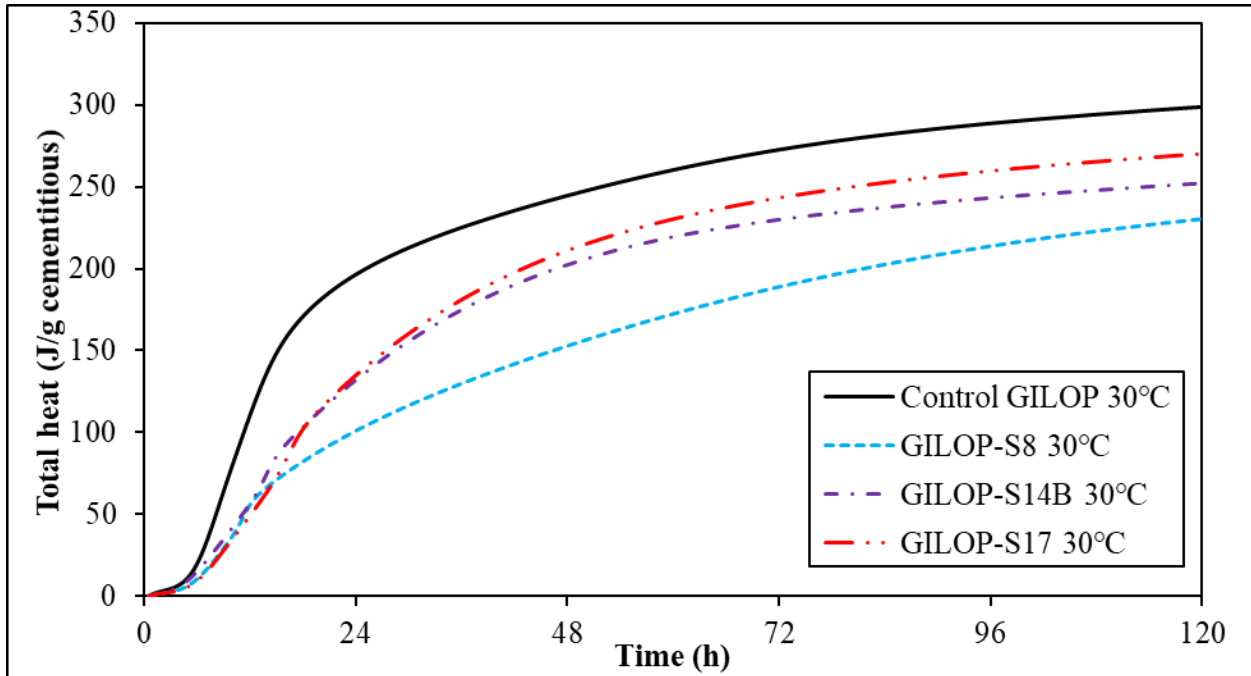
Figure 4-19: Heat of hydration of paste mixtures with cement GIL-OP at 30°C (86°F)
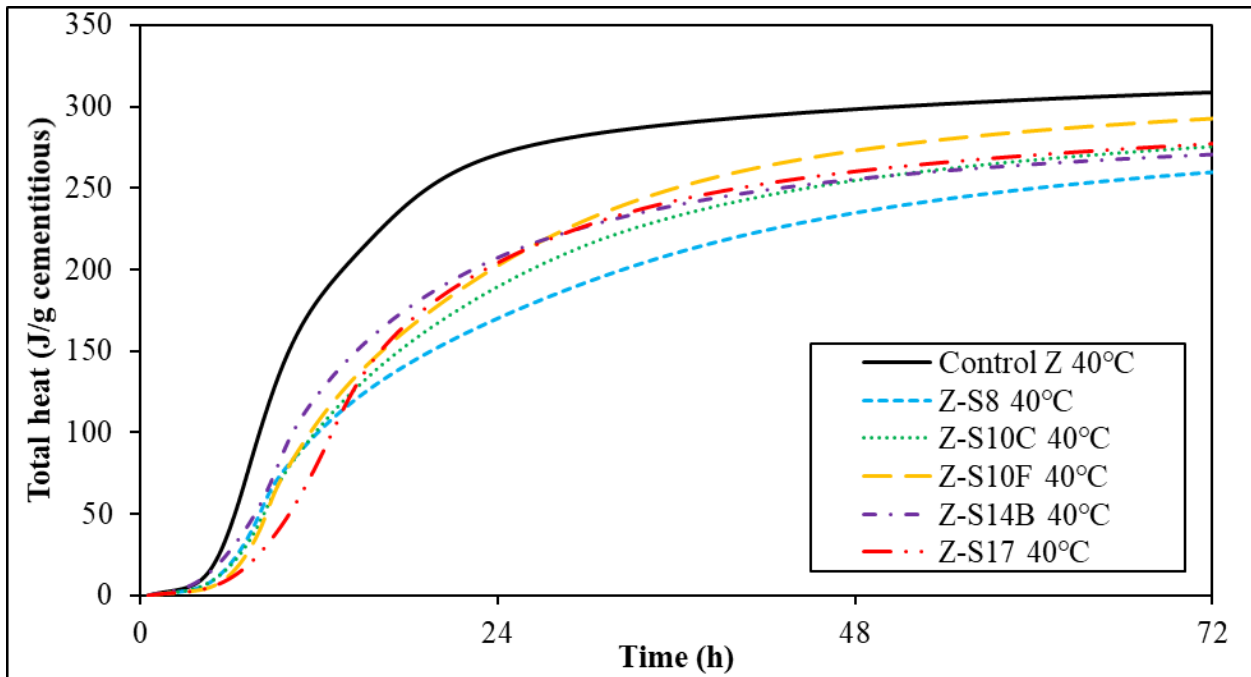
Figure 4-20: Heat of hydration of paste mixtures with cement Z at 40°C (104°F)
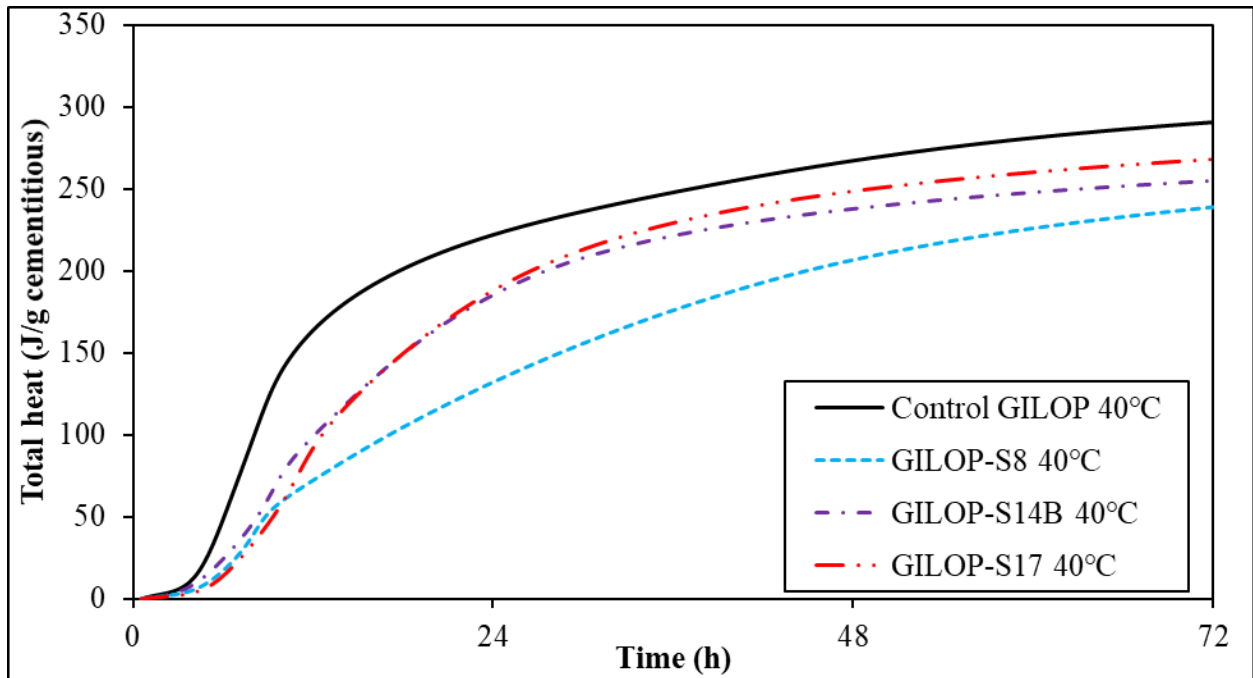
Figure 4-21: Heat of hydration of paste mixtures with cement GIL-OP at 40°C (104°F)

Table 4-8: Heat of hydration of paste at 23°C (73.4°F)

Mix ID	Heat of hydration at 3 days (J/g cementitious)
Control Z	286
Control GILOP	248
Z-S8	179
Z-S10C	199
Z-S10F	208
Z-S14B	212
Z-S17	222
GILOP-S8	156
GILOP-S14B	201
GILOP-S17	209

Typically, E_a is calculated by only varying τ, while keeping α_u and β fixed. This method assumes that the ultimate degree of hydration of a mixture is not affected by the curing temperature. However, to eliminate this assumption, several studies [29], [30] calculated the E_a by

135

varying the three parameters; α_u, β, and τ. In the current study, the same method was used to determine E_a, and the calculated E_a values and the hydration parameters are listed in Table 4-9 and Table 4-10. The variation of β and τ with the curing temperature is consistent with the literature [29], [30]. The β value which corresponds to the slope of the major linear part of the hydration curve appeared to increase with increasing the slag alumina content indicating a higher rate of hydration. As expected, τ values are higher in the slag mixes owing to the slower hydration of the slag-blended systems. In terms of E_a values, and similar to the published literature [10], [31], [32], the incorporation of slag increased the E_a compared to their respective control mixtures.

Table 4-9: HOH based activation energy for cement Z mixes

Mix ID	Temp(°C)	α_u	β	τ	Ea (kJ/mol)	R^2
Control Z	23	0.826	1.371	16.133	28.337	1.00
	30	0.819	1.504	12.439		
	40	0.793	1.838	8.637		
Z-S8	23	0.833	0.624	39.04	43.765	0.99
	30	0.779	0.737	23.45		
	40	0.738	0.981	14.72		
Z-S10C	23	0.863	0.719	37.01	45.483	1.00
	30	0.801	0.870	23.38		
	40	0.726	1.212	13.52		
Z-S10F	23	0.822	0.796	32.77	39.975	1.00
	30	0.788	0.942	21.71		
	40	0.757	1.311	13.52		
Z-S14B	23	0.710	0.957	25.25	37.641	0.99
	30	0.674	1.139	16.73		
	40	0.667	1.407	10.94		
Z-S17	23	0.688	1.203	25.66	30.220	1.00
	30	0.702	1.280	19.37		
	40	0.663	1.789	13.18		

Table 4-10: HOH based activation energy for cement GILOP mixes

Mix ID	Temp(°C)	α_u	β	τ	Ea (kJ/mol)	R^2
Control GILOP	23	0.986	0.882	18.050	31.461	1.00
	30	0.940	1.043	13.117		
	40	0.895	1.177	8.994		
GILOP-S8	23	1.000	0.494	65.70	38.714	1.00
	30	0.983	0.562	44.82		
	40	0.983	0.686	27.91		
GILOP-S14B	23	0.778	0.836	29.92	39.285	0.99
	30	0.706	1.044	18.86		
	40	0.683	1.296	12.46		
GILOP-S17	23	0.753	0.996	29.06	34.476	1.00
	30	0.753	1.099	20.51		
	40	0.708	1.423	13.55		

4.3.4 Sensitivity Analysis

As it was observed from the adiabatic calorimetry results, the differences in slag chemistry affect the temperature rise of the slag-blended systems. These effects can be magnified in the mass concrete elements and subsequently result in thermal cracking. The effect can vary depending on the volume of the concrete element. Therefore, a sensitivity analysis was performed using ConcreteWorks software [33]. To this end, hydration parameters α_u^*, β^*, and τ^* were determined for concrete from the adiabatic calorimetry data and the activation energy determined from isothermal calorimetry. The data were fit to Equation 4-6. The determined adiabatic hydration parameters and the activation energy values are listed in Table 4-11. The change in predicted maximum temperature and maximum temperature difference with variable dimensions of a square column were investigated in the analysis. Moreover, the analyses were performed at two different placement temperatures, 60°F (15.5°C) and 80°F (26.7°C), to account for the differences in weather conditions during construction. The mixture placed at 60°F (15.5°C) was analyzed assuming a placement date of December 1 at 7 am in Jacksonville, FL, while the mixture placed at 80°F (26.7°C) was analyzed assuming a placement of date of August 1 at 7 am in Jacksonville, FL. Uninsulated steel forms removed 14 days after placement were assumed in the analysis.

Table 4-11: Adiabatic hydration parameters

Parameter Mix ID	E_a (J/mol)	$H_u \cdot \alpha_u^*$ (J/kg)	β^*	τ^*
Control Z	28,337	358,400	1.528	12.726
Control GILOP	31,461	362,366	0.980	14.076
Z-S8	43,765	337,405	0.792	26.523
Z-S10C	45,483	319,391	0.863	27.012
Z-S10F	39,975	350,912	0.970	26.030
Z-S14B	37,641	322,879	1.039	21.260
Z-S17	30,220	347,374	1.240	24.047
GILOP-S8	38,714	336,447	0.744	34.001
GILOP-S14B	39,285	315,191	0.982	24.112
GILOP-S17	34,476	357,926	1.021	26.982

Figures Figure 4-22 through Figure 4-24 illustrate the predicted maximum temperature, the difference in maximum temperature compared to control and the maximum temperature difference within the element for cement GILOP mixes at a placement temperature of 60°F (15.5°C). Figures

138

Figure 4-25 through Figure 4-27 show the same predicted output for cement GILOP mixes, but at a placement temperature of 80°F (26.7°C). Predicted results follow the trends observed in the adiabatic calorimetry results. As expected, the larger the concrete element, the higher the temperature within the element as well as the temperature difference between the core and corner. Inclusion of slags substantially decreased the maximum temperature and the temperature difference, especially with smaller elements. However, this benefit decreased with member size, especially for slag S17. Therefore, the use of slags with high alumina contents in larger concrete elements may require more mitigation measures in thermal control plans than those made with lower alumina slags in smaller members. This effect was exaggerated in hot weather.
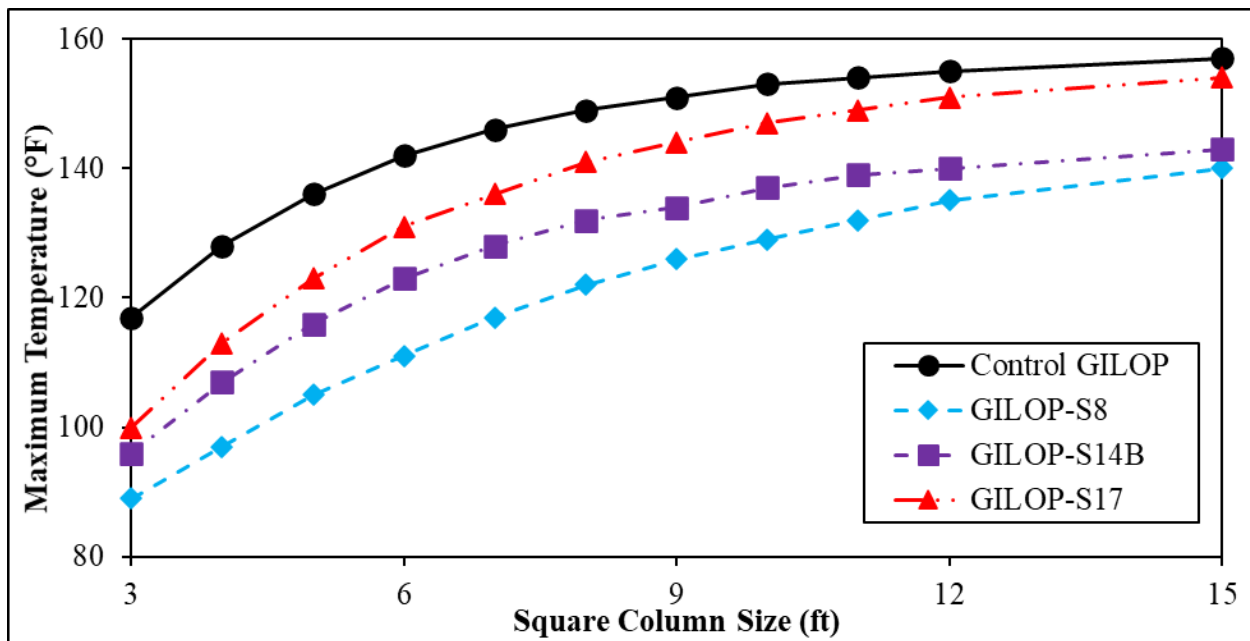
Figure 4-22: Predicted maximum temperature for cement GILOP mixes at 60°F (15.5°C) placement temperature
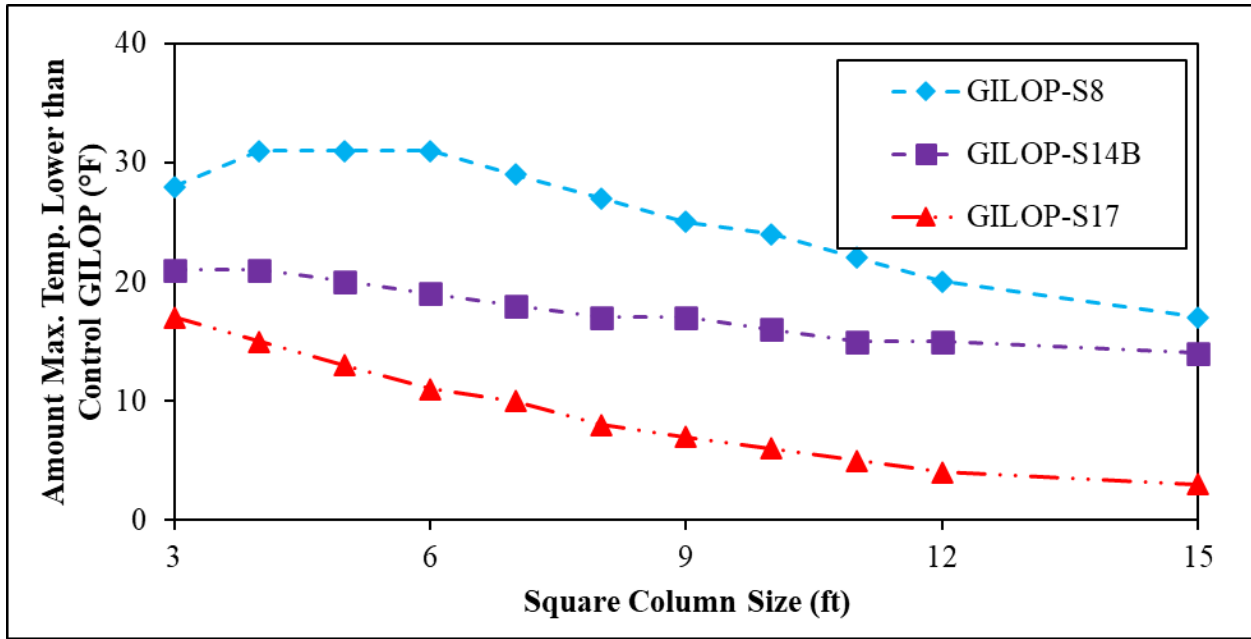
Figure 4-23: Amount maximum temperature for cement GILOP mixes was calculated to be lower than control GILOP at 60°F (15.5°C) placement temperature
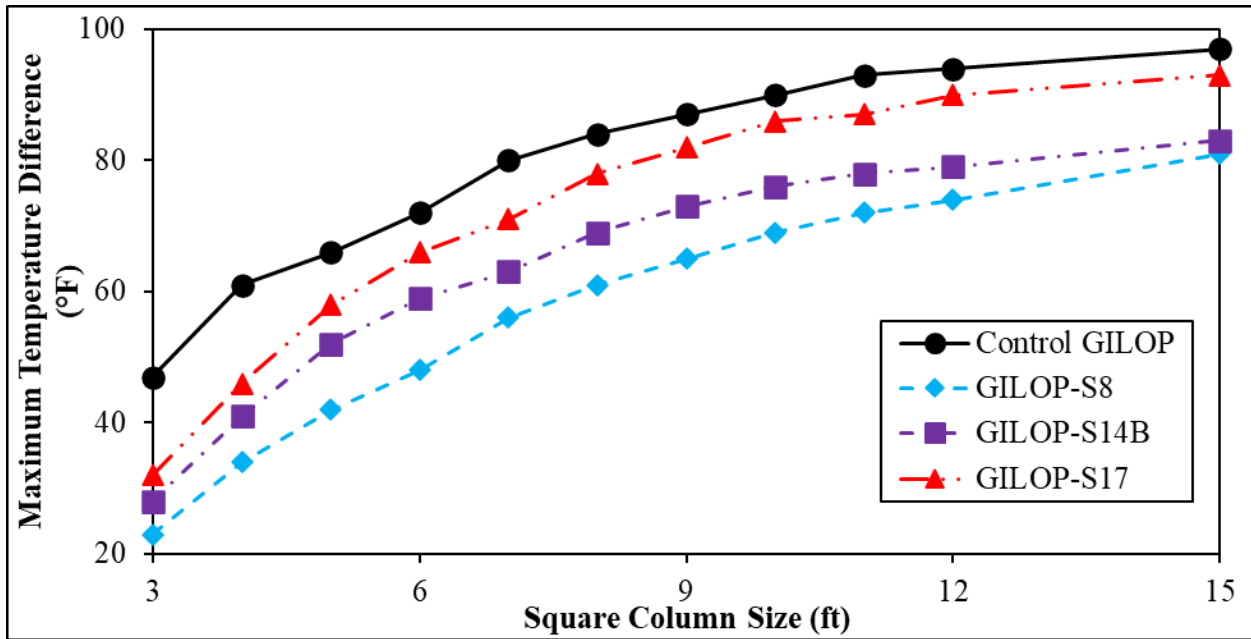
Figure 4-24: Predicted maximum temperature difference for cement GILOP mixes at 60°F (15.5°C) placement temperature
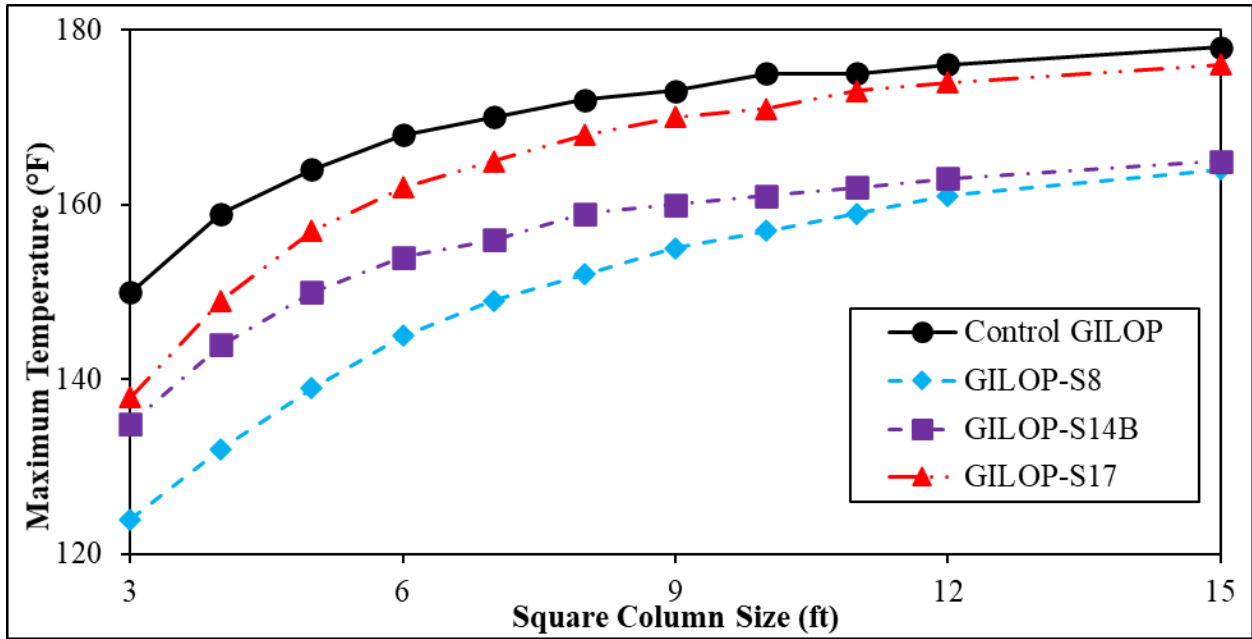
Figure 4-25: Predicted maximum temperature for cement GILOP mixes at 80°F (26.7°C) placement temperature
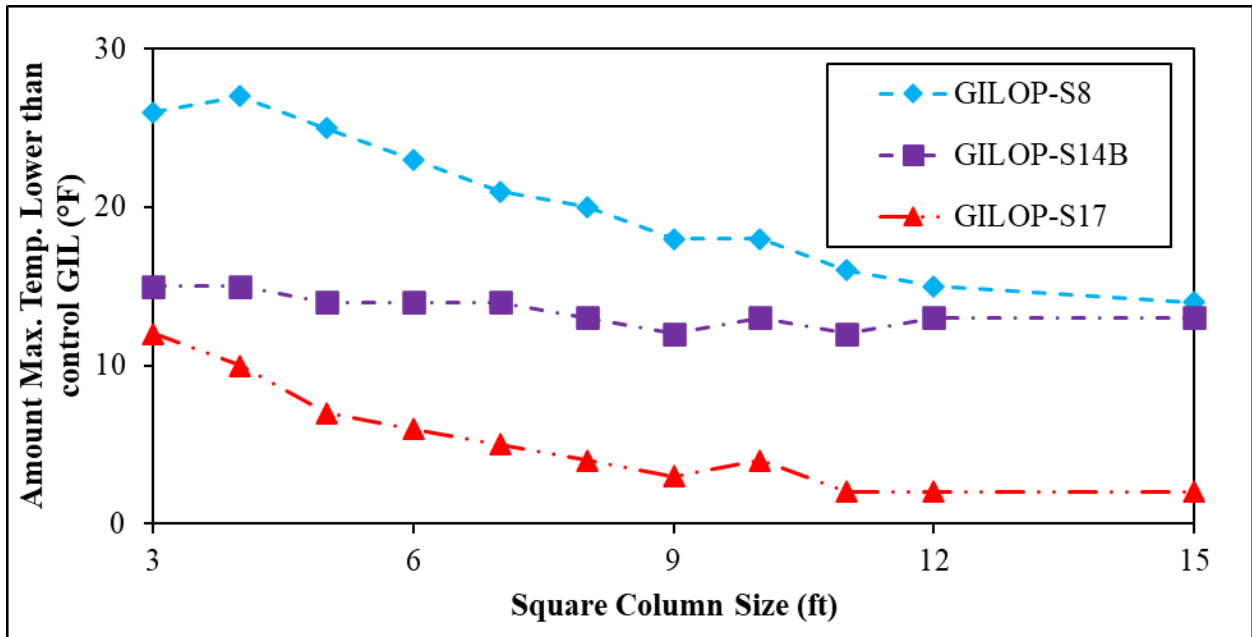
Figure 4-26: Amount maximum temperature for cement GILOP mixes was calculated to be lower than control GIL at 80°F (26.7°C) placement temperature
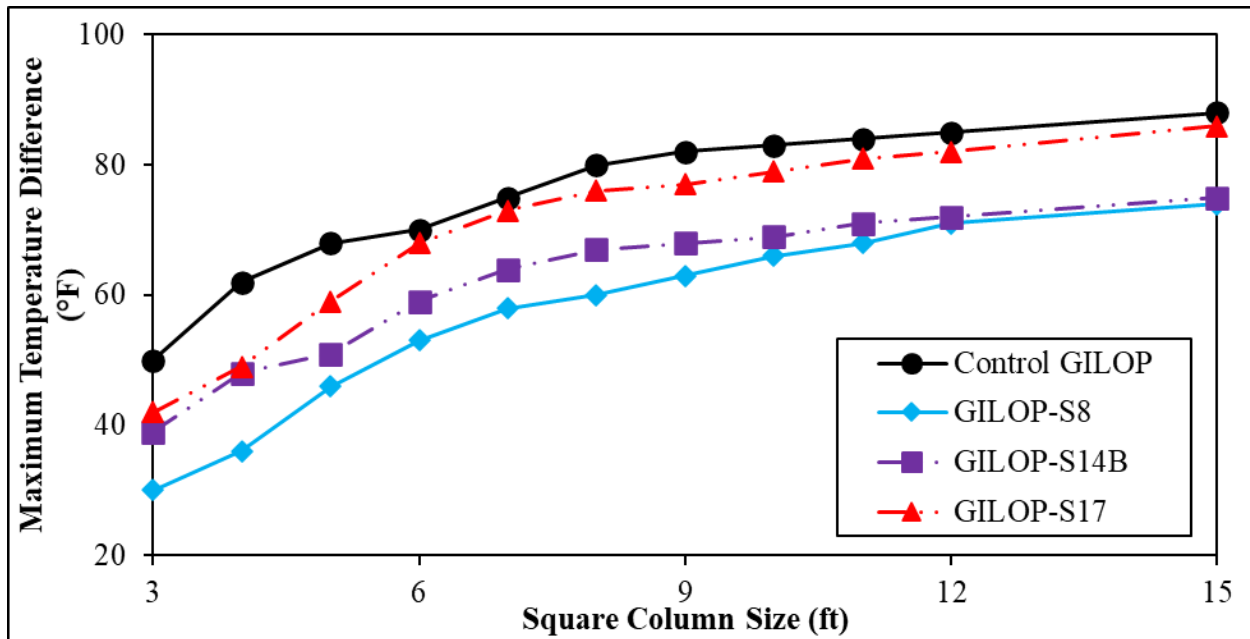
Figure 4-27: Predicted maximum temperature difference for cement GILOP mixes at 80°F (26.7°C) placement temperature

The same parameters were predicted for cement Z mixes at the same placement temperatures. Figures Figure 4-22 through Figure 4-30 illustrate the predicted maximum temperature, the difference in maximum temperature compared to control and the maximum temperature difference within the element for cement Z mixes at the placement temperature of 60°F (15.5°C). Figures Figure 4-31 through Figure 4-33 show the same predicted output for cement Z mixes, but at the placement temperature of 80°F (26.7°C). Similar to cement GILOP mixes, predicted results for cement Z mixes also followed the same trends observed in the adiabatic calorimetry experiments. Use of slags with cement Z clearly reduced the temperature within the element. This temperature drop in cement Z mixes is higher than that of cement GILOP mixes. However, this effect was only significant for smaller elements. Larger elements had temperatures that approached the maximum temperature of the control mix. Moreover, the maximum temperature and temperature difference in Z-S10C and Z-S10F mixes showed very close behavior to those of Z-S17, especially with larger concrete elements indicating the significance of fine grinds even at slag alumina content of 10%.
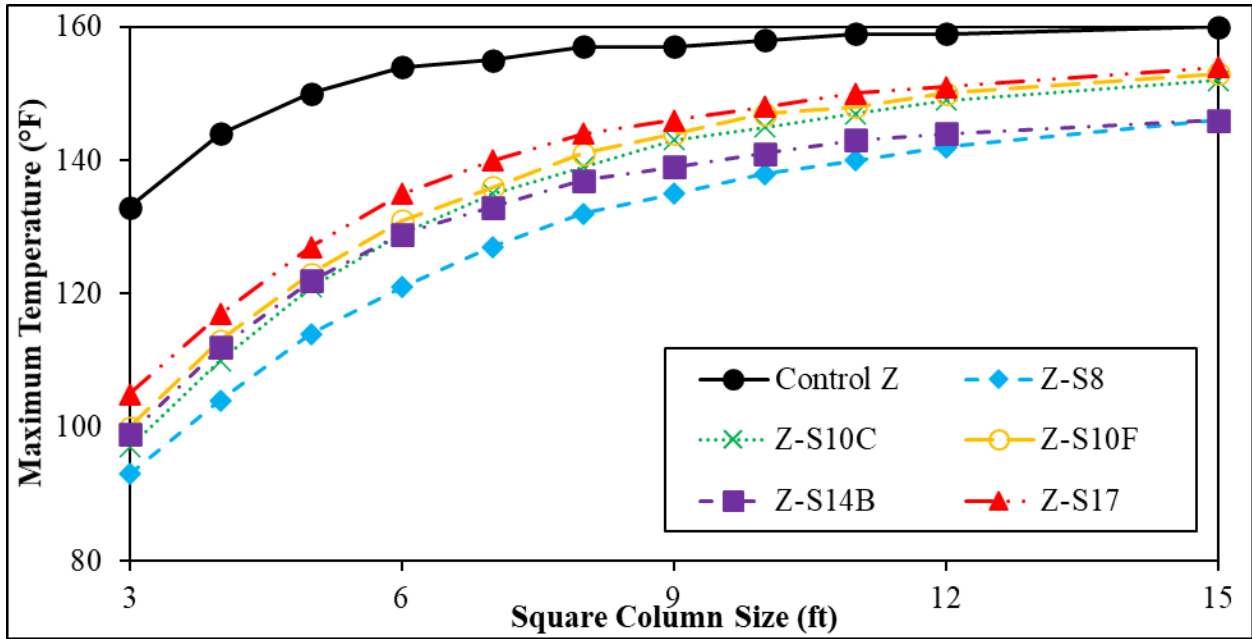
Figure 4-28: Predicted maximum temperature for cement Z mixes at 60°F (15.5°C) placement temperature
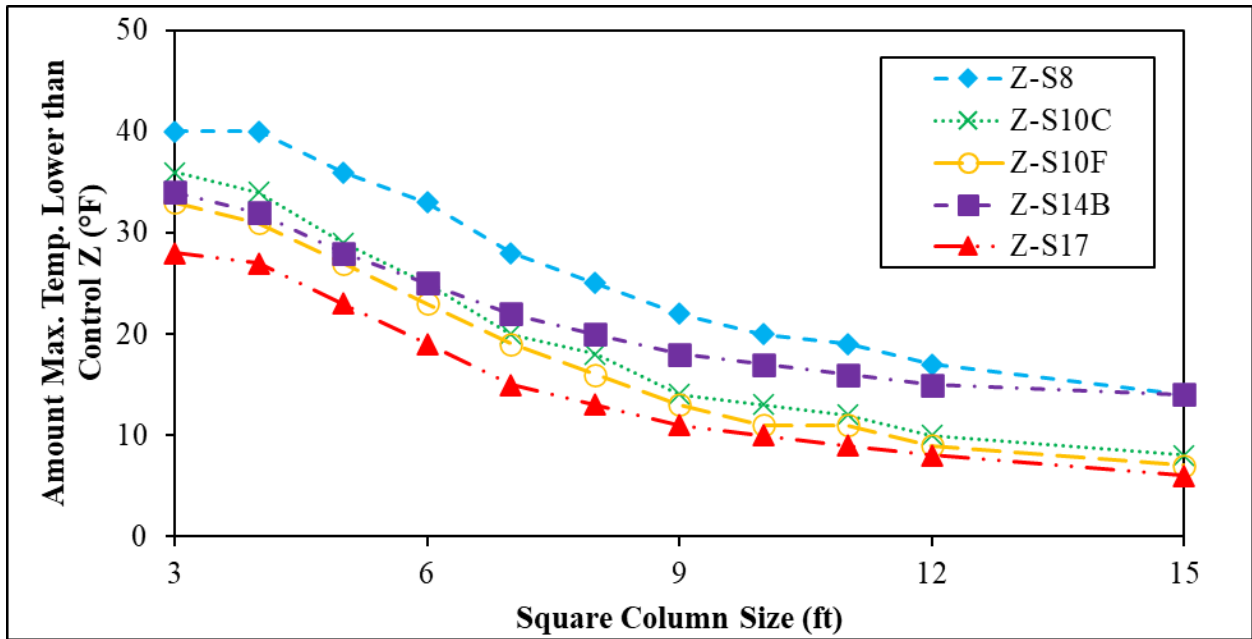
Figure 4-29: Amount maximum temperature for cement Z mixes was calculated to be lower than control Z at 60°F (15.5°C) placement temperature
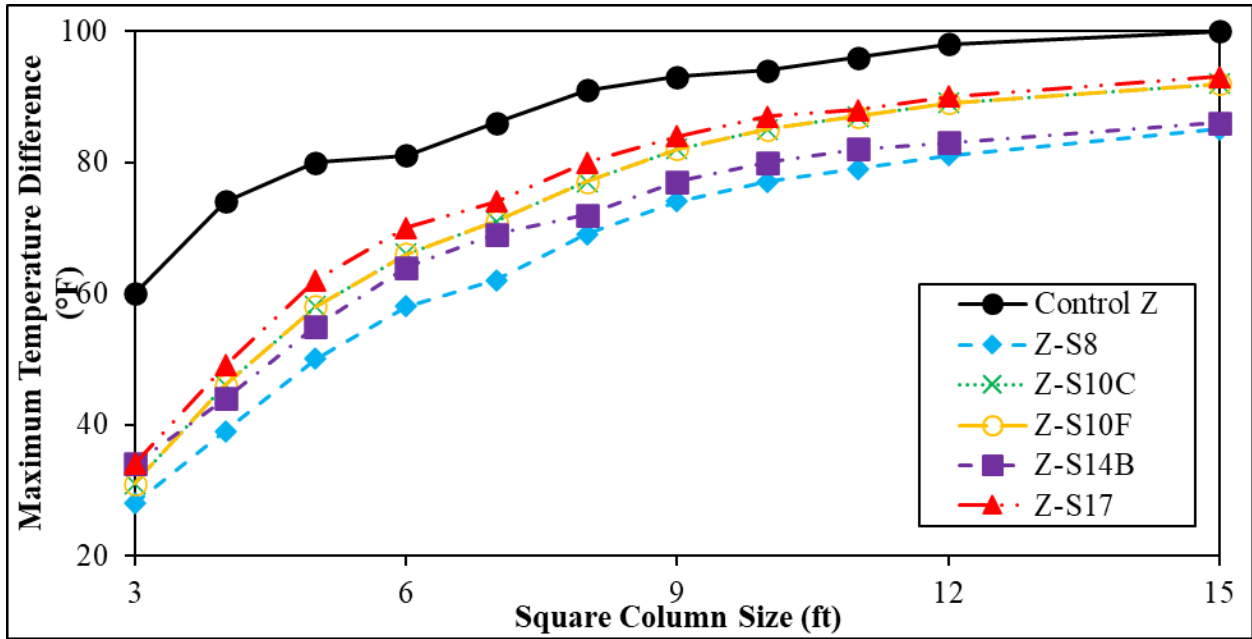
Figure 4-30: Predicted maximum temperature difference for cement Z mixes at 60°F (15.5°C) placement temperature
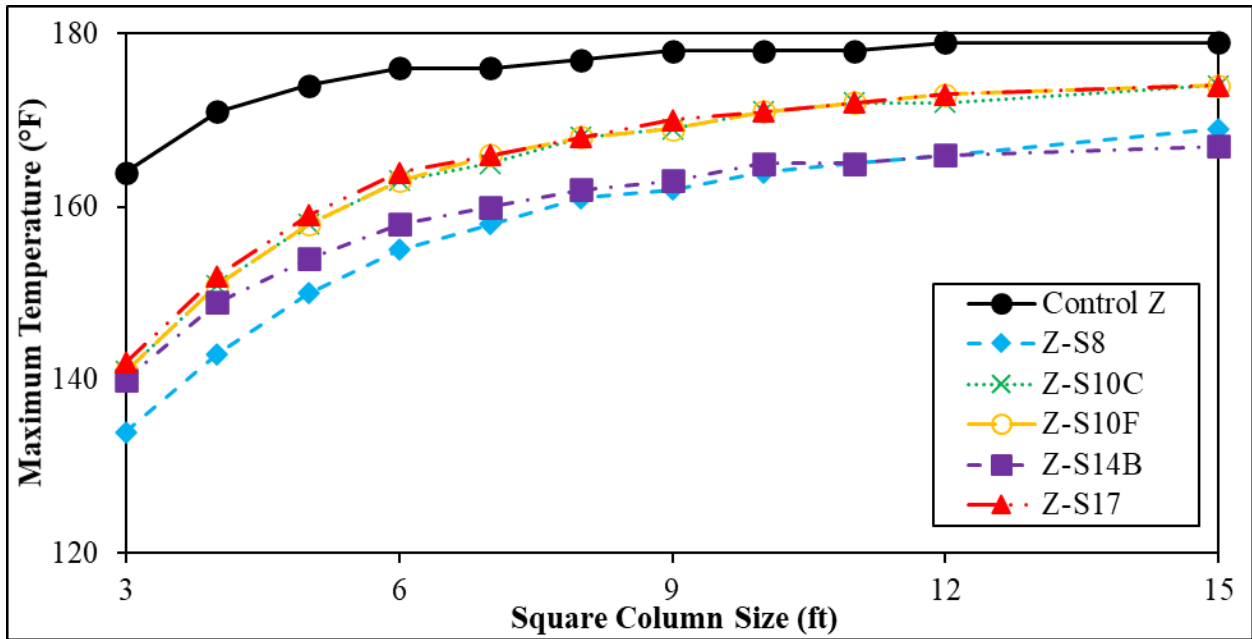
Figure 4-31: Predicted maximum temperature for cement Z mixes at 80°F (26.7°C) placement temperature
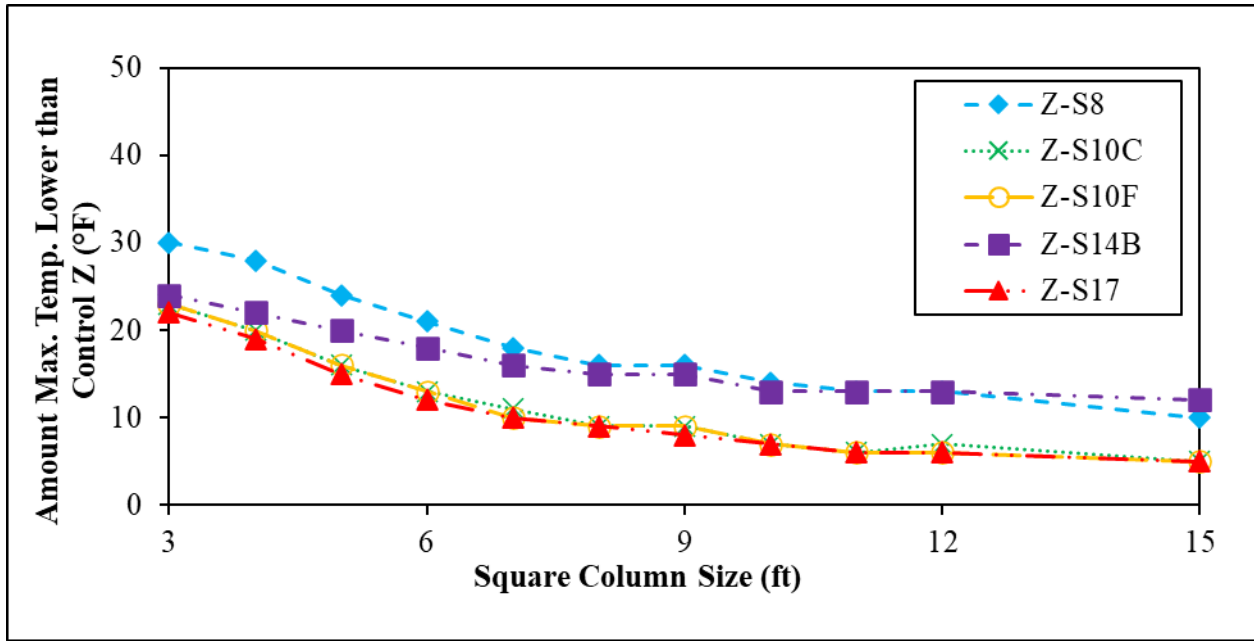
Figure 4-32: Amount maximum temperature for cement Z mixes was calculated to be lower than control Z (at 80°F (26.7°C) placement temperature)
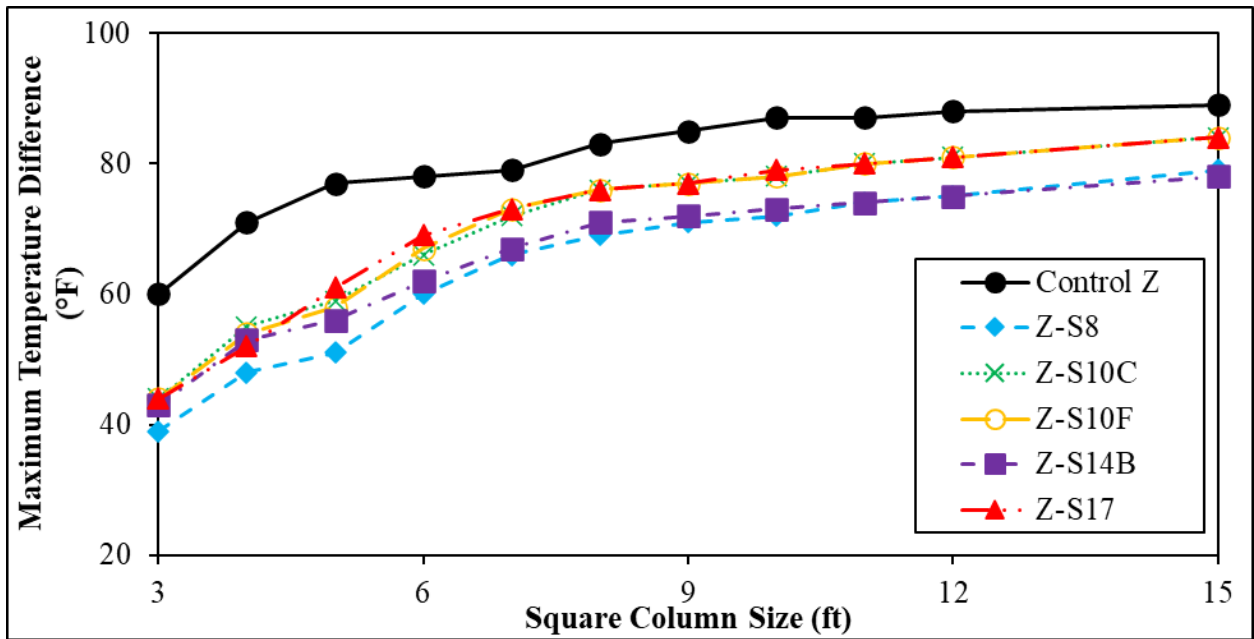
Figure 4-33: Predicted maximum temperature difference for cement Z mixes at 80°F (26.7°C) placement temperature

145

4.4   Conclusions

Based on the analysis of the heat generation of slag-blended concrete, the following conclusions can be made:

- In general, 60% cement replacement with slag reduced the adiabatic temperature rise with both Type II (MH) cement and Type IL(10) cement.

- Varying alumina contents of slags from 8% to 17% indicated a substantial difference in the adiabatic temperature rise.

- Although the slag with 14% alumina content did not have highest temperature rise, it had the highest rate of temperature rise during the initial period (24-36 h) due to an increased reactivity attributing to its lower MgO content.

- In terms of sensitivity analysis, inclusion of slag reduced the temperature rise as well as gradients within the slag-blended concrete element compared to the control mixtures; however, this reduction in temperature diminished as the member size increased, especially with high alumina slag. A large difference was also seen between slags of different compositions. Thermal control plans should use the adiabatic temperature rise parameters associated with the slag intended to be used to avoid unexpected maximum temperatures on site.

- Additional analysis of the adiabatic temperature rise data is presented in Appendix B. It is recommended that the information presented in Appendix B should be implemented in the approval process of MCCP.

- Further research is needed to assess the degree of slag reactivity and its relationship to slag chemical, physical and mineralogical characteristics. This will subsequently improve the adiabatic temperature rise prediction for slag-blended concrete mixtures.

4.5   References

[1]   ACI committee 207, "ACI 207.2R- Report on thermal volume hange effects on cracking of mass concrete," American Concrete Institute, Farmington Hills, MI, 2007.

[2]   M. Whittaker, M. Zajac, M. Ben Haha, F. Bullerjahn, and L. Black, "The role of the alumina content of slag, plus the presence of additional sulfate on the hydration and microstructure of Portland cement-slag blends," *Cem. Concr. Res.*, vol. 66, pp. 91–101, Dec. 2014.

[3]   M. Ben Haha, B. Lothenbach, G. Le Saout, and F. Winnefeld, "Influence of slag chemistry on the hydration of alkali-activated blast-furnace slag — Part I: Effect of MgO," *Cem. Concr. Res.*, vol. 41, no. 9, pp. 955–963, Sep. 2011.

[4]   M. Ben Haha, B. Lothenbach, G. Le Saout, and F. Winnefeld, "Influence of slag chemistry on the hydration of alkali-activated blast-furnace slag — Part II: Effect of Al_2O_3," *Cem. Concr. Res.*, vol. 42, no. 1, pp. 74–83, Jan. 2012.

[5]   A. Zayed, K. Riding, Y. P. Stetsko, N. Shanahan, A. Markandeya, F. Nosouhian, D. Mapa, and M. Fincan, "Final Report Effects of Blast Furnace Slag Characteristics on Durability of Cementitious Systems for Florida Concrete Structures FDOT Contract Number : BDV25-977-28," University of South Florida, Tampa, FL, 2019.

[6]   M. Whittaker, M. Zajac, M. Ben Haha, F. Bullerjahn, and L. Black, "The role of the alumina content of slag, plus the presence of additional sulfate on the hydration and microstructure of Portland cement-slag blends," *Cem. Concr. Res.*, vol. 66, pp. 91–101, Dec. 2014.

[7]   P. Z. Wang, R. Trettin, V. Rudert, and T. Spaniol, "Influence of Al_2O_3 content on hydraulic reactivity of granulated blast-furnace slag, and the interaction between Al_2O_3 and CaO," *Adv. Cem. Res.*, vol. 16, no. 1, pp. 1–7, 2004.

[8]   F. Nosouhian, M. Fincan, N. Shanahan, Y. P. Stetsko, K. A. Riding, and A. Zayed, "Effects of slag characteristics on sulfate durability of Portland cement-slag-blended systems," *Constr. Build. Mater.*, vol. 229, p. 116882, Dec. 2019.

[9]   A. Markandeya, N. Shanahan, D. Mapa, K. A. Riding, and A. Zayed, "Influence of slag composition on cracking potential of slag-portland cement concrete," *Constr. Build. Mater.*, vol. 164, pp. 820–829, 2018.

[10] A. K. Schindler and K. J. Folliard, "Heat of hydration models for cementitious materials," *ACI Mater. J.*, vol. 102, no. 1, pp. 24–33, 2005.

[11] ACI Committee 233, "ACI 233R-03: Slag Cement in Concrete and Mortar," American Concrete Institute, Farmington Hills, MI, 2011.

[12] ASTM C204-16, "Standard Test Method for Fineness of Hydraulic Cement by Air Permeability Apparatus," West Conshohocken, PA: ASTM International, 2016.

[13] ASTM C989 / C989M-17, "Standard Specification for Slag Cement for Use in Concrete and Mortars," West Conshohocken, PA: ASTM International, 2017.

[14] ASTM C192/C192M-16a, "Standard Practice for Making and Curing Concrete Test Specimens in the Laboratory," West Conshohocken, PA: ASTM International, 2016.

[15] ASTM C231/C231M-14, "Standard Test Method for Air Content of Freshly Mixed Concrete by the Pressure Method," West Conshohocken, PA: ASTM International, 2014.

[16] ASTM C143/C143M-15a, "Standard Test Method for Slump of Hydraulic-Cement Concrete," West Conshohocken, PA: ASTM International, 2015.

[17] ASTM C138/C138M-16a, "Standard Test Method for Density (Unit Weight), Yield, and Air Content (Gravimetric)," West Conshohocken, PA: ASTM International, 2016.

[18] USBR 4911-92, "Temperature Rise of Concrete," in *Concrete Manual, Part 2*, 9th ed., Denver, Co: Bureau of Reclamation, 1992.

[19] K. A. Riding, J. Vosahlik, K. Bartojay, C. Lucero, A. Sedaghat, A. Zayed and C. C. Ferraro, "Methodology Comparison for Concrete Adiabatic Temperature Rise," *ACI Mater. J.*, vol. 116, no. 2, pp. 45–53, 2019.

[20] ASTM C1702-17, "Standard Test Method for Measurement of Heat of Hydration of Hydraulic Cementitious Materials Using Isothermal Conduction Calorimetry," West Conshohocken, PA: ASTM International, 2017.

[21] J. L. Poole, K. Riding, M. C. Juenger, K. Folliard, and A. Schindler, "Effect of Chemical Admixtures on Apparent Activation Energy of Cementitious Systems," *J. Mater. Civ. Eng.*, vol. 23, no. 12, pp. 1654–1661, Dec. 2011.

148

[22] A. K. Schindler, "Concrete Hydration, Temperature Development, and Setting at Early-Ages," University of Texas at Austin, Austin, 2002.

[23] J. L. Poole, K. a. Riding, K. J. Folliard, M. C. G. Juenger, and A. K. Schindler, "Methods for calculating activation energy for portland cement," *ACI Mater. J.*, vol. 104, no. 1, pp. 86–94, 2007.

[24] N. Shanahan, A. Markandeya, A. Elnihum, Y. P. Stetsko, and A. Zayed, "Multi-technique investigation of metakaolin and slag-blended portland cement pastes," *Appl. Clay Sci.*, 2016.

[25] B. Lothenbach, G. Le Saout, E. Gallucci, and K. Scrivener, "Influence of limestone on the hydration of Portland cements," *Cem. Concr. Res.*, vol. 38, no. 6, pp. 848–860, 2008.

[26] Y. Wei and W. Hansen, "Early-age strain-stress relationship and cracking behavior of slag cement mixtures subject to constant uniaxial restraint," *Constr. Build. Mater.*, vol. 49, pp. 635–642, 2013.

[27] P. B. Bamforth, "In situ measurement of the effect of partial Portland cement replacement using either fly ash or ground granulated blast-furnace slag on the performance of mass concrete," *Proc. Instn Civ. Engrs*, vol. 69, pp. 777–800, 1980.

[28] M. K. Saeed, M. K. Rahman, and M. H. Baluch, "Early age thermal cracking of mass concrete blocks with Portland cement and ground granulated blast-furnace slag," *Mag. Concr. Res.*, vol. 68, no. 13, pp. 647–663, Nov. 2015.

[29] Q. Xu, J. Hu, J. M. Ruiz, K. Wang, and Z. Ge, "Isothermal calorimetry tests and modeling of cement hydration parameters," *Thermochim. Acta*, vol. 499, pp. 91–99, 2010.

[30] N. Shanahan, A. Bien-aime, D. Buidens, T. Meagher, A. Sedaghat, K. Riding, and A. Zayed, "Combined Effect of Water Reducer – Retarder and Variable Chloride-Based Accelerator Dosage on Rapid Repair Concrete Mixtures for Jointed Plain Concrete Pavement," *J. Mater. Civ. Eng.*, pp. 1–10, 2016.

[31] J. L. Poole, K. a. Riding, M. C. G. Juenger, K. J. Folliard, and A. K. Schindler, "Effects of Supplementary Cementitious Materials on Apparent Activation Energy," *J. ASTM Int.*, vol. 7, no. 9, p. 102906, 2010.

[32] N. J. Carino and R. C. Tank, "Maturity functions for concretes made with various cements and admixtures," *ACI Mater. J.*, vol. 89, no. 2, pp. 188–196, 1992.

[33] Concrete Durability Center, "ConcreteWorks (Version 3.1.0) [Software]," 2007. [Online]. Available: https://www.txdot.gov/inside-txdot/division/information-technology/engineering-software.external.html. [Accessed: 01-Dec-2016].

Chapter 5   Effect of Sulfated Slags on Sulfate Durability, Chloride Binding, and Microstructure Modification in Cementitious Systems

5.1   Introduction

Sulfate and chloride durability of concrete are important issues in mixture design and materials selection in concrete structural elements in Florida. It is typically believed that incorporation of ground granulated blast furnace slag (GGBFS, slag) in concrete enhances durability performance of structures. However, the wide variability in the chemical and physical characteristics of the approved slag sources in the state of Florida may have variable effect on slag-blended concrete performance and therefore must be further investigated. In this chapter the findings on the effect of different slag-blended cementitious combinations on sulfate and chloride durability will be presented; specifically, performance under external sulfate exposure conditions, internal sulfate attack potential of slag-blended systems to experience internal sulfate attack (DEF) if the structural element experiences elevated temperatures, and the efficiency of the slag-blended cementitious system in binding chlorides. The effect of sulfate-optimized slag-blended systems on durability performance was also studied, as the sulfate balance of slag-blended cementitious systems is of significance for the durability of slag-blended concrete.

Sulfate durability of a concrete structure can be affected by internal and/or external sulfate attack and consequently result in secondary or delayed ettringite formation. This may create detrimental effects on concrete durability. The current terminology in the literature identifies secondary ettringite formation due to internal sulfate attack as delayed ettringite formation (DEF) [1]. If the concrete experiences elevated temperatures (> 70ºC ~ 158°F) during its life, ettringite can decompose. Later on, at normal temperatures in a moist environment, ettringite can reform with subsequent expansion and cracking.

On the other hand, external sulfate attack occurs when sulfate in soil, groundwater or water in contact with the structural element enters concrete [2]. Three mechanisms have been proposed to explain the damage in concrete due to external sulfate attack, (i) conversion of monosulfoaluminate to ettringite, (ii) secondary gypsum formation due to the reaction between calcium hydroxide (CH) and sulfates, and (iii) decalcification of the calcium silicate hydrate gel (C-S-H) [3], [4]. For cementitious systems, where the sulfate-to-aluminate ratio is low or if the

availability of sulfate ions is not adequate for ettringite formation, monosulfoaluminate forms during the initial stages of hydration. When sulfate ion ingress occurs, monosulfoaluminate reacts with these ions and converts to ettringite, causing expansion [5]–[7]. Additionally, secondary gypsum formation can also result in expansion [3], [8]. Decalcification of C-S-H is more common in the presence of magnesium sulfate and is not accompanied by an increase in volume, but it can result in loss of strength and cohesion [3].

Partial portland cement replacement by supplementary cementitious materials (SCMs) often improves resistance of concrete exposed to sulfate environments due to lime consumption and pore size refinement. Slag can be used in concrete to enhance sulfate resistance. However, experience showed that the sulfate resistance can be dependent on the slag composition, fineness, and dosage. As described in ASTM C989 [9], cement replacement with low-alumina slags (11% Al_2O_3) can improve sulfate resistance but use of high-alumina slags (18% Al_2O_3) may require high replacement levels to achieve sulfate resistance. According to the studies by Whittaker [10], [11] slag-blended cementitious systems demonstrated greater resistance to sulfate attack compared to the plain cement systems in terms of expansion measurements, but visual observations indicated poor performance in alumina-rich slags. Slags with Al_2O_3 contents of 7.36%, 11.6% and 12.33% were used in that study at a cement replacement level of 40%. The same study reported that a slag with high magnesia (MgO, M) content can increase sulfate resistance by binding alumina (Al_2O_3, A) to hydrotalcite and making it less available to form ettringite. Hydrotalcite has been shown to be stable during sulfate attack as more alumina was bound as hydration progressed.

In another study, Ogawa et al. [12] suggested addition of sulfate to improve sulfate resistance in blended cements with high-alumina slags. This study used two cements, ASTM C150 Type I ordinary portland cement (OPC) (8.7% tricalcium aluminate (C_3A)) and ASTM C150 Type V portland cement (4.9% C_3A). A high-alumina slag of 15.2% Al_2O_3 and a low alumina slag of 10.7% Al_2O_3 were also used. When the total SO_3 content of OPC blended with 40% high-alumina slag increased from 2.6% to 4.2% and 5.8%, mortar bar expansion according to ASTM C1012 [13] was significantly suppressed. For the same system, when 4% limestone powder was incorporated along with 4.2% sulfate content, sulfate resistance further improved. Both of these methods delayed ettringite formation to later ages. Increasing the total sulfate content of the cementitious system minimized monosulfoaluminate content and in the presence of limestone, carboaluminate phases formed, which stabilized ettringite at early age. Additionally, use of Type V cement with

60% low-alumina slag demonstrated stable sulfate resistance without any sulfate or limestone additions, however, use of high-alumina slag with the same cement required sulfate (4% total SO_3) and limestone (4%) additions to improve sulfate resistance.

DEF was observed in cast-in-place mass concrete elements which experienced internal temperatures above 85ºC (185°F) due to the heat released from cement hydration [14]. At temperatures between 70ºC (158°F) and 90ºC (194°F), ettringite is unstable and transforms to monosulfoaluminate [15]. This was confirmed by XRD investigations performed on samples directly after heat treatment [14]. Monosulfoaluminate is metastable at normal temperatures but becomes stable at temperatures above 50ºC (122°F) [16]. Simultaneously, during heat curing, sulfates are also adsorbed by C-S-H. In laboratory experimental investigation of DEF, the heat-treated specimens are submerged in water or in a moist environment to accelerate the DEF process. Although these conditions do not necessarily represent field conditions, the chemical changes occurring in these laboratory studies are believed to be applicable to field concrete, but in an accelerated manner (due to alkali leaching) [15]. As reported by several researchers [17]–[19], the presence of alkalis in the system and subsequent leaching of alkalis significantly affect ettringite stability and DEF formation. During storage, leaching of alkalis causes a reduction in pH of the pore solution. This is counteracted by the increase in calcium ion concentration in the pore solution, which promotes ettringite formation and removes sulfates from the pore solution. Lowering sulfate ion concentration in the pore solution creates a gradient between the sulfates in the pore solution and the sulfates adsorbed in C-S-H. Consequently, sulfates are desorbed from C-S-H, and DEF occurs [14]. In addition to alkalis, cement fineness, C_3A content, C_3S content, and MgO content were reported to increase the expansion caused by DEF [17].

At elevated temperatures, higher degree of hydration can be achieved during initial curing, and consequently more C-S-H amounts can be formed, increasing the sulfate uptake by C-S-H. Subsequently, more sulfates can be desorbed later after heat curing which may increase ettringite content. However, as reported by Ramlochan et al. [20], incorporation of SCMs could reduce the long-term expansion, slow the rate of expansion, and delay the onset of expansion depending on the amount of reactive alumina in the SCM. Interestingly, ettringite formation in heat-cured SCM blended systems was believed not to cause expansion. As explained by Ramlochan et al. [20], there is no general relationship between expansion and ettringite formation. Expansion only occurs when the sulfates react with monosulfoaluminate, finely intermixed with the outer product of C-S-H,

and converts to ettringite. When alumina-bearing SCMs are incorporated, this reaction is prevented and ettringite precipitates in any available void space due to the reaction between sulfates and alumina contributed by SCMs. It is likely in the presence of sulfates, but in the absence of other sources of alumina, monosulfoaluminate gradually converts to more stable ettringite and consequently results in physical expansion. It was speculated that the difference in densities of monosulfoaluminate and ettringite and changes in crystal structure were reasons for such expansion [14]. Moreover, it was stated that if alumina contributed from an SCM is completely consumed before all the sulfates are desorbed from C-S-H, there is a possibility of conversion of monosulfoaluminate to ettringite even in SCM blended systems. Although expansion can be expected in this instance, it is likely to be very much delayed.

Chloride ingress in reinforced concrete elements can cause corrosion of the steel reinforcement. Although corrosion initially only occurs in a localized cross-sectional area of the rebar, it can be aggravated to a level in which the load carrying capacity of the reinforced element is compromised. In marine environments, this can be attributed to chloride ion penetration which can adversely affect the passive iron oxide film that protects the rebar. Transport of chloride ions in concrete exposed to a marine environment occurs primarily through diffusion. Chloride ion penetration in concrete is controlled by the pore structure characteristics and connectivity. Therefore, corrosion resistance can be improved by decreasing concrete permeability and therefore chloride diffusivity. It is to be noted that chloride ions that penetrate into concrete can be also bound in the hydration products either by chemical reactions or physical adsorption. This can result in a lower concentration of free chlorides available for steel depassivation. Chemical binding of chlorides by alumina-bearing phases such as Aluminate-Ferrite-monosubstituted (AFm) phases and hydrotalcite result in the formation of Kuzel's salt ($C_3A \cdot (0.5CaCl_2)(0.5CaSO_4) \cdot 12H_2O$) and Friedel's salt ($C_3A.CaCl_2.10H_2O$) [21], [22]. At lower chloride ion concentrations, monosulfate is transformed to Kuzel's salt [23], [24] whereas at higher concentrations it is transformed to Friedel's salt [22], [23], [25]. At high chloride concentrations (2-3M) ettringite may also transform to Friedel's salt [22]. Several other alumina-bearing phases such as hemicarboaluminate, monocarboaluminate and stratlingite may also be transformed partially or completely to Friedel's salt depending on the chloride ion concentration. Additionally, chlorides can be physically adsorbed to C-S-H [22], [25].

As documented in the literature [21], [22], the chloride binding capacity of concrete is affected by w/cm ratio, temperature, pH, carbonation, and sulfate content. Higher w/cm ratios increase the porosity and therefore the binding sites appear to be more accessible to chloride ion ingress. Both chemical and physical binding capacities are affected by the pH of the pore solution. Hydroxyl and chloride ions seem to compete for the adsorption sites on the surface of C-S-H and therefore at higher pH levels fewer chloride ions will be physically bound to C-S-H [23], [26]. Carbonation is also reported to have severe effects on chloride binding as CO_2 can react with and decompose calcium silicate and aluminate hydrates to form $CaCO_3$. The effect of temperature on chloride binding is reported to be dependent on chloride concentration. At chloride concentrations below 1M, chloride binding decreased with increasing temperatures; however, at 3M chloride concentration, binding increased at higher temperatures [22].

Additionally, the sulfate content of the cement was reported to have adverse effects on chloride binding [22]. Ettringite conversion to Friedel's salt only happens at higher chloride concentrations. Incorporation of slag and other SCMs into concrete can influence the chloride binding capacity of the system and consequently affect the chloride ion transport in concrete [27]. As stated by Zibara et al. [28], it is not just the alumina content of the SCM which influences the binding capacity, but also the overall lime-to-alumina (C/A) and lime-to-silica (C/S) ratios of the SCM-cement system. The C/A and C/S ratios affect the formation of calcium aluminate hydrate (C-A-H) and C-S-H phases and consequently will affect the chloride binding capacity. Moreover, increasing slag replacement levels have shown to increase the binding capacity [29], [30].

As discussed, sulfate and chloride durability of concrete are affected by various factors such as the chemical and physical properties of the cementitious system, SCM substitution levels, w/cm ratio, etc. In the following sections, the findings on the influence of slag cementitious blends characteristics on external sulfate attack, internal sulfate attack in heat-cured systems, and chloride binding capacity will be presented.

5.2   Materials and Methods

5.2.1   Materials

Six cements (BB, C, TTC, Z, TIL and THIL) and six slags (S8, S10C, S10F, S14A, S14B, S17) were used in this part of the study. Cements BB and C are Type I cements, but the latter is a

high alkali cement (1.05% Na_2O_{eq}). Cements TTC and Z are Type II moderate heat cements (Type II(MH)) with cement Z having a higher alkali content (0.65% Na_2O_{eq}). Cements TIL and THIL are Type IL cements with approximately 10% and 14% limestone contents, respectively. Slags were selected based on Al_2O_3 contents (8-17%), MgO content, SO_3 content and fineness. The chemical and physical properties of the as-received cements, and as-received slags are listed in Table 5-1, Table 5-2, Table 5-3 and Table 5-4.

Table 5-1: Chemical oxide composition and physical properties of cements

Analyte	BB I	C I(HA)	TTC II(MH)	Z II(MH)(HA)	TIL IL(10)	THIL IL(14)
SiO_2	19.53	19.00	20.21	19.41	19.16	19.14
Al_2O_3	5.51	5.90	5.00	4.64	4.61	4.52
Fe_2O_3	1.79	2.80	3.78	3.06	3.74	3.54
CaO	64.27	60.80	63.60	62.77	62.40	62.11
MgO	1.05	2.50	0.32	3.01	1.12	1.08
SO_3	3.93	4.00	2.55	3.25	2.47	2.44
Na_2O	0.11	0.32	0.01	0.02	0.17	0.17
K_2O	0.41	1.10	0.32	0.95	0.32	0.29
TiO_2	0.26	0.26	0.36	0.35	0.23	0.22
P_2O_5	0.27	0.26	0.10	0.05	0.09	0.09
Mn_2O_3	0.02	0.11	0.13	0.09	0.15	0.14
SrO	0.07	0.28	0.13	0.04	0.12	0.12
Cr_2O_3	0.01	0.01	0.03	0.01	0.02	0.02
ZnO	0.00	0.07	0.05	0.04	0.05	0.04
L.O.I. (550°C)	-	-	1.34	0.75	0.76	0.69
L.O.I. (950°C)	2.60	2.40	2.85	2.53	5.35	5.99
Total	99.83	99.82	99.44	100.21	99.98	99.91
Na_2O_{eq}	0.38	1.05	0.22	0.65	0.38	0.36
Blaine Fineness, (m^2/kg)	356	436	428	412	483	488
Mean Particle Size (MPS), (µm)	14.03	16.50	12.29	13.46	10.80	12.75

Table 5-2: Mineralogical composition of cements determined by Rietveld analysis

Analyte	BB I	C I(HA)	TTC II(MH)	Z II(MH)(HA)	TIL IL(10)	THIL IL(14)
Alite	49.1	49.5	49.6	54	44.5	40.3
Belite	15.6	13.7	19.1	7.2	16.1	16.9
Aluminate	8.6	8.3	3.3	5.6	2.3	2.9
Ferrite	4.2	7.5	11.3	7.7	11.8	10.8
Gypsum	5.7	3.8	3.2	0.3	1.5	1.5
Hemihydrate	0.2	1.7	0.2	2.5	1.4	2
Anhydrite	0.1	-	-	-	-	-
Calcite	0.2	1.8	2.8	3.4	8.8	11.4
Portlandite	1.1	0.2	-	-		
Quartz	0	0.2	0.3	0.2	1.2	1.4
Dolomite	-	1.3	-	0.5	-	-
Periclase	0.1	1.3	-	1.8	-	-
Syngenite	0.5	0.9	-	1.1	-	-
Aphthitalite	0.3	0.6	-	-	-	-
Amorphous content (AC) / unidentified	14.2	9.4	10.2	15.7	12.5	12.8

Table 5-3: Chemical oxide composition and physical properties of slags

Analyte	S8	S10C	S10F	S14A	S14B	S17
SiO_2	38.44	36.34	36.67	34.39	33.39	30.47
Al_2O_3	7.82	10.69	10.09	13.95	13.80	17.07
Fe_2O_3	0.47	0.79	1.06	0.54	0.84	0.46
CaO	39.18	39.23	38.33	42.15	42.00	35.49
MgO	10.71	10.70	10.81	5.14	5.60	10.96
Total SO_3	2.18	2.03	2.17	2.96	3.10	2.87
Sulfide, Sulfur	0.59	0.86	0.79	0.54	0.60	0.59
SO_3 as sulfate	0.18	0.05	0.11	1.03	1.22	1.39
Na_2O	0.28	0.26	0.30	0.24	0.23	0.48
K_2O	0.42	0.22	0.33	0.29	0.28	0.30
TiO_2	0.39	0.44	0.41	0.57	0.53	1.63
P_2O_5	0.00	0.00	0.00	0.01	0.00	0.00
Mn_2O_3	0.53	0.28	0.28	0.25	0.19	0.35
SrO	0.05	0.04	0.05	0.07	0.07	0.07
Cr_2O_3	0.00	0.00	0.00	0.00	0.00	0.00
ZnO	0.00	0.00	0.00	0.00	0.00	0.00
BaO	0.04	0.03	0.03	0.08	0.06	0.08
L.O.I. (950°C)	-0.77	-1.20	-0.06	-0.73	0.09	0.17
Total	99.73	99.84	100.21	99.89	100.17	100.39
Na_2O_{eq}	0.56	0.40	0.52	0.42	0.41	0.68
Blaine Fineness (m^2/kg)	617	485	600	551	553	510
MPS (µm)	9.49	10.29	9.03	10.97	12.55	9.79

Table 5-4: Mineralogical composition of slags determined by Rietveld analysis

Analyte	S8	S10	S10F	S14A	S14B	S17
Calcite	0.9	0.2	0.2	0.2	1.4	0.2
Melilite	0.4	0.4	0.3	0.3	0.3	1.4
Merwinite	-	1.1	1.1	-	0.1	-
Quartz	-	-	-	-	-	0.1
Gypsum	-	-	-	0.2	2.0	2.6
Hemihydrate	-	-	-	0.7	-	-
AC/ unidentified	98.7	98.3	98.4	98.5	96.1	95.7

5.2.2 Expansion Measurements for External Sulfate Attack

The effect of cement and slag characteristics on sulfate durability were investigated considering both internal and external sulfate attack phenomena. Length change of mortar bars stored in a 5% sodium sulfate solution was monitored in order to assess the effects of external sulfate ion ingress. Cements BB, C, TTC, TIL and THIL were blended with all the slags used in this study. Mortar bars were prepared and tested in accordance with ASTM C1012 [31], except the water-cementitious material ratio (w/cm) was maintained constant at 0.485. Immediately after molding, the specimens were placed in sealed curing containers and the containers were stored in a water bath maintained at 35 ± 3ºC for initial curing for 23.5 h $\pm$ 0.5 h. Mortar cubes of the same mixture design, subjected to the same curing conditions as the mortar bars, attained a compressive strength of 2,850 psi before the mortar bars were exposed to sulfate solution. Mortar bar mixtures of the as-received cements and slag were prepared at 60% cement replacement. Moreover, to assess the effect of sulfate optimization of slag on sulfate durability, additional mixtures with slag optimized sulfate contents were also prepared. The optimized sulfate contents were determined using isothermal calorimetry. The optimum was based on the sulfate content generating the highest cumulative heat of hydration at 2 days (Chapter 3 (Table 5-5)). Hemihydrate was used as the external sulfate source and was added as a partial replacement of slag. For all the mortar bars, length change measurements were taken at 1, 2, 3, 4, 8, 13, and 15 weeks, and also at 4, 6, 9, and 12 months after immersion in the sulfate solution as stated in ASTM C1012 [31]. The sulfate solution was changed at the same ages as well. The pH of the freshly prepared sulfate solution was

measured using a pH meter each time the solution was changed, in order to ensure that the pH of the solution was within the specified range of 6 to 8.

Table 5-5: Optimized SO_3 contents of the mixtures studied for external sulfate attack

Cement	Slag	2-day Optimum SO_3%
BB	S8	2.49
	S10C	3.26
	S10F	3.25
	S14B	4.31
TTC	S10F	2.79
	S14B	3.91
TIL	S10F	2.68
	S14B	3.78

5.2.3   Expansion Measurements for Internal Sulfate Attack

In order to assess the effect of slag-blended cementitious system characteristics on delayed ettringite formation (DEF) caused by internal sulfate attack, mortar mixtures with cements BB, C, Z, TIL and THIL were made with blends of the different slags. Mortar bars were prepared following ASTM C1012 [31] at a w/cm of 0.485. ASTM C778 Standard Ottawa sand (20-30) was used in mortar bars preparation, as it was reported to cause greater expansion in heat-cured mortar bars than graded standard sand [32]. Four bars were cast for each mixture. The curing procedure adopted was a modified procedure based on the curing regime established by Fu [32] for accelerating internal sulfate attack using a high temperature moist cycle at 95°C (203°F) and 100% relative humidity along with a drying cycle. This curing regime was modified to simulate the temperature evolution experienced by mass concrete structures in Florida [33] [34]. Immediately after casting, the mortar bars were placed in curing containers and stored in an environmental chamber. First, the mortar bars were pre-cured at 23°C (73.4°F) for 4 h (heat cure regime 1 - HCR1), as depicted in Figure 5-1. The temperature was then increased to 95 °C (203°F) at a rate of 20 °C/h (68°F/h) (HCR2). The mortar bars were heat treated at this temperature using a soak time of 36 h (HCR3). Finally, the temperature was decreased to 23°C (73.4°F) at a rate of 20°C/h (68°F/h) (HCR4). Throughout the curing regime, the relative humidity was maintained at 100%. At HCR4, the mortar specimens were taken out of the environmental chamber and were stored in the saturated lime solution at 23°C (73.4°F). Initial length measurement was taken after 1 day of

immersion in the lime solution. The saturated lime solution contains 3 g of calcium hydroxide per liter of deionized water. Subsequently, length change measurements were carried out at 7, 21, and 28 days of storage in saturated lime water and then measured every month thereafter. Moreover, additional mixtures with optimized sulfate contents were also prepared (Table 5-6).
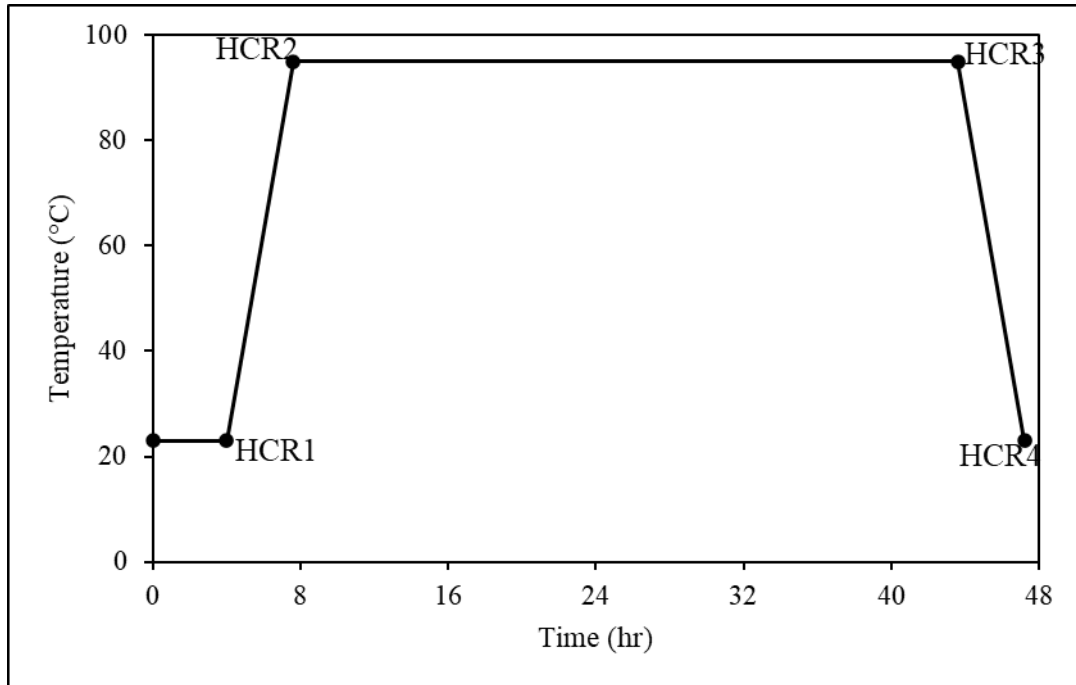
Figure 5-1: Adopted curing regime for DEF mortar specimens

Table 5-6: Optimized SO_3 contents of the mixtures studied for internal sulfate attack

Cement	Slag	2-day Optimum SO_3%
BB	S8	2.49
	S10C	3.26
	S14B	4.31
C	S10F	3.20
Z	S10F	2.82
	S14B	3.89
TIL	S10F	2.68
	S14B	3.78

5.2.4 Chloride Binding

To investigate the effect of slag-blended cementitious mixtures characteristics on chloride binding, cements BB, C, TTC, TIL, THIL were blended with three slags (S8, S14B, S17) at a 60% cement replacement level and w/cm ratio of 0.402. The method detailed by Zibara et al. [28] was adopted here. Paste samples were mixed in accordance with ASTM C305 [35] and were cast into 50 ml cylindrical plastic vials with screw caps. The vials were cured sealed for 24 h while being rotated at 8 rpm in a rotator to prevent segregation. The sealed vials were then transferred to a sealed curing container of saturated lime solution for a period of two months for curing and to avoid carbonation. Subsequently, the specimens were demolded, and 2-mm thick disks were cut from the central part of the specimen using a wet diamond saw in which deionized (DI) water was the lubricant. Sliced samples were vacuum dried in a desiccation chamber which contained silica gel and soda lime to prevent carbonation at $23°C \pm 2°C$ ($73.4°F \pm 35.6°F$) for 7 days. Afterwards, the discs were conditioned in another chamber which was maintained at 11% RH using silica gel, soda lime and saturated lithium chloride solution. After three weeks of conditioning, paste samples weighing approximately 25 g were placed in 100 ml NaCl solutions with chloride concentrations of 0.1M, 0.3M, 0.5M, 1M and 3M. These solutions were saturated with calcium hydroxide to prevent leaching [28] and subsequently were sealed and stored at $23°C \pm 2°C$ ($73.4°F \pm 35.6°F$) for two months to ensure that the equilibrium was reached. Since the Cl^- concentration of the host solution was high, a diluted solution was prepared prior to performing potentiometric titration using 0.1N $AgNO_3$ solution. First, the sample of the host solution was vacuum filtered using grade 41 filter paper and transferred to a 100 ml volumetric flask. Next, 1 ml of 15% KNO_3 solution was added as an ionic strength adjuster (ISA) and subsequently the remainder of the flask was filled with DI water. The diluted solution was left to rest for 30 mins before titration. The concentration of free chloride in the diluted solution was then determined using an EasyPlus Cl Auto-titrator and 0.1 N $AgNO_3$ as titrant. The concentration of the host solution was calculated using Equation 5-1.

$$C_f V_1 = C_2 V_2 \qquad \text{Equation 5-1}$$

$$C_2 = \frac{V_e C_{Ag} AW_{Cl} * 10^3}{V_2'} \qquad \text{Equation 5-2}$$

Where, C_f is the free chloride concentration of the host solution at equilibrium (ppm), V_1 is the volume of the host solution (ml), C_2 is the chloride concentration of the diluted solution (ppm),

V_2 is the total volume of the diluted solution, V_e is the volume of silver nitrate at the equivalence point (ml), C_{Ag} is the molarity of silver nitrate (mol/l), AW_{Cl} is the atomic weight of chloride (35.45 g/mol), V'_2 is the volume of the titrated diluted solution (ml).

The reduced concentration of the host solution is believed to be due to the chloride being bound into the cementitious system [36], [22], [23]. The amount of bound chloride was calculated using Equation 5-3.

$$C_b = \frac{(C_i - C_f) * V_1 * 10^{-3}}{m} \qquad \text{Equation 5-3}$$

Where, C_b is the amount of bound chloride (mg Cl$^-$/g of paste), C_i is the initial chloride concentration of the host solution (ppm) C_f is the free chloride concentration of the host solution at equilibrium (ppm), V_1 is the volume of the host solution (ml) and m is the dry mass of the paste samples (g).

In order to determine chloride binding isotherms, the bound chloride concentrations normalized to the dry mass of the paste were calculated using Equation 5-3, plotted against free chloride concentration and fit to a Freundlich isotherm denoted by Equation 5-4.

$$\text{Freundlich isotherm: } C_b = \alpha C_f^{\beta} \qquad \text{Equation 5-4}$$

Where C_b is bound chloride (mg Cl$^-$/g paste), C_f is free chloride (mol Cl$^-$/l) and α and β are binding coefficients.

5.2.5 X-ray Diffraction Analysis

The effect of cement and slag characteristics on microstructure evolution due to external sulfate attack, internal sulfate attack, and chloride binding was studied using quantitative x-ray diffraction (QXRD). Paste or mortar samples were crushed and gently ground by hand with mortar and pestle in order to minimize formation of additional x-ray amorphous content due to the grinding effects [37]–[39]. The material was then sieved through a 45 µm sieve and the fraction passing the 45 µm sieve was used for the analysis.

In order to identify the phase assemblage prior to sulfate exposure, pastes were prepared by hand mixing for 5 mins and subsequently cured at the same conditions as the mortar bars at 35ºC (95°F) during the first 24 h and then at 23ºC (73.4°F) until the age of sulfate exposure. In

addition, QXRD were performed on mortar bars after about 1 year of exposure or at the age of failure. Samples were taken from the surface which is exposed to high concentration of sulfate ions and the core of the bar which contains background levels of sulfate ions. The fraction passing 45 μm was then mixed with an internal standard in order to determine the amorphous/unidentified content of each sample. Standard reference material (SRM) 676a obtained from the National Institute of Standards and Technology was used as an internal standard in this study. To characterize the phases, during and after heat curing, pastes were prepared and cured using the same curing regime as the heat-cured mortar bars (Figure 5-1). Pastes were prepared by mixing for 1 min using a mixing blade attached to a power drill (Dewalt DC759). QXRD analysis was performed at each HCR (HCR1 through HCR4) and also at 4 months of storage. In terms of chloride binding, QXRD analysis was performed on paste samples prepared as discussed in 5.2.4, immediately before chloride exposure and for the paste samples stored in solutions of 0.1, 0.5 and 3 M NaCl concentrations, at the age of titration after chloride exposure.

XRD measurements were performed using a Phillips X'Pert PW3040 Pro diffractometer equipped with the X'Celerator Scientific detector and a CuKα x-ray source. Tension and current were set to 45 kV and 40 mA, respectively. Scans were performed in the range of 7 - 70° 2θ, with a step size of 0.0167° 2θ. Samples were then loaded into the sample holder using a back-loading technique in order to minimize preferred orientation, and placed onto a spinner stage that was rotating at 30 rpm in order to improve counting statistics [40]. Phase quantification was performed using the Rietveld refinement functionality of the PANalytical HighScore Plus 4.5 software.

5.2.6   Thermodynamic Modeling

Thermodynamic modeling was performed to simulate external sulfate attack and chloride binding, using the Gibbs free energy minimization software (GEMS 3) [41]. Thermodynamic data was taken from the default Nagra-PSI database [42] and CEMDATA14 [43] for cement-specific compounds. GEMS predicts phase assemblage based on equilibrium reactions.

External sulfate attack was modeled considering 100% and 70% hydration for cement and slag, respectively. When performing GEMS modeling for cement-slag systems, 70% degree of hydration of slag has been widely considered in the literature [44], [45] as it can be expected in samples about 1 year old [46]. Sulfate ingress was simulated by varying the cementitious material-

to-Na$_2$SO$_4$ solution ratio. Nosouhian et al. [47] used a similar modeling approach to simulate sulfate attack in slag-blended mortar bars immersed in sulfate solution.

In order to simulate the chloride binding effect at varying NaCl concentrations (0, 0.1, 0.5 and 3M), the degree of hydration (DOH) of cement was calculated using XRD analysis by rescaling the quantification results on an anhydrous basis [48]. The DOH of slag was assumed to be 50% considering the DOH reported in the literature for similar ages [49], [50]. The effect of NaCl solution was simulated employing the same amount of water as in the experiments. Moreover, thermodynamic modeling was also performed to simulate the ingress of 3M NaCl into the specimen. In this analysis, at ultimate equilibrium, 100% and 70% hydration was assumed for ordinary portland cement (OPC) and slag, respectively [47].

5.3   Results and Discussion

5.3.1   Length Change Measurements in Sulfate Solution according to ASTM C1012

5.3.1.1 As-Received Cement Systems

Figure 5-2 shows the length change of control mortar bars prepared with as-received cements BB, C, TTC, TIL and THIL after immersion in 5% sodium sulfate solution following ASTM C1012 [31]. Table 5-7 summarizes the expansion of the control mixtures at 180 days. Control BB had a well-defined induction period of approximately 30 days prior to the onset of expansion. Subsequently, the rate of expansion of control BB indicated a drastic increase in reaction. However, the control BB bars were broken at the age of 91 days as depicted in the Figure 5-2 with a 'X', after which the length change of the bars could not be measured. This behavior in control BB was not surprising due to the high amounts of monosulfoaluminate expected prior to sulfate exposure as a result of the high C$_3$A content in cement BB. The induction period of control C was not well-distinguished but was approximately 60 days. Control C had a somewhat slower rate of expansion compared to that of control BB, yet it also showed a rapid increase in length. Although, both cement BB and C had similar C$_3$A contents, the alkali content, sulfate content and fineness of cement C were higher. These factors may have contributed to the delayed expansion of control C compared to control BB. According to Stark and Bollmann [15], Na$_2$O$_{eq}$ levels between 0.8% and 1.2% may lead to pH values between 13.5 and 14 during initial hydration which makes primary ettringite more stable and consequently less monosulfoaluminate would be

165

available to react with external sulfate ions. Moreover, the higher fineness of cement C could reduce the permeability of mortar and slow down the sulfate ion ingress, provided the as-received cement is sulfate balanced. However, the control C bars broke at the age of 270 days, after which the length change was not measured. In terms of the other control mixtures, well-defined induction periods cannot be observed, but the expansion appeared to be substantially lower. Among these, expansion was slightly higher in control TTC mortar bars, due to its moderate C_3A content. Control TIL and control THIL indicated lower expansions. Reduced expansion in IL cement mixtures can be attributed to a lower clinker factor as well as the stability of primary ettringite due to the formation of carboaluminate phases in presence of limestone prior to sulfate exposure [12], [51].
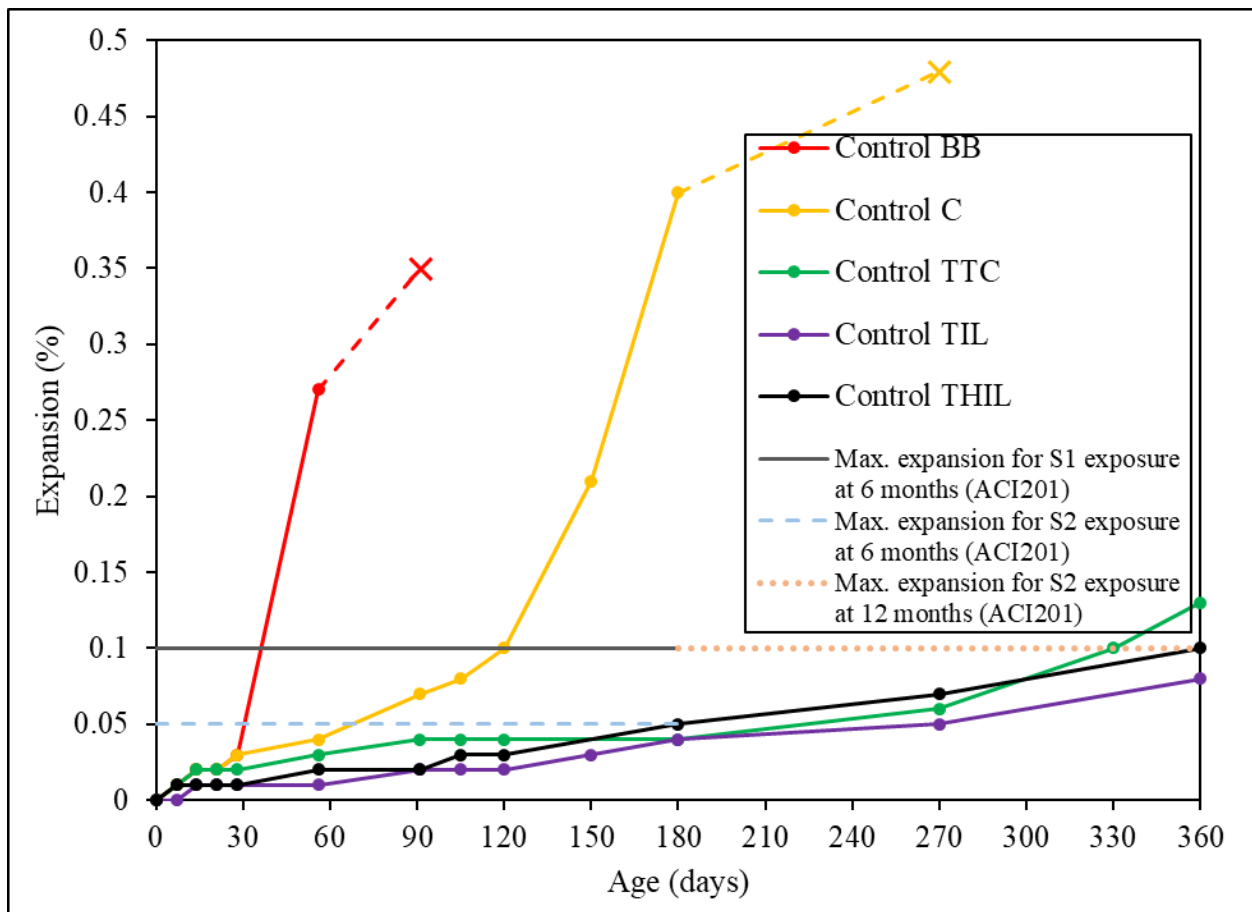
Figure 5-2: Length change of as-received cements mortar bars in 5% sodium sulfate solution

Table 5-7: Expansion of control mixtures at 180 days

Mixture ID	Expansion at 180 days (%)
Control BB	Broken
Control C	0.40
Control TTC	0.04
Control TIL	0.04
Control THIL	0.05

5.3.1.2 As-Received Slag-Blended Systems

Figure 5-3 through Figure 5-5 illustrate the expansion of slags blended with cements BB, TTC and TIL, respectively. Table 5-8 summarizes the expansion of the as-received slag mixtures at 180 days. The (L0) in the mixture identification indicates no sulfate addition and the sulfate level in the cementitious mixture is that of the as-received cement and as-received slag.

A significant reduction in expansion can be observed with the addition of slags (60% replacement), in cement BB blends, compared to its control BB (Figure 5-3). In general, the highest expansion was observed in slag S17 blend, which had the highest Al_2O_3 content (17.07%). Although it is difficult to differentiate the length change between other slags at the current testing age, a lower expansion is expected in low-alumina slags. According to the findings in a previous project [52], [47] increasing Al_2O_3 in slag decreased the sulfate durability. In terms of cements TTC and TIL, no significant difference can be seen with incorporation of slags at the current testing age. Lower C_3A contents in both of these cements can be one of the reasons for such behavior. Additionally, the presence of higher amounts of calcite in cement TIL could have formed carboaluminate phases and stabilized ettringite at early age. This may have minimized and controlled the formation monosulfoaluminate which contributes to external sulfate attack. However, due to the limited testing age, among the slag-blended mixtures, a clear distinction in the length change cannot be observed at 180 days.
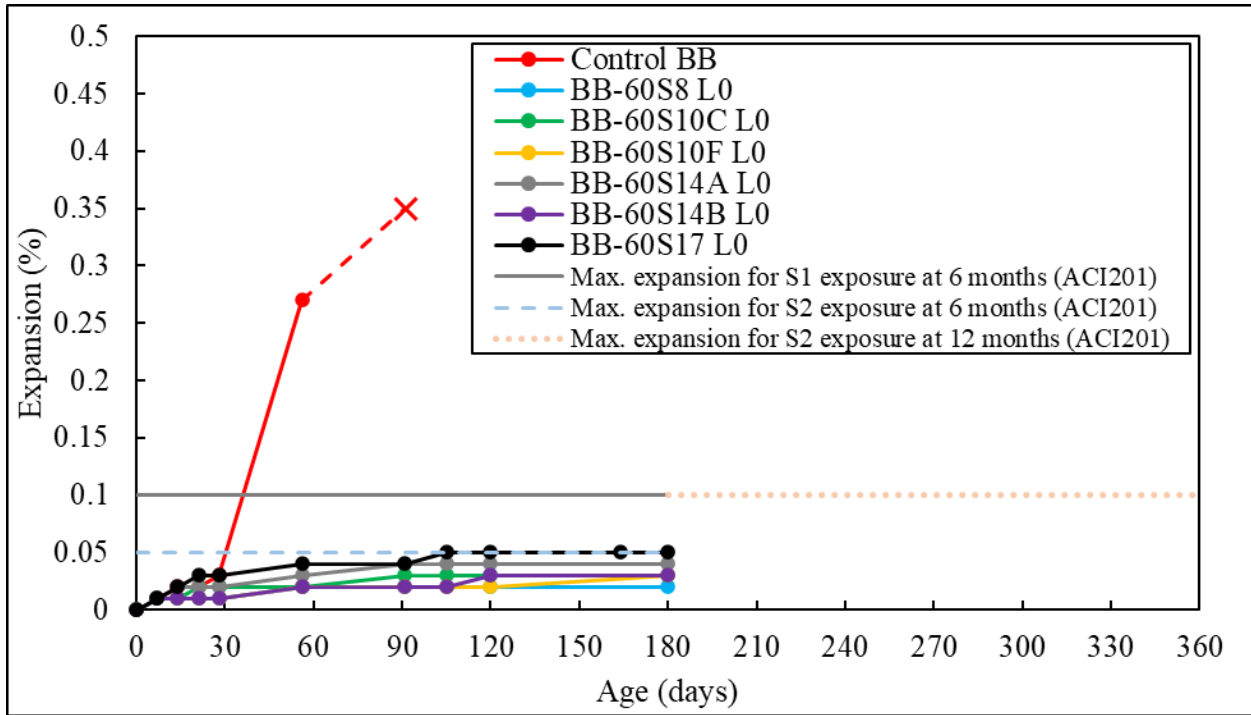
Figure 5-3: Length change of slag mortar bars blended with cement BB in 5% sodium sulfate solution
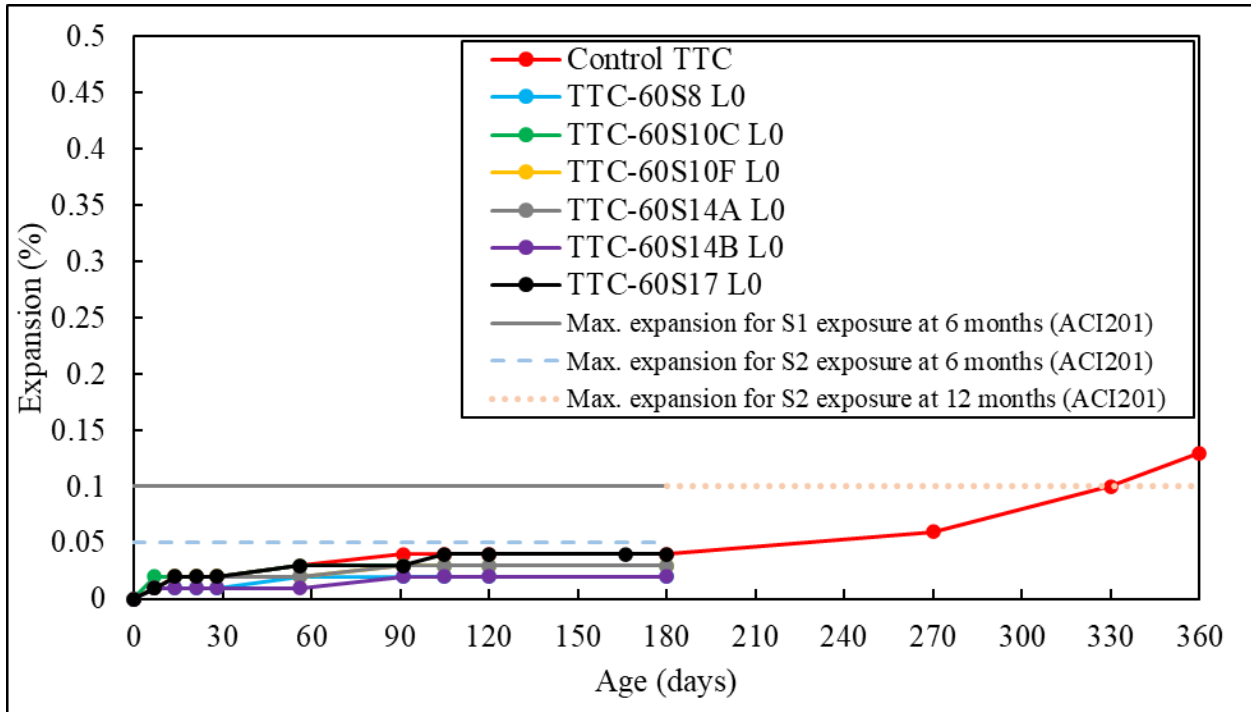
Figure 5-4: Length change of slag mortar bars blended with cement TTC in 5% sodium sulfate solution

168
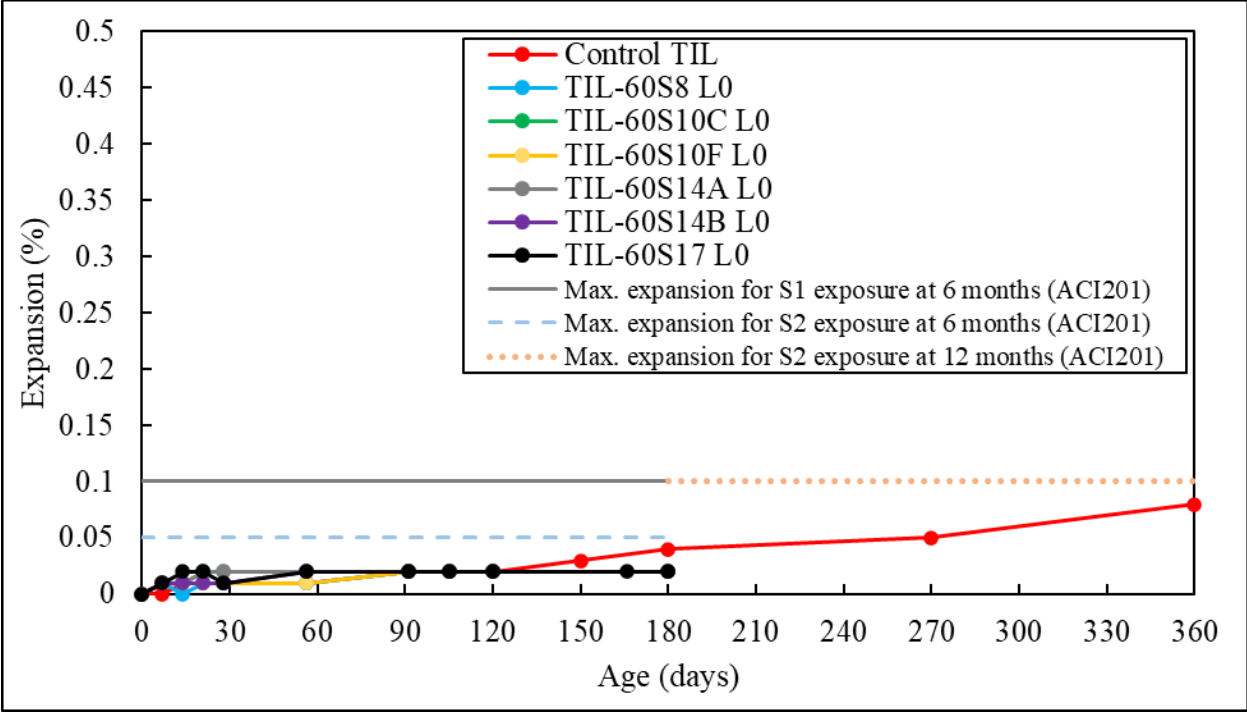
Figure 5-5: Length change of slag mortar bars blended with cement TIL in 5% sodium sulfate solution

Yu et al. [53] stated that the deterioration mechanism of slag-blended systems exposed to sulfate environments is different to that of pure cement systems. Apparently, slag-blended systems deteriorate more through loss of surface due to the refined pore system than macroscopic expansion. Close to the surface of slag-blended systems, a buffering effect is created as sulfates penetrating the samples are fixed by aluminate phases such as AFm and anhydrous slag. Further ingress takes place once the phases in the buffering region react and the sulfate ions in the pore solution increase. Thus, expansion occurs in a thin layer due to ettringite formation which would cause cracking and surface spalling. High-alumina slag blends have been reported to have higher surface spalling. As a consequence, high-alumina slag blends could demonstrate lower expansion while experiencing material loss due to surface spalling.

Figure 5-6 shows the length change of slag S17 blends with different cements. Although the mixtures are still in the induction period at this age, the highest expansion was observed when slag S17 was blended with cement BB due to the high C_3A content in cement BB. Therefore, it is expected that BB-60S17 mortar bars would fail earlier than the rest as a result of surface spalling. The expansion of BB-60S17 was followed by blends with cement C, TTC and Z. Both IL cement

mixtures indicated the lowest expansions, due to a reduced clinker factor in limestone cements. Among the two mixtures, expansion was lower when slag S17 was blended with cement THIL which has a higher limestone content.
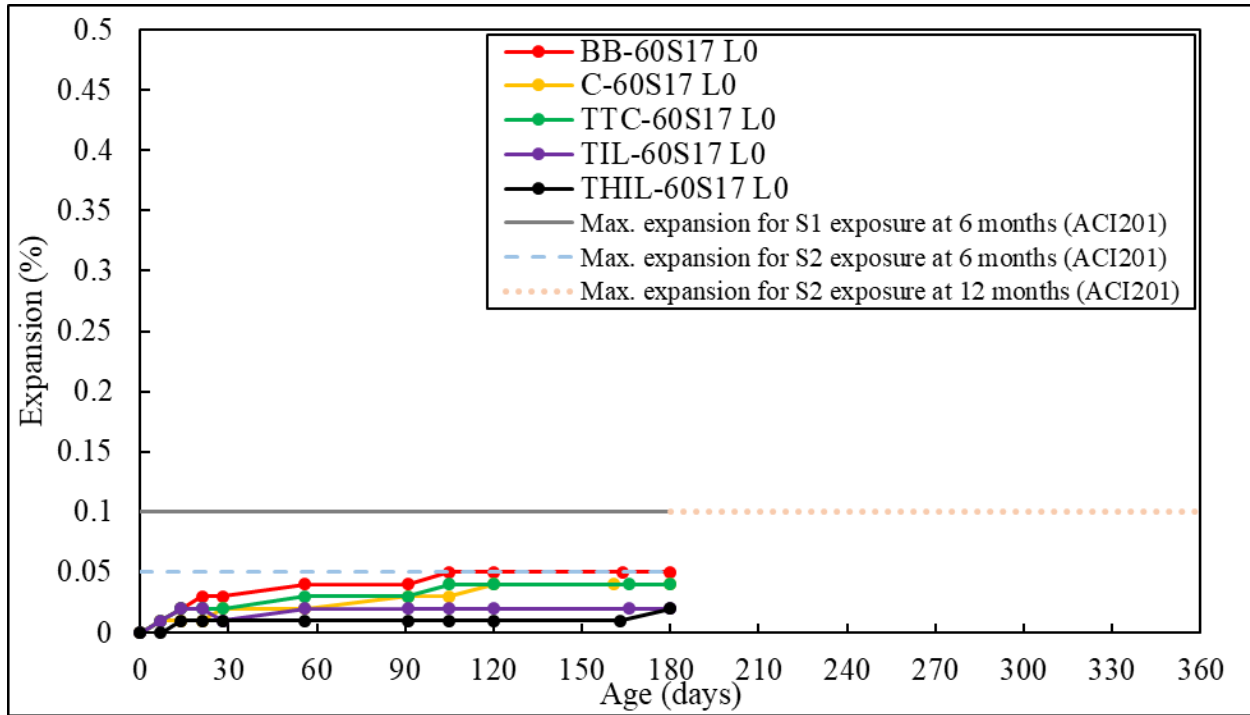
Figure 5-6: Length change of slag S17 mortar bars blended with cements in 5% sodium sulfate solution

Table 5-8: Expansion of as-received slag-blended mixtures at 180 days

Mixture ID	Expansion at 180 days (%)
BB-60S8 L0	0.02
BB-60S10C L0	0.03
BB-60S10F L0	0.03
BB-60S14A L0	0.04
BB-60S14B L0	0.03
BB-60S17 L0	0.05
TTC-60S8 L0	0.02
TTC-60S10C L0	0.03
TTC-60S10F L0	0.03
TTC-60S14A L0	0.03
TTC-60S14B L0	0.02
TTC-60S17 L0	0.04
TIL-60S8 L0	0.02
TIL-60S10C L0	0.02
TIL-60S10F L0	0.02
TIL-60S14A L0	0.02
TIL-60S14B L0	0.02
TIL-60S17 L0	0.02
C-60S17 L0	0.04
THIL-60S17 L0	0.02

5.3.1.3 Sulfate-Optimized Slag-Blended Systems

Figure 5-7 through Figure 5-14 illustrate the expansion of sulfate-optimized mixtures. Table 5-9 summarizes the expansion of sulfate-optimized slag-blended mixtures at 180 days. In the mixture ID, L2 denotes the SO_3 content obtained from sulfate optimum determined at a hydration time of 2 days and using isothermal calorimetry, while the first parenthesis indicates the optimized SO_3 content in the slag, whereas the second parenthesis indicates the total SO_3 content in the optimized blended cementitious system. At the maximum reported testing age of 180 days, sulfate-optimized mixtures showed slightly lower expansion compared to their respective as-received systems. Therefore, it is likely that the onset of expansion of these mixtures will be delayed; however, expansion measurements to an age of 18 months are necessary for appropriate sulfate exposure classification.
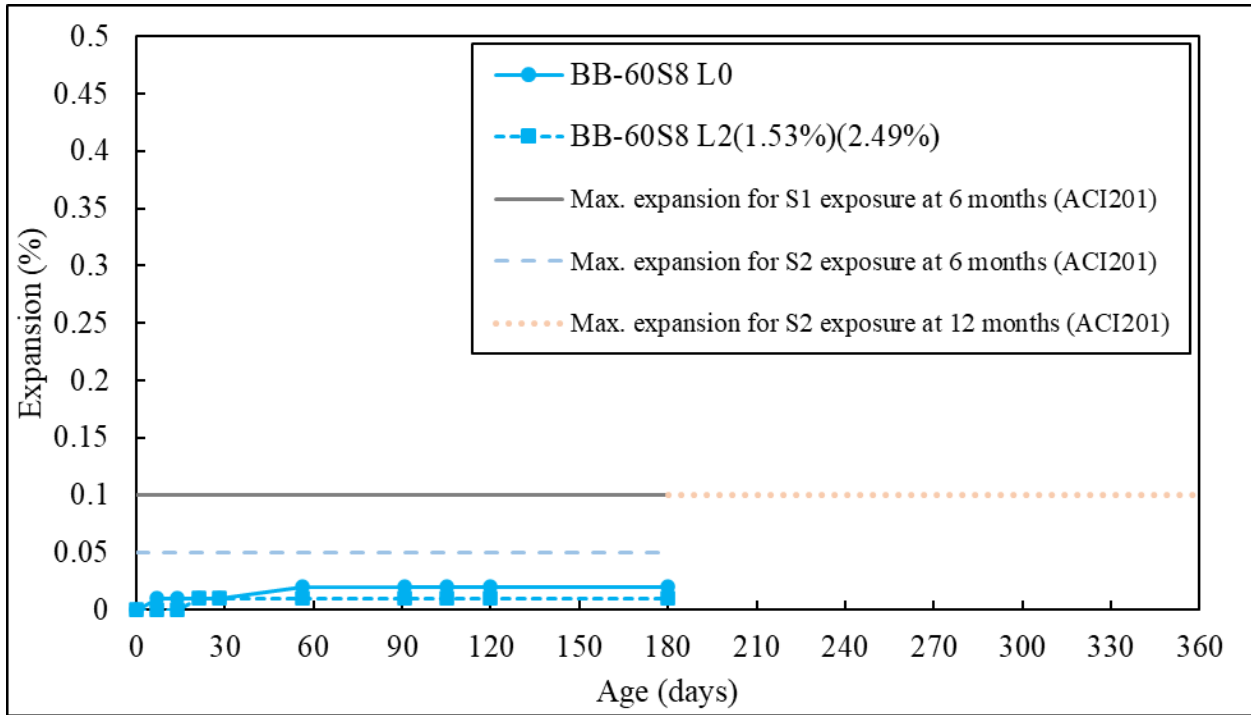
Figure 5-7: Length change of sulfate-optimized slag S8 mortar bars blended with cement BB
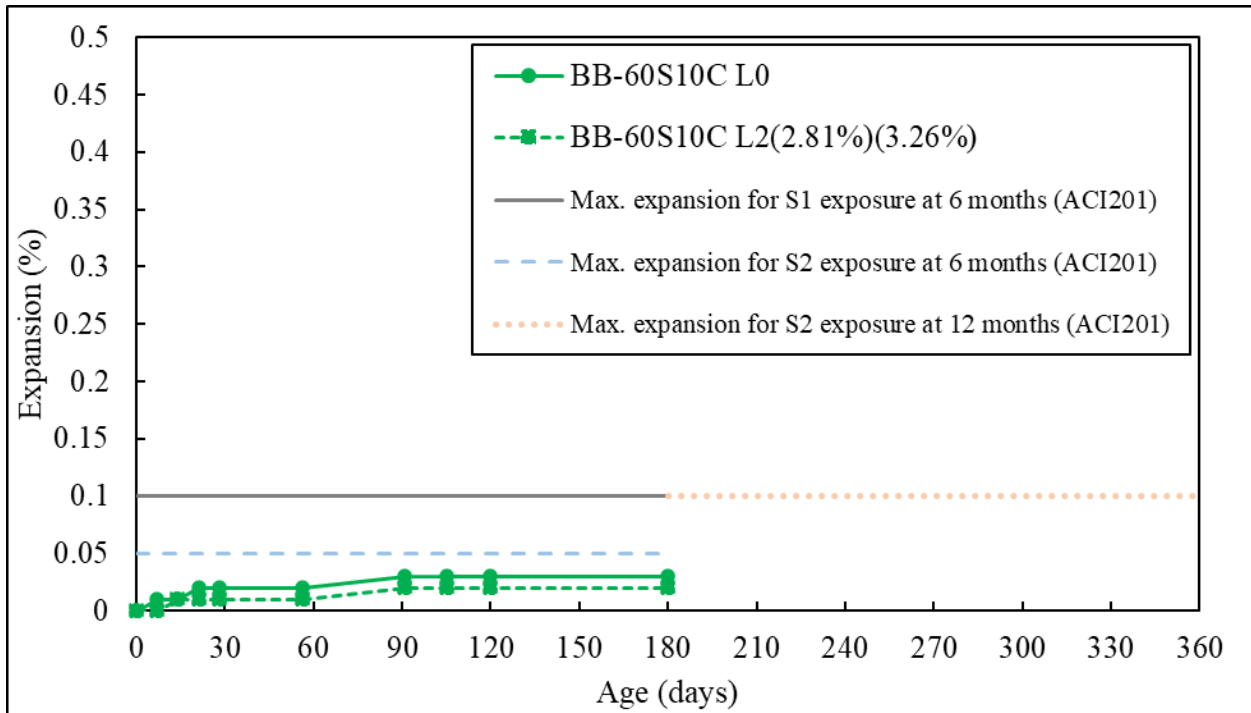
Figure 5-8: Length change of sulfate-optimized slag S10C mortar bars blended with cement BB
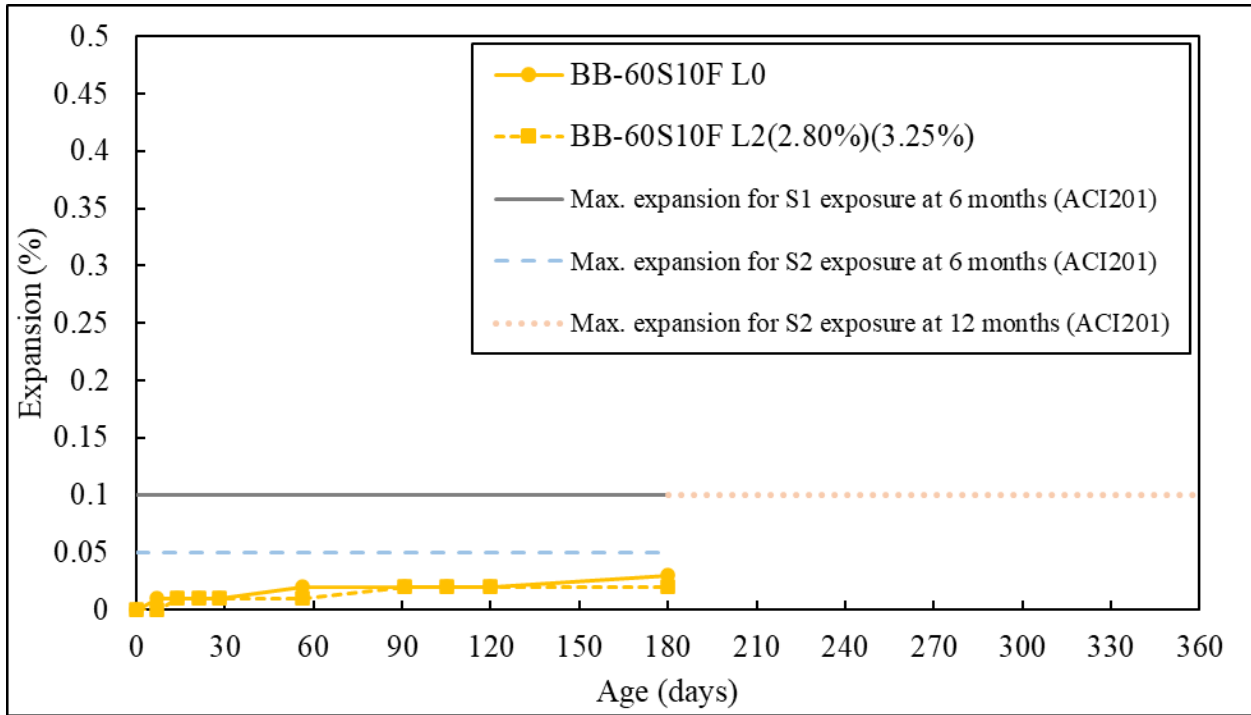
Figure 5-9: Length change of sulfate-optimized slag S10F mortar bars blended with cement BB
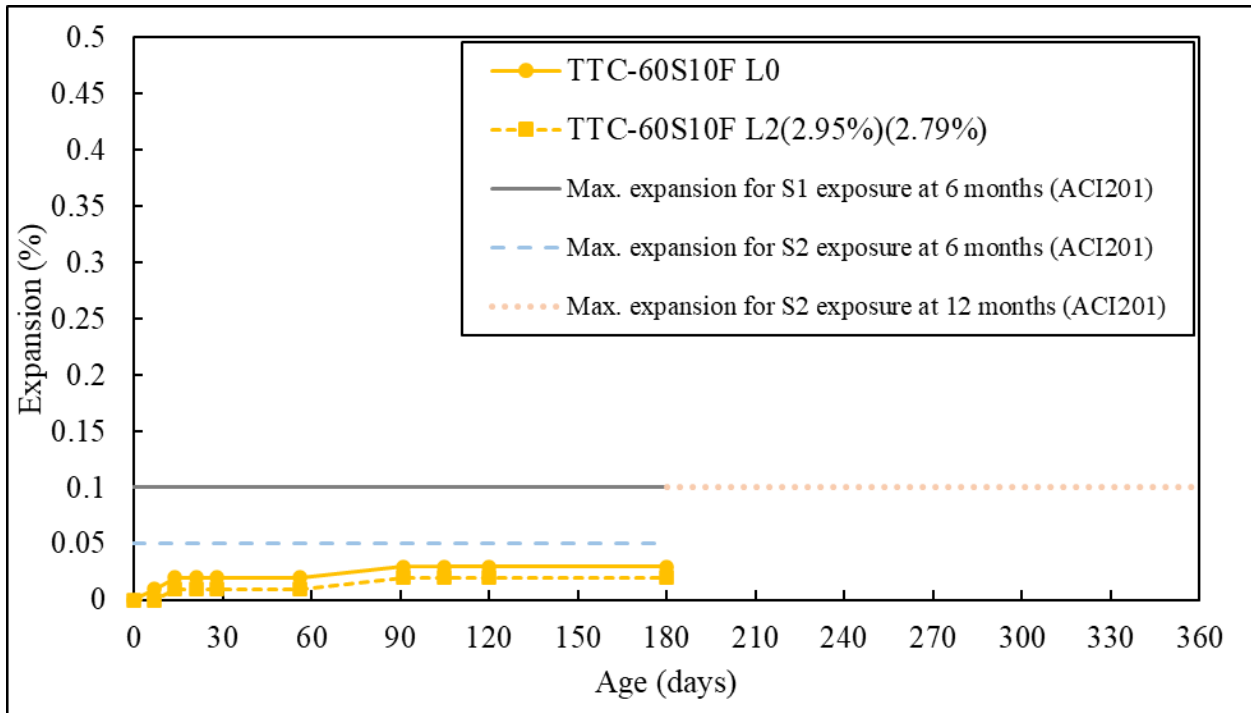
Figure 5-10: Length change of sulfate-optimized slag S10F mortar bars blended with cement TTC
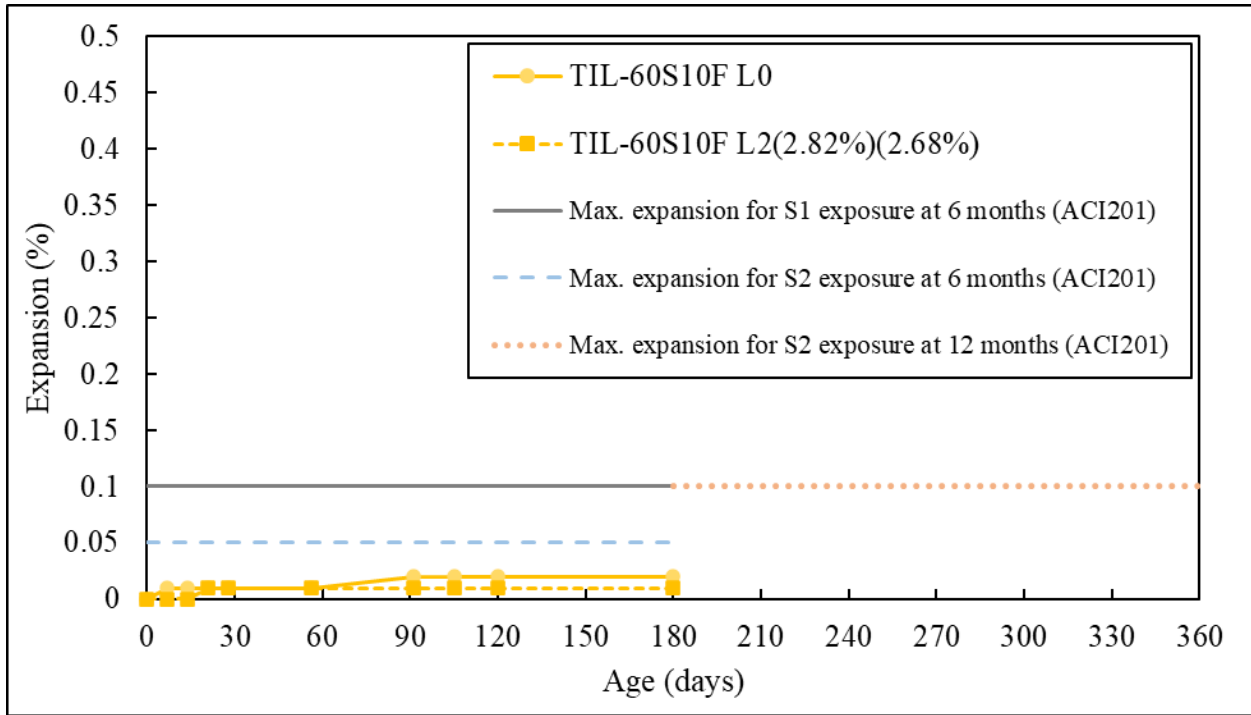
Figure 5-11: Length change of sulfate-optimized slag S10F mortar bars blended with cement TIL
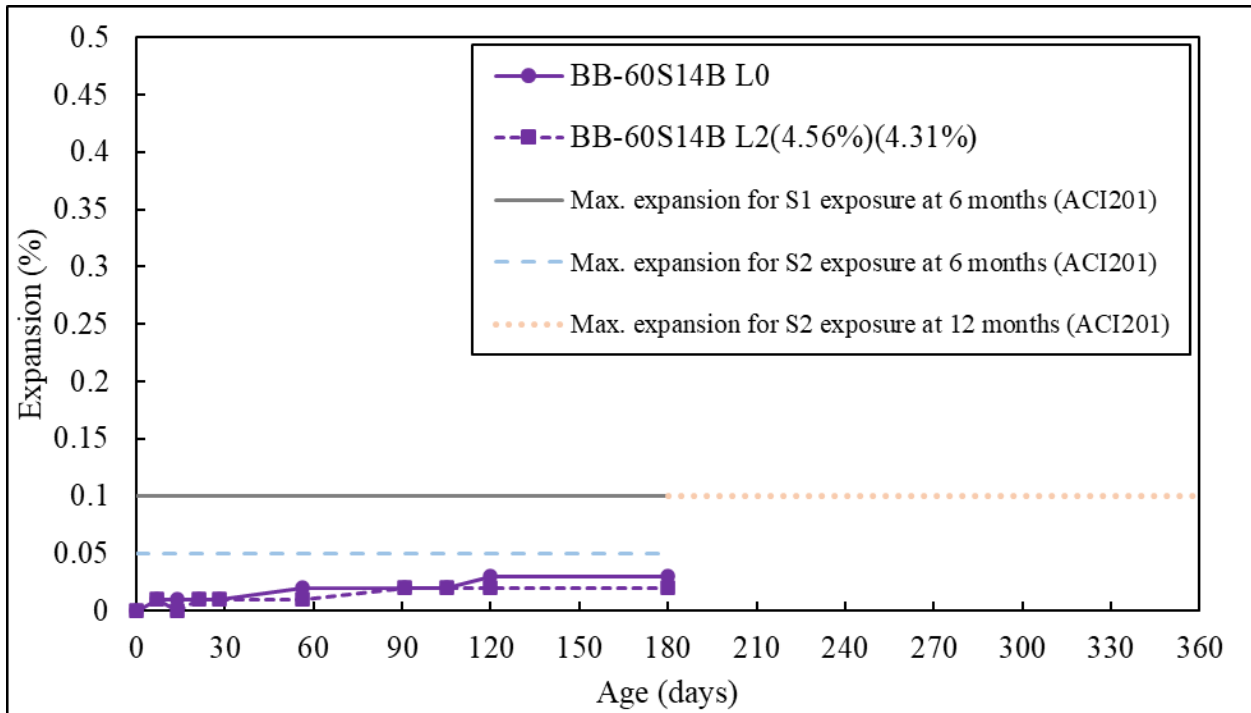
Figure 5-12: Length change of sulfate-optimized slag S14B mortar bars blended with cement BB
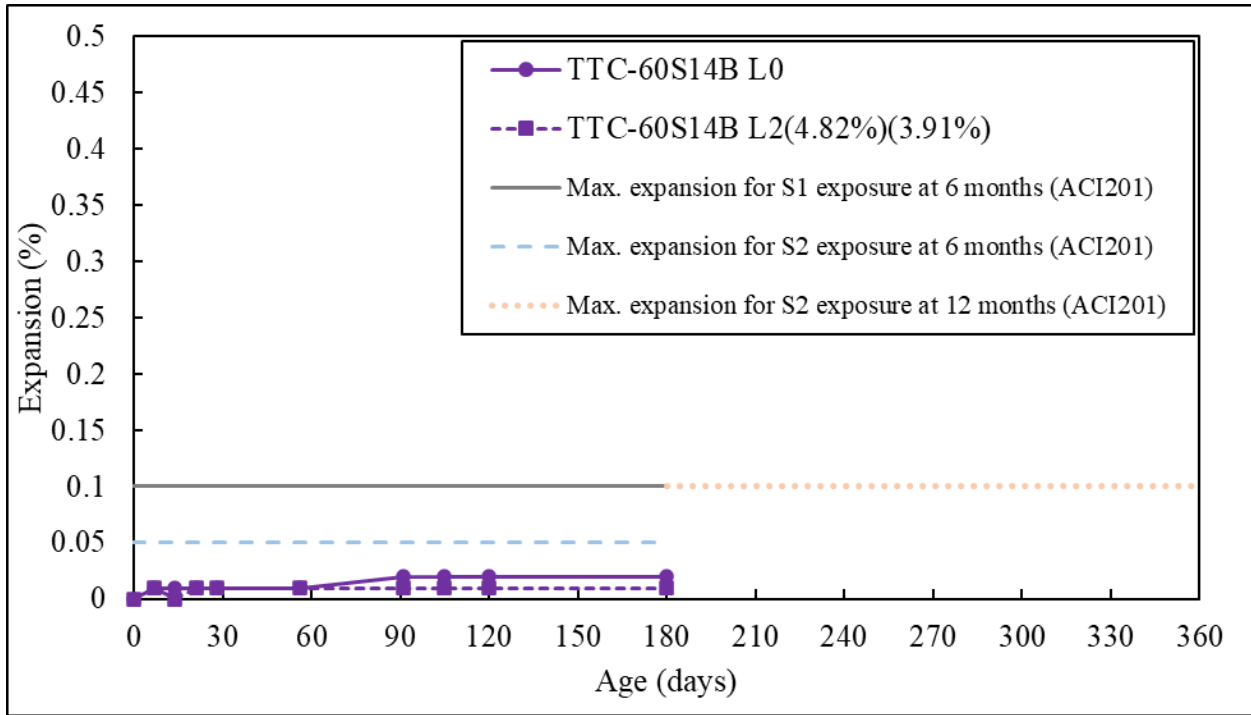
Figure 5-13: Length change of sulfate-optimized slag S14B mortar bars blended with cement TTC
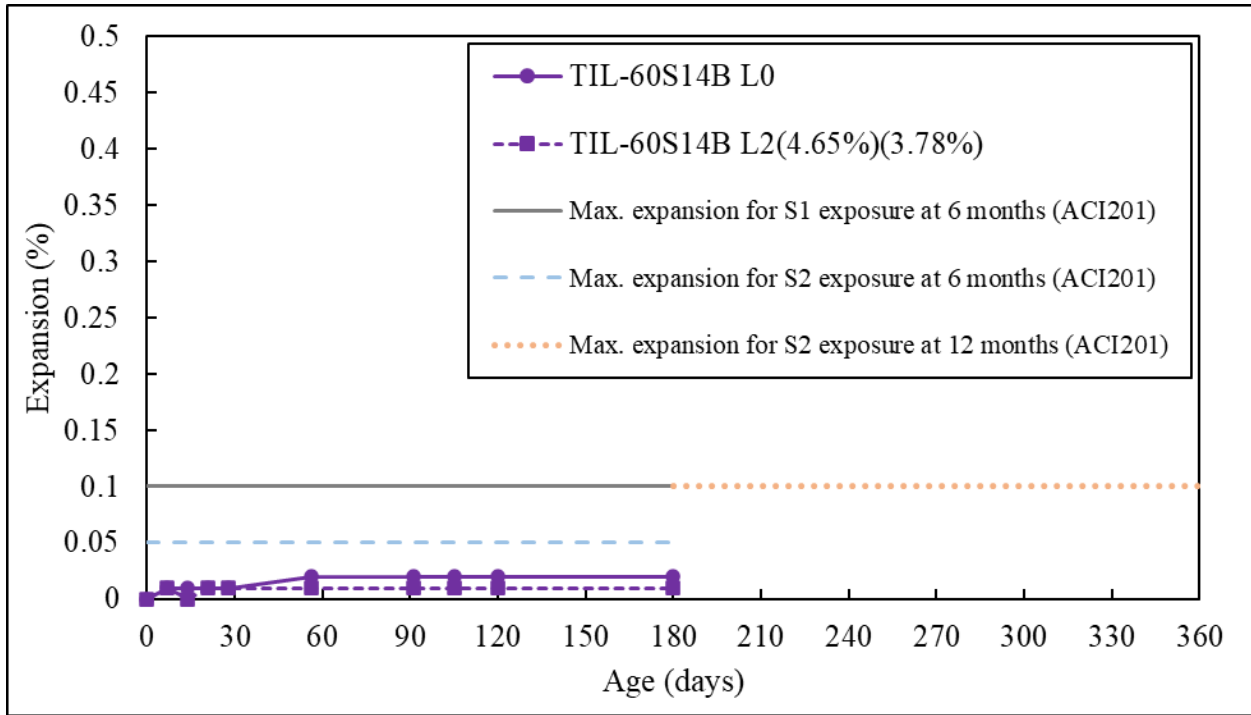
Figure 5-14: Length change of sulfate-optimized slag S14B mortar bars blended with cement TIL

Table 5-9: Expansion of sulfate-optimized slag-blended mixtures at 180 days

Mixture ID	Expansion at 180 days (%)
BB-60S8 L2	0.01
BB-60S10C L2	0.02
BB-60S10F L2	0.02
BB-60S14B L2	0.02
TTC-60S10F L2	0.02
TTC-60S14B L2	0.01
TIL-60S10F L2	0.01
TIL-60S14B L2	0.01

Ogawa et al. [12] reported that the addition of sulfate and limestone is effective in delaying expansion due to sulfate attack. They studied sulfate resistance of Type V cement (4.9% C_3A) with 60% slag substitution and plain OPC (8.7% C_3A) with 40% slag substitution. Two slags with high-alumina (15.2% Al_2O_3) and low alumina (10.7% Al_2O_3) content were used. Since the current study used 60% cement replacement level, the expansion results obtained for Type V cement blended with slags can be used for comparison. The total SO_3 content in Type V cement blended with high-alumina slag system was 1% and these mortar bars exceeded 0.1% expansion and failed at around 6 months. Addition of 4% limestone to this mix delayed the time to 0.1% expansion, which was about 7 to 8 months. This can be attributed to carboaluminate formation which delayed the formation of ettringite. Carboaluminate phases are expected to convert to ettringite in the presence of excessive sulfate, which explains the limited sulfate improvement. On the other hand, increasing the total SO_3 content to 4 % by adding calcium sulfate to the Type V + high-alumina slag system significantly improved the sulfate resistance as indicated by the expansion at 18 months which was less than 0.1%. Moreover 4% limestone powder was added to the same system with 4% total SO_3 and the sulfate resistance was further improved. The SO_3/Al_2O_3 mass ratios of these mixtures, which showed improved sulfate resistance, were around 0.4-0.43. In the current study, except for mixtures BB-60S8, TTC-60S10F and TIL-60S10F, all other sulfate-optimized mixtures had SO_3/Al_2O_3 mass ratios approximately similar to 0.4 (based on the 2-day sulfate optimum level) as listed in Table 5-10. Therefore, delayed or controlled long term expansion can be expected in the sulfate-optimized mixtures compared to their respective as-received systems. Among these, mixtures with 1L cement are expected to show the most enhanced sulfate resistance.

Table 5-10: SO_3/Al_2O_3 (by mass) of the sulfate-optimized mixtures

Slag [as-received SO_3 %]	Cement (Type) [as-received SO_3 %]	as-received SO_3/Al_2O_3 in the system	2-day optimum SO_3/Al_2O_3 in the system
S8 [0.18]	BB (Type I) [3.93]	0.24	0.37
S10C [0.05]	BB (Type I) [3.93]	0.19	0.39
S10F [0.11]	BB (Type I) [3.93]	0.20	0.41
	TTC (Type II (MH)) [2.55]	0.13	0.36
	TIL (Type IL) [2.47]	0.13	0.35
S14B [1.22]	BB (Type I) [3.93]	0.22	0.43
	TTC (Type II (MH)) [2.55]	0.17	0.40
	TIL (Type IL) [2.47]	0.17	0.39

5.3.1.4 X-Ray Diffraction Analysis of Pastes Prior to Sulfate Exposure

Table 5-11 presents the phase assemblage of the control mixtures prior to sulfate immersion at an age of 1 day. The phase assemblage of selected slag-blended mixtures prior to sulfate exposure are listed in Table 5-12. The corresponding exposure age of each mixture is also listed in the same table. This is the age at which the specimens reached the specified strength requirement per ASTM C1012 for sulfate immersion. Substantial amounts of portlandite were detected in all the control systems. Ettringite was observed in all the control mixtures; controls BB and C showed higher amounts of ettringite as expected due to their high C_3A contents. No monosulfoaluminate was detected. Only the controls prepared with IL cements (Controls TIL and THIL) indicated small amounts of hemicarboaluminate at the age of 1 day.

Table 5-11: Phase quantification of control mixture paste samples before sulfate exposure

Mix ID	Control BB	Control C	Control TTC	Control T1L	Control TH1L
Age at sulfate exposure (days)	1	1	1	1	1
Alite	6.2	5.8	6.5	3.8	4.1
Belite	5.5	3.8	4.6	4.2	5
Aluminate	0.5	0.5	0	0	0
Ferrite	0.1	0.5	2.1	2	1.8
Calcite	0.1	0.4	0.6	2.2	3.2
Quartz	0	0.1	0	0.8	0.6
Portlandite	8.2	6.8	7.5	8	6.4
Periclase	0	0.3	0	0	0
Dolomite	0	0.5	0	0	0
Ettringite	5.3	5.9	4.4	3.7	4.6
Hemicarboaluminate	0	0	0	0.1	0.4
AC/ Unidentified	74.2	75.6	74.4	75.1	73.8

Table 5-12: Phase quantification of slag-blended mixture paste samples before sulfate exposure

Mix ID	BB-60S8	TTC-60S8	T1L-60S8	BB-S14B	TTC-S14B	T1L-S14B	BB-60S17	C-60S17	TTC-60S17	T1L-60S17	TH1L-60S17
Age at sulfate exposure (days)	4	4	4	2.75	2	2	2	3	2.75	2	2.25
Alite	0.6	0.4	0.3	1.2	1.5	0.3	1.3	1.4	0.8	0.3	0.6
Belite	2.6	1.4	2	3	1.9	1.8	2.6	1	2.4	1.9	1.5
Aluminate	0	0	0	0	0	0	0	0	0	0	0
Ferrite	0	0.1	0.2	0	0.7	0.4	0	0.1	0.4	0.3	0.2
Calcite	0.1	0.2	1.1	0.2	0.5	1.2	0.1	0.3	0.1	0.8	1
Quartz	0	0	0.3	0	0	0.3	0	0	0	0.2	0.2
Portlandite	2.5	2.6	2.4	1.4	2.8	1.8	1.2	0.9	1.6	1.8	1.2
Periclase	0	0	0	0	0	0	0	0.1	0	0	0
Dolomite	0	0	0	0	0	0	0	0.3	0	0	0
Melilite	0.1	0	0.1	0.1	0	0	0.4	0.3	0.3	0.3	0.3
Ettringite	2.5	2.1	2	2.9	3.2	3.6	2.2	2.2	2.4	3.8	3.7
Monosulfate	1.2	0	0	1.1	0	0	2.4	2.2	1.3	0.2	0.1
Hydrotalcite	0.2	0.2	0.2	0.1	0	0.1	0.2	0.3	0.3	0.4	0.4
Hemicarboaluminate	0	1.2	1.7	0.5	0.5	2	0	0	0.1	1.5	2.1
AC/Unidentified	90.2	91.9	89.8	89.5	89	88.4	89.4	91	90.4	88.6	88.8

In terms of blended mixtures, addition of slag lowered the amounts of portlandite, ettringite, and unreacted clinker phases due to reduced cement fraction. Monosulfoaluminate was observed in all the systems except TTC-60S8, TIL-60S8, TTC-60S14B and TIL-60S14B. Cementitious system blends made with cements TTC or TIL showed hemicarboaluminate formation. Apparently, the systems which showed monosulfoaluminate at early age were either cement BB with any slag or slag S17 with any cement, due to the high levels of alumina present. Additionally, hydrotalcite was detected in the blended mixtures, with lower amounts found with slag S14B blends due to its low MgO content. Formation of monosulfoaluminate and hydrotalcite in slag-blended mixtures due to slag hydration has been reported in the literature [54], [55]. Hemicarboaluminate formation in the presence of limestone in slag-blended systems has been reported in [12], [56]; however, the presence of monosulfoaluminate at early age is not desirable for sulfate durability as it can be converted to ettringite when exposed to external sulfate ions. Only very small amounts of monosulfoaluminate can be observed in TIL-60S17 and THIL-60S17 due to the calcite content in cements TIL and THIL. As a consequence, the high-alumina slag system at high replacement levels may show better sulfate resistance (Figure 5-6). However, some studies [11] in the literature speculated that monosulfoaluminate formation due to slag hydration may not necessarily mean that it will be converted to ettringite and cause damage in sulfate environments. It was stated that less ettringite was formed in slag systems, despite the higher AFm contents before sulfate exposure.

5.3.1.5 X-Ray Diffraction Analysis of Mortar Bars after Sulfate Exposure

Phase quantification results of core and surface samples of the control mortar bar mixtures are listed in Table 5-13. The samples from controls BB and C were taken at the ages the bars were broken whereas the samples from unbroken bar mixtures were taken at 1 year. From the unhydrated clinker phases only small amounts of belite were detected indicating a very high degree of hydration. When comparing the cores and the surfaces of the samples, a higher amount of portlandite was detected in the cores, whereas gypsum and ettringite were higher at the surface. This is expected during external sulfate attack [57], [58]. Monosulfoaluminate was observed only in the core of control BB. The highest ettringite content was observed in the control BB mortar bar surface which deteriorated at an age of 91 days of sulfate exposure. Although control C mortar bars were broken at 270 days, they showed the lowest ettringite content at the surface.

Additionally, the portlandite content at the surface of both these systems was very low, which implies that it reacted with sulfate to form gypsum. Controls TTC, TIL and THIL showed considerable amount of ettringite at the surface of the bars which explains the observed mortar bar expansion (Figure 5-2). Although the expansion of controls TTC, TIL and THIL were similar, ettringite contents detected in IL systems were higher than that in control TTC. This can be attributed to the higher initial ettringite formation prior to sulfate exposure in controls TIL and THIL (Table 5-11). As stated in the literature [51], ettringite is more stable in the presence of limestone.

Table 5-13: Phase quantification of the core and surface samples of control mortar bars stored in 5% Na$_2$SO$_4$ solution

Mix ID	Control BB		Control C		Control TTC		Control T1L		Control TH1L	
Age (days)	91		270		360		360		360	
Condition of bar	Broken		Broken		Not Broken		Not Broken		Not Broken	
	Surface	Core	Surface	Core	Surface	Core	Surface	Core	Surface	Core
Belite	0.9	1.1	0.4	1	0.9	1	1.3	1.3	1.2	1.1
Calcite	1	0	26.4	1.7	10.8	0.3	4.9	3.3	9.4	5.1
Portlandite	0.8	17.7	0.2	16.6	5.6	14.9	11.3	15.1	6.2	15.9
Periclase	0	0	0.1	0.1	0	0	0	0	0	0
Dolomite	0	0	0.1	0.1	0	0	0	0	0	0
Gypsum	5	0.5	5.7	0.5	2.6	0.5	2.6	0.5	7.2	0.9
Ettringite	29.5	8.8	9.6	7.5	10.6	4.3	13.2	4.7	16.7	6.1
Monosulfate	0	1	0	0	0	0	0	0	0	0
AC/Unidentified	62.6	71	57.3	72.4	69.5	79.2	66.6	74.9	59.4	70.9

Table 5-14 through Table 5-16 list the phase quantification of slags S8, S14B and S17 blends immersed in sulfate solution. It is noteworthy that these samples were taken from a duplicate batch of the same mortar bar mixtures, which was discussed in section 5.3.1.2, as the duplicate batch had reached approximately 1 year of age. Slag S8 and S14B mixtures were tested after 300 days of exposure, whereas unbroken slag S17 mixtures were tested after 360 days of exposure. The samples from BB-60S17 and C-60S17 were tested at the broken age. Amorphous content refers to the sum of C-S-H and unhydrated slag. Only a small amount of belite was observed in all the samples indicating a high degree of cement hydration. Similar to the control mixtures, portlandite content was lower and gypsum and ettringite contents were higher at the

surface compared to the core of the slag-blended mortar bars. However, both portlandite and ettringite contents in core samples of the blended mixtures were lower compared to their respective controls. These lower ettringite contents can be attributed to the reduced cement content and also due to the pozzolanic reaction of slag with portlandite. Monosulfoaluminate was nevertheless observed in all the core samples, except for TIL-60S8 and TIL-60S14B, and it increased with increasing slag alumina contents. It appears that because of the presence of limestone, noticeable amounts of carboaluminate phases were formed in the cores of the mortar bars prepared with IL cements, but were lower at the surface which implies decomposition of carboaluminates to form ettringite when exposed to excessive sulfate ions [12]. Moreover, unlike in control mixtures, hydrotalcite was detected in all the systems; very low amounts were observed in the surface due to sulfate attack. It is noteworthy that the hydrotalcite content observed in slag S14B blended mixtures were lower due to its lower MgO content. Whittaker et al. [11] stated that the quantity of hydrotalcite formed and its Mg/Al ratio depends on the Mg and Al content in the slags and therefore a slag with higher Mg could enhance resistance to sulfate attack by binding more Al to form hydrotalcite.

Table 5-14: Phase quantification of the core and surface samples of slag S8 blended mortar bars stored in 5% Na_2SO_4 solution

Mix ID	BB-60S8		TTC-60S8		TIL-60S8	
Age (days)	300		300		300	
Condition of bar	Not Broken		Not Broken		Not Broken	
	Surface	Core	Surface	Core	Surface	Core
Belite	0.4	0.6	0.4	0.5	0.4	0.4
Calcite	10.1	0.1	11	0.4	14.7	0.5
Portlandite	0.9	3.8	0.3	4.1	0.6	3.6
Gypsum	1.5	0.3	1.8	0.4	0.9	0.2
Ettringite	3.4	1.6	1.7	1.1	1.8	1.2
Monosulfate	0	0.7	0	0.3	0	0
Hemicarboaluminate	0	0	0	0.2	0.1	1.8
Monocarboaluminate	0	0	0	0	0.1	0.1
Hydrotalcite	0.4	1.2	0.6	1.6	0.3	1.6
Melilite	0	0.1	0.1	0	0.1	0
AC/Unidentified	83.1	91.7	84	91.4	81.1	90.4

Table 5-15: Phase quantification of the core and surface samples of slag S14B blended mortar bars stored in 5% Na$_2$SO$_4$ solution

Mix ID	BB-60S14B		TTC-60S14B		TIL-60S14B	
Age (days)	300		300		300	
Condition of bar	Not Broken		Not Broken		Not Broken	
	Surface	Core	Surface	Core	Surface	Core
Belite	0.4	0.7	0.4	0.5	0.3	0.5
Calcite	9.5	0.2	10.3	0.4	12.9	0.6
Portlandite	0.1	2.4	0.2	2.7	0.2	2.7
Gypsum	0.9	0.5	1.6	0.3	1.5	0.4
Ettringite	4.8	1.9	3.5	2.4	4.5	2.7
Monosulfate	0	1.6	0	0.6	0	0
Hemicarboaluminate	0	0.7	0	2.7	0.1	2.3
Monocarboaluminate	0	0	0	0	0	0.4
Hydrotalcite	0.2	0.3	0.1	0.6	0.1	0.5
Melilite	0.1	0.1	0	0.1	0	0
AC/Unidentified	83.9	91.5	83.9	89.4	80.3	89.7

Table 5-16: Phase quantification of the core and surface samples of slag S17 blended mortar bars stored in 5% Na_2SO_4 solution

Mix ID	BB-60S17		C-60S17		TTC-60S17		TIL-60S17		THIL-60S17	
Age (days)	330		330		360		360		360	
Condition of bar	Broken		Broken		Not Broken		Not Broken		Not Broken	
	Surface	Core	Surface	Core	Surface	Core	Surface	Core	Surface	Core
Belite	0.5	0.9	0.3	0.6	0.5	0.6	0.4	0.4	0.3	0.6
Calcite	6.5	0.1	5.6	0.1	6	0.2	8.3	0.5	14.2	0.6
Portlandite	0.5	2	0.3	1.7	0.2	2.8	0.3	2.2	0.1	2.1
Dolomite	0	0	0.2	0.3	0	0	0	0	0	0
Gypsum	0.5	0.2	0.6	0.3	0.5	0.2	1.2	0.3	0.9	0.2
Ettringite	9.5	1.1	6.9	1.5	5.9	1.2	6.2	2.3	4.5	2.9
Monosulfate	0.2	3.5	1.1	2.0	0.5	2.1	0	0.5	0	0.4
Hemicarboaluminate	0	0	0	0	0	0	0.1	2.3	0	2.7
Monocarboaluminate	0	0	0	0	0	0	0.1	0.2	0	0.2
Hydrotalcite	0.4	2	0.6	2.6	0.5	2.2	0.9	2	0.6	1.8
Melilite	0.2	0.3	0.2	0.3	0.3	0.3	0.3	0.3	0.2	0.2
AC/Unidentified	81.6	90	84.1	90.4	85.3	90.5	82.2	88.7	78.9	88

Among all the slag blends, the highest ettringite contents were observed at the surface of slag S17 mixtures, which implies poor sulfate resistance of slag S17. Out of these, ettringite was the highest in the BB-60S17 system followed by C-60S17 at 330 days (broken age) which explains mortar bar failure in the duplicate batch, due to higher alumina content contributed from both cement and slag. The ettringite content at the surface was then followed by TIL-60S17 and TTC-60S17 mixtures. However, similar to IL control mixtures, primary ettringite formed prior to sulfate exposure was higher in IL cements + slag S17 blends compared to the TTC-60S17 mix as listed in Table 5-12. Therefore, secondary ettringite formation appeared to be higher in the TTC-60S17 blend, coinciding with possible earlier bar failure according to ASTM C1012. In all slag S17 mixtures except for TIL-60S17 and THIL-60S17, substantial amounts of monosulfoaluminate were detected at the surface even at 1 year of exposure. This implies further potential expansion and deterioration of those bars, when the remaining monosulfoaluminates convert to ettringite. However, in IL cement blends, no monosulfoaluminate was observed at the surface and only traces of monosulfoaluminate were detected at the core, which implies delay and/or suppression of bar expansion even further.

5.3.1.6 Thermodynamic Modeling

Figure 5-15 through Figure 5-18 illustrate the phase assemblage predicted for controls BB, C, TTC and TIL mixtures immersed in 5% Na_2SO_4 solution. The left side of the plots indicate the phases at the core of the bars while the right side corresponds to the surface of the bars in contact with the sulfate solution. The main phases predicted at the core of the control mixtures were C-S-H, ettringite, hemi- and monocarboaluminate, portlandite and Fe-siliceous hydrogarnet ($C_3FS_{0.84}H_{4.32}$). No carboaluminate phases were detected however by XRD analysis for the control mixtures, possibly due to their low amounts. Monosulfoaluminate was only observed in the control BB mixture due to its high C_3A content. Although both cement BB and cement C have approximately similar C_3A contents, no monosulfoaluminate was predicted at the core of the control C mix, instead, considerably higher ettringite content was predicted similar to QXRD findings. Cement C has a higher alkali content which may have increased the stability of ettringite as discussed before. Additionally, small amounts of hydrotalcite and unhydrated calcite were also predicted in all the control mixtures. Predicted hydrotalcite content in control C was the highest due to its higher MgO content (2.5%) in cement C. However, no hydrotalcite was detected by QXRD analysis likely due to its small amounts. Unhydrated calcite content increased with increasing limestone contents of cements.
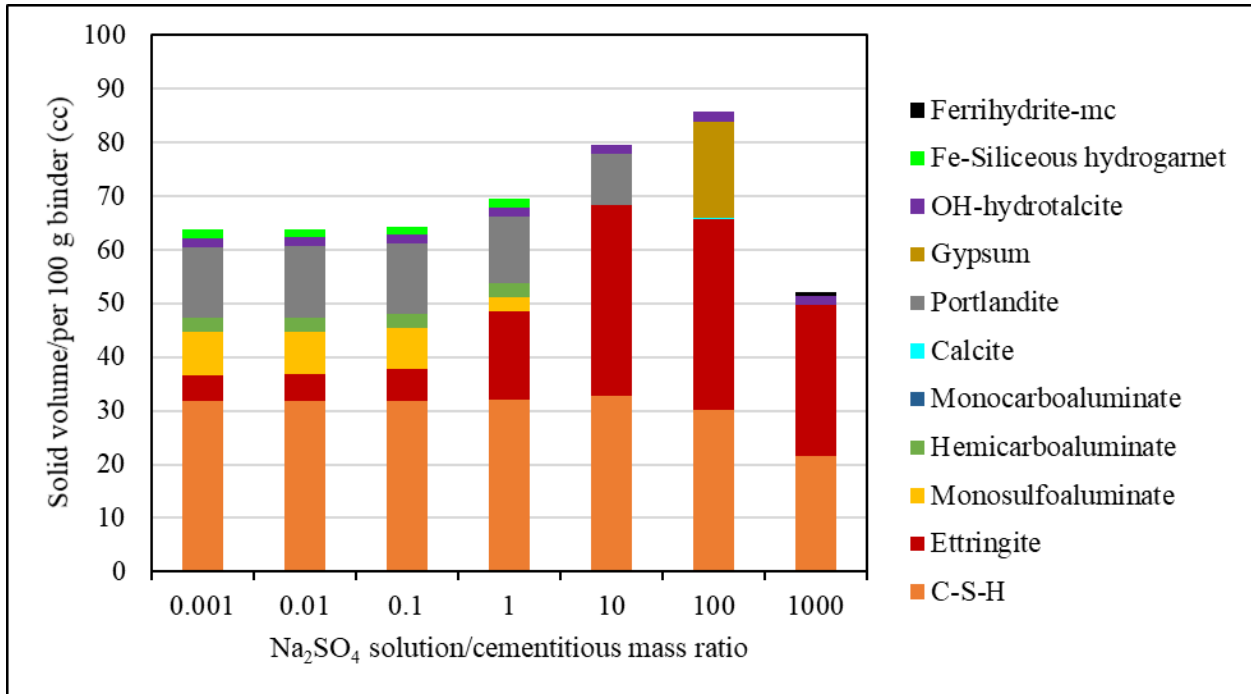
Figure 5-15: Predicted phase assemblage for control BB mixture immersed in 5% Na_2SO_4 solution
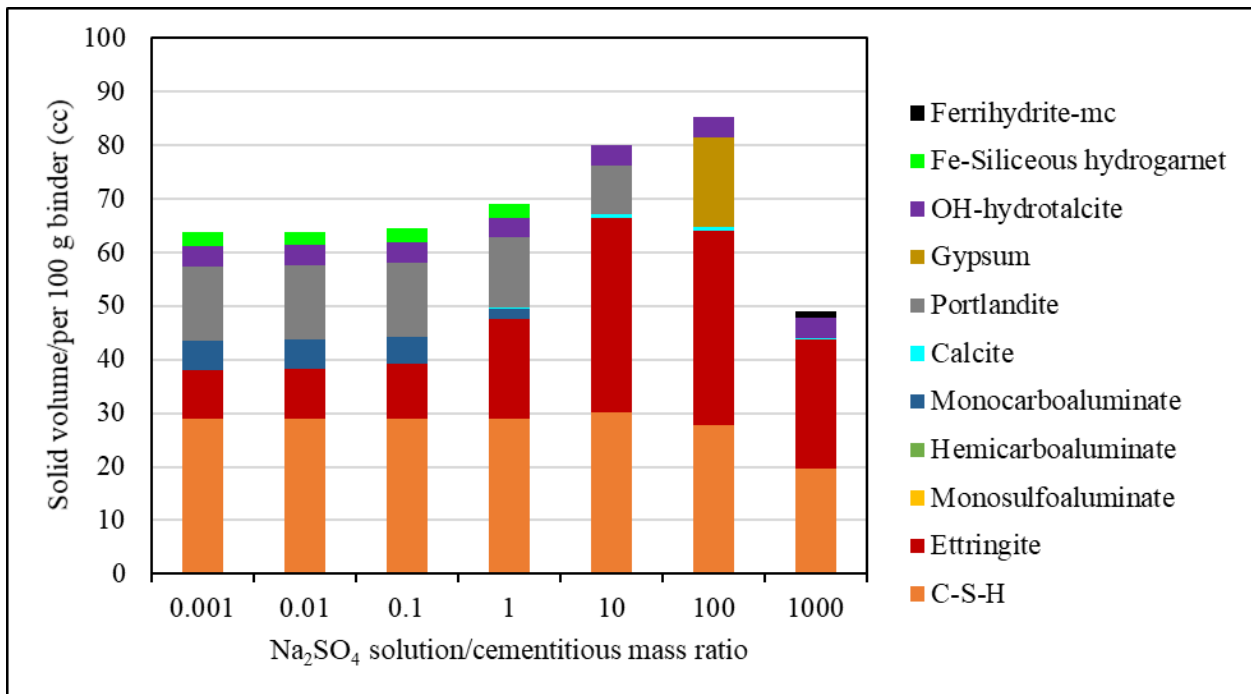
Figure 5-16: Predicted phase assemblage for control C mixture immersed in 5% Na_2SO_4 solution
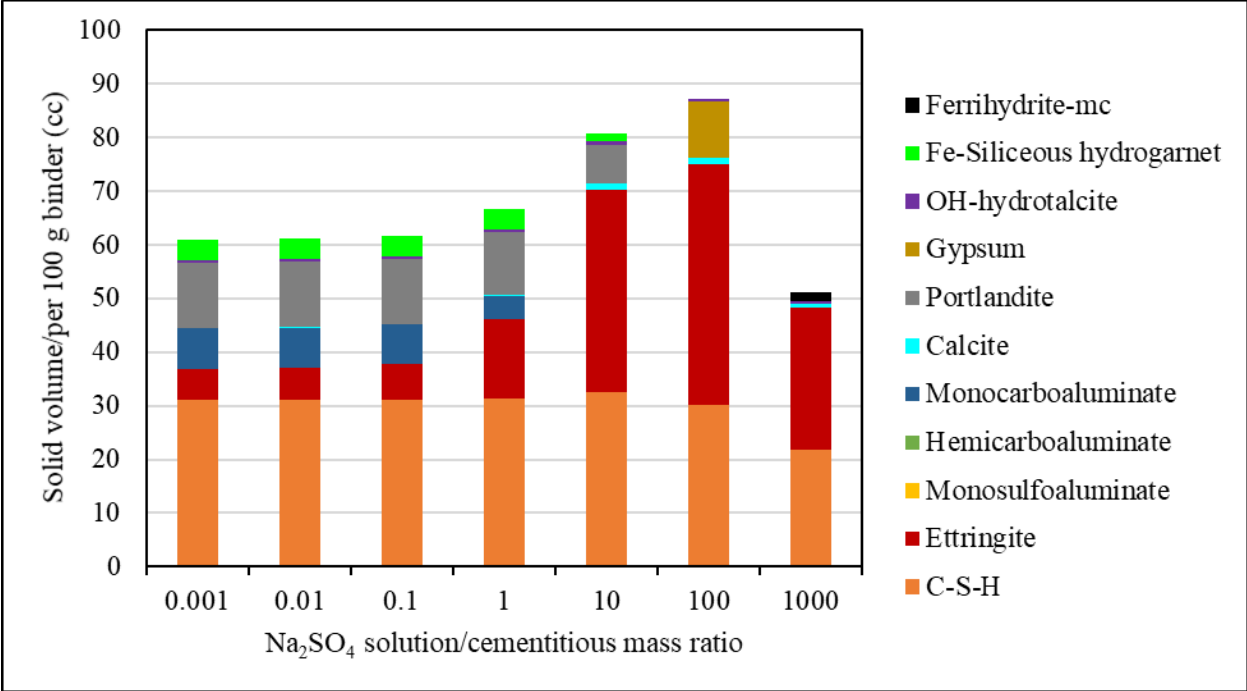
Figure 5-17: Predicted phase assemblage for Control TTC mixture immersed in 5% Na_2SO_4 solution
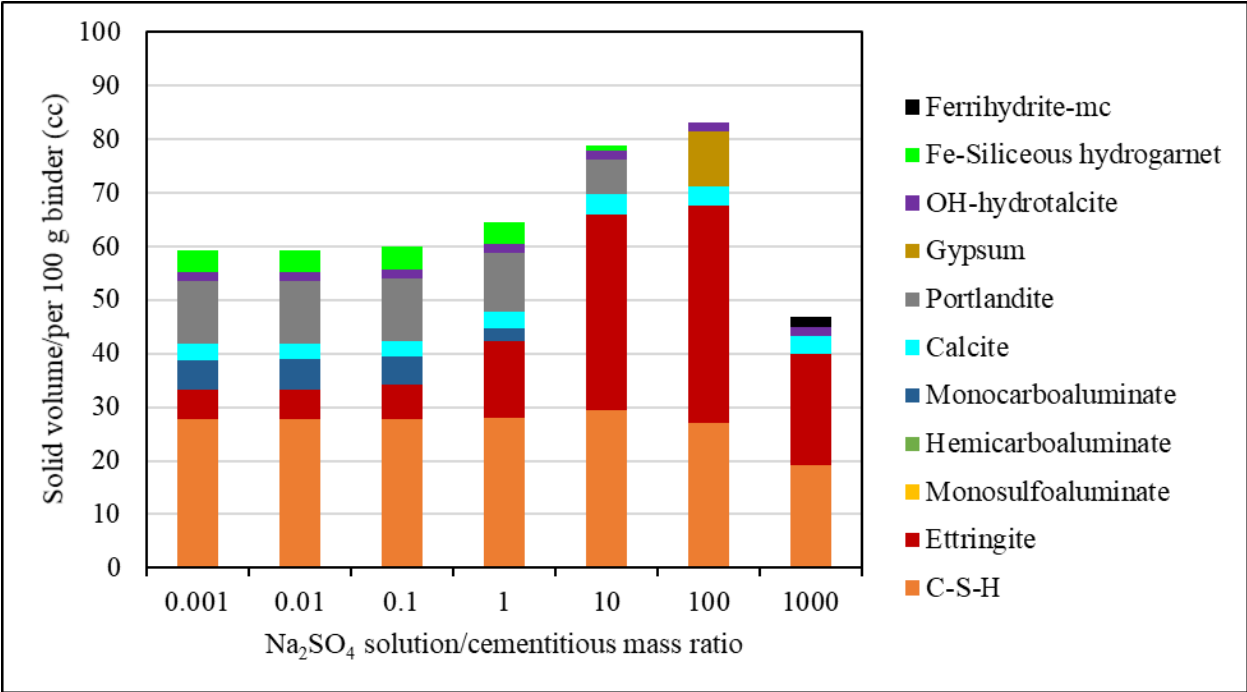
Figure 5-18: Predicted phase assemblage for Control TIL mixture immersed in 5% Na_2SO_4 solution

As the surface of the mortar bars is approached, a significant increase in ettringite volume can be observed, which caused an increased total solid volume, as expected. The conversion of monosulfoaluminate to ettringite was observed in the control BB mix. Moreover, as stated in the literature [59], decomposition of alumina-bearing phases such as hemicarboaluminate and monocarboaluminate, in presence of an external sulfate source, to form ettringite was apparent. This was further supported by the formation of calcite. Furthermore, decomposition of portlandite and formation of secondary gypsum were also seen near the surface of the control mortar bars, in agreement with QXRD findings.

Figure 5-19 through Figure 5-28 show that the addition of slag changed the phase assemblage and the total solid volume. Addition of slag is expected to increase the C-S-H volume and decrease the portlandite content. Portlandite was not predicted in any of the blended systems, due to the pozzolanic reaction. Increase in C-S-H volume was observed in slag S8 blends. However, in high-alumina slag mixtures, at the core of the mortar bars, no such increase in C-S-H volume was seen, but notable amounts of stratlingite were predicted. It implies that these mixtures had more alumina than could be incorporated into C-S-H [60] structure. It is likely because the slag DOH assumed in modeling was higher than what the slag had in reality. Furthermore, monosulfoaluminate was predicted in all the slag-blended systems, except in TTC-60S8, TIL-60S8 and TIL-60S17 mixtures. Formation of monosulfoaluminate can be attributed to the alumina from slags. The higher the slag alumina content, the more monosulfoaluminate formed. In low-alumina slag (S8) mixtures with cements TTC and TIL, no monosulfoaluminate was observed due to the lower alumina content in the slag and the lower C_3A contents in cements. Instead, ettringite and carboaluminate phases were formed. However, in the mixture with sulfated slag S17 and cement TIL (Type IL cement), no monosulfoaluminate was predicted. This is likely due to the presence of sulfate in slag and limestone in cement. On the other hand, in the TIL-60S14B mix, a small amount of monosulfoaluminate was predicted. In general, slightly higher monosulfoaluminate and/or carboaluminates were observed in slag S14B blends compared to those of slag S17. This can be attributed to the lower amount of hydrotalcite formed in slag S14B mixtures due to its low MgO content. Typically, the Mg/Al ratio of hydrotalcite formed in slag blends is approximately 2 [54]. However, XRD analysis did not detect such a trend in monosulfoaluminate at the core of the mortar bars, though for S14B mixtures the amounts of carboaluminates and ettringite were slightly higher while hydrotalcite content was lower.
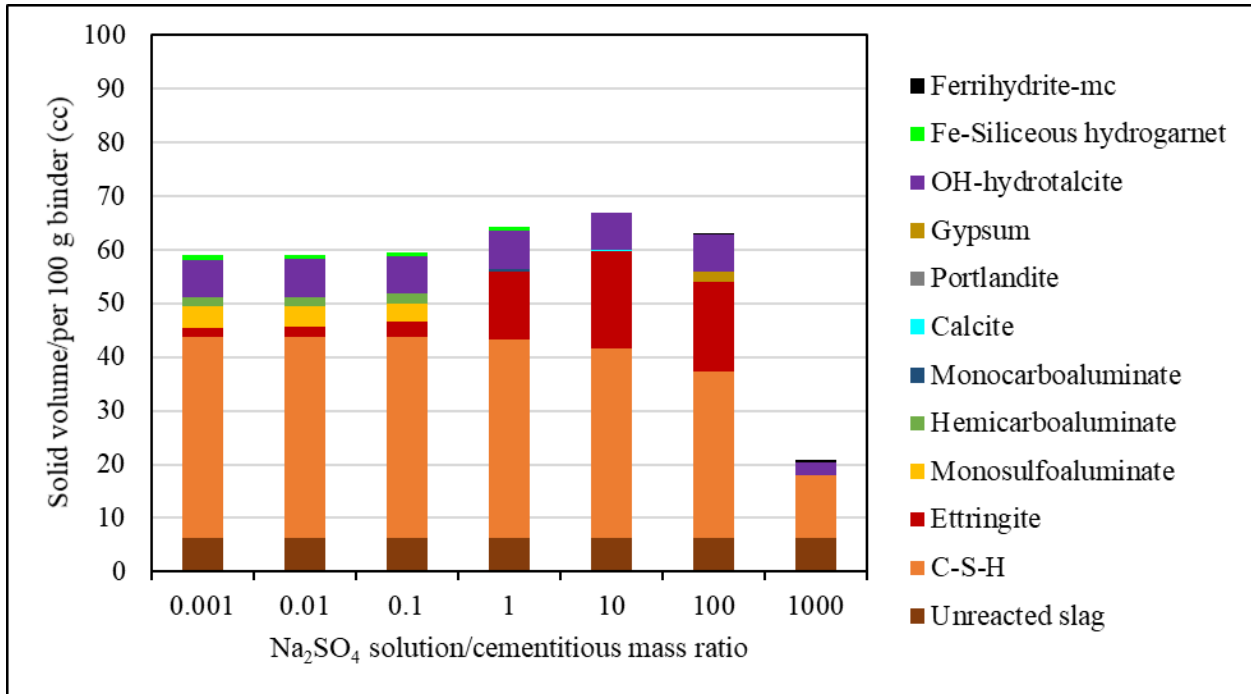
Figure 5-19: Predicted phase assemblage for BB-60S8 mixture immersed in 5% Na_2SO_4 solution
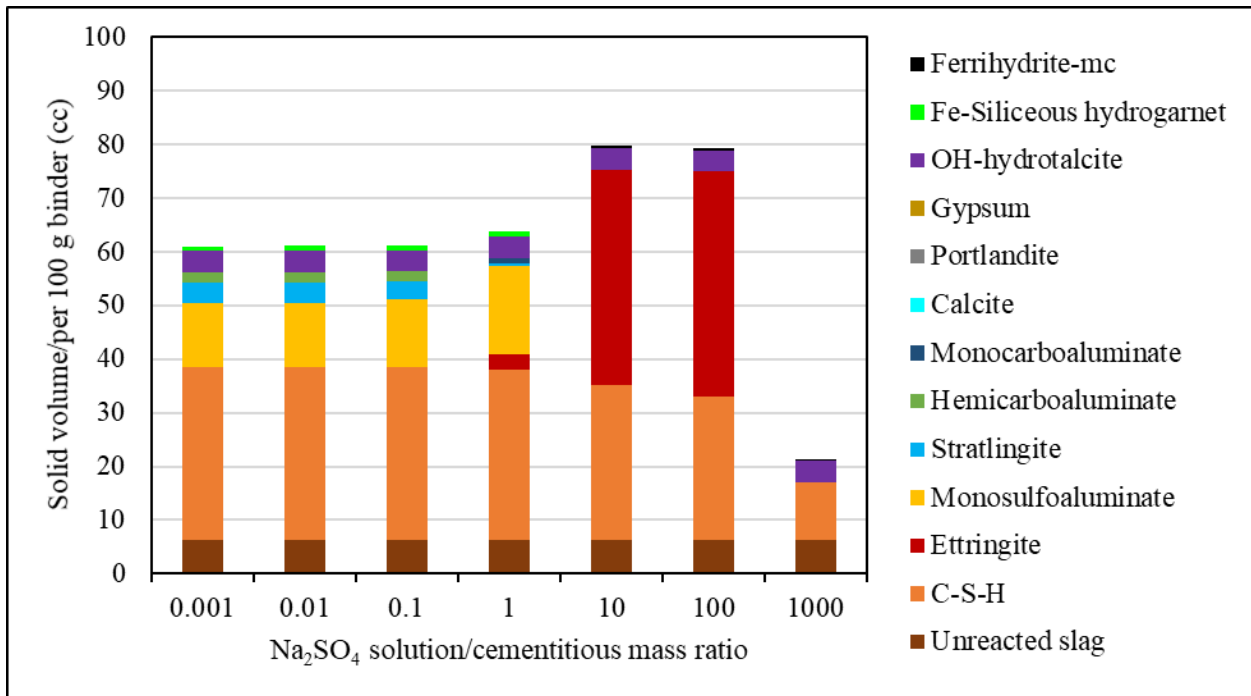
Figure 5-20: Predicted phase assemblage for BB-60S14B mixture immersed in 5% Na_2SO_4 solution
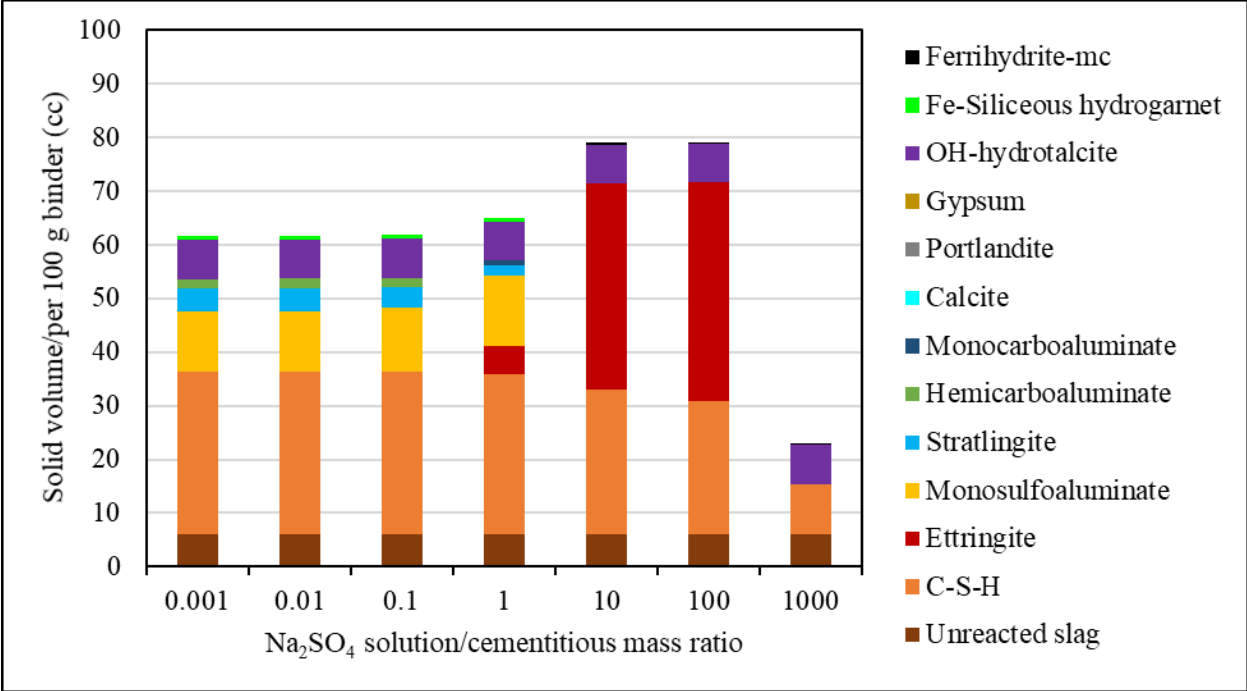
Figure 5-21: Predicted phase assemblage for BB-60S17 mixture immersed in 5% Na_2SO_4 solution
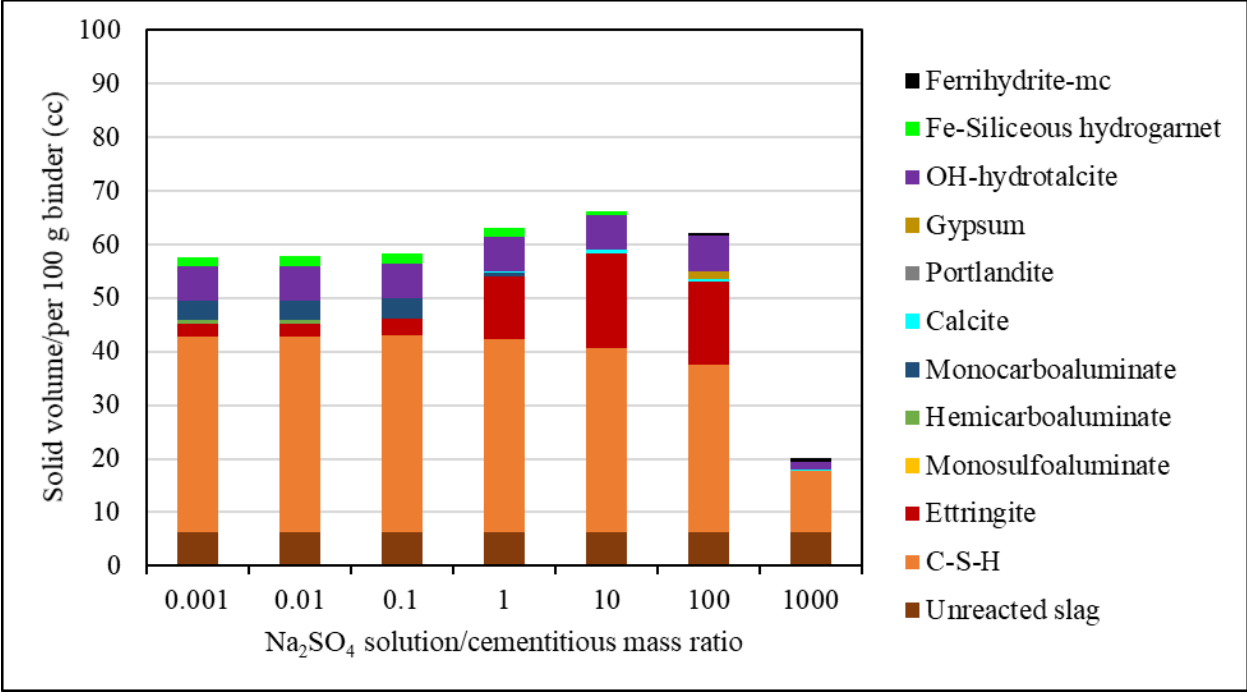
Figure 5-22: Predicted phase assemblage for TTC-60S8 mixture immersed in 5% Na_2SO_4 solution
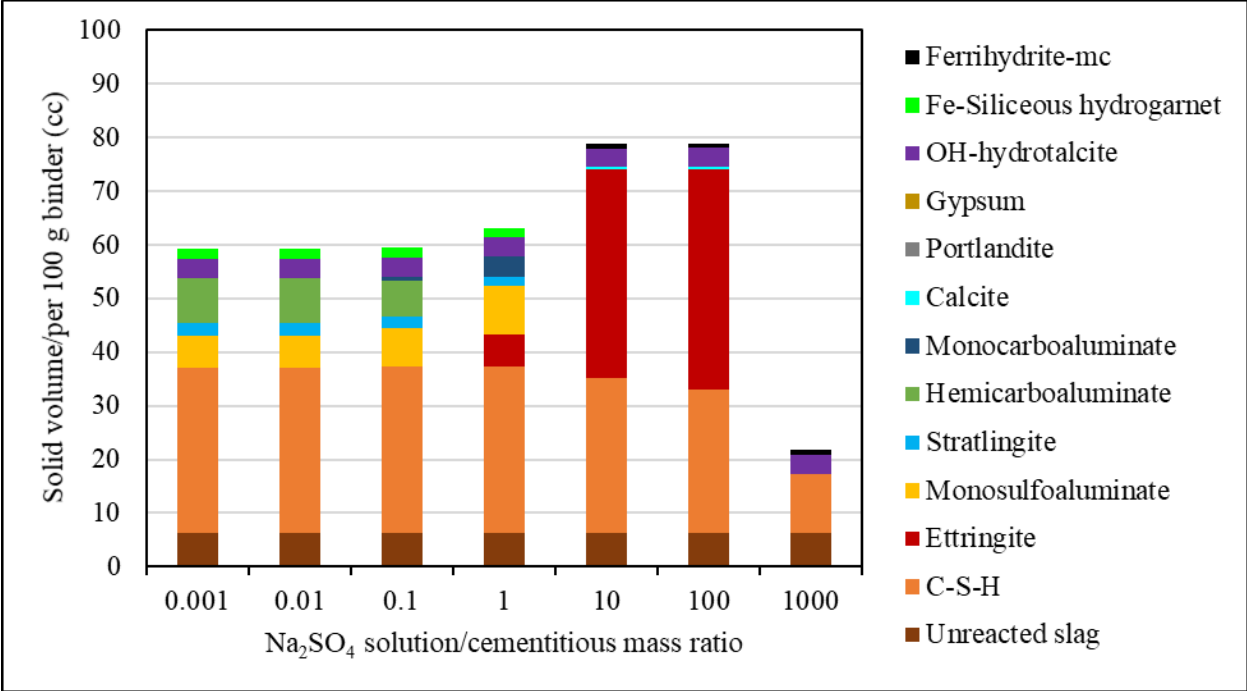
Figure 5-23: Predicted phase assemblage for TTC-60S14B mixture immersed in 5% Na_2SO_4 solution
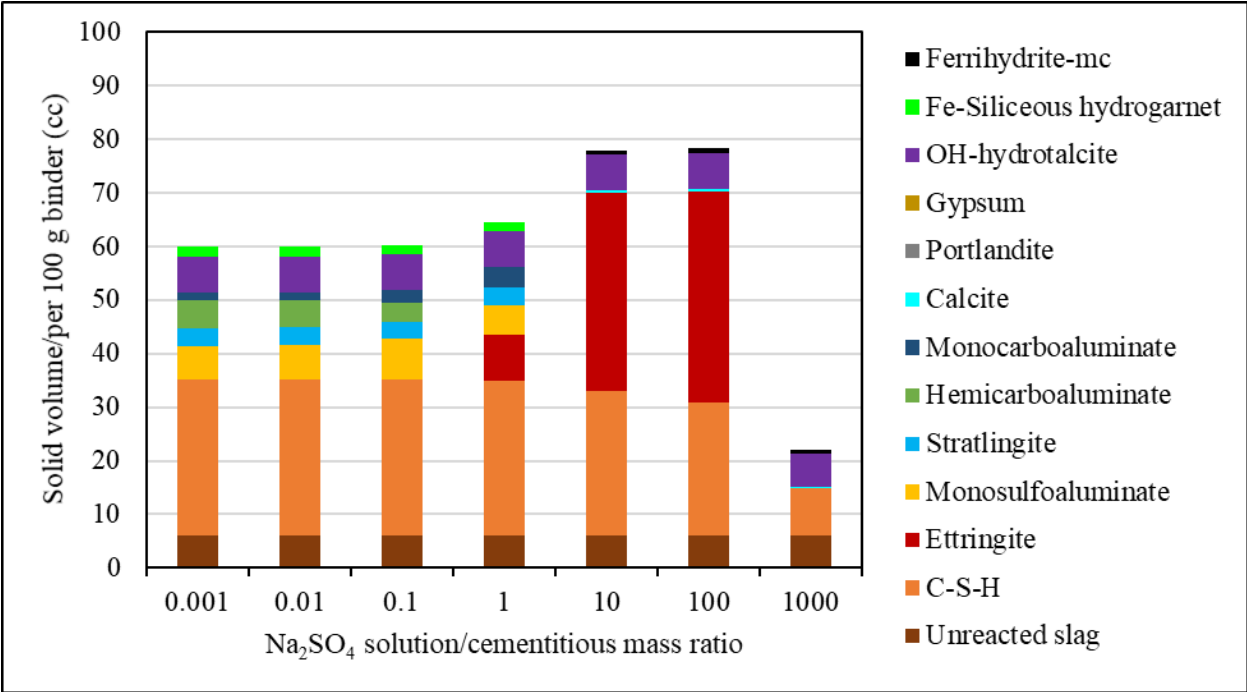
Figure 5-24: Predicted phase assemblage for TTC-60S17 mixture immersed in 5% Na_2SO_4 solution
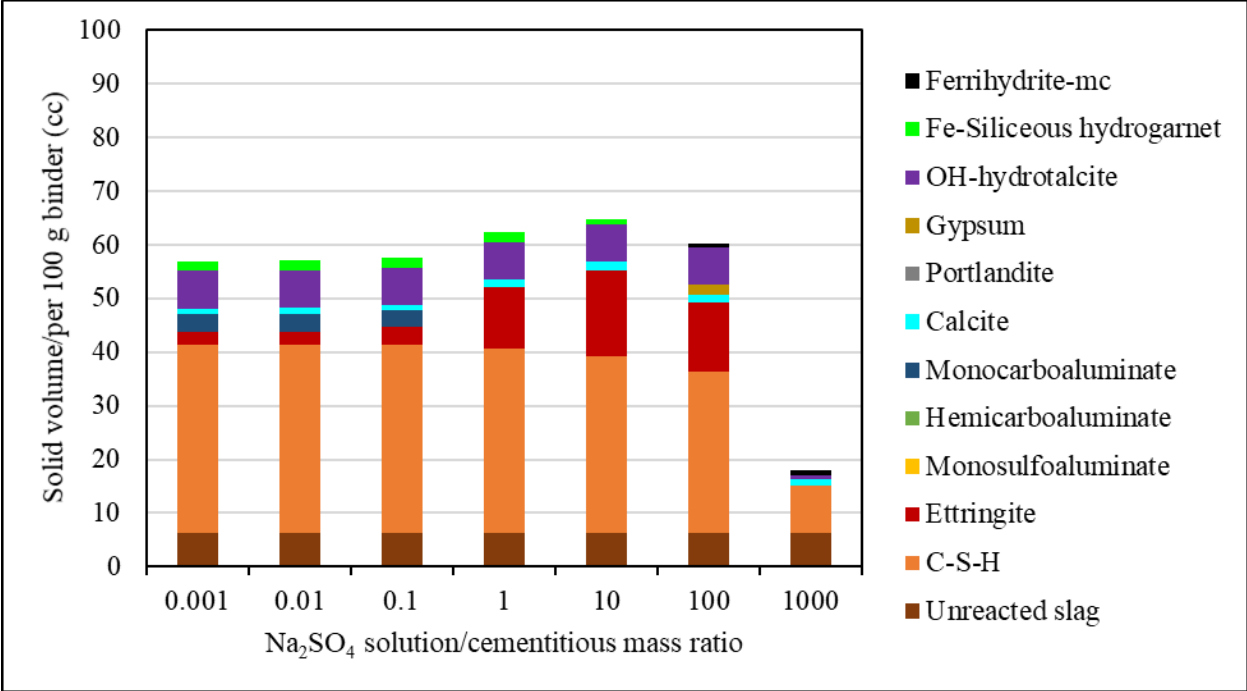
Figure 5-25: Predicted phase assemblage for TIL-60S8 mixture immersed in 5% Na_2SO_4 solution
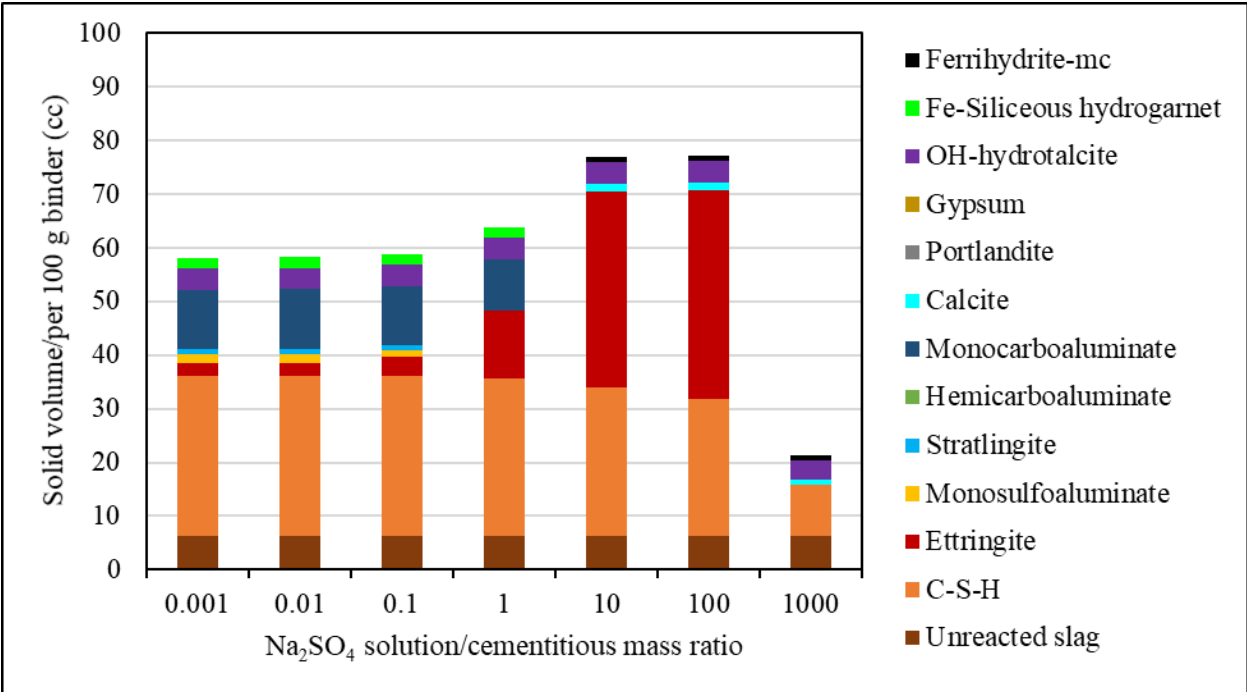
Figure 5-26: Predicted phase assemblage for TIL-60S14B mixture immersed in 5% Na_2SO_4 solution
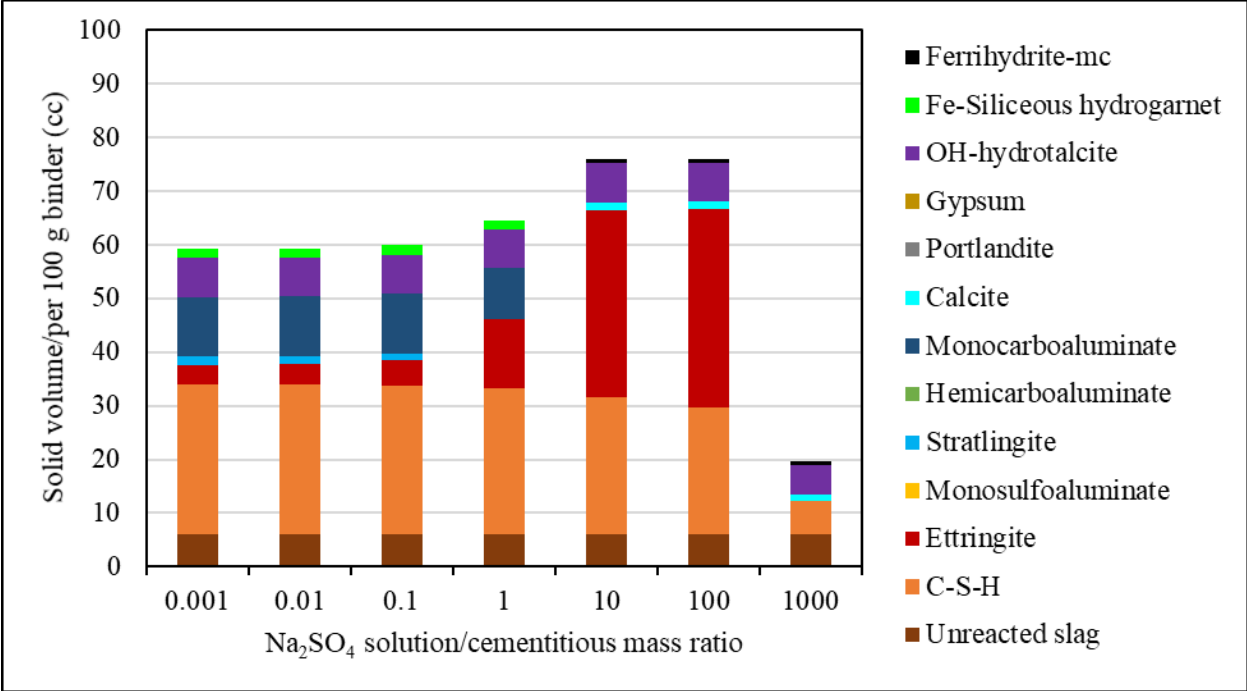
Figure 5-27: Predicted phase assemblage for TIL-60S17 mixture immersed in 5% Na_2SO_4 solution
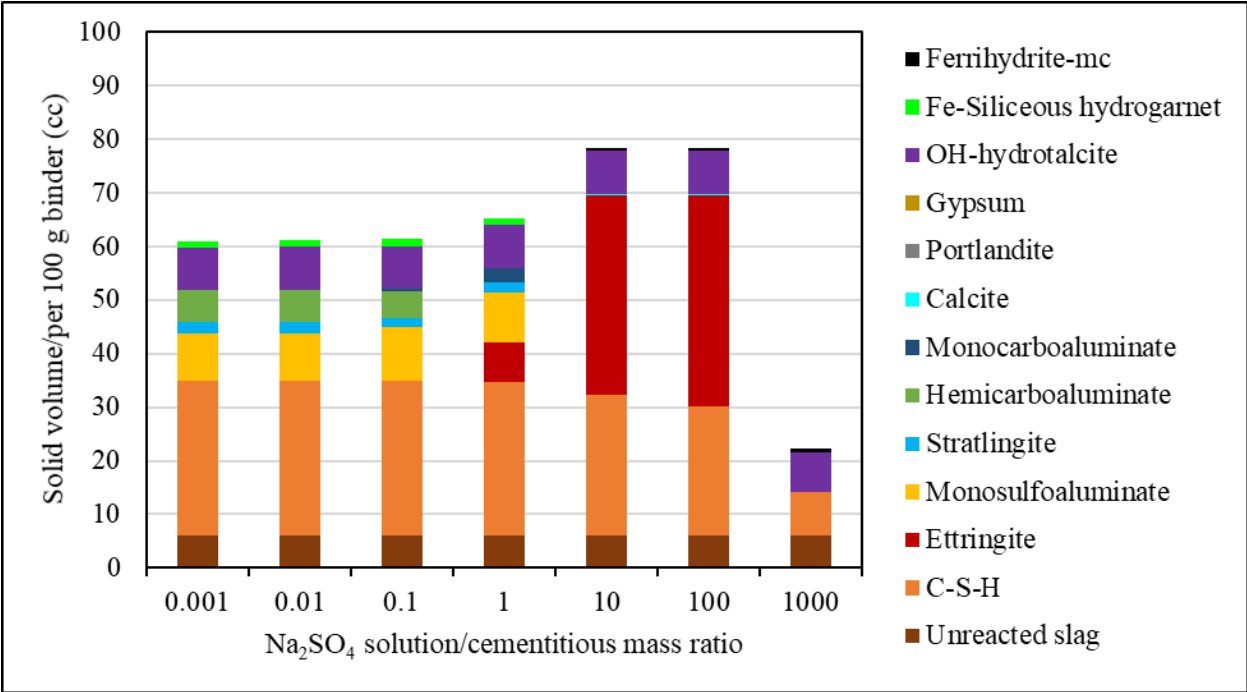
Figure 5-28: Predicted phase assemblage for C-60S17 mixture immersed in 5% Na_2SO_4 solution

Similar to the control mixtures, as the surface of the slag-blended mortar bars is approached, a substantial increase in ettringite volume was observed with a corresponding increase in the total solid volume. This can be due to the conversion of monosulfoaluminate and decomposition of carboaluminate phases in the presence of external sulfate source. Moreover, a leaching effect was observed in both control and blended systems, as indicated by the decreased volumes of C-S-H, ettringite, and gypsum with increasing sulfate solution volume [47]. It is interesting to see the predicted decrease in C-S-H volume around a solution-to-binder mass ratio of 0.5 for BB-60S14B and BB-60S17, while this decrease in other mixtures was observed at a solution-to-binder mass ratio of 1. This implies faster deterioration of BB-60S14B and BB-60S17 mixtures in sulfate environments at the same concentration. This also implies that a large part of the benefits seen by slag comes from a reduction in transport properties to keep the sulfate ions out of the concrete.

Predicted volume change of the studied mixtures are listed in Table 5-17. Solid volume increase was calculated considering the difference between the maximum and the initial solid volumes of the system. Initial total volume includes the solid volume as well as the pore volume in the system. When comparing the maximum solid volume and the initial total volume, clearly the controls BB, C, TTC and TIL exceeded their initial total volumes, which indicates expansion. Moreover, the least solid volume increase was observed in slag S8 blends while the highest was observed in slag S14B mixtures.

Table 5-17: Predicted volume changes for mixtures immersed in 5% Na_2SO_4 solution

Mix ID	Initial total volume (cc/100g binder)	Initial solid volume (cc/100g binder)	Max solid volume (cc/100g binder)	Solid volume increase (cc/100g binder)
Control BB	81	64	87	23
Control C	80	64	86	23
Control TTC	81	61	89	28
Control TIL	81	59	85	26
BB-60S8	82	59	67	8
BB-60S14B	82	61	80	19
BB-60S17	82	62	80	18
TTC-60S8	82	58	68	11
TTC-60S14B	82	59	80	21
TTC-60S17	82	60	79	19
TIL-60S8	82	57	67	10
TIL-60S14B	82	58	78	20
TIL-60S17	82	59	77	17
C-60S17	82	61	79	18

The phase assemblage of selected sulfate-optimized mixtures was also modeled using GEMS. Figure 5-29 and Figure 5-30 illustrates the predicted the phases of sulfate-optimized BB-60S14B and TIL-60S14B mixtures. Clearly, addition of sulfate to the blends affects the phases formed and their quantities. When additional sulfate is incorporated in slag, an increase in ettringite volume is expected in the core of the bars. While this was predicted in both optimized BB-60S14B and TIL-60S14B systems, a small increase in monosulfoaluminate was also observed only in the optimized BB-60S14B mix. This was the opposite in the TIL-60S14B mix, in which monosulfoaluminate decreased and was completely eliminated at 3.78% total SO_3 in the system. It is interesting to see stratlingite disappear with sulfate addition to the slag, which may have contributed to the increase in monosulfoaluminate volume in the optimized BB-60S14B mix. A considerable amount of stratlingite was predicted in cement BB blends due to its high C_3A content, whereas only a trace amount of stratlingite was predicted in cement TIL blends. Nevertheless, sulfate-optimized mixtures showed lower solid volume increase close to the surface when exposed to sulfate solution and compared to their respective as-received systems. This implies less expansion is expected to occur in the sulfate-optimized mixtures. This effect was more significant in the IL cement systems, due to the formation of monocarboaluminate which stabilized initial

195

ettringite. As stated in the literature [12], [54], additions of limestone and calcium sulfate allow for and/or increase the formation of monocarboaluminate and ettringite prior to sulfate exposure. As discussed previously in section 5.3.1.3, the onset of expansion is delayed when the total SO_3 was increased to 4% (using 6.5% gypsum addition) in a system with Type V cement (4.9% C_3A) and 60% high-alumina slag (15.2% Al_2O_3) [12]. Addition of 4% limestone to the sulfated mixture further suppressed expansion and improved sulfate resistance. Therefore, it appears when high-alumina slags are blended with Type I cements, addition of sulfate and/or limestone powder would be desirable to enhance sulfate resistance.
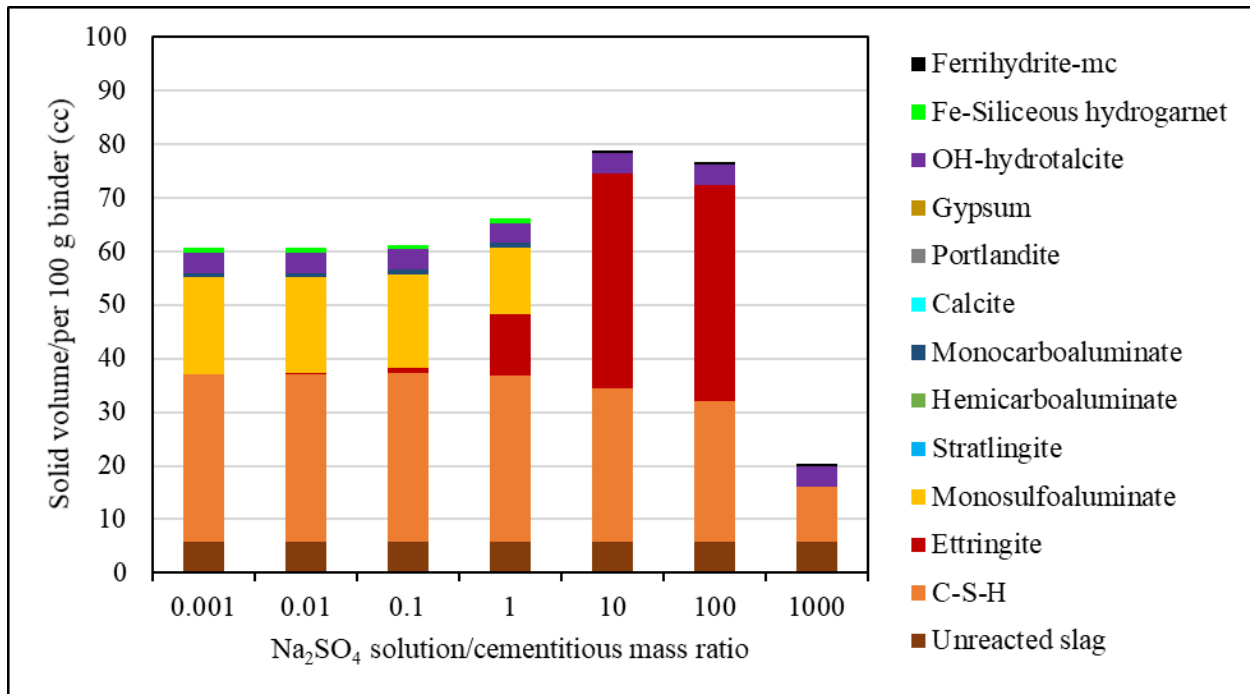
Figure 5-29: Predicted phase assemblage for 2-day optimized BB-60S14B (Total SO_3 4.31%) mixture immersed in 5% Na_2SO_4 solution
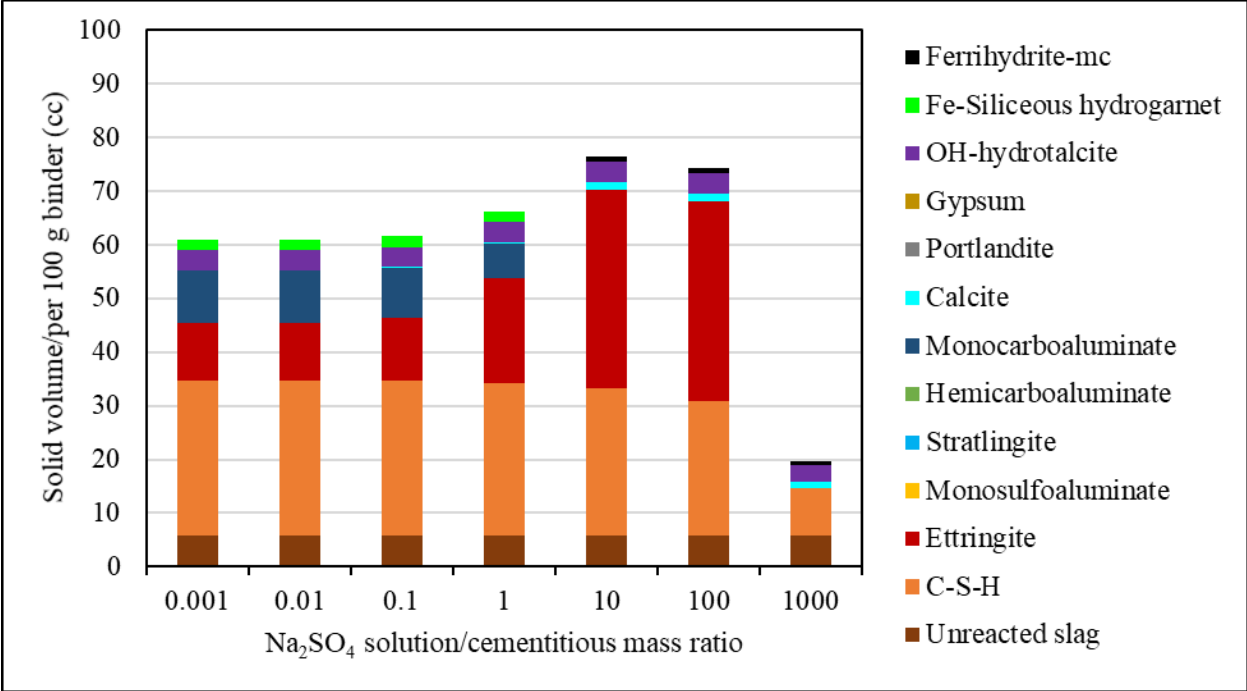
Figure 5-30: Predicted phase assemblage for 2-day optimized TIL-60S14B (Total SO_3 3.78%) mixture immersed in 5% Na_2SO_4 solution

5.3.1.7 Summary

The findings indicate the significance of the cement and slag characteristics on the sulfate durability of plain cement and slag-blended mortar bars tested in accordance with ASTM C1012 [31]. Earlier failure of mortar bars prepared with Type I cements (BB and C) of higher C_3A content indicate poor sulfate resistance when compared to the other cements. The delayed expansion and subsequent failure of Type I (HA) cement (C) mortar bars, compared to cement B, is likely due to the initial ettringite stability caused by higher pH levels. Type IL cements (TIL and THIL) followed by Type II (MH) cement (TTC) showed substantially lower expansion indicating moderate sulfate resistance. This is due to the moderate C_3A content of Type II (MH) cement and the reduced clinker fraction in Type IL cements. Additionally, formation of carboaluminates in IL cement systems stabilized the primary ettringite and lowered monosulfoaluminate content.

In terms of blended systems, addition of any slag at a 60% replacement level, regardless of its characteristics, enhanced sulfate resistance in Type I cement blends by delaying the onset of expansion compared to the respective control mixtures of plain cement. Additionally, expansion was similar or slightly lower in blends with Type II(MH) and Type IL up to 6 months. Moreover,

197

due to the limited testing age, no significant trends were observed in expansion among the slag blends, but at the current age the high-alumina slag S17 showed the highest length change when blended with all cement types (I, II(MH), IL). This effect was more noticeable when slag S17 was blended with Type I cements, possibly due to higher amounts of monosulfoaluminate detected by QXRD prior to sulfate exposure. Thermodynamic modeling also demonstrated higher susceptibility to sulfate attack in high-alumina slag systems (S14B and S17) when blended with Type I cement (BB). This was confirmed by the higher amounts of ettringite at the surface of mortar bars of Type I cement and high-alumina slag blends as detected by QXRD after about 1 year of exposure. Moreover, Type II(MH) cement-slag blends demonstrated moderate sulfate resistance as indicated by XRD analysis and thermodynamic modeling. Conversely, the phases assemblage determined from QXRD and predicted from GEMS analysis indicate IL blended cements provide higher resistance to sulfate attack due to carboaluminate formation which suppresses and/or controls monosulfoaluminate formation.

In terms of the sulfate-optimized mixtures, most mixtures showed lower expansions at the current testing age compared to their respective as-received systems indicating a delayed onset of expansion. Thermodynamic modeling demonstrated a decrease in solid volume increase in the optimized systems close to the surface when exposed to sulfate solution compared to their respective as-received systems, which is indicative of lowered expansion. This effect was more noticeable in IL cement blends. Apparently, the addition of sulfate to slag-blended mixtures improved sulfate resistance while the combined addition of sulfate and limestone was more effective in enhancing sulfate durability.

5.3.2   Length Change Measurements after Heat Treatment

5.3.2.1 As-Received Cement Systems

Figure 5-31 shows the expansion of control mortar bar mixtures prepared with cements BB, C, Z, TIL and THIL. Table 5-18 summarizes the expansion of the control mixtures at 180 days. The maximum expansion was observed in control BB, followed by control C, both of which are Type I cements. This was expected because of their high C_3A contents [17]. It has been reported that high C_3S contents result in rapid formation of C-S-H at high temperatures and can decrease ettringite stability by acting as a 'sink' for aluminates due to substitution of silicates and for sulfates

due to adsorption [17]. As a result of ettringite decomposition, higher amounts of monosulfoaluminate can be available in these systems after heat treatment and can potentially form ettringite during storage. On the other hand, the expansion of control Z and control TIL were substantially lower. The lowest expansion was observed for control THIL. The lower expansion in IL cements can be attributed to the lower C_3A contents due to a reduced clinker fraction. Control BB showed the highest expansion, Control C had a smaller induction period of approximately 30 days before the onset of expansion whereas the induction period of control BB was approximately 60 days. It is likely the higher alkali content present in cement C (1.05 Na_2O_{eq}%), triggered DEF and caused expansion at an earlier age. However, the rate of expansion of control BB was higher and surpassed the expansion of control C at around 90 days of storage. Although well-distinguished induction periods were not observed in the control mixtures of Z, TIL, and THIL cements, those were approximately 30, 60, and 60 days, respectively. The shorter induction period of control Z can also be attributed to accelerated DEF due to the higher alkali content (0.65 Na_2O_{eq}%) in the cement.
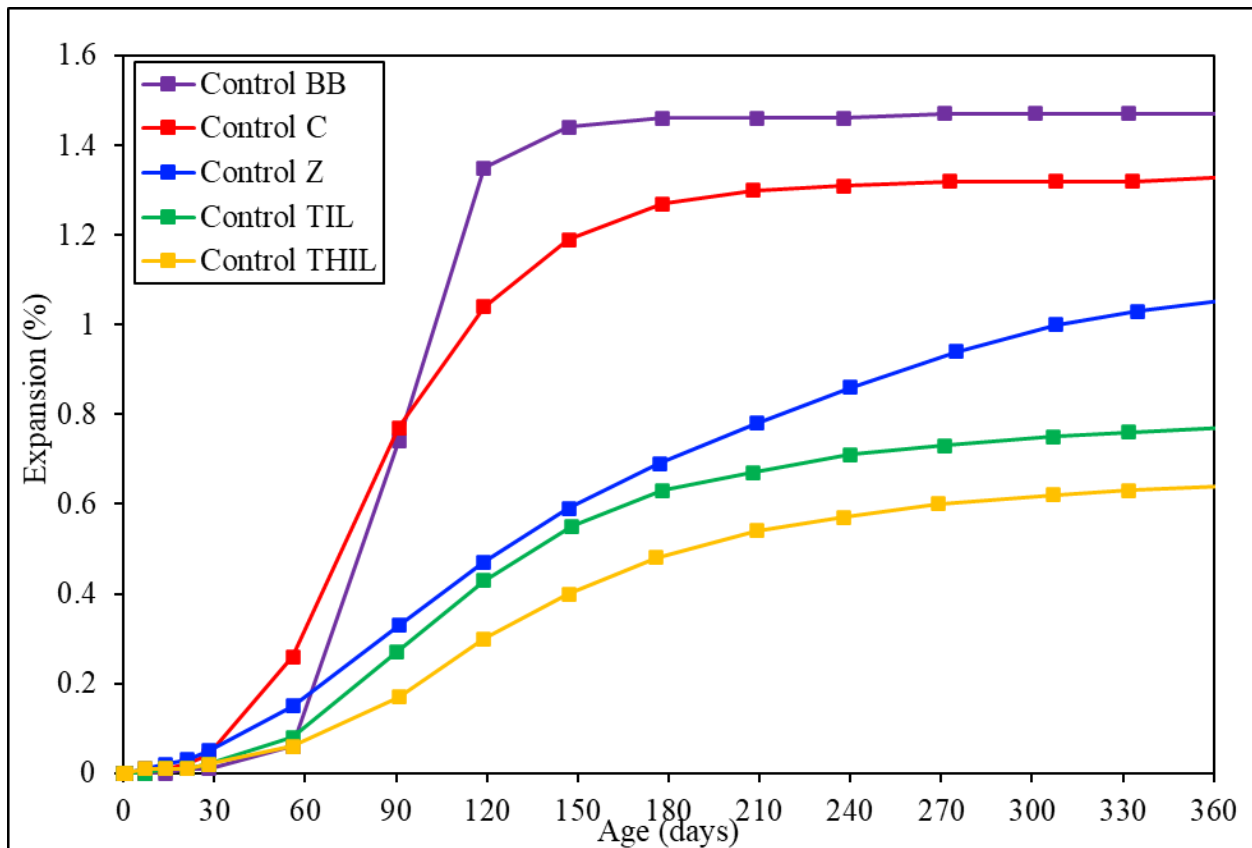
Figure 5-31: Length change of as-received cement mortar bars after heat treatment

Table 5-18: Expansion of control mixtures at 180 days

Mixture ID	Expansion at 180 days (%)
Control BB	1.46
Control C	1.27
Control Z	0.69
Control TIL	0.63
Control THIL	0.48

5.3.2.2 As-Received Slag-Blended Systems

The length change of the as-received slag-blended systems are illustrated in Figure 5-32 through Figure 5-36. Table 5-19 summarizes the expansion of slag-blended mixtures at 180 days. L0 in the mixture ID denotes the as-received blended system. Clearly, incorporation of slag-blended mixtures significantly reduced expansion compared to their respective control mixtures. This is in agreement with what is reported in the literature [14], [20], [61]. These studies considered slag substitution levels of 25% and 35% and heat curing at 95 °C, in which an expansion of 0.2% and 0.01% were reported for 25% and 35% slag-blended system at 1,200 days, respectively. Apparently, higher slag substitution levels gave lower expansion caused by DEF. Thus, Ramlochan et al. [20] stated that "a replacement level of 25% may suppress long-term expansion with most cements, but higher levels may be required when used with cements having very high sulfate or alkali contents". Nevertheless, ACI committee 201 [62] has recommended slag substitution levels greater than or equal to 35% with any ASTM C150/C150M portland cement to reduce damage caused by DEF. The fact that any cement with a minimum of 35% slag would control DEF is questionable and requires further investigation because cement and slag characteristics such as high alkali and sulfate levels, presence of limestone, and high fineness may influence the expansion caused by DEF. However, in the current study, no expansion was observed in the 60% slag-blended systems during the reported testing period.

The reason for controlled and delayed expansion in the slag-blended systems was explained as a result of the dilution effect, increased Al_2O_3 content and the low concentration of the $(SO_4)^{2-}$ in the pore solution. To the best of the authors' knowledge, there is no study currently available which has discussed the effect of slag alumina contents or slag with added sulfates on expansion caused by DEF. However, high alumina levels contributed by SCMs appear to suppress the long

term expansion after heat treatment. Addition of SCMs such as metakaolin, that have very high alumina levels have been reported to control or eliminate the expansion even at cement replacement levels as low as 8% [20]. As stated by Ramlochan [14], incorporation of alumina-bearing SCMs prevents the conversion from monosulfoaluminate to ettringite, and instead the sulfates and alumina react to form ettringite which will be precipitated in any available void space. Therefore, it is likely that slags may delay the onset of expansion or suppress the expansion. However, the slag used in Ramlochan study had a low alumina content of 9.42% and was not sulfated; therefore, the findings of that study might not be predictive of the currently available sulfated slags in the state of Florida with alumina content that can be above 17%.

The presence of limestone is expected to delay or suppress expansion caused by DEF because of the reduced clinker fraction and also the formation of carboaluminate phases due to the reaction between alumina and calcite. Deboucha et al. [63] studied the combined effect of limestone filler and slag on DEF in heat-cured mortar using a slag with 7.35% Al_2O_3. The findings indicated that 10% and 20% slag ternary cements with 5% limestone filler delayed onset of expansion and lowered long-term expansion. Moreover, 40% slag with 5% limestone filler suppressed the expansion caused by DEF. Therefore, it is possible that mixtures with IL cement and slags (Figure 5-35 and Figure 5-36) may have lower or suppressed long-term expansion.
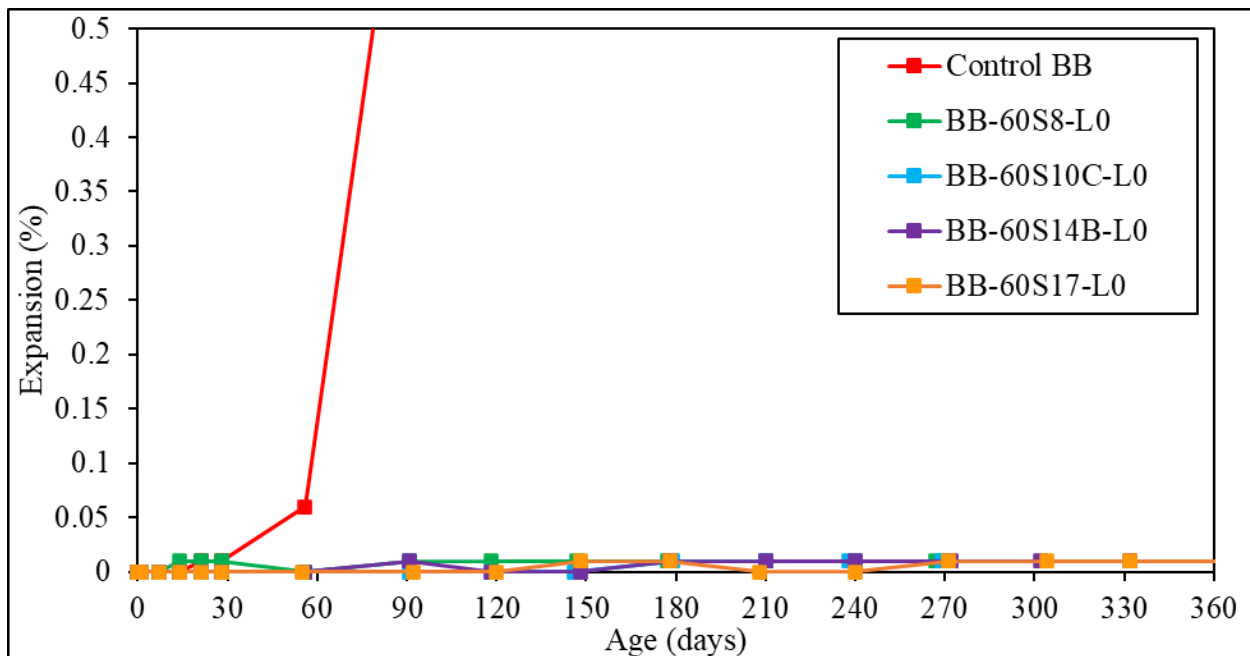
Figure 5-32: Length change of slag-blended mortar bars with cement BB after heat treatment
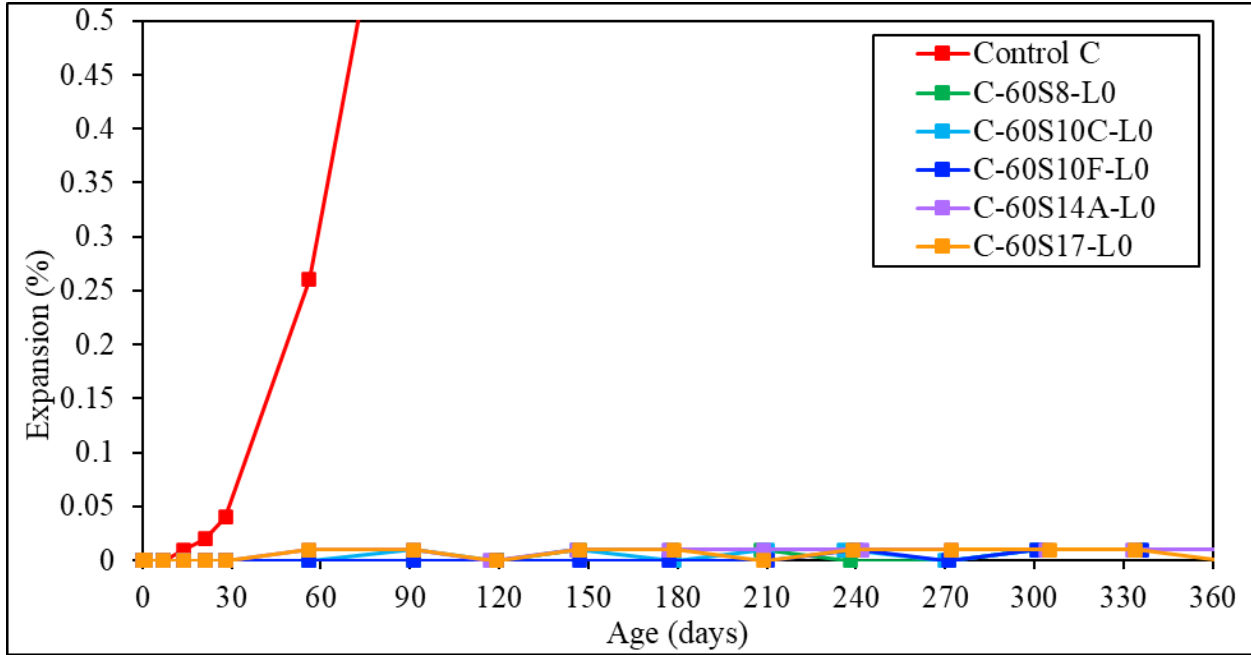
Figure 5-33: Length change of slag-blended mortar bars with cement C after heat treatment
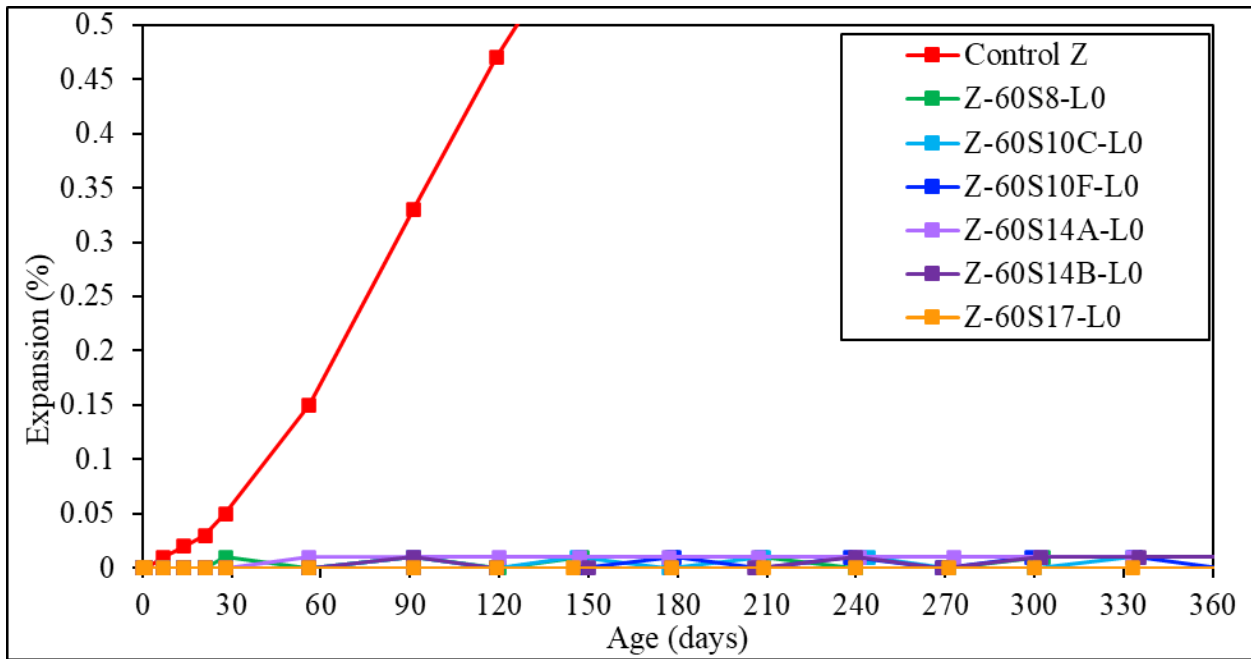
Figure 5-34: Length change of slag-blended mortar bars with cement Z after heat treatment
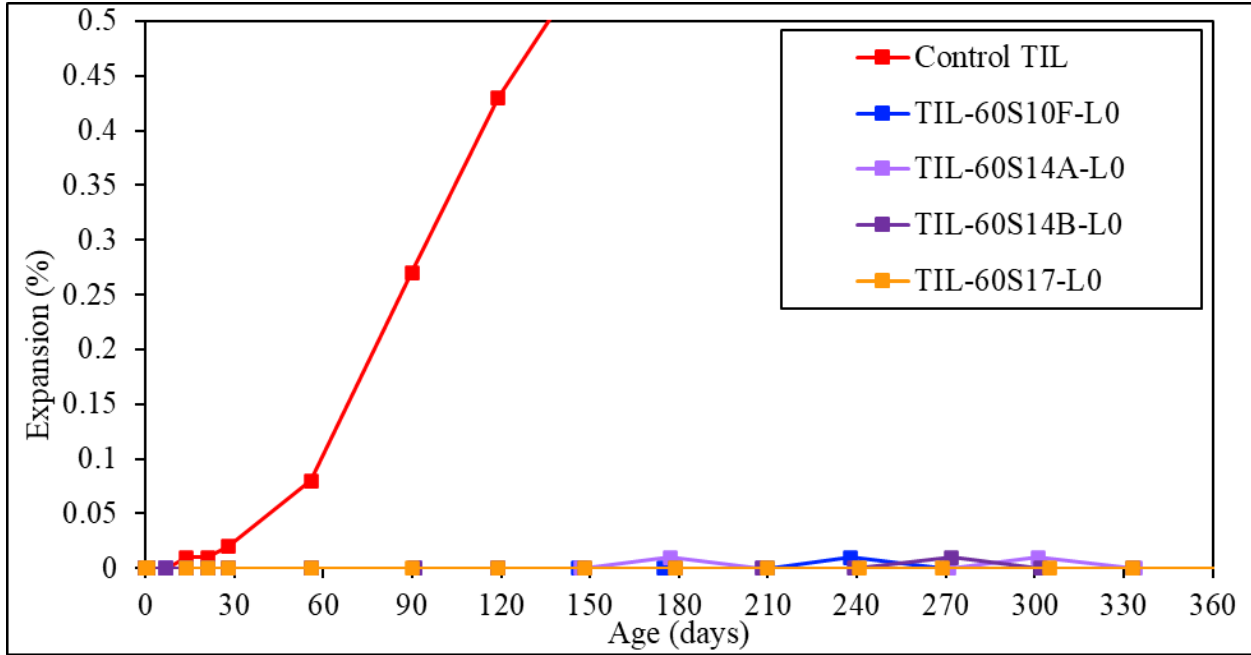
Figure 5-35: Length change of slag-blended mortar bars with cement TIL after heat treatment
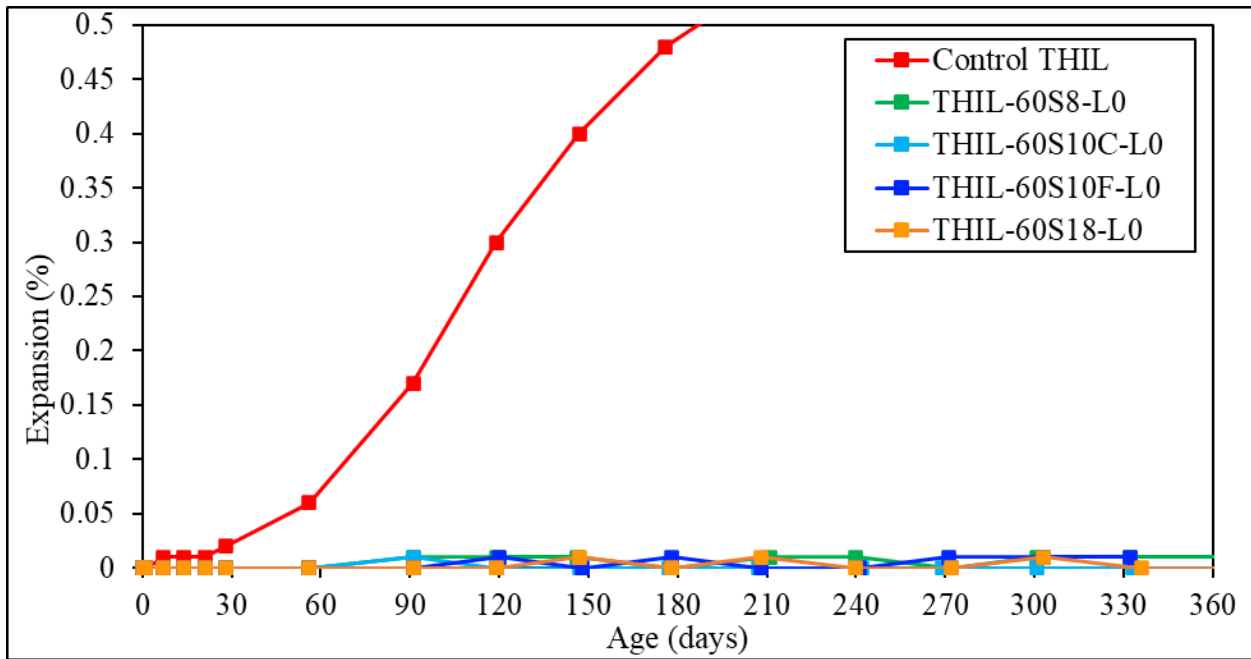
Figure 5-36: Length change of slag-blended mortar bars with cement THIL after heat treatment

Table 5-19: Expansion of as-received slag-blended mixtures at 180 days

Mixture ID	Expansion at 180 days (%)
BB-60S8-L0	0.01
BB-60S10C-L0	0.01
BB-60S14B-L0	0.01
BB-60S17-L0	0.01
C-60S8-L0	0.01
C-60S10C-L0	0.00
C-60S10F-L0	0.00
C-60S14A-L0	0.01
C-60S17-L0	0.01
Z-60S8-L0	0.01
Z-60S10C-L0	0.00
Z-60S10F-L0	0.01
Z-60S14A-L0	0.01
Z-60S14B-L0	0.00
Z-60S17-L0	0.00
TIL-60S10F-L0	0.00
TIL-60S14A-L0	0.01
TIL-60S14B-L0	0.00
TIL-60S17-L0	0.00
THIL-60S8-L0	0.00
THIL-60S10C-L0	0.00
THIL-60S10F-L0	0.01
THIL-60S17-L0	0.00

5.3.2.3 Sulfate-Optimized Slag-Blended Systems

The SO_3/Al_2O_3 molar ratio of a system was considered as the critical parameter that determines the potential for expansion. It is stated that the expansion caused by DEF was greatest when the SO_3/Al_2O_3 molar ratio was close to 1.0 [14], [64]. Heinz et al. [65] reported that sulfate contents ≥ 3 wt. % and SO_3/Al_2O_3 mass ratios > 0.45 in cementitious systems are more susceptible to DEF. However, it is not accurate to assume that all the Al_2O_3 and SO_3 available would form sulfoaluminate phases, because some SO_3 is contained in major cement phases and some Al_2O_3 is contained in ferrite and may not be released even after several years of hydration. Additionally, there may be some Al_2O_3 bound to non-sulfate phases such as a hydrogarnet or hydrotalcite-type phase. The mass ratio $(SO_3)^2/Al_2O_3$ (where Al_2O_3 is only alumina present in C_3A) was shown to

relate to expansion [14], [66]. Although this did not show a great improvement compared to the SO_3/Al_2O_3 molar ratio, it indicated a pessimum value close to 6.0. Certainly, the SO_3 content in the system affects the amount of sulfoaluminate phases formed and consequently the expansion caused by DEF.

Figure 5-37 through Figure 5-44 show the expansion of sulfate-optimized slag-cement blended systems after heat treatment. Table 5-20 summarizes the expansion of sulfate-optimized slag-blended mixtures at 180 days. As stated in section 5.3.1.3, L2 in the mixture ID denotes the SO_3 levels optimized at 2 days, the first parenthesis indicates the optimized SO_3 level in the slag, whereas the second parenthesis indicates the optimized SO_3 level in the total system. At the current reported test age, no significant difference was observed in the length change of sulfate-optimized slag blends compared to their respective as-received systems. However, the expansions in sulfate-optimized BB-60S14B, C-60S10F, Z-60S10F, Z-60S14B, TIL-60S10F and TIL-60S14B mixtures were slightly higher than their corresponding as-received counterparts, although not problematic. It is possible that this could be problematic at lower slag replacement levels or later ages.
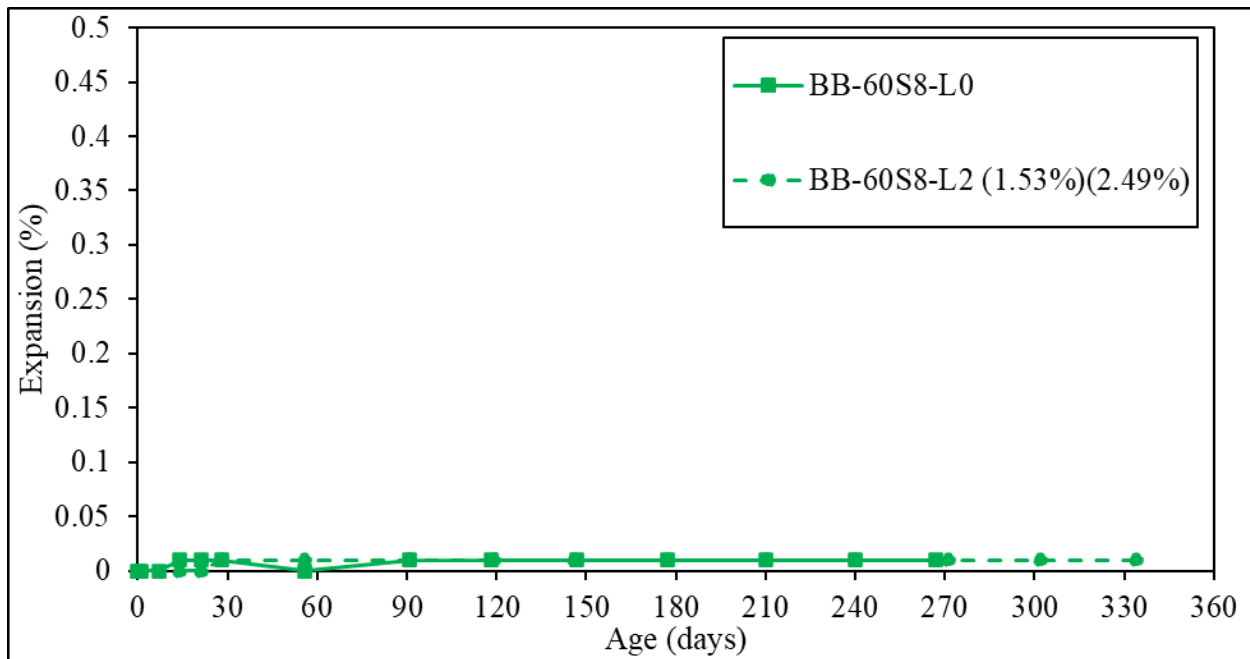
Figure 5-37: Length change of sulfate-optimized slag S8 mortar bars blended with cement BB
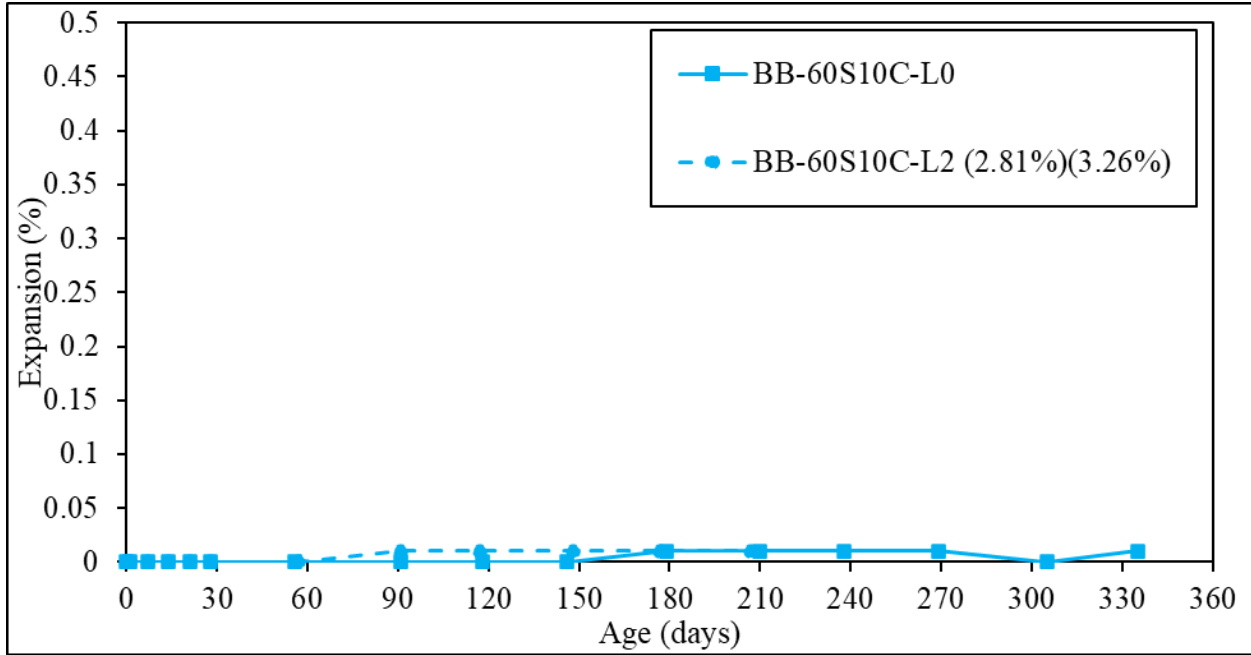
Figure 5-38: Length change of sulfate-optimized slag S10C mortar bars blended with cement BB
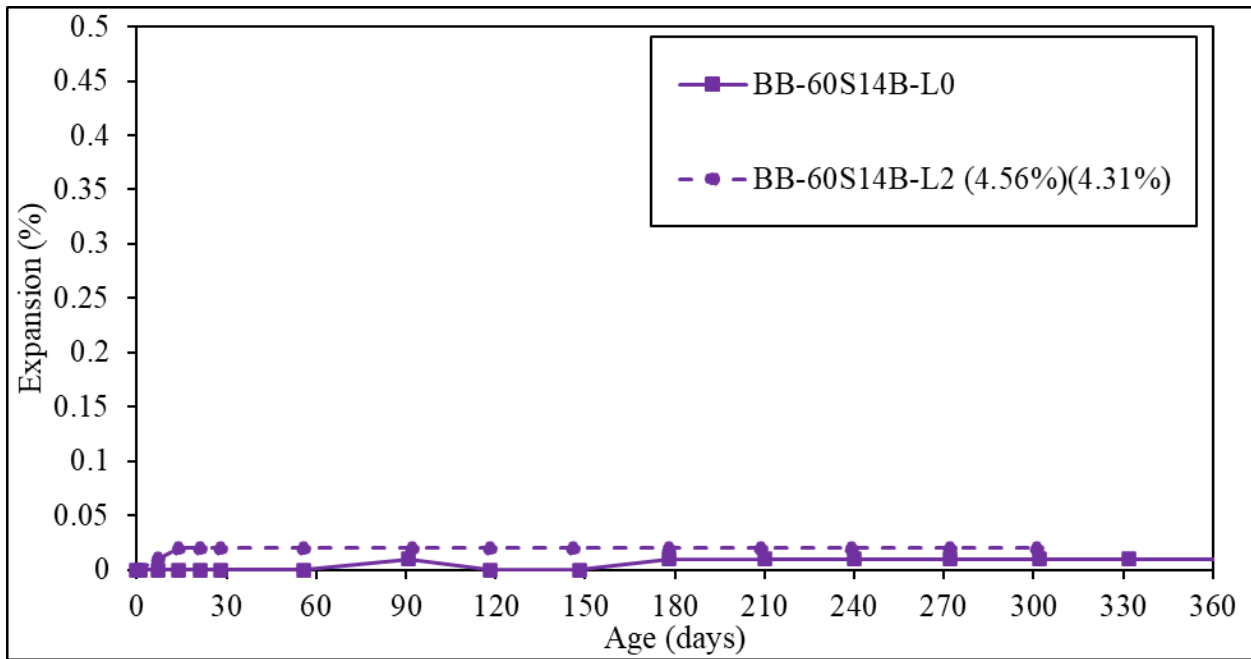
Figure 5-39: Length change of sulfate-optimized slag S14B mortar bars blended with cement BB
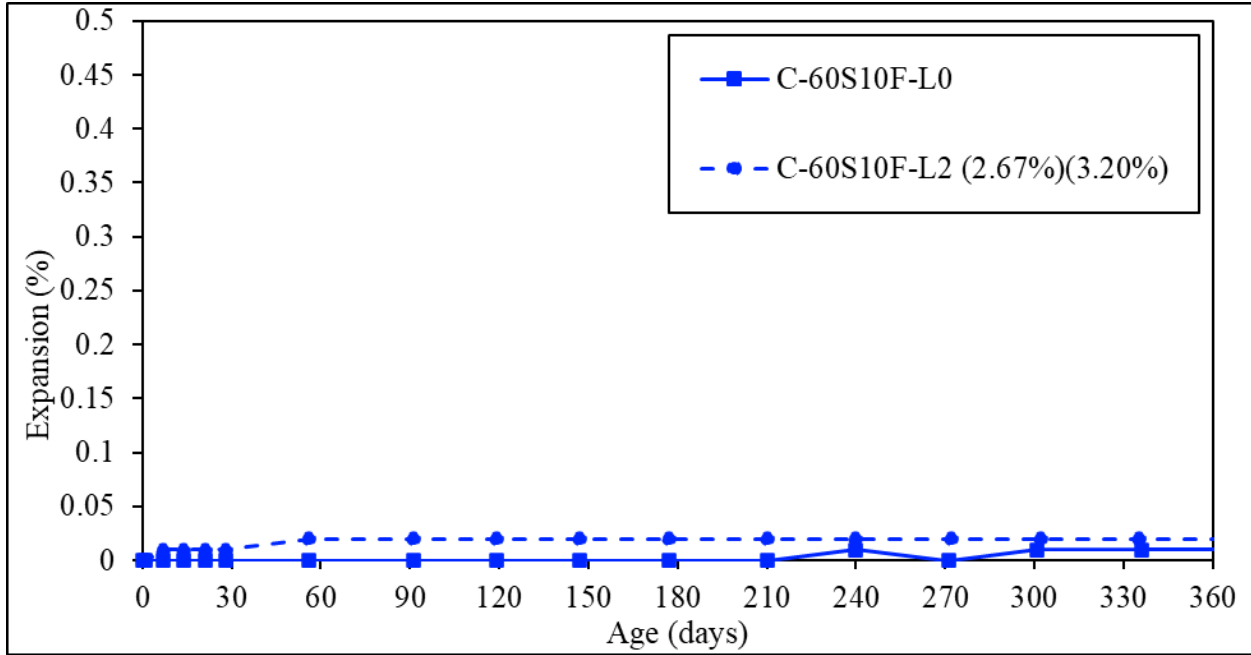
Figure 5-40: Length change of sulfate-optimized slag S10F mortar bars blended with cement C
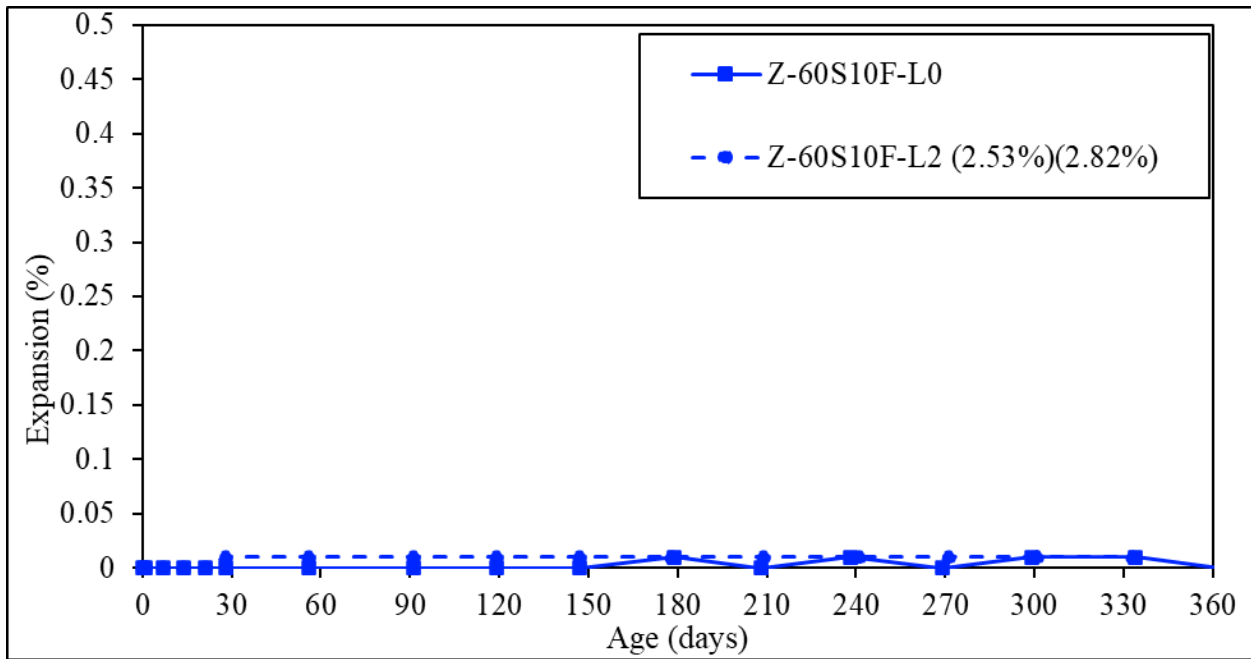
Figure 5-41: Length change of sulfate-optimized slag S10F mortar bars blended with cement Z
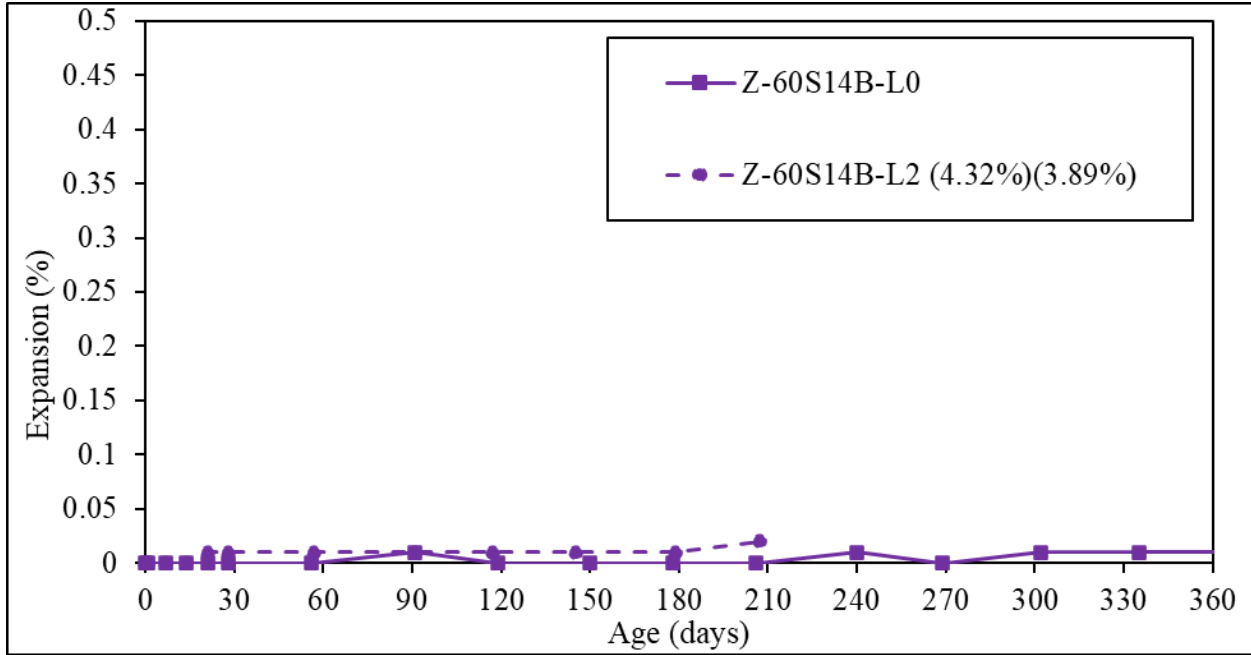
Figure 5-42: Length change of sulfate-optimized slag S14B mortar bars blended with cement Z
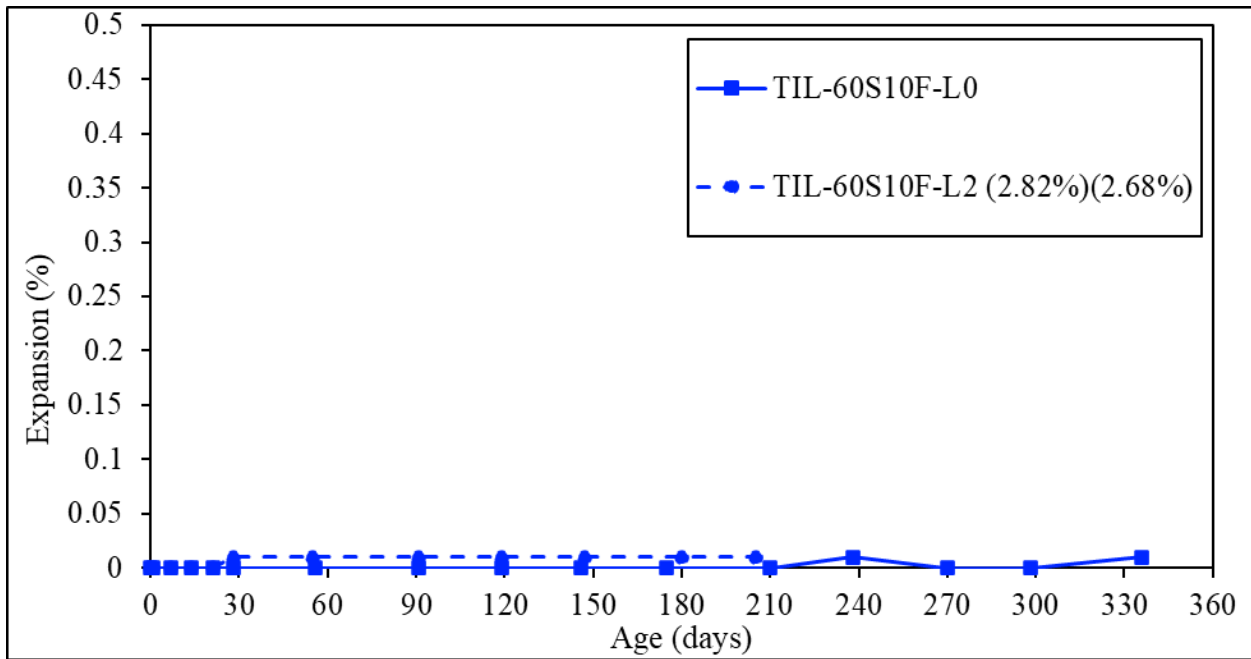
Figure 5-43: Length change of sulfate-optimized slag S10F mortar bars blended with cement TIL
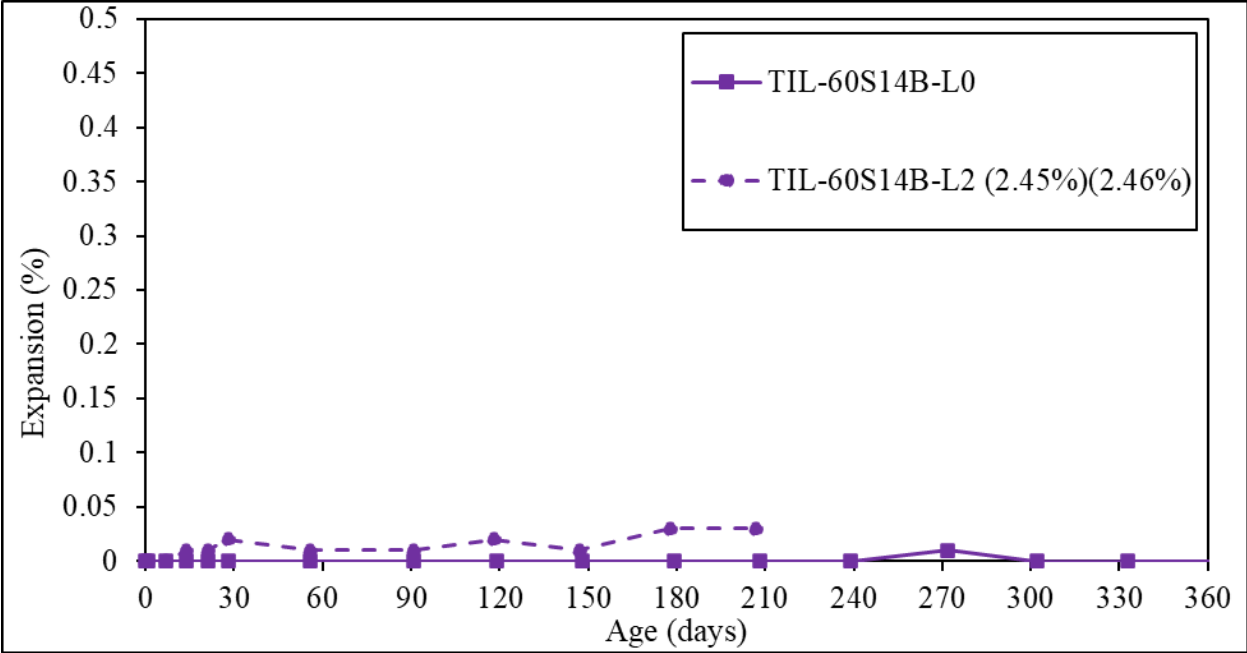
Figure 5-44: Length change of sulfate-optimized slag S14B mortar bars blended with cement TIL

Table 5-20: Expansion of sulfate-optimized slag-blended mixtures at 180 days

Mixture ID	Expansion at 180 days (%)
BB-60S8-L2	0.01
BB-60S10C-L2	0.01
BB-60S14B-L2	0.02
C-60S10F-L2	0.02
Z-60S10F-L2	0.01
Z-60S14B-L2	0.01
TIL-60S10F-L2	0.01
TIL-60S14B-L2	0.03

5.3.2.4 X-Ray Diffraction Analysis of Pastes before and after Heat Treatment

The change in phase assemblage of the mixtures during heat treatment determined using QXRD analysis is discussed in this section. Table 5-21 through Table 5-26 present the phases detected in mixtures at selected ages before (at HCR1) and just after (at HCR4) heat treatment. Appendix C shows the phase assemblage of the mixtures at more ages (at HCR2 and HCR3) during heat treatment and after until 4 months. In general, ettringite was detected in all the mixtures prior

to heat treatment (at 4 h). When the temperature was increased to 95℃ (203°F), ettringite content increased due to accelerated hydration. However, curing at 95℃ (203°F) for 36 h resulted in ettringite decomposition while phases such as monosulfoaluminate and hydrogarnet were formed. Ettringite is typically expected to decompose at temperatures above 74℃ (165°F) [67]. After experiencing the heat curing cycle and subsequent storage, ettringite reformed in all the mixtures and continued to increase overtime which may eventually cause expansion. However, no significant change was observed in the hydrogarnet content with time after the temperature was decreased to 23℃ (73.4°F). This can imply that it is not an active aluminate-bearing phase in reactions with sulfate ions [68]. Formation of hydrogarnet in heat-cured cement systems at temperatures from 80°C–100°C (176°F–212°F) was reported in the literature where it was indicated that increasing curing temperatures increased the amount of hydrogarnet [68], [19]. It was stated that most of the aluminate species resulting from ettringite and monosulfoaluminate decomposition at 85℃ (185°F) and above form hydrogarnet. Apparently, hydrogarnet formation during heat curing significantly reduces the amount of active alumina in the system. As explained by Yang and Sharp [68], the active SO_3/Al_2O_3 ratio in OPC cured at room temperature is typically much lower than that of ettringite (which is 1.5), which favors the formation of monosulfoaluminate and other AFm phases. However, "potential for formation of ettringite in the heat-cured system subsequently stored at room temperature is much enhanced by raising the active SO_3/Al_2O_3 ratio because of increased formation of the inert hydrogarnet" [68].

Table 5-21: Phase quantification of control mixtures before and after heat treatment by XRD

Mix ID	Control BB		Control C		Control Z		Control T1L		Control TH1L	
Curing age / Analyte	HCR1	HCR4	HCR1	HCR4	HCR1	HCR4	HCR1	HCR4	HCR1	HCR4
Alite	23.6	0.9	23.1	3.8	28.1	2.2	20.9	0.5	19.2	0.7
Belite	5	1.4	3	1.4	2.3	1.8	2.8	1.3	3.9	1.6
Aluminate	3.6	1.1	2.4	0.5	1.4	0.3	0.4	0	0.6	0
Ferrite	0.4	0.2	1.5	0.6	1.8	1	3	2.8	3	2.4
Calcite	0.1	0.3	0.7	1.5	0.9	1.7	2.4	3.4	2.4	4.2
Quartz	0	0.1	0.1	0.2	0.1	0.2	0.7	0.6	0.6	0.6
Portlandite	1.1	7.8	0.4	7.4	0.2	6.8	1.2	10	0.9	10
Periclase	0	0	0.3	0.2	0.5	0.4	0	0	0	0
Dolomite	0	0	0.4	0.5	0.1	0.2	0	0	0	0
Ettringite	1.9	0	0.4	0	1	0	1.5	0	1	0
Monosulfate	0	0.9	0	0.3	0	0	0	0	0	0
Hydrogarnet	0	4.1	0	3.2	0	2.8	0	3	0	4
Hemicarboaluminate	0	0	0	0	0	0	0	0	0	0
Gypsum	0.4	0	0.4	0	0	0	0	0	0.1	0
AC/Unidentified	63.9	83.4	65.7	81.8	63.7	82.6	67.1	79.6	68.3	76.3

In the control mixtures (Table 5-21), ettringite was detected but no monosulfoaluminate was observed prior to heat treatment. However, at HCR4 ettringite was decomposed and a substantial amount of hydrogarnet as well as portlandite were formed in all the mixtures. Additionally, small amount of monosulfoaluminate was formed only in controls BB and C. Therefore, control BB and C mixtures were more susceptible to ettringite reformation during storage because of their higher C_3A content, which explains the higher expansion observed in Figure 5-31. In IL cement mixtures, this process was hindered due to the reduced clinker factor and a corresponding lower C_3A content.

In the as-received slag-blended mixtures (Table 5-22 through Table 5-26), low amounts of ettringite were detected at HCR1, similar to the control mixtures. After heat treatment, phases such as monosulfoaluminate, hydrogarnet and hydrotalcite were formed. The presence of hydrotalcite with slags in heat-cured systems has been documented in the literature [14], [69]. While hydrogarnet and hydrotalcite were observed in almost every mixture, monosulfoaluminate was

only formed in systems with high-alumina slag and high C_3A cement. As it appears, not only hydrogarnet but also hydrotalcite did not react with the sulfate present in the system [69]. Although it is likely for the monosulfoaluminate available in HCR4 to convert to ettringite in the presence of sulfate, no significant length change was observed in the slag-blended mixtures during a period of 1 year as discussed in section 5.3.2.2. According to Ramlochan et al. [20], expansion only occurs when monosulfate intermixed in outer C-S-H is converted to ettringite, and no expansion occurs when excess alumina present in the system reacts with sulfate to form ettringite. Therefore, it is possible that the ettringite detected in the blended systems after 4 months (Appendix C) was non-expansive ettringite. Moreover, hydrogarnet contents at HCR4 increased with increasing slag alumina contents. The presence of high amounts of hydrogarnet and hydrotalcite may lower the active alumina in the system and increase the potential for ettringite formation.

On a different note, initial ettringite content (at HCR1) was higher in blends with high alkali cements (C and Z), which can be attributed to a faster hydration. After heat treatment, hydrogarnet contents were higher in the same blends. Phase assemblage of IL slag-blended cementitious systems before and after heat treatment also followed the same trends which were observed in any other slag blend. However, the amounts of ettringite, hydrogarnet, and monosulfoaluminate were comparatively lower due to the lower clinker fraction in IL cement.

Table 5-22: Phase quantification of as received slag-cement BB mixtures before and after heat treatment by XRD

Mix ID	BB-60S8		BB-60S10C		BB-60S14B		BB-60S17	
Curing age / Analyte	HCR1	HCR4	HCR1	HCR4	HCR1	HCR4	HCR1	HCR4
Alite	9.9	0.8	9.3	1.2	8.8	0.7	9.8	1.4
Belite	1.6	1.4	1.7	1.5	2.4	2.2	2.5	2.2
Aluminate	1.4	0.1	1.5	0.2	1.5	0.2	1.7	0.3
Ferrite	0	0	0.1	0	0.1	0	0	0
Calcite	0.2	0.3	0.1	0.2	0.2	0.5	0.1	0.5
Portlandite	0.4	1	0.4	1	0.5	0.4	0.3	0.4
Melilite	0.1	0.1	0.1	0.1	0.1	0.1	0.3	0.3
Merwinite	0	0	0.1	0.1	0	0	0	0
Ettringite	0.6	0	0.5	0	1	0	0.5	0
Monosulfate	0	0.2	0	0.2	0	1.2	0	0.6
Hydrogarnet	0	0.2	0	1.1	0	3.4	0	4.4
Hydrotalcite	0	0.2	0	0.2	0	0.3	0	0
Hemicarboaluminate	0	0	0	0	0	0	0	0
Gypsum	0.4	0	0.2	0	0.3	0	1	0
AC/Unidentified	85.3	95.6	85.9	94	85.1	90.8	83.8	89.7

Table 5-23: Phase quantification of as received slag-cement C mixtures before and after heat treatment by XRD

Mix ID	C-60S8		C-60S10C		C-60S10F		C-60S14A		C-60S17	
Curing age Analyte	HCR1	HCR4	HCR1	HCR4	HCR1	HCR4	HCR1	HCR4	HCR1	HCR4
Alite	8.4	0.9	8.2	1.6	8.3	1.9	8.9	1.6	8.5	2.1
Belite	1.5	1	1.1	0.7	1.5	0.9	1.5	1.2	1.9	1.6
Aluminate	0.8	0.1	0.7	0	0.9	0	0.8	0	0.5	0
Ferrite	0.3	0.1	0.5	0.1	0.6	0.3	0.5	0.2	0.4	0
Calcite	0.5	1.1	0.5	0.7	0.8	0.5	0.3	0.9	0.3	0.9
Quartz	0.1	0.1	0	0.1	0	0.1	0	0.1	0	0
Portlandite	0.1	0.5	0.1	0.1	0	0.2	0	0.2	0.2	0.2
Periclase	0.2	0.2	0.2	0.1	0.1	0.1	0.1	0.1	0.2	0.1
Dolomite	0.2	0.2	0.2	0.1	0.2	0.2	0.3	0.3	0.2	0.3
Melilite	0	0	0.1	0.1	0.1	0.1	0.1	0.1	0.3	0.3
Merwinite	0	0	0.1	0.1	0.1	0.1	0	0	0	0
Ettringite	1.1	0	1.9	0	1.4	0	1.3	0	0.8	0
Monosulfate	0	0	0	0	0	0.2	0	1.2	0	1.3
Hydrogarnet	0	0.7	0	2.2	0	1.4	0	3.1	0	3.1
Hydrotalcite	0	0.9	0	0.8	0	0.7	0	0.2	0	0.5
Hemicarboaluminate	0	0	0	0	0	0.1	0	0	0	0
Gypsum	0.1	0	0	0	0.1	0	0.3	0	0.2	0
AC/Unidentified	86.8	94.2	86.4	93.4	85.9	93.3	85.9	90.8	86.6	91.2

Table 5-24: Phase quantification of as received slag-cement Z mixtures before and after heat treatment by XRD

Mix ID	Z-60S8		Z-60S10C		Z-60S10F		Z-60S14A		Z-60S14B		Z-60S17	
Curing age Analyte	HCR1	HCR4	HCR1	HCR4	HCR1	HCR4	HCR1	HCR4	HCR1	HCR4	HCR1	HCR4
Alite	9.3	1.2	10.7	1.1	9.1	1.6	9.4	1.2	9.4	1.1	10.9	2
Belite	0.9	0.5	1.2	0.9	0.9	0.7	1.1	0.8	1.2	0.8	1.3	1
Aluminate	0.5	0	0.5	0	0.6	0	0.5	0	0.5	0	0.2	0
Ferrite	0.5	0.1	0.5	0.3	0.5	0.3	0.5	0.1	0.5	0.3	0.3	0.2
Calcite	1.6	1.7	0.9	1.5	0.9	0.6	0.2	1.8	0.6	1.7	0.3	1
Quartz	0	0.1	0	0.1	0	0.1	0.1	0	0	0	0	0.1
Portlandite	0.2	0.5	0.1	0.5	0.2	0.4	0.1	0.4	0.1	0.4	0.2	0.7
Periclase	0.2	0.2	0.2	0.2	0.3	0.3	0.2	0.1	0.2	0.1	0.2	0.1
Dolomite	0.1	0.2	0.1	0.2	0.1	0.2	0.1	0.2	0.1	0.2	0.1	0.1
Melilite	0	0	0.1	0.1	0.1	0.1	0.1	0.1	0.1	0.1	0.3	0.3
Merwinite	0	0	0.1	0.1	0.1	0.1	0	0	0	0	0	0
Ettringite	1.4	0	0.9	0	0.9	0	0.5	0	0.8	0	1.6	0
Monosulfate	0	0.1	0	0	0	0	0	0.7	0	0.3	0	1.1
Hydrogarnet	0	1.1	0	2.4	0	1.6	0	3.9	0	5.1	0	4.4
Hydrotalcite	0	1	0	1.4	0	1.4	0	0.3	0	0.5	0	1.4
Hemicarboaluminate	0	0	0	0	0	0	0	0	0	0	0	0
Gypsum	0	0	0	0	0	0	0	0	0.1	0	0.1	0
AC/Unidentified	85.3	93.3	84.8	91.3	86.5	92.6	87.2	90.4	86.4	89.4	84.7	88.5

Table 5-25: Phase quantification of as received slag-cement TIL mixtures before and after heat treatment by XRD

Mix ID	TIL-60S10F		TIL-60S14B		TIL-60S14A		TIL-60S17	
Curing age / Analyte	HCR1	HCR4	HCR1	HCR4	HCR1	HCR4	HCR1	HCR4
Alite	6.7	0.6	7.3	0.4	7.1	0.3	7.4	1
Belite	1.6	0.8	1.5	1.3	1.6	1.3	1.5	1.3
Aluminate	0.3	0	0.1	0	0.1	0	0.1	0
Ferrite	1.1	0.3	1.1	0.5	1.1	0.5	1	0.4
Calcite	1.5	1	1.3	2.8	1.1	2.1	0.9	1.1
Quartz	0.2	0.2	0.2	0.3	0.2	0.2	0.2	0.3
Portlandite	0.3	1	0.8	0.4	0.6	0.9	0.4	1.1
Melilite	0.1	0.1	0.1	0.1	0.1	0.1	0.3	0.3
Merwinite	0.1	0.1	0	0	0	0	0	0
Ettringite	0.9	0	1.3	0	0.8	0	0.7	0
Monosulfate	0	0.2	0	0	0	1	0	0.8
Hydrogarnet	0	0.1	0	4.8	0	3.6	0	3.2
Hydrotalcite	0	1.3	0	0.4	0	0.3	0	1.5
Hemicarboaluminate.	0	0	0	0	0	0	0	0
Gypsum	0	0	0.2	0	0.1	0	0.3	0
AC/Unidentified	87.3	94.3	86.2	88.5	87.1	90	87.3	90.4

Table 5-26: Phase quantification of as received slag-cement THIL mixtures before and after heat treatment by XRD

Mix ID	THIL-60S8		THIL-60S10C		THIL-60S10F		THIL-60S17	
Curing age / Analyte	HCR1	HCR4	HCR1	HCR4	HCR1	HCR4	HCR1	HCR4
Alite	7.2	0.6	6.3	0.4	6.9	0.3	7.3	0.8
Belite	1.8	1.5	1.5	1.1	1.8	1.1	1.6	1.2
Aluminate	0.2	0	0.3	0	0.3	0	0.1	0
Ferrite	0.9	0.5	1	0.4	0.9	0.3	0.9	0.3
Calcite	1.3	1.9	1.3	2.8	0.8	1.8	1	1.6
Quartz	0.3	0.3	0.3	0.2	0.3	0.2	0.3	0.2
Portlandite	0.6	1.2	0.6	0.5	0.4	0.9	0.4	0.2
Melilite	0	0	0.1	0.1	0.1	0.1	0.3	0.3
Merwinite	0	0	0.1	0.1	0.1	0.1	0	0
Ettringite	0.5	0	0.9	0	0.7	0	0.6	0
Monosulfate	0	0	0	0	0	0.2	0	0.8
Hydrogarnet	0	0	0	1.3	0	0.7	0	3.6
Hydrotalcite	0	1.4	0	2.8	0	2.3	0	1.4
Hemicarboaluminate	0	0	0	0	0	0.1	0	0
Gypsum	0	0	0	0	0	0	0.5	0
AC/Unidentified	87.2	92.7	87.5	90.4	87.7	91.9	86.9	89.7

In terms of sulfate-optimized mixtures, no significant difference was observed in the ettringite content of the mix with added sulfates at HCR1 compared to that in the respective as-received system; however, the gypsum content increased (Table 5-27 through Table 5-33). Apparently, the added hemihydrate was first converted to gypsum during the first 4 hours before it reacted with alumina. Moreover, it is interesting to observe reduction in hydrogarnet and hydrotalcite in the sulfate-optimized mixtures. The additional sulfate, however, resulted in substantial increase of monosulfoaluminates in slags blended with any cement. It is likely that more alumina was consumed to form monosulfoaluminate rather than hydrogarnet and hydrotalcite. Within the experimental error, no significant difference can be observed between the ettringite contents in sulfate-optimized mixtures and as-received mixtures. However, as discussed in section 5.3.2.3, a small increase in length change was observed in the sulfate-optimized mixtures.

Table 5-27: Phase quantification of as-received (L0) and sulfate-optimized (L2) cement BB-slag

S8 mixtures before and after heat treatment by XRD

Mix ID	BB-60S8-L0		BB-60S8-L2(1.53[*])(2.49[+])	
Curing age Analyte	HCR1	HCR4	HCR1	HCR4
Alite	9.9	0.8	9.2	0.2
Belite	1.6	1.4	2.4	2
Aluminate	1.4	0.1	1.4	0.1
Ferrite	0	0	0	0
Calcite	0.2	0.3	0.1	0.4
Portlandite	0.4	1	0.5	0.7
Melilite	0.1	0.1	0.1	0.1
Merwinite	0	0	0	0
Ettringite	0.6	0	0.8	0
Monosulfate	0	0.2	0	0
Hydrogarnet	0	0.2	0	0
Hydrotalcite	0	0.2	0	0
Hemicarboaluminate	0	0	0	0
Gypsum	0.4	0	0.9	0
AC/Unidentified	85.3	95.6	84.4	96.3

[*] Optimized SO_3 level in the slag

[+] Optimized SO_3 level in the total system

Table 5-28: Phase quantification of as-received (L0) and sulfate-optimized (L2) cement BB-slag S10C mixtures before and after heat treatment by XRD

Mix ID	BB-60S10C-L0		BB-60S10C-L2(2.81*)(3.26+)	
Curing age / Analyte	HCR1	HCR4	HCR1	HCR4
Alite	9.3	1.2	9.7	0.9
Belite	1.7	1.5	2.3	1.9
Aluminate	1.5	0.2	1.3	0.1
Ferrite	0.1	0	0.1	0
Calcite	0.1	0.2	0.3	1.9
Portlandite	0.4	1	0.2	0.6
Melilite	0.1	0.1	0.1	0.1
Merwinite	0.1	0.1	0.1	0.1
Ettringite	0.5	0	0.7	0
Monosulfate	0	0.2	0	1.9
Hydrogarnet	0	1.1	0	0.2
Hydrotalcite	0	0.2	0	0
Hemicarboaluminate	0	0	0	0
Gypsum	0.2	0	1.9	0
AC/Unidentified	85.9	94	83.4	92.4

* Optimized SO_3 level in the slag

+Optimized SO_3 level in the total system

Table 5-29: Phase quantification of as-received (L0) and sulfate-optimized (L2) cement BB-slag S14B mixtures before and after heat treatment by XRD

Mix ID	BB-60S14B-L0		BB-60S14B-L2(4.56[*])(4.31[+])	
Curing age Analyte	HCR1	HCR4	HCR1	HCR4
Alite	8.8	0.7	9.1	1
Belite	2.4	2.2	1.9	1.6
Aluminate	1.5	0.2	1.4	0.1
Ferrite	0.1	0	0	0
Calcite	0.2	0.5	0.2	0.2
Portlandite	0.5	0.4	0.3	0.8
Melilite	0.1	0.1	0	0.1
Merwinite	0	0	0	0
Ettringite	1	0	1	0
Monosulfate	0	1.2	0	3.4
Hydrogarnet	0	3.4	0	0.1
Hydrotalcite	0	0.3	0	0
Hemicarboaluminate	0	0	0	0
Gypsum	0.3	0	1.8	0
AC/Unidentified	85.1	90.8	84.2	92.8

[*] Optimized SO_3 level in the slag

[+] Optimized SO_3 level in the total system

Table 5-30: Phase quantification of as-received (L0) and sulfate-optimized (L2) cement C-slag S10F mixtures before and after heat treatment by XRD

Mix ID	C-60S10F-L0		C-60S10F-L2(2.67*)(3.20+)	
Curing age / Analyte	HCR1	HCR4	HCR1	HCR4
Alite	8.3	1.9	10.6	1.2
Belite	1.5	0.9	1.1	0.9
Aluminate	0.9	0	1	0
Ferrite	0.6	0.3	0.4	0
Calcite	0.8	0.5	0.4	0.2
Quartz	0	0.1	0	0
Portlandite	0	0.2	0	0.2
Periclase	0.1	0.1	0.1	0.1
Dolomite	0.2	0.2	0.1	0.3
Melilite	0.1	0.1	0.1	0.1
Merwinite	0.1	0.1	0.1	0.1
Ettringite	1.4	0	1.9	0
Monosulfate	0	0.2	0	1.4
Hydrogarnet	0	1.4	0	0
Hydrotalcite	0	0.7	0	0
Hemicarboaluminate	0	0.1	0	0
Gypsum	0.1	0	0.3	0
AC/Unidentified	85.9	93.3	83.9	95.6

* Optimized SO_3 level in the slag

+Optimized SO_3 level in the total system

Table 5-31: Phase quantification of as-received (L0) and sulfate-optimized (L2) cement Z-slag S10F mixtures before and after heat treatment by XRD

Mix ID	Z-60S10F-L0		Z-60S10F-L2(2.53[*])(2.82[+])	
Curing age Analyte	HCR1	HCR4	HCR1	HCR4
Alite	9.1	1.6	11.7	1
Belite	0.9	0.7	0.5	0.3
Aluminate	0.6	0	0.6	0
Ferrite	0.5	0.3	0.5	0.1
Calcite	0.9	0.6	0.3	0.5
Quartz	0	0.1	0	0
Portlandite	0.2	0.4	0.1	0.3
Periclase	0.3	0.3	0.2	0.1
Dolomite	0.1	0.2	0.1	0.2
Melilite	0.1	0.1	0.1	0.1
Merwinite	0.1	0.1	0.1	0.1
Ettringite	0.9	0	0.7	0
Monosulfate	0	0	0	0.7
Hydrogarnet	0	1.6	0	0.6
Hydrotalcite	0	1.4	0	0
Hemicarboaluminate	0	0	0	0
Gypsum	0	0	0.6	0
AC/Unidentified	86.5	92.6	84.5	96.2

[*] Optimized SO_3 level in the slag

[+] Optimized SO_3 level in the total system

Table 5-32: Phase quantification of as-received (L0) and sulfate-optimized (L2) cement Z-slag S14B mixtures before and after heat treatment by XRD

Mix ID	Z-60S14B-L0		Z-60S14B-L2(4.32*)(3.89+)	
Curing age Analyte	HCR1	HCR4	HCR1	HCR4
Alite	9.4	1.1	10.3	1.3
Belite	1.2	0.8	0.9	0.6
Aluminate	0.5	0	0.4	0
Ferrite	0.5	0.3	0.5	0
Calcite	0.6	1.7	0.6	1.8
Quartz	0	0	0	0
Portlandite	0.1	0.4	0.2	0.6
Periclase	0.2	0.1	0.3	0.2
Dolomite	0.1	0.2	0.2	0.3
Melilite	0.1	0.1	0.1	0.1
Merwinite	0	0	0	0
Ettringite	0.8	0	0.6	0
Monosulfate	0	0.3	0	2.9
Hydrogarnet	0	5.1	0	0.5
Hydrotalcite	0	0.5	0	0.1
Hemicarboaluminate	0	0	0	0
Gypsum	0.1	0	0.9	0
AC/Unidentified	86.4	89.4	85.1	91.6

* Optimized SO_3 level in the slag

+Optimized SO_3 level in the total system

Table 5-33: Phase quantification of as-received (L0) and sulfate-optimized (L2) cement TIL-slag S10F mixtures before and after heat treatment by XRD

Mix ID	T1L-60S10F-L0		T1L-60S10F-L2(2.82*)(2.68+)	
Curing age / Analyte	HCR1	HCR4	HCR1	HCR4
Alite	6.7	0.6	8.8	0.7
Belite	1.6	0.8	1.6	1.3
Aluminate	0.3	0	0.1	0
Ferrite	1.1	0.3	1	0.4
Calcite	1.5	1	1	2.3
Quartz	0.2	0.2	0.2	0.3
Portlandite	0.3	1	0.3	1.2
Melilite	0.1	0.1	0.1	0.1
Merwinite	0.1	0.1	0.1	0.1
Ettringite	0.9	0	0.5	0
Monosulfate	0	0.2	0	1.3
Hydrogarnet	0	0.1	0	0
Hydrotalcite	0	1.3	0	0.7
Hemicarboaluminate	0	0	0	0
Gypsum	0	0	1.1	0
AC/Unidentified	87.3	94.3	85.1	91.6

* Optimized SO_3 level in the slag

+Optimized SO_3 level in the total system

5.3.2.5 Summary

Length change and the phase assemblage of the heat-cured mortar bars appeared to be affected by the cement and slag characteristics. The control mixtures showed the highest expansion associated with DEF. Type I cements (BB and C) showed the highest expansion (higher C_3A) followed by Type II(MH) with Type IL cements (TIL and THIL) showing the lowest expansion (low clinker factor). It is noteworthy that these trends were similar to those of external sulfate attack.

When 60% slag was incorporated in the cementitious binder, and regardless of the slag source or the cement type, a significant drop and a delay in expansion was observed. However, the limited test duration was not sufficient to identify the effects of varying slag characteristics on DEF. As stated in the literature, high alumina levels contributed by SCMs are believed to suppress the long-term expansion of heat-cured specimens. Therefore, it is likely that high-alumina slags will have more resistance to internal sulfate attack. Although the ACI 201 Guide to Durable Concrete [62] recommends slag substitution levels greater than or equal to 35% with any ASTM C150/C150M portland cement, in order to mitigate/suppress DEF, further investigation is required to assess performance of high alumina slags of different characteristics. Cement and slag properties such as high alkali and sulfate levels, presence of limestone, and high fineness may affect DEF in heat-cured systems. Moreover, slightly higher length change was observed in the sulfate-optimized mixtures compared to their respective as-received mixtures at the current testing age, which is opposite to the trends observed in terms of external sulfate attack. However, it is noteworthy that the length change of sulfate-added slag mixtures at high substitution levels may not be as significant as the length change of sulfate-added slag mixtures at low substitution levels.

QXRD analysis indicate ettringite decomposed in all control and blended mixtures during curing at 95ºC (203°F) for a period of 36 hours. After heat treatment and during storage, hydrogarnet was formed in all the mixtures making less alumina available to react with sulfates. However, ettringite reformed in all the systems. Additionally, monosulfoaluminate was detected, especially in mixtures with high-alumina slags and high C_3A cements. It appears that ettringite formation in the control mixtures caused significant expansion. Although ettringite was detected in slag-blended systems, no expansion was observed at 6 months. The literature suggests two types of ettringite formation; conversion of monosulfoaluminate to ettringite, which causes expansion,

and non-expansive ettringite formation due to the reaction between excess alumina and sulfate in the system. Thus, high alumina levels contributed by slags may not cause expansion due to DEF at 60% replacement; however, expansion monitoring for extended age (900-1000 days) is necessary to verify such conclusion.

5.3.3   Chloride Binding

5.3.3.1 Binding Isotherms

Freundlich chloride binding isotherms and corresponding coefficients of determination (R^2) obtained for all mixtures are presented in   Table 5-34. The bound chloride contents when mixtures are exposed to NaCl solutions of different concentrations are listed in Table 5-35. The chloride binding isotherms of the control mixtures are presented in Figure 5-45. A similar binding capacity was observed in all mixtures at 0.1M chloride concentration. Nevertheless, the highest chloride binding capacity was observed with cement BB, which is a Type I cement with the highest C_3A content (8.5%). This behavior was expected as it is well established that cements with higher C_3A contents bind more chlorides due to the formation of Friedel's salt and Kuzel's salt [22]. Additionally, higher C-S-H amounts can be expected in control BB due to its higher C_3S content. This could have contributed to the increased binding capacity of control BB possibly due to the physical adsorption of Cl^- ions to C-S-H. The second highest binding capacity was observed with cement TTC, which is a Type II(MH) cement (3.3% C_3A), followed by cement C, which has a C_3A content of 8.3%. The high alkali content (1.05% Na_2O_{eq}) of Cement C affected the chloride binding capacity and resulted in a lower bound chloride content compared to that of cement TTC, although its C_3A content is higher. Previous studies indicate the higher solubility of Friedel's salt at high pH which results in reducing the chloride binding capacity [22], [23], [70].

Type IL cements (TIL and THIL) had the lowest chloride binding capacity. Cements TIL and THIL have approximately 10% and 14% limestone contents, respectively. Cement THIL, with the highest limestone content, had the lowest bound chloride content. This is in agreement with the published literature which indicates that the presence of limestone in cements decreases chloride binding capacity [71]. Dilution of clinker in limestone cements can result in lower C-S-H formation and consequently fewer chloride binding sites for physical adsorption. 25% to over 50% of binding capacity can be attributed to C_3S [72], which is a substantial contribution. Sui et al. [73]

226

quantified the free chloride, chemically bound chloride in AFm phases, and physically bound chloride to C-(A)-S-H in cement paste systems with varying limestone contents of 0-55%. The findings indicated that increasing limestone contents decreased the physically bound chloride content, which resulted in a decreased chloride binding capacity.

Table 5-34: Binding coefficients of Freundlich isotherms and corresponding coefficients of determination (R^2)

Mix ID	α	β	R^2
Control BB	13.6925	0.3096	0.9832
Control C	11.5866	0.3257	0.9993
Control TTC	12.5616	0.3478	0.9997
Control TIL	11.0992	0.3452	0.9976
Control THIL	10.2454	0.3217	0.9920
C-60S8	12.4210	0.3714	0.9864
C-60S14B	17.1438	0.4499	0.9967
C-60S17	17.0757	0.4626	0.9953
TTC-60S8	13.4101	0.3398	0.9689
TTC-60S14B	17.2426	0.4819	0.9988
TTC-60S17	16.9649	0.4628	0.9958
THIL-60S8	11.4730	0.3854	0.9967
THIL-60S14B	13.4653	0.4415	0.9976
THIL-60S17	13.6292	0.4192	0.9983

Table 5-35: Bound chloride contents when exposed to NaCl solutions of different concentrations

	Bound chloride content (mg Cl-/g of paste)				
NaCl conc. (M) Mix ID	0.1	0.3	0.5	1	3
Control BB	4.83	9.20	10.88	13.59	18.61
Control C	4.64	7.50	8.88	11.23	16.34
Control TTC	4.89	7.69	9.24	12.23	18.11
Control TIL	4.65	6.88	8.07	10.80	16.07
Control THIL	4.74	6.46	7.73	9.64	14.65
C-60S8	3.73	8.06	9.30	12.07	18.21
C-60S14B	4.53	8.63	11.96	16.68	27.02
C-60S17	4.34	8.50	11.45	17.00	27.16
TTC-60S8	3.92	9.10	10.44	13.30	18.78
TTC-60S14B	4.79	9.21	11.60	15.17	27.57
TTC-60S17	4.46	8.93	11.54	15.85	28.38
THIL-60S8	4.43	6.84	7.95	11.10	17.37
THIL-60S14B	4.48	6.81	9.34	13.08	21.34
THIL-60S17	4.67	7.23	9.51	13.29	21.09
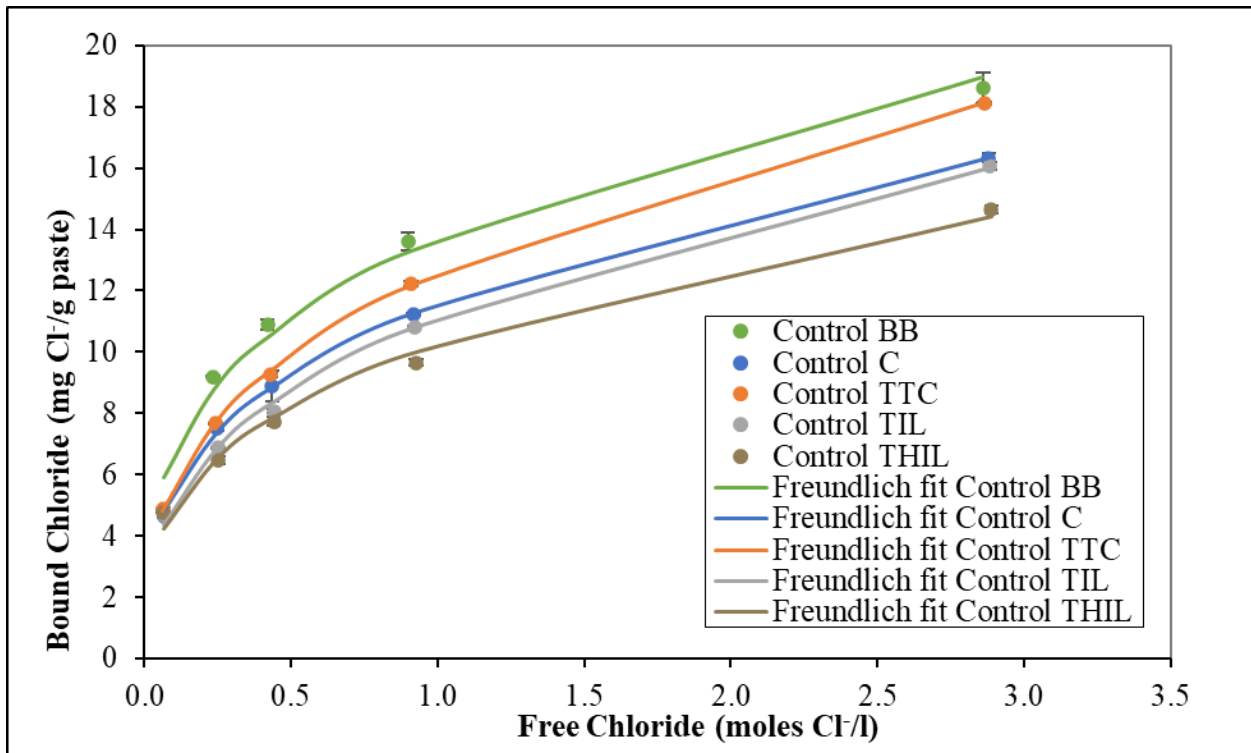
Figure 5-45: Chloride binding isotherms of control mixtures

Chloride binding isotherms of the slag-blended cementitious systems are shown in Figure 5-46 through Figure 5-48. In general, partial replacement of cement with slag increased the chloride binding capacity. This can be attributed to the formation of additional AFm phases, due to the slag alumina content, which transforms to Friedel's salt when exposed to chlorides. Moreover, increased formation of C-(A)-S-H can also enhance the physical chloride binding capacity of these mixtures. Similar to the control mixtures, bound chloride content at 0.1M NaCl concentration was similar for all the mixtures; however, at higher concentrations, bound chloride content was affected by the slag characteristics. Clearly, increasing slag alumina content from 8% to 14% and/or 17% influenced the chloride binding capacity of the cementitious system. While the difference in bound chloride content between slag S8 blends and their respective controls were not that significant, high alumina levels in slags (slags S14B and S17) corresponded with higher chloride binding capacities. Moreover, the influence of cement characteristics on the binding capacity of the blended systems followed trends similar to those observed in the control mixtures.
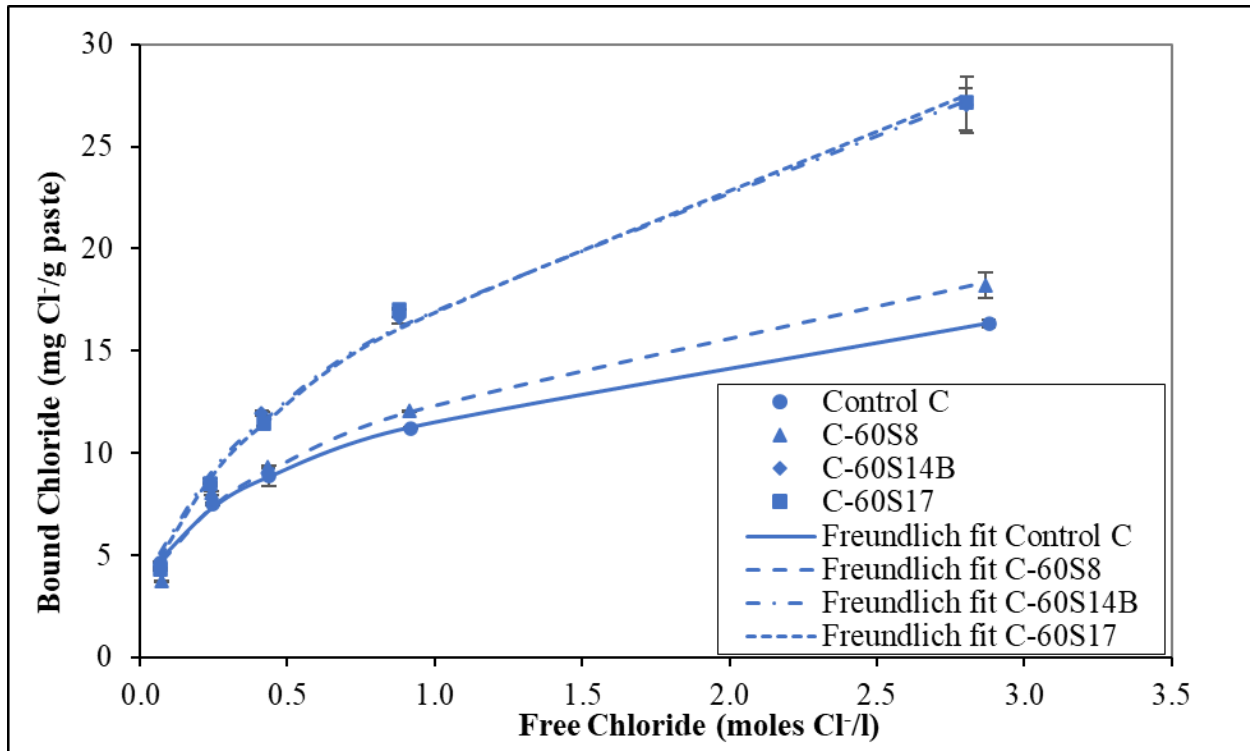
Figure 5-46: Chloride binding isotherms of slags blended with cement C
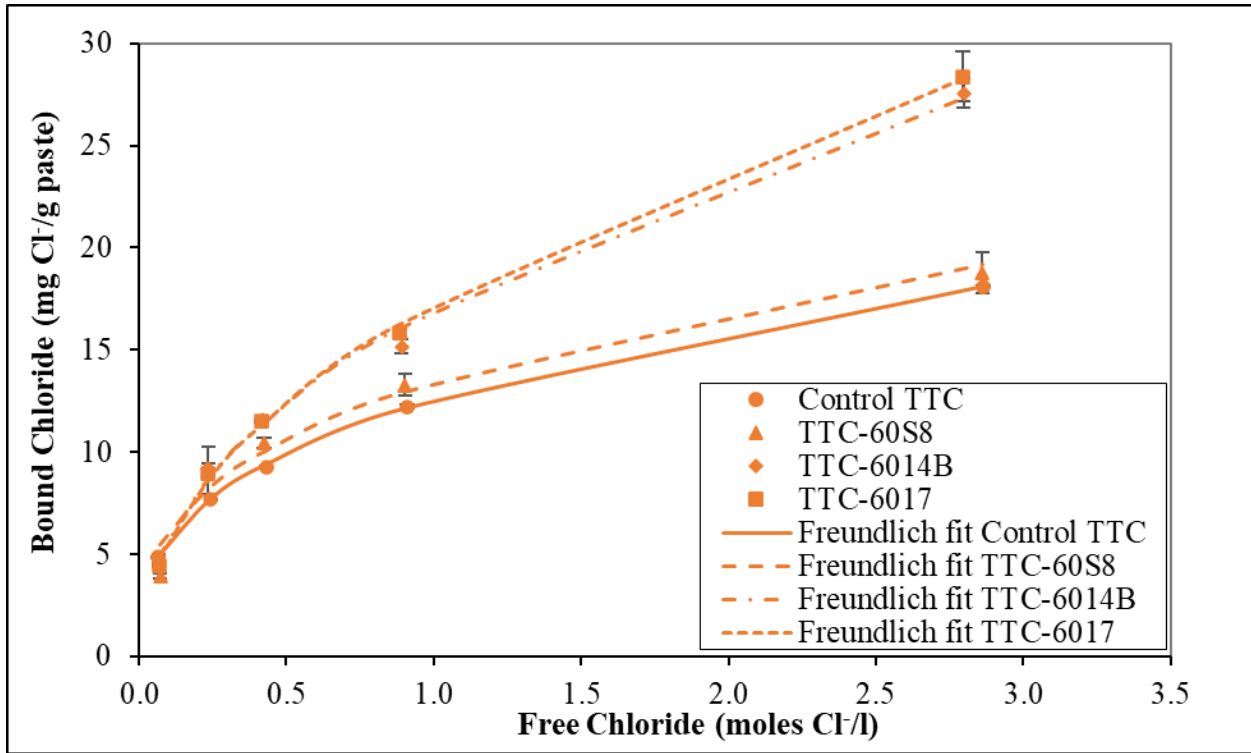
Figure 5-47: Chloride binding isotherms of slags blended with cement TTC
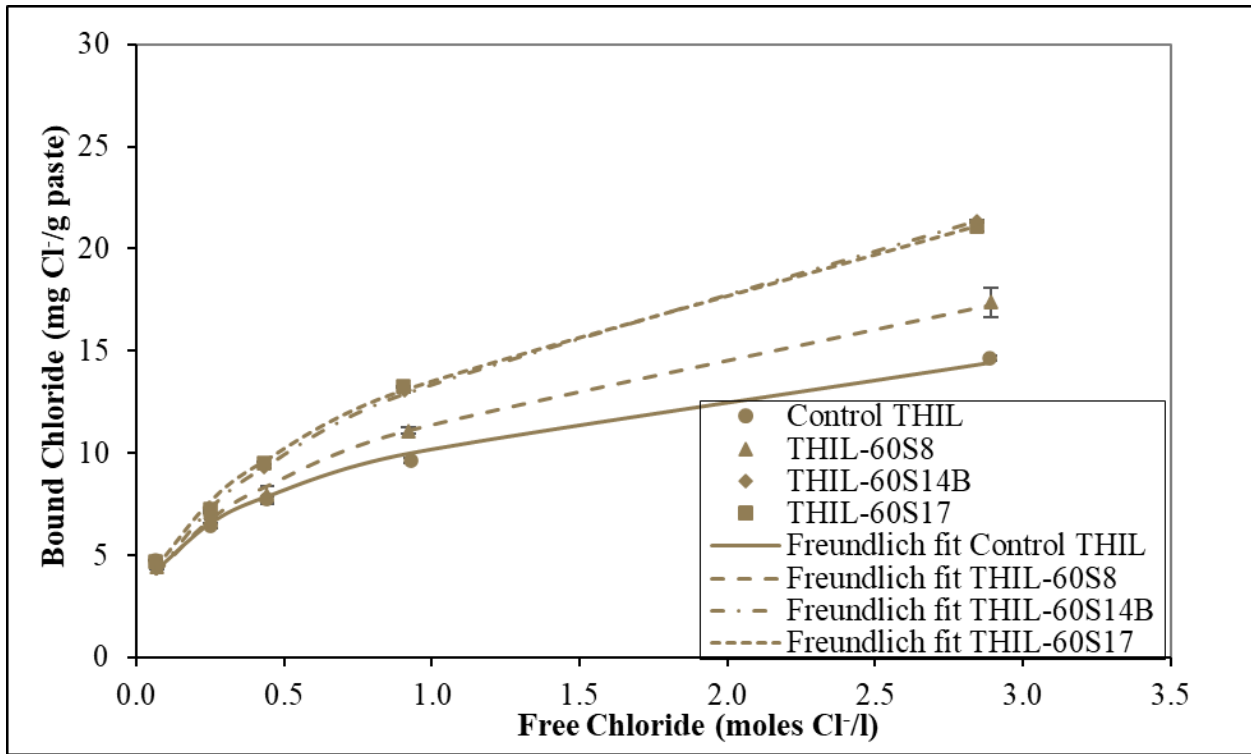
Figure 5-48: Chloride binding isotherms of slags blended with cement THIL

5.3.3.2 X-Ray Diffraction Analysis

Cement paste phase assemblage was quantified using XRD coupled with Rietveld analysis in order to understand the influence of cement composition on chloride ion ingress. Table 5-36 lists the phase assemblage determined from QXRD analysis of cement pastes before and after chloride exposure. In general, portlandite, ettringite, and hemi/mono carboaluminates were the main phases detected prior to chloride exposure in all systems. Monosulfate was only observed in the control BB system due to its high C_3A content and lower sulfate content. Carboaluminate phases were observed in all other systems due to the calcite present in cements. Higher quantities of carboaluminate phases were seen in Type IL cements, whereas the same phases were detected in lower amounts in control C and TTC. The trends observed in the phase assemblage of the control paste systems matched well with the trends observed in the bound chloride contents. After chloride exposure, Friedel's salt can be observed in all systems. Friedel's salt content increased with increasing NaCl concentration for each system while the amount of ettringite, monosulfate, and carboaluminate phases decreased, indicating the chemical binding of chlorides. In the control BB system, Kuzel's salt can also be observed at lower NaCl concentrations (0.1-0.5M). Transformation of monosulfate to Kuzel's salt at low NaCl concentrations was also reported by Zibara [22]. It is likely that Kuzel's salt transformed to Friedel's salt at higher chloride concentrations. Moreover, the increase in ettringite and carboaluminate phases at low NaCl concentrations compared to before exposure is noteworthy. When comparing control C and control TTC mixtures, similar or slightly higher Friedel's salt amounts were observed in the control C system, while the binding capacity was notably lower than that of control TTC (Figure 5-45). As it appears, physical binding was considerably reduced due to the high pH levels in control C [23], [26]. Despite the higher Friedel's salt quantities detected, lower bound chloride contents were observed in control TIL and THIL mixtures (Figure 5-45). This can be attributed to the reduction in the physically bound chlorides due to a lower clinker factor in limestone cements.

Table 5-36: Phase quantification of control mixtures before and after two months of chloride exposure by XRD

Sampe ID	Control BB				Control C				Control TTC				Control TIL				Control THIL			
Cl conc. (M) / Phase (%)	0^*	0.1	0.5	3	0^*	0.1	0.5	3	0^*	0.1	0.5	3	0^*	0.1	0.5	3	0^*	0.1	0.5	3
Alite	0.4	0.2	0.2	0.3	2.7	2	2	2	1.3	0.7	0.7	0.8	0.3	0.1	0.2	0.2	0.1	0	0	0
Belite	3.2	1.8	1.6	1.5	2.2	0.9	1	1.1	3.1	1	1.1	1.2	2.3	1.4	1.3	1.3	3.1	1.9	1.6	1.7
Aluminate	0	0	0	0	0	0	0	0	0	0	0	0	0	0	0	0	0	0	0	0
Ferrite	0	0	0	0	0.1	0	0	0	1.7	0.7	0.8	0.7	1.6	1	1.1	1	1.3	0.9	0.7	0.6
Calcite	0.1	0.1	0.1	0.2	0.7	0.8	0.9	0.3	0.3	0.5	0.3	0.4	3.1	3.3	3.3	3	3.1	4	3.9	3.9
Quartz	0.1	0.1	0	0.1	0.2	0.1	0.1	0.1	0.3	0.2	0.2	0.2	0.9	1	0.9	1	1	1.1	1.1	1.1
Portlandite	14	13	13	12	11	11	11	11	12	12	12	11	11	12	11	10	6	11	11	10
Periclase	0	0	0	0	0.5	0.4	0.3	0.3	0	0	0	0	0	0	0	0	0	0	0	0
Dolomite	0	0	0	0	0.5	0.4	0.4	0.4	0	0	0	0	0	0	0	0	0	0	0	0
Ettringite	1.5	7.1	7.9	4.3	3.5	8.3	7.8	5.9	1.7	5.8	4.8	3.5	2.3	4.8	4.4	3.3	2.2	5.2	5.2	3.4
Monosulfate	3.2	0.1	0	0	0	0	0	0	0	0	0	0	0	0	0	0	0	0	0	0
Hydrotalcite	0	0	0	0	0	0	0	0	0	0	0	0	0	0	0	0	0	0	0	0
Hemicarboaluminate	0	0.4	0.3	0.1	0	0.8	0.5	0.3	0.1	0.3	0.2	0	0	0.3	0.2	0.1	0.1	0.3	0.2	0.2
0.8 Carboaluminate	0	0	0	0.1	0.2	0.2	0.2	0.1	0	0	0	0	0.1	0.1	0	0	0.2	0.2	0.1	0.1
Monocarboaluminate	0	0	0	0	0.4	0	0	0	0.5	0	0	0	0.6	0.1	0	0	0.9	0.1	0	0
Friedel's Salt	0	0.7	2.4	5.3	0	1.2	2.7	3.8	0	1.5	2.3	3	0	1.4	2.4	3.5	0	1.7	3.2	4.5
Kuzel's Salt	0	1.2	0.1	0	0	0	0	0	0	0	0	0	0	0	0	0	0	0	0	0
AC//Unidentified	78.0	75.4	74.6	76.4	77.6	74.0	73.2	75.1	79.2	77.6	78.1	79.4	77.8	75.0	75.3	76.0	82.0	73.6	73.4	74.0

* Before chloride exposure

In terms of the phase assemblage detected by XRD for the slag-blended mixtures, the trends are in general agreement with the chloride binding capacities (Table 5-37 through Table 5-39). Prior to chloride exposure, ettringite was detected in all systems, although monosulfate was only formed in control BB prior to chloride exposure. In slag-blended mixtures, and prior to chloride exposure, monosulfate was detected in all the blended systems except cement THIL blends. Small amounts of carboaluminate phases were also detected in the same blends. In cement THIL blends, notable amounts of carboaluminate phases were observed as expected due to the presence of calcite in cement. Ettringite, monosulfate and carboaluminate contents were higher in the high-alumina slags prior to chloride exposure. AFm phases and ettringite can chemically bind chlorides, therefore higher amounts of these phases are desirable for chloride binding. In addition, hydrotalcite was also detected in the blended systems prior to exposure. While the hydrotalcite contents were similar in slag S8 and S17 blends, in slag S14B blends, hydrotalcite contents were lower, due to the lower magnesia content of this slag.

On exposure to chloride solutions, phase assemblage data indicate that the alumina-bearing phases transformed to Friedel's salt and Kuzel's salt. Increasing NaCl concentrations increased the formation of Friedel's salt and Kuzel's salt and reduced the quantities of alumina-bearing phases. Systems with high-alumina slags formed higher amounts of Friedel's salt and Kuzel's salt, following the trends observed in the binding isotherms. It is noteworthy that the Friedel's salt contents observed in slag S14B mixtures were either similar to or higher than those of slag S17 mixtures. However, ettringite, carboaluminate and hydrotalcite were notably higher at low NaCl concentrations compared to those observed prior to exposure.

Table 5-37: Phase quantification of cement C mixes before and after two months of chloride exposure by XRD

Sampe ID	C-60S8				C-60S14B				C-60S17			
Cl conc. (M) / Phase (%)	0[*]	0.1	0.5	3.0	0[*]	0.1	0.5	3.0	0[*]	0.1	0.5	3.0
Alite	0.6	0.2	0.3	0.4	1.1	0.4	0.3	0.4	1.1	0.6	0.6	0.5
Belite	1.1	0.6	0.6	0.5	1.2	0.7	0.6	0.6	1.4	0.7	0.6	0.6
Aluminate	0	0	0	0	0	0	0	0	0	0	0	0
Ferrite	0	0	0	0	0	0	0	0	0	0	0	0
Calcite	0.1	0.1	0.3	0.1	0.1	0.3	0.5	0.3	0.1	0.1	0.1	0.2
Quartz	0	0	0	0	0	0	0	0	0	0	0	0
Portlandite	3.2	2.8	2.5	2.3	2.1	1.5	0.9	0.9	2.0	1.1	1.1	0.7
Periclase	0.1	0.1	0.1	0.1	0.1	0.1	0.1	0.1	0.2	0.1	0.1	0.1
Dolomite	0.3	0.3	0.3	0.3	0.4	0.4	0.4	0.4	0.4	0.4	0.4	0.4
Melilite	0.1	0.1	0.1	0.1	0.1	0.1	0.1	0.1	0.3	0.4	0.4	0.4
Merwinite	0	0	0	0	0	0	0	0	0	0	0	0
Ettringite	0.4	2.2	2.2	1.4	1.3	3.7	3.9	2.2	1.0	2.3	2.2	1.6
Monosulfate	1.3	0.7	0.1	0	1.0	0.3	0	0	2.7	2.2	0.2	0
Hydrotalcite	0.7	1.7	1.1	0.4	0.2	0.4	0.4	0.3	1.0	2.6	2.6	1.6
Hemicarboaluminate	0	0.3	0.6	0.5	0.8	1.4	0.9	0.4	0	0.8	1.2	0.5
0.8 Carboaluminate	0.1	0.1	0.1	0.2	0	0.3	0.1	0.2	0.2	0.1	0.3	0.2
Monocarboaluminate	0.1	0	0	0	0.1	0	0	0	0.6	0	0	0
Friedel's Salt	0	0.7	1.5	4.0	0	1.4	3.9	6.8	0	1.0	1.6	4.1
Kuzel's Salt	0	0.5	0.4	0	0	1.0	0.1	0	0	0.2	0.9	0.1
AC//Unidentified	91.8	89.6	89.9	89.8	91.5	88.3	87.9	87.3	88.9	87.4	87.8	88.9

* Before chloride exposure

Table 5-38: Phase quantification of cement TTC mixes before and after two months of chloride exposure by XRD

Sampe ID	TTC-60S8				TTC-60S14B				TTC-60S17			
Cl conc. (M) / Phase (%)	0^*	0.1	0.5	3.0	0^*	0.1	0.5	3.0	0^*	0.1	0.5	3.0
Alite	0.3	0.2	0.2	0.2	0.3	0.3	0.3	0.2	0.4	0.2	0.1	0.1
Belite	1.2	0.8	0.8	0.7	1.5	1.1	0.9	0.8	1.7	1.2	1.3	1.1
Aluminate	0	0	0	0	0	0	0	0	0	0	0	0
Ferrite	0	0	0	0	0	0	0	0	0	0	0	0
Calcite	0.1	0.1	0.2	0.4	0.1	0.2	0.3	0.1	0.1	0.1	0.1	0.2
Quartz	0	0	0	0	0	0	0	0	0.1	0	0	0
Portlandite	4.2	3.5	3.2	2.9	3.2	2.2	2.0	1.5	2.7	2.0	1.9	1.0
Melilite	0.1	0.1	0.1	0.1	0.1	0.1	0.1	0.1	0.4	0.4	0.4	0.4
Merwinite	0	0	0	0	0	0	0	0	0	0	0	0
Ettringite	0.6	1.3	1.3	1.1	1.0	2.7	3.2	1.4	0.7	1.1	1.2	1.3
Monosulfate	0.4	0	0	0	0.3	0	0	0	2.4	1.3	0.1	0
Hydrotalcite	1.1	0.8	0.9	0.3	0.2	0.4	0.5	0.1	1.1	2.2	1.7	1.1
Hemicarboaluminate	0.2	0.4	0.5	0.6	1.2	1.4	1.8	1.5	0.1	0.1	0.2	0.3
0.8 Carboaluminate	0.2	0.1	0.1	0.1	0.1	0.1	0.2	0.3	0.4	0.2	0.3	0.4
Monocarboaluminate	0	0	0	0	0.2	0	0	0	0.5	0.2	0.2	0
Friedel's Salt	0	0.3	1.6	3.4	0	2.4	3.0	5.1	0	1.1	1.6	6.1
Kuzel's Salt	0	0.3	0	0	0	0	0	0	0	0.5	0.7	0
AC//Unidentified	91.6	92.1	91.1	90.1	91.7	89.0	87.7	88.9	89.5	89.5	90.0	87.9

* Before chloride exposure

Table 5-39: Phase quantification of slag THIL cement mixes before and after two months of chloride exposure by XRD

Sampe ID	THIL-60S8				THIL-60S14B				THIL-60S17			
Cl conc. (M) / Phase (%)	0*	0.1	0.5	3.0	0*	0.1	0.5	3.0	0*	0.1	0.5	3.0
Alite	0.7	0.2	0.3	0.3	0.5	0.2	0.3	0.3	0.4	0.2	0.2	0.2
Belite	1.6	0.9	0.7	0.6	1.9	1.2	1.2	1.0	1.8	0.9	1.1	0.9
Aluminate	0	0	0	0	0	0	0	0	0	0	0	0
Ferrite	0	0	0	0	0	0	0	0	0.3	0	0	0
Calcite	0.8	1.0	1.0	1.0	1.2	1.3	1.5	1.4	0.8	0.8	1.0	0.6
Quartz	0.3	0.3	0.3	0.2	0.4	0.3	0.4	0.4	0.3	0.2	0.3	0.2
Portlandite	3.2	2.8	2.8	2.4	2.0	1.6	1.5	1.1	2.1	1.4	1.2	1.0
Melilite	0.1	0.1	0.1	0.1	0.1	0.1	0.1	0.1	0.3	0.4	0.4	0.4
Merwinite	0	0	0	0	0	0	0	0	0	0	0	0
Ettringite	0.6	1.5	1.7	1.0	1.8	3.6	3.4	2.4	2.8	4.1	3.3	3.1
Monosulfate	0	0	0	0	0	0	0	0	0	0	0	0
Hydrotalcite	1.2	1.8	1.8	0.3	0.3	0.4	0.4	0.3	1.1	2.0	1.4	0.9
Hemicarbonate	1.2	0.8	0.3	0.4	1.4	1.5	0.9	0.3	1.5	2.0	0.9	0.9
0.8 Carboaluminate	0.5	0	0	0	0.1	0	0	0	0.4	0	0	0
Monocarbonate	0.1	0.1	0	0	0.8	0	0	0	0.3	0	0	0
Friedel's Salt	0	2.1	3.5	4.8	0	2.6	4.7	6.5	0	1.9	3.9	5.1
Kuzel's Salt	0	0	0	0	0	0	0	0	0	0	0	0
AC//Unidentified	89.7	88.5	87.5	88.7	89.5	87.2	85.8	86.2	87.9	86.1	86.2	86.6

* Before chloride exposure

5.3.3.3 Thermodynamic Modeling

The predicted phase assemblages of the control mixtures with cements BB, C, TTC and THIL exposed to varying concentrations of NaCl solutions are shown in Figure 5-49 through Figure 5-52. Before chloride exposure (0M NaCl), C-S-H, ettringite, monosulfoaluminate, carboaluminates, portlandite, hydrotalcite and Fe-siliceous hydrogarnet ($C_3FS_{0.84}H_{4.32}$) were predicted in all control mixtures. Monosulfoaluminate was only predicted in the control BB system, in agreement with QXRD findings, due to its higher C_3A and lower sulfate content. Although hemicarboaluminate was predicted in control BB, monocarboaluminate was observed in all other control mixtures due to the higher calcite contents in the cements. As stated in the literature [54], [74], monocarboaluminate was calculated to be the more thermodynamically stable phase in the presence of calcite, while hemicarboaluminate was calculated only if the calcite content present in hydrated cements was substantially lower. Moreover, the highest ettringite content was predicted in control C prior to chloride exposure, in agreement with QXRD findings. Additionally, unhydrated calcite was predicted in control THIL due to its higher calcite content.
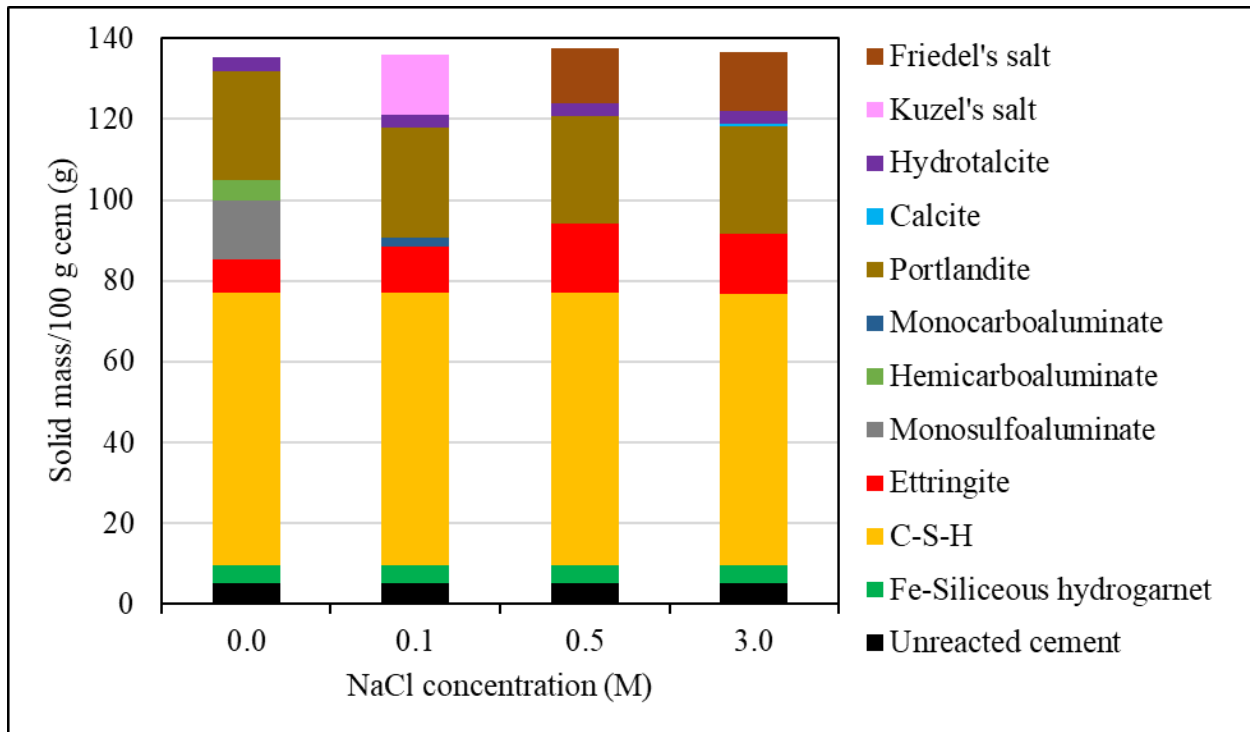
Figure 5-49: Predicted phase assemblage of control BB at variable NaCl solution concentrations
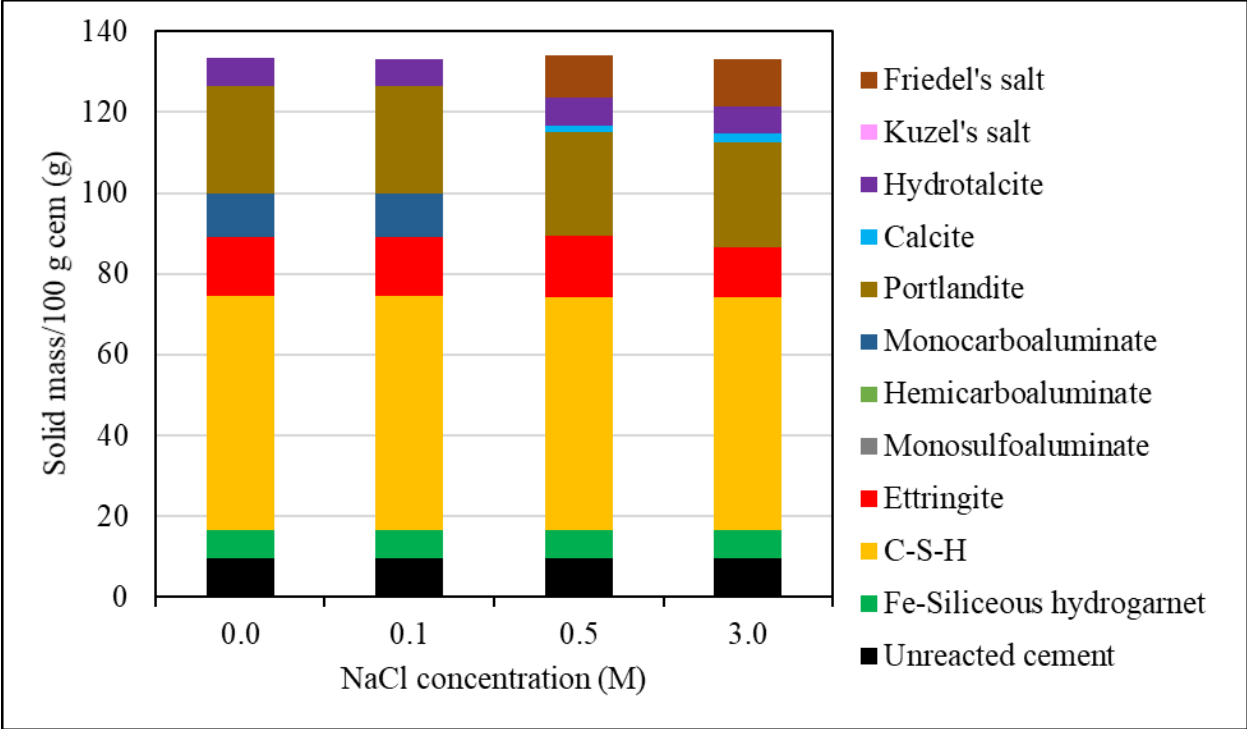
Figure 5-50: Predicted phase assemblage of control C at variable NaCl solution concentrations
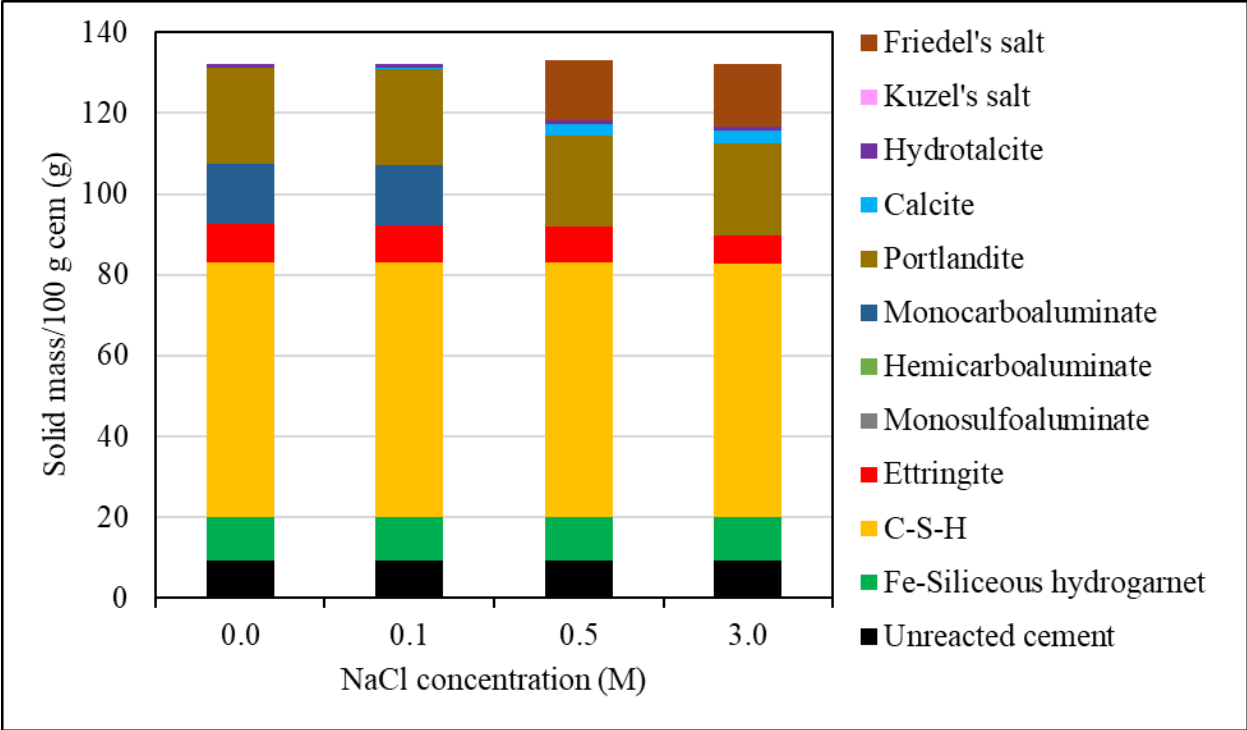
Figure 5-51: Predicted phase assemblage of control TTC at variable NaCl solution concentrations
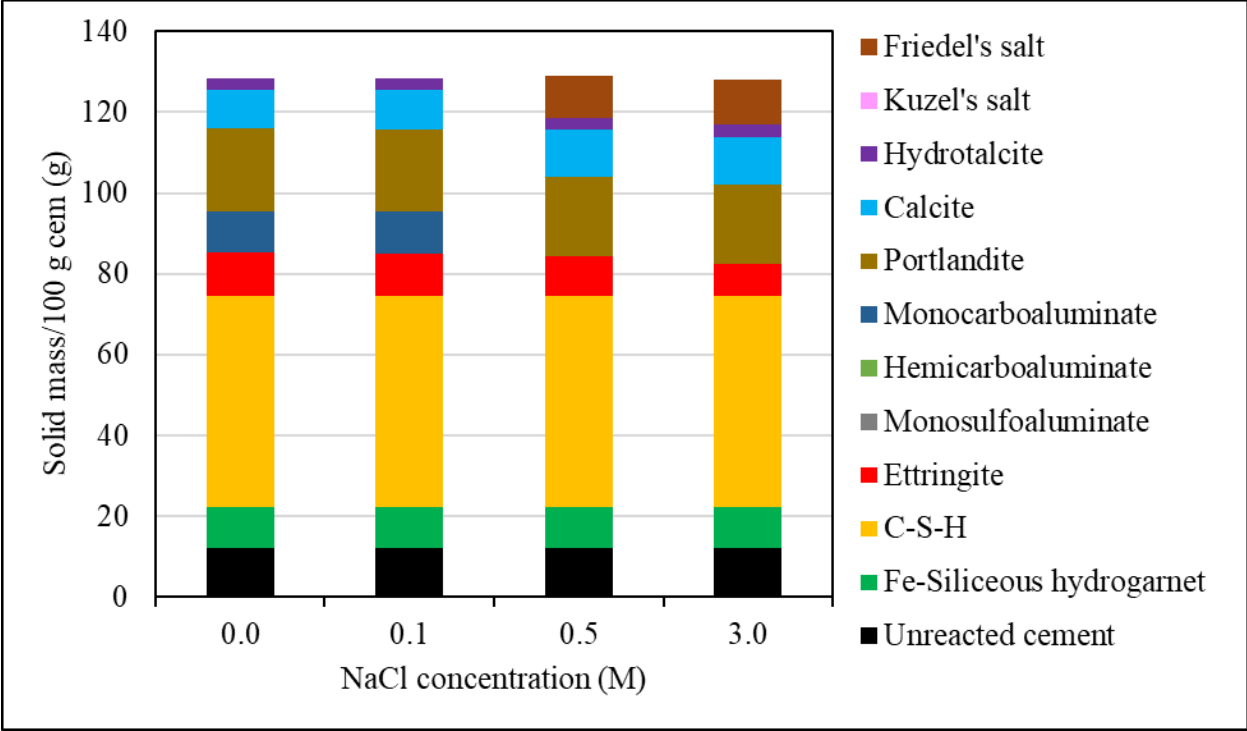
Figure 5-52: Predicted phase assemblage of control THIL at variable NaCl solution concentrations

After chloride exposure, Friedel's salt was predicted in all control mixtures at NaCl concentrations above 0.5 M. However, small amounts of Friedel's salt were detected by QXRD even at 0.1M NaCl concentration. As stated by Zibara [22], at low chloride concentrations (0.1M), sulfates react with alumina present in the system and form ettringite and monosulfate. Ettringite and monocarboaluminate in the control mixtures, except control BB, appeared to be stable at 0.1 M NaCl, similar to the before exposure condition. Kuzel's salt was predicted in control BB at 0.1 M NaCl concentration, similar to that observed in QXRD analysis. With the formation of Friedel's salt and Kuzel's salt, the carboaluminate phases and monosulfoaluminate disappeared, which indicates phase transformation possibly due to chloride binding. Simultaneously, calcite was observed which further indicated carboaluminate decomposition in the presence of chlorides. With increasing NaCl concentrations, the predicted ettringite content showed a small increase followed by a decrease in most of the mixtures which was similar to the trends observed in the reported QXRD results. Moreover, it is noteworthy that hydrotalcite was not detected by QXRD for any of the control mixtures, although it was predicted by GEMS. The highest hydrotalcite content was

predicted in control C whereas the lowest was predicted in control TTC, which corresponds to their respective MgO contents (2.5% in cement C and 0.32% in cement TTC).

The phase assemblages predicted for slag-blended mixtures are shown in Figure 5-53 through Figure 5-61. While the phases predicted in slag-blended mixtures were similar to those observed in control mixtures, addition of slags clearly affected their quantities. In terms of cement C and TTC blends, ettringite was only observed in C-60S8 and TTC-60S8 systems before exposure. When blended with slag S14B and S17, monosulfoaluminate, hemicarboaluminate, and traces of stratlingite were predicted due to their higher alumina content. On the other hand, when cement THIL was blended with slags S8, S14B, and S17, only ettringite and monocarboaluminate were predicted prior to chloride exposure. Additionally, little to no portlandite was observed in the slag-blended mixtures due to the consumption of portlandite.

After chloride exposure, Friedel's salt and Kuzel's salt were predicted. Kuzel's salt was only observed in C-60S14B, C-60S17, TTC-60S14B and TTC-60S17 at 0.1 M NaCl concentration. However, QXRD analysis detected small amounts of Kuzel's salt even at 0.5 M NaCl concentration for some of the mixtures. It is possible that the assumed slag degree of hydration (50%) was higher for these mixtures and might have caused this discrepancy. At NaCl concentrations above 0.5M, Friedel's salt was predicted in all the blended systems. In general, higher alumina slags corresponded with high amounts of Friedel's and Kuzel's salts. Compared to slag S17 blends, Friedel's salt predicted in slag S14B blends were slightly higher. This can be attributed to the lower MgO content in slag S14B which can also explain the lower predicted amounts of hydrotalcite compared to that of slag S17 blends. As slag S17 has a higher amount of MgO, more alumina was used to form more hydrotalcite. Similar trends were detected by QXRD for slag S14B blends as well. Nevertheless, no significant differences were observed in the binding isotherms of slag S14B and S17 blends (Figure 5-46 through Figure 5-48).
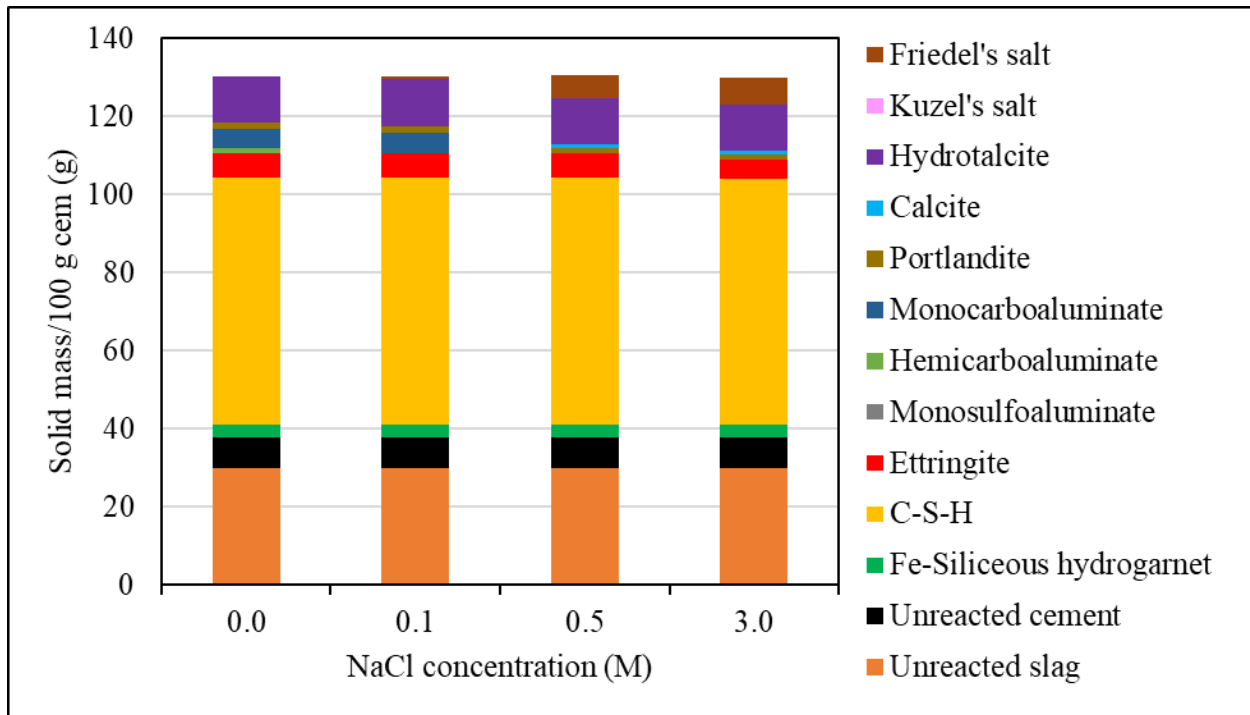
Figure 5-53: Predicted phase assemblage of C-60S8 mixture at variable NaCl solution concentrations
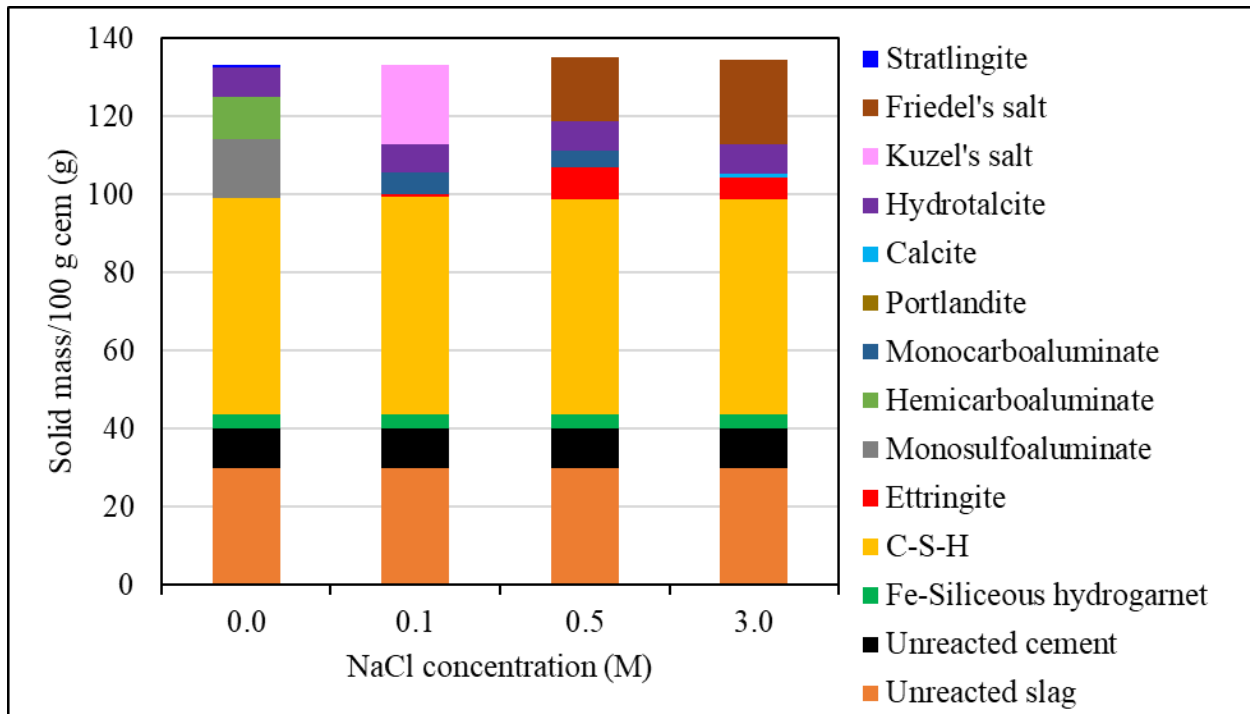
Figure 5-54: Predicted phase assemblage of C-60S14B mixture at variable NaCl solution concentrations
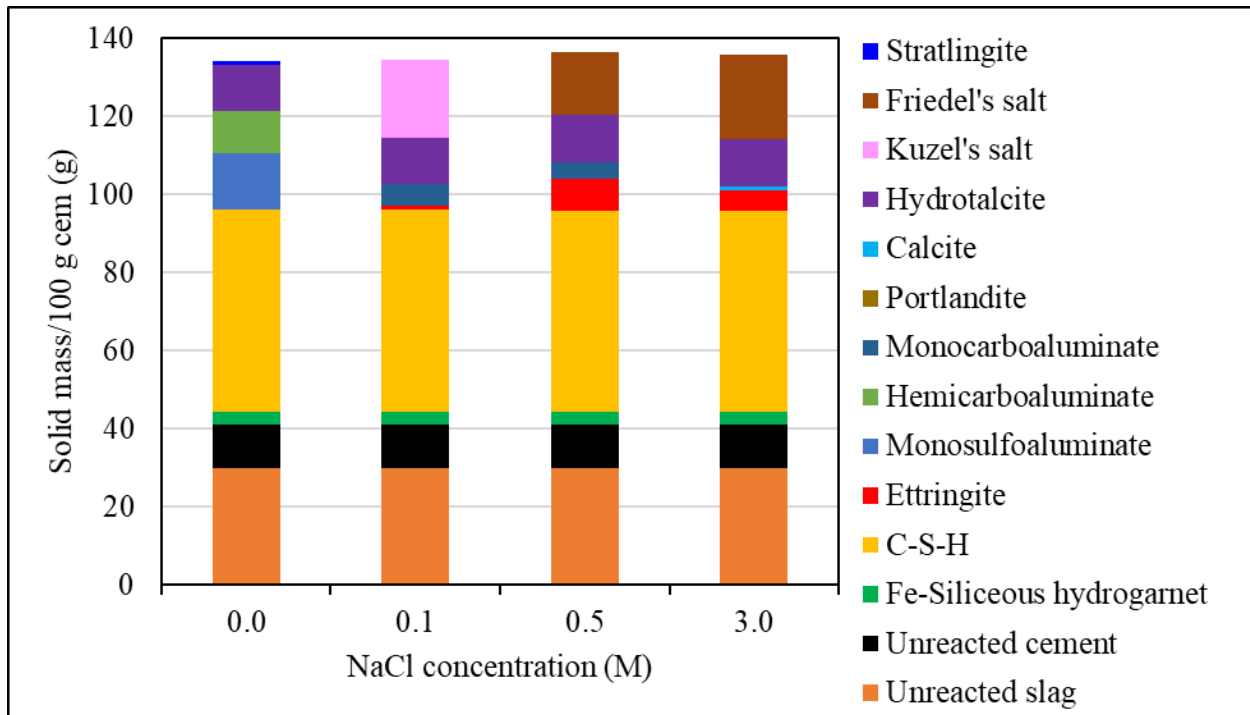
Figure 5-55: Predicted phase assemblage of C-60S17 mixture at variable NaCl solution concentrations
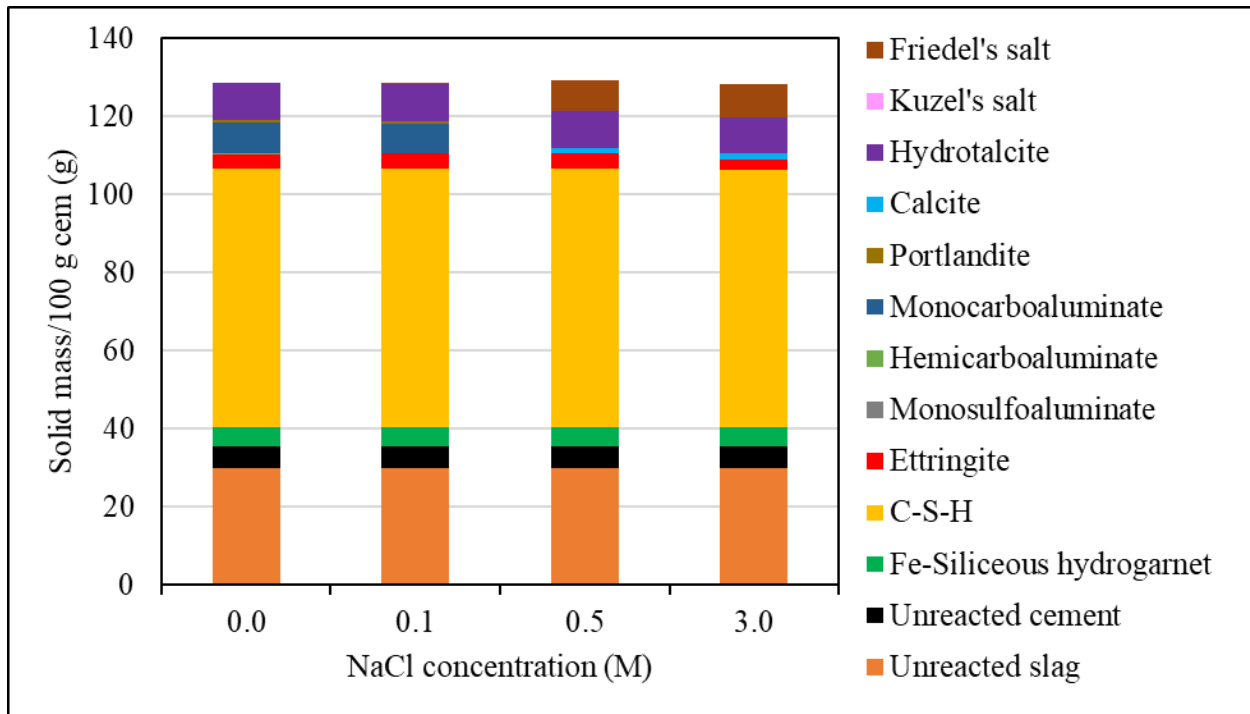
Figure 5-56: Predicted phase assemblage of TTC-60S8 mixture at variable NaCl solution concentrations

242
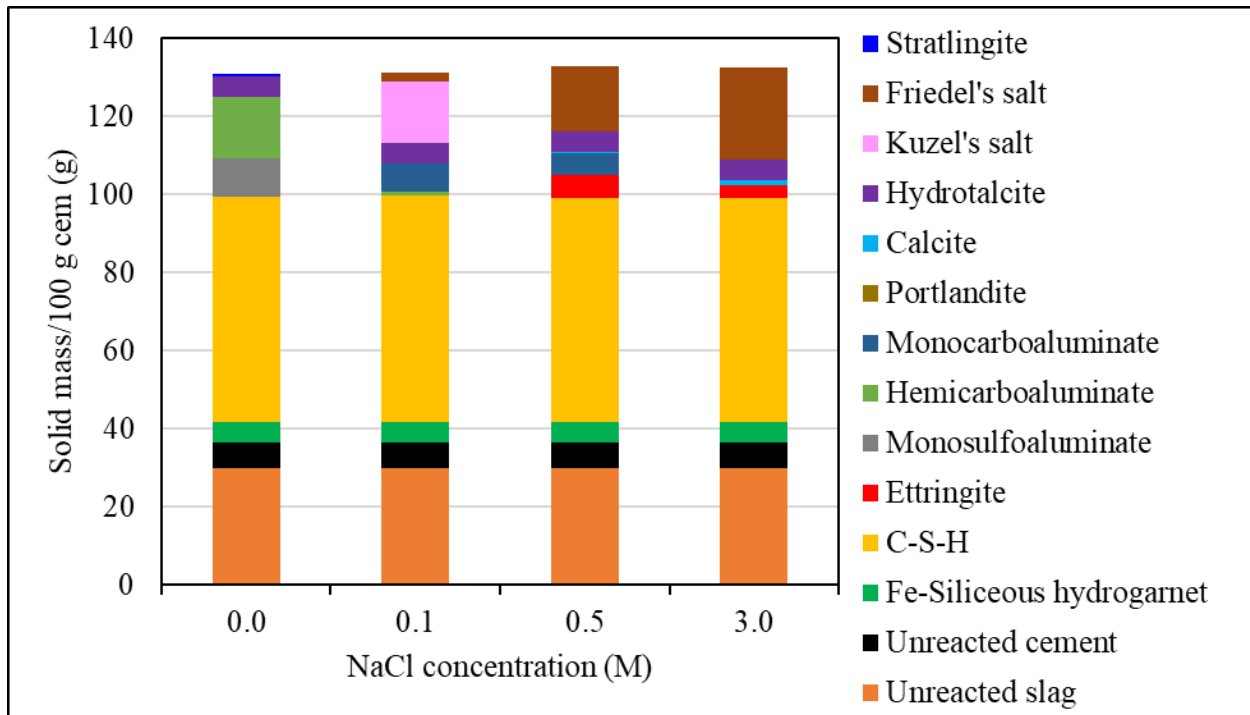
Figure 5-57: Predicted phase assemblage of TTC-60S14B mixture at variable NaCl solution
concentrations
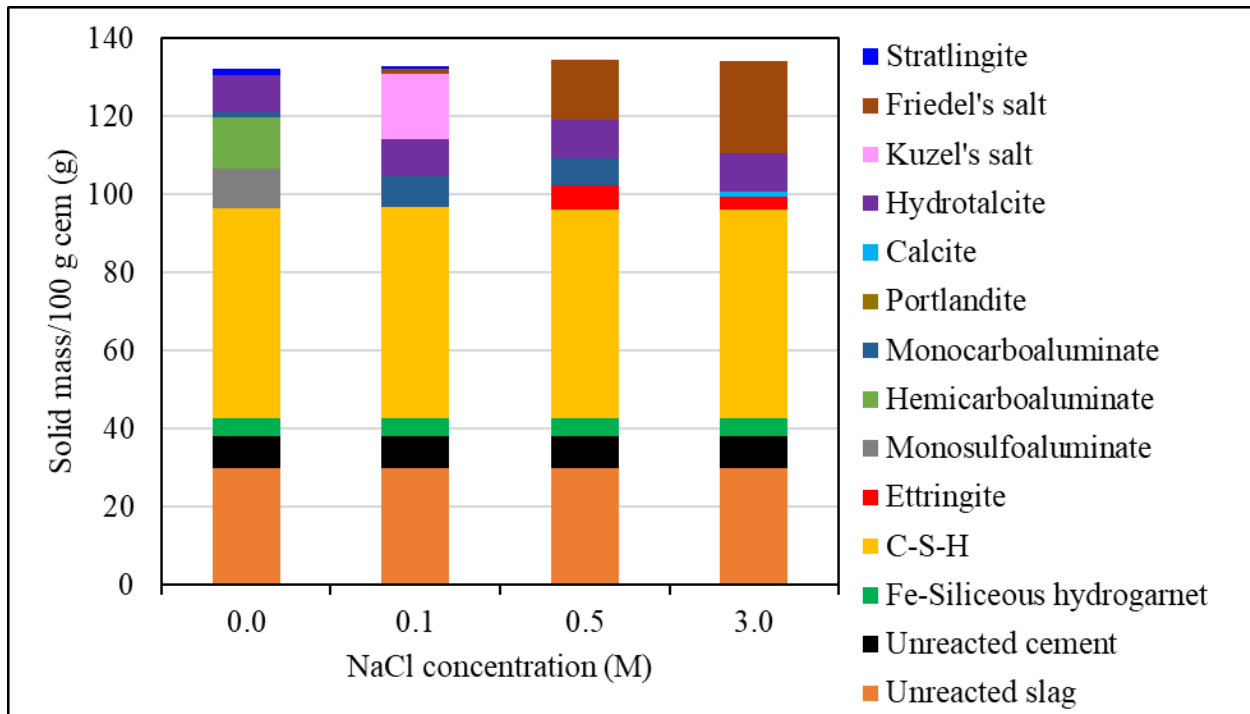
Figure 5-58: Predicted phase assemblage of TTC-60S17 mixture at variable NaCl solution
concentrations
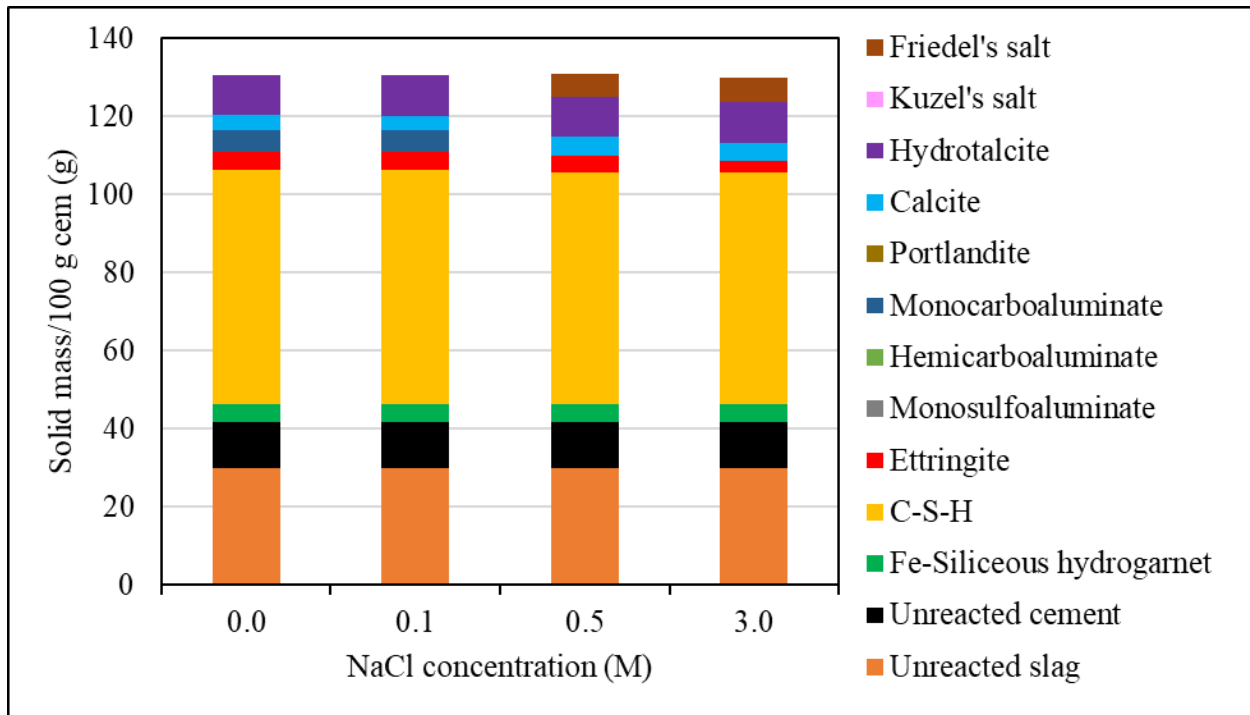
Figure 5-59: Predicted phase assemblage of THIL-60S8 mixture at variable NaCl solution concentrations
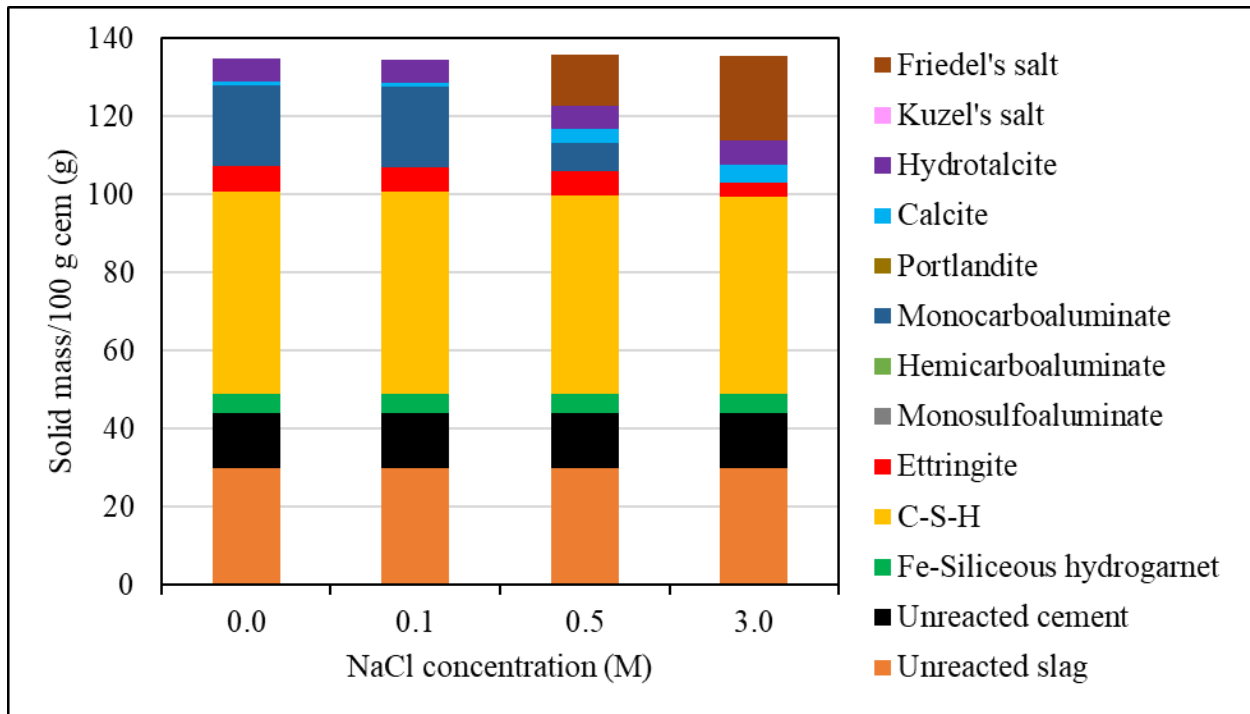
Figure 5-60: Predicted phase assemblage of THIL-60S14B mixture at variable NaCl solution concentrations
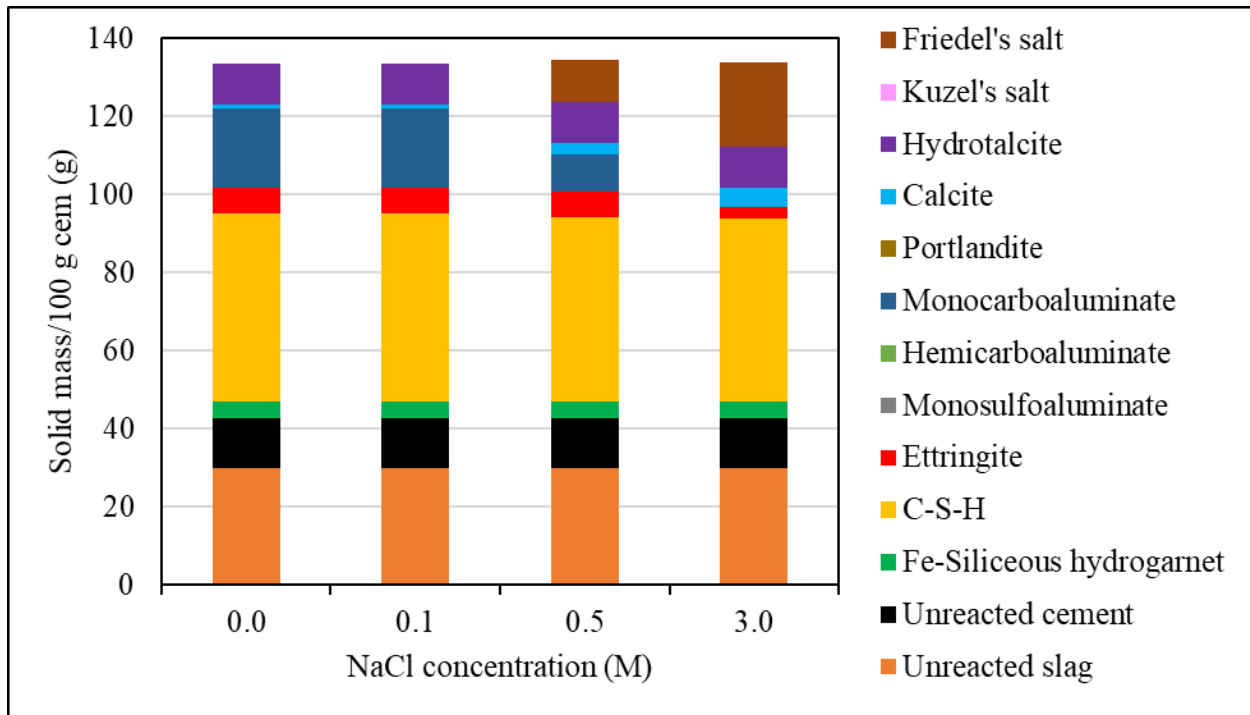
Figure 5-61: Predicted phase assemblage of THIL-60S17 mixture at variable NaCl solution concentrations

Based on the predicted Friedel's and Kuzel's salt contents, theoretical chemically bound chloride contents were calculated for each system (Table 5-40). With increasing NaCl concentrations, chemically bound chloride content increased. As physically adsorbed chloride contents were not considered in the calculation, chemically bound Cl content was expected to be lower than the experimentally determined bound chloride content. However, in some mixtures, the calculated bound chloride contents were higher. It is likely the assumed slag degree of hydration (50%) for modeling was higher in such cases and consequently resulted in an overestimation of chemically bound chlorides. Moreover, bound Cl contents of slag S8 blends were lower than those observed for their respective controls. When slags S14B and S17 were blended with the same cement, chemically bound Cl contents were similar, as indicated from the binding isotherms. Moreover, there was a substantial difference between the chemically bound chloride contents of low-alumina slag (S8) and high-alumina slags (S14B and S17), similar to that observed in binding isotherms data.

Table 5-40: Theoretical chemically bound chloride content

Mix ID	Chemically bound Cl (mg Cl-/g paste)		
	0.1 M NaCl	0.5 M NaCl	3.0 M NaCl
Control BB	6.1	12.1	13.0
Control C	0.0	9.5	10.4
Control TTC	0.0	13.5	14.2
Control THIL	0.0	9.4	10.1
C-60S8	0.8	5.4	6.0
C-60S14B	8.4	14.7	19.6
C-60S17	8.3	14.4	19.5
TTC-60S8	0.3	7.1	7.6
TTC-60S14B	8.7	15.3	21.4
TTC-60S17	8.2	13.8	21.3
THIL-60S8	0.0	5.3	5.8
THIL-60S14B	0.0	12.0	19.7
THIL-60S17	0.0	9.7	19.6

In order to further understand the effect of chloride ingress on phase formation, Figure 5-62 through Figure 5-64 show the effect of 3M NaCl penetration into cement C mixtures as modeled by GEMS. In the control C and C-60S8 system, the monocarboaluminate was transformed to Kuzel's and/or Friedel's salt and calcite with increasing NaCl concentration [50]. In the C-60S8 system, at first a small amount of Kuzel's salt was formed and subsequently transformed to Friedel's salt. In the C-60S17 system, high amounts of monosulfoaluminate, hemicarboaluminate, and a small amount of stratlingite were present at the core of the specimen which first transformed to Kuzel's salt and then to Friedel's salt. Although, ettringite was available at low volumes of NaCl in the control C and C-60S8 systems, it was not predicted in the C-60S17 system. However, with the formation of Kuzel's and Friedel's salt, ettringite appeared in C-60S17 towards the surface of the specimen. While substantially high amounts of portlandite were predicted in control C mix, little to no amounts were predicted in the slag mixtures. Near the surface with high amounts of NaCl, portlandite, C-S-H and Friedel's salt decomposed. Loser et al. [50] indicated similar behavior and observed a decrease in chloride binding at higher total chloride contents. However, in all the systems, hydrotalcite appeared to remain stable with varying NaCl contents [50].
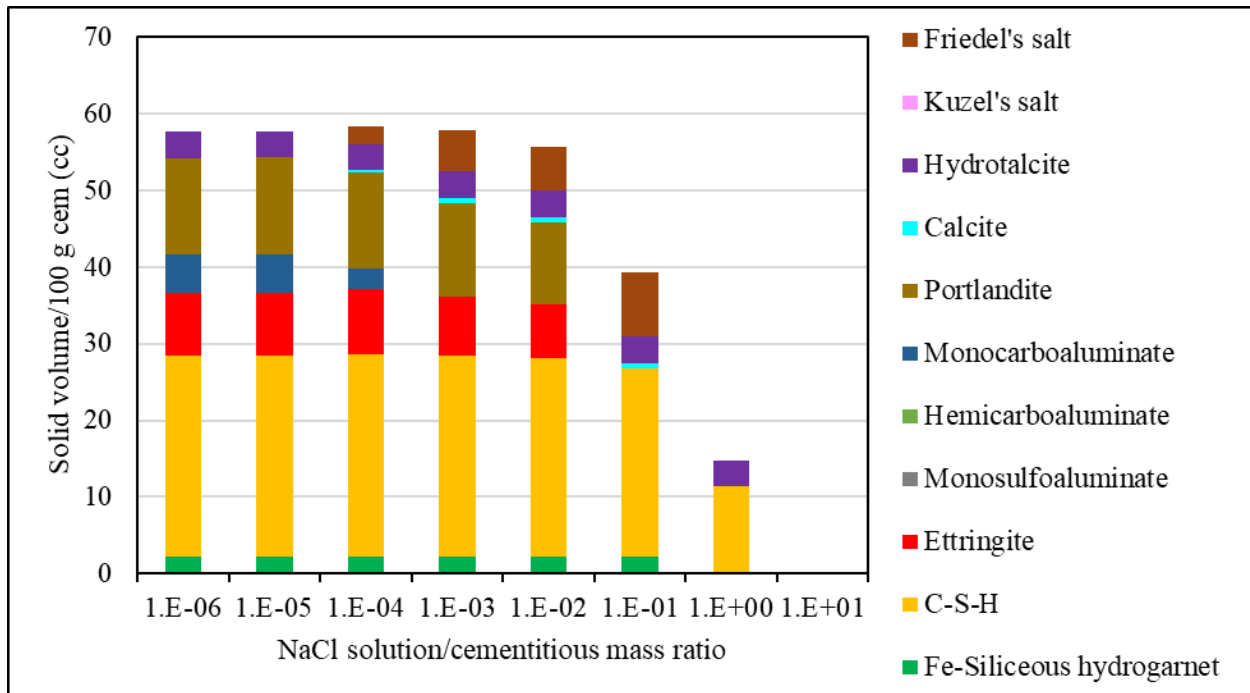
Figure 5-62: Predicted phase assemblage of control C mixture exposed to increasing amounts of NaCl solutions
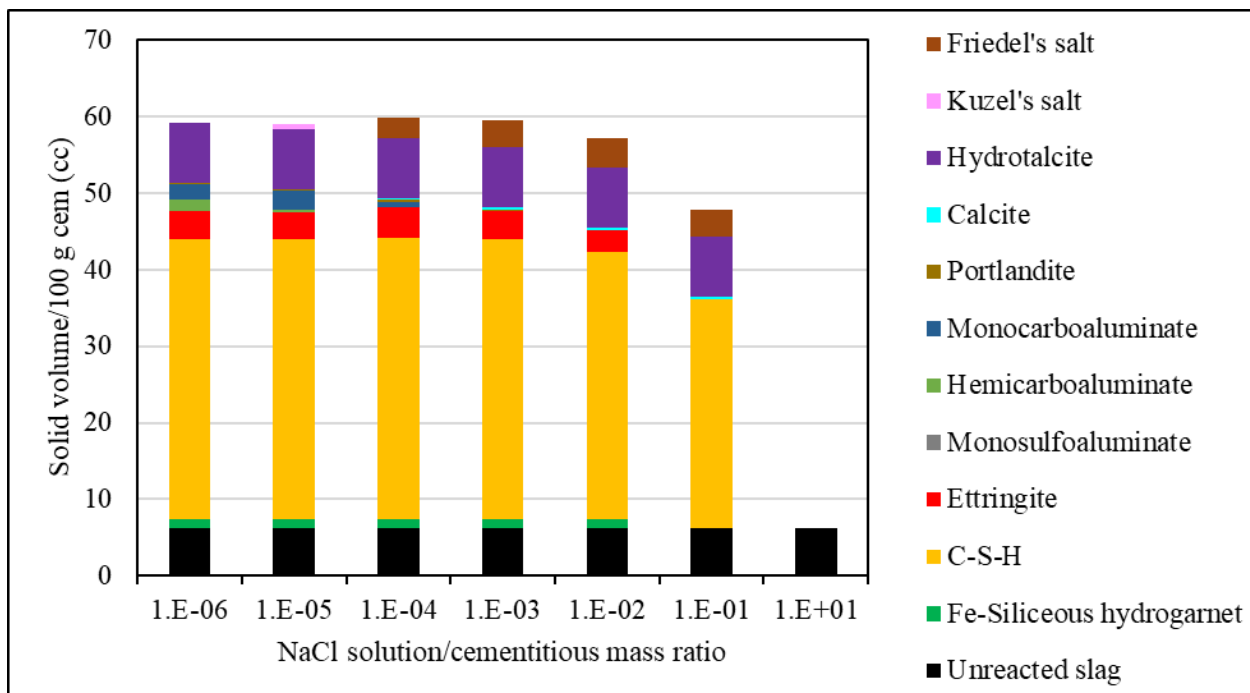
Figure 5-63: Predicted phase assemblage of C-60S8 mixture exposed to increasing amounts of NaCl solutions
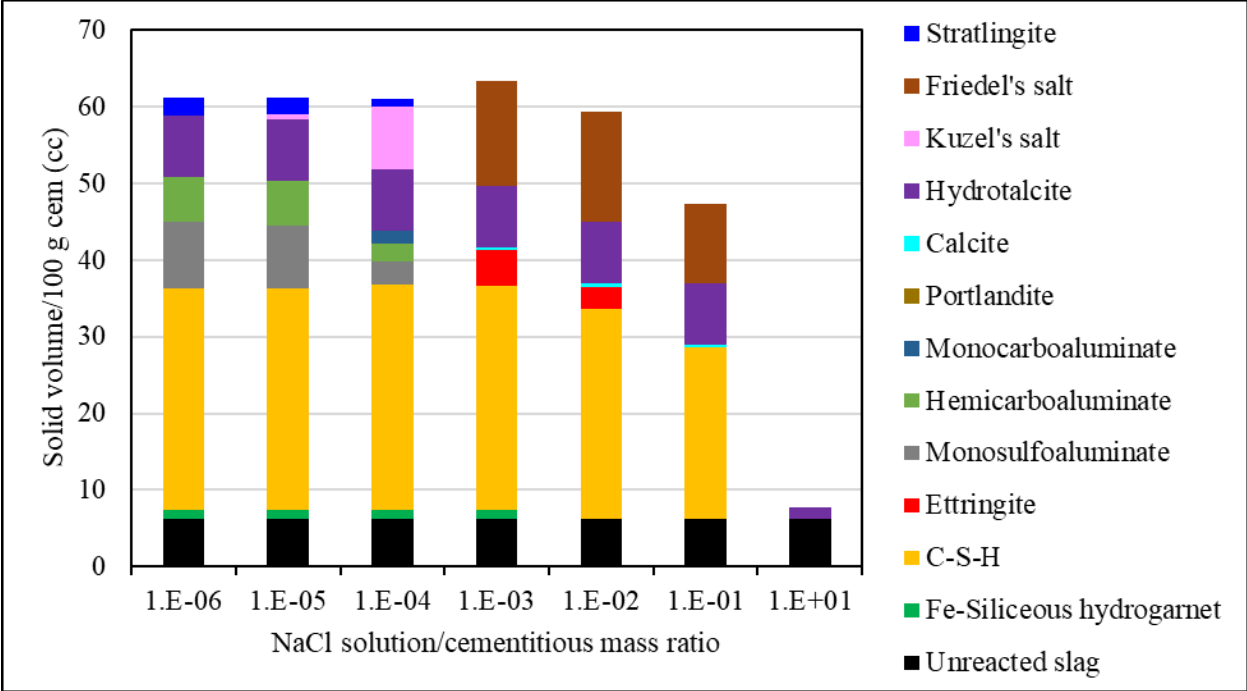
Figure 5-64: Predicted phase assemblage of C-60S17 mixture exposed to increasing amounts of NaCl solutions

Predicted volume changes of control C, C-60S8 and C-60S17 are reported in Table 5-41. No significant difference was observed between the initial pore volumes of the mixtures; however, the S17 blend indicated a slightly lower pore volume compared to the control C and C-60S8 mix. Therefore, it is likely that the C-60S17 blend was less permeable. Moreover, maximum solid volume increase was observed in C-60S17, which is in agreement with its higher chloride binding capacity. This can be attributed to the conversion of monosulfoaluminate and carboaluminate phases to Kuzel's salt and Friedel's salt [30].

Table 5-41: Predicted volume changes for cement C mixtures immersed in 3M NaCl solution

Mix ID	Initial total volume (cc/100g binder)	Initial solid volume (cc/100g binder)	Initial pore volume (cc/100g binder)	Max solid volume (cc/100g binder)
Control C	72	58	14	59
C-60S8	74	59	14	60
C-60S17	73	61	12	64

5.3.3.4 Summary

Chloride binding capacity of the paste mixtures was greatly influenced by cement and slag characteristics. For plain cement mixtures, chloride binding was the highest in Type I cement (BB) due to its higher C_3A and C_3S contents. This was supported by the high amounts of Friedel's salt detected by QXRD and thermodynamic modeling at all NaCl concentrations, although physically adsorbed chlorides are not directly identified by those techniques. Kuzel's salt was only observed in low NaCl concentrations. Binding capacity of Type I(HA) (cement C) was lower than that of Type II(MH) (cement TTC) due to the solubility of Friedel's salt at higher pH levels. The lowest binding capacity was observed in Type IL cement mixtures (TIL, THIL) although QXRD analysis detected high Friedel's salt contents. This could be attributed to a lower C-S-H formation caused by the dilution effect and a corresponding reduction in chlorides binding sites available through physical adsorption.

Partial replacement of cement with 60% slag enhanced the chloride binding capacity, with higher chloride binding noted for the high-alumina slags. This was due to the formation of more AFm phases from the additional alumina in slags, which later transformed to Friedel's salt during chloride exposure. Moreover, increased formation of C-(A)-S-H may also have contributed to improve physical chloride binding capacity. High-alumina slag (S14B and S17) mixtures indicated substantially higher binding capacities compared to their respective controls, although the difference in bound chloride content between the slag S8 blends and controls were lower. Both QXRD and thermodynamic modeling showed higher and similar Friedel's salt contents in slag S14B and slag S17 mixtures. Moreover, the effect of cement type on the binding capacity of slag mixtures demonstrated trends similar to those observed in the control mixtures.

As it appears, high alumina levels in cements and slags increase chloride binding capacity, which in turn reduces free chloride content and may improve corrosion resistance of reinforced concrete. Although, this is in line with what is stated in the literature, few studies [75], [76] questioned this hypothesis and reported certain risks on corrosion associated with chloride binding. Chloride ion penetration is dependent on the diffusivity of concrete, which is affected by its pore structure characteristics, connectivity, and pH of the pore solution. Therefore, in order to obtain a comprehensive knowledge of the effect of cement and slag characteristics on corrosion resistance

of concrete, further investigation of chloride ion penetration and concrete chloride diffusivity is required.

5.4   Conclusions and Recommendations

Different cement-slag combinations demonstrated variable effects on concrete durability in terms of external sulfate attack, internal sulfate attack in heat-cured systems, and chloride binding. Based on the current investigation, several conclusions can be made.

Mixtures prepared with Type I cements indicated potential for failure under conditions of external sulfate exposure as well as heat treatment at elevated temperatures. This is due to their higher C_3A contents, which leads to the formation of high amounts of ettringite after sulfate exposure and heat treatment. It is noteworthy that the expansion from exposure to sulfates for the Type I(HA) mixture was slightly delayed, possibly due to initial ettringite stability caused by higher pH levels. The expansion of the heat-cured Type I(HA) mixture occurred earlier likely due to the high alkali levels but was surpassed eventually by the Type I mixture. Additionally, Type II(MH) cement indicated moderate resistance to external sulfate attack, while Type II(MH)(HA) cement showed some resistance to internal sulfate attack, both because of their moderate C_3A contents. Among the control mixtures, Type IL cements demonstrated the highest resistance to both internal and external sulfate attack. This can be attributed to the lower C_3A and C_3S contents due to the reduced clinker factor. Additionally, formation of carboaluminates in IL cement systems may have stabilized the primary ettringite making less monosulfoaluminate available for further reaction in sulfate environments.

Chloride binding of Type I (low alkali) cement was the highest due to its higher C_3A and C_3S contents, and the formation of higher amounts of Friedel's salt. However, chloride binding for Type I(HA) cement was lower than that of Type II(MH), likely due to a reduced physical binding capacity at higher pH levels. Additionally, Type IL cements showed slightly lower chloride binding capability, mostly due to the reduced physical adsorption as a result of lower C-S-H formation caused by the dilution effect.

Incorporation of slags at 60% replacement level, regardless of their characteristics, enhanced the durability of the mixtures for the reported test ages, as indicated by lower expansion in sulfate solutions, lower expansion for heat-cured specimens, as well as an increased chloride

250

binding capacity. In terms of specimens exposed to sulfate solution, the most significant reduction and delay in expansion was observed for blends with Type I cement. However, the limited testing duration was not sufficient to be conclusive about the effect of different slags on both external and internal sulfate attack. Nevertheless, QXRD analysis (after one year of sulfate exposure) as well as thermodynamic modeling indicated differences in phase assemblage for different cement-slag combinations. Both analysis techniques indicate that blending high-alumina slags with Type IL cements would result in higher sulfate resistance. This is due to carboaluminate formation which may delay/suppress secondary ettringite formation.

Most of the sulfate-optimized mixtures (based on 2-day optimum level), when exposed to sulfate environment, showed lower expansions compared to their respective as-received systems indicating the possibility of improved sulfate resistance with optimized the sulfate content of the blended cementitious systems. This was supported by lower solid volume increases (thermodynamic modeling) on exposure to a sulfate environment. The effect was more significant in Type IL cement blends. Therefore, sulfate resistance of slag blends can be improved by sulfate addition. However, the effect of sulfate additions on DEF must be further studied to allow rendering scientific conclusions and recommendations pertaining to identifying any potential durability issue, especially at lower slag replacement levels.

As for chloride binding, high-alumina slags demonstrated higher chloride binding capacities. The highest binding capacity was observed for Type I cement and high-alumina slags. This is due to high amounts of Friedel's salt formation and enhanced C-(A)-S-H formation. However, simple assessment of chloride binding capacity might not provide conclusive information in regards to corrosion resistance of reinforced concrete. Further investigation on chloride ion penetration and chloride diffusivity in blended concrete are recommended to fully understand the effect of slag-blended cementitious systems characteristics on corrosion resistance.

5.5   References

[1]   M. Collepardi, "A state-of-the-art review on delayed ettringite attack on concrete," *Cem. Concr. Compos.*, vol. 25, no. 4–5, pp. 401–407, May 2003.

[2]   A. M. Neville, *Properties of Concrete*, 4th ed. Harlow, England: Pearson Education Limited, 2006.

[3]   A. Neville, "The confused world of sulfate attack on concrete," *Cem. Concr. Res.*, vol. 34, no. 8, pp. 1275–1296, 2004.

[4]   P. K. Mehta and P. J. M. Monteiro, *Concrete: Microstructure, Properties, and Materials*, Fourth Edi. McGraw-Hill Education, 2014.

[5]   P. K. Mehta, "Mechanism of expansion associated with ettringite formation," *Cem. Concr. Res.*, vol. 3, pp. 1–6, 1973.

[6]   N. Shanahan and A. Zayed, "Cement composition and sulfate attack," *Cem. Concr. Res.*, vol. 37, no. 4, pp. 618–623, Apr. 2007.

[7]   I. Odler and J. Colán-Subauste, "Investigations on cement expansion associated with ettringite formation," *Cem. Concr. Res.*, vol. 29, no. 5, pp. 731–735, 1999.

[8]   B. Tian and M. D. Cohen, "Does gypsum formation during sulfate attack on concrete lead to expansion?," *Cem. Concr. Res.*, vol. 30, no. 1, pp. 117–123, Jan. 2000.

[9]   ASTM C989/C989M-17, "Standard Specification for Slag Cement for Use in Concrete and Mortars," West Conshohocken, PA: ASTM International, 2017.

[10]   M. J. Whittaker, "The Impact of Slag Composition on the Microstructure of Composite Slag Cements Exposed to Sulfate Attack," The University of Leeds, 2014.

[11]   M. Whittaker, M. Zajac, M. Ben Haha, and L. Black, "The impact of alumina availability on sulfate resistance of slag composite cements," *Constr. Build. Mater.*, vol. 119, pp. 356–369, 2016.

[12]   S. Ogawa, T. Nozaki, K. Yamada, H. Hirao, and R. D. Hooton, "Improvement on sulfate resistance of blended cement with high alumina slag," *Cem. Concr. Res.*, vol. 42, no. 2, pp. 244–251, Feb. 2012.

[13]   ASTM C1012/C1012M-15, "Standard test method for length change of hydraulic-cement mortars exposed to sulfate solution," West Conshohocken, PA: ASTM International, 2015.

[14]   T. Ramlochan, "The Effect of Pozzolans and Slag on the Expansion of Mortars and Concrete Cured at Elevated Temperature," University of Toronto, 2003.

[15]   J. Stark and K. Bollmann, "Delayed Ettringite Formation in Concrete," *ZKG Int.*, vol. 53, no. 4, pp. 1–25, 2000.

[16]   F. P. Glasser, D. Damidot, and M. Atkins, "Phase development in cement in relation to the secondary ettringite problem," *Adv. Cem. Res.*, vol. 7, no. 26, pp. 57–68, 1995.

[17]   S. Kelham, "The Effect of Cement Composition and Fineness on Expansion Associated with Delayed Ettringite Formation," *Cem. Concr. Compos.*, vol. 18, pp. 171–179, 1996.

[18]   G. Escadeillas, J. E. Aubert, M. Segerer, and W. Prince, "Some factors affecting delayed ettringite formation in heat-cured mortars," *Cem. Concr. Res.*, vol. 37, no. 10, pp. 1445–1452, 2007.

[19]   H. F. W. Taylor, C. Famy, and K. L. Scrivener, "Delayed Ettringite Formation," *Cem. Concr. Res.*, vol. 31, pp. 683–693, 2001.

[20]   T. Ramlochan, P. Zacarias, M. D. A. Thomas, and R. D. Hooton, "The effect of pozzolans and slag on the expansion of mortars cured at elevated temperature: Part I: Expansive behaviour," *Cem. Concr. Res.*, vol. 33, no. 6, pp. 807–814, Jun. 2003.

[21]   O. R. Ogirigbo and L. Black, "Chloride binding and diffusion in slag blends: Influence of slag composition and temperature," *Constr. Build. Mater.*, vol. 149, pp. 816–825, Sep. 2017.

[22]   H. Zibara, "Binding of external chlorides by cement pastes," University of Toronto, 2001.

[23]   M. D. A. Thomas, R. D. Hooton, A. Scott, and H. Zibara, "The effect of supplementary cementitious materials on chloride binding in hardened cement paste," *Cem. Concr. Res.*, vol. 42, no. 1, pp. 1–7, 2012.

[24]   P. Brown and J. Bothe, "The system CaO-Al2O3-CaCl2-H2O at 23±2 °C and the mechanisms of chloride binding in concrete," *Cem. Concr. Res.*, vol. 34, no. 9, pp. 1549–1553, 2004.

[25]   A. Delagrave, J. Marchand, J. Ollivier, S. Julien, and K. Hazrati, "Chloride binding capacity

of various hydrated cement paste systems," *Adv. Cem. Based Mater.*, vol. 6, no. 2, pp. 28–35, 1997.

[26]   H. Zibara, "Binding of External Chlorides by Cement Pastes," 2001.

[27]   M. D. A. Thomas, R. D. Hooton, A. Scott, and H. Zibara, "The effect of supplementary cementitious materials on chloride binding in hardened cement paste," *Cem. Concr. Res.*, vol. 42, no. 1, pp. 1–7, Jan. 2012.

[28]   H. Zibara, R. D. Hooton, M. D. A. Thomas, and K. Stanish, "Influence of the C/S and C/A ratios of hydration products on the chloride ion binding capacity of lime-SF and lime-MK mixtures," *Cem. Concr. Res.*, vol. 38, no. 3, pp. 422–426, 2008.

[29]   K. Y. Yeau and E. K. Kim, "An experimental study on corrosion resistance of concrete with ground granulate blast-furnace slag," *Cem. Concr. Res.*, vol. 35, no. 7, pp. 1391–1399, Jul. 2005.

[30]   M. Otieno, H. Beushausen, and M. Alexander, "Effect of chemical composition of slag on chloride penetration resistance of concrete," *Cem. Concr. Compos.*, vol. 46, pp. 56–64, Feb. 2014.

[31]   ASTM C1012/C1012M-18b, "Standard test method for length change of hydraulic-cement mortars exposed to sulfate solution," West Conshohocken, PA: ASTM International, 2018.

[32]   Y. Fu, "Delayed Ettringite Formation in Portland Cement Products," University of Ottawa, 1996.

[33]   T. Whitfield, "Effect of Tricalcium Silicate Content on Expansion in Internal Sulfate Attack," University of South Florida, 2006.

[34]   D. E. Kennedy, "Evaluation and Development of a Test Method for Delayed Ettringite Formation in Mass Concrete," University of Florida, 2017.

[35]   ASTM C305-14, "Standard Practice for Mechanical Mixing of Hydraulic Cement Pastes and Mortars of Plastic Consistency," West Conshohocken, PA: ASTM International, 2014.

[36]   T. Luping and L.-O. Nilsson, "Chloride binding capacity and binding isotherms of OPC pastes and mortars," *Cem. Concr. Res.*, vol. 23, no. 2, pp. 247–253, 1993.

[37]   D. Jansen, F. Goetz-Neunhoeffer, C. Stabler, and J. Neubauer, "A remastered external

standard method applied to the quantification of early OPC hydration," *Cem. Concr. Res.*, vol. 41, no. 6, pp. 602–608, Jun. 2011.

[38] D. Jansen, S. T. Bergold, F. Goetz-Neunhoeffer, and J. Neubauer, "The hydration of alite: A time-resolved quantitative XRD approach using the G-factor method compared with heat release," *J. Appl. Crystallogr.*, vol. 44, no. 5, pp. 895–901, 2011.

[39] D. Jansen, C. Stabler, F. Goetz-Neunhoeffer, S. Dittrich, and J. Neubauer, "Does Ordinary Portland Cement Contain Amorphous Phase? A Quantitative Study Using an External Standard Method," *Powder Diffr.*, vol. 26, no. 1, pp. 31–38, Mar. 2011.

[40] D. Bish and R. J. Reynolds, "Sample Preparation for X-Ray Diffraction," in *Modern Powder Diffraction*, D. Bish and J. Post, Eds. Washington, DC: The Mineralogical Society of America, 1989, pp. 73–99.

[41] Paul Scherrer Institut (PSI), "GEMS 3 [Software]." .

[42] W. Hummel, U. Berner, E. Curti, F. J. Pearson, and T. Thoenen, "Nagra/PSI chemical thermodynamic data base 01/01," *Radiochim. Acta*, vol. 90, no. 9–11, pp. 805–813, 2002.

[43] EMPA, "CEMDATA14." [Online]. Available: https://www.empa.ch/web/s308/cemdata.

[44] A. Schöler, B. Lothenbach, F. Winnefeld, and M. Zajac, "Hydration of quaternary Portland cement blends containing blast-furnace slag, siliceous fly ash and limestone powder," *Cem. Concr. Compos.*, vol. 55, pp. 374–382, 2015.

[45] W. Kunther, B. Lothenbach, and K. L. Scrivener, "On the relevance of volume increase for the length changes of mortar bars in sulfate solutions," *Cem. Concr. Res.*, vol. 46, pp. 23–29, 2013.

[46] V. Kocaba, E. Gallucci, and K. L. Scrivener, "Methods for determination of degree of reaction of slag in blended cement pastes," *Cem. Concr. Res.*, vol. 42, no. 3, pp. 511–525, 2012.

[47] F. Nosouhian, M. Fincan, N. Shanahan, Y. P. Stetsko, K. A. Riding, and A. Zayed, "Effects of slag characteristics on sulfate durability of Portland cement-slag-blended systems," *Constr. Build. Mater.*, vol. 229, p. 116882, Dec. 2019.

[48] R. Snellings, "X-ray powder diffraction applied to cement," in *A Practical Guide to*

Microstructural Analysis of Cementitious Materials, 2016, pp. 107–176.

[49]   J. S. Lumley, R. S. Gollop, G. K. Moir, and H. F. W. Taylor, "Degrees of reaction of the slag in some blends with Portland cements," *Cem. Concr. Res.*, vol. 26, no. 1, pp. 139–151, 1996.

[50]   R. Loser, B. Lothenbach, A. Leemann, and M. Tuchschmid, "Chloride resistance of concrete and its binding capacity – Comparison between experimental results and thermodynamic modeling," *Cem. Concr. Compos.*, vol. 32, no. 1, pp. 34–42, Jan. 2010.

[51]   S. Adu-Amankwah, L. Black, J. Skocek, M. Ben Haha, and M. Zajac, "Effect of sulfate additions on hydration and performance of ternary slag-limestone composite cements," *Constr. Build. Mater.*, vol. 164, pp. 451–462, 2018.

[52]   A. Zayed, K. A. Riding, Y. Stetsko, N. Shanahan, A. Markandeya, F. Nosouhian, D. Mapa and M. Fincan, "Final Report Effects of Blast Furnace Slag Characteristics on Durability of Cementitious Systems for Florida Concrete Structures FDOT Contract Number : BDV25-977-28," University of South Florida, Tampa, FL, 2019.

[53]   C. Yu, W. Sun, and K. Scrivener, "Degradation mechanism of slag-blended mortars immersed in sodium sulfate solution," *Cem. Concr. Res.*, vol. 72, pp. 37–47, Jun. 2015.

[54]   M. Whittaker, M. Zajac, M. Ben Haha, F. Bullerjahn, and L. Black, "The role of the alumina content of slag, plus the presence of additional sulfate on the hydration and microstructure of Portland cement-slag blends," *Cem. Concr. Res.*, vol. 66, pp. 91–101, Dec. 2014.

[55]   R. S. Gollop and H. F. W. Taylor, "Microstructural and microanalytical studies of sulfate attack. IV. Reactions of a slag cement paste with sodium and magnesium sulfate solutions," *Cem. Concr. Res.*, vol. 26, no. 7, pp. 1013–1028, 1996.

[56]   S. Adu-Amankwah, M. Zajac, C. Stabler, B. Lothenbach, and L. Black, "Influence of limestone on the hydration of ternary slag cements," *Cem. Concr. Res.*, vol. 100, pp. 96–109, Oct. 2017.

[57]   R. S. Gollop and H. F. W. Taylor, "Microstructural and microanalytical studies of sulfate attack. II. Sulfate-resisting portland cement: Ferrite composition and hydration chemistry," *Cem. Concr. Res.*, vol. 24, no. 7, pp. 1347–1358, 1994.

[58] E. F. Irassar, V. L. Bonavetti, and M. González, "Microstructural study of sulfate attack on ordinary and limestone Portland cements at ambient temperature," *Cem. Concr. Res.*, vol. 33, no. 1, pp. 31–41, 2003.

[59] E. F. Irassar, "Sulfate attack on cementitious materials containing limestone filler - A review," *Cem. Concr. Res.*, vol. 39, no. 3, pp. 241–254, 2009.

[60] M. C. G. Juenger and R. Siddique, "Recent advances in understanding the role of supplementary cementitious materials in concrete," *Cem. Concr. Res.*, vol. 78, pp. 71–80, 2015.

[61] W. Deboucha, N. Leklou, and A. Khelidj, "Blast Furnace Slag Addition Effects on Delayed Ettringite Formation in Heat-cured Mortars," *KSCE J. Civ. Eng.*, vol. 22, no. 9, pp. 3484–3490, Sep. 2018.

[62] ACI Committee 201, "ACI 201.2R - 16 Guide to Durable Concrete," American Concrete Institute, Farmington Hills, MI, 2016.

[63] W. Deboucha, D. Ph, N. Leklou, A. Khelidj, O. Plé, and U. J. Alengaram, "Combination Effect of Limestone Filler and Slag on Delayed Ettringite Formation in Heat-Cured Mortar," vol. 32, no. 2017, pp. 1–6, 2020.

[64] Z. Zhang, J. Olek, and S. Diamond, "Studies on delayed ettringite formation in heat-cured mortars II: Characteristics of cement that may be susceptible to DEF," *Cem. Concr. Res.*, vol. 32, no. 11, pp. 1737–1742, 2002.

[65] D. Heinz, M. Kalde, U. Ludwig, and I. Ruediger, "Present State of Investigation on Damaging Late Ettringite Formation (DLEF) in Mortars and Concrete," in *SP-177: Ettringite-The Sometimes Host of Destruction*, B. Erlin, Ed. ACI Committee 201, 1999, pp. 1–13.

[66] D. Heinz, U. Ludwig, and I. Rüdger, "Delayed ettringite formation in heat treated mortars and concretes," *Concr. Precast. Plant Technol.*, no. 11, pp. 56–61, 1989.

[67] P. W. Brown and J. V. Bothe, "The stability of ettringite," *Adv. Cem. Res.*, vol. 5, no. 18, pp. 47–63, 1993.

[68] R. Yang and J. H. Sharp, "Hydration Characteristics of Portland Cement after Heat Curing:

II, Evolution of Crystalline Aluminate-Bearing Hydrates," *J. Am. Ceram. Soc.*, vol. 84, no. 5, pp. 1113–1119, 2001.

[69]   T. Ramlochan, M. D. A. Thomas, and R. D. Hooton, "The effect of pozzolans and slag on the expansion of mortars cured at elevated temperature: Part II: Microstructural and microchemical investigations," *Cem. Concr. Res.*, vol. 34, no. 8, pp. 1341–1356, 2004.

[70]   Z. Shi, M. Geiker, K. De Weerdt, T. A. Ostnor, B. Lothenbach, F.Winnefeld, J.Skibsted, "Role of calcium on chloride binding in hydrated Portland cement–metakaolin–limestone blends," *Cem. Concr. Res.*, 2017.

[71]   A. Ipavec and R. Gabrov, "Cement and Concrete Research Chloride binding into hydrated blended cements : The influence of limestone and alkalinity," *Cem. Concr. Res.*, vol. 48, pp. 74–85, 2013.

[72]   Q. Yuan, C. Shi, G. De Schutter, K. Audenaert, and D. Deng, "Chloride binding of cement-based materials subjected to external chloride environment - A review," *Constr. Build. Mater.*, vol. 23, no. 1, pp. 1–13, 2009.

[73]   S. Sui, W. Wilson, F. Georget, H. Maraghechi, H. Kazemi-Kamyab, W. Sun, K. Scrivener, "Quantification methods for chloride binding in Portland cement and limestone systems," *Cem. Concr. Res.*, vol. 125, no. March, p. 105864, 2019.

[74]   M. Zajac, A. Rossberg, G. Le Saout, and B. Lothenbach, "Influence of limestone and anhydrite on the hydration of Portland cements," *Cem. Concr. Compos.*, vol. 46, pp. 99–108, Feb. 2014.

[75]   G. K. Glass and N. R. Buenfeld, "The influence of chloride binding on the chloride induced corrosion risk in reinforced concrete," *Corros. Sci.*, vol. 42, no. 2, pp. 329–344, 2000.

[76]   B. Reddy, G. K. Glass, P. J. Lim, and N. R. Buenfeld, "On the corrosion risk presented by chloride bound in concrete," vol. 24, pp. 1–5, 2002.

Chapter 6   Summary, Conclusions, and Recommendations

6.1   Summary and Conclusions

A battery of experiments was conducted in order to assess the durability of slag-blended cementitious systems in terms of sulfate balance, temperature rise, external sulfate durability, DEF caused by internal sulfate attack, chloride binding. The cements studied here included Type I, Type I(Ha), Type II(MH), Type II(MH)(Ha) and Type IL cements, which showed the effect of varying C_3S, C_3A, alkalis, sulfates, limestone contents and fineness. The selected slags were predominantly varied based on their alumina content, while differences in magnesia contents, sulfates and fineness were observed. The as-received cementitious materials were characterized with XRF, XRD, Blaine fineness, laser particle size analysis and specific gravity. The blended cementitious systems incorporated a slag substitution of 60%. Adiabatic calorimetry was conducted on slag-blended concrete mixtures to assess the adiabatic heat generation.

The findings indicate that adiabatic temperature rise, and the rate of temperature rise of slag-blended mixtures depend on slag chemical composition; namely, alumina and magnesia content as well as the cement type. The findings also indicate that adiabatic temperature rise predictions using ACI 207.2R underestimate the adiabatic temperature rise in mass concrete using Type II(MH) and Type IL(10) cements. Type IL concrete mixture showed lower adiabatic temperature rise during the first 48 hours compared to Type II(MH) concrete mixture. At 60% slag replacement, concrete blended with high alumina slag did not provide significant reduction in the adiabatic temperature rise compared to the control mixtures. The findings indicate the significance of the cement and slag chemical and physical characteristics on adiabatic temperature rise in slag-blended concrete mixtures. Mass concrete control plans (MCCP) must be developed based on the specific cement and slag used in the mixture.

The findings of the current research provided the State Materials Office with adiabatic temperature rise curves for concrete made with Type IL(10) and Type II(MH) cements which can be implemented in the approval process of MCCP and subsequently offer a better prediction for field concrete temperature rise in structural elements. Additionally, the current research provided values for equivalent cement factors for different slags (B) which are required for adiabatic temperature prediction in concrete mixtures incorporating slags of variable chemical composition.

Again, the provided scientific data, when implemented in MCCP approval protocols, would minimize related to underpredicting temperature rise in mass concrete elements and therefore enhance the service life of massive structural elements.

Sulfate optimization studies indicate that the sulfate balance of slag-blended cementitious mixtures was affected by the cementitious materials particle size as well as the cement composition (alumina bearing compounds and calcite content) and slag composition (alumina, magnesia and calcite). Isothermal calorimetry was found to be an accurate technique to identify sulfate optimum for slag-blended cementitious systems.

In terms of external sulfate durability, slags blended with IL(10,14) cements showed better durability than mixtures with Type II(MH) or Type I cements. The limestone content was also found to affect durability with higher limestone content showing better durability (up to 11% calcite content). Additionally, sulfate durability experiments conducted on sulfate-optimized slag mixtures, suggest that sulfate durability, assessed using ASTM C1012 for a period of 6 months, improved with sulfate optimization. However, extending the exposure time to 18 months might be critical for proper classification of the appropriate sulfate exposure class.

Internal sulfate attack or delayed ettringite formation (DEF) studies were conducted on plain and slag-blended mortar (60% replacement). The findings indicate that for the control mixtures prepared with Type I (moderate and high alkali content (HA)), Type II moderate heat (MH), Type IL(10), Type IL(14) cements all showed DEF within 120 days. No signs of delayed ettringite formation (DEF) were identified here for mixtures incorporating slag at 60% replacement level whether the slag had the as-received or optimized sulfate content. However, longer monitoring times are needed to verify this conclusion.

The findings also indicate that high alumina slag cementitious systems have higher chloride binding capacities than low alumina slag systems. Further research is needed to assess the effectiveness of slags of variable chemical composition, at different replacement levels, on chloride diffusivity in slag-blended concrete (FDOT Road and Bridge Construction Specification). This is a critical study which is necessary for specifying the minimum slag replacement levels in reinforced structural elements to minimize incidents of reinforcement corrosion and enhance corrosion performance and durability of the infrastructure in the state of Florida.

6.2   Recommendations

Based on the findings of this study, the following recommendations can be made:

1. Proposed specification changes to the following current FDOT specifications:

    a. Specification 929-4 Ground Granulated Blast Furnace Slag: The recommended modification to the specification language is as follows:

Ground granulated blast furnace slag (GGBFS, slag cement, slag) is the quenched, ground by-product of the iron ore refinement process conducted in blast furnaces. It is primarily an amorphous material of calcium aluminosilicate constituents.

929-4 Slag Cement.

   Sub-article 929-4.1 General: Slag and reference cement used for the determination of slag activity tests shall meet the requirements of ASTM C989. Sampling and testing procedures shall follow the requirements of ASTM C989. Calcium sulfate or calcium sulfate and limestone additions are required for slags with alumina content greater than 11%. Addition amounts shall be determined in accordance with ASTM C563 using isothermal calorimetry and a 50:50 cement-GGBFS blend.

   Sub-article 929-4.2 Acceptance Testing of Slag: Acceptance of slag from sources operating under an accepted QC Plan shall be based on the monthly test reports meeting the chemical and physical requirements of ASTM C989 and this Section. Acceptance testing documentation shall include:

1. Reporting results of all testing listed under Section 10 of ASTM C989.
2. Report results of the following elemental oxide content: CaO, SiO_2, Al_2O_3, MgO, MnO, TiO_2, total SO_3, Fe_2O_3, Na_2O and K_2O. Report any limestone addition content, including $CaCO_3$ content.
3. Report any calcium sulfate addition content, including SO_3 content.
4. Report any inorganic processing additions content. If inorganic processing additions are used, report compliance with Section 6.1.2. of ASTM C989.

   Corresponding samples along with monthly test reports shall be submitted to the Department, upon request.

   Sub-article 929-4.3 Exceptions: Slag alumina content shall not exceed 18%. Slags with alumina content $\geq 15\%$ but not exceeding 18% must have an expansion $\leq 0.1\%$ at 365

days when tested in accordance with ASTM C1012 using Type I/II portland cement with an equivalent alkali content of ≤ 0.6%, fixed w/cm of 0.485, and slag content of 50% to be approved for use.

b. Recommended modifications for Standard Specification, Section 346 Table 346-2 for Structural Portland Cement Concrete: The recommended changes to Tables 346-2 and 346-3 are shown below in red, bold, and underlined:

Recommended Modifications to Table 346-2 Cementitious Materials Concrete Mix Proportions (%) (Environmental classification is extremely aggressive, unless otherwise noted)					
Application	Portland Cement	Fly Ash Type F	Slag	Highly Reactive Pozzolans [4]		
				Silica Fume	Metakaolin	Ultra-Fine Fly Ash
General Use	70-82	18-30				
	66-78	15-25		7-9		
	66-78	15-25			8-12	
	66-78	15-25				8-12
	30-40	10-20	50-60			
	30-75 [1]		25-70 [1]			
	41-50		**50-59 [5]**			
	30-40		**60-70**			
	36-43		50-55	7-9		
	33-42		50-55		8-12	
	33-42		50-55			8-12
Precast / Prestressed	70-85 [1]	15-30 [1]				
	70-82	18-30				
	66-78	15-25		7-9		
	66-78	15-25			8-12	
	66-78	15-25				8-12
	30-40	10-20	50-60			
	41-50		**50-59 [5]**			
	30-40		**60-70**			
	36-43		50-55	7-9		
	33-42		50-55		8-12	
	33-42		50-55			8-12
Drilled Shaft	63-67	33-37				
	38-42		58-62			
	30-40	10-20	50-60			
Mass Concrete	50-82 [2]	18-50 [2]				
	50-65 [3]	35-50 [3]				
	66-78	15-25		7-9		
	66-78	15-25			8-12	
	66-78	15-25				8-12
	30-40	10-20	50-60			
	41-50		**50-59 [5]**			
	30-40		**60-70**			
	36-43		50-55	7-9		
	33-42		50-55		8-12	
	33-42		50-55			8-12

Notes:
(1) Slightly Aggressive and Moderately Aggressive environments. For Moderately Aggressive environment, water to cementitious materials ratio (w/cm) must be less than or equal to 0.50.
(2) For Concrete with Core Temperature T≤160°F.
(3) For Concrete with Core Temperature T>160°F.
(4) Highly reactive pozzolans may be used below the specified ranges to enhance strength and workability.
(5) Concrete in contact with soil or water using slag with Al$_2$O$_3$≥15%, requires maximum w/cm = 0.40 and minimum f$_c$′=5,000 psi or demonstrate that slag at 50% replacement of Type II portland cement (ASTM C150), tested in accordance to ASTM C1012 at a fixed w/cm ratio of 0.485, does not exceed 0.1% expansion at 12 months. Report the chemical and physical properties of the cement and slag (according to relevant FDOT reporting requirements on cement and slag) used in ASTM C1012 testing.

Recommended Modifications to Table 346-3 Master Proportion Table			
Class of Concrete	28-day Specified Minimum Compressive Strength **(7)** (f$_c$′) (psi)	Maximum Water to Cementitious Materials Ratio **(7)** (pounds per pounds)	Target Slump Value (inches) [3]
I [1]	3,000	0.53**(8)**	3 [2]
I (Pavement)	3,000	0.50	1.5 or 3 [5]
II [1]	3,400	0.53[8]	3 [2]
II (Bridge Deck)	4,500	0.44	3 [2]
III [4]	5,000	0.44	3 [2]
III (Seal)	3,000	0.53**(8)**	8
IV	5,500	0.41[6]	3 [2]
IV (Drilled Shaft)	4,000	0.41	8.5
V (Special)	6,000	0.37[6]	3 [2]
V	6,500	0.37[6]	3 [2]
VI	8,500	0.37[6]	3 [2]
VII	10,000	0.37[6]	3 [2]

Notes:
(1) For precast three-sided culverts, box culverts, endwalls, inlets, manholes and junction boxes, the target slump value and air content will not apply. The maximum allowable slump is 6 inches, except as noted in (2). The Contractor is permitted to use concrete meeting the requirements of ASTM C478 (4,000 psi) in lieu of the specified Class I or Class II concrete for precast endwalls, inlets, manholes and junction boxes.
(2) The Engineer may allow a maximum target slump of 7 inches when a Type F, G, I or II admixture is used.
(3) For a reduction in the target slump for slip-form operations, submit a revision to the mix design to the Engineer. The target slump for slip-form mix is 1.50 inches.
(4) When precast three-sided culverts, box culverts, endwalls, inlets, manholes or junction boxes require a Class III concrete, the minimum cementitious materials content is 470 pounds per cubic yard. Do not apply the air content range and the maximum target slump shall be 6 inches, except as allowed in (2).
(5) Meet the requirements of Section 350.
(6) When silica fume or metakaolin is required, the maximum water to cementitious material ratio will be 0.35. When ultrafine fly ash is used, the maximum water to cementitious material ratio will be 0.30.
(7) When slag is used as supplementary cementitious materials in structures located in a very severe sulfate environment (S3) according to ACI 201.2 classification, use slag with Al$_2$O$_3$ ≤15%, f$_c$′ > 5,000 psi and maximum w/cm of 0.40.
(8) When used in structures located in a moderate sulfate environment (S1) according to ACI 201.2, the w/cm must not exceed 0.50. When used in structures located in a severe sulfate environment (S2) according to ACI 201.2, the w/cm must not exceed 0.45 and fc' > 4500.

2. For structural concrete elements, where temperature rise is a concern, require use of Figure B2 (Appendix B) for concrete mixtures made with ASTM C595 Type IL cement and Figure B3 for concrete mixtures made with an ASTM C150 Type II(MH) cement in the MCCP in lieu of Figure 4.3 of ACI 207.2. Use of this data can be enforced during MCCP approval process.

3. Require use of B values in MCCP analysis of 0.85 for slags with alumina content of 8% and 14% and 1.0 for slags with alumina content of 10% and 17%. Use of the specified B values can be enforced during the MCCP approval process.

4. In lieu of Figure B2 or Figure B3 and use of B values, allow specialty engineers to use adiabatic temperature rise values taken from test data from adiabatic or semi-adiabatic temperature rise tests conducted by USBR or a licensed professional engineer. This allowance can be enforced during the MCCP approval process.

5. Require optimization of slag sulfate levels based on the cement intended to be blended with. Perform heat of hydration measurements using isothermal calorimetry to optimize slag sulfate levels.

6. Require testing for external sulfate durability according to ASTM C1012, for a period of 18 months, as part of the approval process for sulfate-optimized slag mixtures.

6.3 Suggestions for Future Work

Based on the findings of this study, the following is recommended;

1. Initiate a study to assess chloride ingress in slag-blended concrete using slag sources of different chemical composition. In addition to assessing the effectiveness of slags of different chemical composition on chloride ingress, the study must also assess the effectiveness of different slag replacement levels on chloride diffusivity. This is a critical study that will directly impact the current specifications pertaining to minimum slag content and subsequently the appropriate use of slag-blended concrete.

2. Initiate a study to assess the degree of slag reactivity and its relationship to chemical, physical and mineralogical characteristics of slags. This will be beneficial to further improve the adiabatic temperature rise prediction for slag-blended concrete mixtures.

3. Initiate a study to assess the sulfate optimization with an expanded matrix of slags and cements currently available in the state of Florida. The study must cover, at a

minimum, the currently approved replacement levels of slags in slag-blended concrete under FDOT Road and Bridge Construction Specification.

4. Initiate a study to investigate the effect of sulfate and limestone content in slag on sulfate durability (external and internal (DEF)) and chloride ingress in slag-blended systems at different replacement levels.

Figure A1: Heat flow of cement BB and S8 with variable sulfate levels
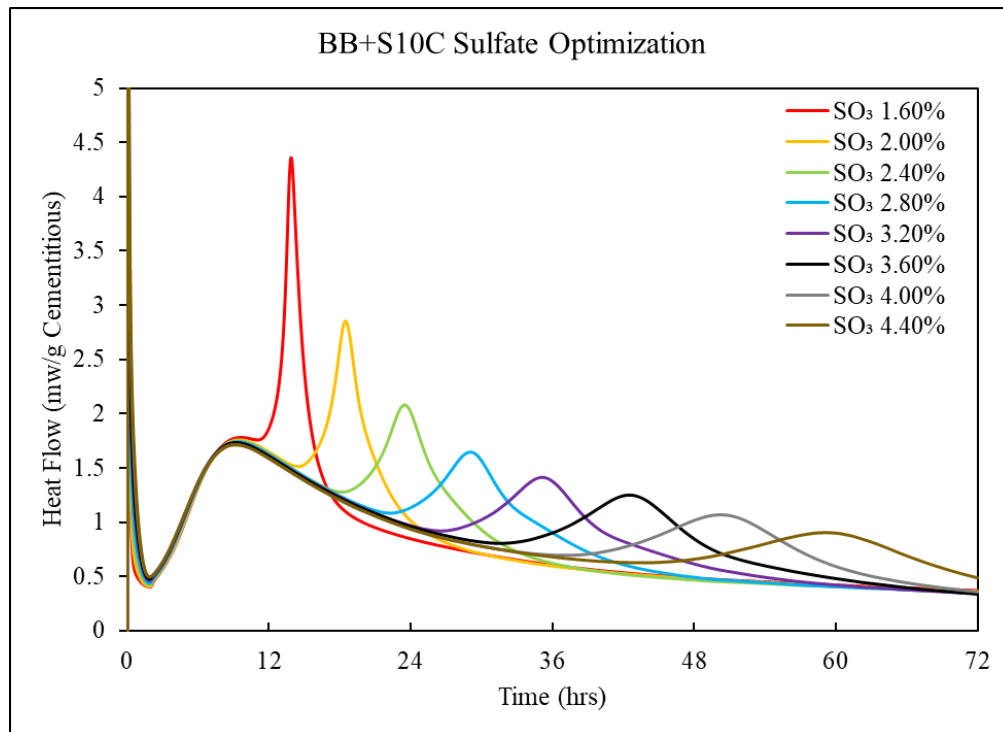
Figure A2: Heat flow of cement BB and S10C with variable sulfate levels
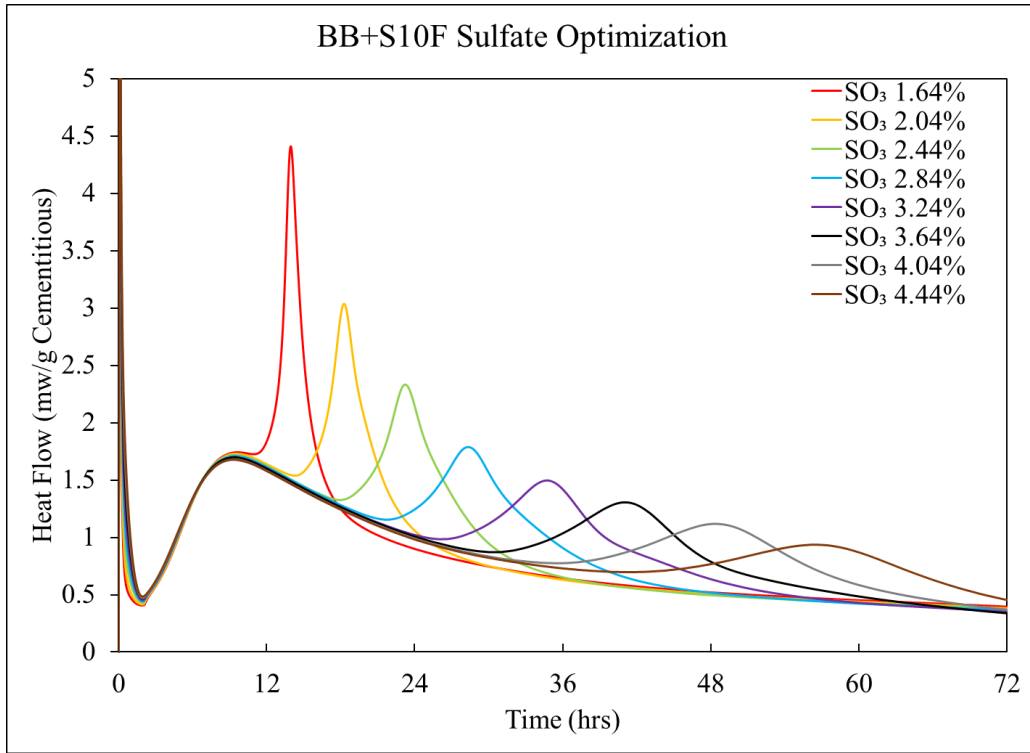
Figure A3: Heat flow of cement BB and S10F with variable sulfate levels
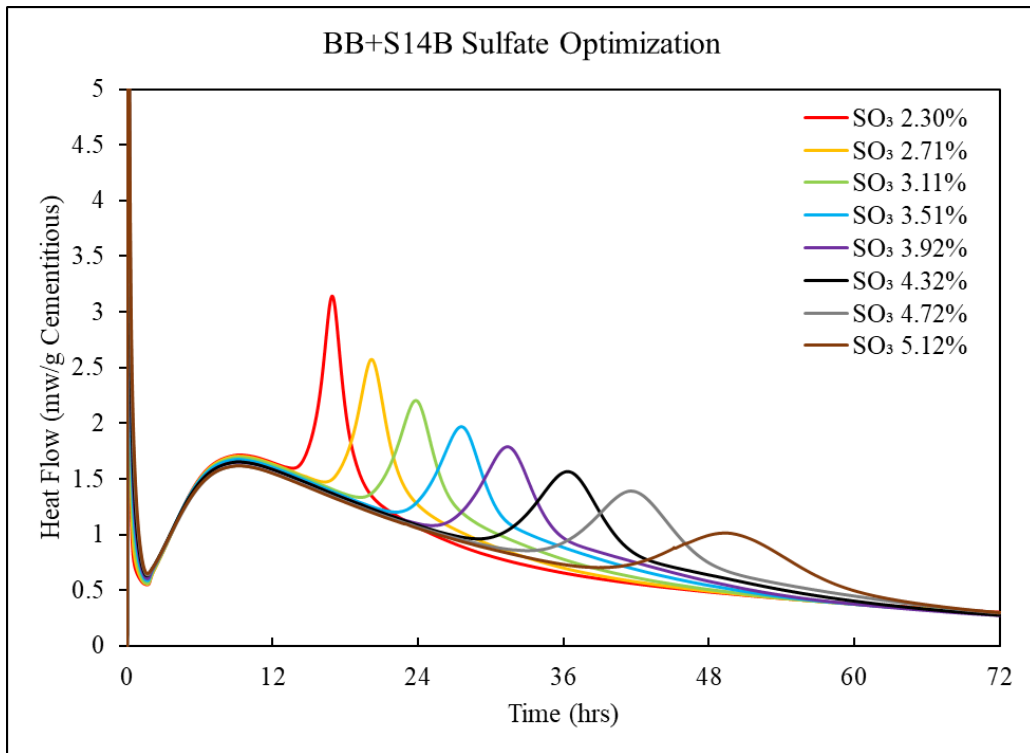
Figure A4: Heat flow of cement BB and S14B with variable sulfate levels
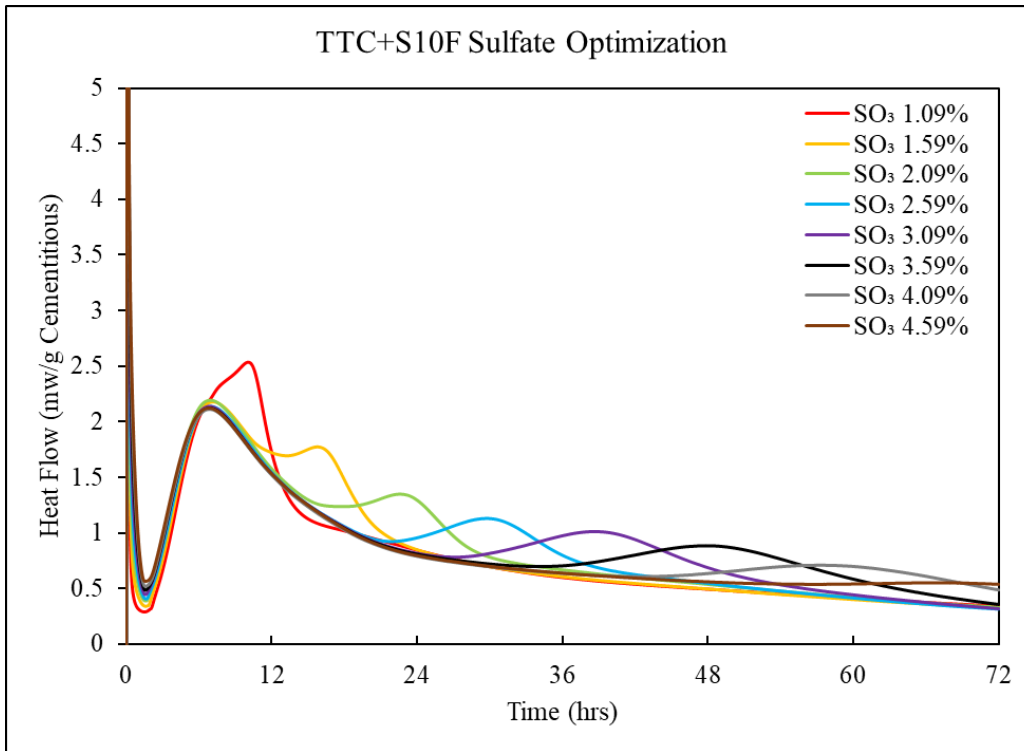
Figure A5: Heat flow of cement TTC and S10F with variable sulfate levels
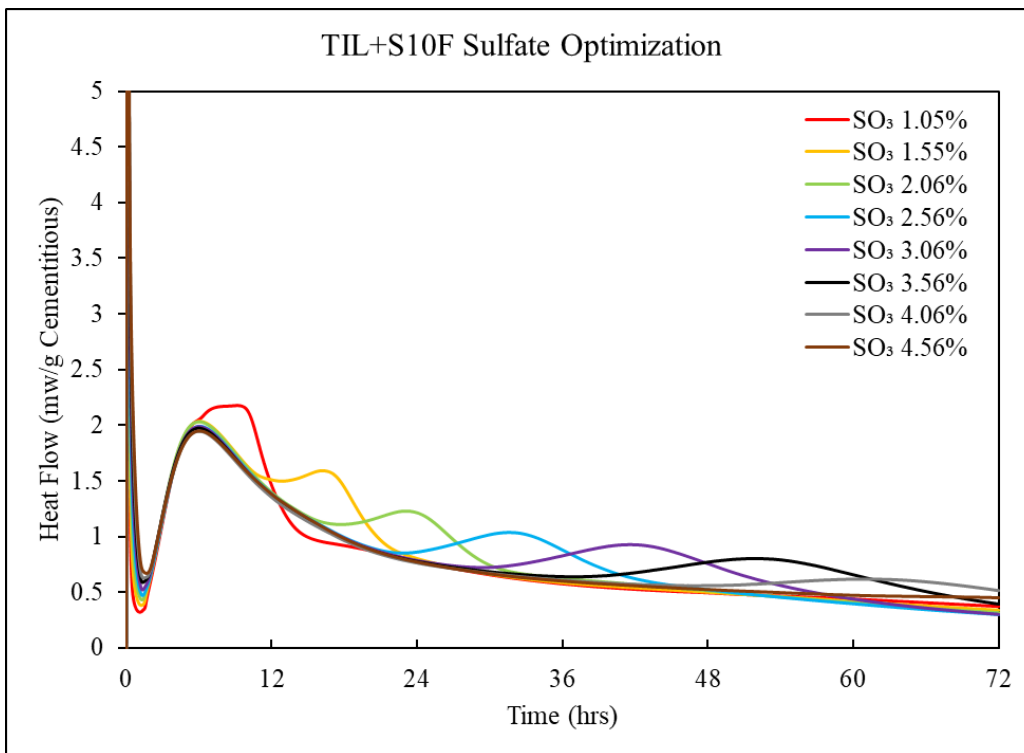
Figure A6: Heat flow of cement TIL and S10F with variable sulfate levels
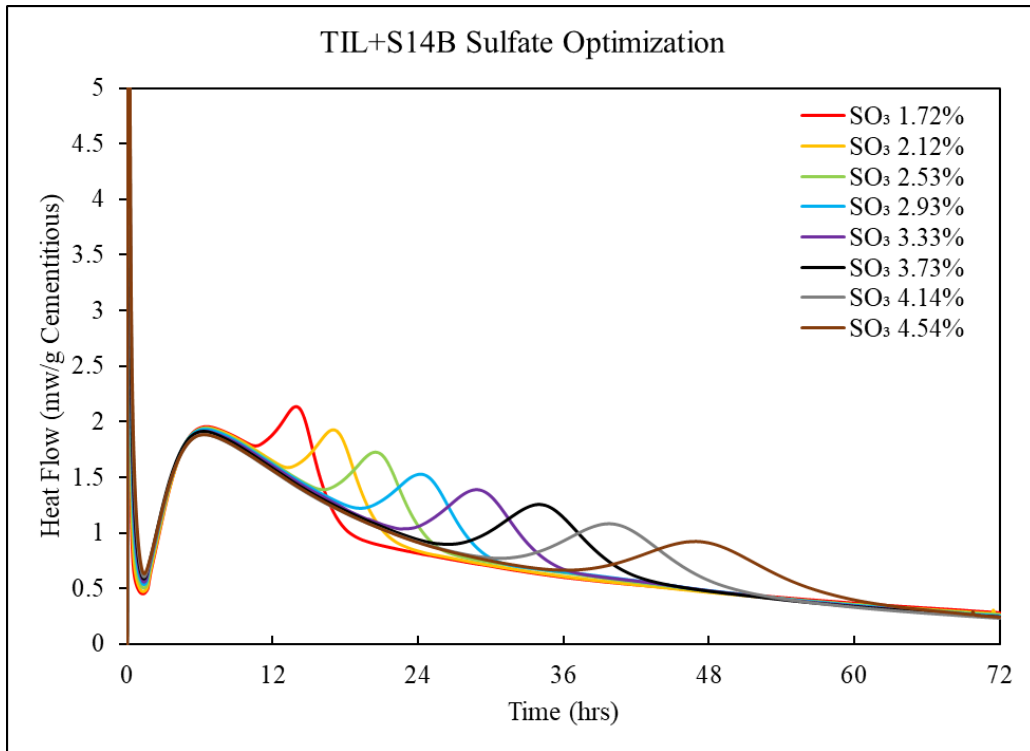
Figure A7: Heat flow of cement TIL and S14B with variable sulfate levels

Appendix B – Mass Slag-Blended Concrete Recommendations

Background

Mass concrete control plans (MCCP) are required by specification 346-3.3 to be developed by a specialty engineer and accepted by the Florida Department of Transportation for all structures designated as mass concrete [1]. As part of the mass concrete control plan, prepared according to ACI 207.2 [2], the concrete member temperature is simulated using as an input the concrete adiabatic temperature rise for a given placement temperature as given in Figure 4.3 of ACI 207.2.

The adiabatic temperature rise given in Figure 4.3 is for 376 lb/yd^3 of ASTM C150 [3] ASTM C150 [4] Type I cement based on extrapolated data from a study performed starting in 1940 and published in 1950 [5]. In that study, cement paste heat of hydration values were collected using conduction calorimetry for 3 days and heat of solution calorimetry [6] at 3 days, 7 days, 28 days, 3 months, 1 year, and 6.5 years. Samples were cured either isothermally or at 70°F for 1 day, followed by 100°F for 27 days, followed by 70°F until the end of testing. There are several reasons why the adiabatic temperature rise values given in Figure 4.3 may not be representative of the adiabatic temperature rise of concrete currently used in Florida Department of Transportation (FDOT) structures. These reasons can be summarized as follows:

1. The test methods and extrapolations used in the 1940s to measure the cement paste heat of hydration did not take into account the effects of a rising temperature from the concrete heat release on the rate of hydration. Since the tests were not performed under adiabatic conditions, and little information is known on any adjustments for this effect, the concrete rate of heat generation may not have been properly accounted for.

2. The 12 Type I cements used in the study to develop the adiabatic temperature rise curves had a Wagner turbidimeter fineness measured according to ASTM C115 [7] between 166.5 and 201 m^2/kg [5]. Equivalent ASTM C204 [8] Blaine fineness values were estimated using an empirical relationship shown in Equation B1 [3]:

$$BF = \frac{WT - 61.123}{0.3858}$$
<div align="right">Equation B1</div>

Where *BF* is the ASTM C204 Blaine fineness (m^2/kg) and *WT* is the ASTM C115 Wagner Turbidimeter measurement in (m^2/kg). The estimated Blaine fineness values ranged from 273 to 363 m^2/kg, with an average of 312 m^2/kg. The cements used were considerably

coarser than modern cements currently used. In addition, the Type I cements used had C_3S content that ranged between 42.5 and 64.5%, with and average value of 49.6%. The C_2S content ranged between 10 and 32%, with an average value of 24%. The lower fineness, C_3S content, and higher C_2S than currently used cements would greatly affect the adiabatic temperature rise rate especially during the first 3 days of curing.

3. The adiabatic temperature rise curves in Figure 4.3 assume a cement content of 376 lb/yd^3, a value appropriate for dam construction or other large hydraulic structures. Concrete mixtures used in FDOT structures use considerably more cementitious materials than 376 lb/yd^3. In order to account for this, the adiabatic temperature rise is typically scaled according to Equation B2:

$$ATR_{CC}(t) = ATR_{207}(t)\frac{C_C}{376}$$ Equation B2

Where $ATR_{CC}(t)$ is the adiabatic temperature rise for the mixture used (°F) at time t (hrs), $ATR_{207}(t)$ is the adiabatic temperature rise for the mixture from Figure 4.3 in ACI 207.2 (°F) at time t, and C_C is the portland cement content in the mixture used (lb/yd^3). ACI 207.2 says that for low and medium cement contents the adiabatic temperature rise is directly proportional to that with 376 lb/yd^3 [2]. High cement contents such as those used in FDOT structures may not be directly proportional, however. Scaling mixture adiabatic temperature rise values does not account for how the increased cement content would cause the temperature to rise faster, increasing the rate of rise faster than what is shown in Figure 4.3. Figure B1 illustrates the differences seen between the predicted adiabatic temperature rise using Figure 4.3 in ACI 207.2 and Equation B2 and measured values from tests performed at the U.S. Bureau of Reclamation (USBR) on an ASTM C150 Type II(MH) cement and an ASTM C595 Type IL(10) cement. Modern cements show a much higher rate of heat generation during the first 36 hours than predicted by ACI 207.2 Figure 3.4 and Equation B2.
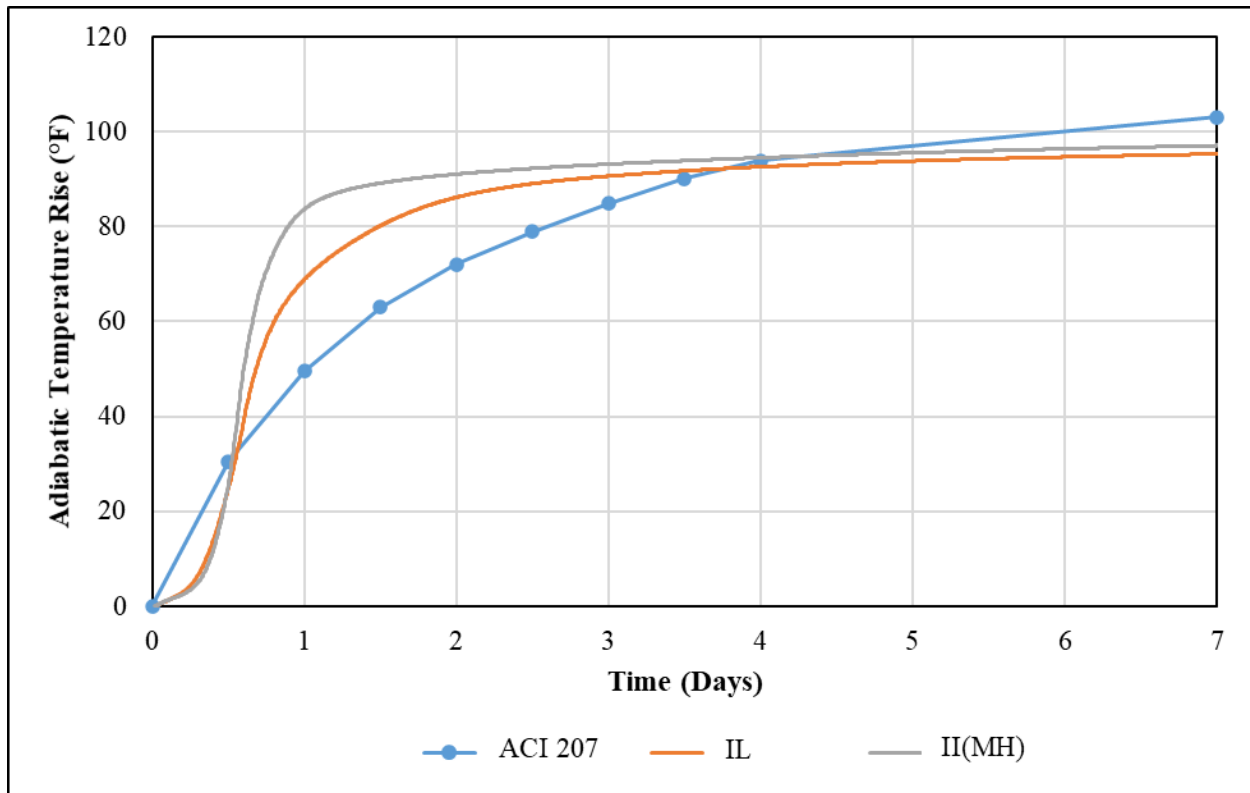
Figure B1: Adiabatic temperature rise predicted using ACI 207 and measured for an ASTM
C595 Type IL(10) and an ASTM C150 Type II(MH) cement

4. ACI 207.2R does not specify how to account for slag heat of hydration when estimating
the concrete adiabatic temperature rise. No directions are given in ACI 207 for IL cements
either. Many specialty engineers estimate the adiabatic temperature rise of mixtures that
contain slag by using an equivalent cement factor B for slag cement. In this case, they
calculate an equivalent cement content CC_{eq} (lb/yd^3) to use in the analysis according to
Equation B3:

$$CC_{eq} = C_C + B \cdot SC \hspace{3cm} \text{Equation B3}$$

Where SC is the slag content (lb/yd^3). A constant value is often used regardless of
slag composition, fineness, or percentage of total cementitious materials, or concrete age.
Slag can retard the cement hydration and may react at a slower rate than portland cement.
This could reduce the accuracy of the analysis with time and could result in inappropriate
amounts of insulation being used, higher than predicted temperatures in the field, and peak
temperatures occurring later than predicted. This may result in concrete forms needing to

273

stay on the concrete member longer than anticipated in the MCCP or cracking of the concrete when they are removed too early.

Proposed Method to Account for Slag in MCCP

Current specifications direct the specialty engineer to develop their own plan based on their preferred construction means and methods. Because ACI 207.2 does not provide recommendations on how to account for slag in the adiabatic temperature rise, engineers to date have been filling in this gap with assumptions that do not always result in accurate temperature predictions in MCCPs. Recommendations are provided to assist FDOT in approving MCCPs and guiding specialty engineers in developing more accurate future MCCPs. The recommended changes are not intended to result in changes to FDOT specifications, only in the practice of MCCP acceptance by FDOT when slag is used.

Based on adiabatic temperature rise testing performed at the USBR on 10 different concrete mixtures and isothermal calorimetry testing performed at the University of South Florida (USF), new charts are proposed to replace Figure 4.3 in ACI 207.2R, along with updated B values based on the slag composition used in MCCPs. While the simplifications proposed to model the adiabatic temperature rise will result in some deviations from the actual adiabatic temperature rise, they provide a significant improvement over what is currently used.

Adiabatic temperature rise curves were calculated by first calculating the activation energies E_a for cements IL and Z from isothermal calorimetry performed at three different temperatures (Chapter 4). The activation energy value used for cement IL was 29,359 J/mol and for cement Z was 28,152 J/mol. Next, coefficients in Equation B4 were fit by simulating the measured concrete adiabatic temperature using the heat generation equation and assumed concrete specific heat values [9]:

$$Q_h(t) = H_u \cdot C_c \cdot \left(\frac{\tau}{t_e}\right)^\beta \cdot \left(\frac{\beta}{t_e}\right) \cdot \alpha_u \cdot \exp\left(-\left[\frac{\tau}{t_e}\right]^\beta\right) \cdot \exp\left(\frac{E_a}{R}\left(\frac{1}{T_r} + \frac{1}{T_c}\right)\right) \qquad \text{Equation B4}$$

Where $Q_h(t)$ is the heat generated with time t (h), where τ is the hydration time parameter (hours), β is the hydration slope parameter, α_u is the ultimate degree of hydration, t_e is the concrete equivalent age (h), H_u is the total heat available for reaction (J/gram) as calculated from the cement composition shown in Equation B5:

$$H_{cem} = 500 \cdot p_{C_3S} + 260 \cdot p_{C_2S} + 866 \cdot p_{C_3A} + 420 \cdot p_{C_4AF} \qquad \text{Equation B5}$$
$$+ 624 \cdot p_{SO_3} + 1186 \cdot p_{FreeCa} + 850 \cdot p_{MgO}$$

Where p_i is the cement component mass-to-total cement content ratio for the ith cement component and H_{cem} = total heat of hydration of the cement (J/gram). The concrete fresh temperature was then changed to be 40, 50, 60, 70, 80, 90, and 100°F while using the fit τ, β, and α_u, values to model the concrete heat generation term. Figure B2 shows the adiabatic temperature rise by placement temperature calculated for cement IL(10), while Figure B3 shows the adiabatic temperature rise by placement temperature for cement II(MH) for 665 lb/yd^3 of cement.

Figure B2: Adiabatic temperature rise by placement temperature calculated using parameters fit from Equation B4 for Type IL(10) cement at 665 lb/yd^3 of cement

Figure B3: Adiabatic temperature rise by placement temperature calculated using parameters fit from Equation B4 for Type II(MH) cement at 665 lb/yd^3 of cement

It is recommended for FDOT to provide Figure B2 and Figure B3 and datasets in Table B1 and **Error! Reference source not found.** to contractors and specialty engineers in Florida that prepare MCCP to use to calculate the adiabatic temperature rise of concrete containing IL cements, information that does not exist in ACI 207.2R. The use of higher adiabatic temperature rise values for Type IL cements than that calculated from Figure 4.3 in ACI 207.2R might disincentive contractors from using Type IL cements, even though they can produce less heat than a Type II(MH) cement, as shown in Figure B1. In order to eliminate this perverse incentive, it is recommended that the adiabatic temperature rise for Type II(MH) seen in Figure B3 also be provided, with approval of the MCCP plan contingent on using this data or equivalent data from tests performed by the contractor.

It is recommended that contractors not be required to change the methods they use to account for slag in the concrete on the adiabatic temperature rise, only the values used. This should simplify adoption by contractors and specialty engineers. To provide updated B values for

Equation B3, they were calculated with age of the concrete by using the ratio of concrete adiabatic temperature rise for the slag mixture and control mixture with time. This ratio was considered to be equal to the ratio of the CC_{eq} for the slag mixture and C_C for the control mixture with time. C_C was set equal to 665 lb/yd^3. B was then calculated from CCeq with time using Equation B3. Adiabatic temperature rise tests were performed on concrete mixtures that contained 60% slag at USBR for different slags. Figure B4 shows the development of B with age. Because specialty engineers currently use a constant B value in their analysis and use of a changing B value would complicate the analysis, it is recommended that conservative values be selected by specialty engineers. For slags S8 and S14, a B value of 0.85 is recommended. For slags S10 and S17, it is recommended to use a B value of 1.0. Use of these B values assumes that Figure B2 and Figure B3 are used in lieu of Figure 4.3 in ACI 207.2. It is recommended that enforcement of these B values be done during the MCCP approval process. Equation B4
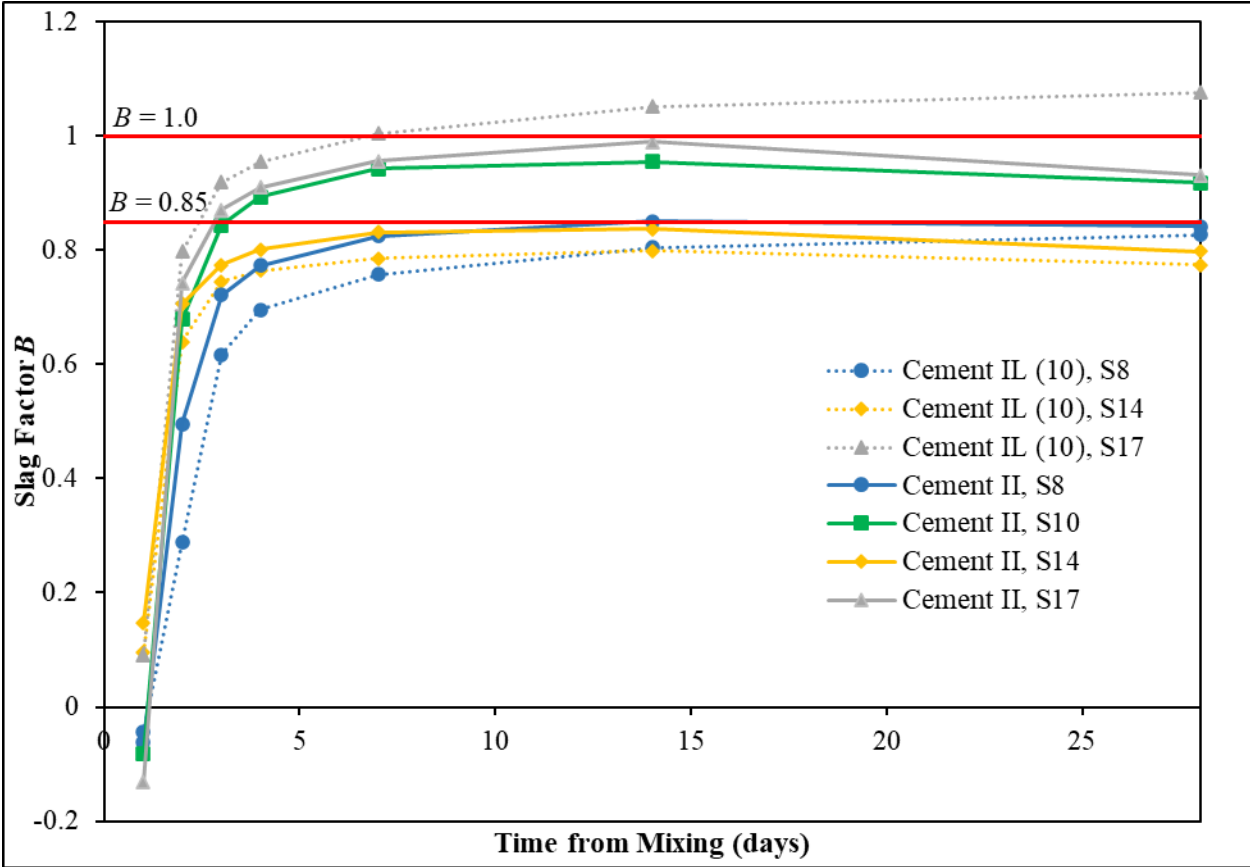
Figure B4: *B* values for slag calculated from adiabatic temperature rise curves for mixtures with slag and the control mixtures

277

Table B1: Adiabatic temperature rise by placement temperature calculated using parameters fit from Equation B4 for Type IL(10) cement at 665 lb/yd^3 of cement

Time		Adiabatic Temperature Rise (deg F)						
		Starting Temp (deg F)						
Days	Hours	40°F	50°F	60°F	70°F	80°F	90°F	100°F
0.1	2.4	0.00018	0.00346	0.03165	0.16944	0.61396	1.6727	3.69522
0.2	4.8	0.12307	0.55021	1.71111	4.11462	8.2185	14.2827	22.2237
0.3	7.2	1.20909	3.33327	7.31392	13.5963	22.2202	32.5954	43.5128
0.4	9.6	3.85884	8.50442	15.8165	25.7388	37.3512	49.0074	59.1655
0.5	12	7.94782	15.3824	25.7645	38.1105	50.4848	61.0697	69.1458
0.6	14.4	13.1528	23.2681	35.9331	49.1188	60.5823	69.2883	75.4372
0.7	16.8	18.9283	31.2448	45.0911	57.8199	67.7192	74.697	79.4384
0.8	19.2	25.3815	39.3487	53.3655	64.8571	73.0746	78.6094	82.2991
0.9	21.6	32.0182	46.8772	60.2408	70.2241	76.9759	81.4134	84.3477
1.0	24	38.5643	53.5752	65.8006	74.3152	79.8781	83.4898	85.8712
1.1	26.4	44.792	59.349	70.2449	77.465	82.088	85.0736	87.0407
1.2	28.8	50.3488	64.0702	73.6842	79.8502	83.7564	86.2749	87.9339
1.3	31.2	55.54	68.1658	76.5552	81.8188	85.1355	87.2739	88.6818
1.4	33.6	60.1266	71.5701	78.8804	83.4057	86.2518	88.088	89.2955
1.5	36	64.1251	74.4013	80.7834	84.7044	87.1704	88.7624	89.8071
1.6	38.4	67.5818	76.7649	82.3581	85.7819	87.9373	89.329	90.2396
1.7	40.8	70.4619	78.6865	83.6336	86.6583	88.5649	89.7957	90.5976
1.8	43.2	73.0337	80.3738	84.7531	87.4316	89.1222	90.2124	90.9189
1.9	45.6	75.2473	81.8105	85.7082	88.0951	89.6032	90.5741	91.1991
2.0	48	77.1578	83.0427	86.5302	88.6695	90.0222	90.8907	91.4454
2.1	50.4	78.813	84.1073	87.2437	89.1711	90.39	91.1701	91.6636
2.2	52.8	80.2069	85.0037	87.8473	89.5979	90.7047	91.4101	91.8517
2.3	55.2	81.4719	85.8185	88.399	89.9902	90.9953	91.6326	92.0267
2.4	57.6	82.5832	86.5363	88.8878	90.3396	91.2555	91.8326	92.1844
2.5	60	83.5643	87.1725	89.3233	90.6527	91.4895	92.0132	92.3273
2.6	62.4	84.4345	87.7393	89.7136	90.9346	91.7012	92.177	92.4573
2.7	64.8	85.1848	88.2302	90.0534	91.1812	91.8871	92.3214	92.5721
2.8	67.2	85.8817	88.6886	90.3723	91.4137	92.0629	92.4584	92.6813
2.9	69.6	86.5081	89.1027	90.6619	91.6258	92.2239	92.5841	92.7817
3.0	72	87.0735	89.4785	90.926	91.8199	92.3717	92.6999	92.8744
3.1	74.4	87.5858	89.8207	91.1677	91.9983	92.508	92.8068	92.9602
3.2	76.8	88.0363	90.1232	91.3822	92.1572	92.6297	92.9026	93.0371
3.3	79.2	88.4627	90.4109	91.5872	92.3095	92.7468	92.9949	93.1114
3.4	81.6	88.853	90.6756	91.7765	92.4507	92.8555	93.0808	93.1807

Table B1 (Continued): Adiabatic temperature rise by placement temperature calculated using parameters fit from Equation B4 for Type IL(10) cement at 665 lb/yd^3 of cement

		Adiabatic Temperature Rise (deg F)						
Time		Starting Temp (deg F)						
Days	Hours	40°F	50°F	60°F	70°F	80°F	90°F	100°F
3.5	84	89.2113	90.9197	91.9518	92.5819	92.9568	93.161	93.2455
3.6	86.4	89.5413	91.1456	92.1147	92.7041	93.0514	93.236	93.3061
3.7	88.8	89.8359	91.3481	92.2612	92.8143	93.1369	93.304	93.3612
3.8	91.2	90.1187	91.5434	92.403	92.9213	93.2201	93.3701	93.4149
3.9	93.6	90.3811	91.7254	92.5355	93.0216	93.2982	93.4324	93.4654
4.0	96	90.6251	91.8953	92.6597	93.1157	93.3717	93.4911	93.5131
4.1	98.4	90.8526	92.0543	92.7762	93.2043	93.441	93.5465	93.5582
4.2	100.8	91.058	92.1983	92.8822	93.285	93.5042	93.5971	93.5995
4.3	103.2	91.2573	92.3387	92.9856	93.364	93.5662	93.6468	93.64
4.4	105.6	91.4442	92.4707	93.0832	93.4387	93.6249	93.6939	93.6785
4.5	108	91.6197	92.5951	93.1754	93.5094	93.6805	93.7386	93.715
4.6	110.4	91.7848	92.7125	93.2627	93.5764	93.7334	93.7812	93.7498
4.7	112.8	91.9352	92.8198	93.3425	93.6379	93.7819	93.8203	93.7818
4.8	115.2	92.0823	92.925	93.4211	93.6985	93.8298	93.8589	93.8135
4.9	117.6	92.2213	93.0248	93.4958	93.7561	93.8754	93.8957	93.8437
5.0	120	92.3529	93.1195	93.5668	93.8111	93.919	93.9309	93.8726
5.1	122.4	92.4777	93.2095	93.6344	93.8635	93.9606	93.9645	93.9002
5.2	124.8	92.592	93.2923	93.6967	93.9118	93.999	93.9956	93.9258
5.3	127.2	92.7047	93.3739	93.7583	93.9597	94.037	94.0265	93.9512
5.4	129.6	92.8118	93.4518	93.8171	94.0055	94.0735	94.0561	93.9755
5.5	132	92.9138	93.5261	93.8734	94.0493	94.1085	94.0845	93.9989
5.6	134.4	93.011	93.5972	93.9272	94.0913	94.142	94.1117	94.0213
5.7	136.8	93.1007	93.6628	93.9771	94.1303	94.1731	94.137	94.0422
5.8	139.2	93.1894	93.7279	94.0266	94.169	94.2041	94.1622	94.063
5.9	141.6	93.2742	93.7902	94.0741	94.2062	94.2339	94.1864	94.083
6.0	144	93.3554	93.85	94.1198	94.242	94.2625	94.2098	94.1023
6.1	146.4	93.4332	93.9074	94.1636	94.2764	94.2901	94.2323	94.1209
6.2	148.8	93.5052	93.9606	94.2043	94.3085	94.3158	94.2533	94.1383
6.3	151.2	93.5768	94.0137	94.245	94.3404	94.3415	94.2742	94.1556
6.4	153.6	93.6455	94.0647	94.2841	94.3713	94.3663	94.2945	94.1724
6.5	156	93.7115	94.1137	94.3218	94.401	94.3902	94.314	94.1886
6.6	158.4	93.775	94.161	94.3582	94.4297	94.4133	94.3329	94.2042
6.7	160.8	93.834	94.205	94.3921	94.4565	94.4349	94.3506	94.2189
6.8	163.2	93.8929	94.249	94.426	94.4833	94.4565	94.3683	94.2336

Table B1 (Continued): Adiabatic temperature rise by placement temperature calculated using parameters fit from Equation B4 for Type IL(10) cement at 665 lb/yd³ of cement

		Adiabatic Temperature Rise (deg F)						
Time		Starting Temp (deg F)						
Days	Hours	40°F	50°F	60°F	70°F	80°F	90°F	100°F
6.9	165.6	93.9497	94.2914	94.4588	94.5092	94.4774	94.3854	94.2478
7.0	168	94.0044	94.3324	94.4905	94.5343	94.4976	94.402	94.2616
7.1	170.4	94.0571	94.372	94.5211	94.5586	94.5172	94.4181	94.2749
7.2	172.8	94.1063	94.409	94.5497	94.5813	94.5356	94.4331	94.2874
7.3	175.2	94.1555	94.446	94.5785	94.6041	94.554	94.4483	94.3
7.4	177.6	94.2031	94.4818	94.6063	94.6262	94.5719	94.463	94.3122
7.5	180	94.2491	94.5165	94.6333	94.6476	94.5893	94.4772	94.3241
7.6	182.4	94.2936	94.5501	94.6594	94.6684	94.6061	94.4911	94.3356
7.7	184.8	94.3352	94.5816	94.6839	94.6879	94.6219	94.5041	94.3464
7.8	187.2	94.3769	94.6132	94.7085	94.7076	94.6379	94.5172	94.3573
7.9	189.6	94.4174	94.6439	94.7324	94.7266	94.6533	94.5299	94.368
8.0	192	94.4566	94.6736	94.7556	94.7451	94.6684	94.5423	94.3783
8.1	194.4	94.4946	94.7025	94.7782	94.7631	94.683	94.5544	94.3883
8.2	196.8	94.5302	94.7296	94.7994	94.7801	94.6967	94.5657	94.3978
8.3	199.2	94.566	94.7568	94.8207	94.7971	94.7106	94.5771	94.4073
8.4	201.6	94.6008	94.7833	94.8415	94.8137	94.7241	94.5883	94.4166
8.5	204	94.6345	94.8091	94.8617	94.8299	94.7373	94.5991	94.4257
8.6	206.4	94.6674	94.8342	94.8813	94.8456	94.7501	94.6097	94.4345
8.7	208.8	94.6982	94.8577	94.8998	94.8605	94.7622	94.6197	94.4428
8.8	211.2	94.7292	94.8815	94.9185	94.8754	94.7744	94.6297	94.4512
8.9	213.6	94.7594	94.9046	94.9367	94.89	94.7863	94.6396	94.4594
9.0	216	94.7888	94.9271	94.9544	94.9042	94.7979	94.6491	94.4674
9.1	218.4	94.8174	94.9491	94.9717	94.9181	94.8092	94.6585	94.4753
9.2	220.8	94.8443	94.9698	94.9879	94.9312	94.8199	94.6673	94.4826
9.3	223.2	94.8715	94.9906	95.0044	94.9444	94.8307	94.6763	94.4901
9.4	225.6	94.8979	95.011	95.0204	94.9573	94.8412	94.685	94.4974
9.5	228	94.9237	95.0309	95.0361	94.9699	94.8515	94.6935	94.5046
9.6	230.4	94.9489	95.0502	95.0514	94.9822	94.8616	94.7019	94.5115
9.7	232.8	94.9726	95.0685	95.0659	94.9939	94.8711	94.7097	94.5181
9.8	235.2	94.9965	95.087	95.0805	95.0056	94.8807	94.7177	94.5248
9.9	237.6	95.0199	95.105	95.0948	95.0172	94.8901	94.7255	94.5313
10.0	240	95.0427	95.1227	95.1087	95.0284	94.8994	94.7332	94.5377
10.1	242.4	95.065	95.1399	95.1224	95.0394	94.9084	94.7406	94.544
10.2	244.8	95.086	95.1562	95.1352	95.0498	94.9169	94.7477	94.5499

Table B1 (Continued): Adiabatic temperature rise by placement temperature calculated using parameters fit from Equation B4 for Type IL(10) cement at 665 lb/yd^3 of cement

Time		Adiabatic Temperature Rise (deg F)						
		Starting Temp (deg F)						
Days	Hours	40°F	50°F	60°F	70°F	80°F	90°F	100°F
10.3	247.2	95.1073	95.1726	95.1483	95.0604	94.9255	94.7549	94.5559
10.4	249.6	95.1281	95.1888	95.1611	95.0707	94.934	94.7619	94.5618
10.5	252	95.1484	95.2045	95.1736	95.0808	94.9423	94.7688	94.5676
10.6	254.4	95.1682	95.2199	95.1858	95.0907	94.9504	94.7755	94.5732
10.7	256.8	95.187	95.2345	95.1974	95.1001	94.9581	94.7819	94.5786
10.8	259.2	95.206	95.2493	95.2092	95.1096	94.9659	94.7884	94.584
10.9	261.6	95.2246	95.2638	95.2207	95.1189	94.9735	94.7947	94.5893
11.0	264	95.2428	95.2779	95.2319	95.128	94.981	94.8009	94.5946
11.1	266.4	95.2606	95.2918	95.243	95.1369	94.9884	94.807	94.5997
11.2	268.8	95.2775	95.3049	95.2534	95.1454	94.9953	94.8128	94.6045
11.3	271.2	95.2946	95.3182	95.264	95.154	95.0024	94.8187	94.6095
11.4	273.6	95.3113	95.3313	95.2744	95.1624	95.0093	94.8245	94.6143
11.5	276	95.3277	95.3441	95.2847	95.1707	95.0161	94.8301	94.6191
11.6	278.4	95.3438	95.3566	95.2947	95.1788	95.0228	94.8357	94.6237
11.7	280.8	95.359	95.3685	95.3041	95.1865	95.0291	94.841	94.6282
11.8	283.2	95.3744	95.3806	95.3138	95.1944	95.0356	94.8463	94.6327
11.9	285.6	95.3896	95.3924	95.3232	95.202	95.0419	94.8516	94.6371
12.0	288	95.4044	95.4041	95.3325	95.2096	95.0481	94.8567	94.6414
12.1	290.4	95.419	95.4155	95.3416	95.217	95.0542	94.8618	94.6457
12.2	292.8	95.4328	95.4263	95.3503	95.224	95.06	94.8666	94.6498
12.3	295.2	95.4468	95.4373	95.3591	95.2312	95.0659	94.8715	94.6539
12.4	297.6	95.4606	95.4481	95.3677	95.2382	95.0717	94.8764	94.6579
12.5	300	95.4741	95.4587	95.3762	95.2451	95.0773	94.8811	94.6619
12.6	302.4	95.4873	95.4691	95.3845	95.2519	95.0829	94.8858	94.6658
12.7	304.8	95.4999	95.4789	95.3924	95.2583	95.0882	94.8902	94.6696
12.8	307.2	95.5127	95.489	95.4005	95.2648	95.0936	94.8947	94.6734
12.9	309.6	95.5253	95.4988	95.4084	95.2713	95.099	94.8991	94.6771
13.0	312	95.5376	95.5085	95.4162	95.2776	95.1042	94.9035	94.6808
13.1	314.4	95.5497	95.5181	95.4238	95.2838	95.1093	94.9078	94.6844
13.2	316.8	95.5612	95.5271	95.4311	95.2898	95.1142	94.9118	94.6878
13.3	319.2	95.5729	95.5363	95.4385	95.2958	95.1192	94.916	94.6913
13.4	321.6	95.5844	95.5454	95.4457	95.3017	95.1241	94.9201	94.6947
13.5	324	95.5957	95.5543	95.4529	95.3076	95.1289	94.9241	94.6981
13.6	326.4	95.6069	95.5631	95.4599	95.3133	95.1336	94.9281	94.7015

Table B1 (Continued): Adiabatic temperature rise by placement temperature calculated using parameters fit from Equation B4 for Type IL(10) cement at 665 lb/yd^3 of cement

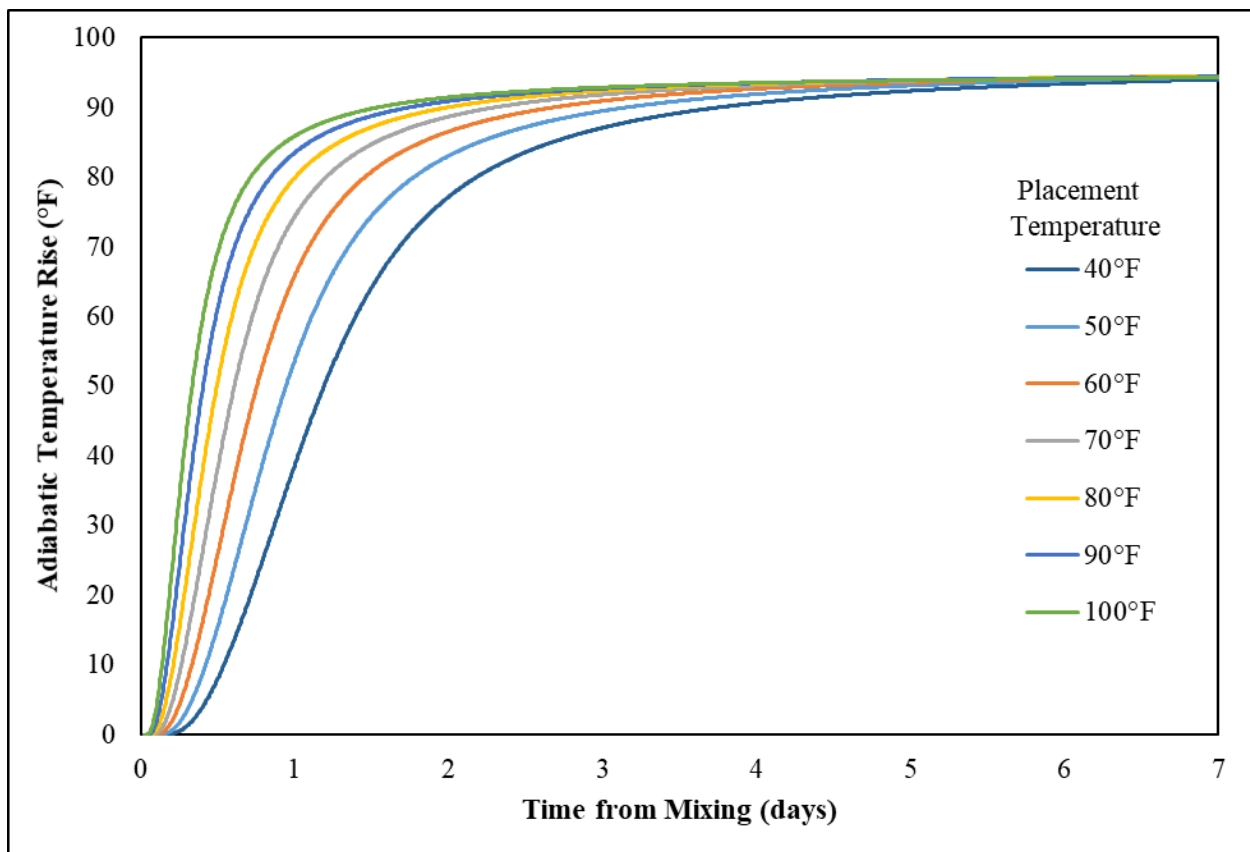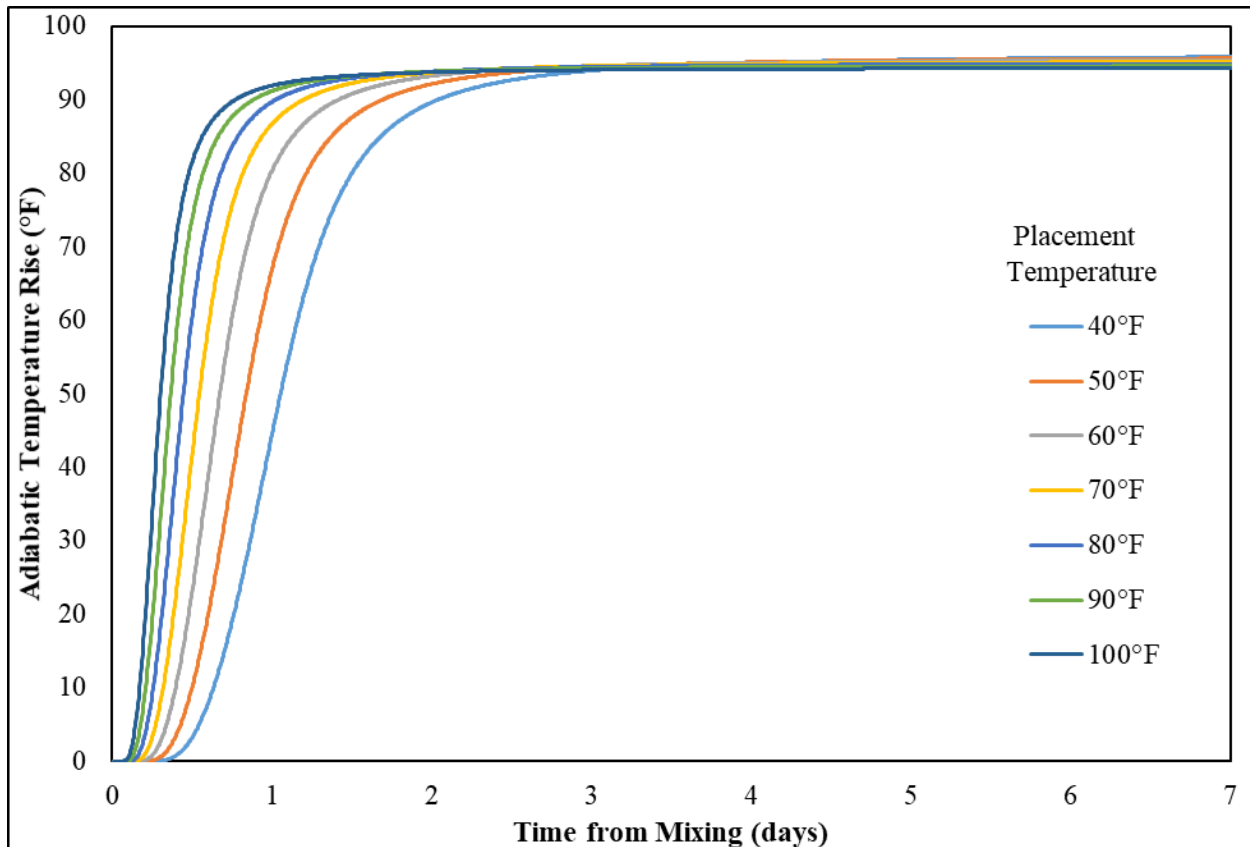| Time		Adiabatic Temperature Rise (deg F)						
		Starting Temp (deg F)						
Days	Hours	40°F	50°F	60°F	70°F	80°F	90°F	100°F
13.7	328.8	95.6174	95.5714	95.4666	95.3188	95.1382	94.9318	94.7046
13.8	331.2	95.6282	95.5799	95.4735	95.3243	95.1428	94.9357	94.7079
13.9	333.6	95.6388	95.5882	95.4802	95.3298	95.1473	94.9395	94.7111
14.0	336	95.6492	95.5965	95.4868	95.3352	95.1517	94.9432	94.7142

Table B2: Adiabatic temperature rise by placement temperature calculated using parameters fit from Equation B4 for Type II(MH) cement at 665 lb/yd^3 of cement

Time		Adiabatic Temperature Rise (deg F)						
		Starting Temp (deg F)						
Days	Hours	40°F	50°F	60°F	70°F	80°F	90°F	100°F
0.1	2.4	0	2.6E-11	1.4E-07	4.9E-05	0.00277	0.04633	0.34143
0.2	4.8	6.6E-05	0.00512	0.09458	0.69479	2.81529	7.76753	16.5577
0.3	7.2	0.04834	0.49743	2.43657	7.51358	17.1801	31.5988	48.3111
0.4	9.6	0.73568	3.41106	10.0971	22.3463	39.554	57.3643	70.8608
0.5	12	3.1442	9.91427	22.8379	41.3566	60.1732	73.6408	81.4287
0.6	14.4	7.62036	19.4082	37.9277	58.2709	73.2637	81.7574	86.2193
0.7	16.8	14.4873	31.6477	53.2834	70.88	81.0091	86.1715	88.8232
0.8	19.2	23.3268	44.7609	65.6902	78.7903	85.3899	88.653	90.3249
0.9	21.6	33.5551	56.8922	74.4449	83.6234	88.007	90.1677	91.2683
1.0	24	44.2839	66.7642	80.2652	86.6582	89.6706	91.1573	91.901
1.1	26.4	54.15	73.9003	84.0061	88.5922	90.7561	91.8201	92.3342
1.2	28.8	63.0494	79.203	86.6419	89.9733	91.5514	92.3172	92.6652
1.3	31.2	70.2375	82.9459	88.4766	90.9565	92.132	92.6876	92.9159
1.4	33.6	75.7713	85.6137	89.7949	91.6807	92.5694	92.9717	93.1108
1.5	36	79.9333	87.5517	90.7704	92.2296	92.9077	93.1949	93.2657
1.6	38.4	82.9547	88.9479	91.4889	92.643	93.1669	93.3682	93.3873
1.7	40.8	85.3228	90.0507	92.0695	92.9839	93.3841	93.515	93.4911
1.8	43.2	87.1272	90.9048	92.5296	93.2591	93.5618	93.6365	93.5777
1.9	45.6	88.5227	91.579	92.9006	93.4847	93.7093	93.7382	93.6507
2.0	48	89.6186	92.1202	93.2044	93.6722	93.8333	93.8244	93.713
2.1	50.4	90.4654	92.5474	93.4485	93.8249	93.9352	93.8958	93.7649
2.2	52.8	91.1771	92.914	93.6615	93.9597	94.026	93.9598	93.8116

Table B2 (Continued): Adiabatic temperature rise by placement temperature calculated using parameters fit from Equation B4 for Type II(MH) cement at 665 lb/yd^3 of cement

Time		Adiabatic Temperature Rise (deg F)						
		Starting Temp (deg F)						
Days	Hours	40°F	50°F	60°F	70°F	80°F	90°F	100°F
2.3	55.2	91.7601	93.2203	93.8421	94.0754	94.1045	94.0155	93.8524
2.4	57.6	92.2433	93.479	93.9968	94.1754	94.1729	94.0642	93.8883
2.5	60	92.6483	93.6997	94.1305	94.2626	94.2329	94.1073	93.9201
2.6	62.4	92.9802	93.8834	94.243	94.3366	94.2842	94.1442	93.9475
2.7	64.8	93.2746	94.0488	94.3454	94.4044	94.3315	94.1783	93.9729
2.8	67.2	93.528	94.1932	94.4357	94.4647	94.3736	94.2089	93.9957
2.9	69.6	93.7479	94.3201	94.5157	94.5185	94.4115	94.2365	94.0163
3.0	72	93.94	94.4323	94.5871	94.5667	94.4455	94.2614	94.035
3.1	74.4	94.1034	94.5287	94.6489	94.6087	94.4754	94.2832	94.0514
3.2	76.8	94.2533	94.6181	94.7066	94.6481	94.5034	94.3039	94.067
3.3	79.2	94.3865	94.6983	94.7587	94.6839	94.529	94.3227	94.0812
3.4	81.6	94.5055	94.7706	94.806	94.7165	94.5524	94.34	94.0943
3.5	84	94.6123	94.836	94.849	94.7463	94.5738	94.3559	94.1063
3.6	86.4	94.7053	94.8934	94.887	94.7727	94.5929	94.37	94.117
3.7	88.8	94.7925	94.9477	94.9231	94.7979	94.6111	94.3835	94.1273
3.8	91.2	94.8718	94.9973	94.9563	94.8211	94.6279	94.3961	94.1369
3.9	93.6	94.9439	95.0428	94.9868	94.8426	94.6435	94.4077	94.1458
4.0	96	95.0098	95.0846	95.015	94.8624	94.658	94.4185	94.154
4.1	98.4	95.0682	95.1218	95.0402	94.8803	94.671	94.4283	94.1615
4.2	100.8	95.1239	95.1575	95.0644	94.8974	94.6836	94.4377	94.1687
4.3	103.2	95.1752	95.1906	95.087	94.9135	94.6953	94.4466	94.1755
4.4	105.6	95.2225	95.2212	95.108	94.9284	94.7063	94.4548	94.1818
4.5	108	95.2664	95.2498	95.1276	94.9424	94.7166	94.4626	94.1878
4.6	110.4	95.3057	95.2755	95.1453	94.9551	94.7259	94.4696	94.1932
4.7	112.8	95.3436	95.3004	95.1624	94.9674	94.7351	94.4765	94.1985
4.8	115.2	95.379	95.3236	95.1786	94.979	94.7436	94.483	94.2035
4.9	117.6	95.4119	95.3454	95.1937	94.9899	94.7517	94.4891	94.2082
5.0	120	95.4427	95.3659	95.208	95.0002	94.7593	94.4949	94.2127
5.1	122.4	95.4706	95.3845	95.2209	95.0096	94.7663	94.5002	94.2167
5.2	124.8	95.4978	95.4026	95.2336	95.0188	94.7731	94.5054	94.2208
5.3	127.2	95.5233	95.4197	95.2456	95.0275	94.7796	94.5103	94.2246
5.4	129.6	95.5472	95.4358	95.257	95.0357	94.7858	94.515	94.2282
5.5	132	95.5698	95.4511	95.2677	95.0435	94.7916	94.5194	94.2316
5.6	134.4	95.5904	95.465	95.2775	95.0507	94.797	94.5235	94.2348

283

Table B2 (Continued): Adiabatic temperature rise by placement temperature calculated using parameters fit from Equation B4 for Type II(MH) cement at 665 lb/yd^3 of cement

Time		Adiabatic Temperature Rise (deg F)						
		Starting Temp (deg F)						
Days	Hours	40°F	50°F	60°F	70°F	80°F	90°F	100°F
5.7	136.8	95.6106	95.4787	95.2872	95.0578	94.8022	94.5276	94.2379
5.8	139.2	95.6297	95.4917	95.2964	95.0645	94.8073	94.5314	94.2409
5.9	141.6	95.6478	95.504	95.3051	95.0709	94.8121	94.5351	94.2437
6.0	144	95.6649	95.5157	95.3135	95.077	94.8166	94.5386	94.2465
6.1	146.4	95.6806	95.5264	95.3211	95.0826	94.8209	94.5418	94.249
6.2	148.8	95.696	95.537	95.3287	95.0882	94.825	94.545	94.2515
6.3	151.2	95.7108	95.5472	95.3359	95.0935	94.829	94.5481	94.2539
6.4	153.6	95.7247	95.5568	95.3428	95.0986	94.8329	94.551	94.2561
6.5	156	95.7381	95.566	95.3494	95.1034	94.8365	94.5538	94.2583
6.6	158.4	95.7504	95.5745	95.3555	95.1079	94.8399	94.5564	94.2604
6.7	160.8	95.7625	95.5829	95.3616	95.1124	94.8433	94.559	94.2624
6.8	163.2	95.7741	95.591	95.3674	95.1167	94.8465	94.5615	94.2643
6.9	165.6	95.7852	95.5987	95.3729	95.1208	94.8497	94.5639	94.2662
7.0	168	95.7958	95.6061	95.3783	95.1247	94.8526	94.5662	94.268
7.1	170.4	95.8057	95.613	95.3832	95.1284	94.8554	94.5683	94.2697
7.2	172.8	95.8154	95.6198	95.3881	95.1321	94.8582	94.5705	94.2713
7.3	175.2	95.8248	95.6263	95.3929	95.1356	94.8609	94.5725	94.2729
7.4	177.6	95.8337	95.6326	95.3974	95.139	94.8634	94.5745	94.2745
7.5	180	95.8423	95.6387	95.4018	95.1422	94.8659	94.5764	94.276
7.6	182.4	95.8503	95.6443	95.4059	95.1453	94.8682	94.5782	94.2774
7.7	184.8	95.8583	95.6499	95.41	95.1483	94.8705	94.58	94.2788
7.8	187.2	95.8659	95.6553	95.4139	95.1512	94.8727	94.5817	94.2801
7.9	189.6	95.8733	95.6605	95.4177	95.1541	94.8749	94.5833	94.2814
8.0	192	95.8804	95.6655	95.4214	95.1568	94.877	94.585	94.2827
8.1	194.4	95.887	95.6702	95.4248	95.1593	94.8789	94.5865	94.2838
8.2	196.8	95.8936	95.6749	95.4282	95.1619	94.8808	94.588	94.285
8.3	199.2	95.9	95.6794	95.4315	95.1644	94.8827	94.5894	94.2862
8.4	201.6	95.9061	95.6837	95.4347	95.1668	94.8846	94.5908	94.2873
8.5	204	95.912	95.6879	95.4378	95.1691	94.8863	94.5922	94.2883
8.6	206.4	95.9176	95.6919	95.4406	95.1712	94.888	94.5935	94.2893
8.7	208.8	95.9231	95.6958	95.4435	95.1734	94.8896	94.5947	94.2903
8.8	211.2	95.9284	95.6996	95.4463	95.1755	94.8912	94.596	94.2913
8.9	213.6	95.9336	95.7033	95.449	95.1775	94.8928	94.5972	94.2923
9.0	216	95.9386	95.7069	95.4517	95.1795	94.8943	94.5984	94.2932

Table B2 (Continued): Adiabatic temperature rise by placement temperature calculated using parameters fit from Equation B4 for Type II(MH) cement at 665 lb/yd^3 of cement

Time		Adiabatic Temperature Rise (deg F)						
		Starting Temp (deg F)						
Days	Hours	40°F	50°F	60°F	70°F	80°F	90°F	100°F
9.1	218.4	95.9433	95.7103	95.4541	95.1814	94.8957	94.5995	94.2941
9.2	220.8	95.948	95.7136	95.4566	95.1832	94.8971	94.6006	94.2949
9.3	223.2	95.9526	95.7169	95.459	95.185	94.8985	94.6017	94.2958
9.4	225.6	95.957	95.7201	95.4614	95.1868	94.8999	94.6027	94.2966
9.5	228	95.9613	95.7231	95.4636	95.1885	94.9012	94.6037	94.2974
9.6	230.4	95.9653	95.726	95.4657	95.1901	94.9024	94.6047	94.2981
9.7	232.8	95.9693	95.7289	95.4679	95.1917	94.9036	94.6056	94.2989
9.8	235.2	95.9732	95.7317	95.47	95.1933	94.9048	94.6066	94.2996
9.9	237.6	95.977	95.7345	95.472	95.1948	94.906	94.6075	94.3004
10.0	240	95.9807	95.7371	95.4739	95.1963	94.9071	94.6084	94.301
10.1	242.4	95.9842	95.7396	95.4758	95.1977	94.9082	94.6092	94.3017
10.2	244.8	95.9876	95.7421	95.4777	95.1991	94.9093	94.61	94.3024
10.3	247.2	95.991	95.7446	95.4795	95.2004	94.9103	94.6108	94.303
10.4	249.6	95.9943	95.747	95.4812	95.2018	94.9114	94.6116	94.3036
10.5	252	95.9975	95.7493	95.483	95.2031	94.9124	94.6124	94.3043
10.6	254.4	96.0005	95.7515	95.4846	95.2043	94.9133	94.6132	94.3048
10.7	256.8	96.0036	95.7537	95.4862	95.2055	94.9143	94.6139	94.3054
10.8	259.2	96.0065	95.7558	95.4878	95.2067	94.9152	94.6146	94.306
10.9	261.6	96.0094	95.7579	95.4893	95.2079	94.9161	94.6153	94.3065
11.0	264	96.0122	95.7599	95.4909	95.2091	94.917	94.616	94.3071
11.1	266.4	96.0149	95.7619	95.4923	95.2102	94.9178	94.6167	94.3076
11.2	268.8	96.0175	95.7638	95.4937	95.2112	94.9186	94.6173	94.3081
11.3	271.2	96.0201	95.7657	95.4951	95.2123	94.9195	94.618	94.3086
11.4	273.6	96.0227	95.7675	95.4965	95.2134	94.9203	94.6186	94.3091
11.5	276	96.0251	95.7693	95.4979	95.2144	94.9211	94.6192	94.3096
11.6	278.4	96.0275	95.771	95.4991	95.2153	94.9218	94.6198	94.3101
11.7	280.8	96.0298	95.7727	95.5004	95.2163	94.9225	94.6204	94.3105
11.8	283.2	96.0321	95.7744	95.5016	95.2173	94.9233	94.6209	94.311
11.9	285.6	96.0344	95.7761	95.5029	95.2182	94.924	94.6215	94.3114
12.0	288	96.0366	95.7777	95.5041	95.2191	94.9247	94.622	94.3118
12.1	290.4	96.0386	95.7792	95.5052	95.2199	94.9254	94.6226	94.3123
12.2	292.8	96.0407	95.7807	95.5063	95.2208	94.926	94.6231	94.3127
12.3	295.2	96.0428	95.7822	95.5075	95.2217	94.9267	94.6236	94.3131
12.4	297.6	96.0448	95.7837	95.5085	95.2225	94.9273	94.6241	94.3135

Table B2 (Continued): Adiabatic temperature rise by placement temperature calculated using parameters fit from Equation B4 for Type II(MH) cement at 665 lb/yd^3 of cement

		Adiabatic Temperature Rise (deg F)						
Time		Starting Temp (deg F)						
Days	Hours	40°F	50°F	60°F	70°F	80°F	90°F	100°F
12.5	300	96.0467	95.7851	95.5096	95.2233	94.928	94.6246	94.3139
12.6	302.4	96.0486	95.7864	95.5106	95.2241	94.9285	94.6251	94.3142
12.7	304.8	96.0504	95.7878	95.5117	95.2249	94.9291	94.6255	94.3146
12.8	307.2	96.0523	95.7891	95.5127	95.2256	94.9297	94.626	94.315
12.9	309.6	96.0541	95.7905	95.5136	95.2264	94.9303	94.6264	94.3153
13.0	312	96.0558	95.7917	95.5146	95.2271	94.9309	94.6269	94.3157
13.1	314.4	96.0575	95.793	95.5155	95.2278	94.9314	94.6273	94.316
13.2	316.8	96.0591	95.7942	95.5164	95.2285	94.932	94.6277	94.3163
13.3	319.2	96.0608	95.7954	95.5173	95.2292	94.9325	94.6281	94.3167
13.4	321.6	96.0624	95.7966	95.5182	95.2299	94.933	94.6286	94.317
13.5	324	96.064	95.7977	95.5191	95.2305	94.9335	94.629	94.3173
13.6	326.4	96.0655	95.7988	95.5199	95.2312	94.934	94.6293	94.3176
13.7	328.8	96.067	95.7999	95.5208	95.2318	94.9345	94.6297	94.3179
13.8	331.2	96.0685	95.801	95.5216	95.2324	94.935	94.6301	94.3182
13.9	333.6	96.0699	95.8021	95.5224	95.233	94.9355	94.6305	94.3185
14.0	336	96.0713	95.8032	95.5232	95.2336	94.9359	94.6308	94.3188

Summary of Recommendations

The following changes in FDOT policies, procedures, or specifications are made:

1. No changes are recommended for FDOT specification 346- 3.3.
2. Require use of Figure B2 for concrete made with an ASTM C595 Type IL cement, and Figure B3 for concrete made with an ASTM C150 Type II(MH) cement in the MCCP in lieu of Figure 4.3 of ACI 207. Use of this data can be enforced during the MCCP approval process.
3. Require use of *B* values in MCCP analysis of 0.85 for slags S8 and S14 and 1.0 for slags S10 and S17. Use of these values can be enforced during the MCCP approval process.
4. In lieu of Figure B2 or Figure B3 and use of B values, allow specialty engineers to use adiabatic temperature rise values taken from test data from adiabatic or semi-adiabatic

temperature rise tests conducted by USBR or a licensed professional engineer. This allowance can be enforced during the MCCP approval process.

References

[1]   Florida Department of Transportation, "Standard Specifications for Road and Bridge Construction," Tallahassee, FL, 2020.

[2]   ACI 207.2, "Report on Thermal and Volume Change Effects on Cracking of Mass Concrete," Farmington Hills, MI, 2007.

[3]   J. I. Bhatty and P. D. Tennis, "U.S. and Canadian Cement Characteristics: 2004," *PCA R&D SN2879*. Portland Cement Association, Skokie, Illinois, pp. 1–67, 2008.

[4]   ASTM C150, "Standard Specification for Portland Cement," West Conshohocken, PA: ASTM International, 1947.

[5]   G. J. Verbeck and C. W. Foster, "Long-Time Study of Cement Performance in Concrete. Chapter 6 - The Heats of Hydration of the Cements," *Proceedings, ASTM*, vol. 50, pp. 1235–1262, 1950.

[6]   ASTM C186-44T, "Standard Test Method for Heat of Hydration of Hydraulic Cement," West Conshohocken, PA: ASTM International, 1944.

[7]   ASTM C115/C115M, "Standard Test Method for Fineness of Portland Cement by the Turbidimeter 1," West Conshohocken, PA: ASTM International, 2010.

[8]   ASTM C204, "Standard Test Methods for Fineness of Hydraulic Cement by Air-Permeability," West Conshohocken, PA: ASTM International, 2018.

[9]   K. A. Riding, J. L. Poole, K. J. Folliard, M. C. G. Juenger, and A. K. Schindler, "Modeling Hydration of Cementitious Systems," *ACI Mater. J.*, vol. 109, no. 2, p. 24, 2012.

Appendix C – Phase Quantification of Mixtures before and after Heat Treatment by XRD

Table C1: Phase quantification of control mixtures before and after heat treatment by XRD

Mix ID	BB					C						Z					
Curing age / Analyte	HCR1	HCR2	HCR4	3 months	4 months	HCR1	HCR2	HCR3	HCR4	3 months	4 months	HCR1	HCR2	HCR3	HCR4	3 months	4 months
Alite	23.6	10.9	0.9	0.4	0	23.1	11.7	3.9	3.8	1.5	0.9	28.1	11.7	2.4	2.2	0.4	0.2
Belite	5	4.6	1.4	0.8	0.5	3	2.9	1.5	1.4	1.3	1.3	2.3	2.1	1.9	1.8	0.8	0.8
Aluminate	3.6	1.7	1.1	0.9	0.7	2.4	0.8	0.5	0.5	0.4	0.3	1.4	0.6	0.4	0.3	0.2	0.2
Ferrite	0.4	0.3	0.2	0	0	1.5	0.8	0.6	0.6	0.6	0.4	1.8	1.2	1.1	1	0.9	0.8
Calcite	0.1	0.8	0.3	0	0	0.7	1.5	1.8	1.5	0.8	1	0.9	2.4	2.6	1.7	1.5	1.6
Quartz	0	0	0.1	0	0.1	0.1	0.1	0.1	0.2	0.1	0.2	0.1	0.2	0.1	0.2	0.2	0.2
Portlandite	1.1	4.4	7.8	12.2	11	0.4	2.9	5.6	7.4	7.5	9.1	0.2	4.8	6.6	6.8	10.1	9.5
Periclase	0	0	0	0	0	0.3	0.3	0.3	0.2	0.3	0.3	0.5	0.5	0.5	0.4	0.4	0.4
Dolomite	0	0	0	0	0	0.4	0.5	0.5	0.5	0.4	0.5	0.1	0.1	0.1	0.2	0.1	0.1
Ettringite	1.9	6	0	2.2	5	0.4	3.1	0	0	2.4	3.2	1	2.2	0	0	1.9	2.3
Monosulfate	0	0	0.9	0	0	0	0	0.6	0.3	0	0	0	0	0	0	0	0
Hydrogarnet	0	0	4.1	4.3	5.3	0	0	2.2	3.2	6.9	6.1	0	0	1.8	2.8	4.5	6.4
Hydrotalcite	0	0	0	0	0	0	0	0	0	0	0	0	0	0	0	0	0
Hemicarboaluminate	0	0	0	0	0	0	0	0	0	0	0.1	0	0	0	0	0	0
Gypsum	0.4	0	0	0	0	0.4	0	0	0	0	0	0	0	0	0	0	0
AC/Unidentified	63.9	71.3	83.4	79	77.4	65.7	75.4	82.3	81.8	77.8	76.7	63.7	74.2	82.5	82.6	78.9	77.4

Table C2: Phase quantification of control mixtures before and after heat treatment by XRD

Mix ID	T1L					TH1L				
Curing age / Analyte	HCR1	HCR2	HCR3	HCR4	4 months	HCR1	HCR2	HCR3	HCR4	4 months
Alite	20.9	8.6	0.6	0.5	0.1	19.2	7.2	0.8	0.7	0.2
Belite	2.8	2.7	1.4	1.3	0.7	3.9	3.6	1.7	1.6	0.8
Aluminate	0.4	0	0	0	0	0.6	0	0	0	0
Ferrite	3	2.9	2.8	2.8	2.2	3	2.8	2.5	2.4	2
Calcite	2.4	3.2	3.9	3.4	3.2	2.4	3.6	4.5	4.2	4.3
Quartz	0.7	0.7	0.7	0.6	0.6	0.6	0.6	0.6	0.6	0.7
Portlandite	1.2	4.4	8.2	10	9.5	0.9	4.1	8.8	10	9.9
Ettringite	1.5	2.6	0	0	2.5	1	1.8	0	0	1.7
Monosulfate	0	0	0	0	0	0	0	0.1	0	0
Hydrogarnet	0	0	2.1	3	2.7	0	0	2.3	4	5.3
Hydrotalcite	0	0	0	0	0	0	0	0	0	0
Hemicarboaluminate	0	0	0	0	0	0	0	0	0	0
Gypsum	0	0	0	0	0	0.1	0	0	0	0
AC/Unidentified	67.1	74.8	80.3	79.6	78.3	68.3	76.2	78.6	76.3	75.3

Table C3: Phase quantification of as received slag-cement BB mixtures before and after heat treatment by XRD

Mix ID	BB-60S8					BB-60S10C					BB-60S10F					BB-60S14B				BB-60S17			
Curing age / Analyte	HCR1	HCR2	HCR3	HCR4	4 months	HCR1	HCR2	HCR3	HCR4	4 months	HCR1	HCR2	HCR3	HCR4	4 months	HCR1	HCR2	HCR4	4 months	HCR1	HCR2	HCR4	4 months
Alite	9.9	2.24	0.9	0.8	0.3	9.3	2.5	1.5	1.2	0.4	9.1	2.8	0.8	0.8	0.6	8.8	3.4	0.7	0.4	9.8	3.2	1.4	0.8
Belite	1.6	1.5	1.4	1.4	1.1	1.7	1.6	1.5	1.5	1.3	2.1	2	1.4	1.3	1.1	2.4	2.2	2.2	2	2.5	2.3	2.2	1.9
Aluminate	1.4	0.2	0.1	0.1	0	1.5	0.3	0.2	0.2	0	1.4	0.4	0.1	0.1	0	1.5	0.4	0.2	0	1.7	0.5	0.3	0.1
Ferrite	0	0	0	0	0	0.1	0	0	0	0	0.2	0	0	0	0	0.1	0	0	0	0	0	0	0
Calcite	0.2	1.2	0.6	0.3	0.1	0.1	0.9	0.2	0.2	0.5	0.1	1.6	0.2	0.2	0.2	0.2	3.1	0.5	0.1	0.1	2.6	0.5	0.1
Quartz	0	0	0	0	0	0	0	0	0	0	0	0	0	0	0	0	0	0	0	0	0	0	0
Portlandite	0.4	1.3	1.1	1	1.5	0.4	0.8	1.2	1	1	0.3	0.7	0.6	0.7	1.1	0.5	0.5	0.4	0.6	0.3	0.4	0.4	0.5
Melilite	0.1	0.1	0.1	0.1	0.1	0.1	0.2	0.2	0.1	0.1	0.1	0.1	0.1	0.1	0.1	0.1	0.1	0.1	0.1	0.3	0.3	0.3	0.3
Merwinite	0	0	0	0	0	0.1	0.1	0.1	0.1	0	0.1	0.1	0.1	0.1	0	0	0	0	0	0	0	0	0
Ettringite	0.6	1.6	0	0	0.7	0.5	1.5	0	0	1.3	0.4	0.7	0	0	0.2	1	2.3	0	0.8	0.5	3.7	0	0.4
Monosulfate	0	0	0.1	0.2	0.2	0	0	0.2	0.2	0.3	0	0	0.1	0.2	0.5	0	0	1.2	1	0	0	0.6	0.6
Hydrogarnet	0	0	0.2	0.2	0.3	0	0	1.2	1.1	1.5	0	0	0.3	0.5	1.1	0	0	3.4	3.1	0	0	4.4	4.8
Hydrotalcite	0	0	0.2	0.2	0.7	0	0	0.2	0.2	0.6	0	0	0	0	0.4	0	0	0.3	0.6	0	0.2	0	0.5
Hemicarboaluminate	0	0	0	0	0	0	0	0	0	0	0	0	0	0	0	0	0.1	0	0	0	0.1	0	0
Gypsum	0.4	0	0	0	0	0.2	0	0	0	0	0.2	0	0	0	0	0.3	0	0	0	1	0	0	0
Stratlingite	0	0	0	0	1	0	0	0	0	1.1	0	0	0	0	1.5	0	0	0	0	0	0	0	0
AC/Unidentified	85.3	91.8	95.2	95.6	93.9	85.9	92.2	93.5	94	92	86.3	91.7	96.4	95.9	93.3	85.1	88	90.8	91.2	83.8	86.8	89.7	90.0

Table C4: Phase quantification of as received slag-cement C mixtures before and after heat treatment by XRD

Mix ID	C-60S8				C-60S10C				C-60S10F				C-60S14A				C-60S17			
Curing age / Analyte	HCR1	HCR2	HCR4	4 months	HCR1	HCR2	HCR3	4 months	HCR1	HCR2	HCR4	4 months	HCR1	HCR2	HCR4	4 months	HCR1	HCR2	HCR4	4 months
Alite	8.4	5.8	0.9	0.6	8.2	4.3	1.6	1.1	8.3	4.6	1.9	1.7	8.9	4.3	1.6	0.9	8.5	4	2.1	1.2
Belite	1.5	1.4	1	0.9	1.1	1	0.7	0.5	1.5	1.4	0.9	0.7	1.5	1.3	1.2	0.6	1.9	1.8	1.6	1.3
Aluminate	0.8	0.2	0.1	0	0.7	0.2	0	0	0.9	0.3	0	0	0.8	0.2	0	0	0.5	0.3	0	0
Ferrite	0.3	0.2	0.1	0	0.5	0.3	0.1	0	0.6	0.4	0.3	0.2	0.5	0.3	0.2	0.1	0.4	0.2	0	0
Calcite	0.5	1.6	1.1	0.7	0.5	1.3	0.7	0.1	0.8	1.4	0.5	0.1	0.3	1.6	0.9	0.5	0.3	1.4	0.9	0.9
Quartz	0.1	0.1	0.1	0.1	0	0	0.1	0.1	0	0	0.1	0.1	0	0	0.1	0.1	0	0	0	0
Portlandite	0.1	0.8	0.5	0.3	0.1	0.4	0.1	0.2	0	0.2	0.2	0.3	0	0.2	0.2	0.1	0.2	0.2	0.2	0.3
Periclase	0.2	0.3	0.2	0.2	0.2	0.2	0.1	0.2	0.1	0.1	0.1	0.1	0.1	0.1	0.1	0.1	0.2	0.2	0.1	0.1
Dolomite	0.2	0.2	0.2	0.2	0.2	0.2	0.1	0.2	0.2	0.2	0.2	0.2	0.3	0.2	0.3	0.4	0.2	0.2	0.3	0.3
Melilite	0	0	0	0	0.1	0.1	0.1	0.1	0.1	0.1	0.1	0.1	0.1	0.1	0.1	0.1	0.3	0.3	0.3	0.3
Merwinite	0	0	0	0	0.1	0.1	0.1	0.1	0.1	0.1	0.1	0.1	0	0	0	0	0	0	0	0
Ettringite	1.1	1.3	0	1.1	1.9	1.1	0	0.4	1.4	1.3	0	0.4	1.3	2.9	0	0.7	0.8	3.4	0	0.3
Monosulfate	0	0	0	0	0	0	0	0	0	0	0.2	0.2	0	0	1.2	1.4	0	0	1.3	0.5
Hydrogarnet	0	0	0.7	1	0	0	2.2	3	0	0	1.4	1.3	0	0	3.1	3	0	0	3.1	3.7
Hydrotalcite	0	0	0.9	1.5	0	0	0.8	1.6	0	0	0.7	0.9	0	0	0.2	0.6	0	0	0.5	0.8
Hemicarboaluminate	0	0	0	0	0	0.2	0	0	0	0.1	0.1	0.1	0	0.1	0	0	0	0.2	0	0
Gypsum	0.1	0	0	0	0	0	0	0	0.1	0	0	0	0.3	0	0	0	0.2	0	0	0
Stratlingite	0	0	0	0	0	0	0	0	0	0	0	0	0	0	0	0	0	0	0	0
AC/Unidentified	86.8	88.2	94.2	93.3	86.4	90.6	93.4	92.5	85.9	89.9	93.3	93.5	85.9	88.7	90.8	91.3	86.6	87.9	91.2	90.3

Table C5: Phase quantification of as received slag-cement Z mixtures before and after heat treatment by XRD

Mix ID	Z-60S8				Z-60S10C				Z-60S10F				Z-60S14A				Z-60S14B				Z-60S17			
Curing age / Analyte	HCR1	HCR2	HCR4	4 months	HCR1	HCR2	HCR4	4 months	HCR1	HCR2	HCR4	4 months	HCR1	HCR2	HCR4	4 months	HCR1	HCR2	HCR4	4 months	HCR1	HCR2	HCR4	4 months
Alite	9.3	4.9	1.2	0.6	10.7	5.5	1.1	0.5	9.1	4.6	1.6	1.2	9.4	3.8	1.2	1	9.4	4	1.1	0.7	10.9	3.7	2	1
Belite	0.9	0.7	0.5	0.4	1.2	1.1	0.9	0.3	0.9	0.8	0.7	0.3	1.1	0.9	0.8	0.6	1.2	0.9	0.8	0.6	1.3	1.2	1	0.8
Aluminate	0.5	0.2	0	0	0.5	0.2	0	0	0.6	0.1	0	0	0.5	0.1	0	0	0.5	0.2	0	0	0.2	0.1	0	0
Ferrite	0.5	0.3	0.1	0.1	0.5	0.4	0.3	0.2	0.5	0.4	0.3	0.2	0.5	0.3	0.1	0	0.5	0.4	0.3	0.2	0.3	0.2	0.2	0.1
Calcite	1.6	2.1	1.7	0.7	0.9	2.1	1.5	0.6	0.9	2.1	0.6	0.1	0.2	2.5	1.8	0.4	0.6	2.4	1.7	0.6	0.3	1.9	1	0.8
Quartz	0	1	0.1	0.1	0	0.1	0.1	0.1	0	0	0.1	0.1	0.1	0.1	0	0.1	0	0	0	0.1	0	0.1	0.1	0.1
Portlandite	0.2	1	0.5	0.9	0.1	0.3	0.5	0.5	0.2	0.6	0.4	0.8	0.1	0.4	0.4	0.2	0.1	0.4	0.4	0.6	0.2	0.6	0.7	0.2
Periclase	0.2	0.2	0.2	0.2	0.2	0.2	0.2	0.2	0.3	0.3	0.3	0.2	0.2	0.2	0.1	0.1	0.2	0.3	0.1	0.2	0.2	0.2	0.1	0.1
Dolomite	0.1	0.1	0.2	0.2	0.1	0.1	0.2	0.1	0.1	0.2	0.2	0.2	0.1	0.2	0.2	0.3	0.1	0.1	0.2	0.2	0.1	0.1	0.1	0.1
Melilite	0	0	0	0	0.1	0.1	0.1	0.1	0.1	0.1	0.1	0.1	0.1	0.1	0.1	0.1	0.1	0.1	0.1	0.1	0.3	0.3	0.3	0.3
Merwinite	0	0	0	0	0.1	0.1	0.1	0.1	0.1	0.1	0.1	0.1	0	0	0	0	0	0	0	0	0	0	0	0
Ettringite	1.4	1.2	0	0.4	0.9	0.7	0	0.6	0.9	1.1	0	0.4	0.5	1	0	0.6	0.8	2.2	0	0.6	1.6	3.2	0	0.2
Monosulfate	0	0	0.1	0	0	0	0	0	0	0	0	0	0	0.4	0.7	0.5	0	0	0.3	0.3	0	0	1.1	0.3
Hydrogarnet	0	0	1.1	0.9	0	0	2.4	2.4	0	0	1.6	1.5	0	0	3.9	3.7	0	0	5.1	5.4	0	0	4.4	4.6
Hydrotalcite	0	0	1	1.7	0	0	1.4	2.1	0	0	1.4	2.1	0	0	0.3	0.5	0	0	0.5	1	0	0.1	1.4	1.6
Hemicarboaluminate	0	0	0	0.1	0	0	0	0	0	0.1	0	0	0	0	0	0	0	0	0	0	0	0.2	0	0
Gypsum	0	0	0	0	0	0	0	0	0	0	0	0	0	0	0	0	0.1	0	0	0	0.1	0	0	0
Stratlingite	0	0	0	0	0	0	0	0.7	0	0	0	0	0	0	0	0.6	0	0	0	0	0	0	0	0
AC/Unidentified	85.3	89.3	93.3	93.8	84.8	89	91.3	91.5	86.5	89.6	92.6	92.6	87.2	90.2	90.4	91.4	86.4	89.1	89.4	89.3	84.7	88	88.5	89.6

Table C6: Phase quantification of as received slag-cement TIL mixtures before and after heat treatment by XRD

Mix ID	TIL-60S10F					TIL-60S14B				TIL-60S14A				TIL-60S17			
Curing age / Analyte	HCR1	HCR2	HCR3	HCR4	4 months	HCR1	HCR2	HCR4	4 months	HCR1	HCR2	HCR4	4 months	HCR1	HCR2	HCR4	4 months
Alite	6.7	1.4	0.8	0.6	0.2	7.3	2.3	0.4	0.3	7.1	2	0.3	0.2	7.4	2.6	1	0.6
Belite	1.6	1.5	1	0.8	0.6	1.5	1.4	1.3	1.1	1.6	1.5	1.3	1.1	1.5	1.4	1.3	0.7
Aluminate	0.3	0	0	0	0	0.1	0	0	0	0.1	0	0	0	0.1	0	0	0
Ferrite	1.1	0.7	0.3	0.3	0.2	1.1	0.7	0.5	0.4	1.1	0.8	0.5	0.4	1	0.8	0.4	0.3
Calcite	1.5	1.3	1.2	1	1.8	1.3	2.7	2.8	1.9	1.1	2.9	2.1	1.3	0.9	2.2	1.1	1.6
Quartz	0.2	0.3	0.2	0.2	0.3	0.2	0.3	0.3	0.3	0.2	0.2	0.2	0.3	0.2	0.2	0.3	0.3
Portlandite	0.3	0.9	1	1	1.3	0.8	0.9	0.4	0.6	0.6	0.7	0.9	0.6	0.4	1	1.1	0.4
Melilite	0.1	0.1	0.1	0.1	0.1	0.1	0.1	0.1	0.1	0.1	0.1	0.1	0.1	0.3	0.3	0.3	0.3
Merwinite	0.1	0.1	0.1	0.1	0	0	0	0	0	0	0	0	0	0	0	0	0
Ettringite	0.9	0.6	0	0	0.5	1.3	1.5	0	0.3	0.8	0.6	0	0.3	0.7	2.3	0	0.7
Monosulfate	0	0	0.3	0.2	0.2	0	0	0	0	0	0	1	0.6	0	0	0.8	0.3
Hydrogarnet	0	0	0.2	0.1	0.6	0	0	4.8	4.8	0	0	3.6	3.7	0	0	3.2	3.4
Hydrotalcite	0	0	1.5	1.3	2.5	0	0	0.4	0.8	0	0	0.3	0.9	0	0.1	1.5	2.8
Hemicarboaluminate	0	0.1	0	0	0	0	0.1	0	0	0	0	0	0.1	0	0.2	0	0
Gypsum	0	0	0	0	0	0.2	0	0	0	0.1	0	0	0	0.3	0	0	0
Stratlingite	0	0	0	0	0	0	0	0	0	0	0	0	0.9	0	0	0	0
AC/Unidentified	87.3	93.1	93.2	94.3	91.8	86.2	89.9	88.5	88.7	87.1	91.2	90	89.4	87.3	88.9	90.4	88.6

Table C7: Phase quantification of as received slag-cement THIL mixtures before and after heat treatment by XRD

Mix ID	THIL-60S8				THIL-60S10C				THIL-60S10F				THIL-60S17			
Curing age / Analyte	HCR1	HCR2	HCR4	4 months	HCR1	HCR2	HCR4	4 months	HCR1	HCR2	HCR4	4 months	HCR1	HCR2	HCR4	4 months
Alite	7.2	2.5	0.6	0.4	6.3	1.8	0.4	0.3	6.9	2.5	0.3	0.1	7.3	2.8	0.8	0.5
Belite	1.8	1.7	1.5	1	1.5	1.4	1.1	0.9	1.8	1.6	1.1	0.6	1.6	1.5	1.2	0.7
Aluminate	0.2	0	0	0	0.3	0.1	0	0	0.3	0	0	0	0.1	0	0	0
Ferrite	0.9	0.7	0.5	0.4	1	0.6	0.4	0.3	0.9	0.6	0.3	0.2	0.9	0.5	0.3	0.2
Calcite	1.3	2.2	1.9	1.2	1.3	2.7	2.8	1.4	0.8	2.7	1.8	1.7	1	3.5	1.6	1.8
Quartz	0.3	0.3	0.3	0.4	0.3	0.3	0.2	0.3	0.3	0.3	0.2	0.3	0.3	0.3	0.2	0.3
Portlandite	0.6	1.4	1.2	1.6	0.6	0.4	0.5	1.2	0.4	0.6	0.9	1	0.4	0.8	0.2	0.4
Melilite	0	0	0	0	0.1	0.1	0.1	0.1	0.1	0.1	0.1	0.1	0.3	0.3	0.3	0.3
Merwinite	0	0	0	0	0.1	0.1	0.1	0.1	0.1	0.1	0.1	0.1	0	0	0	0
Ettringite	0.5	0.7	0	0	0.9	0.1	0	0.3	0.7	0.5	0	0.9	0.6	2.4	0	0.6
Monosulfate	0	0	0	0	0	0	0	0	0	0	0.2	0.2	0	0	0.8	0.4
Hydrogarnet	0	0	0	0.2	0	0	1.3	1.2	0	0	0.7	1.2	0	0	3.6	3.4
Hydrotalcite	0	0	1.4	1.9	0	0	2.8	3	0	0	2.3	3.2	0	0.1	1.4	2.5
Hemicarboaluminate	0	0	0	0.1	0	0.1	0	0.1	0	0	0.1	0.2	0	0.1	0	0.1
Gypsum	0	0	0	0	0	0	0	0	0	0	0	0	0.5	0	0	0
AC/Unidentified	87.2	90.4	92.7	92.7	87.5	92.4	90.4	90.9	87.7	91.1	91.9	90.2	86.9	87.7	89.7	88.8

Table C8: Phase quantification of as-received (L0) and sulfate-optimized (L2) cement BB-slag S8 mixtures before and after heat treatment by XRD

Mix ID	BB-60S8-L0					BB-60S8-L2(1.53[*])(2.49[+])			
Curing age / Analyte	HCR1	HCR2	HCR3	HCR4	4 months	HCR1	HCR2	HCR4	4 months
Alite	9.9	2.24	0.9	0.8	0.3	9.2	3.3	0.2	0.1
Belite	1.6	1.5	1.4	1.4	1.1	2.4	2.2	2	1.3
Aluminate	1.4	0.2	0.1	0.1	0	1.4	0.5	0.1	0
Ferrite	0	0	0	0	0	0	0	0	0
Calcite	0.2	1.2	0.6	0.3	0.1	0.1	0.3	0.4	0.3
Quartz	0	0	0	0	0	0	0	0	0
Portlandite	0.4	1.3	1.1	1	1.5	0.5	1.6	0.7	1.3
Melilite	0.1	0.1	0.1	0.1	0.1	0.1	0.1	0.1	0.1
Merwinite	0	0	0	0	0	0	0	0	0
Ettringite	0.6	1.6	0	0	0.7	0.8	4.2	0	0.7
Monosulfate	0	0	0.1	0.2	0.2	0	0	0	0.1
Hydrogarnet	0	0	0.2	0.2	0.3	0	0	0	0.3
Hydrotalcite	0	0	0.2	0.2	0.7	0	0	0	0.2
Hemicarboaluminate	0	0	0	0	0	0	0	0	0
Gypsum	0.4	0	0	0	0	0.9	0	0	0
Stratlingite	0	0	0	0	1	0	0	0	0.6
AC/Unidentified	85.3	91.8	95.2	95.6	93.9	84.4	87.8	96.3	94.7

[*] Optimized SO_3 level in the slag

[+] Optimized SO_3 level in the total system

Table C9: Phase quantification of as-received (L0) and sulfate-optimized (L2) cement BB-slag S10C mixtures before and after heat treatment by XRD

Mix ID	BB-60S10C-L0					BB-60S10C-L2(2.81*)(3.26+)				
Curing age / Analyte	HCR1	HCR2	HCR3	HCR4	4 months	HCR1	HCR2	HCR3	HCR4	4 months
Alite	9.3	2.5	1.5	1.2	0.4	9.7	3.3	1	0.9	0.6
Belite	1.7	1.6	1.5	1.5	1.3	2.3	2.1	2	1.9	1.1
Aluminate	1.5	0.3	0.2	0.2	0	1.3	0.4	0.2	0.1	0.0
Ferrite	0.1	0	0	0	0	0.1	0	0	0	0.0
Calcite	0.1	0.9	0.2	0.2	0.5	0.3	0.2	2.6	1.9	0.2
Quartz	0	0	0	0	0	0	0	0	0	0.0
Portlandite	0.4	0.8	1.2	1	1	0.2	0.7	0.8	0.6	1.3
Melilite	0.1	0.2	0.2	0.1	0.1	0.1	0.1	0.1	0.1	0.0
Merwinite	0.1	0.1	0.1	0.1	0	0.1	0.1	0.1	0.1	0.1
Ettringite	0.5	1.5	0	0	1.3	0.7	5.5	0	0	1.1
Monosulfate	0	0	0.2	0.2	0.3	0	0	1.8	1.9	1.7
Hydrogarnet	0	0	1.2	1.1	1.5	0	0	0.1	0.2	0.3
Hydrotalcite	0	0	0.2	0.2	0.6	0	0	0	0	0.2
Hemicarboaluminate	0	0	0	0	0	0	0	0	0	0.0
Gypsum	0.2	0	0	0	0	1.9	0	0	0	0.0
Stratlingite	0	0	0	0	1.1	0	0	0	0	1.0
AC/Unidentified	85.9	92.2	93.5	94	92	83.4	87.6	91.3	92.4	92.4

* Optimized SO_3 level in the slag

+Optimized SO_3 level in the total system

Table C10: Phase quantification of as-received (L0) and sulfate-optimized (L2) cement BB-slag S14B mixtures before and after heat treatment by XRD

Mix ID	BB-60S14B-L0				BB-60S14B-L2(4.56*)(4.31+)				
Curing age Analyte	HCR1	HCR2	HCR4	4 months	HCR1	HCR2	HCR3	HCR4	4 months
Alite	8.8	3.4	0.7	0.4	9.1	3.6	1.1	1	0.4
Belite	2.4	2.2	2.2	2	1.9	1.8	1.8	1.6	1.4
Aluminate	1.5	0.4	0.2	0	1.4	0.6	0.1	0.1	0
Ferrite	0.1	0	0	0	0	0	0	0	0
Calcite	0.2	3.1	0.5	0.1	0.2	1.1	0.2	0.2	0.1
Quartz	0	0	0	0	0	0	0	0	0
Portlandite	0.5	0.5	0.4	0.6	0.3	1.3	0.7	0.8	0.8
Melilite	0.1	0.1	0.1	0.1	0	0.1	0.1	0.1	0.1
Merwinite	0	0	0	0	0	0	0	0	0
Ettringite	1	2.3	0	0.8	1	8.9	0	0	2.6
Monosulfate	0	0	1.2	1	0	0	3.4	3.4	2.6
Hydrogarnet	0	0	3.4	3.1	0	0	0.2	0.1	0.4
Hydrotalcite	0	0	0.3	0.6	0	0	0	0	0.1
Hemicarboaluminate	0	0.1	0	0	0	0	0	0	0
Gypsum	0.3	0	0	0	1.8	0	0	0	0
Stratlingite	0	0	0	0	0	0	0	0	0
AC/Unidentified	85.1	88	90.8	91.2	84.2	82.6	92.5	92.8	91.4

* Optimized SO_3 level in the slag

+Optimized SO_3 level in the total system

Table C11: Phase quantification of as-received (L0) and sulfate-optimized (L2) cement C-slag S10F mixtures before and after heat treatment by XRD

Mix ID	C-60S10F-L0				C-60S10F-L2(2.67*)(3.20+)				
Curing age / Analyte	HCR1	HCR2	HCR4	4 months	HCR1	HCR2	HCR3	HCR4	4 months
Alite	8.3	4.6	1.9	1.7	10.6	3.3	1.3	1.2	0.5
Belite	1.5	1.4	0.9	0.7	1.1	1	0.9	0.9	0.6
Aluminate	0.9	0.3	0	0	1	0.2	0	0	0
Ferrite	0.6	0.4	0.3	0.2	0.4	0.3	0.1	0	0
Calcite	0.8	1.4	0.5	0.1	0.4	1.5	0.4	0.2	0.3
Quartz	0	0	0.1	0.1	0	0	0	0	0.1
Portlandite	0	0.2	0.2	0.3	0	0.3	0.3	0.2	0.5
Periclase	0.1	0.1	0.1	0.1	0.1	0.1	0.1	0.1	0.1
Dolomite	0.2	0.2	0.2	0.2	0.1	0.2	0.3	0.3	0.3
Melilite	0.1	0.1	0.1	0.1	0.1	0.1	0.1	0.1	0.1
Merwinite	0.1	0.1	0.1	0.1	0.1	0.1	0.1	0.1	0.1
Ettringite	1.4	1.3	0	0.4	1.9	6.4	0	0	1.1
Monosulfate	0	0	0.2	0.2	0	0	1.3	1.4	1.2
Hydrogarnet	0	0	1.4	1.3	0	0	0	0	0.4
Hydrotalcite	0	0	0.7	0.9	0	0	0	0	0.3
Hemicarboaluminate	0	0.1	0.1	0.1	0	0	0	0	0
Gypsum	0.1	0	0	0	0.3	0	0	0	0
Stratlingite	0	0	0	0	0	0	0	0	0.9
AC/Unidentified	85.9	89.9	93.3	93.5	83.9	86.4	95.2	95.6	93.6

* Optimized SO_3 level in the slag

+ Optimized SO_3 level in the total system

Table C12: Phase quantification of as-received (L0) and sulfate-optimized (L2) cement Z-slag S10F mixtures before and after heat treatment by XRD

Mix ID	Z-60S10F-L0				Z-60S10F-L2(2.53[*])(2.82[+])			
Curing age Analyte	HCR1	HCR2	HCR4	4 months	HCR1	HCR2	HCR4	4 months
Alite	9.1	4.6	1.6	1.2	11.7	4.8	1	0.8
Belite	0.9	0.8	0.7	0.3	0.5	0.4	0.3	0.2
Aluminate	0.6	0.1	0	0	0.6	0.2	0	0
Ferrite	0.5	0.4	0.3	0.2	0.5	0.3	0.1	0
Calcite	0.9	2.1	0.6	0.1	0.3	0.9	0.5	1.4
Quartz	0	0	0.1	0.1	0	0	0	0.1
Portlandite	0.2	0.6	0.4	0.8	0.1	0.7	0.3	0.2
Periclase	0.3	0.3	0.3	0.2	0.2	0.2	0.1	0.2
Dolomite	0.1	0.2	0.2	0.2	0.1	0.1	0.2	0.2
Melilite	0.1	0.1	0.1	0.1	0.1	0	0.1	0.1
Merwinite	0.1	0.1	0.1	0.1	0.1	0.1	0.1	0.1
Ettringite	0.9	1.1	0	0.4	0.7	4.2	0	0.5
Monosulfate	0	0	0	0	0	0	0.7	0.5
Hydrogarnet	0	0	1.6	1.5	0	0	0.6	1.1
Hydrotalcite	0	0	1.4	2.1	0	0	0	0.7
Hemicarboaluminate	0	0.1	0	0	0	0	0	0.1
Gypsum	0	0	0	0	0.6	0	0	0
Stratlingite	0	0	0	0	0	0	0	1
AC/Unidentified	86.5	89.6	92.6	92.6	84.5	88.2	96.2	92.7

[*] Optimized SO_3 level in the slag

[+] Optimized SO_3 level in the total system

Table C13: Phase quantification of as-received (L0) and sulfate-optimized (L2) cement Z-slag S14B mixtures before and after heat treatment by XRD

Mix ID	Z-60S14B-L0				Z-60S14B-L2(4.32*)(3.89+)				
Curing age / Analyte	HCR1	HCR2	HCR4	4 months	HCR1	HCR2	HCR3	HCR4	4 months
Alite	9.4	4	1.1	0.7	10.3	3.9	1.4	1.3	0.5
Belite	1.2	0.9	0.8	0.6	0.9	0.7	0.7	0.6	0.6
Aluminate	0.5	0.2	0	0	0.4	0.2	0	0	0.0
Ferrite	0.5	0.4	0.3	0.2	0.5	0.3	0	0	0.0
Calcite	0.6	2.4	1.7	0.6	0.6	1.3	1.8	1.8	1.5
Quartz	0	0	0	0.1	0	0	0	0	0.1
Portlandite	0.1	0.4	0.4	0.6	0.2	0.7	0.7	0.6	0.3
Periclase	0.2	0.3	0.1	0.2	0.3	0.3	0.2	0.2	0.2
Dolomite	0.1	0.1	0.2	0.2	0.2	0.2	0.3	0.3	0.3
Melilite	0.1	0.1	0.1	0.1	0.1	0.1	0.1	0.1	0.0
Merwinite	0	0	0	0	0	0	0	0	0.1
Ettringite	0.8	2.2	0	0.6	0.6	6.9	0	0	1.7
Monosulfate	0	0	0.3	0.3	0	0	2.9	2.9	2.3
Hydrogarnet	0	0	5.1	5.4	0	0	0.5	0.5	1.2
Hydrotalcite	0	0	0.5	1	0	0	0.1	0.1	0.3
Hemicarboaluminate	0	0	0	0	0	0	0	0	0.0
Gypsum	0.1	0	0	0	0.9	0	0	0	0.0
Stratlingite	0	0	0	0	0	0	0	0	0.2
AC/Unidentified	86.4	89.1	89.4	89.3	85.1	85.5	91.4	91.6	90.7

* Optimized SO_3 level in the slag
+Optimized SO_3 level in the total system

Table C14: Phase quantification of as-received (L0) and sulfate-optimized (L2) cement TIL-slag S10F mixtures before and after heat treatment by XRD

Mix ID	T1L-60S10F-L0					T1L-60S10F-L2(2.82*)(2.68+)				
Curing age Analyte	HCR1	HCR2	HCR3	HCR4	4 months	HCR1	HCR2	HCR3	HCR4	4 months
Alite	6.7	1.4	0.8	0.6	0.2	8.8	2	0.8	0.7	0.2
Belite	1.6	1.5	1	0.8	0.6	1.6	1.5	1.4	1.3	1.0
Aluminate	0.3	0	0	0	0	0.1	0	0	0	0.0
Ferrite	1.1	0.7	0.3	0.3	0.2	1	0.8	0.5	0.4	0.4
Calcite	1.5	1.3	1.2	1	1.8	1	1.3	1.8	2.3	1.7
Quartz	0.2	0.3	0.2	0.2	0.3	0.2	0.1	0.2	0.3	0.4
Portlandite	0.3	0.9	1	1	1.3	0.3	1	1.1	1.2	0.8
Melilite	0.1	0.1	0.1	0.1	0.1	0.1	0.1	0.1	0.1	0.0
Merwinite	0.1	0.1	0.1	0.1	0	0.1	0.1	0.1	0.1	0.0
Ettringite	0.9	0.6	0	0	0.5	0.5	3.9	0	0	1.6
Monosulfate	0	0	0.3	0.2	0.2	0	0	1.3	1.3	0.8
Hydrogarnet	0	0	0.2	0.1	0.6	0	0	0	0	0.1
Hydrotalcite	0	0	1.5	1.3	2.5	0	0	0.7	0.7	0.9
Hemicarboaluminate	0	0.1	0	0	0	0	0	0	0	0.0
Gypsum	0	0	0	0	0	1.1	0	0	0	0.0
AC/Unidentified	87.3	93.1	93.2	94.3	91.8	85.1	89.1	91.9	91.6	92.1

* Optimized SO_3 level in the slag

+Optimized SO_3 level in the total system